Chiral perturbation theory for heavy hadrons and chiral effective field theory for heavy hadronic molecules

Lu Meng [1a], Bo Wang [1b,c,d], Guang-Juan Wang [1e,f], Shi-Lin Zhu [g,*]

[a]*Institute of theoretical physics II, Department of physics and astronomy, Ruhr-University Bochum, 44780 Bochum, Germany*
[b]*School of Physical Science and Technology, Hebei University, Baoding 071002, China*
[c]*Key Laboratory of High-precision Computation and Application of Quantum Field Theory of Hebei Province, Baoding 071002, China*
[d]*Research Center for Computational Physics of Hebei Province, Baoding, 071002, China*
[e]*Advanced Science Research Center, Japan Atomic Energy Agency, Tokai, Ibaraki 319-1195, Japan*
[f]*KEK Theory Center, Institute of Particle and Nuclear Studies (IPNS), High Energy Accelerator Research Organization (KEK), 1-1 Oho, Tsukuba, Ibaraki, 305-0801, Japan*
[g]*School of Physics and Center of High Energy Physics, Peking University, Beijing 100871, China*

Abstract

Chiral symmetry and its spontaneous breaking play an important role both in the light hadron and heavy hadron systems. The chiral perturbation theory (χPT) is the low energy effective field theory of the Quantum Chromodynamics. In this work, we shall review the investigations on the chiral corrections to the properties of the heavy mesons and baryons within the framework of χPT. We will also review the scatterings of the light pseudoscalar mesons and heavy hadrons, through which many new resonances such as the $D_{s0}^*(2317)$ could be understood.

Moreover, many new hadron states were observed experimentally in the past decades. A large group of these states is near-threshold resonances, such as the charged charmoniumlike Z_c and Z_{cs} states, bottomoniumlike Z_b states, hidden-charm pentaquark P_c and P_{cs} states and the doubly charmed T_{cc} state, etc. They are very good candidates of the loosely bound molecular states composed of a pair of charmed (bottom) hadrons, which are very similar to the loosely bound deuteron. The modern nuclear force was built upon the chiral effective field theory (χEFT), which is the extension of the χPT to the systems with two matter fields. The long-range and medium-long-range interactions between two nucleons arise from the single- and double-pion exchange respectively, which are well constrained by the chiral symmetry and its spontaneous breaking. The short-distance interactions can be described by the low energy constants. Such a framework works very well for the nucleon-nucleon scattering and nuclei. In this work, we will perform an extensive review of the progress on the heavy hadronic molecular states within the framework of χEFT. We shall emphasize that the same chiral dynamics not only govern the nuclei and forms the deuteron, but also dictates the shallow bound states or resonances composed of two heavy hadrons.

Keywords: Chiral perturbation theory, Effective field theory, Heavy quark symmetry, Heavy hadrons, Heavy hadronic molecules, Phenomenological models
PACS: 21.10.-k, 21.10.Pc, 21.60.Jz, 11.30.Pb, 03.65.Pm

Contents

---

[1]These authors equally contribute to this work.
[*]Corresponding author.
  Email addresses: lu.meng@rub.de (Lu Meng), wangbo@hbu.edu.cn (Bo Wang), wgj@post.kek.jp (Guang-Juan Wang), zhusl@pku.edu.cn (Shi-Lin Zhu)

1. Brief overview of the heavy hadron spectroscopy

Quantum chromodynamics (QCD) is the theory of the strong interaction. Its basic constituents are the quarks and gluons. They carry the color degrees of freedom of the non-Abelian SU(3) color gauge group and interact with each other through the exchange of the gluons. QCD has three salient features: color confinement, asymptotic freedom, chiral symmetry and its spontaneous breaking. No isolated quarks and gluons have been observed. Instead, the quarks and gluons are confined within the colorless mesons and baryons. The interaction strength between the quarks and gluons increases as the energy scale of the interaction decreases. The perturbation in terms of the coupling constant is invalid in the low energy region. The QCD Lagrangian exhibits the exact $SU(3)_L \otimes SU(3)_R$ chiral symmetry when the current quark masses of the up, down and strange quarks vanish, which is spontaneously broken to the $SU(3)_V$. With the small current quark masses, QCD also exhibits the approximate SU(3) flavor symmetry. When the masses of the charm, bottom and top quarks become very large, QCD exhibits the approximate heavy quark spin and

flavor symmetries. These symmetries play a crucial role in our understanding of the heavy hadrons and their strong interactions.

The hadrons encode the underlying information of the QCD dynamics in the nonperturbative region. The hadron spectroscopy tightly connects the experimental measurements with various theoretical frameworks, such as the *ab-initio* lattice QCD simulations, the quark models, QCD sum rule, etc. In the traditional quark model, the mesons and baryons are composed of the quark-antiquark pair ($q\bar{q}$) and three quarks (qqq), respectively. Most of the ground-state and excited hadrons can be successfully described by such a simple framework.

In the past decades, the hadron spectroscopy has been revived by the observation of many excited heavy hadrons [1], the exotic X, Y, Z states [1], and the hidden-charm pentaquark states [2, 3] as well as the doubly charmed teraquark state T_{cc} [4, 5], etc. Readers may find more experimental and theoretical details in the reviews [6, 7, 8, 9, 10, 11, 12, 13, 14, 15, 16, 17]. The traditional quark model failed badly for most of these states. In general, QCD allows the existence of the more complicated forms of structures for the hadrons, such as the hybrid meson, the glueball, the tetraquark state, the pentaquark state, and hadronic molecule, etc. In fact, the multiquark states ($qq\bar{q}\bar{q}$) and ($qqqq\bar{q}$) were proposed together with the conventional mesons and baryons by Gell-Mann [18] and Zweig [19]. These newly observed structures might be the good candidates of the exotic states and contain the missing piece of knowledge about the nonperturbative strong interactions.

Most of the new hadron states are in the heavy sector. Thus, the heavy hadron spectroscopy is of great interest. The heavy hadrons are composed of the light quarks $q = u, d, s$ ($m_q \ll \Lambda_\chi$), and the heavy quarks $Q = c, b$ ($m_Q \gg \Lambda_{\rm QCD}$). Note that the top quark is not considered because it decays into the bottom quark and W boson rapidly and its life time is much shorter than the typical hadronization time scale. Therefore, the heavy hadrons synchronously possess the chiral symmetry for the light quarks as well as the heavy quark symmetry for the heavy quarks. The heavy hadrons are ideal objects to study the dynamics between the light and heavy quarks, and explore the chiral symmetry and heavy quark symmetry simultaneously. In the following, we will give a brief review about the heavy hadron spectroscopy, especially the states which will be analyzed carefully in the following sections.

1.1. Singly heavy mesons

A singly heavy meson is composed of a heavy quark Q and a light antiquark $\bar{q}$ from the perspective of the quark model. From the point of view of heavy quark effective field theory (HQEFT), an open flavor meson contains a heavy quark and a light quark cloud with the quantum numbers of a light antiquark. In Fig. 1, we present the masses of the heavy mesons collected from the Review of Particle Physics (RPP) [1]. For comparison, we also list the predictions of the Godfrey-Isgur quark model (GI model) [20]. The hyperfine splittings between the ground 1^- and 0^- heavy mesons are measured precisely [1]

$$m_{D^*(2007)^0} - m_{D^0} = (142.014 \pm 0.030) \text{ MeV}, \tag{1}$$

$$m_{D^*(2010)^+} - m_{D^+} = (140.603 \pm 0.015) \text{ MeV}, \tag{2}$$

$$m_{D_s^{*\pm}} - m_{D_s^\pm} = (143.8 \pm 0.4) \text{ MeV}, \tag{3}$$

$$m_{B^*} - m_B = (45.21 \pm 0.21) \text{ MeV}, \tag{4}$$

$$m_{B_s^*} - m_{B_s} = (48.6^{+1.8}_{-1.5}) \text{ MeV}, \tag{5}$$

where the ratio between the hyperfine splitting for the charmed and the bottom mesons is around m_c/m_b. The strange quark mass is around 90 MeV, which induces the SU(3) flavor symmetry breaking mass

$$m_{D_s^\pm} - m_{D^\pm} = (98.69 \pm 0.05)\text{MeV}, \tag{6}$$

$$m_{B_s^0} - m_{B^0} = (87.38 \pm 0.16) \text{ MeV}. \tag{7}$$

The P-wave excited states are of special interest. In the quark model, there are four possible spin-orbital configurations $^{(2S+1)}L_J^P = {}^1P_1^+, {}^3P_0^+, {}^3P_1^+, {}^3P_2^+$ for the P-wave heavy mesons with $J^P = 1^+, 0^+, 1^+, 2^+$. The $^1P_1^+$ and $^3P_1^+$ components may mix with each other to form the $J^P = 1^+$ states through the spin-orbital potential. Since the heavy quark is much heavier than the light quarks, the heavy quark symmetry (HQS) is a good symmetry, especially for the bottom hadrons. In the heavy quark limit $m_Q \to \infty$, the light spin j_ℓ decouples with the heavy quark spin s_Q, where $\boldsymbol{j}_\ell = \boldsymbol{s}_q + \boldsymbol{L}$. The quantum numbers j_ℓ^P, s_Q and J are conserved separately. Therefore, one can categorize the

4

heavy mesons with the light j_ℓ and heavy degrees of freedom (d.o.f) s_Q. The two categorization methods based on different bases can always be related to each other through the Clebsch–Gordan (CG) coefficients. For the P-wave heavy mesons,

$$P\text{-wave}: \quad j_\ell^P = \frac{1}{2}^+, \quad J^P = 0^+ \text{ or } 1^+, \tag{8}$$

$$j_\ell^P = \frac{3}{2}^+, \quad J^P = 1^+ \text{ or } 2^+. \tag{9}$$

In the heavy quark limit, the mesons with the same j_ℓ^P are degenerate and can be treated as the heavy spin doublet (see Sec. 2.6). The decay behavior of the two doublets could be distinct. For instance, given large enough phase space, the $j_\ell^P = \frac{1}{2}^+$ and $j_\ell^P = \frac{3}{2}^+$ $c\bar{q}$ doublets decay into the $D^{(*)}\pi$ modes via S-wave and D-wave in the heavy quark limit, respectively. Hence, the $j_\ell^P = \frac{1}{2}^+$ doublet is generally expected to be broad while the $j_\ell^P = \frac{3}{2}^+$ doublet is narrow.

There are four non-strange P-wave charm mesons, the $D_0^*(2300)$ [known as $D_0^*(2400)$ previously], $D_1(2420)$, $D_1(2430)^0$ and $D_2^*(2460)$ [1]. The $D_1(2420)$ is narrow with a width around (31.3 ± 1.9) MeV, while the $D_1(2430)$ is very broad with a width around (314 ± 29) MeV. The $D_0^*(2300)$ is also very broad and its mass from different experimental collaborations varies from 2300 MeV to 2400 MeV [1].

In the charm-strange sector, the four P-wave states are $D_{s0}^*(2317)$, $D_{s1}(2460)$, $D_{s1}(2536)$, $D_{s2}^*(2573)$. All the four states are very narrow. The masses and narrow widths of the $D_{s1}(2536)$ and $D_{s2}^*(2573)$ are consistent with the theoretical predictions for the $(1^+, 2^+)$ doublet [21]. But the low mass and extremely narrow width of the $D_{s0}^*(2317)$ and $D_{s1}(2460)$ states are very puzzling.

In 2003, the $D_{s0}^*(2317)$ was first observed in the $D_s^+\pi^0$ channel by BaBar Collaboration [22]. Later, its axial-vector partner state $D_{s1}(2460)$ was observed by the CLEO Collaboration [23]. They were confirmed by Belle and BaBar Collaborations [24, 25, 26]. Their masses are (2317.8 ± 0.5) MeV and (2459.5 ± 0.6) MeV, respectively [1]. In particular, the $D_{s0}^*(2317)$ and $D_{s1}(2460)$ lie below the DK and D^*K thresholds, respectively. The only allowed strong decay channels are the $D_s^{(*)}\pi$ which break the isospin symmetry and their decay widths are therefore extremely narrow. Since the discoveries, these two states inspired strong interests in the charm-strange mesons due to the following puzzles: (i) the masses of the $D_{s0}^*(2317)$ and $D_{s1}(2460)$ states are significantly lighter than the quark model predictions; (ii) the mass splitting $m_{D_{s1}(2460)} - m_{D_{s0}^*(2317)} = 141.7$ MeV is equal to $m_{D^*} - m_D$ within 2 MeV [(]the P-wave $(0^+, 1^+)$ states and the ground D_s states belong to different heavy quark spin doublets and their hyperfine splittings are unrelated by any symmetry]; (iii) the mass hierarchy $m_{D_{s0}^*(2317)} - m_{D_0^*(2300)} = -25.2$ MeV and $M_{D_{s1}(2460)} - M_{D_1(2430)} = 47.5$ MeV are unnatural.

In order to unveil the mysteries of the $D_{s0}^*(2317)$ and $D_{s1}(2460)$, there exist a lot of investigations in literature, including the quenched and unquenched $c\bar{s}$ quark model [27, 28, 29, 30, 31, 32, 33, 34, 35, 36], the hadronic molecules [37, 38, 39, 40, 41, 42, 43, 44, 45, 46, 47, 48, 49, 50, 51, 52, 53, 54, 55, 56, 57, 58], the compact tetraquark states [59, 60, 61, 62, 63], and the mixing of the $c\bar{s}$ state and tetraquark state [64, 65, 66, 32]. The readers may consult the reviews [7, 67, 11, 68, 17] for more details. We will review the P-wave states with the chiral unitary approaches in Sec. 4.

1.2. Heavy baryons

In the language of the quark model, the heavy baryons are composed of three quarks, which give rises to a very intricate spectroscopy. According to the number of the heavy quarks, the heavy baryons can be classified into the singly heavy baryon Qqq (B_Q), doubly heavy baryon QQq (B_{QQ}) and triply heavy baryon QQQ (B_{QQQ}), respectively. In the view of HQEFT, these three types of heavy baryons consist of the singly, doubly and triply heavy quarks accompanied by the light quark cloud.

For the singly heavy baryons, the two light quarks are in the antisymmetric $\bar{\mathbf{3}}_f$ or the symmetric $\mathbf{6}_f$ flavor representations in the SU(3) flavor symmetry. Experimentally, 30 singly charmed baryons and 22 bottom baryons have been established now [1], which are shown in Fig. 2. In the review, we focus on the ground-state singly/doubly heavy baryons (see Sec. 3) and the possible hadronic molecules composed of the singly/doubly heavy baryons and other hadrons (see Sec. 5.7 and Sec. 5.8).

In the ground-state S-wave singly heavy baryons, the two light quarks form the diquark with the total spin 0 and 1 as shown in Table 1. The diquark then combines with the heavy quark to form the spin-$\frac{1}{2}$ anti-triplet heavy baryons
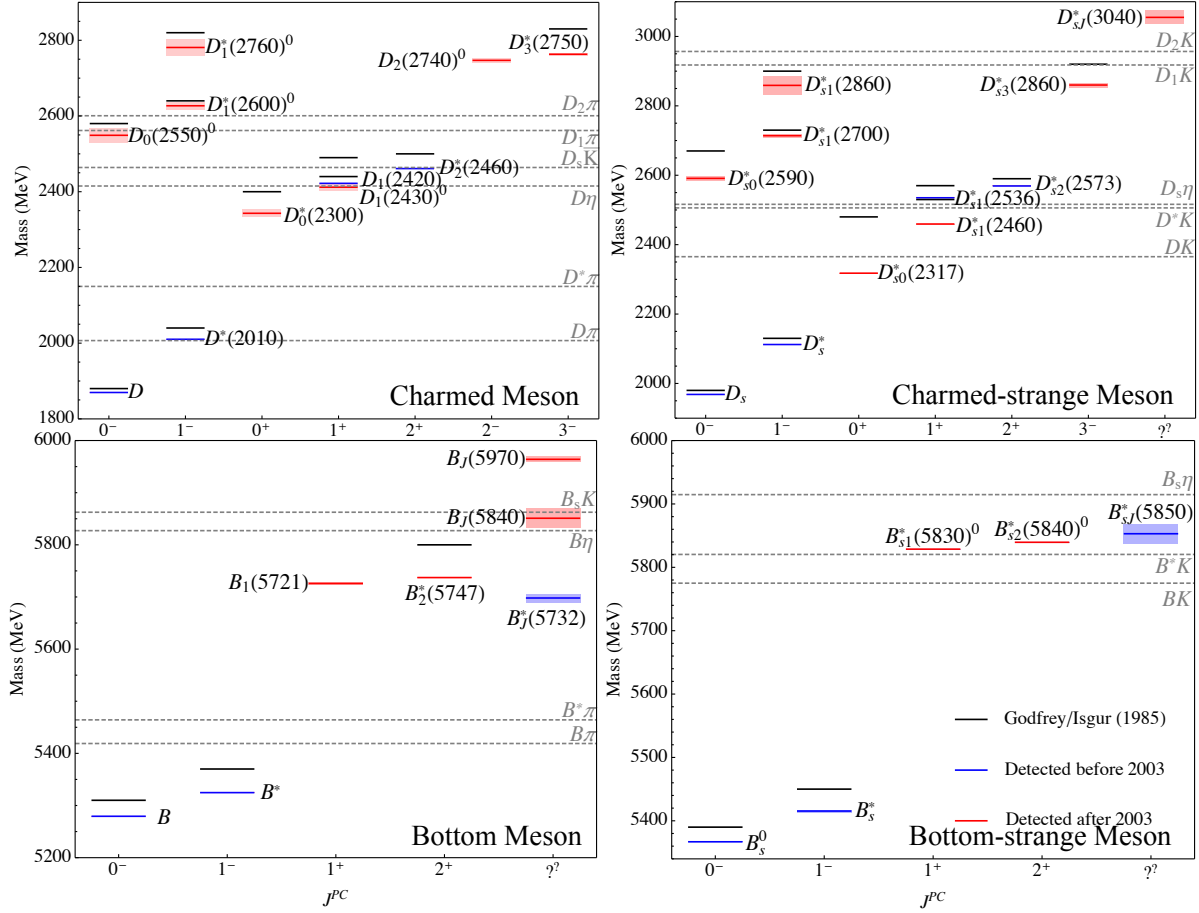
Figure 1: The charmed and bottom mesons from the Review of Particle Physics [1]. The colored band denotes the error of the mass. The dashed horizontal line stands for the threshold. The x- and y-axis represent the J^P quantum numbers and masses (in units of MeV), respectively.

which include the $(\Lambda_c^+, \Xi_c^0, \Xi_c^+)/(\Lambda_b^0, \Xi_b^-, \Xi_b^0)$, and the sextet spin-$\frac{1}{2}$ or $\frac{3}{2}$ heavy baryons which are denoted as the $(\Sigma_c^{++}, \Sigma_c^+, \Sigma_c^0, \Xi_c'^+, \Xi_c'^0, \Omega_c^0)/(\Sigma_b^+, \Sigma_b^0, \Sigma_b^-, \Xi_b'^0, \Xi_b'^-, \Omega_b^-)$ in the charmed/bottom sectors.

In the Σ_Q sector, the $(\Sigma_c(2455), \Sigma_c(2520))$ and (Σ_b, Σ_b^*), form the S-wave doublet $(\frac{1}{2}^+, \frac{3}{2}^+)$ as listed in Table 1. In the Ξ_Q sector, since the three quarks in the Ξ_Q heavy baryons are different, the possible configurations are quite rich. The Ξ_Q can be in the antisymmetric $\bar{\mathbf{3}}_f$ or symmetric $\mathbf{6}_f$ flavor representations as shown in Table 1, which are analogous to the Λ_Q and Σ_Q, respectively. The two lowest Ξ_Q baryons are in the $\bar{\mathbf{3}}_f$ representation and can only decay weakly. The Ξ_c' and $\Xi_c(2645)$, as well as $\Xi_b'(5935)$ and $\Xi_b(5955)^-/\Xi_b(5945)^0$ are in the symmetric $\mathbf{6}_f$ representation and form the S-wave $\Xi_c' \left(\frac{1}{2}^+, \frac{3}{2}^+\right)$ doublet. Constrained by the phase space, the Ξ_c' has no strong decay modes but can decay radiatively. In the Ω_c sector, the lowest Ω_c and $\Omega_c(2770)^0$ form the S-wave doublet $\left(\frac{1}{2}^+, \frac{3}{2}^+\right)$ as shown in Table 1. The former one can only decay weakly, and the latter one mainly decays into the $\Omega_c^0 \gamma$ since the mass difference between the $\Omega_c(2770)^0$ and Ω_c^0 is too small to permit the strong decays. In the bottom sector, only the lowest Ω_b^- with $J^P = \frac{1}{2}^+$ state was observed [69] while its partner state with $J^P = \frac{3}{2}^+$ is still absent. These ground-state singly heavy baryons are understood very well as the conventional Qqq baryons in the quark model.

In quark model, a heavy baryon, composed of three quarks Qqq, has two orbital excitation modes, the ρ-mode with the orbital excitation (L_ρ) between the two light quarks, and the λ-mode one with the orbital excitation L_λ between the heavy quark and the light diquark. They combine to form the total orbital angular momentum $L = L_\rho + L_\lambda$, which then couples with the spin of the two light quarks (s_{qq}) and the heavy quarks (s_Q) to form the total spin J of the heavy

6

baryon. Due to the different excitation modes, there are multiple candidates for the singly baryons with specific $I(J^P)$ quantum numbers as shown in Table 1. In the HQEFT, only the quantum numbers of the light quark cloud j_ℓ^P matter.

Up to now, the knowledge about the excited singly heavy baryons is still quite poor. Among them, the $\Lambda_c(2940)^+$ and $\Sigma_c(2800)$ attracted much attention since they are located very close to the ND^* (2946 MeV) and ND (2805 MeV) thresholds, respectively, which leads to the molecular interpretations as discussed in Sec. 5.8.1.

The $\Lambda_c(2940)^+$ was reported by the BaBar Collaboration in the invariant mass spectrum of the D^0p channel [70]. No signal was seen in the D^+p final state. Therefore the isospin of the $\Lambda_c(2940)^+$ equals 0. Later, the Belle Collaboration confirmed the $\Lambda_c(2940)^+$ in the $\Lambda_c^+\pi^+\pi^-$ final state [71]. In 2017, the LHCb Collaboration analyzed the amplitude of the decay $\Lambda_b^0 \to D^0 p\pi^-$ and found the most likely spin-parity assignment of the $\Lambda_c(2940)^+$ is $\frac{3}{2}^-$, but the assignments with spin $\frac{1}{2}$ to $\frac{7}{2}$ cannot be excluded [72]. Recently, the $\Lambda_c(2910)$ was reported by the Belle Collaboration in the decay process $\bar{B}^0 \to \Sigma_c(2455)\pi\bar{p}$ [73]. Its mass and width are measured to be $2913.8 \pm 5.6 \pm 3.8$ MeV and $51.8 \pm 20.0 \pm 18.8$ MeV, respectively.

In 2005, the Belle Collaboration observed the $\Sigma_c(2800)$ in the $\Lambda_c\pi$ channel [74], which was confirmed by BaBar Collaboration in the $\Lambda_c^+\bar{p}$ channel [75], but with the measured mass about 50 MeV larger. Up to now, the spin-parity quantum numbers of the $\Sigma_c(2800)$ have not been determined yet.

The interpretations of the $\Lambda_c(2940)$ and $\Sigma_c(2800)$ are still controversial. The mass of the $\Lambda_c(2940)^+$ is consistent with the first radial or P-wave excitation of the Λ_c considering the uncertainty of the quark model around tens of MeV [76, 77, 78, 79]. The $\Sigma_c(2800)$ may be the P-wave excitation [80, 81, 82, 83, 84]. However, the $\Lambda_c(2940)^+$ is only 6 MeV lower than the $D^{*0}p$ threshold, which inspired various D^*N molecular interpretations [85, 86, 87, 88, 89, 90, 91, 92, 93]. Similar to the $\Lambda_c(2940)^+$, the $\Sigma_c(2800)$ is located just below the DN threshold and was proposed as a candidate of the DN molecule [91, 92, 93, 94, 95]. More discussions are referred to reviews [96, 97, 98, 7, 99, 100, 17]. In the past several years, many excited heavy baryons including some P-wave states have been observed by LHCb Collaboration. An extensive review of these states can be found in Ref. [17].

In literature, the singly heavy baryon spectroscopy have been studied in different frameworks, such as the various quark models [101, 77, 102, 103, 80, 77, 104, 105, 106, 107, 108, 78, 101, 83, 109, 110], QCD sum rule [111, 112, 113, 114, 115, 116, 117], bag models [118, 119, 120, 121], nonperturbative string approach [122], effective field theory incorporating different symmetries [123, 124, 125, 126, 127], Skyrme model [128], the Faddeev method [76], the relativistic flux tube model [129], lattice QCD [130, 131, 132, 133, 134, 135, 136, 137, 138, 139, 140, 141, 142, 139, 143, 144, 137, 145, 146, 147, 148, 149, 150, 151, 152] and so on. Besides the mass spectrum, the other properties, such as the strong and radiative decays, magnetic moments have also been widely studied [81, 153, 154, 155, 156, 157, 158, 79, 159, 160, 153, 161, 162, 163, 164, 165]. More detailed discussions about the singly heavy baryons can be found in Refs. [7, 97, 166, 98, 17].
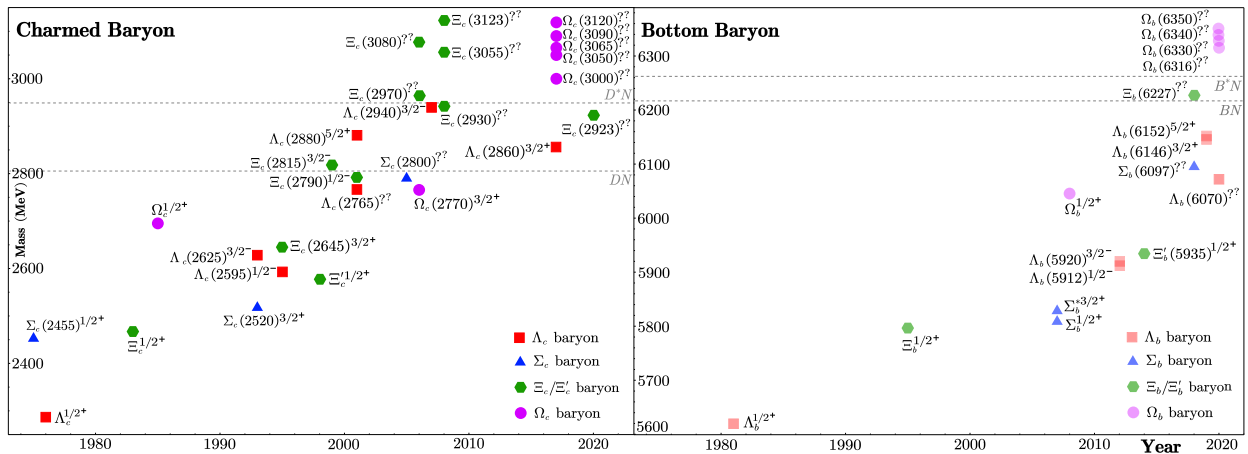

Figure 2: The charmed and bottom baryons from the Review of Particle Physics [1]. The x- and y-axis denote the year of the observation and mass (in units of MeV), respectively. Here, the mass errors are not presented.

For the doubly heavy baryons, the SELEX Collaboration reported the $\Xi_{cc}(3520)^+$ in the $\Lambda_c^+ K^- \pi^+$ [167] as well

Table 1: The possible configurations of the two light quarks in the singly heavy baryon in the quark model. The first five columns are the flavor-color-spatial-spin configurations of the two light quarks, which are antisymmetric under the light quark interchange. The L_ρ and L_λ are the orbital angular momentum between the two light quarks and that between the light quark cluster and the heavy quark, respectively. The j_ℓ^P and s_Q denote the light and heavy d.o.f, respectively. The scripts "S" and "A" represent the exchange symmetry and antisymmetry for the identical particles, respectively.

S-wave

Flavor	Color	L_ρ	s_{qq}	J_{qq}^P	L_λ	j_ℓ^P	s_Q	State	J^P
$\bar{\mathbf{3}}_f$ (A)	$\bar{\mathbf{3}}_c$ (A)	0(S)	0 (A)	0^+	0	0^+	$\frac{1}{2}$	Λ_Q, Ξ_Q	$\frac{1}{2}^+$
$\mathbf{6}_f$ (S)	$\bar{\mathbf{3}}_c$ (A)	0 (S)	1 (S)	1^+	0	1^+	$\frac{1}{2}$	$\Sigma_Q, \Xi'_Q, \Omega_Q$	$(\frac{1}{2}^+, \frac{3}{2}^+)$

λ-mode P-wave

Flavor	Color	L_ρ	s_{qq}	J_{qq}^P	L_λ	j_ℓ^P	s_Q	State	J^P
$\bar{\mathbf{3}}_f$ (A)	$\bar{\mathbf{3}}_c$ (A)	0 (S)	0 (A)	0^+	1	1^-	$\frac{1}{2}$	Λ_{QS}, Ξ_{QS}	$(\frac{1}{2}^-, \frac{3}{2}^-)$
$\mathbf{6}_f$ (S)	$\bar{\mathbf{3}}_c$ (A)	0 (S)	1 (S)	1^+	1	$0^-/1^-/2^-$	$\frac{1}{2}$	$\Sigma_{QA}, \Xi'_{QA}, \Omega_{QA}$	$\frac{1}{2}^-/(\frac{1}{2}^-, \frac{3}{2}^-)/(\frac{3}{2}^-, \frac{5}{2}^-)$

ρ-mode P-wave

Flavor	Color	L_ρ	s_{qq}	J_{qq}^P	L_λ	j_ℓ^P	s_Q	State	J^P
$\bar{\mathbf{3}}_f$ (A)	$\bar{\mathbf{3}}_c$ (A)	1 (A)	1 (S)	0^-	0	0^-	$\frac{1}{2}$	Λ_{QP}, Ξ_{QP}	$\frac{1}{2}^-$
				1^-	0	1^-	$\frac{1}{2}$	Λ_{QV}, Ξ_{QV}	$(\frac{1}{2}^-, \frac{3}{2}^-)$
$\mathbf{6}_f$ (S)	$\bar{\mathbf{3}}_c$ (A)	1 (A)	0 (A)	1^-	0	1^-	$\frac{1}{2}$	$\Sigma_{QV}, \Xi'_{QV}, \Omega_{QV}$	$(\frac{1}{2}^-, \frac{3}{2}^-)$

2-orbital excitations

Flavor	Color	L_ρ	s_{qq}	J_{qq}^P	L_λ	j_ℓ^P	s_Q	State	J^P
$\bar{\mathbf{3}}_f$ (A)	$\bar{\mathbf{3}}_c$ (A)	2 (S)	0 (A)	2^+	0	2^+	$\frac{1}{2}$	Λ_{Q2}, Ξ_{Q2}	$(\frac{3}{2}^+, \frac{5}{2}^+)$
$\mathbf{6}_f$ (S)	$\bar{\mathbf{3}}_c$ (A)	2 (S)	1 (S)	$1^+/2^+/3^+$	0	$1^+/2^+/3^+$	$\frac{1}{2}$	$\Sigma_{Q1/2/3}, \Xi'_{Q1/2/3}, \Omega_{Q1/2/3}$	$(\frac{1}{2}^+, \frac{3}{2}^+)/(\frac{3}{2}^+, \frac{5}{2}^+)/(\frac{5}{2}^+, \frac{7}{2}^+)$

Flavor	Color	L_ρ	s_{qq}	J_{qq}^P	L_λ	j_ℓ^P	s_Q	State	J^P
$\bar{\mathbf{3}}_f$ (A)	$\bar{\mathbf{3}}_c$ (A)	0 (S)	0 (A)	0^+	2	2^+	$\frac{1}{2}$	$\tilde{\Lambda}_{Q2}, \tilde{\Xi}_{Q2}$	$(\frac{3}{2}^+, \frac{5}{2}^+)$
$\mathbf{6}_f$ (S)	$\bar{\mathbf{3}}_c$ (A)	0 (S)	1 (S)	1^+	2	$1^+/2^+/3^+$	$\frac{1}{2}$	$\tilde{\Sigma}_{Q1/2/3}, \tilde{\Xi}'_{Q1/2/3}, \tilde{\Omega}_{Q1/2/3}$	$(\frac{1}{2}^+, \frac{3}{2}^+)/(\frac{3}{2}^+, \frac{5}{2}^+)/(\frac{5}{2}^+, \frac{7}{2}^+)$

Flavor	Color	L_ρ	s_{qq}	J_{qq}^P	L_λ	j_ℓ^P	s_Q	State	J^P
				0^-	1	1^+	$\frac{1}{2}$	$\tilde{\Lambda}^0_{Q1}, \tilde{\Xi}^0_{Q1}$	$(\frac{1}{2}^+, \frac{3}{2}^+)$
$\bar{\mathbf{3}}_f$ (A)	$\bar{\mathbf{3}}_c$ (A)	1 (A)	1 (S)	1^-	1	$0^+/1^+/2^+$	$\frac{1}{2}$	$\tilde{\Lambda}^1_{Q0/1/2}, \tilde{\Xi}^1_{Q0/1/2}$	$\frac{1}{2}^+/(\frac{1}{2}^+, \frac{3}{2}^+)/(\frac{3}{2}^+, \frac{5}{2}^+)$
				2^-	1	$1^+/2^+/3^+$	$\frac{1}{2}$	$\tilde{\Lambda}^2_{Q1/2/3}, \tilde{\Xi}^2_{Q1/2/3}$	$(\frac{1}{2}^+, \frac{3}{2}^+)/(\frac{3}{2}^+, \frac{5}{2}^+)/(\frac{5}{2}^+, \frac{7}{2}^+)$
$\mathbf{6}_f$ (S)	$\bar{\mathbf{3}}_c$ (A)	1 (A)	0 (A)	1^-	1	$0^+/1^+/2^+$	$\frac{1}{2}$	$\tilde{\tilde{\Sigma}}_{Q0/1/2}, \tilde{\tilde{\Xi}}'_{Q0/1/2}, \tilde{\tilde{\Omega}}_{Q0/1/2}$	$\frac{1}{2}^+/(\frac{1}{2}^+, \frac{3}{2}^+)/(\frac{3}{2}^+, \frac{5}{2}^+)$

as the pD^+K^- channels [168]. They also reported the $\Xi_{cc}^{++}(3460)$ and $\Xi_{cc}^{++}(3780)$ in the $\Lambda_c^+K^-\pi^+\pi^+$ channel [169]. However, none of them has been confirmed by the other experimental collaborations [170, 171, 172, 173].

In 2017, the LHCb Collaboration reported the Ξ_{cc}^{++} in the $\Lambda_c^+K^-\pi^+\pi^+$ decay mode [174] and one year later in the $\Xi_c^+\pi^+$ decay mode [175]. Its mass is [176]

$$m_{\Xi_{cc}^{++}} = 3621.55 \pm 0.23 \text{ (stat) } \pm 0.30 \text{ (syst) MeV}, \tag{10}$$

and its lifetime [177] is

$$\tau = (2.56 \pm 0.27) \times 10^{-13} \text{ s}. \tag{11}$$

There have been extensive theoretical efforts to study the mass spectrum, the strong decay patterns, the electromagnetic properties, the life time and other properties of the doubly heavy baryon in different frameworks, such as the bag models [178, 179, 180, 181], various quark models [182, 183, 184, 185, 186, 109, 78], Bethe-Salpeter equation [187], Born-Oppenheimer EFT [188, 189], the Regge phenomenology [190, 191], QCD sum rule [192, 193, 194, 195, 196, 197, 160], heavy diquark effective theory [198], and lattice QCD [132, 146, 147].

In Sec. 3, we will review the investigations of the doubly heavy baryons using the chiral perturbative theory. Under the heavy diquark-antiquark symmetry (HDAS) [199], the interactions between the doubly heavy baryons with the other hadrons can be related to the interactions of the heavy mesons. The doubly heavy baryons may interact with other hadrons to form the exotic molecules similar to the heavy mesons. We will review these theoretical studies about the $B_{QQ}\varphi$ system in Sec. 4.3, and the $B_{QQ}D^{(*)}$, $B_{QQ}B_Q$ as well as $B_{QQ}B_{QQ}$ systems in Sec. 5.8, respectively.

1.3. Heavy hadronic molecule candidates

1.3.1. X(3872) and T_{cc}^+

We focus on the experimental progresses after 2015. For the previous experimental results and huge theoretical efforts, we refer to Refs. [6, 9, 8, 10, 11, 200, 13, 14] for reviews.

The $\chi_{c1}(3872)$, also known as $X(3872)$, was first observed by Belle Collaboration in 2003 [201]. With the tremendous efforts of many experimental collaborations, its quantum numbers were measured to be $J^{PC} = 1^{++}$ [1, 202]. The $X(3872)$ is an excellent candidate of the exotic states. Its mass coincides exactly with the $\bar{D}^{*0}D^0/\bar{D}^0D^{*0}$ threshold as $m_{D^0} + m_{D^{*0}} - m_{X(3872)} = (0.00 \pm 0.18)$ MeV with a very narrow width $\Gamma = (1.19 \pm 0.21)$ MeV [1]. Whether the $X(3872)$ lies below or above the $\bar{D}^{*0}D^0/\bar{D}^0D^{*0}$ threshold is still a pending question. In fact, the above decay width was extracted from the Breit-Wigner fits [203, 204]. Using a Flàtte-inspired model, the full width at the half maximum (FWHM) of the lineshape was determined to be FWHM = $0.22^{+0.07+0.11}_{-0.06-0.13}$ MeV [203]. As the $\chi_{c1}(2P)$ state, there is large discrepancy between the experimental mass of $X(3872)$ and the quark model predictions (e.g. [20]). Another important feature of the $X(3872)$ is the large isospin violating decay patterns [205, 206, 207],

$$\frac{\mathcal{B}[X \to J/\psi\pi^+\pi^-\pi^0]}{\mathcal{B}[X \to J/\psi\pi^+\pi^-]} = 1.0 \pm 0.4 \pm 0.3 \quad \text{Belle}; \qquad \frac{\mathcal{B}[X \to J/\psi\omega]}{\mathcal{B}[X \to J/\psi\pi^+\pi^-]} = \begin{cases} 1.6^{+0.4}_{-0.3} \pm 0.2 & \text{BESIII,} \\ 0.7 \pm 0.3 & B^+ \text{ events, BaBar,} \\ 1.7 \pm 1.3 & B^0 \text{ events, BaBar,} \end{cases} \tag{12}$$

where the final states $J/\psi\pi^+\pi^-\pi^0$ and $J/\psi\pi^+\pi^-$ are mainly driven by the intermediate states $J/\psi\omega$ and $J/\psi\rho$, respectively.

The theoretical interpretations of the $X(3872)$ include the $\chi_{c1}(2P)$ state, the $D^*\bar{D}/\bar{D}^*D$ molecular state, the mixing of the $c\bar{c}$ core with the $D^*\bar{D}/\bar{D}^*D$ component, the compact tetraquark state and so on. Obviously, in the pure $c\bar{c}$ picture and compact tetraquark picture, it is hard to understand the puzzles of its mass coincidence with the threshold and large isospin violation. In the $\bar{D}^{*0}D^0/\bar{D}^0D^{*0}$ molecular picture, the proximity of the $X(3872)$ mass to the threshold is natural although such an exact coincidence is still confusing (see Sec. 5.5 for the discussion of the fine-tuning problem). The mass of the $X(3872)$ exactly coincides with the neutral threshold $D^0\bar{D}^{*0}/D^{*0}\bar{D}^0$ and is about 8 MeV below the charged threshold $D^{*-}D^+/D^-D^{*+}$. In Sec. 5.5.5, we will review the theoretical interpretations of the large ratio in Eq. (12) based on the fine-tuning mass of the $X(3872)$. Meanwhile, we will see the kinematic mechanisms due to the threshold of the $J/\psi\rho(\omega)$ and the $\rho(\omega)$ widths will also contribute to the large ratio in Eq. (12). Another experimental evidence supporting the molecular picture is the dominant decay mode of $X(3872)$ [1],

$$\Gamma(X \to D^0\bar{D}^0\pi^0)/\Gamma_{\text{total}} = (49^{+18}_{-20})\%, \qquad \Gamma(X \to \bar{D}^{*0}D^0)/\Gamma_{\text{total}} = (37 \pm 9)\%, \tag{13}$$

where the branch fractions were extracted from $\mathcal{B}(B^+ \to D^0\bar{D}^0\pi^0 K^+)\Gamma(X \to D^0\bar{D}^0\pi^0)/\Gamma_{\text{total}}$, $\mathcal{B}(B^+ \to \bar{D}^{*0}D^0 K^+)\Gamma(X \to \bar{D}^{*0}D^0)/\Gamma_{\text{total}}$ and $\mathcal{B}(B^+ \to X(3872)K^+)$. The phase spaces of the above decay modes are severely suppressed. The large fractions indicate the strong coupling between the $X(3872)$ and the $\bar{D}^{*0}D^0/\bar{D}^0 D^{*0}$ channels.

The experimental progresses inspired the heated debates about the nature of $X(3872)$. The authors of Ref. [208] argued that the experimental prompt production data of the $X(3872)$ [209, 210, 211, 212, 213, 214] challenged the hadronic molecule interpretation. The prompt and non-prompt contributions are discriminated by analyzing displacement of the production vertex. In Sec. 5.5.5, we will review the discussions [208, 215, 216, 217]. In order to pin down the nature of the $X(3872)$, its heavy quark flavor partner was searched in CMS [218], ATLAS [219] and Belle [220]. No evidence for the X_b was observed. In Ref. [203], the lineshape of the $X(3872) \to J/\psi\pi^+\pi^-$ was investigated in a Flatté inspired model by LHCb Collaboration. The pole structure analysis indicated the $X(3872)$ is consistent with the $D^0\bar{D}^{*0}/D^{*0}\bar{D}^0$ with the molecular component $\gtrsim 70\%$ in the context of Weinberg's compositeness criterion [221]. The lineshape analysis results incited a debate on discerning the structure of the $X(3872)$ with the sign of the effective range in Ref. [222, 223], which will be discussed in Sec. 5.1.1. In Ref. [213], the LHCb Collaborations investigated the multiplicity-dependence of the prompt production of the $X(3872)$, $\psi(2S)$ and their ratio in pp collisions and found that the ratio decreased with the multiplicity. Based on the Comover Interaction Model, the authors of Ref. [224] argued that the above observation disfavored the molecular picture of the $X(3872)$, which was challenged by Ref. [225]. The CMS Collaboration reported the evidence of the $X(3872)$ production in relativistic heavy ion collisions for the first time [226], which provides a novel insight into the nature of $X(3872)$ [227, 228, 229, 230].

Very recently, the LHCb Collaboration observed the first doubly charmed tetraquark state T_{cc}^+ in the prompt production of the pp collision [4]. Its mass with respect to the $D^{*+}D^0$ threshold and width are

$$\delta m = (-273 \pm 61 \pm 5^{+11}_{-14}) \text{ keV}, \qquad \Gamma = (410 \pm 165 \pm 43^{+18}_{-38}) \text{ keV}. \qquad (14)$$

In the fitting, the quantum number $J^P = 1^+$ is assumed. The LHCb Collaboration also released the analysis in the unitarized Breit-Wigner profile including the $T_{cc}^+ \to D^0D^0\pi^+$, $D^0D^+\pi^0$ and $D^0D^+\gamma$ explicitly in the decay width [5]. The mass with respect to the $D^{*+}D^0$ threshold and width read

$$\delta m_U = (-361 \pm 40) \text{ keV}, \qquad \Gamma_U = (47.8 \pm 1.9) \text{ keV}. \qquad (15)$$

One should notice the discrepancy in the widths from the above two analyses. The conventional Breit-Wigner parameterization in the first analysis works well in the region far away from the thresholds. The T_{cc} state lies very close to the DD^* two-body thresholds and $DD\pi$ three-body thresholds. The second analysis constrained by the unitarity is more reasonable. In Sec. 5.5.4, we will review the related theoretical calculations (some of them were ahead of the second experimental analysis), which also support the narrower width.

The observation of the T_{cc}^+ marks the striking progress in the search of the exotic states. It is the second doubly charmed hadron observed in experiments after the Ξ_{cc}^{++} [174]. Moreover, the T_{cc}^+ is manifestly exotic with four (anti)quarks ($cc\bar{q}\bar{q}$), which has been anticipated and debated for 40 years [231, 232, 233, 234, 235, 236, 237, 238, 239, 240, 241, 242, 243, 244, 245, 246, 247, 248, 249, 250, 251, 252, 253, 254, 255, 256, 257, 258, 259, 260, 261, 262, 263, 264]. The T_{cc}^+ is also the second hadron with the mass almost coinciding with the threshold and a very narrow width after the $X(3872)$. In fact, the T_{cc}^+ and $X(3872)$ share the same fine-tuning problem. In the molecular scheme, the one-pion-exchange interaction of the $\bar{D}^*D/\bar{D}D^*$ system with the quantum numbers of $I(J^{PC}) = 0(1^{++})$ [corresponding to the $X(3872)$] and that of the D^*D system with $I(J^P) = 0(1^+)$ are exactly the same in the isospin symmetry limit. The D^*D molecular states had been predicted [265, 266, 267, 268] before the experimental observations. The discovery of the T_{cc} also inspired huge amounts of investigations [269, 270, 271, 272, 273, 274, 275, 276, 277, 278, 279, 280, 281, 282, 283, 284, 285, 286, 287, 288, 289, 290, 291, 292].

1.3.2. Z_c, Z_{cs} and Z_b

In addition to the isoscalar states $X(3872)$ and T_{cc}^+, there are several well-known isovector states $Z_c(3900)$ and $Z_c(4020)$ in the charmonium energy region, as well as the $Z_b(10610)$ and $Z_b(10650)$ in the bottomonium energy region [1]. The charged charmoniumlike states $Z_c(3900)$ and $Z_c(4020)$ were observed by the BESIII Collaboration in the $J/\psi\pi^\pm$, $(D\bar{D}^*)^\pm$ [293, 294, 295] and $h_c\pi^\pm$, $(D^*\bar{D}^*)^\pm$ [296, 297] channels, respectively. The $Z_c(3900)$ was also confirmed by Belle Collaboration [298] and Xiao et al [299]. The charged bottomoniumlike states $Z_b(10610)$ and $Z_b(10650)$ were observed by the Belle Collaboration in the $\Upsilon(nS)\pi^\pm$ ($n = 1, 2, 3$) and $h_b(mP)\pi^\pm$ ($m = 1, 2$)

invariant mass spectra [300], as well as in the $(B\bar{B}^*)^{\pm}$ and $(B^*\bar{B}^*)^{\pm}$ channels [301], respectively. Besides, the Belle and LHCb Collaborations also observed several other Z_c states with large widths in the B meson decay processes, e.g., the $Z_c(4200)$ [302, 303] and $Z_c(4430)$ [303, 304, 305, 306]. In what follows, we will mainly focus on the $Z_c(3900)$, $Z_c(4020)$, $Z_b(10610)$ and $Z_b(10650)$. For the experimental and theoretical aspects of $Z_c(4200)$ and $Z_c(4430)$, we refer to reviews [6, 11, 14].

The minimal quark content of these charged charmoniumlike and bottomoniumlike states should be $Q\bar{Q}q\bar{q}$ ($Q = c, b$, $q = u, d$), so they are good candidates of the manifestly exotic hadrons. There are many similarities among the $Z_c(3900)$, $Z_c(4020)$ and $Z_b(10610)$, $Z_b(10650)$ from their mass spectra and decay patterns, etc. For example, (i) their masses from Breit-Wigner fits all lie about several MeVs above the corresponding $D\bar{D}^*$, $D^*\bar{D}^*$ and $B\bar{B}^*$, $B^*\bar{B}^*$ thresholds, respectively (see Refs. [307] and [308] for results with other parameterizations); (ii) they both decay into the open and hidden heavy flavor channels, but the open heavy flavor channels are dominant; (iii) their $I^G(J^{PC})$ quantum numbers are measured to be $1^+(1^{+-})$ [the J^P of $Z_c(4020)$ is not determined yet, but 1^+ is presumed in most works]. There have been many efforts toward understanding the internal structures of these charged heavy quarkoniumlike states, such as the lattice QCD simulations, effective field theories (EFTs) (see the reviews in Sec. 5.6) and the phenomenological models, etc. The popular explanations include the molecular states (bound states, virtual states or resonances), compact tetraquarks, hadro-quarkonia and kinetic effects (see reviews [6, 14, 11, 9, 10, 12, 13, 8, 200, 309]). The proximities to the $D^{(*)}\bar{D}^*/B^{(*)}\bar{B}^*$ thresholds indicate that their properties should be strongly correlated with the $D^{(*)}\bar{D}^*/B^{(*)}\bar{B}^*$ interactions. These states provide a very good platform to utilize the EFTs containing both the chiral and heavy quark symmetries.

The strange partner of the Z_c states—the $Z_{cs}(3985)$ was recently observed by the BESIII Collaboration in the $D_s^- D^{*0} + D_s^{*-} D^0$ channel [310]. With the Breit-Wigner parameterization, its mass and width are measured to be

$$m = 3982.5^{+1.8}_{-2.6} \pm 2.1 \text{ MeV}, \qquad \Gamma = 12.8^{+5.3}_{-4.4} \pm 3.0 \text{ MeV}. \qquad (16)$$

Similar to the $Z_c(3900)$, the $Z_{cs}(3985)$ lies about 6 MeV above the $D_s^- D^{*0}/D_s^{*-} D^0$ thresholds. In addition, the mass difference is $m_{Z_{cs}(3985)} - m_{Z_c(3900)} \simeq m_{D_s^{(*)}} - m_{D^{(*)}} \simeq 100$ MeV. These features inspired the interpretations of the $Z_{cs}(3985)$ as the SU(3) partner of the $Z_c(3900)$ [311, 312, 313]. The discovery of the $Z_{cs}(3985)$ has stimulated many works to explain its nature from various aspects [311, 312, 313, 314, 315, 316, 317, 318, 319, 320, 321, 322, 323, 324, 325, 326, 327, 328, 329, 330, 331, 332, 333, 264, 334, 335, 336, 337, 338, 339, 340, 341, 342, 343, 344]. Later, the LHCb Collaboration reported two Z_{cs} states—the $Z_{cs}(4000)$ and $Z_{cs}(4220)$ in the $J/\psi K^+$ channel from the process $B^+ \rightarrow J/\psi K^+ \phi$ [345]. The mass of the $Z_{cs}(4000)$ ($4003 \pm 6^{+4}_{-14}$ MeV) is close to that of $Z_{cs}(3985)$, but its width ($131 \pm 15 \pm 26$ MeV) is about ten times larger than that of $Z_{cs}(3985)$. Whether they are the same state [330] or totally different ones [331, 332, 346] is still under debate. Some important implications for the $Z_{cs}(3985)$ and $Z_{cs}(4000)$ as two different states were derived in Ref. [346].

1.3.3. P_c and P_{cs}

In 2015, the LHCb Collaboration reported two pentaquark states, a broader $P_c(4380)$ with a width $205 \pm 18 \pm 86$ MeV and narrower $P_c(4450)$ with a width $39 \pm 5 \pm 19$ MeV in the $J/\psi p$ invariant mass distribution in the decay process $\Lambda_b^0 \rightarrow J/\psi p K^-$ [2]. In 2019, in the same channel $J/\psi p$ but with larger statistics, the LHCb Collaboration found that the $P_c(4450)^+$ should be dissolved into two substructures $P_c(4440)^+$ and $P_c(4457)^+$ [3]. In addition, another narrow state $P_c(4312)^+$ was observed. Their resonance parameters are [3]

$$P_c^+(4312): \quad M_{P_c^+(4312)} = 4311.9 \pm 0.7^{+6.8}_{-0.6} \text{ MeV}, \qquad \Gamma_{P_c^+(4312)} = 9.8 \pm 2.7^{+3.7}_{-4.5} \text{ MeV}, \qquad (17)$$

$$P_c^+(4440): \quad M_{P_c^+(4440)} = 4440.3 \pm 1.3^{+4.1}_{-4.7} \text{ MeV}, \qquad \Gamma_{P_c^+(4440)} = 20.6 \pm 4.9^{+8.7}_{-10.1} \text{ MeV}, \qquad (18)$$

$$P_c^+(4457): \quad M_{P_c^+(4457)} = 4457.3 \pm 1.3^{+0.6}_{-4.1} \text{ MeV}, \qquad \Gamma_{P_c^+(4457)} = 6.4 \pm 2.0^{+5.7}_{-1.9} \text{ MeV}. \qquad (19)$$

In the new analysis, the evidence of the broad $P_c(4380)$ in Ref. [2] was neither confirmed nor contradicted and awaits for a future complete amplitude analysis of the decay $\Lambda_b^0 \rightarrow J/\psi p K^-$.

The observation of the P_c states confirmed the predictions of the hidden-charm molecular pentaquarks in Refs. [347, 348, 349] and inspired the great enthusiasm about the hidden-charm pentaquark states. Various interpretations have been proposed such as the molecular states [350, 351, 352, 353, 354, 355, 356, 357, 358, 359, 360, 361, 362, 363, 364, 365, 366, 355], the compact pentaquark states [367, 368, 369, 370, 371, 372, 373], the hadro-charmonium states [374, 375, 376, 377], the triangle singularities [378, 379, 380], and the cusp effects [367, 381].

The $P_c(4312)$ and $P_c(4440)/P_c(4457)$ are located only tens of MeV below the $\Sigma_c\bar{D}$ and $\Sigma_c\bar{D}^*$ thresholds, respectively. The molecular scheme is a more natural interpretation and attracted much attention. In the molecular picture, the $P_c(4312)$ is widely accepted as an S-wave $\Sigma_c\bar{D}$ molecule with $J^P = \frac{1}{2}^-$. The $P_c(4440)$ and $P_c(4457)$ are treated as the S-wave $\Sigma_c\bar{D}^*$ molecules. However, there are two possible scenarios of the spin-parity assignments. In scenario I, the $P_c(4440)$ and $P_c(4457)$ are the $\Sigma_c\bar{D}^*$ molecules with the $J^P = \frac{1}{2}^-$ and $\frac{3}{2}^-$, respectively [382, 383, 351, 364, 365]. In scenario II, the J^P quantum numbers of the $P_c(4440)$ and $P_c(4457)$ are the $\frac{3}{2}^-$ and $\frac{1}{2}^-$, respectively [384, 385, 386, 387, 384, 363]. Their decay patterns [388, 389, 366, 365, 390, 391, 392, 360, 393, 394] and productions [395, 396, 397, 398, 399, 400, 401, 392, 377, 402, 403] were also investigated extensively. In Ref. [404], the photo-production of P_c was suggested to testing its multiquark nature in the framework of string-junction picture [405, 406, 407] unifying the baryons and multiquark states.

Recently, the LHCb Collaboration reported the evidence of a new pentaquark state $P_c(4337)^+$ in the $J/\psi p$ invariant mass distribution of the decay $B_s \to J/\psi p\bar{p}$. Its resonance parameters are [408]

$$P_c(4337)^+ : \quad M_{P_c(4337)^+} = 4337^{+7+2}_{-4-2} \text{ MeV}, \qquad \Gamma_{P_c(4337)^+} = 29^{+26+14}_{-12-14} \text{ MeV}. \qquad (20)$$

The $P_c(4337)^+$ lies very close to the $P_c^+(4312)$ state and the $P_c(4380)$ signal. Its interpretations included the compact tetraquark state [373], the cusp effect [381], the hadro-charmonium [409], coupled channel dynamics [409], the $\bar{D}\Sigma_c$ molecule [409], the $\bar{D}\Sigma_c^*$ molecule [$P_c(4380)^+$] [410], etc.

The partners of the P_c states were predicted with the heavy quark spin symmetry, $[\Sigma_c^*\bar{D}]^{I=1/2}_{J=3/2}$ [candidate for the $P_c(4380)^+$] and $[\Sigma_c^*\bar{D}^*]^{I=1/2}_{J=(\frac{1}{2},\frac{3}{2},\frac{5}{2})}$ [364, 387, 411, 412, 385, 359, 356, 384, 352], which await the future experimental scrutiny. The studies of the P_c states can be easily extended to the strange hidden-charm molecular pentaquarks (P_{cs}) under the SU(3) flavor symmetry and the P_{cs} states were predicted in Refs. [348, 413, 414, 415, 416, 417, 416, 418].

In 2020, the LHCb found the evidence of the $P_{cs}(4459)$ in the $J/\psi\Lambda$ invariant mass distribution via the decay $\Xi_b^- \to J/\psi\Lambda K^-$ [419],

$$P_{cs}(4459) : \quad M_{P_{cs}(4459)} = 4458.8 \pm 2.9^{+4.7}_{-1.1} \text{ MeV}, \qquad \Gamma_{P_{cs}(4459)} = 17.3 \pm 6.5^{+8.0}_{-5.7} \text{ MeV}. \qquad (21)$$

which is only about 19 MeV below the $\Xi_c^0\bar{D}^{*0}$ threshold. The experiment did not confirm or contradict the existence of the two-peak hypothesis. The result inspired various theoretical works [420, 340, 421, 373, 422, 423, 424, 425, 426, 427]. Most of them favored the P_{cs} as the $\Xi_c\bar{D}^*$ molecule [422, 420, 423, 424, 425, 426, 427, 428]. Besides the molecular interpretation, there also exist other explanations such as the hadro-charmonium [340], compact pentaquark states [421, 373]. There were intensive discussions of its production, decays and other properties [429, 430, 431]. Similar to the P_c states, various partners of the P_{cs} were also predicted in numerous theoretical works [417, 426, 416, 428, 432, 423, 414, 433, 416], which need to be examined by future experiments.

Very recently, the LHCb Collaboration observed the $P_{cs}(4338)$ (also named as the $P_{\psi s}^\Lambda(4338)^0$ according to the naming convention proposed in Ref. [434]) in the decay $B^- \to J/\psi\Lambda\bar{p}$ [435]. The amplitude analysis prefers the $J^P = \frac{1}{2}^-$ assignment for $P_{cs}(4338)$. Its mass and width in the relativistic Breit-Wigner fits read

$$P_{cs}(4338) : \quad M_{P_{cs}(4338)} = 4338.3 \pm 0.7 \pm 0.4 \text{ MeV}, \qquad \Gamma_{P_{cs}(4338)} = 7.1 \pm 1.2 \pm 1.3 \text{ MeV}. \qquad (22)$$

The $P_{cs}(4338)$ is very close to the $\Xi_c\bar{D}$ threshold (which is about 4336 MeV). In Ref. [436], the authors proposed it is the $\Xi_c\bar{D}$ molecule considering the near-threshold behavior, the spin-parity and the narrow width. In Ref. [437], Meng et al investigated the influence of the double-threshold ($\Xi_c^0\bar{D}^0$ and $\Xi_c^+D^-$) on the line shape (the invariant mass distribution of $J/\psi\Lambda$) of $P_{cs}(4338)$. A comparison between the P_c and P_{cs} states was given in Ref. [438]. Other approaches were also employed to understand this state, such as the one-boson exchange model [439], the triangle singularity [440], the effective field theory [441, 442], the coupled-channel dynamics [443, 444], the quark model [445], etc. Its electromagnetic properties were also studied in Refs. [446, 447].

The discovery of the P_c states and the evidence of the P_{cs} also inspired the investigation of the other pentaquark states, such as $QQqq\bar{q}$ [448, 449, 450, 451, 452, 453, 450, 454], P_{css} [455], the fully heavy pentaquark state [456, 457], the $\bar{Q}qqqq$ [458, 459, 460, 461, 462], $B\Xi_c$ and $B\Xi_c'$ bound states [463], etc.

1.4. A short summary

Quark model inherits some spirits and features of QCD and has been successfully employed to describe the conventional mesons and baryons at the quark level. The hadron spectroscopy had witnessed the success of quark model before 2003. However, the quark model was challenged by many near-threshold exotic states observed since 2003. More and more experimental evidences indicate the relevance and importance of the clustering effect of the quarks, e.g., the heavy hadronic molecules. The loosely bound hadronic molecules are very well known as a building block of the matter, namely the nuclei. The abundant hadron spectra are the opportunities and challenges for us to understand the nonperturbative behaviors of QCD at low energy domains.

The chiral effective theories are built upon the chiral symmetry of QCD with the asymptotic hadronic d.o.f. These powerful tools have been developed and applied in the nuclear sectors with flying colors in the past decades. The heavy hadrons and exotic hadronic molecular states observed in recent years supply the fertile soil for the redevelopment of these effective theories. In this work, we will mainly review the developments and applications of chiral perturbation theory, chiral effective field theory, as well as their ramifications and variants in the heavy flavor sectors together with the heavy quark symmetry. We shall also cover the experimental measurements, lattice QCD simulations, and phenomenological model calculations briefly.

2. Symmetries of low energy QCD and effective field theories

Effective field theory (EFT) is designed for systems with widely separated energy scales. One basic principle of EFT is that the low energy interaction does not depend on the details of dynamics at high energies. The most general Lagrangian contains all terms satisfying the requirements of underlying symmetries of the system, which are organized with increasing number of derivatives [464]. Once the low energy scale Q and high energy scale Λ for such a system are well identified, the amplitude of a soft process can be expanded in powers of Q/Λ, i.e.,

$$\mathcal{A} = \sum_\nu C_\nu(Q/\mu, c_i) \left(\frac{Q}{\Lambda}\right)^\nu, \tag{23}$$

where the expansion coefficients C_ν are the functions of regularization scale μ which arises from the loop diagrams and low energy constants (LECs). For a well-defined EFT, the expansion coefficients are of order unity (naturalness) after separating out the common dimension of the amplitude. The high energy dynamics above the Λ are encoded in the LECs c_i via a series of the local contact terms, which are the functions of Λ in general, i.e., $c_i \equiv c_i(\Lambda)$. The expansion index ν is connected to the power counting given by the EFT. If the energy scale is largely separated in the system, the small value Q/Λ ensures the good convergence of the above expansion, thus only finite terms are needed for a given accuracy in practical calculations. One can consult two recent books [465, 466] for a more comprehensive introduction about EFT.

QCD is one of the main ingredients of the Standard Model. The full Lagrangian of QCD is given in terms of the quark and gluon degrees of freedom, which reads

$$\mathcal{L}_{\text{QCD}} = \bar{q}(i\slashed{D} - \mathcal{M})q - \frac{1}{4}\mathcal{G}_{\mu\nu,a}\mathcal{G}_a^{\mu\nu}, \tag{24}$$

where the quark field is $q \equiv q_f^c$, and the summations over the flavor index f and color index c are implied. The covariant derivative is $\mathcal{D}_\mu = \partial_\mu - ig_s\lambda^a\mathcal{A}_\mu^a/2$, where g_s is the strong coupling constant. λ^a $(a = 1, \ldots, 8)$ represents the Gell-Mann matrix, and $\mathcal{A}_\mu^a$ denotes the gluon field. The quark mass matrix is defined as $\mathcal{M} = \text{diag}(m_u, m_d, m_s, m_c, m_b, m_t)$. The field strength tensor reads $\mathcal{G}_{\mu\nu,a} = \partial_\mu\mathcal{A}_{\nu,a} - \partial_\nu\mathcal{A}_{\mu,a} + g_s f_{abc}\mathcal{A}_{\mu,b}\mathcal{A}_{\nu,c}$ [where f_{abc} denotes the antisymmetric structure constant of SU(3) group], with $\tilde{\mathcal{G}}_a^{\mu\nu} = \epsilon^{\mu\nu\alpha\beta}\mathcal{G}_{\alpha\beta,a}/2$ being its dual. QCD exhibits well separated scales. In the following, we refer to the current quark mass in the $\overline{\text{MS}}$ subtraction scheme at a renormalization scale $\mu = 2$ GeV [1]. The u, d and s quarks are very light

$$(m_u = 2.16^{+0.49}_{-0.26}, \ m_d = 4.67^{+0.48}_{-0.17}, \ m_s = 93^{+11}_{-5}) \text{ MeV} \ll \Lambda_{\text{QCD}}, \tag{25}$$

where $\Lambda_{\text{QCD}} \sim 200$ MeV is the nonperturbative scale of QCD. The c, b and t quarks are very heavy compared with Λ_{QCD},

$$(m_c = 1.27 \pm 0.02, \ m_b = 4.18^{+0.03}_{-0.02}, \ m_t = 172.76 \pm 0.03) \text{ GeV} \gg \Lambda_{\text{QCD}}. \tag{26}$$

Therefore, the u, d and s quarks are generally called as the light quarks, while c, b and t are the heavy quarks. The small mass of the light quarks and the large mass of the heavy quarks stimulate two extreme approximations, i.e., $m_u = m_d = m_s \to 0$ and $m_c = m_b \to \infty$ (the top quarks are generally not considered in hadron physics due to its extremely unstable nature). In these two limits, QCD exhibits chiral symmetry and heavy quark symmetry, respectively.

Due to the nonperturbative nature of QCD at low energy domain, the quarks are confined in the color neutral hadrons with the not-fully-understood nonperturbative dynamics. It is hard to perform thorough analyses in terms of its fundamental d.o.f, i.e., the quarks and gluons. An alternative description for the physics occurring at $E \ll \Lambda_\chi$ is in terms of the asymptotic hadron states, where $\Lambda_\chi \sim 1$ GeV is the chiral symmetry breaking scale [1]. As a full-fledged EFT of QCD at low energies, the chiral perturbation theory (χPT) has been developed in the past decades. Now it has become the common language of nuclear physics and hadron physics when encountering the light quark dynamics. However, the richness of hadron spectrum also calls for combinations of chiral symmetry and HQS in the heavy-light systems (e.g., the singly heavy mesons $Q\bar{q}$, the singly heavy baryons Qqq, where $Q = c, b$ and $q = u, d, s$). The EFT based on the chiral symmetry and heavy quark symmetry for the heavy-light systems is denoted as the heavy hadron chiral perturbation theory (HHχPT). Besides, in recent years, an approximate symmetry, the so-called heavy diquark-antiquark symmetry (HDAS), is proposed for the heavy-heavy-light system (i.e., the doubly heavy baryons QQq), whereas the suitability is still an open question.

In the following, we outline the basic frameworks of χPT, heavy quark effective theory (HQET), HHχPT and chiral effective field theory (χEFT) with two matter fields, respectively. For more comprehensive details of these theories and related topics, we refer to some more specialized reviews [468, 469, 470, 471, 472, 473, 474, 475, 476] and lecture notes [477, 478, 479], and the references therein. The readers who are familiar with these effective theories can skip this chapter and move on to the next one.

2.1. Chiral perturbation theory

2.1.1. Chiral symmetry and its spontaneous breaking

Now we focus on the three flavor (u, d, and s) QCD with massless quarks (chiral limit), and pick out their left-handed ($q_L = P_L q$) and right-handed ($q_R = P_R q$) components with the projection operators

$$P_L = \frac{1}{2}(1 - \gamma^5), \quad P_R = \frac{1}{2}(1 + \gamma^5), \text{ with } P_L + P_R = 1, \ P_R^2 = P_R, \ P_L^2 = P_L, \ P_R P_L = P_L P_R = 0. \tag{27}$$

The Lagrangian (24) is expressed with the q_L and q_R as

$$\mathcal{L}_{\text{QCD}}^0 = \bar{q}_L i \mathcal{D} q_L + \bar{q}_R i \mathcal{D} q_R, \tag{28}$$

where the irrelevant gluon field strength tensor is omitted for this discussion. The Lagrangian (28) is invariant under the global $G = \text{SU}(3)_L \otimes \text{SU}(3)_R$ transformations[2]

$$q_L \xrightarrow{G} g_L q_L = \exp(-i\vartheta_L^a \frac{\lambda^a}{2}) q_L, \qquad q_R \xrightarrow{G} g_R q_R = \exp(-i\vartheta_R^a \frac{\lambda^a}{2}) q_R. \tag{29}$$

According to the Noether's theorem, there are eight conserved left-handed currents $J_L^{\mu,a}$ and right-handed currents $J_R^{\mu,a}$, respectively, with $J_L^{\mu,a} = \bar{q}_L \gamma^\mu \frac{\lambda^a}{2} q_L$, $\partial_\mu J_L^{\mu,a} = 0$, and $J_R^{\mu,a} = \bar{q}_R \gamma^\mu \frac{\lambda^a}{2} q_R$, $\partial_\mu J_R^{\mu,a} = 0$. The vector currents and axial vector currents are the linear combinations of $J_L^{\mu,a}$ and $J_R^{\mu,a}$

$$\begin{aligned} V^{\mu,a} &= J_R^{\mu,a} + J_L^{\mu,a} = \bar{q}\gamma^\mu \frac{\lambda^a}{2} q, & \text{with } \partial_\mu V^{\mu,a} = 0, \\ A^{\mu,a} &= J_R^{\mu,a} - J_L^{\mu,a} = \bar{q}\gamma^\mu \gamma_5 \frac{\lambda^a}{2} q, & \text{with } \partial_\mu A^{\mu,a} = 0. \end{aligned} \tag{30}$$

---

[1] Λ_χ can be chosen either as $4\pi f_\pi$, a factor appearing in the loop diagrams [467] or the mass of the ρ-meson, a natural scale for chiral symmetry breaking.

[2] It is also invariant under the $U(1)_V \otimes U(1)_A$ transformations. The $U(1)_V$ trivially corresponds to the baryon number conservation, while the $U(1)_A$ is broken at quantum level due to the '$U(1)_A$ anomaly'.

The vector charges and axial-vector charges are given as

$$Q_V^a = \int d^3x V^{0,a}(\boldsymbol{x},t) = \int d^3x q^\dagger(\boldsymbol{x},t)\frac{\lambda^a}{2}q(\boldsymbol{x},t), \quad \text{with } \frac{d}{dt}Q_V^a = 0,$$

$$Q_A^a = \int d^3x A^{0,a}(\boldsymbol{x},t) = \int d^3x q^\dagger(\boldsymbol{x},t)\gamma_5\frac{\lambda^a}{2}q(\boldsymbol{x},t), \quad \text{with } \frac{d}{dt}Q_A^a = 0. \tag{31}$$

They obey the following commutation relations,

$$[Q_V^a, Q_V^b] = if^{abc}Q_V^c, \qquad [Q_A^a, Q_A^b] = if^{abc}Q_V^c, \qquad [Q_V^a, Q_A^b] = if^{abc}Q_A^c. \tag{32}$$

Both the Q_V^a and Q_A^a commute with the QCD Hamiltonian H_{QCD}^0, i.e., $[Q_V^a, H_{\text{QCD}}^0] = [Q_A^a, H_{\text{QCD}}^0] = 0$, which implies the existence of degenerate light hadrons with opposite parities, i.e., the parity doublets, if the QCD vacuum satisfies the same symmetry as the Hamiltonian. From the experimental facts, the lightest vector hadron ($J^P = 1^-$) is the ρ meson and its mass is $m_\rho \simeq 770$ MeV. In contrast, the lightest axial-vector state ($J^P = 1^+$) is the a_1 meson and its mass $m_{a_1} \simeq 1230$ MeV is much heavier than m_ρ. Therefore, it is far-fetched to regard the $a_1(1260)$ as the parity partner of the ρ. Moreover, there are eight light pseudoscalar mesons below m_ρ, and their masses are lighter than the scalar states in the hadron spectrum. These facts indicate that the vacuum (ground state) of QCD is not invariant under the continuous $SU(3)_{R-L}$ transformation, i.e.,

$$Q_A^a|0\rangle \neq |0\rangle, \tag{33}$$

where we keep having $Q_V^a|0\rangle = |0\rangle$.

A continuous symmetry is spontaneously broken if this symmetry is not realized in its ground state. Therefore, Eq. (33) implies the spontaneous breaking of chiral symmetry. Then the Goldstone's theorem [480, 481] demands that there should exist massless particles with the same quantum numbers as the broken generators, which are called Goldstone bosons. The number of Goldstone bosons is equal to the number of the broken generators, so there should exist eight Goldstone bosons according to Eq. (33) with $J^P = 0^-$. The eight lightest pseudoscalars $(\pi^+, \pi^-, \pi^0, K^+, K^-, K^0, \bar{K}^0, \eta)$ coincidentally correspond to the eight Goldstone bosons. According to the Lorentz invariance, one can parameterize the following matrix elements,

$$\langle 0|A_\mu^a(0)|\varphi^b(p)\rangle = ip_\mu f_0\delta^{ab}, \tag{34}$$

where φ^a are the Goldstone bosons, and f_0 is the decay constant in the chiral limit [3]. The non-vanishing masses of the Goldstone bosons arise from light quark masses which break the chiral symmetry explicitly.

2.1.2. Explicit breaking of chiral symmetry

In deriving Eq. (28), the approximation $\mathcal{M} \to 0$ is assumed, whereas the light quarks have non-vanishing masses, which explicitly break the chiral symmetry. The mass term results in the mixing of left-handed and right-handed components of the quark fields, $\mathcal{L}_M = -\bar{q}\mathcal{M}q = -(\bar{q}_L\mathcal{M}q_R + \bar{q}_R\mathcal{M}q_L)$. An infinitesimal transformation on the $\mathcal{L}_M$ under chiral group G leads to the divergences of $V^{\mu,a}$ and $A^{\mu,a}$ as

$$\partial_\mu V^{\mu,a} = i\bar{q}[\mathcal{M}, \lambda^a/2]q, \qquad \partial_\mu A^{\mu,a} = i\bar{q}\{\mathcal{M}, \lambda^a/2\}\gamma_5 q. \tag{35}$$

The three flavor light quark mass matrix can be expressed with the λ_a matrix as

$$\mathcal{M} = \begin{bmatrix} m_u & 0 & 0 \\ 0 & m_d & 0 \\ 0 & 0 & m_s \end{bmatrix} = \frac{m_u + m_d + m_s}{\sqrt{6}}\lambda_0 + \frac{(m_u + m_d)/2 - m_s}{\sqrt{3}}\lambda_8 + \frac{m_u - m_d}{2}\lambda_3. \tag{36}$$

Inserting Eq. (36) into Eq. (35) one obtains that:

---

[3] In the weak decay element of pion, $\langle l^-\bar{\nu}|H_W|\pi^-\rangle = \frac{G_F \cos\theta_C}{\sqrt{2}}\langle l^-\nu|j^{-\mu}|0\rangle\langle 0|J_\mu^-|\pi^-\rangle$, the leptonic current and the hadronic currents are $j_\mu^- = \bar{l}\gamma^\mu(1 - \gamma_5)\nu_l$ and $J_\mu^- = V_\mu^+ + A_\mu^+$, respectively, where G_F and θ_C are coupling constants and Cabibbo angle. Because of $\langle 0|V_\mu(0)|\pi\rangle = 0$, only the axial current has contribution. Thus, the matrix element of axial current is related to the leptonic decay constant f_0.

1. When $m_u = m_d = m_s$, the eight vector currents $V^{\mu,a}$ are conserved due to $[1, \lambda^a] = 0$, which corresponds to the emergence of the rigorous $SU(3)_f$ (subscript f denotes flavor) symmetry. In this case, we can define the U-spin and V-spin in the subgroup $[SU(2)_f]$ of $SU(3)_f$, which are analogous to the well-known isospin I,

$$u \overset{I}{\longleftrightarrow} d, \qquad d \overset{U}{\longleftrightarrow} s, \qquad s \overset{V}{\longleftrightarrow} u. \tag{37}$$

Similarly, we can further define the G_U-parity and G_V-parity as the G-parity for isospin symmetry, with the transformation operators

$$\hat{G} = \hat{C}e^{i\pi\hat{I}_2}, \qquad \hat{G}_U = \hat{C}e^{i\pi\hat{U}_2}, \qquad \hat{G}_V = \hat{C}e^{i\pi\hat{V}_2}. \tag{38}$$

The eight axial-vector currents $A^{\mu,a}$ are not conserved anymore, and the chiral symmetry is explicitly broken [in comparison with the hidden (spontaneous) breaking in Sec. 2.1.1]. The non-vanishing divergences of $A^{\mu,a}$ leads to the microscopic interpretation of the partially conserved axial-vector current (PCAC) relation [482, 483, 484].

2. When $m_u = m_d \neq m_s$, the $SU(3)_f$ symmetry group breaks down to its subgroup $SU(2)_f$. Now the isospin symmetry is still exact.

3. When $m_u \neq m_d \neq m_s$, the isospin symmetry is also broken, which leads to the isospin breaking effect [4].

The light masses of these pseudoscalar mesons [especially in the SU(2) sector] are deeply rooted in their nature as the pseudo Goldstone bosons. The quantum fluctuations of these pseudoscalar mesons are very important, which are denoted as chiral dynamics. The χPT is the low-energy effective field theory of the QCD.

2.1.3. Lowest order Lagrangians and power counting

The phenomenological and experimental evidences all suggest that the chiral group $G = SU(3)_L \otimes SU(3)_R$ spontaneously breaks down to its vectorial subgroup $SU(3)_V$ [or say $SU(3)_{R+L}$], i.e.,

$$G = SU(3)_L \otimes SU(3)_R \longrightarrow H = SU(3)_V. \tag{39}$$

The interactions among light Goldstone bosons are described by the χPT [485, 486], in which the light octet are collected in terms of a 3×3 unitary matrix field $U(\varphi)$ transforming under $SU(3)_L \otimes SU(3)_R$ as

$$U(\varphi) \overset{G}{\longrightarrow} g_R U(\varphi) g_L^{-1} \text{ or } g_L U(\varphi) g_R^{-1}, \quad \text{with } (g_L, g_R) \in G. \tag{40}$$

Different parameterizations of $U(\varphi)$ correspond to the different choices of coordinates in coset space G/H, where a commonly used representation is the exponential parametrization,

$$U(\varphi) = \xi^2(\varphi) = \exp\left(i\frac{\varphi}{f_\varphi}\right), \qquad \varphi = \sum_a \lambda_a \varphi_a = \begin{bmatrix} \pi^0 + \frac{1}{\sqrt{3}}\eta_8 & \sqrt{2}\pi^+ & \sqrt{2}K^+ \\ \sqrt{2}\pi^- & -\pi^0 + \frac{1}{\sqrt{3}}\eta_8 & \sqrt{2}K^0 \\ \sqrt{2}K^- & \sqrt{2}\bar{K}^0 & -\frac{2}{\sqrt{3}}\eta_8 \end{bmatrix}, \tag{41}$$

where the coset field $\xi(\varphi)$ is introduced as the square root of $U(\varphi)$, which transforms under the $SU(3)_L \otimes SU(3)_R$ as

$$\xi(\varphi) \overset{G}{\longrightarrow} g_R \xi(\varphi) K^{-1}(\varphi, g) = K(\varphi, g)\xi(\varphi)g_L^{-1}, \text{ with } g = (g_L, g_R) \in G. \tag{42}$$

where the compensator field $K(\varphi, g)$ belongs to the unbroken subgroup $SU(3)_V$. Introducing the coset field $\xi(\varphi)$ ensures the interactions of the Goldstone bosons with themselves and the matter fields (such as baryons, heavy mesons, etc.) can be described by the nonlinear representation theory on quantum fields [487, 488].

---

[4]The other origin of the isospin symmetry breaking effect comes from the electromagnetic interaction.

The leading order (LO) Lagrangian for the interactions among the light Goldstone bosons without the external sources is given as

$$\mathcal{L}_2 = \frac{f_\varphi^2}{4}\text{Tr}\left[\partial_\mu U \partial^\mu U^\dagger\right],$$ (43)

where the decay constant of the light Goldstone bosons f_φ is introduced to yield the canonical kinetic terms (as well as the mass terms in the following).

In quantum field theory, the external fields can be either a computational technique or physical entities. The extended QCD Lagrangian with external fields reads

$$\mathcal{L}_{\text{QCD}}^{\text{ext.}} = \mathcal{L}_{\text{QCD}} + \bar{q}\gamma^\mu(v_\mu + \gamma_5 a_\mu)q - \bar{q}(s - i\gamma_5 p)q,$$ (44)

where the v_μ, a_μ, s and p represent the external vector, axial-vector, scalar and pseudoscalar fields, respectively. The extended Lagrangian (44) is invariant under the local $G_l = \text{SU}(3)_L \otimes \text{SU}(3)_R$ transformations if the quark fields and external fields satisfy the following transformation rules,

$$q_L \xrightarrow{G_l} g_L q_L, \ q_R \xrightarrow{G_l} g_R q_R, \ r_\mu \xrightarrow{G_l} g_R r_\mu g_R^{-1} + ig_R \partial_\mu g_R^{-1}, \ l_\mu \xrightarrow{G_l} g_L l_\mu g_L^{-1} + ig_L \partial_\mu g_L^{-1}, \ s + ip \xrightarrow{G_l} g_R(s + ip)g_L^{-1}, \quad (45)$$

where $g_{L/R} = g_{L/R}(x)$ is the function of x.

In practice, the quarks generally couple to the external sources, such as the electromagnetic field, the weak current, etc. The quark mass matrix $\mathcal{M}$ is contained in the scalar field s. The photon, W boson fields and quark mass terms are embedded in the v_μ, a_μ and s via

$$
\begin{aligned}
r_\mu &= v_\mu + a_\mu = -e\mathcal{Q}A_\mu + \dots, \\
l_\mu &= v_\mu - a_\mu = -e\mathcal{Q}A_\mu - \frac{e}{\sqrt{2}\sin\theta_W}(W_\mu^\dagger T^+ + \text{H.c.}) + \dots, \\
s &= \mathcal{M} + \dots,
\end{aligned}
$$ (46)

where A_μ and W_μ denote the photon and W boson fields, respectively. The quark charge matrix $\mathcal{Q}$, CKM matrix T^+ and quark mass matrix $\mathcal{M}$ are given as, respectively,

$$\mathcal{Q} = \frac{1}{3}\text{diag}(2, -1, -1), \qquad T^+ = \begin{bmatrix} 0 & V_{ud} & V_{us} \\ 0 & 0 & 0 \\ 0 & 0 & 0 \end{bmatrix}, \qquad \mathcal{M} = \text{diag}(m_u, m_d, m_s),$$ (47)

The electromagnetic field and the W boson fields are gauge fields.

The low energy effective field theory of the extended QCD contains the same external fields and has the same local $G_l = \text{SU}(3)_L \otimes \text{SU}(3)_R$ symmetry with extended QCD Lagrangians. The local transformation invariance requires that the fields v_μ and a_μ appear in the covariant derivatives of U,

$$\nabla_\mu U = \partial_\mu U - ir_\mu U + iU l_\mu, \qquad \nabla_\mu U^\dagger = \partial_\mu U^\dagger + iU^\dagger r_\mu - il_\mu U^\dagger, \qquad \nabla_\mu U \xrightarrow{G_l} g_R \nabla_\mu U g_L^{-1}.$$ (48)

We can also introduce the field strength tensors as building blocks,

$$f_R^{\mu\nu} = \partial^\mu r^\nu - \partial^\nu r^\mu - i[r^\mu, r^\nu], \qquad f_L^{\mu\nu} = \partial^\mu l^\nu - \partial^\nu l^\mu - i[l^\mu, l^\nu].$$ (49)

When the gauge field is introduced as the external field, the local group $G_l = \text{SU}(3)_L \otimes \text{SU}(3)_R$ will reduce to the corresponding gauge symmetry. For example, if one introduces the external electromagnetic field, the $f_R^{\mu\nu}$ and $f_L^{\mu\nu}$ degrade into the usual electromagnetic field strength tensor $f_R^{\mu\nu} = f_L^{\mu\nu} = f^{\mu\nu} = -e\mathcal{Q}(\partial^\mu A^\nu - \partial^\nu A^\mu)$. When the external field is switched off, the above local symmetry will degenerate into the global chiral symmetry of QCD.

The most general LO Lagrangian which satisfies the Lorentz invariance and local chiral symmetry reads [486, 489, 490]

$$\mathcal{L}_2 = \frac{f_\varphi^2}{4}\text{Tr}\left[\nabla_\mu U \nabla^\mu U^\dagger + \chi^\dagger U + U^\dagger \chi\right],$$ (50)

17

where the spurion $\chi = 2B_0(s + ip)$, and B_0 is a LEC. The above Lagrangian is the general LO Lagrangian with the external fields. If we focus on the effect induced by the light quark masses, we could set $s = \mathcal{M} = \text{diag}\{m_u, m_d, m_s\}$, $p = l_\mu = r_\mu = 0$, where the scalar field s is the same as that in the extended QCD Lagrangian in Eq. (47). By comparing the vacuum expectation of the EFT Hamiltonian with that of the QCD Hamiltonian with the same external field, one can get $B_0 = -\langle \bar{q}q \rangle/(3f_\varphi^2)$, where $\langle \bar{q}q \rangle$ is the quark condensate [5]. Expanding the Lagrangian containing the spurion χ at the hadronic level, one can see it corresponds to the mass of the pseudoscalar mesons, specifically,

$$\chi = 2B_0 \text{diag}(m_u, m_d, m_s) = \text{diag}(m_\pi^2, m_\pi^2, 2m_K^2 - m_\pi^2). \tag{51}$$

The masses of the pseudoscalar mesons can be related to the quark masses.

The χPT is an EFT of QCD at low energies. Its effective Lagrangians are organized in the same form as given in Eq. (23), where the soft scale Q can be either the external momentum of the Goldstone bosons or their small masses. The expansion index ν (chiral order) is obtained from Weinberg's power counting based on the naive dimensional analysis (NDA) [464]. The building blocks (fields and spurion) in the chiral Lagrangians are counted as

$$O(p^0) : U; \qquad O(p^1) : \nabla_\mu U, \ v_\mu, \ a_\mu; \qquad O(p^2) : f_L^{\mu\nu}, \ f_R^{\mu\nu}, \ s, \ p. \tag{52}$$

In χPT without matter fields, the Lagrangians can be even order only. From Eq. (52) one sees that the LO Lagrangian in Eq. (50) is of order $O(p^2)$. The chiral dimension (order) of a Feynmann diagram is

$$D = 4L - 2I_M + \sum_i V_i d_i, \tag{53}$$

where L and I_M are the numbers of loops and Goldstone boson inner lines, respectively. V_i and d_i are the number of vertex i and number of the derivatives in the vertex i, respectively. With the topological relation, $L = I_M - \sum_i V_i + 1$, one can obtain a more useful power counting,

$$D = 2L + 2 + \sum_i V_i(d_i - 2). \tag{54}$$

For the LO interaction ($d_i = 2$), the amplitudes of Feynman diagrams with an extra loop is suppressed by two extra chiral orders. To achieve a certain precision, one needs to calculate the Feynman diagrams with a finite numbers of loops. With the power counting, one can calculate the amplitude perturbatively (in terms of p/Λ_χ).

2.2. Heavy quark effective theory

In this part, we discuss the infinite heavy quark mass limit of low energy QCD [491, 492, 493, 494, 495, 496, 497, 498]. The masses of the c and b quarks are much larger than the nonperturbative scale Λ_{QCD}. We will see that the dynamics is largely simplified in the approximation $m_Q \to \infty$. For a hadron containing one single heavy quark, the typical transferred momentum p^{ty} between the heavy quark and light d.o.f is of order Λ_{QCD}. The heavy quark is almost on-shell. The variation of the heavy quark velocity $\delta v = p^{\text{ty}}/m_Q$ is very small due to $m_Q \gg p^{\text{ty}}$. In the limit $m_Q \to \infty$, the heavy quark moves with a constant velocity. In the heavy quark limit, the heavy quark is at rest in the hadron rest frame and serves only as a static color source .

2.2.1. Heavy quark flavor and spin symmetries

In the framework of heavy quark effective theory (HQET), the four-momentum p^μ of a heavy quark is split into two parts,

$$p^\mu = m_Q v^\mu + k^\mu, \tag{55}$$

where v^μ is the four velocity of the heavy quark with $v^2 = 1$, k^μ is called the residual momentum. $k \ll m_Q v$ since the heavy quark is almost on-shell. The heavy quark spinor field $Q(x)$ can also be separated into the large component $h_v^{(Q)}(x)$ and small component $H_v^{(Q)}(x)$

$$Q(x) \equiv (P_{v+} + P_{v-})Q(x) = \exp(-im_Q v \cdot x)\left[h_v^{(Q)}(x) + H_v^{(Q)}(x)\right], \tag{56}$$

---

[5] $\langle \mathcal{H}_{\text{EFT}} \rangle = \mathcal{H}_{\text{EFT}}|_{\varphi=0} = -f_\varphi^2 B_0(m_u + m_d + m_s)$ and $\frac{\partial \langle \mathcal{H}_{\text{QCD}} \rangle}{\partial m_q}|_{m_u=m_d=m_s=0} = \frac{1}{3}\langle \bar{q}q \rangle$.

via introducing the projection operators $P_{v\pm}$,

$$P_{v\pm} = \frac{1 \pm \slashed{v}}{2}, \quad \text{with } P_{v+} + P_{v-} = 1, \quad P_{v\pm}^2 = P_{v\pm}, P_{v\pm}P_{v\mp} = 0, \quad \slashed{v}h_v^{(Q)} = h_v^{(Q)}, \quad \slashed{v}H_v^{(Q)} = -H_v^{(Q)}. \tag{57}$$

With $v_\mu = (1, \mathbf{0})$, one can see that the $h_v^{(Q)}(x)$ and $H_v^{(Q)}(x)$ correspond to the large component and small component of the spinor, respectively. $H_v(x, t)$ is suppressed by the factor $1/m_Q$ in comparison with $h_v(x, t)$. The detailed derivation is presented in Appendix B. With Eq. (56), the heavy quark Lagrangian becomes [474]

$$\mathcal{L}_{\text{QCD}}^{(Q)} = \bar{h}_v^{(Q)}(iv \cdot \mathcal{D})h_v^{(Q)} - \bar{H}_v^{(Q)}(iv \cdot \mathcal{D} + 2m_Q)H_v^{(Q)} + \bar{h}_v^{(Q)}i\slashed{\mathcal{D}}_\perp H_v^{(Q)} + \bar{H}_v^{(Q)}i\slashed{\mathcal{D}}_\perp h_v^{(Q)}, \tag{58}$$

where $\mathcal{D}_\perp^\mu = \mathcal{D}^\mu - v^\mu(v \cdot \mathcal{D})$, $v \cdot \mathcal{D}_\perp = 0$. One can see that the h_v and H_v are light and heavy fields with the mass 0 and $2m_Q$, respectively. With the equation of motion or the path integral approach (see Appendix B for details), one can get the effective Lagrangian

$$\mathcal{L}_{\text{eff}} = \bar{h}_v^{(Q)}(iv \cdot \mathcal{D})h_v^{(Q)} + \bar{h}_v^{(Q)}i\slashed{\mathcal{D}}_\perp \frac{1}{(iv \cdot \mathcal{D} + 2m_Q - i\epsilon)}i\slashed{\mathcal{D}}_\perp h_v^{(Q)}. \tag{59}$$

An expansion of Lagrangian in Eq. (59) up to $O(1/m_Q)$ reads

$$\mathcal{L}_{\text{HQET}} = \bar{h}_v^{(Q)}(iv \cdot \mathcal{D})h_v^{(Q)} + \frac{1}{2m_Q}\bar{h}_v^{(Q)}(i\slashed{\mathcal{D}}_\perp)^2 h_v^{(Q)} + \frac{g_s}{4m_Q}\bar{h}_v^{(Q)}\sigma^{\alpha\beta}\mathcal{G}_{\alpha\beta}h_v^{(Q)} + O(1/m_Q^2), \tag{60}$$

where $\mathcal{G}_{\alpha\beta} = \lambda^a \mathcal{G}_{\alpha\beta}^a/2$.

In the heavy quark limit, only the LO term survives. The original quark–gluon vertex $ig_s\gamma^\mu\lambda_a/2$ becomes $ig_s v^\mu\lambda_a/2$, i.e., the interaction is independent of the heavy quark spin. This is called the heavy quark spin symmetry (HQSS). In addition, the heavy quark mass is eliminated thus the reduced Lagrangian is invariant with a global transformation under heavy flavor U(2) group. This is the heavy quark flavor symmetry (HQFS). Therefore, the spin and flavor together form a larger $SU(2) \otimes U(2) \in U(4)$ group.

The physical picture behind the HQSS and HQFS is that the soft gluon as a soft probe can only resolve the dynamics occurring at the scale of $\Lambda_{\text{QCD}}^{-1}$. The light d.o.f can only perceive the color forces induced by the color charge of the heavy quark (chromoelectric interaction), while the chromomagnetic interaction that carries the spin and flavor information of the heavy quark vanishes when $m_Q \rightarrow \infty$.

The HQSS and HQFS lead to interesting spectroscopic implications for the hadrons containing a heavy quark. In the heavy quark limit, the heavy spin j_h (spin of the heavy quark, $j_h = \frac{1}{2}$) and light spin j_ℓ (the total angular momentum of the light d.o.f) are conserved separately. Thus, the singly heavy hadrons can be labeled by its light spin j_ℓ. The states with total spin $J = j_\ell \pm \frac{1}{2}$ should be degenerate. An example is the masses of the ground state heavy mesons,

$$m_{D^*} - m_D \approx 140 \text{ MeV}, \qquad m_{B^*} - m_B \approx 45 \text{ MeV}, \tag{61}$$

where the mass splittings are relatively small compared with the masses of the heavy mesons. The HQSS dictates the mass splittings are inversely proportional to heavy quark masses, namely $(m_{D^*} - m_D)/(m_{B^*} - m_B) = m_b/m_c$ in line with the above experimental results. Meanwhile, HQFS requires that the mass difference between the mesons with different light d.o.f for the charm and bottom systems should be approximately the same. For example

$$m_{B_s^{(*)}} - m_{B^{(*)}} \approx m_{D_s^{(*)}} - m_{D^{(*)}} \approx 100 \text{ MeV}. \tag{62}$$

Apart from the mass spectrum, the HQSS and HQFS could be used to relate the different coupling constants and interactions. For example, in the HQFS, the vertices $BB^*\pi$ and $\bar{D}\bar{D}^*\pi$ can be related to each other. In the heavy quark limit, the interaction between two heavy hadrons is dominated by the interactions of the light d.o.f of the two particles. For example, the HQSS can bridge $D\bar{D}$ interaction and $D^*\bar{D}^*$ interaction. More examples will be discussed in Sec. 5.4.

In fact, the masses of the heavy quarks are finite and $m_c < m_b$, which indicates the HQS is explicitly broken. In Eq. (60), the second and third terms correspond to kinetic energy and chromomagnetic hyperfine interaction, respectively. The second term will break the HQFS while the third term will break both HQSS and HQFS. The chromomagnetic term gives the mass splittings in the spin doublets (D, D^*) and (B, B^*) at $O(1/m_Q)$, respectively. This leads to the refined relation $m_{B^*}^2 - m_B^2 \approx m_{D^*}^2 - m_D^2$.

19

2.2.2. An introduction to the heavy diquark-antiquark symmetry

The HDAS was proposed by Savage and Wise in Ref. [199], which relates the doubly heavy baryons QQq ($\bar{Q}\bar{Q}\bar{q}$) to the heavy mesons $\bar{Q}q$ ($Q\bar{q}$). The basic assumption (approximation) of HDAS is that the QQ pair in color $\bar{\mathbf{3}}$ in the doubly heavy baryons forms a compact object under the attractive color Coulomb interaction. The compact QQ is called the diquark (for more general concepts of the diquark, we refer to Ref. [499]). In the limit $m_Q \to \infty$, the heavy diquark becomes pointlike (the radius is inverse to the m_Q for the Coulomb interaction) and only acts as a static color source in the $\bar{\mathbf{3}}$ channel, which plays the same role as the heavy antiquark in the $\bar{Q}q$ meson.

If we denote the vector diquark as $\mathscr{D}_j$, the LO Lagrangian has the same form as that in Eq. (60)

$$\mathcal{L}_{\mathscr{D}} = \mathscr{D}_j^\dagger (iv \cdot \mathcal{D}) \mathscr{D}_j, \tag{63}$$

with $j = 1, 2, 3$ the spin index for the vector state. The Lagrangian (60) plus (63) is invariant under the U(5) transformation, which is named as the superflavor symmetry [500]. The S-wave QQq and $\bar{Q}q$ form the doublets (Ξ_{QQ}^*, Ξ_{QQ}) and $(\tilde{P}^*, \tilde{P})$ with spins-$(3/2, 1/2)$ and -$(1, 0)$, respectively. When the chromomagnetic interactions at $O(1/m_Q)$ are considered [analogous to Eq. (60)], they give the following relations of the mass splittings [199, 501],

$$m_{\Xi_{QQ}^*} - m_{\Xi_{QQ}} = \frac{3}{4}(m_{\tilde{P}^*} - m_{\tilde{P}}), \tag{64}$$

which is qualitatively supported by the calculations from the potential model [502] and lattice QCD [503, 139, 150]. A similar relation was extended to the singly heavy baryons Qqq and doubly heavy tetraquarks $QQqq$ [504]. The corrections to Eq. (64) from the nonrelativistic QCD (NRQCD) calculation were given in [505]. Eq. (64) implies that the one-pion transition $\Xi_{QQ}^* \to \Xi_{QQ}\pi$ is inaccessible in experiments. Considering $m_{D^*} - m_D \approx m_\pi$, only the radiative and weak decays of the Ξ_{QQ}^* state are allowed. The HDAS was also adopted to relate the axial coupling constant of the doubly heavy baryon to that of the heavy meson [506] because the axial coupling $D^*D\pi$ can be directly extracted from the partial decay width of the D^* in experiments. The details are given in Sec. 2.6.

The HDAS is valid only if the spatial extent cannot be resolved from the perspective of the light d.o.f. If $m_Q v \gg \Lambda_{\text{QCD}}$ [6] and the diquark excitations are suppressed, the HDAS is a good approximation. However, for the doubly charmed baryons, $m_Q v \sim \Lambda_{\text{QCD}} \sim m_Q v^2$, thus one expects that the HDAS breaking effect is sizable in the charmed sector. One can further consult the related discussions and calculations from NRQCD [501, 507, 508].

2.3. Heavy baryon chiral perturbation theory

When we extend the chiral perturbation theory to the heavy-light hadrons, we have to understand the meanings of "heavy" in twofold ways. First, the mass of the matter field is comparable to Λ_χ, which is heavy compared to the pion mass. In this sense, the nucleon mass is also heavy. At the hadronic level, the heavy baryon χPT (HBχPT) for the nucleon (or the matter field without heavy quarks) was invented to perform the chiral expansion. Meanwhile, for the system with a heavy quark, one can perform the heavy quark expansion and adopt the heavy quark symmetry. The heavy field expansion is performed at the quark level. In this subsection and Sec. 2.6, we will focus on twofold meanings in order. In this subsection, we will take the nucleon as an example of the matter field with a large mass but without heavy quarks.

The Weinberg's power counting in Eq. (54) based on the NDA can be extended to the mater fields [509],

$$D = 4L - I_N - 2I_M + \sum_i V_i d_i, \tag{65}$$

where L, I_M and I_N are the numbers of loops, Goldstone boson inner lines and matter field inner lines, respectively. V_i and d_i are the numbers of vertex i and the derivatives in the vertex i, respectively. With two topological relations,

$$L = I_N + I_M - \sum_i V_i + 1, \qquad 2I_N + E_n = \sum_i V_i n_i, \tag{66}$$

---

[6]$m_Q v$ and $m_Q v^2$ are the typical transferred momentum and binding energy between heavy quarks in the NRQCD power counting.

one can obtain a more useful power counting,

$$D = 2L + 2 - \frac{E_n}{2} + \sum_i V_i \Delta_i, \qquad \text{with } \Delta_i \equiv d_i + \frac{n_i}{2} - 2 , \tag{67}$$

where n_i is the number of matter fields connected by the vertex i. E_n is the number of the external matter fields. The power counting can be generalized to the cases with more than one separately connected pieces and more than two matter fields [510, 476, 475]. In this section we focus on the process with one matter field and take $E_n = 2$.

In order to derive (67), we treat the "momentum" of the matter field as a small scale, which is valid only when the mass of the matter field M is removed properly. However, in the practical calculations (e.g., in the dimensional regularization scheme), the mass of the matter field M is comparable to or even larger than Λ_χ, which will make the naive power counting in Eq. (67) fail. In fact, compared to the matter field mass M, the chiral fluctuations involve very soft dynamics. Thus, one can integrate out the hard scale M and recover the Weinberg's power counting. In the HBχPT [511], one can separate the momentum of the matter field into two parts, $p_\mu = M v_\mu + q_\mu$, like the heavy quark expansion in HQET, where $v^2 = 1$. $M v_\mu$ and q_μ are the mass term and residual momentum, respectively. The field is divided into the heavy field and massless light field. One can obtain the action and Lagrangian of the effective field theory by integrating out the heavy field with the assistance of the equation of motion [474] (in the classical sense) or the path integral approach [512] (in the quantum sense), see Appendix B.

We take the LO Lagrangian of the nucleon pion interaction as an example,

$$\mathcal{L}^{(1)} = \bar{\Psi}(i\slashed{D} - M + \frac{g_A}{2}\slashed{u}\gamma_5)\Psi, \qquad u_\mu = \frac{i}{2}\left[\xi^\dagger \partial_\mu \xi - \xi \partial_\mu \xi^\dagger\right], \tag{68}$$

where $\Psi = (p, n)^T$ and $\xi^2 = U$. The complete form of u_μ with the external fields is given in Eq. (A.4). With the heavy field decomposition, the corresponding $\mathcal{A}$, $\mathcal{B}$ and C in Eq. (B.11) read

$$\mathcal{A} = iv \cdot \mathcal{D} + g_A(u \cdot S), \tag{69}$$

$$\mathcal{B} = i\slashed{D}^\perp - \frac{g_A}{2}(v \cdot u)\gamma_5, \tag{70}$$

$$C = i(v \cdot \mathcal{D}) + 2M + g_A(u \cdot S). \tag{71}$$

One can see that there is no mass term for the light field H, while the mass of the heavy field h is $2M$. Expanding the C^{-1} in powers of $1/M$ one obtains that

$$C^{-1} = \frac{1}{2M} - \frac{i(v \cdot \mathcal{D}) + g_A(u \cdot S)}{(2M)^2} + \dots. \tag{72}$$

The contribution of the heavy component will appear as the recoiling effect, which is suppressed by the power of $1/M$. In the HBχPT, one has to perform two expansions, the chiral expansion and heavy baryon expansion. The HBχPT has been widely used to investigate the chiral dynamics of the nucleon systems (e.g., see Refs. [469, 513] for reviews). For the heavy flavor systems, the recoiling effect is less important because of the much larger heavy quark mass M as compared to the nucleon mass. However, the HQS breaking effect will appear as the $1/M$ correction for the heavy flavor system, which is particularly interesting for some systems. We will discuss this issue in Sec. 5.4.

Apart from the nonrelativistic expansion, the infrared regularization scheme [514, 515, 516] and extended on-mass-shell scheme (EOMS) [517] are two Lorentz covariant approaches to performing chiral expansion for the matter fields. The motivation of the infrared regularization is to discern the soft dynamics (typically m_φ) and the hard dynamics (typically M). One can only focus on the soft part, which includes the chiral fluctuation effect. To this end, in the infrared regularization scheme, the loop integral is divided into the infrared singular and regular parts when the mass of the Goldstone boson approaches zero. The infrared singular part is typically the soft dynamics. It was shown that the infrared singular parts do not include the power counting breaking (PCB) effect [514] and thus are kept. The infrared regular terms can be expanded as polynomials of the m_φ and thus are absorbed by the renormalization of the LECs. As shown in Fig. 3, the leading terms in the loop integrals of the infrared regularization are consistent with the Weinberg's power counting in Eq. (67).

In the extended on-mass-shell scheme [517], all the PCB terms are polynomials of small scales (such as the m_φ), which can be absorbed by redefining the LECs. As shown in Fig. 3, in this scheme, some infrared regular terms which

do not violate the power counting are kept. Like the infrared regularization scheme, the remaining terms in the loop integrals are at least at the order given by Eq. (67). The terms with powers beyond the Weinberg's power counting only contribute at higher orders.
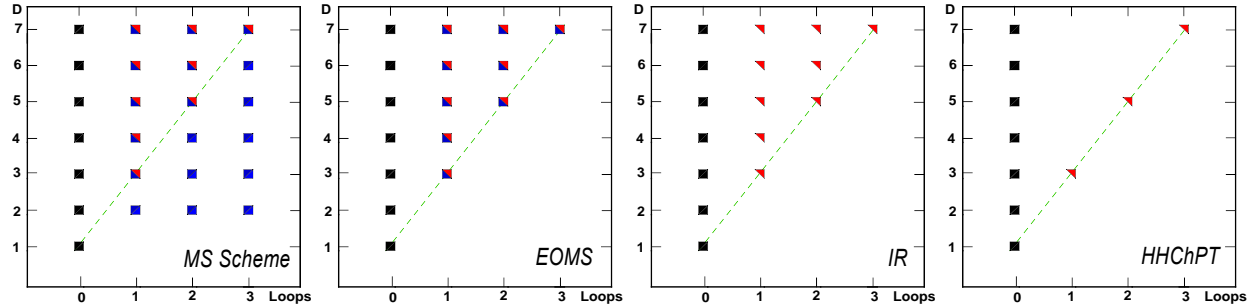

Figure 3: The comparisons of the different regularization schemes in LO Lagrangians [518]. x- and y-axis denote the number of loops and the corresponding chiral order, respectively. The Green dashed lines stand for the Weinberg's power counting. The chiral orders increase linearly with the number of loops according to Eq. (67) if all the vertices are the LO ones. The four subfigures (from left to right) correspond to MS, EOMS, infrared regularization and HHχPT schemes, respectively. The blue lower and red upper triangles represent the infrared regular and singular terms, respectively. The blue squares denote the PCB terms, while the black squares represent tree diagrams and counter terms. A successful subtraction scheme should ensure that there is no contribution below the green dashed line.

2.4. Effective range expansion

Effective range expansion (ERE) is a convenient parameterization scheme of the near-threshold partial wave T-matrix, which was first proposed by Schwinger in an unpublished note and reformulated by Bethe [519]. The ERE has extensive applications in both the experimental and theoretical aspects, such as fitting the scattering data [520], Weinberg compositeness [521], determining the power counting of EFT [522], universality in low energy scattering [523], m_π-dependence [524] and finite volume effect [525, 526] of the lattice QCD simulation and so on.

The partial wave S-matrix and T-matrix are parameterized as functions of the phase shift δ_l,

$$S_l = 1 + 2ikT_l(k) = e^{2i\delta_l(k)}, \qquad T_l(k) = \frac{k^{2l}}{k^{2l+1}\cot\delta_l - ik^{2l+1}}, \tag{73}$$

where the unitarity $S_l S_l^\dagger = 1$ is fulfilled. Here, we use the nonrelativistic formalism. The power of the k for T_l is determined by the asymptotic behavior of the wave functions in the partial wave basis. One can see that the unitary cut of the T-matrix is ensured by introducing the ik^{2l+1} in the denominator. $k^{2l+1}\cot\delta_l$ is a meromorphic function, where we assume that the left-hand cuts are sufficiently far way. Assuming there is no pole for $k^{2l+1}\cot\delta_l$ near the threshold, one can expand it with the Taylor series in powers of k^2,

$$k^{2l+1}\cot\delta_l = -\frac{1}{a_s} + \frac{1}{2}r_0 k^2 + v_2 k^4 + v_3 k^6 + ..., \tag{74}$$

where the coefficients are named as shape parameters. In particular, the leading two order coefficients a_s and r_0 are scattering length and effective range, respectively. The Eq. (74) is called effective range expansion. In the derivation of Bethe's work [519], the above expansion is formulated in the two body systems with a local interaction, namely $V(r, r') = V(r)\delta^3(r - r')$. The r_0 gets its name since its value roughly equals to half of the range of the potential [527]. However, in the modern view, the potentials corresponding to the same scattering data are not unique and there is no good reason to exclude the non-local interactions. It was proven by Ekstein [528] that a large class of unitary transformations can relate the different Hamiltonians producing the same S-matrix. In the modern perspective, the ERE is not relevant to the locality of the interaction but an effective theory to depict the low-energy behavior of the two-body scattering with finite parameters truncated according to the expected precision. It was shown that the ERE is just equivalent to the pionless effective field theory [529]. But, once the one-pion exchange interaction is introduced, the accompanying left-hand cut will invalidate the ERE expansion.
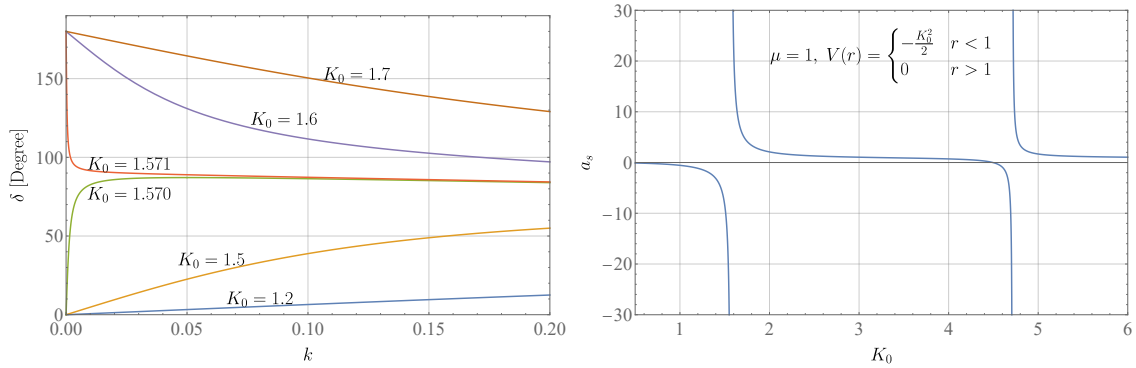
22

Figure 4: Levinson's theorem and scattering lengths with the square well potential as an example (specifically in right panel). The left panel and the right panel illustrate the phase shifts near the threshold and scattering lengths respectively when the interaction becomes more attractive and then bound states appear.

The scattering length encodes important information. According to Levinson's theorem [530, 527], if the potential admits n bound states in the S-wave, the phase shift at zero energy is

$$\delta(0) = n\pi \quad \text{[with the convention } \delta(\infty) = 0]. \tag{75}$$

For the marginal potential that the n_{th} bound state starts to appear, the phase shift is $\delta(0) = (n + \frac{1}{2})\pi$. The phase shifts within the square well potential are shown in Fig. 4 when the potential becomes more attractive and the first bound state starts to appear at $K_0 \sim 1.57$. The scattering lengths will cross the infinity (from the negative one to the positive one or vise verse) when the new bound state appears (see the right panel of Fig. 4). When the interaction is repulsive everywhere or attractive everywhere but too weak to form the bound states, the sign of the scattering lengths can reflect the sign [7] of the potential [531],

$$V > 0 \text{ everywhere} \quad \rightarrow \quad a_s > 0,$$
$$V < 0 \text{ everywhere (but no bound states)} \quad \rightarrow \quad a_s < 0. \tag{76}$$

For the system with the "bare" poles, namely the discrete eigenstates of the free Hamiltonian H_0, the Levinson's theorem is generalized as [532, 533, 534, 535]

$$\delta(0) = (n - n_{\text{bare}})\pi, \tag{77}$$

where n_{bare} is the number of the bare poles, and n is the number of the bound states, namely the discrete eigenstates of the Hamiltonian H.

Landau and Smorodinsky proved that the effective range is always positive $r_0 > 0$ if the local potential is attractive everywhere, i.e. $V(r) < 0$ everywhere in their textbook [536]. The arguments was cited in Ref. [222] to claim that "the molecular case gives always $r_0 > 0$". However, as we mentioned before, the potentials corresponding to the same observable are not unique. The local attractive everywhere potential is not the necessary condition of the hadronic bound states. The statement in Ref. [222] extends the argument of Landau and Smorodinsky without an extra proof. In fact, according to the Wigner's theorem [537] (based on the unitary and causality), the effective range of the zero-range potential is non-positive [538]. From the perspective of the inverse scattering problem, one can construct the non-local potential to permit any given scattering phase shift function (no matter the sign of the effective range) and bound states with given binding energies. For example, one can construct the rank-one separable potential to permit a loosely bound state and arbitrary phase shift [539]. In Sec. 5.1.1, we will construct an example with the non-local interaction admitting the bound state but with negative effective range. See [540] for more detailed discussions on this issue.

---

[7]There are different conventions about the sign of the scattering length. Here, we follow the convention in Eq. (74).

23

The ERE in Eq. (74) is the simplest version, which has been extended to more complicated cases. The single-channel ERE was generalized to the multichannel cases [541, 542, 543]. In fitting the pion-pion scattering, the effect of the inelastic thresholds are considered with ERE supplemented by a conformal expansion, which takes the unitarity and analyticity into account [544]. Meanwhile, the convergence radius of Eq. (74) is determined by the appearance of the left-hand cuts. For example, for the NN scattering systems, the ERE fails at the energy $|E_{lab}| \sim m_\pi^2/(2m_N) = 10.5$ MeV. If one includes the Coulomb interaction, the convergence radius of ERE is zero. In Ref. [545], the modified ERE was proposed to overcome this problem by separating the long-range interaction and the short-range interaction, where the long-range interaction is known explicitly (e.g., OPE and Coulomb interaction). In the modified ERE, the contribution of the long-range interaction is calculated directly and the contribution of the short-range interaction can be expanded in the power of k^2, where the left-hand singularity is absent. It was shown that the effective-range function is actually metamorphic, where the poles might prevent performing the Taylor expansion in Eq. (74). The problem can be solved by replacing the Taylor expansion with the Padé approximation [546].

2.5. Chiral unitary approach

The analyticity and unitarity are important features of the S-matrix, which are closely tied to the causality and conservation of the probability current, respectively. Considering these constraints, many theoretical tools have been invented to explore the nonperturbative dynamics. The chiral unitary approaches combine the χPT, unitarity and analyticity. Compared with the χPT, the chiral unitary formalism satisfies the exact unitary condition, while the χPT satisfies it perturbatively. A dazzling merit of the unitary methods is that they can introduce the bound state or resonance poles in the amplitude, which is impossible in the χPT up to any finite order. In this subsection, we will introduce the basic concepts and frameworks. We refer to Refs. [547, 548, 549, 68] for reviews.

For an elastic scattering process $1 + 2 \to 1 + 2$, its partial wave amplitude is given by

$$T_\ell(s) = \frac{1}{2(\sqrt{2})^\alpha} \int_{-1}^{1} dz T(s, z) P_\ell(z), \tag{78}$$

where $(\sqrt{2})^\alpha$ is the symmetry factor. The α equals 1 or 0 when the two particles are identical and different, respectively. $\sqrt{s}$ is the total energy. $z = \cos\theta$, with θ the relative angle between the initial and final momenta in the center of mass system (c.m.s). P_ℓ is the Legendre polynomial.

The partial wave S-matrix is constrained by the unitary,

$$S_\ell(s) = 1 + 2i\rho(s)T_\ell(s), \qquad S_\ell^* S_\ell = 1, \tag{79}$$

with

$$\rho(s) = \frac{q}{8\pi\sqrt{s}}, \qquad q = \frac{\sqrt{\left(s - (m_1 + m_2)^2\right)\left(s - (m_1 - m_2)^2\right)}}{2\sqrt{s}}, \tag{80}$$

where m_1 and m_2 are the masses of the scattering particles. q is the relative momentum in the c.m.s. The optical theorem $\operatorname{Im} T_\ell(s) = T_\ell^\dagger(s)\rho(s)T_\ell(s)$ leads to the unitary condition

$$\operatorname{Im} T_\ell^{-1}(\sqrt{s}) = -\rho(s), \qquad s \geq s_{\text{th}} = (m_1 + m_2)^2. \tag{81}$$

Based on Eq. (81), one can define the K-matrix, $T_\ell = [K^{-1} - i\rho(s)]^{-1}$, where $K^{-1} = \operatorname{Re}(T_\ell^{-1})$.

The T_ℓ is the function of $\sqrt{s}$, which is real and analytical along some intervals of real $\sqrt{s}$ axis. The T_ℓ can be analytically continued to the whole complex plane except for the poles and cuts. According to the Schwartz reflection principle (see Ref. [549] for details), one gets

$$T_\ell(\sqrt{s}) = T_\ell(\sqrt{s^*})^*. \tag{82}$$

With the unitary condition in (81), we know the discontinuity appears across the real axis for $\sqrt{s} > m_1 + m_2$,

$$T_\ell(\sqrt{s} + i\epsilon) - T_\ell(\sqrt{s} - i\epsilon) = 2i \operatorname{Im} T_\ell(\sqrt{s}), \tag{83}$$

which corresponds to a right-hand cut (named after its approaching to the right), or unitary cut. The unitary cut is independent of the interaction and appears as the threshold opens, which is also classified as the kinetic cut.

Apart from the right-hand cut, there might exist the left-hand cuts (also called the dynamical cuts since they depend on the dynamical details, e.g., see Ref. [550]). For the relativistic systems, the cross symmetry will transform the singularities of the t-channel or u-channel into the left-hand cuts in the s-channel. For the nonrelativistic system, the particle-exchange interaction such as the one-pion-exchange interaction in the NN system will give rise to the left-hand cuts.

When the T_ℓ is continued to the complex plane of $\sqrt{s}$, the q in Eq. (80) is a multivalue function of $\sqrt{s}$. For simplicity, we neglect the existence of the left-hand cuts and focus on the single-channel problem. In this case, the Riemann surface has two sheets. Moving from one sheet to the other one needs to cross the unitary cut and changes the sign of Im q. The conventional definition is

$$\text{sheet I (physical): Im } q > 0, \qquad \text{sheet II: Im } q < 0. \tag{84}$$

The poles on the real axial of sheet I with $\sqrt{s} < m_1 + m_2$ correspond to the bound states. Actually, constrained by the causality, on the first sheet the poles can only appear on the real axis below the lowest threshold. The poles in the sheet II with $\text{Im}(\sqrt{s}) < 0$ correspond to the resonances. We refer to Ref. [547] for the topology of the Riemann surfaces for the coupled-channel problem.

2.5.1. Bethe-Salpeter equation

One may incorporate the unitary condition through the Bethe-Salpeter equation (BSE). For simplicity, we start from the singe-channel scattering amplitude.

The Bethe-Salpeter equation reads

$$T = V + VGT, \tag{85}$$

$$T(q, q', P) = V(q, q', P) + \int \frac{d^4k}{(2\pi)^4} V(q, k, P) \frac{1}{k^2 - m_1^2 + i\epsilon} \frac{1}{(P - k)^2 - m_2^2 + i\epsilon} T(k, q', P), \tag{86}$$

where P, q', and q are the total four-momentum, relative ones in the initial and final states, respectively. G is the hadron-hadron loop function with k the four-momentum in the loop. m_1 and m_2 are the masses of the scattering hadrons. The Lippmann-Schwinger equation has a very similar form but in a nonrelativistic framework where the integral is performed for the three momentum. In Sec. 2.5.2, we will see that Eq. (86) is equivalent to the dispersion relation of the T-matrix [c.f. Eq. (99)] constrained by the unitary condition if the left-hand cut is neglected [551].

The BSE in Eq. (86) can be understood as the nonperturbative resummation of the s-channel loops as shown in Fig. 5. The BSE can generate the poles of the S-matrix corresponding to the bound states or resonances, which is impossible in χPT. Thus, the BSE was widely used to investigated the so-called "dynamically generated" states. These poles originate from the hadron-hadron scattering dynamics and can be understood as the meson-meson/meson-baryon/baryon-baryon molecules to some extent.

One should note that the unitary approach only considers the s-channel loops as shown in Fig. 5, while the χPT has the t-channel and u-channel ones as well, which are not included explicitly in the Bethe-Salpeter equation. If the singularities of the crossed loops locate far away from the concerned energy region, their energy dependency is expected to be smooth. Their contributions can be absorbed by the subtraction terms in regularizing the Bethe-Salpeter equation.

Omitting the off-shell effect, Eq. (85) converts into an algebraic equation

$$T_{\text{on}} = V_{\text{on}} + V_{\text{on}} G T_{\text{on}}. \tag{87}$$

The on-shell approximation T_{on} still satisfies the unitary relation [552, 553, 554]. It was shown that the off-shell contribution could be absorbed by the renormalization of the couplings and masses in the kernel interaction [555, 552]. The loop function G is given by

$$G = i \int \frac{d^4k}{(2\pi)^4} \frac{1}{k^2 - m_1^2 + i\epsilon} \frac{1}{(P - k)^2 - m_2^2 + i\epsilon}. \tag{88}$$
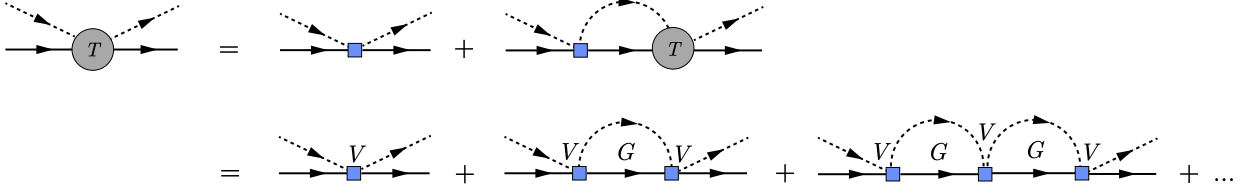
25

Figure 5: The resummation of the *s*-channel diagrams giving rise to the scattering amplitude.

It is divergent and needs to be regularized. In literature, there are two common regularization methods. One is the dimensional regularization [556]

$$G^{\text{DR}}(\sqrt{s}) = \frac{1}{16\pi^2}\left\{a(\mu) + \ln\frac{m_2^2}{\mu^2} + \frac{m_1^2 - m_2^2 + s}{2s}\ln\frac{m_1^2}{m_2^2} + \frac{q}{\sqrt{s}}\left[\ln\frac{\left(s + 2q\sqrt{s}\right)^2 - \left(m_2^2 - m_1^2\right)^2}{\left(s - 2q\sqrt{s}\right)^2 - \left(m_2^2 - m_1^2\right)^2} - 2\pi i\right]\right\}, \quad (89)$$

where μ is the regularization scale and $a(\mu)$ is the subtraction constant to cancel the μ dependence of the loop function. We may also introduce a hard cut-off parameter Λ for the three momentum. The k_0 component in Eq. (88) can be integrated out in the c.m.s, and the loop function reads [557, 552]

$$G^{\text{CR}}(\sqrt{s}) = \int_0^\Lambda \frac{k^2 dk}{4\pi^2}\frac{(\omega_1 + \omega_2)}{\omega_1\omega_2\left[s - (\omega_1 + \omega_2)^2 + i\epsilon\right]}, \qquad \omega_i = \sqrt{k^2 + m_i^2}. \quad (90)$$

Constrained by the unitary relation, the two regularization schemes ensure the same imaginary parts. The analytical continuation to the second Riemann sheet is achieved by

$$G_{\text{II}}(\sqrt{s} + i\epsilon) = G_{\text{I}}(\sqrt{s} + i\epsilon) - 2i\,\text{Im}\,G_{\text{I}}(\sqrt{s} + i\epsilon). \quad (91)$$

However, their real parts depend on $a(\mu)$ or Λ. For such a nonperturbative approach, the renormalization is not transparent. For example, there are no free LECs in the LO Lagrangians contributing to the $\pi\pi$ scattering [557] to absorb the cutoff-dependence in $G(\sqrt{s})$. The $a(\mu)$ or Λ can only be determined phenomenologically [557]. However, in the spirit of EFT, one can expect that the regulator dependence will become weaker as one goes to the high orders. In Ref. [44], the typical value of the Λ was estimated as $\Lambda \sim \sqrt{\Lambda_\chi^2 - m_\varphi^2} \sim 0.8 \pm 0.2$ GeV, where $\Lambda_\chi \sim 1$ GeV and m_φ is the mass of the light mesons such as π, K or η. With the above estimation, the subtraction term in the dimensional regularization can be estimated by requiring the two schemes giving the same results in the low energy region. See Refs. [552, 349] for the discussions on their relations. One can get the regulator-independent results via some other unitary approaches, e.g. the inverse amplitude method in Sec. 2.5.3.

The above equations can be extended to the coupled-channel cases. The T-matrix, the potential V, and G become the $n \times n$ matrix (n is the number of the coupled channels), in which G is a diagonal matrix.

In the chiral unitary method, the kernel interaction V is obtained with the help of the χPT. We use the scattering of the pseduo-Goldstone boson off a matter field as an example. The relativistic G in Eq. (88) is superficially $O(p^0)$. However, the dynamics of the matter field is nonrelativistic. The G function will reduce to $O(p)$ if the propagator of the matter field is nonrelativistic. The unitarized T-matrix within BSE is obtained by

$$T = (1 - VG)^{-1}V. \quad (92)$$

By matching the T with the chiral expansion amplitude $\mathcal{A}$ at low energy regions, the V can be introduced order by order [558, 551, 559],

$$V^{(1)} = \mathcal{A}^{(1)}, \quad V^{(2)} = \mathcal{A}^{(2)}, \quad V^{(3)} = \mathcal{A}^{(3)} - V^{(1)}GV^{(1)}, \quad (93)$$

where the superscript denotes the chiral expansion order. With the kernel potential in Eq. (93), the unitarized T-matrix matches the chiral amplitude $\mathcal{A}$ precisely at a given order and satisfies the unitary condition. One should note

26

that the s-channel loop from the iteration of the lower chiral order amplitudes $\mathcal{A}$ has been subtracted to avoid the double counting. For instance, $V^{(3)} = \mathcal{A}^{(3)} - V^{(1)}GV^{(1)}$ at $O(p^3)$. In Ref. [551], the case with a resonance in the kernel potential was considered. The presence of the resonance arises from the nonperturbative dynamics of chiral Lagrangians [560, 561, 562]. In this case, the power counting method in Eq. (93) should be modified. Recently, the authors in Refs. [563, 564] used an alternative regularization scheme of the HBχPT, infrared regularization scheme, and EOMS in Sec. 2.3. They introduced the renormalized scalar bubble-loop contributions independent of the renormalization scale and replaced the heavy-light field bubble loops subject to certain replacement rules. The renormalization scale dependence of the tadpole integral with only the light mesons is absorbed by the suitable counter terms. The left-hand cuts were also discussed and turned out to be significant.

2.5.2. N/D method

According to the analytic structures in Eq. (81) and Eq. (83), the N/D method is proposed to construct a general solution of the T-matrix [565, 554]. In the following, the "reduced" amplitude $T'_\ell = T_\ell(s)/q^{2\ell}$ is used to remove the vanishing threshold behavior of the partial wave. In the N/D method, the T'_ℓ has the form, $T'_\ell(s) = N'_\ell(s)/D'_\ell(s)$, where N'_ℓ (numerator) and D'_ℓ (denominator) carry the analytic information of the left- and right-hand cuts, respectively. If the left-hand cut is neglected (see Ref. [549] for the derivation of keeping the left-hand cut), N'_ℓ becomes a polynomial.

Dividing the denominator by the numerator, one can set $N'_\ell(s) = 1$ and get [554, 560]

$$T'^{-1}_\ell(s) = D'_\ell(s). \tag{94}$$

With the unitary condition, one has

$$\mathrm{Im}D'_\ell = \begin{cases} 0 & s < s_{th} \\ -\rho(s)q^{2\ell} & s > s_{th} \end{cases}. \tag{95}$$

where ρ is defined in Eq. (80). Using the dispersion relation, the general forms of $D'_\ell(s)$ and $T'_\ell(s)$ are given by

$$T'^{-1}_\ell(s) = D'_\ell(s) = -\frac{(s-s_0)^{\ell+1}}{\pi} \int_{s_{th}}^\infty ds' \frac{q^{2\ell}\rho(s')}{(s'-s)(s'-s_0)^{\ell+1}} + \sum_{m=0}^\ell a_m s^m + \sum_i^{M_\ell} \frac{R_i}{s-s_i}, \tag{96}$$

where s_0 is the subtraction point and a_m stands for the subtraction terms. According to Eq. (95), one has the asymptotic behavior,

$$\lim_{s\to\infty} \frac{\mathrm{Im}D'_\ell}{s^\ell} = -\lim_{s\to\infty} \frac{q^{2\ell}\rho(s)}{s^\ell} = -\frac{1}{4^{\ell+2}\pi}, \tag{97}$$

which requires the $\ell+1$ times subtraction. All the poles (s_i) in Eq. (96) are called the Castillejo–Dalitz–Dyson (CDD) poles [566]. M_ℓ is the number of the CDD poles. When the CDD poles are located far away from the energy region of interest, they can be absorbed into the subtraction terms. However, if they are close to the physical state, one should be much cautious when dealing with the CDD poles. In literature, there are various works where the interplay of the zeros of T-matrix (t-zeros) and poles of T-matrix (t-poles) was discussed in detail [567, 568, 569, 570]. In Ref. [567], the authors used the $X(3872)$ as a paradigm for a two-channel situation and compared the production line shapes in B-meson decays in the near-threshold region with and without the presence of the near-threshold t-zeros and important continuum channel interplay. In the absence of these two factors, the production of the $X(3872)$ is regular and can be described by the simple Flatté formulae. However, if there is a strong channel-entanglement or the presence of near-threshold t-zeros, the line shape can be dramatically distorted and exhibit an irregular behavior. The line shapes can be used to discriminate between the binding mechanisms for the $X(3872)$ as demonstrated in Ref. [570]. Additionally, the presence of the near-threshold t-zeros corresponds to more near-threshold t-poles, as shown in Refs. [568, 567].

The physical resonances or bound states are the poles of T'_ℓ and satisfy $D'_\ell(s_{\mathrm{pole}}) = 0$. In contrast, the CDD poles are the poles of the inverse amplitude T'^{-1}_ℓ and the zeros of $T'_\ell(s) = 0$. In literature, the pole in the interaction potential

was often called the CDD pole, e.g. [571, 572, 573]. One should be cautious about the different meanings of the "CDD pole" according to the context.

If one insists on using the T_ℓ without eliminating the vanishing threshold effect, one obtains the form of the T_ℓ [560] similar to Eq. (96),

$$T_\ell^{-1}(s) = D_\ell(s) = \sum_i \frac{R_i}{s - s_i} + a(s_0) - \frac{s - s_0}{\pi} \int_{s_{th}}^\infty ds' \frac{\rho(s')}{(s' - s)(s' - s_0)}, \tag{98}$$

where the left-hand cut is neglected. The vanishing threshold behaviour of T_ℓ should be introduced as the CDD poles. The $a(s_0)$, s_i and the residue R_i are not known in advance. Their values can be obtained in different ways such as using experimental data, matching to χPT, or fitting lattice data as discussed below.

The Eq. (98) can be written in the generalised form

$$T_\ell^{-1}(s) = \mathcal{V}^{-1}(s) - g(s), \quad \Rightarrow \quad T_\ell(s) = [1 - \mathcal{V}(s)g(s)]^{-1}\mathcal{V}(s), \tag{99}$$

with

$$g(s) = \tilde{a}(s_0) + \frac{s - s_0}{\pi} \int_{s_{th}}^\infty ds' \frac{\rho(s')}{(s' - s)(s' - s_0)}, \tag{100}$$

where the $\tilde{a}(s_0)$ specifies the freedom of choosing subtraction terms. One can see the $\mathcal{V}$ and the $g(s)$ play the same roles as the kernel potential and loop function in BSE in Eq. (86). The explicit calculation shows that $g(s)$ is identical to Eq. (88) up to a constant. Their right-hand cuts and imaginary parts along the cut are the same. In Ref. [551], the interaction kernel is determined by the χPT amplitude to any given chiral expansion order as well as the explicit resonance contributions, see Eq. (93) and the context. The kernel potential $\mathcal{V}(s)$ contains all the contributions except the right-hand cut.

The extension to the coupled-channel cases was given in Ref. [554] with the matrix form, in which the T-matrix satisfies the unitary condition

$$\left[\text{Im } T_\ell^{-1}\right]_{ij} = -\rho_{ii}(s)\delta_{ij}. \tag{101}$$

2.5.3. Inverse amplitude method

The inverse amplitude method (IAM) is another unitarization technique adopting the unitary condition in Eq. (81) for the inverse amplitude rather than the amplitude [574, 575, 576, 577], since they have the same analytic structures except the possible pole contributions. This method has been used to study the light resonances, for instance $f_0(500)$, $K_0^*(700)$, $f_0(980)$, $a_0(980)$, $\rho(770)$ and $K^*(892)$ (see more discussions in Ref. [578]).

Before deriving the formalism of the inverse amplitude method in the unitary perspective, it is instructive to adopt the Padé expansion. The chiral partial wave amplitudes for the scattering of the light pseudoscalar mesons can be expanded as

$$T(s) = T_2(s) + T_4(s) + T_6(s) + \ldots, \tag{102}$$

where the "..." denotes the higher order amplitude $T_{2k} \sim O(p^{2k})$. We can perform the [1, 1] and [1, 2] Padé expansion for the T-matrix,

$$T^{[1,1]} = \frac{N^{(0)} + N^{(2)}}{1 + D^{(2)}} = T_2 + T_4, \quad T^{[1,2]} = \frac{N^{(0)} + N^{(2)}}{1 + D^{(2)} + D^{(4)}} = T_2 + T_4 + T_6, \tag{103}$$

where $[i, j]$ represent that the truncation chiral orders of the expansions of the numerator and denominator are $2i$ and $2j$, respectively. In the above equation, we further match the [1, 1] order and [1, 2] order Padé expansions to the chiral expansions of T to $O(p^4)$ and $O(p^6)$, respectively, which can fix the $N^{(2n)}$ and $D^{(2m)}$ terms. The final results are

$$T^{[1,1]} = \frac{T_2^2}{T_2 - T_4} + O(p^6), \quad T^{[1,2]} = \frac{T_2^2}{T_2 - T_4 + T_4^2/T_2 - T_6} + O(p^8). \tag{104}$$

The Eq. (104) is just the conventional IAM formula to $O(p^4)$ and $O(p^6)$.

Now, we inspect the above results from the unitarity. With the optical theorem, one has

$$\text{Im}\, T_2(s) = 0, \qquad \text{Im}\, T_4(s) = T_2(s)\rho(s)T_2(s), \qquad \text{Im}\, T_6(s) = 2\rho(s)T_2(s)\, \text{Re}\, T_4(s), \ldots \tag{105}$$

The dispersion relations for the amplitudes are

$$T_2(s) = a_0 + a_1 s, \qquad T_4(s) = b_0 + b_1 s + b_2 s^2 + \frac{s^3}{\pi} \int_{s_{th}} ds' \frac{\text{Im}\, T_4(s')}{s'^3(s'-s-i\epsilon)} + \text{LC}(T_4), \tag{106}$$

where $\text{LC}(T_4)$ represents the left-hand cut. a_i $(i=0,1)$ and b_j $(j=0,1,2)$ are the subtraction constants.

To implement unitarity, one defines $g(s) = T_2(s)^2/T(s)$. Since the $T_2(s)$ is real, the $g(s)$ has the same cuts as $T(s)$. One can obtain the integral equation for $g(s)$ with the dispersion relation. For instance, the three times subtracted dispersion relation for $g(s)$ is

$$g(s) = g(0) + g'(0)s + \frac{1}{2}g''(0)s^2 + \frac{s^3}{\pi} \int_{s_{th}} ds' \frac{\text{Im}\, g(s')}{s'^3(s'-s-i\epsilon)} + \text{LC}(g) + \text{PC}(s), \tag{107}$$

where $\text{PC}(s)$ denotes the pole contribution of the $g(s)$. Note that the correct pole contribution of $1/T$ (corresponding to Adler zero) cannot be obtained from the PC term of the $g(s)$ given the appearance of T_2^2 in the numerator. With the unitarity relation in Eq. (81), one obtains

$$\text{Im}\, g(s) = -T_2(s)\rho(s)T_2(s) = -\text{Im}\, T_4(s), \tag{108}$$

on the right-hand cut. The subtraction constants in Eq. (107) are related to the chiral expansions. Up to $O(p^4)$, the $g(s)$ can be expanded in the low energy region using Eq. (106) after neglecting the pole contributions PC,

$$g(s) = \frac{T_2^2}{T_2 + T_4} \simeq a_0 + a_1 s - b_0 - b_1 s - b_2 s^2 - \frac{s^3}{\pi} \int_{s_m} ds' \frac{\text{Im}\, T_4(s')}{s'^3(s'-s-i\epsilon)} - \text{LC}(T_4) = T_2(s) - T_4(s), \tag{109}$$

where one has approximated

$$\text{Im}\, g(s) \simeq -\text{Im}\, T_4(s), \qquad \text{LC}(g) = -\text{LC}(T_4) + \ldots \tag{110}$$

on the left cut. Thus, the elastic formula for IAM reads [574, 575, 576, 577]

$$T(s) \simeq \frac{T_2^2(s)}{T_2(s) - T_4(s)}, \tag{111}$$

which recovers the χPT expansion by expanding Eq. (111) as follows

$$T(s) \simeq \frac{T_2^2(s)}{T_2(s) - T_4(s)} \simeq T_2 + T_4 + O(p^6), \tag{112}$$

The above discussion with the dispersion formalism can be extended to higher orders. For instance, up to the next-to-next-to-leading order (NNLO or N^{2}LO) one reads [577]

$$T(s) \simeq \frac{T_2^2(s)}{T_2(s) - T_4(s) + T_4^2(s)/T_2(s) - T_6(s)}. \tag{113}$$

It should be noticed that the above IAM method neglecting the pole contribution will give the imprecise Adler zeros of the T-matrix. Such a flaw casts some doubts about the robustness of this method [579] given the Adler zeros are zeros of the T-matrix arising from chiral symmetry and its spontaneous breaking [580]. In Ref. [581], the IAM is adjusted to incorporate the Alder zeros correctly.

In Refs. [553, 552, 582], the IAM is generalized to the coupled channels using the matrix formalism,

$$T(s) = T^{(2)}(s) \cdot \left[T^{(2)}(s) - T^{(4)}(s) \right]^{-1} \cdot T^{(2)}(s). \tag{114}$$

The IAM approach can be generalised to study the system with the matter field. In Ref. [583], the authors applied the IAM to derive the scattering amplitude of the pseudo-Goldstone boson off the heavy meson,

$$T(s) = T^{(1)}(s) \cdot \left[T^{(1)}(s) - T^{(2)}(s) - T^{(3)}(s) \right]^{-1} \cdot T^{(1)}(s), \tag{115}$$

where

$$\text{Im}[T^{(1)}(s)] = \text{Im}[T^{(2)}(s)] = 0, \qquad \text{Im}[T^{(3)}(s)] = T^{(1)}(s)\tilde{\rho}(s)T^{(1)}(s). \tag{116}$$

The loop function is $O(p)$ since the propagator of the heavy meson is counted as $O(p^{-1})$ [551] and its imaginary part $\tilde{\rho}(s)$ is $O(p)$ in this case.

2.5.4. Dynamically generated states

The chiral unitary approaches combine the unitary condition with χPT and lead to the nonperturbative resummation of the infinite s-channel loop diagrams. The implementation of the unitary condition extends the applicable range of the χPT to higher energy region and generates the poles for the resonance/bound states in the unitarized scattering amplitudes. Such chiral unitary approaches have been successfully used to describe a variety of scattering processes of the meson-baryon systems [584, 555, 585, 551, 586, 587, 588, 571, 589, 590] and meson-meson systems [577, 557, 553, 552, 591, 556], which can also be extended to the heavy flavor systems in Sec. 4.

In the chiral unitary methods, the poles of the resonances or bound states can be generated by the dynamics of the hadron-hadron scattering. In this context, the poles are called the "dynamically generated" states. These states arise from the hadron-hadron interactions (which definitely happen at the hadron level). They are not the explicit d.o.fs in the free Hamiltonians or Lagrangians. Their properties such as the masses and decay widths are determined by the hadron-hadron scattering potentials.

In contrast to the dynamically generated states, there are literally "preexisting" states, which are assumed to exist as the explicit d.o.fs before the hadron interactions. The "preexisting" states are often associated with the bound states or resonances composed of more fundamental d.o.fs than the scattering d.o.f, and their properties are determined by more fundamental theories. For example, in the meson-meson scattering, the compact quark states such as the $\bar{q}q$ or $qq\bar{q}\bar{q}$ tetraquark state are governed by the direct QCD dynamics. They exist prior to the hadron-hadron interactions and are considered as the preexisting states. There is another potential origin of the "preexisting" states. They can be the dynamically generated states in the other channels, which could be regarded as the preexisting ones in the relevant channels [571, 592, 593, 578].

In Ref. [594], the CDD pole was interpreted as an independent particle participating in the scattering. In literature, the "preexisting" states were associated with the CDD poles which act as the poles of the inverse T-matrix as shown in Eq. (96). Thus, the "preexisting" states were often called the CDD poles directly, e.g. [571, 572]. One should be cautious about the different meanings of the "CDD pole" according to the context. The "preexisting" states are usually introduced explicitly through a bound state or resonance propagators in the effective field theory [571, 593, 595, 595, 572].

However, the above naive distinction (or classification) of the "dynamically generated" and "preexisting" states is model-dependent. From the perspective of the effective field theory, the parameterizations of the kernel potentials which generate the consistent T-matrix at the energy scale of interest are not unique. In some cases, the preexisting states are hidden in the low energy constants (LECs). Within a given energy range, it is possible to replace a theory with the non-perturbative two-particle interactions and no preexisting pole by an effective theory with a preexisting pole and perturbative two-particle interactions [521]. This leads to ambiguity regarding the mechanisms of the resonance generation. Sometimes, it is difficult to distinguish the direct QCD dynamics at the quark level and the hadron-hadron interactions since both of them may contribute simultaneously. Even some well-accepted $\bar{q}q$ mesons could be dynamically generated from the meson-meson interaction at least formally in some frameworks. For example, the pole of the ρ resonance can be reproduced well either from the χPT interaction without the bare pole in the chiral unitary approaches (e.g. [553, 596]) or by introducing the bare pole in the $\pi\pi$ scattering, e.g. [554, 572]. The D^* was also dynamically generated from the $D\pi$ interaction in Ref. [597]. In Sec. 4.3, we will illustrate that the dynamically generated mechanisms and its mixtures with the preexisting states can both reproduce the mass and width of the $D_{s0}^*(2317)$ and are indistinguishable within the current experimental uncertainties.

For the system associated with the meson-meson scattering, to discern the genuine state and the dynamically generated ones, the studies of other properties, such as the trajectories in the large N_C limit, are useful [554]. The latter does not survive in the large N_C limit, since the meson-meson scattering is $O(N_C^{-1})$ [598]. In the large N_C limit, the pole position of the genuine $\bar{q}q$ state $M_{N_C} - i\Gamma_{N_C}/2$ should satisfy M_{N_C}/M_3 being a constant and $\Gamma_{N_C}/\Gamma_3 \sim 3/N_C$, while the dynamically generated two-meson state will disappear [599, 600]. As an example, the studies of the N_C scaling behaviors in Ref. [600] favored the ρ and K^* as the $q\bar{q}$ state, while their results supported the σ and κ as the "dynamically generated" two-meson states as shown in Fig. 6.
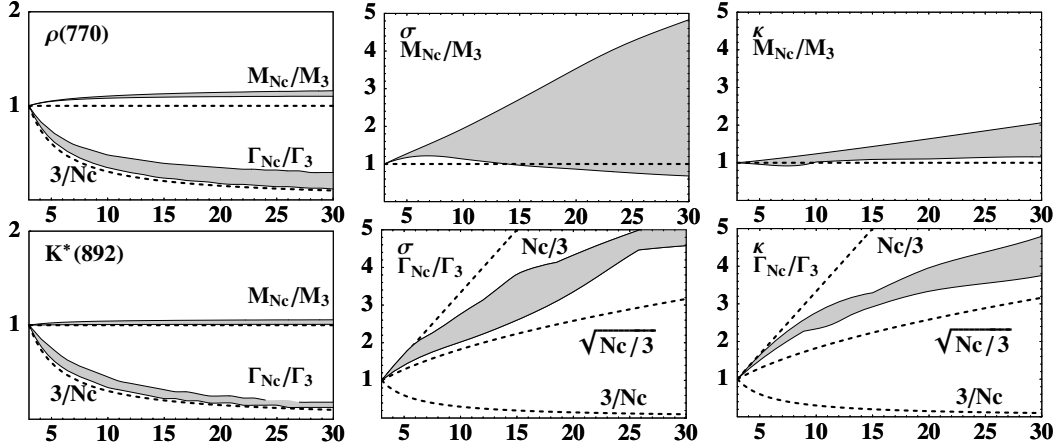

Figure 6: The trajectories of large N_C scaling (dashed line) for the ρ, K^*, σ and κ pole positions ($M_{N_C} - i\Gamma_{N_C}/2$). The gray areas represent the uncertainties induced by the renormalization scale $\mu \simeq 0.5 - 1$ GeV. The figure is taken from Ref. [600].

In fact, many theoretical methods are proposed to define or discern the above two concepts more framework-independently. In principle, the generalized Levinson's theorem [532, 533, 535] in Eq. (77) can tell the number of the "preexisting" states. However, in practice, the phase shifts at the infinite energy are not accessible observables. In the 1960s, Weinberg exploited the relations of the elementary particle and the composite particle [521, 221], which are similar to "preexisting" state and "dynamically generated" state, respectively. For an S-wave shallow bound state, the probability of the hadron-hadron molecule component $(1-Z)$ (where Z is the wave function renormalization constant) is related to the S-wave scattering length a_s and effective range r_e [221],

$$a_s = \frac{2}{\kappa}\frac{1-Z}{2-Z}, \qquad r_e = -\frac{1}{\kappa}\frac{Z}{1-Z}, \qquad (117)$$

where κ is the binding momentum. The above relations provide a criterion of compositeness from the low-energy scattering observables. This relation was used to identify the deuteron as a molecule composed of two nucleons instead an elementary state [221]. Later, this relation has been generalized to describe the unstable resonances in many theoretical works [601, 568, 602, 603, 604, 605, 606, 607, 608]. It should be noticed that the Weinberg compositeness criterion, even the version for the bound states, has its validity range. By construction, one can always get a pure two-body bound state with any given small binding energy with any given phase shifts [539], which means any Z from Weinberg's criterion. The conditions to ensure and validate the Weinberg's criterion include: $\kappa \ll \Lambda$ (where Λ is m_π for the NN system), the non-pole term in the Low equation can be neglected, the form factor $\langle p|V|B \rangle$ is a constant, and so on. In Ref. [609], Li et al investigated the effect of the non-constant form factor. At the same time, the authors demonstrated that the low energy observables (phase shifts) in Weinberg's criterion cannot reveal the short-range structure information of a state. It was pointed that the Weinberg "compositeness" is a measure for the probability to find the constituents separated by a distance greater than the interaction range [610, 611]. In Ref. [612], Song et al also considered the role of the interaction range (the cutoff of the interaction) in the Weinberg's criterion.

2.6. Superfield representations combining the chiral and heavy quark symmetries

For the heavy-light systems, their dynamics are constrained by HQS and chiral symmetry, thus the combination of these two symmetries is necessary. At higher order, the corrections come from two sides: the $1/m_Q$ correction and the chiral expansion. Thus, the HHχPT has a double expansion in $\Lambda_{\rm QCD}/m_Q$ and p/Λ_χ. The Λ_χ and m_Q are identified as the high-energy scale, while the $\Lambda_{\rm QCD}$ and the $p_{\pi,K,\eta} \sim m_{\pi,K,\eta}$ are identified as the low-energy scale. In literature, the two expansions were often combined (treating $\Lambda_{\rm QCD}/m_Q$ as the same order as p/Λ_χ). In this review, we will discuss these corrections separately.

In Sec. 2.2.1, we have discussed the HQSS, which is manifested in heavy hadron spectrum. In the heavy quark limit, these degenerate states are collected in the superfield representation owing to the development of χPT and HQET in 1990s [613, 614, 615, 470, 616]. In the superfield representations, the Lagrangians can be written with a compact form. The LO terms satisfy the HQS and chiral symmetry, while the explicit breaking terms from finite light quark masses and heavy quark masses can be systematically included order by order.

In the following, we outline some basic properties of the superfields. For a heavy-light system, if one assumes the heavy d.o.f is ultra nonrelativistic and decouples from the light d.o.f, the field of this system can be expressed with the product of the heavy and light ones, i.e., $\psi_{hl} \sim \psi_h \psi_l$ [474]. Accordingly, we take the S-wave heavy-light hadrons as an example,

$$\text{heavy mesons: } \mathcal{H} \quad \sim \quad u_h \bar{v}_l, \tag{118}$$

$$\text{singly heavy baryons: } \psi_Q^\mu \quad \sim \quad u_h A_l^\mu, \tag{119}$$

$$\text{doubly heavy baryons: } \psi_{QQ}^\mu \quad \sim \quad u_l A_h^\mu, \tag{120}$$

where u_h and v_l (h and l for heavy and light d.o.f respectively) denote the quark and antiquark. $A_{h/l}^\mu$ represents the vector diquark. The $\mathcal{H}$, ψ_Q^μ and ψ_{QQ}^μ transform as the antitriplet, sextet and triplet under the SU(3)$_L\otimes$SU(3)$_R$ rotations. Meanwhile, they are the linear combinations of the degenerate states in the heavy (di)quark symmetry. Here, we aim to explain the superfield technique to satisfy the heavy (di)quark spin symmetry. However, for the scalar diquarks, there are no heavy (di)quark spin doublets. There is no need to construct the superfields. For the rules to construct the Lagrangians keeping or breaking heavy (di)quark symmetry, see the details in Appendix A and Ref. [615].

In the following, we present the matrix representations of the heavy hadrons as the flavor SU(3) multiplet, and define the superfields of degenerate states under the HQSS. We give the low order Lagrangians to illustrate how to combine the two symmetries for different classes. One can find the definition of building blocks and some technical details in Appendix A.

2.6.1. S-wave heavy mesons

For the ground-state heavy mesons $Q\bar{q}$, $S_Q = \frac{1}{2}$, $j_\ell = \frac{1}{2}$, $J = 0$ and $J = 1$ correspond to the pseudoscalar P and vector meson P^*, respectively. In flavor space, the doublet P with $J^P = 0^-$ and P^* with $J^P = 1^-$ are

$$P = (D^0, D^+, D_s^+) \text{ or } (B^-, \bar{B}^0, \bar{B}_s^0), \qquad P^* = (D^{*0}, D^{*+}, D_s^{*+}) \text{ or } (B^{*-}, \bar{B}^{*0}, \bar{B}_s^{*0}), \tag{121}$$

where the corresponding antiparticle's doublet is denoted as $\tilde{P}$ and $\tilde{P}^*$ (column vector in flavor space), respectively. The degenerate P and P^* ($\tilde{P}$ and $\tilde{P}^*$) are combined into the superfield $\mathcal{H}$ ($\tilde{\mathcal{H}}$) with the form

$$\mathcal{H} = \Lambda_+(P_\mu^* \gamma^\mu + iP\gamma_5), \qquad \tilde{\mathcal{H}} = (\tilde{P}_\mu^* \gamma^\mu + i\tilde{P}\gamma_5)\Lambda_-, \tag{122}$$

where $\Lambda_\pm = (1 \pm \slashed{v})/2$, $v^2 = 1$. The conjugation of $\mathcal{H}$ and $\tilde{\mathcal{H}}$ is defined as $\bar{\mathcal{H}} = \gamma_0 \mathcal{H}^\dagger \gamma_0$ and $\bar{\tilde{\mathcal{H}}} = \gamma_0 \tilde{\mathcal{H}}^\dagger \gamma_0$. The properties of the $\mathcal{H}$ field under the Lorentz, chiral and heavy quark spin transformations can be found in Ref. [478].

With the superfields, the low order Lagrangians read [616, 478]

$$\mathcal{L}_{\mathcal{H}\varphi} = -i\langle \mathcal{H}v \cdot \mathcal{D}\bar{\mathcal{H}}\rangle + g_b\langle \mathcal{H}\slashed{u}\gamma_5\bar{\mathcal{H}}\rangle - \frac{\delta_b}{8}\langle \mathcal{H}\sigma^{\mu\nu}\bar{\mathcal{H}}\sigma_{\mu\nu}\rangle, \tag{123}$$

$$\mathcal{L}_{\tilde{\mathcal{H}}\varphi} = -i\langle \bar{\tilde{\mathcal{H}}}v \cdot \mathcal{D}\tilde{\mathcal{H}}\rangle + g_b\langle \bar{\tilde{\mathcal{H}}}\slashed{u}\gamma_5\tilde{\mathcal{H}}\rangle - \frac{\delta_b}{8}\langle \bar{\tilde{\mathcal{H}}}\sigma^{\mu\nu}\tilde{\mathcal{H}}\sigma_{\mu\nu}\rangle, \tag{124}$$

where $\langle \ldots \rangle$ denotes the trace in spinor space, i.e., for the gamma matrix. If we consider the heavy quark flavor symmetry, the g_b is the same for the charmed and bottom sector. For the mesons, the chiral covariant derivative is defined as $\mathcal{D}_\mu = \partial_\mu + \Gamma_\mu$, and the complete form of chiral connection Γ_μ with the external fields is given in Eq. (A.3). g_b is the axial coupling constant, which can be determined from the decay width of $D^{*+} \to D^0 \pi^+$ [1] for the charmed ones ($|g_b| \simeq 0.59$), or the lattice QCD calculations for the bottom ones [617]. The δ_b terms originate from the chromomagnetic interaction, e.g., see Eq. (60), which contribute to the mass splittings between P and P^*,

$$\delta_b = m_{P^*} - m_P. \tag{125}$$

For the general higher order chiral Lagrangians of the heavy mesons, we refer to Ref. [618].

2.6.2. P-wave heavy mesons

For the P-wave excited heavy mesons, combining the light spin $j_\ell = \frac{1}{2}, \frac{3}{2}$ with the $S_Q = \frac{1}{2}$ yields two spin doublets $(0^+, 1^+)$ and $(1^+, 2^+)$. These two doublets are described by the superfields $\mathcal{S}$ and $\mathcal{T}^\mu$ [615], respectively,

$$\mathcal{S} = \Lambda_+ \left[R^{*\mu} \gamma_\mu \gamma_5 - R \right], \tag{126}$$

$$\mathcal{T}^\mu = \Lambda_+ \left\{ Y^{*\mu\nu} \gamma_\nu - \sqrt{\frac{3}{2}} Y_\nu \gamma_5 \left[g^{\mu\nu} - \frac{1}{3} (\gamma^\mu - v^\mu) \gamma^\nu \right] \right\}. \tag{127}$$

The corresponding low order chiral Lagrangians are given by [619, 620]

$$\mathcal{L}_{\mathcal{S}\varphi} = \langle \mathcal{S} (iv \cdot \mathcal{D} - \delta_{\mathcal{S}}) \bar{\mathcal{S}} \rangle + g_b' \langle \mathcal{S} \slashed{u} \gamma_5 \bar{\mathcal{S}} \rangle + \frac{\delta_b'}{8} \langle \mathcal{S} \sigma^{\mu\nu} \bar{\mathcal{S}} \sigma_{\mu\nu} \rangle, \tag{128}$$

$$\mathcal{L}_{\mathcal{T}\varphi} = \langle \mathcal{T}^\mu (iv \cdot \mathcal{D} - \delta_{\mathcal{T}}) \bar{\mathcal{T}}_\mu \rangle + g_b'' \langle \mathcal{T}^\nu \slashed{u} \gamma_5 \bar{\mathcal{T}}_\nu \rangle + \frac{3\delta_b''}{16} \langle \mathcal{T}^\rho \sigma^{\mu\nu} \bar{\mathcal{T}}_\rho \sigma_{\mu\nu} \rangle, \tag{129}$$

$$\mathcal{L}_{\mathcal{S}\mathcal{H}\varphi} = h \langle \mathcal{H} \slashed{u} \gamma_5 \bar{\mathcal{S}} \rangle + \text{H.c.}, \tag{130}$$

$$\mathcal{L}_{\mathcal{T}\mathcal{H}\varphi} = k_1 \langle \mathcal{T}^\mu \gamma_\lambda \gamma_5 (\mathcal{D}_\mu u^\lambda) \bar{\mathcal{H}} \rangle + k_2 \langle \mathcal{T}^\mu \gamma_\lambda \gamma_5 (\mathcal{D}^\lambda u_\mu) \bar{\mathcal{H}} \rangle + \text{H.c.}, \tag{131}$$

$$\mathcal{L}_{\mathcal{S}\mathcal{T}\varphi} = \tilde{h} \langle \mathcal{T}^\mu u_\mu \gamma_5 \bar{\mathcal{S}} \rangle + \text{H.c.}, \tag{132}$$

where $\delta_{\mathcal{S}}$ and $\delta_{\mathcal{T}}$ contribute to the mass difference with respect to the ground states,

$$\delta_{\mathcal{S}/\mathcal{T}} = \bar{m}_{\mathcal{S}/\mathcal{T}} - \bar{m}_{\mathcal{H}}, \quad \bar{m}_{\mathcal{H}/\mathcal{S}} \equiv \frac{3m_{P^*/R^*} + m_{P/R}}{4}, \quad \bar{m}_{\mathcal{T}} \equiv \frac{5m_{Y^*} + 3m_Y}{8}. \tag{133}$$

The δ_b' and δ_b'' terms produce the mass splittings in the doublets $\mathcal{S}$ and $\mathcal{T}$, respectively,

$$\delta_b' = m_{R^*} - m_R, \quad \delta_b'' = m_{Y^*} - m_Y. \tag{134}$$

2.6.3. Singly heavy baryons

The two light quarks qq in the ground-state singly heavy baryons can form $\mathbf{3} \otimes \mathbf{3} = \bar{\mathbf{3}} \oplus \mathbf{6}$ representations in SU(3) flavor space. The antitriplet have $j_\ell = 0$, while the sextet have $j_\ell = 1$. Therefore, the spin of the antitriplet baryon is $\frac{1}{2}$, while the spins of the sextet are $\frac{1}{2}$ and $\frac{3}{2}$, respectively. In the SU(3) flavor space, the conventional representations of the singly heavy baryons are [621]

$$B_{\bar{3}} = \begin{bmatrix} 0 & \Lambda_c^+ & \Xi_c^+ \\ -\Lambda_c^+ & 0 & \Xi_c^0 \\ -\Xi_c^+ & -\Xi_c^0 & 0 \end{bmatrix}, \quad B_6 = \begin{bmatrix} \Sigma_c^{++} & \frac{\Sigma_c^+}{\sqrt{2}} & \frac{\Xi_c'^+}{\sqrt{2}} \\ \frac{\Sigma_c^+}{\sqrt{2}} & \Sigma_c^0 & \frac{\Xi_c'^0}{\sqrt{2}} \\ \frac{\Xi_c'^+}{\sqrt{2}} & \frac{\Xi_c'^0}{\sqrt{2}} & \Omega_c^0 \end{bmatrix}, \quad B_6^* = \begin{bmatrix} \Sigma_c^{*++} & \frac{\Sigma_c^{*+}}{\sqrt{2}} & \frac{\Xi_c^{*+}}{\sqrt{2}} \\ \frac{\Sigma_c^{*+}}{\sqrt{2}} & \Sigma_c^{*0} & \frac{\Xi_c^{*0}}{\sqrt{2}} \\ \frac{\Xi_c^{*+}}{\sqrt{2}} & \frac{\Xi_c^{*0}}{\sqrt{2}} & \Omega_c^{*0} \end{bmatrix}, \tag{135}$$

where we use the $B_{\bar{3}}$, B_6 and B_6^* to denote the spin-$\frac{1}{2}$ antitriplet, spin-$\frac{1}{2}$ and spin-$\frac{3}{2}$ sextet, respectively.

Without the HQS, the low order Lagrangians are constructed as [621]

$$\mathcal{L}_{B_Q\varphi} = \text{Tr}\left[\bar{B}_6 (i\slashed{D} - m_6) B_6 \right] + \frac{1}{2} \text{Tr}\left[\bar{B}_{\bar{3}} (i\slashed{D} - m_{\bar{3}}) B_{\bar{3}} \right]$$

33

$$+\text{Tr}\left\{\bar{B}_6^{*\mu}\left[-g_{\mu\nu}(i\mathcal{D}-m_6^*)i(\gamma_\mu\mathcal{D}_\nu+\gamma_\nu\mathcal{D}_\mu)-\gamma_\mu(i\mathcal{D}+m_6^*)\gamma_\nu\right]B_6^{*\nu}\right\}$$
$$+g_1\text{Tr}\left[\bar{B}_6\slashed{u}\gamma_5 B_6\right]+g_2\text{Tr}\left[\bar{B}_6\slashed{u}\gamma_5 B_{\bar{3}}\right]+\text{H.c.}+g_3\text{Tr}\left[\bar{B}_6^{*\mu}u_\mu B_6\right]+\text{H.c.}$$
$$+g_4\text{Tr}\left[\bar{B}_6^{*\mu}u_\mu B_{\bar{3}}\right]+\text{H.c.}+g_5\text{Tr}\left[\bar{B}_6^{*\nu}\slashed{u}\gamma_5 B_{6\nu}^*\right]+g_6\text{Tr}\left[\bar{B}_{\bar{3}}\slashed{u}\gamma_5 B_{\bar{3}}\right], \tag{136}$$

where the chiral covariant derivative is

$$\mathcal{D}_\mu B=\partial_\mu B+\Gamma_\mu B+B\Gamma_\mu^T. \tag{137}$$

The Lagrangian (136) is reduced to a compact form with the superfield representation, where the B_6 and B_6^* are described by the superfield ψ_Q^μ via

$$\psi_Q^\mu=\mathcal{B}_6^{*\mu}+\sqrt{\frac{1}{3}}(\gamma^\mu+v^\mu)\gamma^5\mathcal{B}_6,\text{ and its conjugate }\bar{\psi}_Q^\mu=\bar{\mathcal{B}}_6^{*\mu}-\sqrt{\frac{1}{3}}\bar{\mathcal{B}}_6\gamma^5(\gamma^\mu+v^\mu), \tag{138}$$

with $\mathcal{B}_6\,(\equiv\Lambda_+ B_6)$ and $\mathcal{B}_6^*\,(\equiv\Lambda_+ B_6^*)$ the nonrelativistic reduced fields of B_6 and B_6^*, respectively, see Appendix B. Then the Lagrangian (136) is reexpressed as

$$\begin{aligned}\mathcal{L}_{\psi_Q\varphi}&=-\text{Tr}\left[\bar{\psi}_Q^\mu iv\cdot\mathcal{D}\psi_{Q\mu}\right]+ig_a\epsilon_{\mu\nu\rho\sigma}\text{Tr}\left[\bar{\psi}_Q^\mu u^\rho v^\sigma\psi_Q^\nu\right]+i\frac{\delta_a}{2}\text{Tr}\left[\bar{\psi}_Q^\mu\sigma_{\mu\nu}\psi_Q^\nu\right]\\&+\frac{1}{2}\text{Tr}\left[\bar{\mathcal{B}}_{\bar{3}}(iv\cdot\mathcal{D}+\delta_c)\mathcal{B}_{\bar{3}}\right]+g_c\text{Tr}\left(\bar{\psi}_Q^\mu u_\mu\mathcal{B}_{\bar{3}}+\text{H.c.}\right),\end{aligned} \tag{139}$$

where g_a and g_c are two independent axial couplings, and the δ_a term is proportional to the mass splitting between the spin-$\frac{3}{2}$ sextet and spin-$\frac{1}{2}$ sextet. The δ_c contributes to the mass splitting between the flavor antitriplet and sextet. Unfolding Eq. (139) one obtains the following relations

$$g_1=-\frac{2}{3}g_a,\quad g_3=-\frac{1}{\sqrt{3}}g_a,\quad g_5=g_a;\quad g_2=-\frac{1}{\sqrt{3}}g_c,\quad g_4=g_c,\quad g_6=0, \tag{140}$$

in which the g_2 and g_4 can be extracted from the partial decay widths of $\Sigma_c\to\Lambda_c\pi$ and $\Sigma_c^*\to\Lambda_c\pi$, respectively. $g_6=0$ is due to the fact that the interactions between the pseduscalar meson and the spin-0 diquark are forbidden because of the conservation of the parity and angular momentum. Meanwhile, the couplings g_1, g_3 and g_5 are determined with the quark model [622, 623, 624],

$$\begin{aligned}g_2&=-0.60,&g_4&=-\sqrt{3}g_2=1.04;\\g_1&=-\sqrt{\tfrac{8}{3}}g_2=0.98,&g_3&=\tfrac{\sqrt{3}}{2}g_1=0.85,&g_5&=-\tfrac{3}{2}g_1=-1.47.\end{aligned} \tag{141}$$

It should be noticed that, for the SU(2) case, there are two conventional representations for the isospin triplet Σ_c,

$$\Sigma_c^{\text{I}}=\left[\begin{array}{cc}\Sigma_c^{++}&\frac{\Sigma_c^+}{\sqrt{2}}\\\frac{\Sigma_c^+}{\sqrt{2}}&\Sigma_c^0\end{array}\right],\quad\Sigma_c^{\text{II}}=\boldsymbol{\Sigma}_c\cdot\boldsymbol{\tau}=\sqrt{2}\left[\begin{array}{cc}\frac{\Sigma_c^+}{\sqrt{2}}&\Sigma_c^{++}\\\Sigma_c^0&-\frac{\Sigma_c^+}{\sqrt{2}}\end{array}\right]. \tag{142}$$

The different representations will not change the physical results so long as they are used consistently. The first one is the direct reduction of B_6 and the covariant derivative is similar to Eq. (137) but transformed into the SU(2) case. The second representation is like the Σ in the nucleon octet. The corresponding covariant derivative in the Lagrangian becomes $\mathcal{D}_\mu\Sigma_c^{\text{II}}=\partial_\mu+[\Gamma_\mu,\Sigma_c^{\text{II}}]$. The isospin triplet with specific $I_3=(+1,0,-1)$ is also different in the two representations, e.g., $(\Sigma_c^{++},\Sigma_c^+,\Sigma_c^0)^{\text{I}},(-\Sigma_c^{++},\Sigma_c^+,\Sigma_c^0)^{\text{II}}$.

2.6.4. Doubly heavy baryons

For the ground-state doubly heavy baryons QQq, $j_\ell=\frac{1}{2}$, and $S_{QQ}=1$, there exist two multiplets, the B_{QQ} with spin-$\frac{1}{2}$ and the B_{QQ}^* with spin-$\frac{3}{2}$,

$$B_{QQ}=\left[\begin{array}{c}\Xi_{cc}^{++}\\\Xi_{cc}^+\\\Omega_{cc}^+\end{array}\right],\qquad B_{QQ}^*=\left[\begin{array}{c}\Xi_{cc}^{*++}\\\Xi_{cc}^{*+}\\\Omega_{cc}^{*+}\end{array}\right]. \tag{143}$$

The low order Lagrangians after heavy baryon reduction reads (see Ref. [625] for higher order Lagrangians)

$$
\begin{aligned}
\mathcal{L}_{\mathcal{B}_{QQ}\varphi} &= \bar{\mathcal{B}}_{QQ} iv \cdot \mathcal{D} \mathcal{B}_{QQ} - \bar{\mathcal{B}}_{QQ}^{*\mu} (iv \cdot \mathcal{D} - \delta_4) \mathcal{B}_{QQ\mu}^* + 2\tilde{g}_1 \bar{\mathcal{B}}_{QQ} (S \cdot u) \mathcal{B}_{QQ} \\
&\quad + 2\tilde{g}_2 \bar{\mathcal{B}}_{QQ}^{*\mu} (u \cdot S) \mathcal{B}_{QQ\mu}^* + \tilde{g}_3 (\bar{\mathcal{B}}_{QQ}^{*\mu} u_\mu \mathcal{B}_{QQ} + \bar{\mathcal{B}}_{QQ} u_\mu \mathcal{B}_{QQ}^{*\mu}),
\end{aligned}
\tag{144}
$$

where the covariant derivative is the same as that in Eqs. (123) and (124), $\mathcal{D}_\mu = \partial_\mu + \Gamma_\mu$. The mass splitting δ_4 is given as $\delta_4 = m_{B_{QQ}^*} - m_{B_{QQ}}$. $S^\mu = \frac{i}{2} \gamma_5 \sigma^{\mu\nu} v_\nu$ is the covariant spin operator.

If one assumes the heavy diquark as a compact and heavy object, one can adopt the HDAS to treat the (B_{QQ}, B_{QQ}^*) pair as a spin doublet. They can be uniformly depicted by the superfield

$$
\psi_{QQ}^\mu = \mathcal{B}_{QQ}^{*\mu} + \sqrt{\frac{1}{3}} (\gamma^\mu + v^\mu) \gamma^5 \mathcal{B}_{QQ}, \text{ and its conjugate } \bar{\psi}_{QQ}^\mu = \bar{\mathcal{B}}_{QQ}^{*\mu} - \sqrt{\frac{1}{3}} \bar{\mathcal{B}}_{QQ} \gamma^5 (\gamma^\mu + v^\mu).
\tag{145}
$$

The Lagrangian (144) is expressed with the ψ_{QQ}^μ as

$$
\mathcal{L}_{\psi_{QQ}\varphi} = -\bar{\psi}^\mu iv \cdot \mathcal{D} \psi_\mu + \tilde{g}_b \bar{\psi}^\mu \slashed{u} \gamma_5 \psi_\mu + \frac{i\tilde{\delta}_b}{4} \bar{\psi}^\mu \sigma_{\mu\nu} \psi^\nu,
\tag{146}
$$

where there exists only one coupling $\tilde{g}_b$ within the HDAS, and the $\tilde{\delta}_b$ term breaks the heavy diquark symmetry and contributes to the mass splitting of spin-$\frac{1}{2}$ and spin-$\frac{3}{2}$ multiplets. The couplings $\tilde{g}_i$ ($i = 1, 2, 3$) and mass splitting δ_4 in Eq. (144) can be related to $\tilde{g}_b$ and $\tilde{\delta}_b$ via

$$
\tilde{g}_1 = \frac{1}{3} \tilde{g}_b, \qquad \tilde{g}_2 = \tilde{g}_b, \qquad \tilde{g}_3 = 2\sqrt{\frac{1}{3}} \tilde{g}_b, \qquad \delta_4 = \frac{3}{4} \tilde{\delta}_b.
\tag{147}
$$

As discussed in Sec. 2.2.2, the Lagrangians of the doubly heavy baryons can be related to those of the singly heavy mesons with the HDAS. In the superfield formalism, we have $\psi_{QQ}^\mu \sim u_l A_h^\mu$ and $\tilde{\mathcal{H}} \sim u_l \bar{v}_h$. For the Lagrangians with the heavy d.o.f as the spectator, we have

$$
\begin{aligned}
\mathcal{L}_{\tilde{\mathcal{H}}} &= \xi (\bar{u}_l \Gamma u_l) \left(A_h^{*\mu} A_{h\mu} \right) = \xi \bar{\psi}^\mu \Gamma \psi_\mu, \\
\mathcal{L}_{\psi_{QQ}} &= \xi (\bar{u}_l \Gamma u_l) (\bar{v}_h v_h) = \xi \bar{\tilde{\mathcal{H}}} \Gamma \tilde{\mathcal{H}},
\end{aligned}
\tag{148}
$$

where the Lagrangians for the singly heavy meson and doubly heavy baryons share the same coupling constant ξ in HDAS once the heavy parts are normalized properly. Therefore, comparing Eqs. (124) and (146), one can obtain the relation [506],

$$
\tilde{g}_b = g_b.
\tag{149}
$$

Moreover, assuming only the chromomagnetic interaction [the third term in Eq. (60)] breaks the heavy (di)quark symmetry, the δ_b and $\tilde{\delta}_b$ terms in Eqs.(124) and (146) can be related to each other as well [199],

$$
\delta_b = \tilde{\delta}_b.
\tag{150}
$$

2.7. KSW and Weinberg schemes for two matter field systems

For the system with one matter field, one can perform the perturbative expansion with the guideline of the Weinberg's power counting and heavy hadron expansion. However, when one adopts the same scheme in the two matter field system, one has to overcome two obstacles at least.

We use the two nucleon system to illustrate the first obstacle—the pinched singularity [509]. For the box diagram as shown in Fig. 7(a), if we take the leading order of the heavy baryon expansion, the amplitude reads

$$
\mathcal{A} \sim \int dl^0 \frac{1}{v \cdot l + i\varepsilon} \frac{1}{-v \cdot l + i\varepsilon},
\tag{151}
$$

35

where only the two propagators of the intermediate nucleons are presented. The contour of the integration is pinched by the two poles, $l_0 = \pm i\varepsilon$. It is impossible to avoid the singularities by distorting the contour. In order to eliminate the pinched singularity, one has to keep the kinetic terms in the Lagrangian: $\mathcal{L} = \bar{\mathcal{N}}(i\partial_0 + \frac{\partial^2}{2M})\mathcal{N}$. The amplitude becomes

$$\mathcal{A} \sim \int dl^0 \frac{1}{v \cdot l + \frac{p_1'^2}{2M} + i\varepsilon} \frac{1}{-v \cdot l + \frac{p_2'^2}{2M} + i\varepsilon} \sim \frac{1}{\frac{p_2'^2}{2M} + \frac{p_1'^2}{2M}} \sim \frac{1}{|\boldsymbol{p}|}\frac{M}{|\boldsymbol{p}|}. \tag{152}$$

Although the pinched singularity is cured by including the kinetic energy of the nucleon in the leading terms, the amplitude is enhanced by a large factor $M/|\boldsymbol{p}|$. This strong enhancement explicitly breaks the naive power counting with which the l_0 integral should be of $O(1/|\boldsymbol{p}|)$. It is worthwhile to notice that the pinched singularity will appear not only in the box diagrams but also in the triangle diagrams [Fig. 7(b), (c)] and bubble diagram [Fig. 7(d)] in the two nucleon scattering.
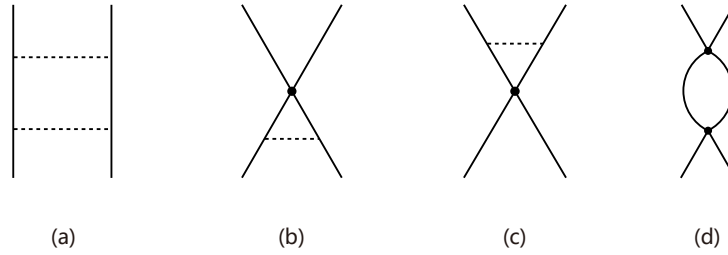

Figure 7: Three types of Feynmann diagrams that contain the pinched singularities for the *NN* scattering at the leading order of the heavy baryon expansion. The (a), (b)/(c) and (d) represent the box, triangle and bubble diagrams, respectively. The solid and dashed lines denote the nucleon and pion, respectively.

The pinched singularity is a typical feature of the nonrelativistic two-body systems. An analog is the heavy quarkonium in the NRQCD [626, 627]. One can first separate the nonrelativistic kinetic energy q^0 and momentum $\boldsymbol{q}$ from the mass in the relativistic momentum $p^\mu = (m_Q, \boldsymbol{0}) + (q^0, \boldsymbol{q})$. For the system with two heavy quarks, a different power counting is adopted in NRQCD . In the NRQCD, q^0 and $\boldsymbol{q}^2/m_Q$ is counted as the same order, while in the HQET the q^0 and $\boldsymbol{q}$ are regarded as the same order. In the NRQCD, the calculation is organized in power of the velocity $v \equiv |\boldsymbol{q}|/m_Q$ [8]. In the nonrelativistic theory, the kinetic energy is at the order of $m_Q v^2$ and the three momentum is at the order of $m_Q v$. One can see that keeping the kinetic term in Eq. (152) essentially takes the similar power counting with NRQCD.
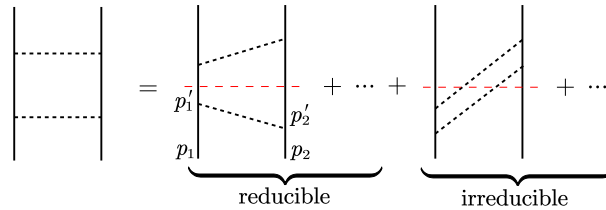
Figure 8: Box diagrams in the time-ordered perturbation theory.

The unnaturalness is the second obstacle preventing the two matter field systems from suiting Weinberg's power counting. The Weinberg's power counting is based on the NDA. An important prerequisite of its validity is the naturalness, which implies all the dimensionless parameters of the expansion is at order of unity. The dimensionless parameter is obtained by factoring out Λ^n, where Λ is the breaking scale of the effective field theory. The opposite of the naturalness is the unnaturalness or the fine tuning. A typical example of the fine tuning is the nuclear force. At

---

[8]One should not confuse the velocity here with that in HQET and heavy field expansion.

the scale $p \ll m_\pi$, one can integrate out the pion by treating it as a hard scale. It is expected that the pionless effective field theory (πEFT) is valid, which is equivalent to the ERE [628]. For example, the ERE for the S-wave NN system is

$$p \cot \delta = -\frac{1}{a_s} + \frac{1}{2} r_0 p^2 + \dots, \tag{153}$$

where δ is the phase shift and p is the magnitude of three momentum. a_s and r_0 are the scattering length and effective range, respectively. In the expansion, the large scale is the pion mass m_π. By assuming naturalness, the scattering length a_s should be of order $1/m_\pi \approx 1.4$ fm. However, the experimental neutron-proton scattering lengths for the $^1S_0$ and $^3S_1$ channels are

$$a_{^1S_0} \simeq -23.76 \text{ fm}, \qquad a_{^3S_1} \simeq 5.42 \text{ fm}. \tag{154}$$

Thus, the loss of the naturalness indicates the failure of Weinberg's power counting for the NN systems.

The unnaturalness of the NN interaction can be attributed to the appearance of the bound state or virtual state, like the deuteron as the $^3S_1$ bound state. The bound state, virtual state and the resonance are all nonperturbative phenomena, which indicate the failure of the perturbative framework conducted by Weinberg's power counting. One has to face the same obstacle of unnaturalness in the heavy hadron systems. The main motivation of investigating the two matter filed system in the heavy flavor sector is to decode the nature of the exotic hadrons in experiments. In the molecular scheme, the exotic hadrons are interpreted as the bound state, virtual state or resonance of two heavy hadrons. Therefore, the same unnaturalness will appear. For the NN systems, there are two types of frameworks to perform the effective field theory properly, the Kaplan-Savage-Wise (KSW) scheme [522, 629] and the Weinberg scheme [630, 509] [9]. They were widely used for the heavy hadron systems as well.

2.7.1. KSW scheme

Kaplan, Savage and Wise proposed an elegant approach to reformulating the power counting of the NN systems considering the unnatural large scattering length [522, 629]. The scheme starts from the scale less than the pion mass in the $^1S_0$ channel. Then the tree level amplitude from the contact interaction reads

$$i\mathcal{A}_{\text{tree}} = -i(\mu/2)^{4-d} \sum_{n=0}^{\infty} C_{2n}(\mu) p^{2n} = -i(\mu/2)^{4-d} C(p^2, \mu), \tag{155}$$

where p is the nucleon momentum in the center of mass frame. M and μ are the nucleon mass and subtraction scale. d is the dimension of space-time. C_{2n} are the LECs and C is the polynomial of C_{2n}. In the Table 2, we present the dimension of the corresponding LECs. For such a nonrelativistic system, the double expansions in power of $1/M$ and p/Λ are performed. In Eqs. (152), every loop will contribute a factor M. In order to ensure the diagrams with arbitrary loops have the same counting of $1/M$ as the tree-level diagrams, we count C_{2n} as order of $1/M$. With the common factor of $1/M$, we can focus on the p/Λ expansion. For example, the dimension of C_0 is -2. Thus, one expects $C_0 \sim 1/(M\Lambda)$ from NDA. With the vertices, the amplitude of the one-loop bubble diagram reads

$$
\begin{aligned}
I_n &= -i(\mu/2)^{4-d} \int \frac{d^d q}{(2\pi)^d} \boldsymbol{q}^{2n} \frac{i}{(E/2 - q^0 - \boldsymbol{q}^2/2M + i\varepsilon)} \frac{i}{(E/2 + q^0 - \boldsymbol{q}^2/2M + i\varepsilon)} \\
&= -M(ME)^n (-ME - i\varepsilon)^{\frac{d-3}{2}} \Gamma\left(\frac{3-d}{2}\right) \frac{(\mu/2)^{4-d}}{(4\pi)^{(d-1)/2}}.
\end{aligned}
\tag{156}
$$

In the calculation, the kinetic energy terms are kept to eliminate the pinched singularity. In the conventional dimensional regularization, the pole at $d = 4$ is subtracted to track the logarithmic ultraviolet divergence $\ln \mu$. However, if one calculates the above integration in a hard cutoff regularization, one can find the linear ultraviolet divergence μ. To track the power ultraviolet divergence, an extra subtraction at $d = 3$ was made by the counter term

$$\delta I_n = -\frac{M(ME)^n \mu}{4\pi(d-3)}. \tag{157}$$

---

[9]One should not confuse with the Weinberg scheme in calculating the nuclear force with the Weinberg's power counting.

Table 2: Power counting and dimensions of the contact terms in Eq. (155) for both natural and unnatural cases.

	C_0	C_2	C_4		C_{2n}	$C_{2n}p^{2n}$
Dimension	-2	-4	-6	$\cdots$	$-2(n+1)$	-2
Natural	$\frac{1}{M}\frac{1}{\Lambda^1}$	$\frac{1}{M}\frac{1}{\Lambda^3}$	$\frac{1}{M}\frac{1}{\Lambda^5}$	$\cdots$	$\frac{1}{M}\frac{1}{\Lambda^{2n+1}}$	$\frac{1}{M}\frac{p^{2n}}{\Lambda^{2n+1}}$
Unnatural	$\frac{1}{M}\frac{1}{p}$	$\frac{1}{M}\frac{1}{p^2\Lambda^1}$	$\frac{1}{M}\frac{1}{p^3\Lambda^2}$	$\cdots$	$\frac{1}{M}\frac{1}{p^{n+1}\Lambda^n}$	$\frac{1}{M}\frac{p^{n-1}}{\Lambda^n}$

The above procedure was called the power divergence substation (PDS) scheme. The regularized amplitude becomes

$$I_n^{\text{PDS}} = I_n + \delta I_n = -(ME)^n \left(\frac{M}{4\pi}\right)(\mu + ip). \tag{158}$$

The amplitude considering bubble diagrams nonperturbatively then becomes

$$i\mathcal{A} = \frac{-iC(p^2,\mu)}{1 + MC(p^2,\mu)(\mu + ip)/4\pi}. \tag{159}$$

In order to investigate the effect of the unnatural scattering length, one can match the above amplitude to the effective range expansion,

$$p\cot\delta = -\frac{4\pi}{MC(p^2,\mu)} - \mu = -\frac{1}{a_s} + \frac{1}{2}r_0 p^2 + \dots. \tag{160}$$

Then the first two LECs read

$$C_0(\mu) = \frac{4\pi}{M}\left(\frac{1}{-\mu + 1/a_s}\right), \qquad C_2(\mu) = \frac{2\pi}{M}\left(\frac{1}{-\mu + 1/a_s}\right)^2 r_0, \dots. \tag{161}$$

Taking $\mu \sim p$, one can obtain the power counting either in the natural or unnatural cases. In the natural case $1/a_s \sim \Lambda$, the powers of C_{2n} satisfy the naive counting in Table 2. In the unnatural case, $a \gg 1/\Lambda$, the power counting is presented in Table 2. The powers of the LECs are increased by the unnaturalness. From Eq. (158), one can see that adding an extra loop (see Fig. 9) will introduce a factor of order Mp from the integration. For the natural case, taking the extra vertex in the loop into consideration, the extra loop will introduce a factor of order p/Λ at most (for the LO vertex, see Fig. 9). Thus, one can perform the calculation perturbatively for the natural case. For the unnatural case, introducing an extra loop with the LO vertex will introduce a factor of order 1. Thus, one has to include the C_0 nonperturbatively. Although the higher order vertices (C_2, C_4,...) were enhanced by the unnaturalness, one can still deal with them perturbatively.
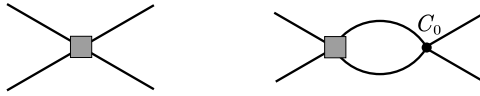

Figure 9: The effect of an extra loop with the LO vertex. In the natural case, the right diagram is suppressed by an extra factor Mp compared with the left one. In the unnatural case, the right one has the same order with the left one.

It is worthwhile to stress that the validity of the above power counting is independent of the specific regularization scheme—PDS. In Refs. [631, 632, 633, 634, 635], the alternative but equivalent regularization schemes were adopted to obtain the same power counting. The key point of choosing the regularization scheme is to track the power divergence. In Ref. [529], the author illustrated the same power counting without specific regularization scheme. In Ref. [636], the equivalent power counting was obtained by performing the Wilsonian renormalization group equation to the Lippmann-Schwinger equation.

The power counting can be extended to $p \sim m_\pi$. In the $^1S_0$ channel, the one-pion exchange (OPE) interaction is

$$V_\pi(\boldsymbol{p}, \boldsymbol{p}') = -\frac{g_A^2}{2f^2}\left(\frac{m_\pi^2}{\boldsymbol{q}^2 + m_\pi^2} - 1\right), \tag{162}$$

where $\boldsymbol{q} = \boldsymbol{p}' - \boldsymbol{p}$. The counting of the OPE interaction is p^0, which is of the same order as the C_2 term, thus can be treated perturbatively.
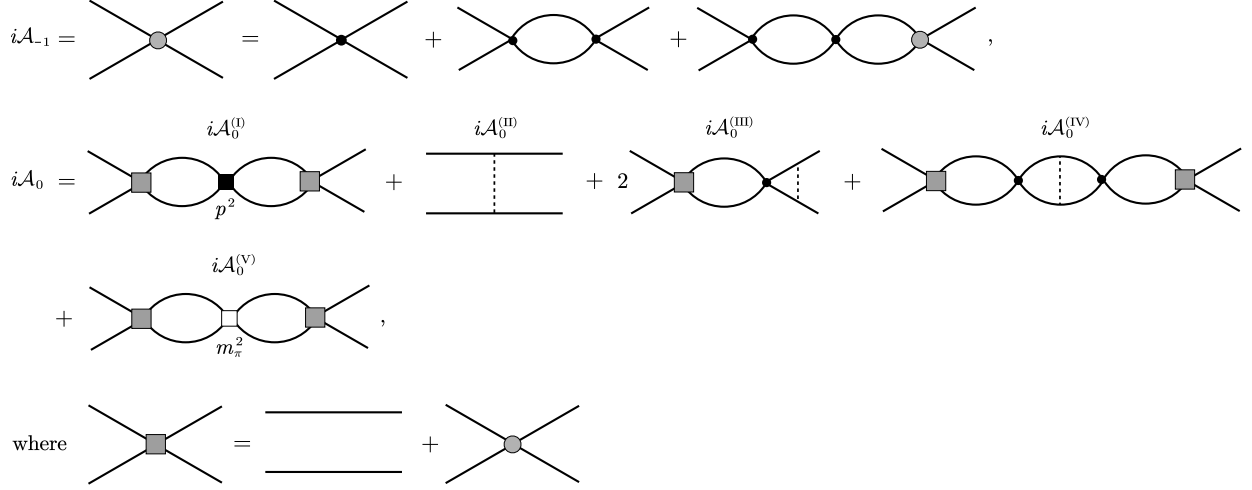

Figure 10: Feynman diagrams for KSW. The LO vertices are represented by the solid dot. The NLO vertices are labeled by solid square and empty square.

The KSW scheme is an elegant framework to treat the unnatural *NN* systems with very clear power counting. In this framework, the renormalization is very transparent. However, the resulting scattering amplitudes didn't converge in certain spin-triplet channels [637, 638] for the nucleon momenta around the pion mass (the subsequent improvements seemed to yield a convergent expansion [639, 640]). It was shown that the breakdown of the KSW expansion arises from the perturbative treatment of the pion exchange contributions [641, 642, 638, 643]. The proper scale where the OPE is perturbative was obtained in Ref. [644].

The KSW type scheme was also applied in the heavy hadronic systems. Using the XEFT to investigate the $X(3872)$ inherits the characters of the KSW scheme—the nonperturbative LO contact interaction and the perturbative OPE and higher contact interactions. We will discuss the relevant EFT in Sec. 5.2 and explain why the perturbative OPE works for the $X(3872)$ although it failed for the NN system.

2.7.2. Weinberg scheme

The state-of-the-art nuclear forces (see Refs. [645, 646, 647, 648] for recent progresses and see Refs. [476, 475, 649, 650] for reviews) are based on the Weinberg's seminal works [630, 509]. Weinberg proposed to adopt the power counting law to calculate the *NN* potentials perturbatively. The *NN* potentials are regarded as the effective potential of the Schrödinger equation or the kernel of the Lippmann-Schwinger equations (LSEs). From the perspective of the time-ordered perturbation theory as shown in Fig. 8, the contribution of the loop diagrams (e.g. box diagrams) is divided into the two-particle-reducible (2PR) part and two-particle-irreducible (2PIR) part. The 2PR part is subtracted in the *NN* potential. The remaining 2PIR part is iterated to all orders by solving the Schrödinger equation or Lippmann-Schwinger equation. The 2PR part is recovered by iterating the tree diagrams automatically.

In the practical calculation, one can obtain the 2PIR contribution by subtracting the contribution of the poles of the nucleons [651, 652] rather than the time-ordered perturbation theory [653]. For the heavy hadron systems, the subtraction becomes more subtle due to the appearance of the mass splitting, see the Appendix of Ref. [364].

Compared with the KSW scheme, the renormalization of Weinberg scheme is less transparent. The amplitudes are nonperturbative expressions obtained by solving the integral equations with ultraviolet (UV) divergences. For example, one usually introduces regulators to the *NN* potential to render the solutions of LSEs or Schrödinger equation finite. Sometimes the Gauss form regulator is used in the calculation

$$V(\boldsymbol{p}, \boldsymbol{p}') \rightarrow V(\boldsymbol{p}, \boldsymbol{p})e^{\frac{-(p^n + p'^n)}{\Lambda^n}}. \tag{163}$$

In such a nonperturbative renormalization, the cutoff independence is implicit. In Refs. [654, 655, 656], several conceptional ambiguities in the renormalization of the nuclear forces in Weinberg scheme were clarified. Though the Weinberg scheme is not as elegant as KSW scheme, it turns out to be convergent and practical in calculating high-precision nuclear forces [476, 475, 649]. In the Weinberg scheme, the OPE interaction is iterated to all orders. In the heavy hadron systems, the Weinberg scheme was also used to identity the hadronic molecules by calculating the mass spectrum (e.g. [355, 364]) and fitting the experimental line shapes [356, 283]. We will discuss this formalism in Sec. 5.

3. Masses, axial charges, strong and electromagnetic decays of heavy hadrons

The HHχPT was developed to investigate the heavy-light hadrons incorporating the chiral symmetry and the heavy quark symmetry consistently. It has successfully described the properties of the heavy-light systems, including the spectra, form factors, decay patterns, etc. In this section, we will review the chiral corrections to the masses, axial currents, magnetic moments, electromagnetic decays and strong decays of the heavy mesons, singly heavy baryons and doubly heavy baryons within the framework of HHχPT. The cross-talk between HHχPT and other frameworks will also be discussed.

3.1. Heavy hadron masses

In this subsection, we briefly introduce the application of the HHχPT in the study of the mass spectroscopy of the heavy mesons and baryons with the help of the experimental data and lattice QCD simulations. In the HHχPT, the propagator of the meson is proportional to

$$\frac{i}{2(v \cdot k - \delta^{\text{tree}}) - \Sigma(v \cdot k)}, \tag{164}$$

where the factor 2 results from the normalization of the heavy meson field (see Appendix B). The heavy meson momentum p is split into the large component with velocity v and small residue momentum k with $p = m_0 v + k$ and m_0 being the bare mass of the reference heavy meson. δ^{tree} denotes the tree-level mass difference of the particle relative m_0. The $-i\Sigma(v \cdot k)$ is the sum of all the one-particle irreducible (1PIR) self-energy contribution. In general, it is complex and the imaginary part is related to the decay width. The on-shell renormalization condition is given by,

$$2(v \cdot \tilde{k} - \delta^{\text{tree}}) - \Sigma(v \cdot \tilde{k}) = 0, \tag{165}$$

The physical mass corresponds the position of the pole of the propagator in Eq. (164) and is given by,

$$m_H^{\text{phy}} = m_0 + v \cdot \tilde{k} = m_0 + \delta^{\text{tree}} + \frac{1}{2}\text{Re}\left[\Sigma(v \cdot \tilde{k})\right], \tag{166}$$

The propagators of the singly and doubly heavy baryons are similar to those of the mesons after the heavy field expansion. Their mass expressions can be written as

$$M = M_0 + \delta^{\text{tree}} + \text{Re}\left[\Sigma(v \cdot \tilde{k})\right], \tag{167}$$

where M_0 is the bare mass of the heavy baryon.

3.1.1. Heavy mesons

As shown in Sec. 1.1, the heavy mesons can be labeled with the light and heavy d.o.f in the heavy quark spin basis. In the heavy quark limit, the mesons with the same j_ℓ^P are degenerate and they can be embedded into the superfields as shown in Eqs. (122), (126) and (127).

Constrained by the heavy quark symmetry and the chiral symmetry, the low order Lagrangians for the heavy mesons $Q\bar{q}$ are given in Eqs. (123), (128)-(132). Among them, we have included the $1/m_Q$ corrections which break the heavy quark symmetry,

$$\mathcal{L}_{1/m_Q} = -\frac{\delta_b}{8}\langle \mathcal{H}\sigma^{\mu\nu}\bar{\mathcal{H}}\sigma_{\mu\nu}\rangle + \frac{\delta_b'}{8}\langle \mathcal{S}\sigma^{\mu\nu}\bar{\mathcal{S}}\sigma_{\mu\nu}\rangle + \frac{3\delta_b''}{16}\langle \mathcal{T}^\rho\sigma^{\mu\nu}\bar{\mathcal{T}}_\rho\sigma_{\mu\nu}\rangle, \tag{168}$$

where the constant $\delta_b/\delta_b'/\delta_b''$ is responsible for the mass splitting, $\delta_b/\delta_b'/\delta_b'' = (M_{P^*/R^*/Y^*} - M_{P/R/Y})$ in the $\mathcal{H}/\mathcal{S}/\mathcal{T}$ multiplets [657], which is suppressed by $1/m_Q$ and vanishes in the heavy quark limit.

At $O(p^2)$ of the chiral expansion, the chiral Lagrangians with the light quark masses read [658, 659, 33, 660, 621, 619, 661, 662, 663, 664, 618]

$$
\begin{aligned}
\mathcal{L}_{\text{chiral}}^{(2)} &= a_H \left\langle \mathcal{H} m^\xi \bar{\mathcal{H}} \right\rangle + \sigma_H \left\langle \mathcal{H}\bar{\mathcal{H}} \right\rangle \text{Tr}(m^\xi) - a_S \left\langle \mathcal{S} m^\xi \bar{\mathcal{S}} \right\rangle - \sigma_S \left\langle \mathcal{S}\bar{\mathcal{S}} \right\rangle \text{Tr}(m^\xi) \\
&\quad - a_T \left\langle \mathcal{T}_\rho m^\xi \bar{\mathcal{T}}^\rho \right\rangle - \sigma_T \left\langle \mathcal{T}_\rho \bar{\mathcal{T}}^\rho \right\rangle \text{Tr}(m^\xi) \\
&\quad - \frac{\Delta_H^{(a)}}{8} \left\langle \mathcal{H}\sigma_{\mu\nu} m^\xi \bar{\mathcal{H}}\sigma^{\mu\nu} \right\rangle - \frac{\Delta_H^{(\sigma)}}{8} \left\langle \mathcal{H}\sigma_{\mu\nu} \bar{\mathcal{H}}\sigma^{\mu\nu} \right\rangle \text{Tr}(m^\xi) \\
&\quad + \frac{\Delta_S^{(a)}}{8} \left\langle \mathcal{S}\sigma_{\mu\nu} m^\xi \bar{\mathcal{S}}\sigma^{\mu\nu} \right\rangle + \frac{\Delta_S^{(\sigma)}}{8} \left\langle \mathcal{S}\sigma_{\mu\nu} \bar{\mathcal{S}}\sigma^{\mu\nu} \right\rangle \text{Tr}(m^\xi) \\
&\quad + \frac{3}{16}\Delta_T^{(a)} \left\langle \mathcal{T}_\rho \sigma_{\mu\nu} m^\xi \bar{\mathcal{T}}^\rho \sigma^{\mu\nu} \right\rangle + \frac{3}{16}\Delta_T^{(\sigma)} \left\langle \mathcal{T}_\rho \sigma_{\mu\nu} \bar{\mathcal{T}}^\rho \sigma^{\mu\nu} \right\rangle \text{Tr}(m^\xi),
\end{aligned}
\tag{169}
$$

where $m^\xi = \chi^+/4B_0 = \text{diag}\{m_u, m_d, m_s\} + O(p^4)$. In the above interaction, the $\Delta_{H/S/T}^{(a)}$ and $a_{H/S/T}$ terms contribute to the SU(3) flavor breaking effect, while the $\Delta_{H/S/T}^{(\sigma)}$ and $\sigma_{H/S/T}$ terms keep the SU(3) flavor symmetry. The terms in $\mathcal{L}_{\text{chiral}}^{(2)}$ will contribute to the mass spectrum of the heavy mesons through Fig. 11(a) at $O(p^2)$ of the chiral expansion. The contributions from $\Delta_{H/S/T}^{(a/\sigma)}$ are further suppressed by $1/m_Q$.

Up to the order of $1/m_Q$ and up to the NLO chiral expansion [$O(p^2)$], the mass corrections come from the tree diagrams [661, 662, 663, 664],

$$
\delta_{P_q}^{\text{tree}} = \sigma_H \bar{m} + a_H m_q - \frac{3}{4}\left(\delta_b + \Delta_H^{(\sigma)}\bar{m} + \Delta_H^{(a)}m_q\right),
\tag{170}
$$

$$
\delta_{P_q^*}^{\text{tree}} = \sigma_H \bar{m} + a_H m_q + \frac{1}{4}\left(\delta_b + \Delta_H^{(\sigma)}\bar{m} + \Delta_H^{(a)}m_q\right),
\tag{171}
$$

$$
\delta_{R_q}^{\text{tree}} = \delta_S + \sigma_S \bar{m} + a_S m_q - \frac{3}{4}\left(\delta_b' + \Delta_S^{(\sigma)}\bar{m} + \Delta_S^{(a)}m_q\right),
\tag{172}
$$

$$
\delta_{R_q^*}^{\text{tree}} = \delta_S + \sigma_S \bar{m} + a_S m_q + \frac{1}{4}\left(\delta_b' + \Delta_S^{(\sigma)}\bar{m} + \Delta_S^{(a)}m_q\right),
\tag{173}
$$

$$
\delta_{Y_q}^{\text{tree}} = \delta_T + a_T m_q + \sigma_T \bar{m} - \frac{5}{8}\left(\delta_b'' + \Delta_T^{(a)}m_q + \Delta_T^{(\sigma)}\bar{m}\right),
\tag{174}
$$

$$
\delta_{Y_q^*}^{\text{tree}} = \delta_T + a_T m_q + \sigma_T \bar{m} + \frac{3}{8}\left(\delta_b'' + \Delta_T^{(a)}m_q + \Delta_T^{(\sigma)}\bar{m}\right),
\tag{175}
$$

where $\bar{m} = m_u + m_d + m_s$. The subscript q denotes different light quarks u, d and s.

The one-loop diagrams start to contribute at $O(p^3)$ of the chiral expansion. The $O(p^3)$ contributions come from the wave function renormalization diagram in Fig. 11(b). The axial coupling vertices in the loops arise from the Lagrangians in Eqs. (123), (128)-(132). The intermediate states in the loop can be the same as or different from the external states. The different intermediate states will include the mass corrections from the other kinds of heavy mesons. The other one-loops in Fig. 11 will contribute at $O(p^4)$. In Fig. 11(c) and (d) diagrams, there are three types of the $O(p^2)$ vertices which stem from $a_{H/S/T}$, $\sigma_{H/S/T}$ and $\Delta_{H/S/T}^{(a/\sigma)}$ terms. The $a_{H/S/T}$ terms keep the HQSS but break the SU(3)$_V$ symmetry. The $\sigma_{H/S/T}$ terms keep the HQSS and yield the flavor-independent contributions to the masses of the pseudoscalar and vector mesons in the same heavy quark spin doublet. The $\Delta_{H/S/T}^{(a/\sigma)}$ terms breaks the HQSS and their loop corrections will be further suppressed by $1/m_Q$. At $O(p^4)$, the tree diagram in Fig. 11(e) is governed by the Lagrangians with two insertions of the light quark mass matrix [660]. As an example, the Lagrangians of the $\mathcal{H}$ multiplet at $O(p^4)$ are given by

$$
\begin{aligned}
\mathcal{L}_{\text{chiral}}^{(4)} &= b \left\langle \mathcal{H} m_\xi m_\xi \bar{\mathcal{H}} \right\rangle + c\,\text{Tr}(m_\xi) \left\langle \mathcal{H} m_\xi \bar{\mathcal{H}} \right\rangle + d\,\text{Tr}(m_\xi m_\xi) \left\langle \mathcal{H}\bar{\mathcal{H}} \right\rangle \\
&\quad - \frac{1}{8}\Delta^{(b)} \left\langle \mathcal{H}\sigma_{\mu\nu} m_\xi m_\xi \bar{\mathcal{H}}\sigma^{\mu\nu} \right\rangle - \frac{1}{8}\Delta^{(c)}\,\text{Tr}(m_\xi) \left\langle \mathcal{H}\sigma_{\mu\nu} m_\xi \bar{\mathcal{H}}\sigma^{\mu\nu} \right\rangle
\end{aligned}
$$

41

$$-\frac{1}{8}\Delta^{(d)}\,\mathrm{Tr}(m_\xi m_\xi)\left\langle \mathcal{H}\sigma_{\mu\nu}\bar{\mathcal{H}}\sigma^{\mu\nu}\right\rangle + \dots, \tag{176}$$

where b, c, d, and $\Delta^{(b/c/d)}$ are the LECs. The Lagrangians for the $\mathcal{S}$ and $\mathcal{T}$ multiplets are similar.

So far, there exist many theoretical predictions for the heavy mesons using the HHχPT. The early studies only considered the ground state D and B mesons. The mass splittings of these heavy mesons have been studied in the heavy quark limit and SU(3) flavor symmetry [492, 495], and receive the $1/m_Q$ and the light quark mass corrections [665, 660, 621, 659, 620, 666, 667, 668, 669, 670, 671, 672] (see Ref. [620] for a review). For instance, the leading mass splittings $m_{D^*} - m_D$ and $m_{B^*} - m_B$ are proportional to δ_b as shown in Eq. (170) and Eq. (171). Since δ_b is proportional to $1/m_Q$, one has

$$\frac{m_{D^*} - m_D}{m_{B^*} - m_B} = \frac{m_b}{m_c}. \tag{177}$$

Its leading corrections come from the mass corrections of the heavy quarks and have been studied in HQET [665, 669, 474]

$$\frac{m_{D^*} - m_D}{m_{B^*} - m_B} = \frac{m_b}{m_c}\left(\frac{\alpha_s(m_b)}{\alpha_s(m_c)}\right)^{-9/25} \simeq \frac{m_B}{m_D}\left(\frac{\alpha_s(m_B)}{\alpha_s(m_D)}\right)^{-9/25}, \tag{178}$$

with the α_s the running coupling constant.

Another popular hyperfine mass splitting is [660, 659, 620, 666, 667, 668]

$$\Delta M_D = \left(M_{D_s^*} - M_{D_s}\right) - \left(M_{D^{*+}} - M_{D^+}\right), \tag{179}$$

$$\Delta M_B = \left(M_{B_s^*} - M_{B_s}\right) - \left(M_{B^{*0}} - M_{B^0}\right). \tag{180}$$

The leading order electromagnetic corrections from the s and d quarks are the same due to their equal electric charges. Hence, both ΔM_D and ΔM_B vanish in the chiral and heavy quark limit.

In the HHχPT formalism, the lowest order contribution arises from the $\Delta_H^{(a)}$ term in $\mathcal{L}_{\mathrm{chiral}}^{(2)}$ through the diagram in Fig. 11(a) at the order $1/m_Q$. The mass splittings then satisfy the following relation [666],

$$\frac{\Delta M_B}{\Delta M_D} = \frac{m_c}{m_b}, \tag{181}$$

which is a direct consequence of Eq. (177).

The one-loop diagram in Fig. 11 will provide corrections to ΔM_D and ΔM_B. In the loop diagrams, the different masses of the pseudoscalar mesons, $m_\pi/m_K/m_\eta$, the mass splittings between the heavy spin doublets $\delta_b/\delta_b'/\delta_b''$, the mass splittings between the non-strange and strange mesons $\Delta_s = \Delta_H^{(a)}(m_s - m_{u/d})$, as well as the different axial couplings for the $P^*P^*\pi$ and $P^*P\pi$ vertex may contribute to the ΔM_D and ΔM_B. The one-loop correction was given by [660, 620, 667, 668, 659]

$$\begin{aligned}
\Delta M_{D/B}^{(b)} &= \frac{g_b^2\delta_b}{16\pi^2 f_\varphi^2}\left[m_K^2\log\left(\Lambda_\chi^2/m_K^2\right) + \frac{1}{2}m_\eta^2\log\left(\Lambda_x^2/m_\eta^2\right) - \frac{3}{2}m_\pi^2\log\left(\Lambda_\chi^2/m_\pi^2\right)\right] \\
&\quad + \frac{g_b^2\delta_b}{16\pi^2 f_\varphi^2}\left(6\pi m_K\Delta_s\right) - \frac{g_b^2}{24\pi f_\varphi^2}\frac{\Delta_{g_b}}{g_b}\left(m_K^3 + \frac{1}{2}m_\eta^3 - \frac{3}{2}m_\pi^3\right),
\end{aligned} \tag{182}$$

where the terms in the first line is the so-called chiral logarithm. The terms in the second line are both of order $m_q^{3/2}$. Δ_{g_b} represents the difference between the axial coupling in the $\mathcal{H}$ multiplet and stems from the Lagrangian at the order $1/m_Q$ [668],

$$\mathcal{L}_{1/m_Q}^{g_b} = i\frac{\xi_1}{m_Q}\left\langle\mathcal{H}\gamma_\mu\gamma_5 u^\mu\bar{\mathcal{H}}\right\rangle + i\frac{\xi_2}{m_Q}\left\langle\mathcal{H}\bar{\mathcal{H}}u^\mu\gamma_\mu\gamma_5\right\rangle, \tag{183}$$

The ξ_1 term is the recoil correction to the leading order interaction term g_b in Eq. (123) and leads to a deviation of the $DD^*\pi$ and $BB^*\pi$ couplings. However, the ξ_1 term keeps the HQSS and does not contribute to the Δ_{g_b}. On the

other hand, the ξ_2 term breaks the HQSS, hence is forbidden in the leading order, which contributes to the coupling difference as

$$\Delta_g = 2\frac{\xi_2}{m_Q}. \tag{184}$$

The calculation can be generalized to the analogous $d - u$ type hyperfine splitting $(D^{*+} - D^+) - (D^{*0} - D^0)$. Both the electromagnetic interaction and the current quark mass difference contribute to the isospin violation. Their effects are quantitatively of the same order. Fortunately, the dominant contribution to the isospin violation from $m_d - m_u$ can be easily accounted for through the spurion χ so long as one keeps $m_d \neq m_u$ from the beginning. In the leading order, the spurion χ leads to the mass splitting of the heavy mesons and baryons, and also the mass splitting of the eight pseudoscalar mesons. The higher order isospin violating corrections to the heavy hadron masses may arise from the chiral loop contributions where the intermediate isospin multiplets of the pions or kaons have different masses with $m_{\pi^+} \neq m_{\pi^0}$ etc. Another source of higher order correction is the multiple insertions of the spurion χ in the construction of higher order Lagrangians. However, both types of higher order corrections are much smaller than the leading order term. Therefore, one generally considers the leading order correction due to $m_d - m_u$ in literature.

Apart from the light quark mass difference , the electromagnetic effect was also important [660]. The Lagrangians contributing to the isospin hyperfine splittings read

$$\mathcal{L}_{\text{QED}}^{\mathcal{Q}_h \mathcal{Q}_h \mathcal{S}} = -\frac{1}{8}\Delta_{\text{em}}\alpha_{\text{em}}\left\langle \mathcal{Q}_h^2 \mathcal{H}\sigma_{\mu\nu}\bar{\mathcal{H}}\sigma^{\mu\nu}\right\rangle, \tag{185}$$

$$\mathcal{L}_{\text{QED}}^{\mathcal{Q}_h Q} = a_{\text{em}}\alpha_{\text{em}}\left\langle \mathcal{Q}_h \mathcal{H}Q_+\bar{\mathcal{H}}\right\rangle, \tag{186}$$

$$\mathcal{L}_{\text{QED}}^{\mathcal{Q}_h Q \mathcal{S}} = -\frac{1}{8}\Delta_{\text{em}}^{(a)}\alpha_{\text{em}}\left\langle \mathcal{Q}_h \mathcal{H}Q_+\sigma_{\mu\nu}\bar{\mathcal{H}}\sigma^{\mu\nu}\right\rangle, \tag{187}$$

$$\mathcal{L}_{\text{QED}}^{QQ} = b_{\text{em}}\alpha_{\text{em}}\left\langle \mathcal{H}Q_+Q_+\bar{\mathcal{H}}\right\rangle + d_{\text{em}}\alpha_{\text{em}}\text{Tr}(Q_+Q_+)\left\langle \mathcal{H}\bar{\mathcal{H}}\right\rangle, \tag{188}$$

$$\mathcal{L}_{\text{QED}}^{QQ\mathcal{S}} = -\frac{1}{8}\Delta_{\text{em}}^{(b)}\alpha_{\text{em}}\left\langle \mathcal{H}\sigma_{\mu\nu}Q_+Q_+\bar{\mathcal{H}}\sigma^{\mu\nu}\right\rangle - \frac{1}{8}\Delta_{\text{em}}^{(d)}\alpha_{\text{em}}\text{Tr}(Q_+Q_+)\left\langle \mathcal{H}\sigma_{\mu\nu}\bar{\mathcal{H}}\sigma^{\mu\nu}\right\rangle, \tag{189}$$

where $\mathcal{Q}_h$ is the heavy quark electric charge and equal to $\frac{2}{3}$ and $-\frac{1}{3}$ for the charmed and bottom quarks, respectively. The $Q_+ = \xi^\dagger \mathcal{Q}_l \xi + \xi \mathcal{Q}_l \xi^\dagger$ with $\mathcal{Q}_l = \text{diag}(2/3, -1/3, -1/3)$ is the light quark electric charge. The charge factor e^2 has been absorbed in α_{em}. The above Lagrangians are suppressed by α_{em}, which are counted as $O(p^2)$ in Refs. [673, 674]. The Lagrangians with the heavy quark charge $\mathcal{Q}_h$ will contribute to the masses of the charmed and bottom hadrons due to their different electric charges. The Lagrangians $\mathcal{L}_{\text{QED}}^{\mathcal{Q}_h Q}$, $\mathcal{L}_{\text{QED}}^{\mathcal{Q}_h Q \mathcal{S}}$, the b_{em} term in $\mathcal{L}_{\text{QED}}^{QQ}$, as well as the $\Delta_{\text{em}}^{(b)}$ term in $\mathcal{L}_{\text{QED}}^{QQ\mathcal{S}}$ will contribute to the isospin breaking effect. The Lagrangians with the superscript $\mathcal{S}$ will break the HQSS and other ones without the $\mathcal{S}$, i.e., $\mathcal{L}_{\text{QED}}^{\mathcal{Q}_h Q}$ and $\mathcal{L}_{\text{QED}}^{QQ}$, conserve the HQSS.

The Lagrangians in Eqs. (185)-(189) will contribute to the $d-u$ type hyperfine splitting at the tree level through the Fig. 11(a) at $O(p^2)$ and up to $1/m_Q$. The $\mathcal{L}_{\text{QED}}^{\mathcal{Q}_h Q}$ and $\mathcal{L}_{\text{QED}}^{QQ}$ contribute to the electromagnetic mass splittings at $O(p^2)$, which are of order $2 - 5$ MeV for the charmed mesons. The contributions from other Lagrangians $\mathcal{L}_{\text{QED}}^{\mathcal{Q}_h \mathcal{Q}_h \mathcal{S}}$, $\mathcal{L}_{\text{QED}}^{\mathcal{Q}_h Q \mathcal{S}}$, and $\mathcal{L}_{\text{QED}}^{QQ\mathcal{S}}$ will be further suppressed by the $1/m_Q$. The electromagnetic correction may also appear at $O(p^3)$ through the photon loop as illustrated in Fig. 12, where the meson-photon interaction vertex arises from the chiral connection Γ_μ [given in Eq. (A.3)] in the chiral covariant derivative of the LO Lagrangians. This loop correction vanishes at $O(p^3)$ in heavy hadron regularization and infrared regularization schemes [675]. Up to $O(p^3)$ and up to the order $1/m_Q$, the electromagnetic contributions to the isospin mass splitting arise from the Lagrangians in Eqs. (186)-(189) at the tree level.

After the observation of the $D_{s0}^*(2317)$ and $D_{s1}(2460)$, the HHχPT has been extended to discuss the mass corrections of the excited heavy mesons with spin-parity 0^+ and 1^+ [618, 661, 662, 676, 30, 677, 678, 679, 680, 663]. In these works, the two even-parity states $[D_{s0}^*(2317), D_{s1}(2460)]$ and their non-strange partner states $[D_0^*(2300), D_1(2430)]$ were treated as the spin doublets $(0^+, 1^+)$ with $j_\ell^P = \frac{1}{2}^+(L = 1)$, which were described by the superfield $\mathcal{S}$. As mentioned in Sec.1.1, one mystery of the excited charmed mesons is their surprising mass degeneracy,

$$m_{D_{s0}^*(2317)} - m_{D_0^*(2300)} = -25.2\,\text{MeV}, \tag{190}$$

$$m_{D_{s1}(2460)} - m_{D_1(2430)} = 47.5\,\text{MeV}, \tag{191}$$

while the typical splittings around 100 MeV are naively expected due to the mass of the strange quark.

This mystery was first investigated in Ref. [678]. The authors calculated the mass difference $(m_{D_0^*} - m_D) - (m_{D_{s0}^*} - m_{D_s})$ in the heavy quark limit. Only the Lagrangians preserving the heavy quark symmetry were considered and the power counting was determined by the chiral expansion only. The chiral corrections were calculated up to $O(p^3)$. The LO Lagrangians in Eqs. (123), (128)-(132) and the $a_{H/S}$ as well as $\sigma_{H/S}$ terms in the next-to-leading order $\mathcal{L}_{\text{chiral}}$ [in Eq.(169)] contribute up to $O(p^2)$ at the tree level. The $O(p^3)$ corrections come from the one-loop diagram in Fig. 11(b). The mass difference only depends on the SU(3) breaking counterterm $a_S - a_H$, which was determined by the lattice calculation. The result was obtained as $(m_{D_0^*} - m_D) - (m_{D_{s0}^*} - m_{D_s}) \sim -100$ MeV, which is inconsistent with the experimental value ~ 100 MeV.

Later, the authors in Ref. [661] included both the heavy quark symmetry breaking effect up to $1/m_Q$ and the SU(3) breaking effects with the Lagrangians $\mathcal{L}_{1/m_Q}$ in Eq. (168) and $\mathcal{L}_{\text{chiral}}^{(2)}$ in Eq. (169), respectively. They derived the mass spectrum of the $\mathcal{H}$ and $\mathcal{S}$ multiplets up to $O(p^3)$ and to $O(1/m_Q)$ in the HHχPT. There are totally eleven LECs: three coupling constant g_b, g_b', h and eight combinations of the other LECs which appear in the $\mathcal{L}_{\text{chiral}}^{(2)}$ [Eq. (169)] and $\mathcal{L}_{1/m_Q}$ [Eq. (168)]. There are different combinations of the LECs as shown in Ref. [661] and Refs. [662, 681, 664]. Since the number of the LECs exceeds that of the experimental data (eight charmed mesons), there are multiple fitting solutions [661, 663]. Therefore, it is impossible to draw firm conclusions. The two fits in Ref. [661] either underestimate the excited non-strange meson or have unnaturally large LECs at $O(1/m_Q)$. Thus the mass difference $(m_{D_0^*} - m_D) - (m_{D_{s0}^*} - m_{D_s})$ still remains a big puzzle.

In Ref. [676], Guo *et al* pointed out that the bare mass of the heavy-light scalar mesons obtained in the quark model was pulled down significantly by the hadron loop with the HHχPT formalism. The authors in Ref. [30] calculated the self-energy corrections arising from the hadronic loop in Fig. 11(b) for both the charmed-strange mesons and their nonstrange partners. They considered the LO Lagrangians in Eqs. (123), (128)-(132) and the $1/m_Q$ correction $\mathcal{L}_{1/m_Q}$ in Eq. (168). However, their results showed that the mass degeneracy and the physical masses of D_{s0}^* and D_0^* cannot be achieved simultaneously in the HHχPT formalism.

In Refs. [662, 664], the authors used the similar framework as in Ref. [661] and calculated the expressions for the heavy meson masses up to $O(p^3)$. Compared with Ref. [661], the additional loop corrections with the intermediate spin-3/2 $\mathcal{T}$ mesons were considered in calculating the $\mathcal{S}$ multiplet masses due to their small mass splitting ($\lesssim 130$ MeV) and the considerable LO couplings. With the masses of the odd-parity and even-party charmed mesons as inputs, they predicted the near degeneracy of the nonstrange and strange scalar B mesons. The authors also pointed out that the calculations in Refs. [676, 30] were not complete since they only included the hadronic loops with the ground mesons in the $\mathcal{H}$ doublet but missed the contribution from the $\mathcal{S}$ doublets to the self-energy corrections of the scalar $D_{(s)0}^*$. In addition, they criticized that the physical masses rather than the bare masses should be used in evaluating loop functions. Later, the authors in Ref. [30] revisited their calculations in Ref. [33]. Their results showed that the unsatisfactory mass degeneracy in Ref. [30] can be implemented by adjusting the g_b', h, and the renormalization scale Λ. The mass degeneracy of the D_{s0}^* and D_0^* can be quantitatively understood as a consequence of the self-energy corrections from the hadronic loop. More technical differences in the approach of the HHχPT among Refs. [620, 661, 676, 658, 30, 33, 662, 663] were given in Refs. [662, 33].

Another mystery of the $D_{s0}^*(2317)$ and $D_{s1}^*(2460)$ is the fine-tuning problem

$$\left(m_{D_{s1}(2460)} - m_{D_{s0}^*(2317)}\right) - (m_{D^*} - m_D) \leq 2\,\text{MeV}, \tag{192}$$

which cannot be dictated by the QCD symmetries alone. With the parity doubling model—an analog of the linear Σ-model for the heavy mesons, the equality was obtained at the tree level [682, 683, 684, 685]. The parity doubling model embeds the chiral symmetry, its spontaneous breaking and heavy quark symmetry. The heavy spin multiplet $(0^+, 1^+)$ with $j_\ell = 1/2$ is assumed to be the chiral partner of the ground doublet $(0^-, 1^-)$. Their linear combinations $D(0^+, 1^+) + D(0^-, 1^-)$ and $D(0^+, 1^+) - D(0^-, 1^-)$ transform as (approximately) pure $(1, 3)$ and $(3, 1)$, respectively, under $\text{SU}(3)_L \otimes \text{SU}(3)_R$ chiral symmetry. The Σ transforms as $(\bar{3}, 3)$. With the spontaneously broken chiral symmetry, the vacuum expectation of the Σ is nonzero leading to the similar effective Lagrangians to those in HHχPT. Compared with HHχPT, the parity doubling model predicts the same hyperfine splittings in the $\mathcal{H}$ and $\mathcal{S}$ doublets, for example, $m_{D^*} - m_D = m_{D_1^*} - m_{D_0^*}$, at the tree level, i.e., $\delta_b' = \delta_b$. In Ref. [661], Mehen *et al* proved that the equality will survive in the one-loop level with $|g_b| = |g_b'|$. It seems that this model explained the relation in Eq. (192).

In the section, all the discussions are performed assuming the $D_{s0}^*(2317)/D_{s1}^*(2460)$ states as the P-wave quark-antiquark mesons. In the same picture, their analogous partner states in the bottom sector, especially the not yet observed heavy bottom mesons $B_{(s)0}^*$ and $B_{(s)1}'$, were discussed with heavy quark flavor symmetry in many theoretical works, such as Refs. [661, 33, 30, 682, 686, 687, 677]. Since the two positive parity D_s reside very close to the DK/D^*K thresholds, other explanations, such as the molecular states composed of $D^{(*)}$ and K mesons, are also quite popular and will be discussed in Sec. 4.
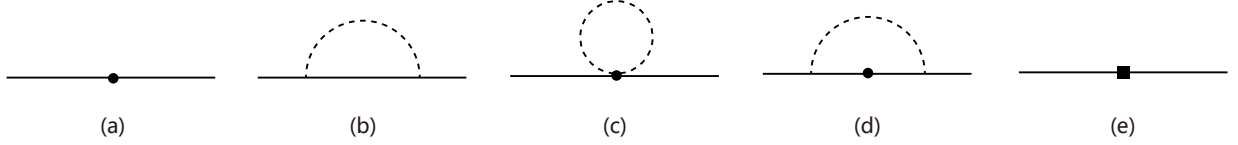

Figure 11: The Feynman diagrams contributing to the mass corrections of the heavy hadrons. The solid and dashed lines represent the heavy hadrons and the Goldstone bosons, respectively. In the loop diagrams, the external and the internal heavy hadrons can be the same or different. The solid dot and black square denote the vertices at $O(p^2)$ and $O(p^4)$, respectively. The one-loop diagram (b) is at $O(p^3)$ while the other one-loop diagrams are at $O(p^4)$.

Figure 12: The QED one-loop self-energy diagram at $O(p^3)$.

3.1.2. Singly heavy baryons

The χPT was first employed to investigate the heavy baryons containing a heavy quark in Refs. [616, 621, 688, 689, 690, 470, 691]. The one-loop chiral corrections to their masses were given in Refs. [692, 693, 675, 694]. In Ref. [694], Jiang *et al* systematically calculated the chiral corrections to the heavy baryon masses as well as the axial charges up to $O(p^3)$ using the HHχPT formalism. In this section, we follow their framework to illustrate the calculation of the heavy baryon masses.

The mass corrections at $O(p)$ come from the Lagrangians in Eq. (136) and Eq. (144) [or Eq. (139) in the superfield formalism]. At $O(p^2)$, the mass splittings arise from the light quark mass difference as well as the electromagnetic effects due to different electric charges. The Lagrangians at $O(p^2)$ contain both the SU(3) flavor breaking Lagrangian $\mathcal{L}_{bc}^{(2)}$ and the QED Lagrangian $\mathcal{L}_{QED}^{(2)}$ as follows [689, 675, 694, 692]

$$
\begin{aligned}
\mathcal{L}_{bc}^{(2)} &= b_1 \text{Tr}\left(\bar{B}_6 \chi_+ B_6\right) + b_5 g_{\mu\nu} \text{Tr}\left(\bar{B}_6^{*\mu} \chi_+ B_6^{*\nu}\right) + b_6 \text{Tr}\left(\bar{B}_{\bar{3}} \chi_+ B_{\bar{3}}\right) \\
&\quad + c_1 \text{Tr}\left(\bar{B}_6 B_6\right) \text{Tr}(\chi_+) + c_5 g_{\mu\nu} \text{Tr}\left(\bar{B}_6^\mu B_6^{*\nu}\right) \text{Tr}(\chi_+) + c_6 \text{Tr}\left(\bar{B}_{\bar{3}} B_{\bar{3}}\right) \text{Tr}(\chi_+),
\end{aligned} \tag{193}
$$

$$
\mathcal{L}_{QED}^{(2)66} = e_1^{66} \text{Tr}\left(\bar{B}_6 Q_+^2 B_6\right) + e_2^{66} \text{Tr}\left(\bar{B}_6 Q_+ B_6\right) \text{Tr}(Q_+) + e_3^{66} \text{Tr}\left(\bar{B}_6 B_6\right) \text{Tr}(Q_+^2) + e_4^{66} \text{Tr}\left(\bar{B}_6 Q_+ B_6 Q_+^T\right), \tag{194}
$$

$$
\mathcal{L}_{QED}^{(2)\bar{3}\bar{3}} = e_1^{\bar{3}\bar{3}} \text{Tr}\left(\bar{B}_{\bar{3}} Q_+^2 B_{\bar{3}}\right) + e_2^{\bar{3}\bar{3}} \text{Tr}\left(\bar{B}_{\bar{3}} Q_+ B_{\bar{3}}\right) \text{Tr}(Q_+) + e_3^{\bar{3}\bar{3}} \text{Tr}\left(\bar{B}_{\bar{3}} B_{\bar{3}}\right) \text{Tr}(Q_+^2), \tag{195}
$$

$$
\begin{aligned}
\mathcal{L}_{QED}^{(2)6^*6^*} &= e_1^{6^*6^*} g_{\rho\sigma} \text{Tr}\left(\bar{B}_6^{*\rho} Q_+^2 B_6^{*\sigma}\right) + e_2^{6^*6^*} g_{\rho\sigma} \text{Tr}\left(\bar{B}_6^{*\rho} Q_+ B_6^{*\sigma}\right) \text{Tr}(Q_+), \\
&\quad + e_3^{6^*6^*} g_{\rho\sigma} \text{Tr}\left(\bar{B}_6^{*\rho} B_6^{*\sigma}\right) \text{Tr}(Q_+^2) + e_4^{6^*6^*} g_{\rho\sigma} \text{Tr}\left(\bar{B}_6^{*\rho} Q_+ B_6^{*\sigma} Q_+^T\right).
\end{aligned} \tag{196}
$$

Here, the $Q_+ = \xi^\dagger \mathcal{Q} \xi + \xi \mathcal{Q} \xi^\dagger$ with $\mathcal{Q} = \mathcal{Q}_h + \mathcal{Q}_l = e\,\text{diag}(2,0,0)$ or $e\,\text{diag}(1,-1,-1)$ the charge matrix of the charmed or bottom baryons. These Lagrangians will contribute to the mass corrections at $O(p^2)$ through diagram in Fig. 11(a). One should note that the above Lagrangians are constructed in the heavy quark limit and no recoil effects are considered.

The chiral one-loop corrections start to contribute at $O(p^3)$ through the diagram in Fig. 11(b). The tree-level QED contributions Σ_{QED} are at $O(p^2)$. The one-loop QED corrections as shown in Fig. 12 stem from the chiral connection

45

term Γ_μ in the leading order Lagrangians and vanish as in the heavy meson case [675]. All the QED effects may be very small due to the double expansion in the chiral order and fine-structure constant.

In Ref. [694], the authors derived the chiral corrections up to $O(p^3)$ with the contributions from the tree diagrams in Fig. 11(a) and (b). They determined the values of the involved LECs with the experimental masses as input in five cases to investigate the role of the different corrections. The LEC values agreed with those in the study of the light-meson-heavy-baryon scattering lengths [695, 696]. The results for the mass spectrum as well as the decay widths were consistent with the experimental data.

In Ref. [675], the authors calculated the isospin mass splitting of the spin-$\frac{1}{2}$ heavy baryons in the isospin multiplets $\Sigma_{c(b)}$ and $\Xi'_{c(b)}$. They calculated the corrections to $O(p^3)$ with the chiral perturbation theory using the infrared regularization. They focused on the isospin splitting and used the experimental splitting values as input. The results showed that the electromagnetic interaction played an important role in turning the mass order of the Σ_c isotriplet into an unnatural pattern (compared with the naive expectation that follows from $m_d > m_u$). For the Σ_b states, the natural mass order is restored.

In Ref. [692], the authors studied the following equal spacing rule between the sextet heavy baryon with the LO Lagrangian in Eq. (136) and the $\mathcal{L}^{(2)}_{bc}$ in Eq. (193),

$$\frac{1}{3}\left(M_{\Sigma_c^{++}} + M_{\Sigma_c^+} + M_{\Sigma_c^0}\right) + M_{\Omega_c^0} - \left(M_{\Xi_c'^+} + M_{\Xi_c'^0}\right) = 0. \tag{197}$$

Up to $O(p^2)$, the relation survives and the $O(p^3)$ corrections from the loop in Fig. 11(b) are small. They also studied the mass splitting between the spin-$\frac{3}{2}$ and spin-$\frac{1}{2}$ sextet heavy baryons. In this case, apart from the above Lagrangians, the δ_a term at $O(1/m_Q)$ as shown in Eq. (139) as well as its chiral corrections at $O(p^2)$ with the insertion of one light quark mass matrix needs to be taken into account [697, 698, 692]. Similar to Eq. (197), the hyperfine splitting $\delta_{\Sigma_c} + \delta_{\Omega_c} - 2\delta_{\Xi_c}$ with $\delta = m_{B^*} - m_B$ equals zero up to $O(p^2)$ and $O(1/m_Q)$, and receives small one-loop corrections from Fig. 11(b) at $O(p^3)$.

In Ref. [693], the authors calculated the masses of the Σ_b, Σ_b^*, Λ_b as well as the mass splitting between the Σ_b and Σ_b^* by extrapolating the lattice QCD data at the unphysical pion mass to the physical region. The Lagrangian in Eq. (139) including the $1/m_Q$ correction and the $\mathcal{L}^{(2)}_{bc}$ in Eq. (193) were considered. Up to $O(p^3)$, the tree diagram (a) and the one-loop diagram (b) in Fig. 11 were calculated and the phenomenological function for the extrapolation of lattice QCD was proposed. They found that the extrapolation was quite different with the naive linear extrapolation when $m_\pi < 500$ MeV.

The parity doubling model mentioned in the heavy meson sector has also been developed to study the heavy baryons (see Refs. [127, 126, 699, 700, 701, 702, 703, 704] and references therein). With the diquarks qq as the building blocks, the chiral diquark effective field theory is built based on the $SU(3)_R \otimes SU(3)_L$ chiral symmetry and its spontaneously breaking induced by the nonvanishing vacuum expectation value of the Σ field. The $0^+(^1S_0)$ and $0^-(^3P_0)$ diquarks are assumed to be the chiral partners and belong to the $(\bar{3}, 1)$ and $(1, \bar{3})$ representations of the $SU(3)_R \otimes SU(3)_L$ symmetry, respectively. Analogous to the heavy mesons, the linear-Σ-model effective Lagrangian is constructed with the Σ field belonging to $(\bar{3}, 3)$ representation. The 1^- diquark and 1^+ diquark form another chiral partner doublet. With the chiral effective model, the mass spectra of the singly heavy baryons have been studied.

In addition to the HHχPT, the investigations of the heavy baryon mass spectrum with other effective field theory methods have been reviewed in Refs. [7, 166], such as the Large N_c, the QCD sum rule in the framework of HQET, and the non-linear chiral SU(3) Lagrangian, etc.

3.1.3. Doubly heavy baryons

In the doubly heavy baryon sector, the first attempt of calculating their masses up to $O(p^4)$ in the baryon chiral perturbation theory was made in Ref. [705] with the HHχPT formalism. Later, the masses of the doubly charmed baryons was also calculated with the EOMS formalism up to $O(p^3)$ [706] and up to $O(p^4)$ [707]. Recently, the authors of Ref. [708] performed a similar calculation up to $O(p^3)$ in HHχPT with new lattice results. The leading order Lagrangian is given in Eq. (144). The higher order Lagrangians up to $O(p^4)$ after the non-relativistic projections read [705, 707, 625]

$$\mathcal{L}^{(2)} = c_1 \bar{\mathcal{B}}_{QQ} \mathcal{B}_{QQ} \text{Tr}(\chi_+) + \frac{c_2}{2} \bar{\mathcal{B}}_{QQ} \mathcal{B}_{QQ} \text{Tr}(v \cdot u)^2 + c_3 \bar{\mathcal{B}}_{QQ} (v \cdot u)^2 \mathcal{B}_{QQ} + \frac{c_4}{2} \bar{\mathcal{B}}_{QQ} \mathcal{B}_{QQ} \text{Tr}(u^2)$$

$$+\frac{c_5}{2}\bar{\mathcal{B}}_{QQ}u^2\mathcal{B}_{QQ}+\frac{c_6}{2}\bar{\mathcal{B}}_{QQ}\left[S^\mu,S^\nu\right]\left[u_\mu,u_\nu\right]\mathcal{B}_{QQ}+c_7\bar{\mathcal{B}}_{QQ}\hat{\chi}_+\mathcal{B}_{QQ}$$

$$+\frac{2}{m}\bar{\mathcal{B}}_{QQ}\left(S\cdot D\right)^2\mathcal{B}_{QQ}-\frac{i\tilde{g}_1}{m}\bar{\mathcal{B}}_{QQ}\{S\cdot D,v\cdot u\}\mathcal{B}_{QQ}-\frac{\tilde{g}_1^2}{2m}\bar{\mathcal{B}}_{QQ}(v\cdot u)^2\mathcal{B}_{QQ}+\dots,\tag{198}$$

$$\mathcal{L}^{(3)}=h_1\bar{\mathcal{B}}_{QQ}S\cdot u\mathcal{B}_{QQ}\mathrm{Tr}(\chi_+)+h_2\bar{\mathcal{B}}_{QQ}S^\mu\left\{\hat{\chi}_+,u_\mu\right\}\mathcal{B}_{QQ}+h_3\bar{\mathcal{B}}_{QQ}S^\mu\mathrm{Tr}(\hat{\chi}_+u_\mu)\mathcal{B}_{QQ}$$

$$-\frac{i}{m^2}\bar{\mathcal{B}}_{QQ}S\cdot Dv\cdot DS\cdot D\mathcal{B}_{QQ}+\dots,\tag{199}$$

$$\mathcal{L}^{(4)}=e_1\bar{\mathcal{B}}_{QQ}\mathcal{B}_{QQ}\mathrm{Tr}(\chi_+)\mathrm{Tr}(\chi_+)+e_2\bar{\mathcal{B}}_{QQ}\hat{\chi}_+\mathcal{B}_{QQ}\mathrm{Tr}(\chi_+)+e_3\bar{\mathcal{B}}_{QQ}\mathcal{B}_{QQ}\mathrm{Tr}(\hat{\chi}_+\hat{\chi}_+)$$

$$+e_4\bar{\mathcal{B}}_{QQ}\hat{\chi}_+\hat{\chi}_+\mathcal{B}_{QQ}+e_5\bar{\mathcal{B}}_{QQ}\mathcal{B}_{QQ}\mathrm{Tr}(\chi_-)\mathrm{Tr}(\chi_-)+e_6\bar{\mathcal{B}}_{QQ}\hat{\chi}_-\mathcal{B}_{QQ}\mathrm{Tr}(\chi_-)$$

$$+e_7\bar{\mathcal{B}}_{QQ}\mathcal{B}_{QQ}\mathrm{Tr}(\hat{\chi}_-\hat{\chi}_-)+e_8\bar{\mathcal{B}}_{QQ}\hat{\chi}_-\hat{\chi}_-\mathcal{B}_{QQ}+\dots.\tag{200}$$

The relativistic forms are referred to Refs. [705, 707, 625, 707]. The last three terms in $\mathcal{L}^{(2)}$ and the last one in $\mathcal{L}^{(3)}$ come from the second term in Eq. (B.11) which is suppressed at least by $1/m$ in the nonrelativistic projections, while the others are the non-relativistic forms of their corresponding relativistic operators. Apart from the contributions in the heavy quark limit, the recoil terms will contribute through the diagrams in Fig. 13. The last term in $\mathcal{L}^{(3)}$ will lead to an additional tree-level diagram at $O(p^3)$ as illustrated in Fig. 13(a_1). The $\tilde{g}_1/m$ term in $\mathcal{L}^{(2)}$ leads to two additional loop diagrams at $O(p^4)$ as shown in Fig. 13(b_1) and (c_1). The physical masses can be obtained with Eq. (167). Up to $O(p^3)$, there are four undetermined LECs involved: the bare mass M_0 in Eq.(167), the $\tilde{g}_1$ in Eq. (144), and the c_1, c_7 in Eq. (198). In Refs. [705, 706, 707], $\tilde{g}_1$ was related to the axial coupling of the singly heavy mesons in the HDAS as shown in Eqs. (148), (149) and (150).
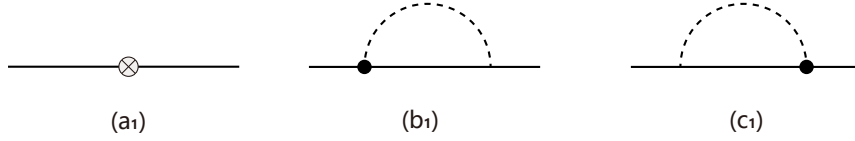

Figure 13: The additional Feynman diagrams contributing to the mass spectrum of the heavy hadrons arising from the recoil effect in the HHχPT formalism. The solid and dashed lines represent the heavy hadrons and the Goldstone bosons, respectively. The solid dot and circled cross denote the vertices from the vertex at $O(p^2)$ and $O(p^3)$, respectively. The two one-loop diagrams are at $O(p^4)$.

In Ref. [506], a superfiled formalism of HDAS was proposed

$$\mathcal{L}=\left\langle\mathcal{H}\left(iD_0\right)\mathcal{H}^\dagger\right\rangle-g\left\langle\mathcal{H}\boldsymbol{\sigma}\cdot\boldsymbol{u}\mathcal{H}^\dagger\right\rangle+\frac{\Delta_H}{4}\left\langle\mathcal{H}_a^\dagger\Sigma^i\mathcal{H}_a\sigma^i\right\rangle,\tag{201}$$

where $\mathcal{H}$ is a 5×2 matrix field formed by the 2×2 matrix field for the heavy baryon $H_a=\boldsymbol{P}_a^*\cdot\boldsymbol{\sigma}+P_a$ and the 3×2 matrix field for the doubly heavy baryon $T_{a,i\beta}=\sqrt{2}\left(\Xi_{a,i\beta}^*+\frac{1}{\sqrt{3}}\Xi_{a,\gamma}\sigma_{\gamma\beta}^i\right)$. The H and T fields are the nonrelativisitc forms of our $\mathcal{H}$ and ψ_{QQ}^μ superfields in Sec. 2.6. The g and Δ_H can be related to the g_b, $\tilde{g}_b$ and δ_b, $\tilde{\delta}_b$ in Sec. 2.6. The Σ^i is an extended Pauli matrix which is determined by assuming the violation of heavy (di)quark spin symmetry only arises from the chromomagnetic interaction in Ref. [506].

The LECs c_1, c_7 and M_0 are determined from the lattice QCD data [136, 709, 503, 133, 710, 147, 139]. In Refs. [705, 706, 707], the authors used the same lattice QCD data for the Ξ_{cc} [136], which were calculated with different m_π and m_c. They introduced the m_c dependence of the doubly heavy baryon masses through the bare mass M_0 in Eq.(167) as follows [705, 706, 707]

$$M_0=\tilde{m}_0+2m_c+\alpha/m_c+O\left(1/m_c^2\right),\tag{202}$$

where two new unknown parameters $\tilde{m}_0$ and α appear to replace M_0. $\tilde{m}_0$ is the mass of the light d.o.f in the doubly charmed baryons. α contains two kinds of $1/m_c$ corrections stemming from the Lagrangian terms at $O(1/m_Q)$ in the HQET as shown in Eq. (60).

In the HHχPT formalism, the contribution from the c_1 term was the same for all the doubly charmed baryons so that it can be absorbed into M_0. In Ref. [705], the authors used the lattice results for the Ξ_{cc} [136] and Ω_{cc} [136, 709, 503, 133, 710] to determine the LECs $\tilde{m}_0$, α and c_7 and obtained the following mass spectrum

$$m_{\Xi_{cc}} = 3.665^{+0.093}_{-0.097} \text{ GeV}, \qquad m_{\Omega_{cc}} = 3.726^{+0.093}_{-0.097} \text{ GeV}. \qquad (203)$$

In the EOMS formalism, the authors in Refs. [706, 707] also fitted four LECs with the same lattice QCD data [136]. In Ref. [707], the authors also took the finite volume effect into consideration and obtained the masses

$$m_{\Xi_{cc}} = 3.591 \pm 0.067 \text{ GeV}, \qquad m_{\Omega_{cc}} = 3.657 \pm 0.100 \text{ GeV}. \qquad (204)$$

The authors of Ref. [708] calculated the masses of the doubly bottom and the charmed-bottom baryons up to $O(p^3)$ with the HHχPT formalism. The authors used the quark model value for $\tilde{g}_1$ from Ref. [711] and determined the LECs M_0, c_7 by fitting the lattice QCD data [147, 139] without considering the mass dependence on the heavy quark. The expressions of the mass corrections up to $O(p^4)$ were also derived in Refs. [705, 707]. Unfortunately, there are too many LECs involved and cannot be determined with the current lattice QCD and experimental data.

The mass splittings of the doubly heavy baryons have been studied with the help of the HDAS [506, 712, 713]. The hyperfine splittings $m_{\Xi_{cc}^*} - m_{\Xi_{cc}} - \frac{3}{4}(m_{P^*} - m_P)$ vanishes at the leading order, which is guaranteed by the Lagrangian constructed in HDAS as illustrated in Eq. (201). In Ref. [506], the authors calculated the one-loop corrections from Fig. 11(b) at $O(p^3)$ and kept the nonanalytic parts. The deviation from the HDAS symmetry was small (< 10 MeV) and changed slightly with different subtraction scale. In Ref. [713], the authors investigated isospin splittings of the doubly charmed baryons up to $O(p^2)$ with the following Lagrangians,

$$\mathcal{L}_{\text{ISV}} = -c\left\langle \mathcal{H}\chi_+ \mathcal{H}^\dagger \right\rangle - d_0 \left\langle \hat{Q}_h \mathcal{H} Q_{l+} \mathcal{H}^\dagger \right\rangle - d_1 \left\langle \mathcal{H}\left(Q_{l+}^2 - Q_{l-}^2\right)\mathcal{H}^\dagger \right\rangle - d_2 \left\langle \mathcal{H} Q_{l+} \mathcal{H}^\dagger \right\rangle \text{Tr}(Q_{l+}), \qquad (205)$$

where $Q_{l\pm}$ is defined with the light quark electric matrix. $\hat{Q}_h$ is the heavy quark charge operator and its projections on the H_a and T_a fields are $\hat{Q}_h H_a = \mathcal{Q}_h H_a$ and $\hat{Q}_h T_a = -2\mathcal{Q}_h T_a$. No loop corrections were considered. They predicted the isospin splittings for the spin-3/2 and -1/2 doubly heavy baryons in the heavy quark spin symmetry

$$M_{\Xi_{cc}^{++}} - M_{\Xi_{cc}^+} = 1.5 \pm 2.7 \text{ MeV}, \quad M_{\Xi_{bb}^-} - M_{\Xi_{bb}^0} = 6.3 \pm 1.7, \text{ MeV}, \quad M_{\Xi_{bc}^+} - M_{\Xi_{bc}^0} = -0.9 \pm 1.8 \text{ MeV}. \qquad (206)$$

In addition to the above formalisms, some other effective field theory, such as the HQET [714], the parity doubling model [715, 716] were also used to study the mass spectroscopy of the doubly heavy baryons.

3.2. Axial vector currents, axial couplings and strong decays

The matrix elements of the axial vector currents involving heavy hadrons are very important in flavor physics and in search for physics beyond the Standard Model. In the weak interaction, the axial charges of the heavy hadrons are associated with many observables at low energies such as the weak transition form factors [717, 688, 718, 719, 720, 721, 722, 723, 724], decay constants [725, 726, 658] and so on. Meanwhile, the coupling constants of the heavy hadrons and pseudoscalar Goldstone bosons (axial coupling for short) can be related to the axial charges through the Goldberger-Treiman relation, which is a natural consequence of the spontaneous breaking of the chiral symmetry. The axial couplings also play important roles in the strong interaction. The pionic strong decays of the heavy hadrons are related to the axial coupling constants. In addition, more and more exotic hadrons were observed as the candidates of the heavy hadronic molecules in the past decades, e.g. the $X(3872)$ as the $\bar{D}^* D / \bar{D} D^*$ molecule [201], the P_c states as the $\Sigma_c^{(*)} \bar{D}^{(*)}$ molecules [2, 3], and the T_{cc} state as the $D^* D$ molecule [5]. In the molecular picture, the exotic hadrons are formed by exchanging the light mesons. Therefore, the precise determination of the axial coupling constants is crucial to understand these molecular structures. The investigations of the molecular hadrons within χEFT will be reviewed in Sec. 5. One can refer to Refs. [6, 11, 14] for general reviews of hadronic molecules. In short, the matrix elements of the axial currents and axial coupling constants are essential for understanding both strong and weak interactions of the heavy hadrons.

We take the axial vector current A_μ between of the pseudoscalar P and vector meson V as an example to illustrate the Goldberger-Treiman relation [727]. In general, the axial current matrix can be parameterized as follows,

$$\langle P(p')|A_\mu^a|V(p)\rangle = \varepsilon_\mu F_1(q^2) + 2(\varepsilon \cdot q)k_\mu F_2(q^2) + (\varepsilon \cdot q)q_\mu F_3(q^2), \qquad (207)$$

where $q = p' - p$ and $k = (p' + p)/2$. ε is the polarization vector of V. F_1, F_2 and F_3 are the scalar functions. From the Goldstone theorem in Sec. 2.1.1, we know the axial current can annihilate the Goldstone bosons in Eq. (34), which is a natural consequence of spontaneous broken chiral symmetry. If we introduce the explicit breaking of chiral symmetry, we can relate the axial current to the pion field with the partially conserved axial current (PCAC) relation $\partial^\mu A_\mu^a = f_\pi m_\pi^2 \pi^a$ as shown in Fig. 14(a). Thus, we can get

$$\langle P(p')|\partial^\mu A_\mu^a|V(p)\rangle = \langle P(p')|\pi^a|V(p)\rangle f_\pi m_\pi^2 + q^\mu N_\mu = (\varepsilon \cdot q) g_{VP\pi}(q^2) \frac{1}{q^2 - m_\pi^2} f_\pi m_\pi^2 + q^\mu N_\mu, \tag{208}$$

where the axial coupling constant $g_{VP\pi}$ is introduced to depict the $VP\pi$ vertex and N_μ term represents the non-pole contribution. In the chiral perturbation theory, the non-pole contribution starts to appear from the $O(p^3)$ Lagrangian [728]. Therefore, in the following derivation, we neglect the non-pole term as shown in Fig. 14(b). Thus, one can relate the axial coupling constant $g_{VP\pi}$ to the axial current matrix elements,

$$g_{VP\pi}(q^2) \frac{1}{q^2 - m_\pi^2} f_\pi m_\pi^2 = \left[F_1(q^2) + 2(q \cdot k) F_2(q^2) + q^2 F_3(q^2) \right]. \tag{209}$$

When $q^2 \to 0$, one can obtain the Goldberger-Treiman relation,

$$g_{VP\pi}(0) = -\frac{1}{f_\pi} F_1(0) \approx g_{VP\pi}(m_\pi^2), \tag{210}$$

where the $F_1(0)$ is the axial charge. The PCAC and Goldberger-Treiman relations are illustrated in Fig. 14. In lattice QCD, the axial coupling constants and strong decays of the ground heavy hadrons were extracted by calculating the matrix element of the light quark axial vector current [138, 729, 730, 731, 727, 732].
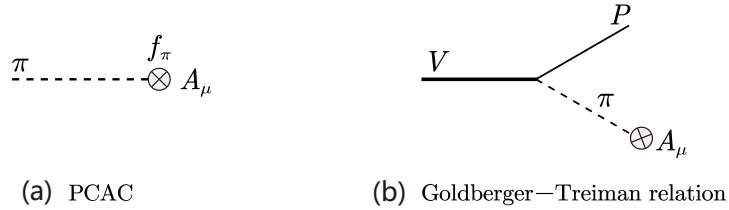

(a) PCAC   (b) Goldberger−Treiman relation

Figure 14: The partially conserved axial current and Goldberger-Treiman relations. The circled cross represents an insertion of the axial current.

Since the Goldstone bosons are very light (massless in chiral limit), the chiral corrections cannot be neglected in the calculation of the axial vector current at low energy (with small q^2) or the axial charges. The χPT was first used to calculate the chiral corrections of the axial vector current of the nucleon systems [511, 733, 734, 735, 736, 737, 738, 739, 740, 741]. The similar formalism combining heavy quark symmetries has been extended to calculate the axial currents of the heavy hadron systems. As for the strong decays of the ground heavy hadrons such as $D^* \to D\pi$, the small phase space for the decays ensures a valid chiral expansion. Therefore, we will review the chiral corrections to the axial vector current and strong decays within HHχPT. In order to avoid the confusions arising from different conventions in literature, we will construct the general Lagrangians contributing to the axial vector currents of the heavy baryons first.

3.2.1. Lagrangians and Feynman diagrams

For the heavy hadrons, the axial coupling terms in the $O(p)$ Lagrangians in Eqs. (124), (139) and (146) will contribute to the LO the axial vector currents of the heavy mesons, singly heavy baryons and doubly heavy baryons, respectively. The NLO [$O(p^3)$] axial vector currents arise from both the tree diagrams and one-loop diagrams. The LO axial vector current multiplied by the wave function renormalization factor of the heavy hadrons will contribute
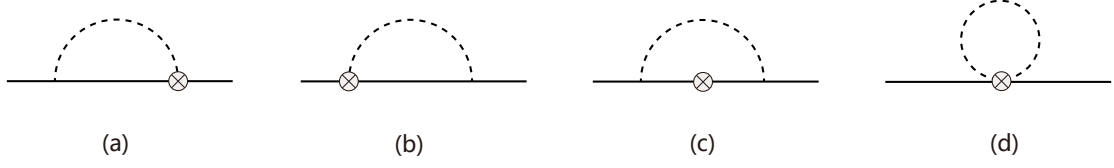
Figure 15: The topological loop diagrams contributing to the axial vector current. The circled cross represents an insertion of the axial vector current.

to the $O(p^3)$ axial vector current. In addition, the loop diagrams in Fig. 15 will contribute to the $O(p^3)$ axial current if the vertices are all LO ones in Eqs. (50), (124), (139) and (146). The chiral correction from the two seagull diagrams contain a factor $v\cdot q$, which is suppressed by $1/M_H$ [734] (M_H is the heavy hadron mass). In literature, this contribution was usually neglected if the recoiling effect was not included.
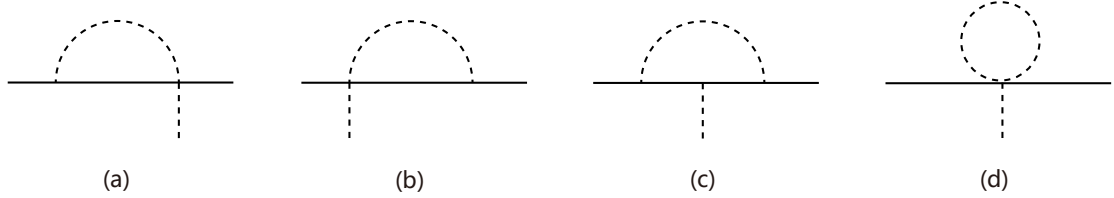

Figure 16: The topological loop diagrams contributing to strong decays.

The $O(p^3)$ Lagrangians will contribute to the $O(p^3)$ axial vector currents at the tree level, which are constructed with the building blocks χ_+ and u_μ. With the knowledge of representations of the SU(3) group as shown in Table A.10, we can construct the Lagrangians as follows,

$$
\begin{aligned}
\mathcal{L}^{(3)}_{\tilde{\mathcal{H}}\varphi} &= h_1\langle\bar{\tilde{\mathcal{H}}}\slashed{u}\gamma_5\tilde{\mathcal{H}}\rangle\mathrm{Tr}(\chi_+) + h_2\langle\bar{\tilde{\mathcal{H}}}\{\hat{\chi}_+,\slashed{u}\}\gamma_5\tilde{\mathcal{H}}\rangle + h_3\langle\bar{\tilde{\mathcal{H}}}\gamma_\mu\gamma_5\tilde{\mathcal{H}}\rangle\mathrm{Tr}(\hat{\chi}_+u^\mu) + ih_4\langle\bar{\tilde{\mathcal{H}}}[\hat{\chi}_+,\slashed{u}]\gamma_5\tilde{\mathcal{H}}\rangle, & (211)
\end{aligned}
$$

$$
\begin{aligned}
\mathcal{L}^{(3)}_{\psi_{QQ}\varphi} &= \tilde{h}_1\bar{\psi}^\nu_{QQ}\slashed{u}\gamma_5\psi_{QQ\nu}\mathrm{Tr}(\chi_+) + \tilde{h}_2\bar{\psi}^\nu_{QQ}\{\hat{\chi}_+,\slashed{u}\}\gamma_5\psi_{QQ\nu} + \tilde{h}_3\bar{\psi}^\nu_{QQ}\gamma_\mu\gamma_5\psi_{QQ\nu}\mathrm{Tr}(\hat{\chi}_+u^\mu) \\
&\quad + i\tilde{h}_4\bar{\psi}^\nu_{QQ}[\hat{\chi}_+,\slashed{u}]\gamma_5\psi_{QQ\nu}, & (212)
\end{aligned}
$$

$$
\begin{aligned}
\mathcal{L}^{(3)}_{\psi_Q\varphi} &= ih_5\epsilon_{\mu\nu\rho\sigma}\mathrm{Tr}\left(\bar{\psi}^\mu_Q u^\rho v^\sigma \psi^\nu_Q\right)\mathrm{Tr}(\chi_+) + ih_6\epsilon_{\mu\nu\rho\sigma}\mathrm{Tr}\left(\bar{\psi}^\mu_Q\{u^\rho,\hat{\chi}_+\}v^\sigma\psi^\nu_Q\right) + h_7\epsilon_{\mu\nu\rho\sigma}\mathrm{Tr}\left(\bar{\psi}^\mu_Q[u^\rho,\hat{\chi}_+]v^\sigma\psi^\nu_Q\right) \\
&\quad + ih_8\epsilon_{\mu\nu\rho\sigma}\mathrm{Tr}\left(\bar{\psi}^\mu_Q v^\sigma\psi^\nu_Q\right)\mathrm{Tr}(u^\rho\hat{\chi}_+) + ih_9\epsilon_{\mu\nu\rho\sigma}\mathrm{Tr}\left(\bar{\psi}^\mu_Q v^\sigma u^\rho\psi^\nu_Q\hat{\chi}^T_+\right), & (213)
\end{aligned}
$$

$$
\begin{aligned}
\mathcal{L}^{(3)}_{\mathcal{B}_{\bar{3}}\varphi} &= h_{10}\mathrm{Tr}\left(\bar{\mathcal{B}}_{\bar{3}}\slashed{u}\gamma_5\mathcal{B}_{\bar{3}}\right)\mathrm{Tr}(\chi_+) + h_{11}\mathrm{Tr}\left(\bar{\mathcal{B}}_{\bar{3}}\{\hat{\chi}_+,\slashed{u}\}\gamma_5\mathcal{B}_{\bar{3}}\right) + h_{12}\mathrm{Tr}\left(\bar{\mathcal{B}}_{\bar{3}}\gamma^\mu\gamma_5\mathcal{B}_{\bar{3}}\right)\mathrm{Tr}(\hat{\chi}_+u_\mu), & (214)
\end{aligned}
$$

$$
\begin{aligned}
\mathcal{L}^{(3)}_{\psi_Q\mathcal{B}_{\bar{3}}\varphi} &= h_{13}\mathrm{Tr}\left(\bar{\psi}^\mu_Q u_\mu\mathcal{B}_{\bar{3}}\right)\mathrm{Tr}(\chi_+) + h_{14}\mathrm{Tr}\left(\bar{\psi}^\mu_Q\{\hat{\chi}_+,u_\mu\}\mathcal{B}_{\bar{3}}\right) + h_{15}\mathrm{Tr}\left(\bar{\psi}^\mu_Q[\hat{\chi}_+,u_\mu]\mathcal{B}_{\bar{3}}\right) + \mathrm{H.c.}. & (215)
\end{aligned}
$$

The $\hat{\chi}_+$ in the above Lagrangians will introduce the SU(3) flavor symmetry violation in the vertices. According to the representation reduction of SU(3) group $\mathbf{8}\otimes\mathbf{8} \to \mathbf{8}_1(\mathbf{8}_2)$, where $\mathbf{8}_1$ and $\mathbf{8}_2$ are two different reduction ways of the octet representation (see Appendix A for details), we introduce $\{\hat{\chi}_+,u_\mu\}$ and $[\hat{\chi}_+,u_\mu]$ as the building blocks. However, in the relativistic Lagrangian with two identical matter fields, e.g., Eq. (214), one of them will be eliminated by the constraint of charge conjugation. Note that the charge conjugation will introduce the transpose of the building blocks $\hat{\chi}_+$ and u_μ as shown in Table A.9. The transpose will introduce an extra sign for $[\hat{\chi}_+,u^\mu]$ but not for $\{\hat{\chi}_+,u^\mu\}$. Therefore, only one of them will survive. However, for the Lagrangians with different matter fields, e.g., Eq. (215), both $\{\hat{\chi}_+,u_\mu\}$ and $[\hat{\chi}_+,u_\mu]$ terms will contribute. In the superfield formalism, we keep both of them in the Lagrangians to include the two different matter field case. However, one should be cautious about these terms for the processes with identical matter fields by checking the C-parity conservation. In the practical calculations, if one does not care about the pion mass dependence, the h_1, $\tilde{h}_1$, h_5, h_{10} and h_{14} terms can be absorbed by the LO Lagrangians, since the building block $\mathrm{Tr}(\chi_+)$ only contributes a constant at the leading order.

50

The Lagrangians and Feynman diagrams which contribute to the strong decays are very similar to those of the axial vector currents. The leading order strong decays arise from the LO axial coupling terms in Eqs. (123), (139) and (146). At $O(p^3)$, the tree level contribution to the strong decays stems from the same Lagrangians of the axial vector currents in Eq. (215). The LO results multiplied by the wave function renormalization factors will contribute to the $O(p^3)$ strong decay amplitudes. The wave function renormalization of the Goldstone bosons will also give rise to the $O(p^3)$ corrections apart from those of the heavy hadrons. The remaining $O(p^3)$ loop corrections arise from the diagrams in Fig. 16. Among them, the contributions of Figs. 16(a) and 16(b) are suppressed by $1/M_H$. The contribution of the diagram 16(d) will be canceled out by the renormalization of the Goldstone bosons [689]. Thus, if one neglects the recoiling effect, only diagram 16(c) and the wave function renormalization of the heavy hadrons contribute to the strong decays at the NLO.

3.2.2. Axial couplings and strong decays of the ground state heavy hadrons

In Ref. [621], the authors constructed the chiral Lagrangians embedding the HQSS, which is in fact the LO Lagrangian of the HHχPT. The axial coupling constants were estimated by relating them to that of the nucleon within the quark model. With the nucleon axial charge $g_A = 1.25$ as input, the coupling constants in Eqs. (123) and (136) were,

$$|g_b| = 0.75, \quad g_1 = \frac{4}{3} \times 0.75, \quad g_2 = -\sqrt{\frac{2}{3}} \times 0.75, \tag{216}$$

and the strong decay widths were estimated to be

$$\Gamma(D^{*-} \to D^0 \pi^-) = 0.10 \text{ MeV}, \quad \Gamma(\Sigma_c^0 \to \Lambda^+ \pi^-) = 2.45 \text{ MeV}. \tag{217}$$

The above calculations were improved by including SU(3) symmetry breaking effect [689] and $1/M_H$ correction [659], respectively. In Ref. [689], the strong decays of the heavy mesons were calculated to the NLO of the chiral expansion including the SU(3) symmetry breaking effect. With the $|g_b| = 0.75$, the strong decay widths of D^{*+} read

$$\Gamma(D^{*+} \to D^0 \pi^+) = 0.276 \text{ MeV}, \quad \Gamma(D^{*+} \to D^+ \pi^0) = 0.125 \text{ MeV}. \tag{218}$$

In Ref. [659], the authors discussed the $1/M_H$ effect by considering the reparametrization invariance of the heavy hadron fields and dynamical effect from the $1/m_Q$ terms in HQET.

In Ref. [742], the author calculated the $D^* \to D\pi$ decay within HHχPT. The chiral expansion is truncated at NLO, which includes the tree and one-loop diagrams. In the analytical calculation, the SU(3) flavor and HQSS breaking effects were included. Apart from the Lagrangians and Feynman diagrams in Sec. 3.2.1, the author also constructed the following $O(p^2)$ terms,

$$\langle \bar{\tilde{\mathcal{H}}} (iv \cdot \nabla \slashed{u}) \gamma_5 \tilde{\mathcal{H}} \rangle, \quad \langle \bar{\tilde{\mathcal{H}}} (i \slashed{\nabla} v \cdot u) \gamma_5 \tilde{\mathcal{H}} \rangle. \tag{219}$$

The two terms give rise to the amplitudes proportional to $v \cdot k_\pi$, which are expected to be tiny, considering the small phase space of $D^* \to D\pi$. In the numerical analysis, the contributions from these two terms were neglected. In addition, the effect of the heavy quark spin and flavor breaking operators in Eq. (60) were included by two operators at the hadron level,

$$\frac{1}{m_Q} \langle \bar{\tilde{\mathcal{H}}} \slashed{u} \gamma_5 \tilde{\mathcal{H}} \rangle, \quad \frac{1}{m_Q} \langle \bar{\tilde{\mathcal{H}}} u^\mu \tilde{\mathcal{H}} \gamma_\mu \gamma_5 \rangle. \tag{220}$$

The first operator only breaks the HQFS due to the different m_Q for the charm and bottom quarks. Apart from the violation of the HQFS, the second term can break the HQSS by flipping the heavy quark spin. With the ratios of $\mathcal{B}(D^{*0} \to D^0 \gamma)/\mathcal{B}(D^{*0} \to D^0 \pi^0)$, $\mathcal{B}(D^{*+} \to D^+ \gamma)/\mathcal{B}(D^{*+} \to D^+ \pi^0)$ and $\mathcal{B}(D_s^* \to D_s \pi^0)/\mathcal{B}(D_s^* \to D_s \gamma)$ [743], the author obtained two solutions, $g_b = 0.27$ or $g_b = 0.76$.

In Ref. [744], the authors studied the decays $B^* \to B\gamma\gamma$ and $D^* \to D\gamma\gamma$ to determine the $g_{B^*(D^*)B(D)\pi}$ and $g_{B^*(D^*)B(D)\gamma}$ with the LO chiral Lagrangians, In the processes, they considered Feynman diagrams including the $B^*(D^*) \to B(D)\gamma$, $B^*(D^*) \to B(D)\pi$, and $\pi^0 \to 2\gamma$ vertices which was fixed by the chiral anomaly.

In Ref. [745], the axial vector current matrix elements of the heavy mesons were calculated to NLO. In order to perform the chiral extrapolation for the partially-quenched lattice QCD simulations, the partially-quenched chiral

perturbation theory was adopted for both SU(4|2) and SU(6|3) symmetries [746]. The finite volume effect was also incorporated. This calculation was used to extrapolate the lattice QCD simulations of the axial couplings of the $B^*B\pi$, $\Sigma_b^*\Sigma_b\pi$ and $\Sigma_b^{(*)}\Lambda_b\pi$ [134, 138]. The numerical results expressed in our conventions in Eqs. (139) and (123) were

$$g_b = 0.449 \pm 0.051, \quad g_a = 0.84 \pm 0.20, \quad g_3 = 0.71 \pm 0.13. \tag{221}$$

In Ref. [694], the axial charges of the ground state heavy baryons were calculated up to NLO within HHχPT in the isospin symmetry limit but with explicit SU(3) breaking. In the calculations, the recoiling corrections were discarded. In the numerical analysis, the authors took the values of the axial charges in the chiral quark model [747] as the pseudo-experimental data. With the pseudo-experimental data as input, the authors determined the LECs and gave the numerical contributions order by order. The results showed that the convergence of the chiral expansion is quite good.

In Ref. [506], the authors constructed the LO chiral Lagrangians for the doubly charmed baryons with the HDAS. The axial coupling constant is related to those of the heavy mesons. Apart from the ground state heavy hadrons, the authors also constructed the chiral Lagrangians for the excited states. The quenched and partially quenched chiral Lagrangians were proposed in Ref. [712] to suit the chiral extrapolation in lattice QCD simulations. Later, Mehen constructed the chiral Lagrangians for the excited doubly heavy baryons and doubly heavy tetarquarks [504].

In Ref. [706], the chiral corrections to the axial vector currents and axial charges of the doubly heavy baryons were investigated to the NLO ($O(p^3)$) of the chiral expansion. The LO axial coupling constant is determined by the HDAS, i.e., $\tilde{g}_b = g_b$ in Eqs. (123) and (146). At the NLO, the loop diagrams and corrections are similar to the discussions in Sec. 3.2.1. At the NLO, the authors also constructed the Lagrangians equivalent to the $\tilde{h}_{1,2,3}$ terms in Eq. (212) to consider the tree-level diagram contributions. If one only considers the spin-$\frac{1}{2}$ doubly charmed baryons, the $\tilde{h}_4$ term vanishes due to the charge conjugation symmetry. In the numerical analysis, the $\tilde{h}_1$ term can be absorbed by the LO axial coupling constant. The remaining LECs $\tilde{h}_2$ and $\tilde{h}_3$ were estimated by the naturalness assumption.

3.2.3. $D_s^* \to D_s\pi^0$ isospin violating decays

In the above discussions of the strong decays, the SU(3) breaking effect is kept but the isospin violating effect is neglected, because it is tiny in general. However, for the specific process $D_s^* \to D_s\pi^0$, the isospin violating effect is significant.

The mass difference between the D_s^* and D_s is slightly larger than the neutral pion mass by about 2 MeV, which makes the $D_s^* \to D_s\pi^0$ and $D_s^* \to D_s\gamma$ the dominant decay modes of the D_s^*. The strong decay process $D_s^* \to D_s\pi^0$ violates the isospin symmetry. The double suppressions from the phase space and the isospin violation make this strong decay width very tiny, around several eVs. The branching fraction of this strong decay mode is $(5.8\pm0.7)\%$. For comparison, the branching fraction of the electromagnetic decay mode $D_s^* \to D_s\gamma$ is about $(93.5\pm0.7)\%$ [748, 749, 1]. The magnitude of the strong decay mode challenges our physical intuitions about the strong decays and deserves a refined investigation.

In Ref. [750], the author calculated the $D_s^* \to D_s\pi^0$ decay rate using HHχPT. The isospin violating effect is attributed to the $\pi^0 - \eta$ mixing as shown in Fig. 17. The $D_s^* D_s\eta$ vertex stems from the LO axial coupling term in Eq. (123). The $\pi^0 - \eta$ mixing effect arises from the mass term in Eq. (50), which reads,

$$\mathcal{L}_{\text{mixing}} = -\frac{B_0}{\sqrt{3}}(m_u - m_d)\eta\pi^0. \tag{222}$$

One can see the mass difference of the up and down quarks drives the $\pi^0 - \eta$ mixing and leads to the isospin violating decays. Another possible origin of the isospin violation is the electromagnetic interaction, which corresponds to the graph (b) in Fig. 17. The $\pi^0\gamma\gamma$ vertex is induced by the axial vector current anomaly in QED. However, the diagram is suppressed by α_{em}^2 and can be neglected safely. In Ref. [750], the author got the ratio

$$\frac{\Gamma(D_s^* \to D_s\pi^0)}{\Gamma(D^{*+} \to D^+\gamma)} \approx 8 \times 10^{-5}. \tag{223}$$

A similar calculation considering the LO contribution was performed in Ref. [751] as well. The result reads

$$\mathcal{R}_{\pi/\gamma} = \frac{\Gamma(D_s^* \to D_s\pi^0)}{\Gamma(D_s^* \to D_s\gamma)} \approx 1.8\%. \tag{224}$$

The calculation of the $D_s^* \to D_s \pi^0$ decay was performed to the NLO in Ref. [742]. The NLO loop diagrams include graphs which allow the direct emission of the π^0 in Fig. 16. If the mass splittings of the intermediate isospin multiplets are neglected, the amplitudes will cancel with each other. In the calculation, the mass splittings of the isospin doublet or triplet in the loops are kept, which give rise to the nonvanishing amplitude. In addition, the loop corrections to the $\pi^0 - \eta$ mixing effect contribute to the decay width as well, which correspond to diagrams replacing the external Goldstone lines in Fig. 16 with the $\pi^0 - \eta$ mixing.
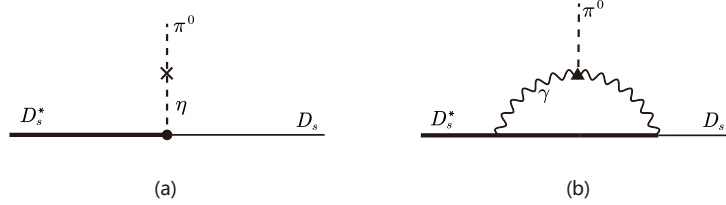
Figure 17: The Feynman diagrams of $D_s^* \to D_s \pi^0$. LO contribution (a) and axial current anomaly contribution (b).

In Ref. [752], the authors calculated the $D_s^* \to D_s \pi^0$ decay to the NLO. Apart from all the diagrams in Ref. [742], the authors also constructed the NLO Lagrangians,

$$\langle \bar{\tilde{\mathcal{H}}} \psi \hat{\chi}_+ \gamma_5 \tilde{\mathcal{H}} \rangle, \ \langle \bar{\tilde{\mathcal{H}}} \psi \gamma_5 \tilde{\mathcal{H}} \rangle \text{Tr} \left[\chi_+ \right], \ i \langle \bar{\tilde{\mathcal{H}}} \slashed{\nabla} \hat{\chi}_- \gamma_5 \tilde{\mathcal{H}} \rangle, \ i \langle \bar{\tilde{\mathcal{H}}} \gamma^\mu \gamma_5 \tilde{\mathcal{H}} \rangle \nabla_\mu \text{Tr} \left[\chi_- \right], \ \langle \bar{\tilde{\mathcal{H}}} \nabla_\nu \slashed{\psi} u^\nu \gamma_5 \tilde{\mathcal{H}} \rangle. \tag{225}$$

In the numerical analysis, two strategies were adopted to estimate the unknown LECs. In the strategy A, the nonanalytic dominant approximation is made. Thus, the NLO result only contains the nonanalytic loop corrections and no contributions from the unknown LECs, which yielded,

$$\Gamma(D_s^* \to D_s \pi^0) = 8.1^{+3.0}_{-2.6} \text{ eV}, \quad \Gamma[D_s^*] = 139.0^{+77.9}_{-54.6} \text{ eV}. \tag{226}$$

Combing the radiative decay $\Gamma(D_s^* \to D_s \gamma) = 0.32^{+0.3}_{-0.3}$ keV in Ref. [753], one can get the ratio defined in Eq. (223) as

$$\mathcal{R}_{\pi/\gamma} \approx 2.5\%. \tag{227}$$

Here we give the value only using the central value and do not give the rigorous uncertainties because the uncertainties of the radiative decay width of D_s^* are too large to use the conventional error propagating formula. In the strategy B, the authors made use of the naturalness assumption. The $\Gamma(D_s^* \to D_s \pi^0)$ was estimated in the range of 5-12 eV. It is worth noticing that the recent experimental value from BESIII of the ratio is $\mathcal{R}_{\pi/\gamma} = (6.16 \pm 0.40 \pm 0.17)\%$ [754]. Apparently, the theoretical results in Eq. (224) and (227) are of the same order as the experimental value. We cannot give more information without the rigorous uncertainties in theoretical calculation.

In Ref. [755], the chiral Lagrangian for the strong and radiative decays of the strange heavy mesons was formulated based on HQET, in which the $1/m_Q$ correction and SU(3) symmetry breaking effect were included. The $\pi^0 - \eta$ mixing vertex was estimated with the new data of $\Gamma(\eta \to 3\pi^0)$ [1].

3.2.4. Strong decays of the excited heavy hadrons

In principle, the χPT cannot be used to investigate the excited heavy hadrons consistently. The mass splittings between the excited and ground heavy mesons do not vanish in the chiral limit, which are numerically much larger than the pion mass. For example $m_{D_0^*} - m_D \approx 470$ MeV $\gg m_\pi$. We cannot expect good convergence in such a high energy scale. Meanwhile, the excited heavy hadrons appear as the resonances in the scattering of the ground state heavy hadrons and pions, which implies the nonperturbative dynamics. However, from the phenomenological perspective, one can still construct the chiral Lagrangians to depict the chiral dynamics of the excited heavy hadrons, discarding the rigorous power counting. For example, in Refs. [81, 153], the authors exploited the chiral Lagrangians to discuss the strong decays of the S-, P-, and higher wave singly charmed baryons. In Refs. [756, 757], the authors investigated the strong decays of the excited charmed mesons with the chiral Lagrangian and heavy quark expansion.

Among the excited heavy hadrons, the nature of the $D_{s0}^*(2317)$ and $D_{s1}(2460)$ remains unsettled decades after their discovery. Whether they are molecule states or conventional P-wave heavy mesons continues to be a heated topic.

In Ref. [657], the authors constructed the chiral Lagrangians in Eqs. (123), (128) and (130). The coupling constant h is extracted from the experimental decay widths of the $D_1(1^+)$ and $D_0(0^+)$ [758, 759, 760], $h^2 = 0.44 \pm 0.11$. With the coupling constants, the authors calculated the isospin violating decays of the $D_{s0}^*(2317)$ and $D_{s1}(2460)$ with the tree level $\pi^0 - \eta$ mixing effect. The results showed that the relevant branching ratios $\mathrm{Br}[D_{s1}(2460) \to D_s^* \gamma]/\mathrm{Br}[D_{s1}(2460) \to D_s^* \pi^0]$ and $\mathrm{Br}[D_{s0}(2317) \to D_s^* \gamma]/\mathrm{Br}[D_{s0}(2317) \to D_s \pi^0]$ deviate significantly from the experimental results [23]. After considering the HQSS violating operators (with the LECs determined by the naturalness) and one-loop chiral corrections to the electromagnetic decays, the theoretical results became consistent with the experimental data. In Ref. [661], the authors calculated the loop corrections to the coupling constants g_b and g_b' and derived their one-loop renormalization group equation as well. This work also investigated the decay patterns in the molecular scheme, see Sec. 3.3.1 for details.

In Ref. [679], the authors considered the one-loop correction to the g_b, g_b' and h in Eqs. (123), (128) and (130) and included the positive parity mesons in the loop diagrams. Although the author also constructed the counter terms, their contributions were neglected due to lacking of input in the numerical analysis. Thus, the results are regularization-scale-dependent. With the regularization scale $\mu \simeq 1$ GeV, they got

$$\text{LO:} \qquad g_b = 0.61, \qquad h = 0.52, \qquad g_b' = -0.15, \tag{228}$$

$$\text{One-loop:} \qquad g_b = 0.66, \qquad h = 0.47, \qquad g_b' = -0.06. \tag{229}$$

In Ref. [761], the isospin violating decays $D_{s1}(2460) \to D_s \pi\pi$, $D_{s1}(2460) \to D_s^* \pi$ and $D_{s0}^*(2317) \to D_s \pi$ were investigated. The g_b, g_b' and h terms in Eqs. (123), (128) and (130) contribute to the $D_{s1}(2460) \to D_s^* \pi$ and $D_{s0}^*(2317) \to D_s \pi$ tree diagrams via the $\pi^0 - \eta$ mixing effect. The one-loop diagrams for the two decays were similar to those for $D_s^* \to D_s \pi^0$. There is no tree-level contribution for the $D_{s1}(2460) \to D_s \pi\pi$ decays. The related one-loop diagrams were presented in Fig. 18. In the calculation, only the diagrams (a), (b) and (c) were taken into consideration. The counter terms were introduced to absorb the divergence of the loop diagrams and estimated with the experimental ratios of the decay widths roughly. The numerical results read

$$\Gamma(D_{s1}(2460)^+ \to D_s^+ \pi^+ \pi^-) \simeq 0.25 \text{ keV}, \qquad \Gamma(D_{s1}(2460)^+ \to D_s^+ \pi^0 \pi^0) \simeq 0.15 \text{ keV}, \tag{230}$$

$$\Gamma(D_{s1}(2460)^+ \to D_s^{*+} \pi^0) = 2.7 \sim 3.4 \text{ keV}, \quad \Gamma(D_{s0}^*(2317)^+ \to D_s^+ \pi^0) = 2.4 \sim 4.7 \text{ keV}. \tag{231}$$

The above results are significantly smaller than the hadronic widths predicted in the molecular pictures, see Refs. [762, 763] for examples. The same framework was used to investigate the isospin violating decays of the positive parity B_s mesons [680]. The numerical results read

$$\Gamma\left(B_{s1}^0 \to B_s^0 \pi\pi\right) \sim 10^{-3}\text{keV}, \quad \Gamma\left(B_{s0}^{*0} \to B_s^0 \pi^0\right) \leq 55\text{keV}, \quad \Gamma\left(B_{s1}^0 \to B_s^{*0} \pi^0\right) \leq 50\text{keV}. \tag{232}$$
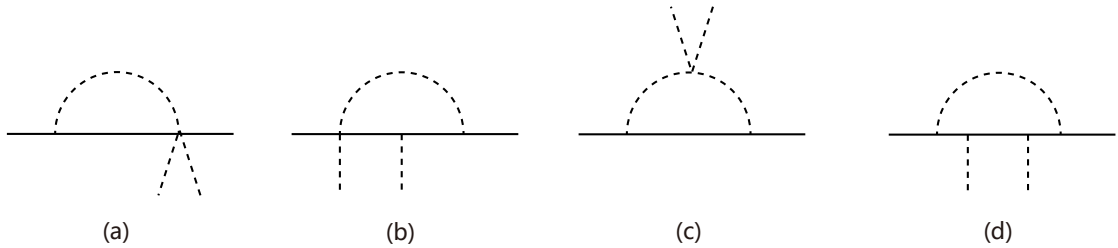

Figure 18: The one-loop diagrams for the $D_{s1}(2460) \to D_s \pi\pi$ decay.

3.3. Magnetic moments and radiative transitions of the heavy hadrons

The mass, charge, spin and magnetic moment are intrinsic characteristics of a particle. The magnetic moment $\boldsymbol{\mu}$ of a particle (e.g., the electron) is related to its charge e, mass m and spin $\boldsymbol{S}$ via

$$\boldsymbol{\mu} = g \frac{e}{2m} \boldsymbol{S}, \tag{233}$$

54

where g is the Landé g-factor, which usually indicates whether a particle is elementary or composite. A renowned example is the neutron's magnetic moment, which is expected to vanish if it is an elementary particle due to its electro-neutral property [see Eq. (233)]. But the experimental measurement told us that the neutron carries a non-zero, large and negative magnetic moment [764, 765, 766], which strongly indicated that the neutron is not an elementary particle. Its inner structure was understood until the quark model was developed in 1960s. Now we know that the neutron is composed of three constituent quarks udd. The sum of their magnetic moments leads to the neutron magnetic moment.

The magnetic moment of a hadron is related to its magnetic form factor $\mathscr{G}_M(q^2)$ at $q^2 = 0$. Generally, the electromagnetic properties of a hadron are encoded in the following matrix element,

$$\left\langle \mathscr{H}(p') \left| \mathscr{J}_{\text{em}}^\mu(q^2) \right| \mathscr{H}(p) \right\rangle, \tag{234}$$

where $\mathscr{J}_{\text{em}}^\mu$ denotes the electromagnetic current and $\mathscr{H}$ is the hadron state. The transferred momentum is $q = p - p'$, with p and p' the 4-momenta of the initial and final states, respectively. The covariant expansion of Eq. (234) depends on the spins of the specified hadrons and is illustrated in Appendix C.

The proton and neutron are stable against the strong and electromagnetic decays. Their long lifetimes allow the direct measurements of their magnetic moments and charge radius [767, 768, 769, 770, 771, 772, 773, 774]. But for the other hadron states, it is generally hard to measure their magnetic moments directly in experiments due to their very short lifetimes. For example, the magnetic moment of the lightest vector meson ρ was extracted from the $e^+e^- \to \pi^+\pi^-\pi^0\pi^0$ process via an indirect way [775], in which the vector meson dominance model was adopted to describe the $\gamma^* \to 4\pi$ vertex. The charge radius of the pion was extracted from the analysis of the $e^+e^- \to \pi^+\pi^-$ data with the help of the dispersion relations [776]. In contrast to the magnetic moment, the radiative decays of the heavy hadrons are more accessible in experiments. For instance, the branching fraction of $D^{*0} \to D^0\gamma$ can reach up to $(35.3 \pm 0.9)\%$. For the D_s^*, B^* and B_s^* mesons, the radiative decays even dominate their decay modes.

For a lepton (e.g., electron and muon), the QED quantum fluctuations can introduce sizable and detectable corrections to its magnetic moment. If a hadron contains the light quarks u, d, s as its components, it will naturally couple to the light Goldstone bosons (such as π, K and η) due to the spontaneous breaking of chiral symmetry in low energy QCD. Apart from the QED, the chiral corrections (fluctuations of the light Goldstone bosons) will make considerable contributions to the magnetic moments.

In this section, we focus on the chiral corrections to the low energy electromagnetic properties (e.g. magnetic moments and electromagnetic decays) of the heavy hadrons within the HHχPT. The tree level and one-loop level Feynman diagrams are given in Fig. 19. The chiral order O of the diagrams in Fig. 19 is organized by the Weinberg power counting scheme in Eq. (67). The order of the (transition) magnetic moment is usually defined as
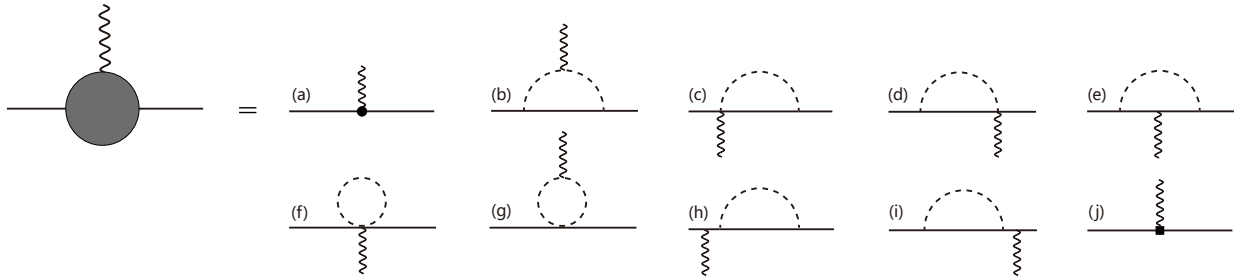
$$O_\mu = O - 1. \tag{235}$$

Figure 19: The tree level and one-loop level diagrams for the magnetic moments and radiative transitions of the heavy hadrons. Each one represents a set of diagrams that have the same topological structure. The solid, dashed and wiggly lines denote the heavy hadrons, light Goldstones and photon, respectively. The solid dot and solid square stand for the $O(p^2)$ and $O(p^4)$ vertices, respectively.

3.3.1. Heavy mesons

The magnetic moments of the charmed and bottom vector mesons were first calculated by Bose and Singh with the Bag model in 1980 [777]. Later, the extended Nambu-Jona-Lasinio model and Bag model were used to study the magnetic moments and radiative transitions of the ground-state vector mesons by Deng *et al* [778, 779] and Šimonis [780, 781], respectively. A systematic study in the framework of χPT up to $O(p^4)$ was performed by Wang *et al* in 2019 [753]. Very recently, Aliev *et al* also investigated the same entities with the light-cone QCD sum rules [782].

The radiative decays of the heavy vector meson $V \to P\gamma$ (V and P are the vector and pseudoscalar mesons, respectively.) were intensively studied in various quark models [783, 784, 785, 786, 787, 788, 789, 790, 791, 792, 793], quark potential models [777, 20, 794, 795, 780, 781], synthesis of heavy quark effective theory and vector meson dominance model [796], QCD sum rules [797, 798, 799, 800], extended Nambu-Jona-Lasinio model [778, 779], lattice QCD simulations [729] and χPT [801, 802, 803, 620, 742, 804, 805, 753]. In χPT, the magnetic moments and radiative transitions are deduced from the same Lagrangians with the same set of parameters. In what follows, we review the results obtained with χPT and summarize the results from other models in Table 3.

Owing to the synthetical development of χPT and HQET in 1990s [616, 688, 621, 690, 811], the electromagnetic interactions are gauged into the Lagrangians of HHχPT by Cho and Georgi [801], in which the LO [$O(p^2)$] contribution [corresponding to Fig. 19(a)] to the $\bar{D}^* \to \bar{D}\gamma$ decay is considered. It is described equivalently by the following Lagrangian,

$$\mathcal{L}_{H\gamma}^{(2)} = a\langle \tilde{\mathcal{H}} \sigma^{\mu\nu} \tilde{\bar{\mathcal{H}}} \rangle \operatorname{Tr}(f_{\mu\nu}^+) + \hat{a}\langle \tilde{\bar{\mathcal{H}}} \sigma^{\mu\nu} \hat{f}_{\mu\nu}^+ \tilde{\mathcal{H}} \rangle, \tag{236}$$

in which the formulations of $f_{\mu\nu}^+$ and $\hat{f}_{\mu\nu}^+$ are given in Eqs. (A.9) and (A.10), respectively. a and $\hat{a}$ are two independent LECs, standing for the coupling strengths of the photon with the heavy and light quark parts, respectively. Therefore, the first and second terms in Eq. (236) represent the heavy quark current and light quark current contributions, respectively. From the properties of the superfields in Eq. (A.25), the first term can flip the heavy spin which breaks the heavy quark spin symmetry and is suppressed by $1/m_Q$.

In the quark model, the transition M1 form factor of $V \to P\gamma$ can be parameterized as [753]

$$\mu'_{\bar{Q}q} = \mathcal{Q}_{\bar{Q}} \frac{1}{\Lambda_{\bar{Q}}} - \mathcal{Q}_q \frac{1}{\Lambda_q}, \tag{237}$$

where $\mathcal{Q}_{\bar{Q}}$ and $\mathcal{Q}_q$ are the charge matrices of the heavy anti-quark $\bar{Q}$ and light quark q, respectively. $\Lambda_{\bar{Q}}$ and Λ_q are the mass parameters that can be understood as the masses of the constituent quarks in the quark model. Heavy quark symmetry guarantees $\Lambda_{\bar{Q}} \approx m_{\bar{Q}}$ (see the discussions in Ref. [478]). In Ref. [753], Wang *et al* adopted the vector meson dominance (VMD) model [770, 796] to estimate the value of Λ_q. It turns out that $\Lambda_u = \Lambda_d = 0.366$ GeV, $\Lambda_s = 0.596$ GeV. These values are very close to the constituent quark masses m_u, m_d, and m_s which are usually adopted in the quark models.

Expanding Eq. (236) and comparing with Eq. (237) one obtains $a \sim 1/m_Q$ and $\hat{a} \sim 1/m_q$. In Ref. [801], Cho *et al* fixed the masses of the c and b quarks, while they left the light quark mass and axial coupling g_b to be determined from the branching ratios of $V \to P\pi$ and $V \to P\gamma$. Cheng *et al* also studied similar processes with the same framework [803], in which the a and $\hat{a}$ were determined from the constituent quark model. Along this line, Wang *et al* obtained [753]

$$a = \frac{1}{24m_Q}, \qquad \hat{a} = -\frac{1}{8m_q}. \tag{238}$$

The NLO contribution comes from the loop diagram in Fig. 19(b) and was first incorporated by Amundson *et al* [802]. In diagram 19(b), the relevant vertices are the $\mathcal{H}\varphi$ coupling from Eq. (124) and $\varphi\gamma$ coupling from Eq. (50), respectively. In principle, the diagrams in Fig. 19(c) and (d) also contribute at this order, but their contributions vanish in the heavy quark limit. We take the Fig. 19(c) as an example. If we are considering the $D^* \to D\gamma$ decay, then the intermediate heavy state is D^*. In this case, its amplitude

$$\mathcal{A} \propto \epsilon_{\mu\nu\alpha\beta} \varepsilon_{D^*}^\mu \varepsilon_\gamma^{*\alpha} v^\beta \int \frac{d^d\ell}{(2\pi)^d} \frac{i\ell_\rho}{\ell^2 - m_\varphi^2 + i\epsilon} \frac{-i(g^{\rho\nu} - v^\rho v^\nu)}{v \cdot \ell + i\epsilon} \sim \epsilon_{\mu\nu\alpha\beta} \varepsilon_{D^*}^\mu \varepsilon_\gamma^{*\alpha} v^\beta v_\rho(g^{\rho\nu} - v^\rho v^\nu) = 0, \tag{239}$$

Table 3: The radiative decay widths of the charmed and bottom vector mesons calculated in various approaches, where Γ^γ_V denotes the decay width of $V \to P\gamma$, while Γ_V represents the total width of meson V. The QM, VMD, QCDSR, NJL, LQCD, and χPT are abbreviations of quark model, vector meson dominance model, QCD sum rule, extended Nambu-Jona-Lasinio model, lattice QCD, and chiral perturbation theory, respectively. The averaged value in the last row is given as an average of the corresponding values calculated in the listed references. Since the pion emission decay for the bottom vector meson is kinematically forbidden, their widths are saturated by the radiative decays, i.e., we approximately have $\Gamma_{B^{*-}} \simeq \Gamma^\gamma_{B^{*-}}$, $\Gamma_{\bar{B}^{*0}} \simeq \Gamma^\gamma_{\bar{B}^{*0}}$ and $\Gamma_{\bar{B}^{*0}_s} \simeq \Gamma^\gamma_{\bar{B}^{*0}_s}$. Although the D^*_s can decay into $D_s\pi^0$ via isospin violating decay, its minor branching ratio [1] makes the approximation $\Gamma_{D^{*+}_s} \approx \Gamma^\gamma_{D^{*+}_s}$ reasonable. The values in this table are all given in units of keV.

Models	Charmed vector mesons						Bottom vector mesons			Refs.
	$\Gamma^\gamma_{D^{*0}}$	$\Gamma^\gamma_{D^{*+}}$	$\Gamma^\gamma_{D^{*+}_s}$	$\Gamma_{D^{*0}}$	$\Gamma_{D^{*+}}$	$\Gamma_{D^{*+}_s}$	$\Gamma^\gamma_{B^{*-}}$	$\Gamma^\gamma_{\bar{B}^{*0}}$	$\Gamma^\gamma_{\bar{B}^{*0}_s}$	
QM	~ 23	~ 0.9	~ 0.1	–	–	~ 0.1	–	–	–	[783]
	35.2	2.4	0.32	78.6	78.0	~ 0.32	1.7	0.5	0.2	[784]
	12.2	4.3	1.1	59.4	79.0	~ 1.1	–	–	–	[787][a]
	21.8	1.7	–	64.2	86.4	–	–	–	–	[788][b]
	17.9	0.36	0.1	56.0	80.5	~ 0.1	0.40	0.13	–	[789][c]
	21.7	0.56	–	65.1	92.0	–	0.43	0.14	–	[790]
	13.1	0.25	–	38.0	62.0	–	–	0.05	–	[791]
	$20.0^{+0.3}_{-0.3}$	$0.9^{+0.02}_{-0.02}$	$0.18^{+0.01}_{-0.01}$	55^{+6}_{-6}	Input [806]	$0.19^{+0.01}_{-0.01}$	$0.4^{+0.03}_{-0.03}$	$0.13^{+0.01}_{-0.01}$	$0.068^{+0.017}_{-0.017}$	[792]
	26.5	0.93	0.21	$99.8^{+19.5}_{-19.5}$	Input [807]	$0.32^{+0.06}_{-0.06}$	0.57	0.18	0.12	[793]
	26.0	0.94	0.2	67.6	94.3	~ 0.2	0.6	0.2	0.1	[794][d]
	11.5	1.04	0.19	–	–	–	0.19	0.07	0.054	[795]
	19.7	1.1	0.4	–	–	–	0.46	0.15	0.10	[780]
VMD	$16.0^{+12.5}_{-9.0}$	$0.51^{+0.69}_{-0.44}$	$0.24^{+0.24}_{-0.24}$	$36.7^{+9.7}_{-9.7}$	$46.1^{+14.2}_{-14.2}$	$\sim 0.24^{+0.24}_{-0.24}$	$0.22^{+0.09}_{-0.09}$	$0.075^{+0.027}_{-0.027}$	–	[796]
	$2.43^{+0.21}_{-0.21}$	$0.22^{+0.06}_{-0.06}$	$0.25^{+0.08}_{-0.08}$	~ 8	~ 12	~ 0.25	–	–	–	[797]
QCDSR	$3.7^{+1.2}_{-1.2}$	$0.09^{+0.40}_{-0.07}$	–	11^{+4}_{-4}	12^{+7}_{-7}	–	$0.10^{+0.03}_{-0.03}$	~ 0.04	–	[798]
	12.9^{+2}_{-2}	$0.23^{+0.1}_{-0.1}$	$0.13^{+0.05}_{-0.05}$	~ 36	~ 46	~ 0.13	$0.38^{+0.06}_{-0.06}$	$0.13^{+0.03}_{-0.03}$	$0.22^{+0.04}_{-0.04}$	[799][e]
NJL	19.4	0.7	0.09	65.9	124.8	~ 0.09	0.25	0.22	0.10	[778]
LQCD	27^{+14}_{-14}	0.8^{+7}_{-7}	–	68^{+17}_{-17}	Input [808]	–	–	–	–	[729]
	$8.8^{+17.1}_{-17.1}$	$8.3^{+8.1}_{-8.1}$	–	$50.6^{+61.9}_{-61.9}$	$97.0^{+95.6}_{-95.6}$	–	$0.66^{+0.93}_{-0.93}$	$0.13^{+0.20}_{-0.20}$	–	[801][f]
χPT	34	2	0.3	102	141	~ 0.3	0.84	0.28	–	[803]
	–	–	–	18	26	0.06	–	–	–	[742][g]
	$16.2^{+6.5}_{-6.0}$	$0.73^{+0.7}_{-0.3}$	$0.32^{+0.3}_{-0.3}$	$77.7^{+26.7}_{-20.5}$	Input [809]	$0.62^{+0.45}_{-0.50}$	$0.58^{+0.2}_{-0.2}$	$0.23^{+0.06}_{-0.06}$	$0.04^{+0.03}_{-0.03}$	[753][h]
Average[i]	18.5	1.4	0.3	55.6	71.8	~ 0.3	0.5	0.2	0.1	

[a] Radiative decays with zero anomalous moment for the charmed quark are quoted.
[b] The results in model (c) of Ref. [788] are quoted.
[c] The results calculated with constituent heavy quark masses $(m_c, m_b) = (1.6, 5.0)$ GeV are quoted.
[d] The results with $\kappa^q = 0.45$ are quoted.
[e] The D^{*0} and D^{*+} widths are inferred by combining the strong decays of those calculated in Ref. [810].
[f] We adopt the results calculated with constituent heavy quark masses $(m_c, m_b) = (1.7, 5.0)$ GeV.
[g] The results with uncertainties from experiment and counter terms are not quoted here.
[g] The results in SU(3) case with $\Delta \neq 0$ are quoted.
[i] Only the central values are used.

where ε_{D^*} and ε_γ denote the polarization vector of D^* and photon, respectively. v and ℓ represent the four-velocity in the superfield notation and the momentum in the loop, in order. One can consult Ref. [812] for the Lorentz structure of the loop integral in Eq. (239). Similar relation holds for the amplitude of Fig. 19(d).

In order to absorb the divergence of the loop correction for Fig. 19(b), Wang *et al* constructed the $O(p^3)$ Lagrangian [753],

$$\mathcal{L}_{H\gamma}^{(3)} = -ic\langle\tilde{\mathcal{H}}\sigma^{\mu\nu}\bar{\tilde{\mathcal{H}}}\rangle v\cdot\nabla\text{Tr}(f_{\mu\nu}^+) - i\hat{c}\langle\bar{\tilde{\mathcal{H}}}\sigma^{\mu\nu}v\cdot\nabla\hat{f}_{\mu\nu}^+\tilde{\mathcal{H}}\rangle. \tag{240}$$

But their contributions can be absorbed by renormalizing the LO LECs a and $\hat{a}$, i.e., $a \to a + cv\cdot q$ and $\hat{a} \to \hat{a} + \hat{c}v\cdot q$.

The Feynman diagrams (e)-(j) in Fig. 19 give the $O(p^4)$ contributions. The vertices in these diagrams are given above except those in diagrams 19(g) and (j). For the diagram 19(g), the $O(p^2)$ two-pion coupling vertex is given by [753]

$$\mathcal{L}_{H\varphi\varphi}^{(2)} = ib\langle\bar{\tilde{\mathcal{H}}}\sigma^{\mu\nu}[u_\mu, u_\nu]\tilde{\mathcal{H}}\rangle, \tag{241}$$

where b is the coupling constant, and its value was phenomenologically determined through the VMD model in Ref. [753]. As the u_μ transforms as an adjoint representation, one may have three terms $\text{Tr}(u_\mu u_\nu)$, $[u_\mu, u_\nu]$ and $\{u_\mu, u_\nu\}$ (they belong to the $\mathbf{1}$, $\mathbf{8}_1$ and $\mathbf{8}_2$ flavor representations, respectively) sandwiched in the paired $\bar{\tilde{\mathcal{H}}}$ and $\tilde{\mathcal{H}}$. However, $\text{Tr}(u_\mu u_\nu)$ and $\{u_\mu, u_\nu\}$ vanish when contracted with $\sigma^{\mu\nu}$ due to their symmetrized Lorentz index. Therefore, only one single term remains in Eq. (241). The general principles to construct the independent Lagrangians are discussed in Appendix A.

The tree-level diagram at $O(p^4)$ in Fig. 19(j) is governed by the following Lagrangians [753],

$$\mathcal{L}_{H\gamma}^{(4)} = \hat{d}\langle\tilde{\mathcal{H}}\sigma^{\mu\nu}\hat{\chi}_+\bar{\tilde{\mathcal{H}}}\rangle\text{Tr}(f_{\mu\nu}^+) + \bar{d}\langle\bar{\tilde{\mathcal{H}}}\sigma^{\mu\nu}\tilde{\mathcal{H}}\rangle\text{Tr}(\hat{f}_{\mu\nu}^+\hat{\chi}_+) + d\langle\bar{\tilde{\mathcal{H}}}\sigma^{\mu\nu}\{\hat{\chi}_+, \hat{f}_{\mu\nu}^+\}\tilde{\mathcal{H}}\rangle, \tag{242}$$

in which the spurion $\hat{\chi}_+$ introduces the SU(3) flavor breaking effect. There are six types of flavor structures constructed with the χ_+ and $f_{\mu\nu}^+$ as listed in Table A.10, but not all of them survive in the Lagrangians. For example, $\text{Tr}(\chi_+)\hat{f}_{\mu\nu}^+$ and $\text{Tr}(\chi_+)\text{Tr}(f_{\mu\nu}^+)$ are assimilated into the $O(p^2)$ Lagrangians (236), thus can be replaced by renormalizing $\hat{a}$ and a, respectively. Besides, both $\hat{\chi}_+$ and $\hat{f}_{\mu\nu}^+$ are diagonal matrices at the LO, which makes the leading term of the $[\hat{\chi}_+, \hat{f}_{\mu\nu}^+]$ vanish after the expansion. Therefore, only three terms survive in Eq. (242) eventually.

Summing up the contributions of all the diagrams in Fig. 19 with all possible intermediate states, one obtains the (transition) magnetic moments of the corresponding vector states (see the analytical expressions in Ref. [753]). In Refs. [801, 803], Cho *et al* and Cheng *et al* calculated the decay widths of $D^* \to D\gamma$ and $B^* \to B\gamma$ at the tree level in HHχPT, respectively. The Lagrangians of Ref. [753] are the same as those in Refs. [801, 803] at the LO. In Ref. [802], Amundson *et al* investigated the same process with the same framework to the NLO, but the heavy quark spin symmetry breaking effect was ignored. In heavy quark limit ($a \to 0$), they found $\mu_V^u : \mu_V^d : \mu_V^s = 2 : -1 : -1$ for the LO results. This ratio relation still holds when the loop corrections are included in the strict SU(3) symmetry [neglecting the mass splitting of SU(3) multiplets] [753, 802, 805]. In particular, the authors of Ref. [753] noticed $|\mu_V| = |\mu_{V\to P\gamma}|$ in the heavy quark limit by taking mass splittings $\delta_b = 0$ in the loops. Because the heavy quark spin completely decouples in the heavy quark limit, the $VV\gamma$ and $VP\gamma$ three point Green functions depict the same light quark dynamics. In a more realistic calculation, the authors of Ref. [753] further showed that the HQSS breaking effect (the physical value of δ_b is used in loop integrals) can induce sizable corrections, especially for the charmed vector mesons, see Table 4.

In Ref. [742], Stewart calculated the decays $D^* \to D\pi$ and $D^* \to D\gamma$ up to the one-loop level within HHχPT, in which the $\mathcal{B}(D^{*+} \to D^+\gamma)$ as well as the ratios of the $D\gamma$ and $D\pi^0$ branching fractions were used to extract the $D^*D\pi$ and $D^*D\gamma$ couplings. The $D^*D\pi$ coupling g_b is determined to be around 0.3, which is close to the current value from the $D^{*+} \to (D\pi)^+$ partial widths.

In addition to the ground state vector states, the excited heavy mesons were also systematically studied in the HHχPT [615, 619, 813, 814, 815, 682, 816]. The radiative decay $D_{s0}^*(2317) \to D_s^*\gamma$ was firstly studied by Colangelo *et al* with the HQS and VMD ansatz [816]. They obtained $\Gamma(D_{s0}^* \to D_s^*\gamma) \simeq 1$ keV (decaying to $D_s\gamma$ is forbidden due to the angular momentum and parity conservation). In Ref. [657], Mehen and Springer studied the electromagnetic decays of the $D_{s0}^*(2317)$ and $D_{s1}(2460)$ in HHχPT considering the chiral loop corrections and HQSS breaking effect.

Table 4: The magnetic moments of the charmed and bottom vector mesons (in units of nucleon magnetons μ_N) calculated with the χPT, Bag model (Bag), extended Bag model (eBag), extended Nambu-Jona-Lasinio model (NJL) and light-cone QCD sum rules (LCSR), respectively. The results from χPT are given in SU(2) and SU(3) symmetries as well as in the cases of the mass splittings $\Delta = 0$ and $\Delta \neq 0$, respectively.

States	SU(2)		SU(3)		The results from other theoretical works			
	$\Delta = 0$	$\Delta \neq 0$	$\Delta = 0$	$\Delta \neq 0$	Bag [777]	eBag [781]	NJL [779]	LCSR [782]
D^{*0}	$-1.38^{+0.25}_{-0.25}$	$-1.60^{+0.25}_{-0.25}$	$-1.18^{+0.25}_{-0.25}$	$-1.48^{+0.38}_{-0.22}$	-0.89	-1.28	$-$	$0.30^{+0.04}_{-0.04}$
D^{*+}	$1.14^{+0.15}_{-0.15}$	$1.39^{+0.15}_{-0.15}$	$1.31^{+0.15}_{-0.20}$	$1.62^{+0.08}_{-0.24}$	1.17	1.13	1.16	$1.16^{+0.08}_{-0.08}$
D_s^{*+}	$-$	$-$	$0.62^{+0.15}_{-0.15}$	$0.69^{+0.10}_{-0.22}$	1.03	0.93	0.98	$1.00^{+0.14}_{-0.14}$
B^{*-}	$-1.86^{+0.25}_{-0.25}$	$-1.90^{+0.20}_{-0.20}$	$-1.71^{+0.25}_{-0.25}$	$-1.77^{+0.30}_{-0.25}$	-1.54	-1.56	-1.47	$-0.90^{+0.19}_{-0.19}$
$\bar{B}^{*0}$	$0.75^{+0.11}_{-0.11}$	$0.78^{+0.11}_{-0.11}$	$0.87^{+0.11}_{-0.13}$	$0.92^{+0.11}_{-0.15}$	0.64	0.69	$-$	$0.21^{+0.04}_{-0.04}$
$\bar{B}_s^{*0}$	$-$	$-$	$0.25^{+0.11}_{-0.11}$	$0.27^{+0.10}_{-0.13}$	0.47	0.51	$-$	$0.17^{+0.02}_{-0.02}$

In the compact meson scenario, the tree level contribution for $\{0^+, 1^+\} \to \{0^-, 1^-\}\gamma$ is mediated by the light quark current coupling with the photon, the Lagrangian reads

$$\mathcal{L}_{\mathcal{SH}\gamma} = \hat{\beta}\langle \mathcal{S}\sigma^{\mu\nu}\hat{f}_{\mu\nu}^+\bar{\mathcal{H}}\rangle. \tag{243}$$

The HQSS violating operators at $O(1/m_c)$ are constructed for the $\mathcal{S} \to \mathcal{H}\gamma$ decay as

$$\mathcal{L} = i\beta' \epsilon^{\mu\nu\alpha\beta}\langle\bar{\mathcal{H}}\sigma_{\mu\nu}\mathcal{S}\gamma_5\rangle\text{Tr}(f_{\alpha\beta}^+) + i\beta''\langle\bar{\mathcal{H}}\sigma^{\mu\nu}\mathcal{S}\gamma^\alpha\rangle\partial_\alpha\text{Tr}(f_{\mu\nu}^+) + \text{H.c.}, \tag{244}$$

where the β' and β'' are proportional to $1/m_c$. The NLO corrections receive contributions from Eq. (244) and the loop diagrams in Fig. 19(b)-(d) with the possible intermediate states in the loops (see Ref. [657]).

For convenience, we define three ratios of the branching fractions for the $\{0^+, 1^+\} \to \{0^-, 1^-\}\gamma$ and $\{0^+, 1^+\} \to \{0^-, 1^-\}\pi$ decays:

$$\mathcal{R}_1 = \frac{\text{Br}\left[D_{s1}(2460) \to D_s^*\gamma\right]}{\text{Br}\left[D_{s1}(2460) \to D_s^*\pi^0\right]}, \quad \mathcal{R}_2 = \frac{\text{Br}\left[D_{s1}(2460) \to D_s\gamma\right]}{\text{Br}\left[D_{s1}(2460) \to D_s^*\pi^0\right]}, \quad \mathcal{R}_3 = \frac{\text{Br}\left[D_{s0}^*(2317) \to D_s^*\gamma\right]}{\text{Br}\left[D_{s0}^*(2317) \to D_s\pi^0\right]}, \tag{245}$$

in which only the $\mathcal{R}_2$ was measured to certain ranges by the Belle Collaboration

$$\mathcal{R}_2 = \begin{cases} 0.38 \pm 0.11 \pm 0.04 \text{ [817]} \\ 0.55 \pm 0.13 \pm 0.08 \text{ [24]} \end{cases}, \tag{246}$$

while for the $\mathcal{R}_1$ and $\mathcal{R}_3$ only the upper limits were estimated with given confidence level [1]. For example, the bounds quoted by the CLEO Collaboration [23]

$$\text{CLEO bounds [23]}: \ \mathcal{R}_1 < 0.16, \qquad \mathcal{R}_3 < 0.059. \tag{247}$$

In the compact-meson scenario, Mehen and Springer [657] calculated the $\mathcal{R}_1$ and $\mathcal{R}_3$ within the LO HHχPT [the $\mathcal{R}_2$ was used as input to determine the $\hat{\beta}$ in Eq. (243)], but the results exceed the CLEO bounds significantly. The ratios can be made consistent with the CLEO bounds when the NLO contributions are included (in which the corresponding LECs are of natural size). They also investigated the electromagnetic decays of the $D_{s0}^*(2317)$ and $D_{s1}(2460)$ and assumed these states are the DK and D^*K hadronic molecules with $I = 0$, respectively. In the molecular scenario, they obtained [657]

$$\mathcal{R}_1 = 3.23, \qquad \mathcal{R}_2 = 2.21, \qquad \mathcal{R}_3 = 2.96. \tag{248}$$

In a recent study [818], Fu et al studied the ratios in the molecular scenario and obtained

$$\mathcal{R}_1 = 0.12 \pm 0.02, \qquad \mathcal{R}_2 = 0.38(\text{fixed}) \pm 0.08, \qquad \mathcal{R}_3 = 0.028 \pm 0.009, \tag{249}$$

in which the central value of $\mathcal{R}_2$ [817] was also used as input to fix the LO counter term in the radiative decays. One can see the ratios obtained from Ref. [818] are about one order of magnitude smaller than those from Ref. [657]. The authors of Ref. [818] considered the extra NLO isospin violating vertices which enhance the strong decay widths of the charmed-strange mesons significantly. A similar investigation was performed by Lutz [762] and Guo [763] to study the decays of the $D^*_{s0}(2317)$ and $D_{s1}(2460)$, as well as the effective Lagrangian approach in Refs. [46, 819].

3.3.2. Singly heavy baryons

As the heavy flavor siblings of the nucleons, the electromagnetic properties of the singly heavy baryons at low energies are sensitive to their inner constituents, structures and corresponding chiral dynamics of the light diquarks. The experimentalists are trying to measure the charm baryon dipole moments (particularly Λ^+_c, Ξ^+_c) at LHC [820]. Before giving the systematic applications of χPT to the electromagnetic properties of the singly heavy baryons, we first briefly review the works from other frameworks in this field. The electromagnetic properties of the singly heavy baryons have been studied with the bag models [777, 781, 821, 822, 823], the various quark models [824, 825, 826, 827, 828, 829, 830, 831, 832, 84, 833], the QCD sum rules [834, 835, 836, 837, 838, 839, 840], the hyper central model [841], the Skyrme model [842, 843], the pion mean-field approach [844, 845, 846], and the bound-state approach [847]. Meanwhile, the *ab initio* calculations in lattice QCD have been performed to investigate the electromagnetic properties of the singly heavy baryons. For example, in Refs. [848, 849], Bahtiyar *et al* studied the $\Omega^*_c \rightarrow \Omega_c \gamma$ and $\Xi'_c \rightarrow \Xi_c \gamma$ transitions in $2+1$-flavor lattice QCD, where the radiative decay widths, electric and magnetic form factors, as well as the magnetic moments are computed (see also [850, 851] for the charmed and charmed-strange baryons).

The χPT was systematically applied to the radiative decays and magnetic moments of the singly heavy baryons in a series of works [803, 852, 853, 854, 855, 856, 857, 624, 858, 859]. The LO calculations were done by Cheng *et al* [803], in which the decay rates of $\Xi'_c \rightarrow \Xi_c \gamma$, $\Sigma_c \rightarrow \Lambda_c \gamma$ and $\Sigma_c \rightarrow \Lambda_c \pi \gamma$ were calculated. The LECs in the chiral Lagrangians were estimated with the constituent quark model, which paved a way for latter works to determine the LECs [753, 856, 857, 624, 858]. Cho extended the chiral Lagrangians to the P-wave $\bar{\mathbf{3}}$ baryons (with the orbital excitation between the heavy quark and light diquark pair, i.e., $j_\ell = 1$, in which the $J^P = \frac{1}{2}^-$ and $\frac{3}{2}^-$ doublets are described with the superfield $\mathcal{R}_{\mu i} = 1/\sqrt{3}(\gamma^\mu + v^\mu)\gamma^5 \mathcal{R}_i + \mathcal{R}^*_{\mu i}$ [852]. The LO expressions for the one-pion, di-pion and one-photon transitions are presented. Savage investigated the magnetic dipole (M1) and electric quadrupole (E2) contributions to the $\Sigma^*_c \rightarrow \Lambda_c \gamma$ process [853]. The E2 contribution in the process of $j_\ell = 1$ to $j_\ell = 0$ is $1/m_c$ suppressed and vanishes in the heavy quark limit. Savage found that the E2 contribution is actually enhanced by a small energy denominator arising from the infrared behaviour of the pion loop graphs, which compensates the suppression and yields a few percent amplitude ratio for $\mathcal{A}_{E2}/\mathcal{A}_{M1}$ (this ratio is also affected by the mass splitting of the Σ^*_c and Σ_c). Bañuls *et al* calculated the $B_6 \rightarrow B_{\bar{\mathbf{3}}} \gamma$, $B_{6^*} \rightarrow B_{\bar{\mathbf{3}}} \gamma$ and $B_{6^*} \rightarrow B_6 \gamma$ decays up to NLO [854], where the magnetic dipole and electric quadrupole contributions were separately computed. Tiburzi studied the same process in a partially quenched approach [855], which allows the pion mass extrapolation and the zero-momentum extrapolation in lattice QCD. The updated calculations to higher orders were performed in Refs. [856, 857, 624, 858]. Here we follow the notations in these references to review how the χPT is employed to study the electromagnetic properties of the heavy baryons.

The chiral Lagrangians contributing to the electromagnetic properties of the singly heavy baryons were constructed in Ref. [856] with the field $B_{\bar{\mathbf{3}}}$, B_6 and B_{6^*} fields. Wang *el al* found the number of LECs can be largely reduced in the superfield formalism with the HQSS [857, 624, 858]. The superfield ψ^μ_Q for the singly heavy baryons is given in Eq. (A.30). A similar form was obtained by Cheng *et al* [803] in heavy quark symmetry and quark model calculation. The LO Lagrangians that contribute to Fig. 19(a) read

$$\begin{aligned}
\mathcal{L}^{(2)}_{\psi_Q \gamma} &= i\kappa_1 \text{Tr}(\bar{\psi}^\mu_Q \hat{f}^+_{\mu\nu} \psi^\nu_Q) + \kappa'_1 \text{Tr}(\bar{\psi}^\lambda_Q \sigma^{\mu\nu} \psi_{Q\lambda}) \text{Tr}(f^+_{\mu\nu}) + \kappa_2 \epsilon^{\mu\nu\alpha\beta} \text{Tr}(\bar{\psi}_{Q\mu} \hat{f}^+_{\alpha\beta} v_\nu B_{\bar{\mathbf{3}}}) + \text{H.c.} \\
&\quad + \kappa'_2 i \text{Tr}(\bar{B}_{\bar{\mathbf{3}}} \gamma^\nu \gamma^5 \psi^\mu_Q) \text{Tr}(f^+_{\mu\nu}) + \text{H.c.} + \kappa'_3 \text{Tr}(\bar{B}_{\bar{\mathbf{3}}} \sigma^{\mu\nu} B_{\bar{\mathbf{3}}}) \text{Tr}(f^+_{\mu\nu}),
\end{aligned} \tag{250}$$

where the $\kappa_{1,2}$ and $\kappa'_{1,2,3}$ terms denote the contributions from the light quark current and heavy quark current, respectively. The $\kappa'_{1,2,3}$ terms can flip the spin of the heavy quark and break heavy quark spin symmetry. There is no contribution from the light quarks for the $B_{\bar{\mathbf{3}}} B_{\bar{\mathbf{3}}} \gamma$, because the spin of the light diquark in the flavor anti-triplet is zero. The $O(p^2)$ di-pion coupling vertices of the heavy baryons in Fig. 19(g) are depicted by

$$\mathcal{L}^{(2)}_{\psi_Q \varphi \varphi} = \kappa_4 \text{Tr}(\bar{\psi}^\mu_Q [u_\mu, u_\nu] \psi^\nu_Q) + i\kappa'_4 \text{Tr}(\bar{B}_{\bar{\mathbf{3}}} \sigma^{\mu\nu} [u_\mu, u_\nu] B_{\bar{\mathbf{3}}}) + i\kappa_5 \epsilon^{\sigma\mu\nu\rho} \text{Tr}(\bar{B}_{\bar{\mathbf{3}}} [u_\mu, u_\nu] v_\rho \psi_{Q\sigma}) + \text{H.c.}$$

$$+i\kappa_6 \, \text{Tr}(\bar{B}_{\bar{3}ab}\epsilon^{\sigma\mu\nu\rho}u_{i\mu}^b u_{j\nu}^a v_\rho \psi_{Q\sigma}^{ij}) + \text{H.c.}. \tag{251}$$

Most of the $O(p^3)$ Lagrangians can be absorbed by renormalizing the $O(p^2)$ ones. The remaining terms may contribute to the lowest-order E2 transitions (see the discussions in Ref. [858]), which read,

$$\mathcal{L}_{\psi_Q\gamma}^{(3)} = n_1 \, \text{Tr}(\bar{B}_3 \nabla_\lambda \tilde{f}_{\mu\nu}^+ S^\lambda v^\mu B_{6^*}^\nu) + m_1 \, \text{Tr}(\bar{B}_6 \nabla_\lambda \tilde{f}_{\mu\nu}^+ S^\lambda v^\mu B_{6^*}^\nu) + \tilde{m}_1 \, \text{Tr}[\bar{B}_6 S^\lambda v^\mu B_{6^*}^\nu] \nabla_\lambda \, \text{Tr}(f_{\mu\nu}^+) + \text{H.c.} + \dots. \tag{252}$$

At N^{2}LO, the Lagrangians for the tree-level transitions in Fig. 19(j) were constructed as

$$\mathcal{L}_{\psi_Q\gamma}^{(4)} = i\kappa_7 \, \text{Tr}(\bar{\psi}_{Q\mu}^{ab}\{\chi_+, \hat{f}_{\mu\nu}^+\}_{ab}^{ij} \psi_{Qij}^\nu) + \kappa_8 \, \text{Tr}(\bar{\psi}_Q^\lambda \chi_+ \sigma^{\mu\nu} \psi_{Q\lambda}) \, \text{Tr}(f_{\mu\nu}^+). \tag{253}$$

In Refs. [854, 857], the Coleman-Glashow relations [860] were obtained at $O(p^2)$ for the singly heavy baryons, which is analogous to that of the octet baryons [861, 862, 863]. But these relations are broken when higher order contributions are involved [857]. The $O(p^4)$ calculations were performed in Refs. [857, 624, 858], in which the LECs were estimated either from the quark model or fitting the results of lattice QCD simulations (one can also consult Refs. [857, 624, 858] for the summarized results from their calculations and the other models). Besides, they also discussed how the inclusion of the $\bar{3}$ baryons as the intermediate states in the loops affects the convergence of the chiral expansion [857, 624, 858].

3.3.3. Doubly heavy baryons

Among the doubly heavy baryons, only the Ξ_{cc}^{++} was observed in experiments [174]. The electromagnetic properties of the doubly heavy baryons have been investigated in various quark models [828, 830, 833, 864, 865, 866, 186, 867, 868], the bag model [777, 821], the Skyrme model [842], the light-cone QCD sum rule [869, 870], and lattice QCD [850, 871].

The HHχPT was used to study the magnetic moments of the spin-$\frac{1}{2}$ [711, 872] and spin-$\frac{3}{2}$ [873] doubly charmed and bottom baryons, as well as the radiative transitions from the spin-$\frac{3}{2}$ to spin-$\frac{1}{2}$ states [874]. The transition amplitudes were calculated up to N^{2}LO in these works, while the numerical results were presented up to NLO, because the LECs at N^{2}LO cannot be fixed well. As for the heavy mesons, the spin-$\frac{1}{2}$ and spin-$\frac{3}{2}$ states can be incorporated in the superfield notations [see the superfield ψ_{QQ}^μ of the doubly heavy baryons in Eq. (A.33)]. The LO Lagrangians for the electromagnetic interaction read

$$\mathcal{L}_{\psi_{QQ}\gamma}^{(2)} = ia'\bar{\psi}_{QQ}^\mu \psi_{QQ}^\nu \text{Tr}(f_{\mu\nu}^+) + \hat{a}'\bar{\psi}_{QQ}^\rho \sigma^{\mu\nu}\hat{f}_{\mu\nu}^+ \psi_{QQ}^\rho, \tag{254}$$

while the NLO dipion Lagrangian reads

$$\mathcal{L}_{\psi_{QQ}\varphi\varphi}^{(2)} = ib'\bar{\psi}_{QQ}^\mu [u_\rho, u_\sigma]\sigma^{\rho\sigma} g_{\mu\nu}\psi_{QQ}^\nu. \tag{255}$$

The N^{2}LO electromagnetic coupling Lagrangians read

$$\mathcal{L}_{\psi_{QQ}\gamma}^{(4)} = i\hat{d}'\bar{\psi}_{QQ}^\mu \hat{\chi}_+ \psi_{QQ}^\nu \text{Tr}(f_{\mu\nu}^+) + \bar{d}'\bar{\psi}_{QQ}^\rho \sigma^{\mu\nu}\psi_{QQ\rho} \text{Tr}(\hat{f}_{\mu\nu}^+ \hat{\chi}_+) + d'\bar{\psi}_{QQ}^\rho \sigma^{\mu\nu}\{\hat{f}_{\mu\nu}^+, \hat{\chi}_+\}\psi_{QQ\rho}. \tag{256}$$

One can see that the structures in Eqs. (254)-(256) are analogous to those for the heavy mesons in Sec. 3.3.1.

In Ref. [711], Li *et al* calculated the magnetic moments of the spin-$\frac{1}{2}$ doubly heavy baryons. The LO tree level contributions as well as the axial coupling $\tilde{g}_b$ are estimated from the quark model. However, the spin-$\frac{3}{2}$ states were not included as the intermediate states of the loops. An improved calculation was performed in Ref. [872], in which the spin-$\frac{3}{2}$ baryons as the intermediate states were considered. They found that the magnetic moment of the Ξ_{cc}^{++} changes acutely from $-0.25\mu_N$ to $0.35\mu_N$ (but note that the positive value is contradictory with the results in other works), and the changes for the magnetic moments of the Ξ_{cc}^+ and Ω_{cc}^+ were also very significant. The magnetic moments of the spin-$\frac{3}{2}$ doubly heavy baryons were calculated in Ref. [873]. The mass splittings of the spin-$\frac{1}{2}$ and spin-$\frac{3}{2}$ doubly heavy baryons are not fixed in experiments, thus a model dependent value was adopted in Refs. [872, 873]. The results in Ref. [873] are compatible with most of the other approaches. The radiative transitions from the spin-$\frac{3}{2}$ to spin-$\frac{1}{2}$ doubly heavy baryons were calculated in Ref. [874], in which the radiative decay widths of the spin-$\frac{3}{2}$ states were estimated to be

$$\Gamma[\Xi_{cc}^{*++} \to \Xi_{cc}^{++}\gamma] = 22.0 \, \text{keV}, \qquad \Gamma[\Xi_{cc}^{*+} \to \Xi_{cc}^+\gamma] = 9.57 \, \text{keV}, \qquad \Gamma[\Omega_{cc}^{*+} \to \Omega_{cc}^+\gamma] = 9.45 \, \text{keV}. \tag{257}$$

A covariant version of χPT with the extended-on-mass-shell renormalization scheme [514] was employed for the doubly heavy baryons in Refs. [875, 876, 164]. In Refs. [875, 876], the authors calculated the magnetic moments of the spin-$\frac{1}{2}$ ones via fitting the lattice data [850, 851, 871]. Since the lattice data were only available for the Ξ_{cc}^+ and Ω_{cc}^+, the two LECs at LO cannot be fixed simultaneously. In Ref. [875], the axial coupling was fixed either by quark model or heavy diquark-antiquark symmetry [506], or fitting the lattice data. By fitting the lattice data, they obtained a relatively smaller axial coupling than that predicted by either the quark model [711] or the heavy diquark-antiquark symmetry [876]. The finite volume effect was not considered in these two works [711, 876]. The follow-up calculations for the spin-$\frac{3}{2}$ ones were provided in Ref. [164], in which the magnetic moments of the spin-$\frac{3}{2}$ doubly charmed baryons as a function of m_π^2 were predicted. The spin-$\frac{3}{2}$ states have not been observed yet. Therefore, the results in all above mentioned works strongly depend on the phenomenological model calculations, such as the mass splittings between the spin-$\frac{3}{2}$ and spin-$\frac{1}{2}$ states appearing in the loops, or the axial coupling constant.

4. Scattering of the Goldstone bosons and heavy hadrons

In this section, we review the theoretical progresses about the scattering of the light Goldstone mesons off the heavy flavor hadrons. In Sec. 4.1, we first review the perturbative calculations of the scattering amplitude for the scattering of the light Goldstone boson off the heavy mesons in χPT. Then we will review the application of the chiral unitary approaches (discussed in Sec. 2.5) to uncover the nature of the $D_{s0}^*(2317)$ and $D_{s1}(2460)$ and related states in Sec. 4.2. We focus on the nonpertubative calculations with the chiral unitary approaches, which incorporate both the low energy dynamics governed by the χPT and the unitary condition in a coupled-channel framework. In Sec. 4.2.1, the scattering amplitudes in χPT are employed as the kernel interactions. The $D_{s0}^*(2317)$ and $D_{s1}(2460)$ are identified as the dynamically generated poles originating from the resummations of the $\mathcal{H}\varphi$ interactions, and are interpreted as the $D^{(*)}K$ molecules. In Sec. 4.2.2, the $c\bar{s}$ cores are included in addition to the $D^{(*)}K$ scattering potential. In Sec. 4.2.3, the two-pole structures of the non-strange charmed mesons in the chiral unitary approaches with the SU(3) flavor symmetry are reviewed. With the HDAS symmetry, the scatterings of the light Goldstone boson off the heavy mesons and doubly heavy baryons are related to each others. In Sec. 4.3, we review the scattering of the light Goldstone mesons off the doubly heavy baryons with the similar frameworks.

4.1. Perturbative scattering amplitude in χPT

We choose the scattering $\mathcal{H}(p_1)\varphi(p_2) \to \mathcal{H}(p_3)\varphi(p_4)$ ($\mathcal{H}$ and φ are the heavy and light mesons, respectively) as an example. The Mandelstam variables are defined as

$$s = (p_1 + p_2)^2, \qquad t = (p_1 - p_3)^2, \qquad u = (p_1 - p_4)^2, \tag{258}$$

where p_i is the momentum of the scattering meson. The power counting rules are

$$m_\mathcal{H} \sim O(p^0), \quad m_\varphi \sim O(p^1), \quad t \sim O(p^2), \quad s - m_\mathcal{H}^2 \sim O(p^1), \quad u - m_\mathcal{H}^2 \sim O(p^1), \tag{259}$$

with p the typical small momentum in the chiral expansion. $m_\mathcal{H} = m_{P/P^*}$ and m_φ denote the masses of the heavy and light mesons, respectively. In the χPT, the naive power counting rule is listed in Eq. (54). As discussed in Sec. 2.3, the $m_\mathcal{H}$ breaks the naive power counting rule in calculating the $\mathcal{H}\varphi$ scattering amplitude. If one adopts Eq. (259), the loop integrals in the relativistic formalism contain the power counting breaking terms which have the lower chiral order than those given by Eq. (54). To deal with the PCB terms, many regularization approaches have been developed. The most well-known ones are the HHχPT, extended on-mass-shell and infrared regularization schemes as discussed in Sec. 2.3.

In the HHχPT, the heavy components of the matter fields are integrated out and only the masses of the light Goldstone mesons appear in the loop calculation. Thus, the PCB terms disappear in the chiral expansion when the heavy hadron mass approaches infinity. At the same time, the Lagrangians in HHχPT are also organized by the inverse of the heavy hadron mass ($1/m_\mathcal{H}$) and the contributions of the heavy components are at least $O(1/m_\mathcal{H})$, which are usually suppressed and can be included as the recoiling corrections. In the heavy meson limit, the pseudoscalar and the vector heavy mesons are degenerate and can be treated as the same spin doublet as shown in Sec. 2.6. The Lagrangians for the $\mathcal{H}\varphi$ scattering read

$$\mathcal{L}_{\mathcal{H}\varphi} = \mathcal{L}_{\varphi\varphi}^{(2)} + \mathcal{L}_{\mathcal{H}\varphi}^{(1)} + \mathcal{L}_{\mathcal{H}\varphi}^{(2)} + \mathcal{L}_{\mathcal{H}\varphi}^{(3)} + \dots, \tag{260}$$

where the numbers in the superscripts denote the chiral orders. The ellipsis represents the higher order Lagrangians. The LO Lagrangian for the pseudoscalar mesons $\mathcal{L}_{\varphi\varphi}^{(2)}$ is given in Eq. (43). In the HHχPT, the LO Lagrangian $\mathcal{L}_{\mathcal{H}\varphi}^{(1)}$ is given in Eq. (50). The NLO and N^{2}LO Lagrangians read [39, 877, 878, 879] [10]

$$
\begin{aligned}
\mathcal{L}_{\mathcal{H}\varphi}^{(2)} &= c_0 \left\langle \mathcal{H}\bar{\mathcal{H}} \right\rangle \mathrm{Tr}\,(\chi_+) + c_1 \left\langle \mathcal{H}\chi_+\bar{\mathcal{H}} \right\rangle - c_2 \left\langle \mathcal{H}\bar{\mathcal{H}} \right\rangle \mathrm{Tr}\left(u^\mu u_\mu\right) - c_3 \left\langle \mathcal{H}u^\mu u_\mu \bar{\mathcal{H}} \right\rangle \\
&\quad - c_4 \left\langle \mathcal{H}\bar{\mathcal{H}} \right\rangle \mathrm{Tr}\,(v\cdot u v\cdot u) - c_5 \left\langle \mathcal{H}v\cdot u v\cdot u\bar{\mathcal{H}} \right\rangle,
\end{aligned}
\tag{261}
$$

$$
\mathcal{L}_{\mathcal{H}\varphi}^{(3)} = k_1 \left\langle \mathcal{H}\left[\chi_-, v\cdot u\right]\bar{\mathcal{H}} \right\rangle + ik_2 \left\langle \mathcal{H}\left[u^\mu,[v\cdot\partial, u_u]\right]\bar{\mathcal{H}} \right\rangle + ik_3 \left\langle \mathcal{H}\left[v\cdot\mu,[v\cdot\partial, v\cdot u]\right]\bar{\mathcal{H}} \right\rangle,
\tag{262}
$$

where the k_2 and k_3 terms are not given explicitly in Refs. [877, 878] since they can be absorbed by the k_1 term at the threshold. The $\mathcal{H}\varphi$ scattering amplitude up to N^{2}LO is given by

$$
\mathcal{A}(s,t) = \mathcal{A}_{\mathrm{LO}}^{(\mathrm{WT})}(s,t) + \mathcal{A}_{\mathrm{LO}}^{(\mathrm{EX})} + \mathcal{A}_{\mathrm{NLO}}^{(\mathrm{Tree})} + \mathcal{A}_{\mathrm{N}^2\mathrm{LO}}^{(\mathrm{Tree})} + \mathcal{A}_{\mathrm{N}^2\mathrm{LO}}^{(\mathrm{Loop})}.
\tag{263}
$$

The corresponding tree and loop Feynman diagrams are shown in Fig. 20, and Figs. 21-22, respectively.

At LO [$O(p)$], the diagram (a) in Fig. 20 stems from the chiral connection term in $\mathcal{L}_{\mathcal{H}\varphi}^{(1)}$ and yields the famous Weinberg–Tomozawa (WT) term [880, 881].

$$
\mathcal{A}_{\mathrm{LO}}^{(\mathrm{WT})} = C_{\mathrm{LO}}\frac{s-u}{4f_\varphi^2},
\tag{264}
$$

where C_{LO} is the flavor coefficient for the different scattering process. The tree diagrams (b) and (c) in Fig. 20 arise from the axial-vector coupling term in $\mathcal{L}_{\mathcal{H}\varphi}^{(1)}$. They contribute to the s- and u-channel exchanging amplitude $\mathcal{A}_{\mathrm{LO}}^{(\mathrm{EX})}$. Compared to $\mathcal{A}_{\mathrm{LO}}^{(\mathrm{WT})}$, the $\mathcal{A}_{\mathrm{LO}}^{(\mathrm{EX})}$ is suppressed by $1/m_\mathcal{H}$ and vanishes in the heavy meson limit. At the threshold, the $\mathcal{A}_{\mathrm{LO}}^{(\mathrm{EX})}$ is actually $O(p^2)$ and can be encoded into the LECs in $\mathcal{L}_{\mathcal{H}\varphi}^{(2)}$ [882, 883, 583].

At NLO [$O(p^2)$], the scattering amplitude $\mathcal{A}_{\mathrm{NLO}}^{(\mathrm{Tree})}$ comes from the tree diagram (d) in Fig. 20 , which stems from the NLO Lagrangian $\mathcal{L}_{\mathcal{H}\varphi}^{(2)}$. The N^{2}LO amplitudes arise from both the tree and loop diagrams. The $\mathcal{L}_{\mathcal{H}\varphi}^{(3)}$ contributes to $\mathcal{A}_{\mathrm{N}^2\mathrm{LO}}^{(\mathrm{Tree})}$ through the tree diagram 20(e). The loop diagrams in Fig. 21 and Fig. 22 contribute to the $\mathcal{A}_{\mathrm{N}^2\mathrm{LO}}^{(\mathrm{Loop})}$. The chiral corrections from Fig. 21 survive in the heavy meson limit, while the corrections from Fig. 22 are proportional to $1/m_\mathcal{H}$ and vanish in the heavy meson limit. All the vertices arise from $\mathcal{L}_{\mathcal{H}\varphi}^{(1)}$ and $\mathcal{L}_{\varphi\varphi}^{(2)}$. One can obtain the $\mathcal{H}\bar{\varphi}$ scattering amplitude using the cross symmetry.

Within the HHχPT scheme, the authors of Ref. [877] calculated the S-wave scattering lengths of the heavy pseudoscalar and Goldstone bosons ($P\varphi$) up to N^{2}LO. They considered only the tree diagrams in Fig. 20 and the loop diagrams in Fig. 21 in the heavy meson limit. The scattering length a was related to the perturbative amplitude at the threshold (T_{th}) by [11]

$$
T_{\mathrm{th}} = 8\pi\left(1+\frac{M_\varphi}{m_\mathcal{H}}\right)a.
\tag{265}
$$

With the scattering lengths from lattice QCD simulations [885], they extracted the LECs and predicted the attractive isoscalar DK interactions. In this work, the scattering lengths were extracted from the perturbative amplitudes. If there exists the bound state or resonance, the perturbative calculation will fail. In this case, the perturbative amplitude can be regarded as the kernel of the nonperturbative calculation. The sign and magnitude of the kernel at threshold [12] still reflect the properties of the interaction and provide the hints for the existence of the possible bound states.

In Ref. [879], the authors applied a similar formalism to study the scattering lengths of the heavy vector and light Goldstone bosons ($P^*\varphi$) up to N^{2}LO. Besides the HHχPT scheme, they also calculated the scattering lengths in the

---

[10]The LECs c_0 and c_1 are equivalent to σ_H and a_H in Eq. (169) up to a constant $4B_0$, respectively.

[11]There are different definitions, for instance, $T_{\mathrm{th}} = -8\pi\left(m_\mathcal{H} + m_\varphi\right)a$ in Refs. [51, 884].

[12]In this case, the experimental scattering lengths cannot be extracted from the perturbative amplitude at the threshold. One can extract the a_{Born} as shown in Eq. (267).

framework of the infrared regularization. The results for the pion scattering channels are similar in the two frameworks and the chiral expansions converge well. The loop contributions for the η and K scattering are large, but canceled by the N²LO tree diagrams, which leads to the convergent results. In particular, they introduced the contribution of the $D_{s1}(2460)$ in the D^*K scattering through the LEC c_3 in $\mathcal{L}_{\mathcal{H}\varphi}^{(2)}$.

In Ref. [878], the authors calculated the $P\varphi$ scattering to N³LO [$O(p^4)$] with the HHχPT scheme without considering the vector P^* meson. The Lagrangian at N³LO reads,

$$\mathcal{L}_{\mathcal{H}\varphi}^{(4)} = e_1 \left\langle \mathcal{H}\bar{\mathcal{H}} \right\rangle \mathrm{Tr}\left[(v \cdot \partial v \cdot u)(v \cdot \partial v \cdot u)\right] + e_2 \left\langle \mathcal{H}(v \cdot \partial v \cdot u)(v \cdot \partial v \cdot u)\bar{\mathcal{H}} \right\rangle, \tag{266}$$

where the terms with the quark mass matrix $\chi_\pm$ in $\mathcal{L}_{\mathcal{H}\varphi}^{(4)}$ are not given explicitly since they can be absorbed by the c_0 and c_1 terms in $\mathcal{L}_{\mathcal{H}\varphi}^{(2)}$ if one is not interested in the light quark mass dependence of the observables. Without the contribution of the vector mesons, the LO interaction comes from the Weinberg-Tomozawa interaction through the tree diagram (a) in Fig. 20, while the diagrams (b) and (c) do not exist. At N²LO, the loop diagrams with the same topological structures as the (a), (b) and (e) diagrams in Fig. 21 contribute and the relevant vertices originate from the kinetic terms of $\mathcal{L}_{\mathcal{H}\varphi}^{(1)}$ and $\mathcal{L}_{\varphi\varphi}^{(2)}$. At N³LO, there are additional diagrams as shown in Fig. 23. The tree diagram stems from $\mathcal{L}_{\mathcal{H}\varphi}^{(4)}$, and the $P^{(*)}P^{(*)}\varphi$ vertices in the loops are from both the $\mathcal{L}_{\mathcal{H}\varphi}^{(1)}$ and $\mathcal{L}_{\mathcal{H}\varphi}^{(2)}$.

The authors of Ref. [878] calculated the scattering amplitude up to N³LO and extracted the scattering lengths with two formalisms: the perturbative one as shown in Eq. (265) and iterated method [584]

$$a = a_{\mathrm{Born}}\left(1 - \frac{1}{2}\mu a_{\mathrm{Born}}\right)^{-1}, \tag{267}$$

where the μ is a cutoff scale. a_{Born} contains the contributions of the diagrams except the s-channel loop diagram (c) in Fig. 21 as well as diagram (d) in Fig. 23, which can be generated through the iteration of the tree diagrams (a) and (d) in Fig. 20. Their isoscalar scattering lengths with Eq. (267) are consistent with the lattice QCD results [884, 886] as well as the results in Refs. [877, 54]. They also obtained the scattering length of the meson and doubly charmed baryon using the heavy diquark-antiquark symmetry. Their results support the existence of the isoscalar $\bar{K}\Xi_{QQ}$ ($Q = c, b$) bound state.

Another approach to eliminate the PCBs is the EOMS scheme. Instead of performing the nonrelativistic projections and integrating out the heavy filed in HHχPT, the EOMS performs the chiral expansion with the covariant Lagrangians. Apart from the substraction of the UV divergences, the extra regularization removing the PCB terms has to be performed. The relevant Lagrangians responsible for the $P\varphi$ and $P^*\varphi$ interactions up to N²LO read [47, 583, 887, 883, 882] [13]

$$
\begin{aligned}
\mathcal{L}_{PP^*\varphi}^{(1)} &= \mathcal{D}_\mu P \mathcal{D}^\mu P^\dagger - m_P^2 P P^\dagger - \frac{1}{2}\mathcal{F}^{\mu\nu}\mathcal{F}_{\mu\nu}^\dagger \\
&\quad + m_{P^*}^2 P^{*\nu} P_\nu^{*\dagger} + ig_0\left(P_\mu^* u^\mu P^\dagger - P u^\mu P_\mu^{*\dagger}\right) + \frac{\tilde{g}_0}{2}\left(P_\mu^* u_\alpha \partial_\beta P_\nu^{*\dagger} - \partial_\beta P_\mu^* u_\alpha P_\nu^{*\dagger}\right)\epsilon^{\mu\nu\alpha\beta}, \tag{268}
\end{aligned}
$$

$$
\begin{aligned}
\mathcal{L}_{PP^*\varphi}^{(2)} &= P\left[-h_0\mathrm{Tr}(\chi_+) - h_1\chi_+ + h_2\mathrm{Tr}(u_\mu u^\mu) - h_3 u_\mu u^\mu\right]P^\dagger + \mathcal{D}_\mu P\left[h_4\mathrm{Tr}(u_\mu u^\nu) - h_5\{u^\mu, u^\nu\}\right]\mathcal{D}_\nu P^\dagger \\
&\quad + P^{*\nu}\left[-\tilde{h}_0\mathrm{Tr}(\chi_+) - \tilde{h}_1\chi_+ + \tilde{h}_2\mathrm{Tr}(u_\mu u^\mu) - \tilde{h}_3 u_\mu u^\mu\right]P_\nu^{*\dagger} + \mathcal{D}_\mu P^{*\alpha}\left[\tilde{h}_4\mathrm{Tr}(u_\mu u^\nu) - \tilde{h}_5\{u^\mu, u^\nu\}\right]\mathcal{D}_\nu P_\alpha^{*\dagger}, \tag{269}
\end{aligned}
$$

$$
\begin{aligned}
\mathcal{L}_{PP^*\varphi}^{(3)} &= g_1 P[\chi_-, u_\nu]\mathcal{D}^\nu P^\dagger + g_2 P[u^\mu, \nabla_\mu u_\nu + \nabla_\nu u_\mu]\mathcal{D}^\nu P^\dagger + g_3 P[u_\mu, \nabla_\nu u_\rho]\mathcal{D}^{\mu\nu\rho} P^\dagger \\
&\quad + i\tilde{g}_1 P^{*\alpha}[\chi_-, u_\nu]\mathcal{D}^\nu P_\alpha^{*\dagger} + \tilde{g}_2 P^{*\alpha}[u^\mu, \nabla_\mu u_\nu + \nabla_\nu u_\mu]\mathcal{D}^\nu P_\alpha^{*\dagger} + \tilde{g}_3 P^{*\alpha}[u_\mu, \nabla_\nu u_\rho]\mathcal{D}^{\mu\nu\rho} P_\alpha^{*\dagger}, \tag{270}
\end{aligned}
$$

where the $\mathcal{D}^{\mu\nu\rho} = \left\{\mathcal{D}_\mu, \left\{\mathcal{D}_\nu, \mathcal{D}_\rho\right\}\right\}$ and $\mathcal{F}_{\mu\nu} = \left(\mathcal{D}_\mu P_\nu^* - \mathcal{D}_\nu P_\mu^*\right)$. m_P and m_{P^*} are the masses of the pseudoscalar and vector heavy mesons, respectively. According to the SU(3) group representation, one has $\mathbf{8} \otimes \mathbf{8} \to \mathbf{8}_1(\mathbf{8}_2)$ as shown in

---

[13]In the heavy quark limit, the Lagrangians recover the formalisms constructed with the superfield as shown in Eq. (50), Eq. (261) and Eq. (262). One has $m_P = m_P^*$, $h_i = \tilde{h}_i$ for ($i = 1, \ldots, 5$), $g_k = \tilde{g}_k$ for $k = 0, \ldots, 3$. The LECs in these two kinds of Lagrangians are related to each other, for instance $h_0 = 2m_{\mathcal{H}}c_0$ and $h_1 = 2m_{\mathcal{H}}c_1$, with $m_{\mathcal{H}}$ the mass of the heavy meson.

Table A.9. Apart from the $\{u^\mu, u^\nu\}$ building block, there is an additional term with the building block $[u^\mu, u^\nu]$ in $\mathcal{L}_{PP^*\varphi}$ [47], which was shown to be $O(p^3)$ and can be absorbed by the $\mathcal{L}^{(3)}_{PP^*\varphi}$ [583, 887].

The calculation of the tree diagrams is independent of the renormalization scheme, and the corresponding tree diagrams are listed in Fig. 20. In the EOMS scheme, at the N^{2}LO, the loop diagrams will generate both the UV divergent and the PCB terms. Taking the $P\varphi$ scattering as an example, the $\mathcal{L}^{(1)}_{PP^*\varphi}$ and the terms with the P field in $\mathcal{L}^{(2)}_{PP^*\varphi}$ and $\mathcal{L}^{(3)}_{PP^*\varphi}$ will contribute to the $P\varphi \to P\varphi$ scattering process up to N^{2}LO, while the terms with the vector meson P^* at the NLO and N^{2}LO Lagrangians do not contribute at this order. The bare LECs can be decomposed into the finite and divergent parts [583, 53]

$$m_P^2 = m_P^{r2}(\mu) + \beta_{m_P^2}\lambda, \qquad m_{P^*}^2 = m_{P^*}^{r2}(\mu) + \beta_{m_{P^*}^2}\lambda, \qquad h_i = h_i^r(\mu) + h_i^0\lambda, \qquad g_j = g_j^r(\mu) + g_j^0\lambda, \qquad (271)$$

where $\lambda = \mu^{d-4}\left[(4\pi)^{d/2}(d-4)\right]^{-1}$ with μ the regularization scale and d the dimension. The UV parts will be absorbed by the divergent term proportional to λ. Up to N^{2}LO, the PCB terms originating from the loop integrals are $O(p^2)$ and can be subtracted by redefining the LECs h_i^r and g_0^r as follows

$$h_i^r(\mu) = \tilde{h}_i + h_i^{\text{PCB}}, \qquad\qquad g_0^r(\mu) = \tilde{g}_0 + g_0^{\text{PCB}}, \qquad (272)$$

while the other g_j^rs do not change. The explicit forms of the coefficients $\beta_{m^2}/\beta_{m^{*2}}/h^0/g^0$ and $h_i^{\text{PCB}}/g_0^{\text{PCB}}$ are referred to Refs. [583, 53]. Eventually, the UV and PCB terms were absorbed by the LECs. With the Lagrangians in Eqs. (268)-(270), the scattering amplitudes of the heavy and light mesons have been calculated up to LO [688, 616, 621], NLO [39, 763, 47, 49, 888, 51], N^{2}LO with the EOMS schemes [883, 583, 53]. In Refs. [583, 53], the authors performed the calculations with and without the contribution of the vector P^* mesons and found the differences were negligible in the vicinity of the thresholds. In the above works, the perturbative scattering amplitudes were used as the kernel interactions in the chiral unitary method and will be discussed in Sec. 4.2.

The Goldstone meson and charmed meson scattering was also investigated in Ref. [42], where the authors studied both the open and the hidden charmed scalar meson resonances. They extended the chiral Lagrangian to study the flavor breaking effect in the Skyrme models. They also considered the SU(4) flavor symmetry and its breaking effect.

The Goldstone meson and heavy hadron interaction Lagrangians may contain many unknown LECs. In general, the LECs should be determined by fitting the experimental data. However, the experimental information of the $\mathcal{H}\varphi$ scattering is still scarce nowadays. One may reduce the number of LECs in the effective field theory by taking approximate limits. In the large N_C limit, the LECs may have different orders. For instance, the $c_1(h_1)$ in Eq. (261) [Eq. (268)] can be obtained by the mass differences between the charmed-strange and charmed non-strange mesons. Furthermore, in Eq. (268), the $h_1/h_3/h_5$ terms at the NLO Lagrangians are $O(N_C^0)$. The $h_0/h_2/h_4$ terms are $O(N_C^{-1})$ and suppressed in the large N_C limit. Their contributions have been neglected in Refs. [762, 49]. In Ref. [883], the authors did not include the h_4 and h_5 terms since their contributions have the same structures as those from the h_2 and h_3 terms in the vicinity of the thresholds. An alternative way is using the lattice QCD data [884, 886, 889, 890, 891, 892], which have been extensively employed to determine the LECs in the perturbative or unitarized χPT calculations [47, 884, 893, 882, 877, 883, 888, 53, 54, 894, 895]. The LECs are also estimated using phenomenological models such as the resonance saturation method [599, 896, 879, 897, 877, 879, 897], where the effective Lagrangians are first constructed with the resonances and then the resonances are integrated out to estimate the LECs for the mesonic Lagrangians. In Ref. [897], the authors constructed the effective Lagrangians with the resonances including the scalar charmed mesons, the light vector mesons, and the tensor mesons. Then they estimated the LECs for the mesonic Lagrangian by integrating out the resonances. The results at NLO were consistent with those obtained by fitting the lattice QCD data, while those at N^{2}LO had a sizable deviation.

The χPT amplitude is valid and useful in the low energy region where the higher resonance/bound states are integrated out. The implementation of the unitarity properties will help to extend the χPT amplitude to the higher regions where the resonances/bound states appear.

4.2. Scatterings of Goldstone bosons off the heavy mesons

As discussed in Sec. 1.1, the $D_{s0}^*(2317)$ and $D_{s1}(2460)$ are two narrow charm strange mesons with the spin-parity $J^P = 0^+$ and $J^P = 1^+$, respectively. They are located around 45 MeV below the DK and D^*K thresholds, respectively.
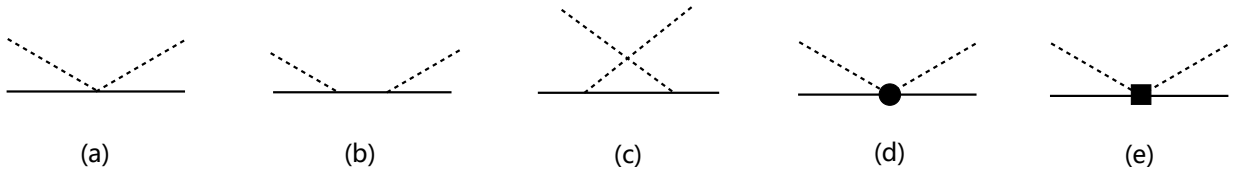
Figure 20: The tree diagrams for the scattering of the pesudoscalar light mesons (dashed line) off the heavy mesons (solid line). Each one represents a set of diagrams which have the same topological structure. The solid dot and square stand for the $O(p^2)$ and $O(p^3)$ vertices. The diagrams (a)-(c) are at LO, while (d) and (e) are at NLO and N^{2}LO, respectively.
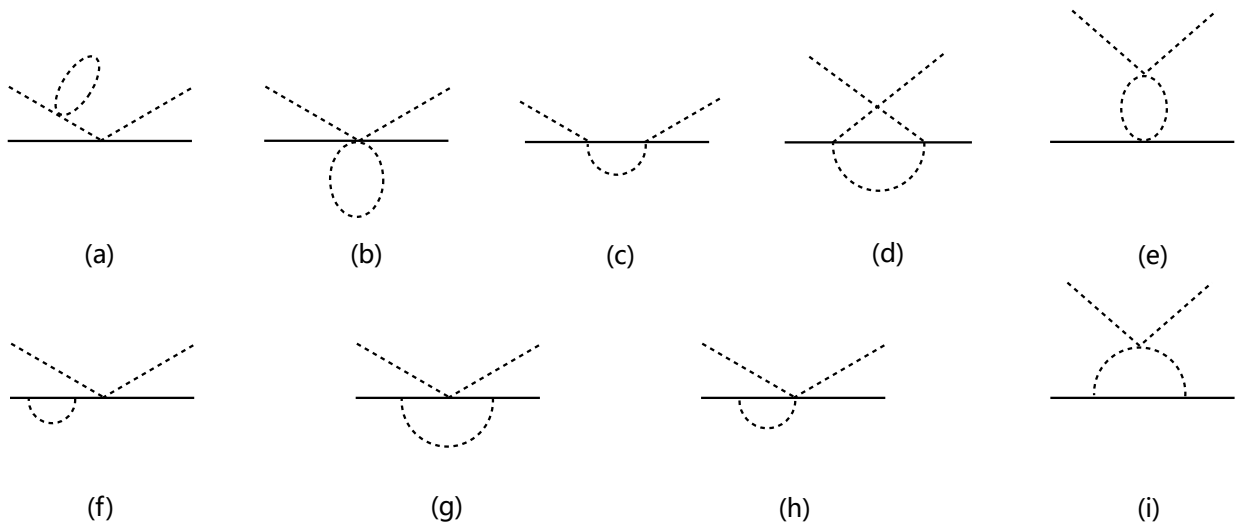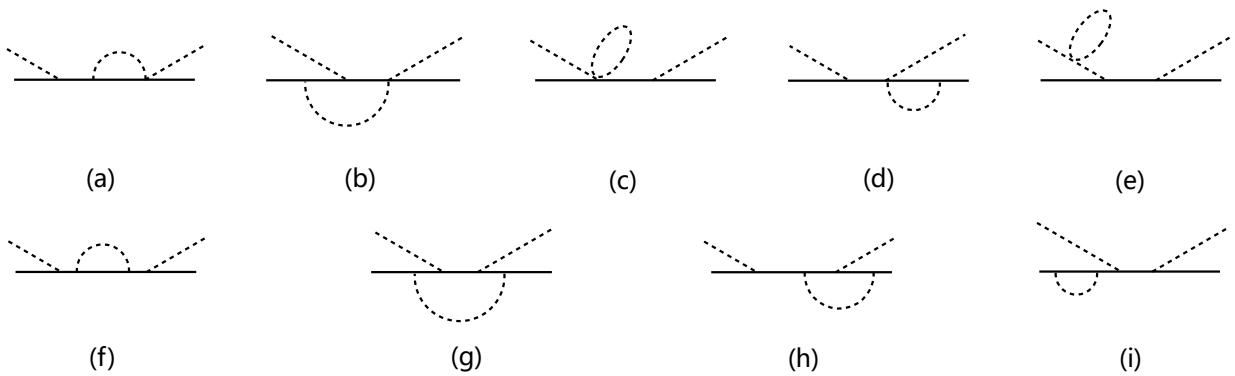

Figure 21: The loop diagrams which survive in the heavy quark limit $m_{\mathcal{H}} \to \infty$ for the scattering of the pesudoscalar light mesons (dashed line) off the heavy mesons (solid line). Each one represents a set of diagrams which have the same topological structure.

Figure 22: The topological loop diagrams for the scattering of the pesudoscalar light mesons (dashed line) and heavy mesons (solid line) that vanish in the heavy quark limit $m_{\mathcal{H}} \to \infty$.
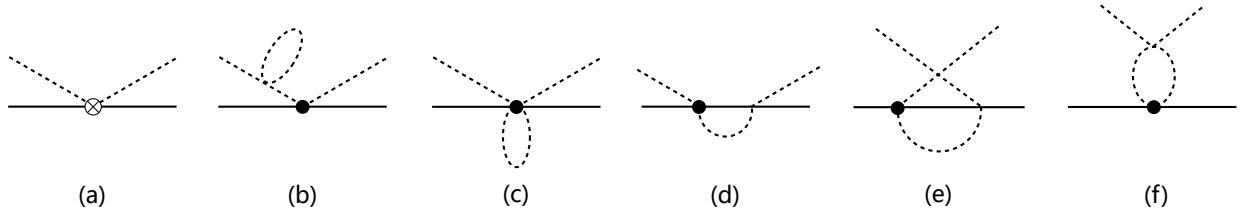
Figure 23: The N³LO topological loop diagrams contributing to the $\mathcal{H}\varphi$ scattering amplitude in the heavy quark limit without the vector P^* meson as the intermediate state in the loop. The solid dot and the crossed circle stand for the $O(p^2)$ and $O(p^4)$ vertices stemming from $\mathcal{L}_{\mathcal{H}\varphi}^{(2)}$ and $\mathcal{L}_{\mathcal{H}\varphi}^{(4)}$, respectively.

Since their observation, their inner structures remain puzzling. The two parity-even D_s states cannot be simply categorized as the $c\bar{s}$ mesons in the quark model, since their masses are much smaller than the quark model predictions. Moreover, the mass splittings between the SU(3) flavor partners are unnatural with $m_{D_{s0}^*(2317)} - m_{D_0^*(2300)} = -25.2$ MeV and $m_{D_{s1}(2460)} - m_{D_1(2430)} = 47.5$ MeV, which are predicted to be around 100 MeV due to the strange quark mass in the conventional quark model. Various explanations have been proposed, including the quenched and unquenched $c\bar{s}$ quark model, the $D^{(*)}K$ hadronic molecules, the $cq\bar{s}\bar{q}$ compact tetraquark states, the mixing of the $c\bar{s}$ state and tetraquark state, and other possibilities (see Sec. 1.1 for more discussions). The proximity of the two $D_s^{(*)}$ states to the $D^{(*)}K$ thresholds has led to the popularity of the $D^{(*)}K$ molecular explanation, which suggests that the dominant component of these mesons is a $D^{(*)}K$ molecule. The molecular explanation was first proposed in Refs. [41, 40] and has been further studied in various works (for more details, see the reviews [7, 67, 11, 68]). The molecular framework provides a consistent explanation of the mass puzzles and the fine-tuning problem in Eq. (192). In this subsection, we will review research works on the formation of the molecular state through two widely used interaction mechanisms and the unitary approach, resulting in the molecular state as a pole of the T matrix.

In Sec. 4.2.1, the $D_{s0}^*(2317)$ and $D_{s1}(2460)$ are identified as the dynamically generated poles originating from the resummations of the $\mathcal{H}\varphi$ interactions, and are interpreted as the $D^{(*)}K$ molecules. The $\mathcal{H}\varphi$ scattering amplitude expanded in χPT (see Sec. 4.1) was used as the kernel interactions in the chiral unitary approaches. The molecular picture seemed to successfully describe the experimental data on the $\mathcal{H}\varphi$ invariant mass distribution as well as the lattice QCD simulations.

In Sec. 4.2.2, the kernel potentials contain both the $\mathcal{H}\varphi$ hadronic potentials and the contributions from the $c\bar{s}$ cores. In this case, the physical states are the mixtures of both the $c\bar{s}$ and the $D^{(*)}K$ components. The contents of the components are vital to identify the nature of the resonance. If the molecular components are dominant in the $D_{s0}^*(2317)$ and $D_{s1}(2460)$ states, they could still owe their origin to the $\mathcal{H}\varphi$ scattering and be understood as the hadronic molecules.

Apart from the successful explanations of the two positive D_s states, the chiral unitary approaches also provide important insights into the non-strange charmed mesons with positive parity. In the SU(3) symmetry limit, the $\mathcal{H}\varphi$ systems can be categorized into the $\mathbf{\bar{3}}_f$, $\mathbf{6}_f$ and $\mathbf{\overline{15}}_f$ flavor representations as illustrated in Fig. 24. In the non-strange sector, the coupled channel effects of $D\pi$, $D_s\bar{K}$ and $D\eta$ are considered. The chiral unitary methods predict the two-pole structures for both the scalar D_0^* and axial-vector D_1^* charmed mesons. Within the two-pole picture, the lower and higher D_0^* mesons are located around 2100 MeV and 2450 MeV, respectively. They mainly couple with the $D\pi$ and $D_s\bar{K}$ channels, respectively. The two-pole picture could accommodate the broad $D_0^*(2300)$ signal and explain the mass splitting puzzle in the quark model.

In contrast, there are only one scalar and axial-vector charmed mesons listed in the Review of Particle Physics (RPP) [1], the $D_0^*(2300)$ [was called as $D_0^*(2400)$ before] and $D_1(2430)$, which are the two lightest scalar and axial-vertor charmed mesons, respectively. The lattice QCD simulations reported only one resonance, but did not exclude the second one [891, 898]. There are many theoretical works to understand the "controversial" results in literature and we will review them in Sec. 4.2.3. With the heavy quark spin symmetry, the similar calculations were generalized to the bottom sectors, especially the unobserved P-wave B_s^* states.
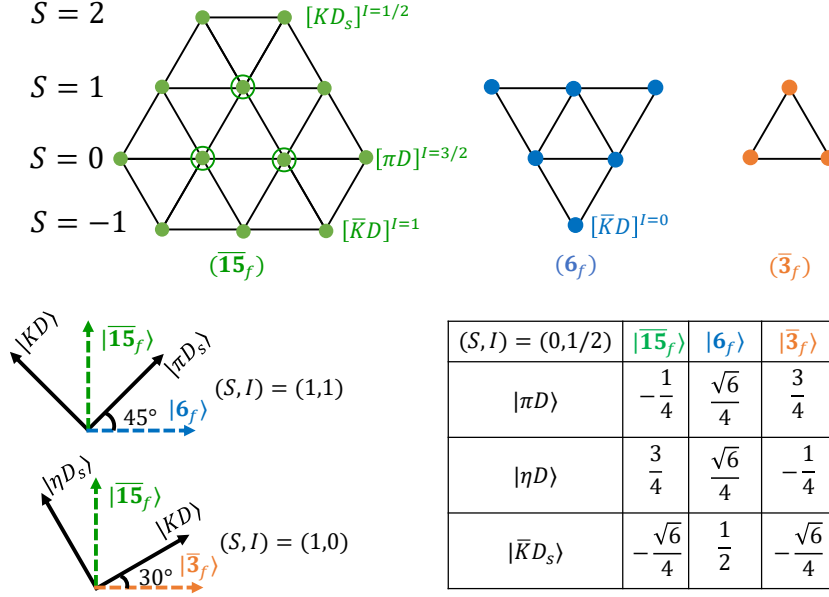
Figure 24: The flavor representations of the $\mathcal{H}\varphi$ system in the SU(3) flavor symmetry and relations with di-hadron basis. The heavy ($\mathcal{H}$) and light (φ) mesons are in the $\bar{\mathbf{3}}_f$ and $\mathbf{8}_f$ representations, respectively. Thus, the possible flavor representations of the $\mathcal{H}\varphi$ system are $\bar{\mathbf{3}}_f \otimes \mathbf{8}_f = \overline{\mathbf{15}}_f \oplus \mathbf{6}_f \oplus \bar{\mathbf{3}}_f$ [899, 42]. "S" is the strange number. The upper panel is the weight diagrams of representation taken from Ref. [899]. For the states in the SU(3) symmetry corresponding to the specific di-hadron system, we label them in the upper panel. For the states corresponding to the mixture of different di-hadron states, we illustrate their mixing angles in the lower panel, including the $(S, I) = (1, 1), (1, 0)$ and $(0, 1/2)$ ones.

4.2.1. $D_{s0}^*(2317)$ and $D_{s1}(2460)$ in the molecular picture

The LO chiral amplitude of the $\mathcal{H}\varphi$ scattering is parameter-free and used as the kernel interactions in the chiral unitary approaches [37, 44, 43, 42, 900, 45]. Kolomeitsev *et al* [37] and Guo *et al* [44, 43] studied the $J^P = 0^+$ and $J^P = 1^+$ heavy mesons with the similar SU(3) chiral Lagrangians. In the charm-strange sector, two bound states were found in the isosinglet DK and D^*K channels and identified as the $D_{s0}^*(2317)$ and $D_{s1}(2460)$ states, respectively. For the heavy non-strange mesons with isospin $I = 1/2$, the two-pole structures were predicted for the scalar D_0^*/B_0^* and axial vector D_1/B_1 mesons, respectively. The lower pole is broad and the higher one is narrow. The two poles belong to the $\bar{\mathbf{3}}_f$ and $\mathbf{6}_f$ representations up to some mixing effects. The partner mesons in the bottom sector were also predicted. Moreover, the decay widths of the isospin violating decays $D_{s0}^{*+}(2317) \to D_s^+\pi^0$ and $B_{s0}^{*0}(5729) \to B_s^0\pi^0$ were calculated to be 8.69 keV and 1.54 keV, respectively [44].

In Ref. [42] and Ref. [900], the authors studied the dynamical generations of the open and hidden charm 0^+ and 1^+ resonances with the SU(4) flavor symmetric Lagrangians. However, the SU(4) flavor symmetry is just an assumption and not a real symmetry of QCD. In their calculations, the exchange of heavy mesons was suppressed, the SU(4) flavor symmetry was broken into the SU(3) symmetry by suppressing the exchange of the heavy mesons. The $D_{s0}^*(2317)$ and $D_{s1}(2460)$ were identified as the DK and D^*K bound states. The two-pole structures were also found for the charmed mesons with the strangeness-isospin number $(S, I) = (0, 1/2)$, similar to Refs. [44, 37, 43]. The lower scalar and the axial vector poles in the $\bar{\mathbf{3}}_f$ representation were identified as the $D_0^*(2300)$ and $D_1(2420)$ in PDG [1], respectively. The other higher poles for the charmed mesons with $J^P = 0^+$ and $J^P = 1^+$ were broader than the predictions in Refs. [44, 37, 43].

To achieve better accuracy, the NLO chiral amplitude was considered in Refs. [39, 47, 49, 893]. With the scattering amplitude up to NLO, the mass dependence of the P-wave heavy mesons on the light Goldstone meson masses can be investigated. In Ref. [47], the authors calculated the S-wave scattering lengths of the $P\varphi$ system with the NLO chiral amplitude as well as its unitarized version. The unitarized one reproduced the quark mass dependence of the scattering lengths from lattice QCD [885]. In Ref. [49], the authors studied the masses of $D_{s0}^*(2317)$ and $D_{s1}(2460)$ as well as

their bottom partner states. They proposed the linear dependence of the heavy meson masses on m_K as a specific character of a molecule, which can be a criterion for investigating the molecular nature. The difference between the S-wave DK and D^*K scattering potentials first arises from the u-channel exchange tree diagram as shown in Fig. 20(c). Compared with the mass splitting of the D and D^* mesons, the difference of the scattering potentials is $O(M_K^2/\Lambda_\chi^2)$. Thus, the hyperfine mass splitting between the $D_{s0}^*(2317)$ and $D_{s1}(2460)$ almost equals the D and D^* mass difference. Later, the authors of Ref. [893] also calculated the $D_{s0}^*(2317)$ scattering length and its mass trajectories of $m_{\pi/K}$ as in Ref. [47]. They determined the LECs with the help of the scattering lengths from lattice QCD simulations [885] rather than applying the large N_c approximation as in Ref. [47].

In 2012, the authors of Ref. [884] studied the $P\varphi$ scattering in lattice QCD simulations and obtained the S-wave scattering lengths of five channels with several m_π without the disconnected contribution: $D\bar{K}$ ($I = 0, 1$), D_sK, $D\pi$ ($I = 3/2$), $D_s\pi$. The chiral extrapolation was incorporated into the unitarized scattering lengths, which were obtained in their previous works [763, 47]. By fitting the lattice QCD data, they determined the unknown LECs and the subtraction constant. Their results favored the DK molecular interpretation of the $D_{s0}^*(2317)$. Moreover, the DK was shown to be dominant in the $D_{s0}^*(2317)$ with the probability 70% by using the Weinberg's compositeness relation. The decay width was $\Gamma[D_{s0}^*(2317) \rightarrow D_s\pi] = (133 \pm 19)$ keV.

With the lattice scattering lengths in Ref. [884] and the data from another group [892, 886, 889] as input, the light-quark mass and the N_C dependencies of the pole positions in the $P\varphi$ channels were analyzed [51]. The pole positions of the $D_{s0}^*(2317)$ as well as the charmed mesons with the strangeness-isospin number $(S, I) = (0, 1/2)$ were found to be not like that of the $c\bar{s}/c\bar{q}$ mesons. They did not tend to fall down to the real axis at large N_C. In contrast, the imaginary part of a genuine $c\bar{s}/c\bar{q}$ states tends to vanish in the large N_C limit.

The fixed LECs and the unitarized NLO $P\varphi$ amplitude in Ref. [884] have been used in the subsequent works [55, 899, 901]. In Ref. [901], the authors summarized the predictions of the pole positions. The results of the lowest positive-parity D_{s0}^*/D_{s1} and B_{s0}^*/B_{s1} were consistent with the available experimental data and the lattice QCD results [890, 902], respectively. For the heavy non-strange ones, two-pole structures were predicted: one flavor antitriplet and a nontrivial sextet meson as shown in Fig. 24. The authors of Ref. [55] calculated the energy levels in the finite volume and compared their results with the lattice QCD simulations. The finite volume effect was taken into consideration. In a finite box with the size L, the finite-volume effects are induced by discretizing the three momentum $\vec{q} \in \mathbb{R}^3$ and its integral as follows

$$\vec{q} \rightarrow \frac{2\pi}{L}\vec{n}, \ (\vec{n} \in \mathbb{Z}^3), \qquad \int_{\mathbb{R}^3} \frac{d^3q}{(2\pi)^3} \rightarrow \frac{1}{L^3}\sum_{n\in\mathbb{Z}^3}. \tag{273}$$

The loop function $G_{ii}(s)$ then transforms into its discrete form $\tilde{G}_{ii}(s, L)$. Correspondingly, the T-matrix $T(s)$ in the discrete form (in the cutoff regularization) reads [903],

$$G_{ii}(s) \quad \rightarrow \quad \tilde{G}_{ii}(s, L) = G_{ii}(s) + \lim_{\Lambda\to\infty}\left(\frac{1}{L^3}\sum_{\vec{n}}^{|\vec{q}|<\Lambda} I_i(\vec{q}) - \int_0^\Lambda \frac{q^2dq}{2\pi^2}I_i(\vec{q})\right), \tag{274}$$

$$V(s) \quad \rightarrow \quad \tilde{V}(s, L) = V(s), \tag{275}$$

$$T^{-1}(s) \quad \rightarrow \quad \widetilde{T}^{-1}(s, L) = V^{-1}(s) - \tilde{G}(s, L), \tag{276}$$

where the integrand $I_i(\vec{q})$ can be read from Eq. (90). This formalism gave a nice description of the energy levels of the 0^+ and 1^+ charmed-strange states in lattice QCD simulations [890] as shown in Fig. 25.

One should note the all the parameters of the unitarized amplitudes have been determined using the scattering lengths in lattice QCD simulations [884] prior to Ref. [890]. The DK ($I = 0$) scattering lengths in the two lattice works are

$$a_s^{\mathrm{I}} = -0.86(3) \text{ fm} \qquad a_s^{\mathrm{II}} = -1.49(0.13)(-0.30) \text{ fm}, \tag{277}$$

where a_s^{I} and a_s^{II} are the results from Refs. [884, 890], respectively.

In Ref. [54], the authors fitted the finite-volume energy levels and scattering lengths from lattice calculations and successfully described the lattice data [884, 902, 891]. After performing the chiral extrapolation, they made predictions of the resonance parameters at the physical m_π, including the phase shifts, the inelasticities, the pole position,
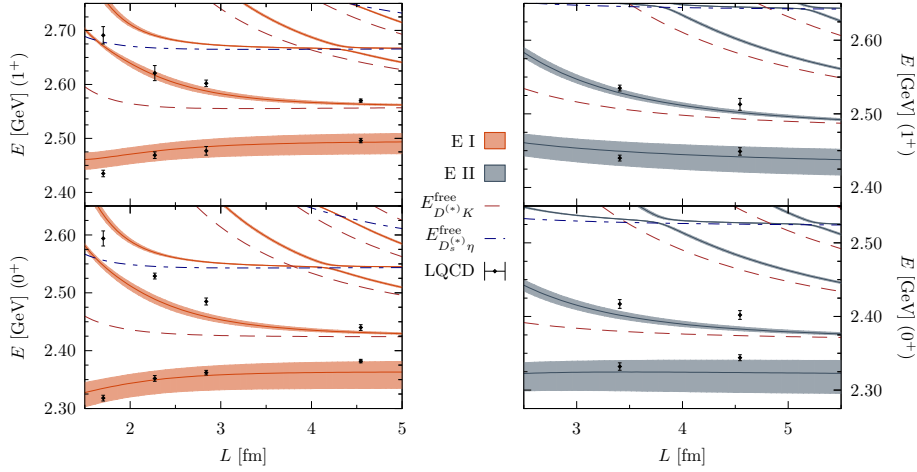
Figure 25: Comparison of the energy levels using the unitarized NLO $P\varphi$ amplitudes of Refs. [884] with the lattice QCD results [890]. The two panels correspond to two sets of lattice QCD data obtained with $m_\pi = 290$ MeV (Ensemble I) and 150 MeV (Ensemble II), respectively. The 68% CL uncertainty bands originate from the errors of the LECs in Ref. [884]. Figures taken from Ref. [55].

and the residues of the pole. They reproduced the $D_{s0}^*(2317)$ mass and found two possible solutions corresponding to the bound and virtual states, respectively. The two poles with the strange-isospin number $(S, I) = (0, 1/2)$ persist. The lower one has the mass around 2100 MeV and width more than 200 MeV, while the higher one has the mass $2300 \sim 2500$ MeV and width $70 \sim 200$ MeV.

The chiral amplitudes were also extended to N²LO [583, 53, 895, 904]. In Ref. [583], the authors calculated the $\mathcal{H}\varphi$ scattering amplitude up to N²LO with the χPT in the EOMS scheme without the contribution of the D^*. With both BSE and the IAM approaches, they obtained the unitarized amplitude and the scattering length. With the chiral extrapolation of the meson masses and the decay constants, they got a good fit to the lattice QCD data of the S-wave scattering lengths [884, 886]. However, most of the parameters suffered from large uncertainties. They also calculated the diagrams with the D^* and found its contribution to be negligible. Later in Ref. [53], they performed a complete calculation with the contribution of the explicit vector charmed meson and used a similar fit procedure as in Ref. [583]. Their results showed that the D^* contribution was negligible for the S-wave scattering near the threshold. They also searched for the $J^P = 0^+$ poles on the Riemann sheets and presented their trajectories with the varying pion mass. The LECs still bear large uncertainties. More lattice data are required to obtain more solid conclusions.

In Refs. [895], the authors used the lattice results of both the heavy meson masses and the S-wave scattering lengths to determine the LECs of the Lagrangians up to $O(p^4)$. They calculated the isospin-violating strong decay width $\Gamma[D_{s0}^*(2317)] = (104 - 106)$ keV and found a clear signal of the exotic sextet charmed meson in the $D\pi$ [895] and $D^*\pi$ [904] S-wave coupled systems, which tended to support the two-pole structure for the charmed meson with $J^P = 0^+$ and 1^+. A similar calculation was extended to the bottom sectors [905].

Besides the lattice data, the B decay process also provided a platform to test the molecular explanation. In Ref. [52], the authors studied the B decays $B^+ \to \bar{D}^0 D^0 K^+$, $B^0 \to D^- D^0 K^+$ [906] and $B_s \to \pi^+ D^0 K$ [907]. The unitarized LO amplitude for the DK scattering [44, 45] was used, which contains an unknown subtraction constant $a(\mu)$ in Eq. (89). The $D_{s0}^*(2317)$ appeared as the DK bound state and their presence led to the enhancement in the DK invariant mass spectra. With the Weinberg's compositeness condition, they extracted the DK component to be $P_{DK} = 70^{+4}_{-6}\,^{+4}_{-8}\%$. In Refs. [901, 908], the authors fitted the LHCb data of $B^- \to D^+\pi^-\pi^-$ [909] and $B_s^0 \to \bar{D}^0 K^-\pi^+$ [907] with the unitarized NLO amplitudes, which will be explained in Sec. 4.2.3.

The chiral unitary methods were also applied to the other open-charm system. For instance, the $X(2900)$ was explained as the dynamically generated DK_1 resonance. More discussions can be found in Refs. [7, 67, 11, 68].

4.2.2. $D_{s0}^*(2317)$ and $D_{s1}(2460)$ with the $(c\bar{s})$ component

In this subsection, we review the works discussing the interplay between the $c\bar{s}$ and D^*K channels in the study

of the D_s^* states. Since the quark model almost successfully explains the spectrum of the conventional ground state hadrons, one naturally expects the existence of the P-wave $c\bar{s}$ mesons. If the masses of the $c\bar{s}$ mesons and $D^{(*)}K$ components are close, their coupled-channel effects may be significant and should be taken into account. The physical state is a mixture of both the conventional $c\bar{s}$ meson and the $D^{(*)}K$ component [40, 910, 911, 65, 912, 595, 886, 889, 55, 890, 894]. The proportion of each component will be related to the strength of their coupling. So far, the interplay of the molecular and compact components is not yet well understood. In literature, there are a lot of works discussing their interplay [567, 913, 604, 914, 602, 608, 915]. If the coupling is weak, the physical state will be dominated by the compact $c\bar{s}$ component, with the D^*K component dressing the $c\bar{s}$ core. Recently, an interesting mechanism was proposed which allows the molecular states to decouple from the compact states in the strong coupling regime [913]. The authors considered N compact resonances and a scattering channel. When these compact resonances strongly interact with the scattering state, $N-1$ compact states are formed as the dressed cores while a single molecular state emerges as a bound or virtual state. In this molecular state, the compact components are suppressed compared to the molecular component, leading to the decoupling of the molecular and compact states.

To understand the structure of a particle and pin down whether it is elementary or composite, the probability of different components is of special importance. As outlined in Sec. 2.5.4, the probability of finding the compact component of the bound states can be quantified using the field renormalization constant Z, which is equivalent to the overlap of the bound state wave function with the bare $c\bar{s}$ core. $1 - Z$ represents the molecular (two-body scattering) component. Z ranges from zero to one. A value close to $Z \sim 0$ indicates that the physical state is primarily molecular, while a value close to $Z \sim 1$ implies that it is predominantly compact. Moreover, the couplings of the T matrix poles to different components are related to Z, which conveys the information of the strength of the coupling.

In some works, the $D_{s0}^*(2317)$ and $D_{s1}(2460)$ states are dominated by the genuine $c\bar{s}$ states but the masses of the bare $c\bar{s}$ core are lowered through their coupling to the $D^{(*)}K$ channels as discussed in Sec. 3.1.1. In Ref. [911], the authors studied the $c\bar{s}$ meson with the quark model [916, 917, 918] and derived its coupling with the $DK(D^*K)$ channels using the $^3P_0$ model [919]. With both the $c\bar{s}$ and D^*K degrees of freedom, they obtained the Hamiltonian with the Resonating Group Method (RGM) [920]. By solving the coupled-channel Schrödinger-type equation, they found that the coupling with the $D^{(*)}K$ scattering states will dress the $c\bar{s}$ state and lead to its mass shift. The dressed state $D_{s0}^*(2317)$ contained around the 34% DK component. The percentages of the D^*K component in the $D_{s1}(2460)$ and $D_{s1}(2536)$ are around 50%.

In Ref. [921], the authors investigated the $D_{s0}^*(2317)$ state using lattice QCD simulations and found that the $D_{s0}^*(2317)$ is mainly the $c\bar{s}$ state in the quark model with a small DK component. However, the DK component was found to be dominant in the $D_{s0}^*(2317)$ from other lattice QCD calculations [890, 886, 922] and in some theoretical works [884, 52, 923, 55, 894] with the probability larger than 60%. In Ref. [923], the extracted percentages of the DK components were 70% in the $D_{s0}^*(2317)$ and $(57\pm21\pm6)$% in the $D_{s1}(2460)$ state, respectively. The authors reanalyzed the three energy levels in the lattice QCD simulations [886, 889] beyond the effective range expansion. They used the auxiliary potentials to construct the unitarized T-matrix in two schemes. In the first scheme, they considered the one-single channel $D^{(*)}K$ with two energy dependent potentials. One potential was the linear function of s and the other one included an additional pole to account for a genuine $c\bar{s}$ contribution explicitly. In the second scheme, the coupled-channel unitarized T-matrix with the $D^{(*)}K$, $D_s^{(*)}\eta$ (energy independent potential) was considered. With an extended Lüscher method as shown in Eq. (274) [903, 595], they determined the two poles of the T-matrix for the $D_{s0}^*(2317)$ and $D_{s1}(2460)$ and identified them as the DK and D^*K bound state. The reformulation of the Weinberg's compositeness condition [221, 601] was used to extract the probability of the meson-meson component and its generalization form reads [924, 925],

$$-\sum_i g_i^2 \frac{\partial G_i}{\partial s} - \sum_{i,j} g_i g_j G_i \frac{\partial V_{ij}}{\partial s} G_j = 1, \tag{278}$$

where G_i is the loop function in the ith two-meson channel. V_{ij} is the potential between the ith and jth two-meson channels and g_i is the coupling of the physical state to the ith two-meson channel. The first term stands for the probabilities of the meson-meson components.

In Ref. [55], the authors considered both the $c\bar{s}$ and two-meson channels such as the $D^{(*)}K$ and $D^{(*)}\eta$ to describe the 0^+ and 1^+ charm-strange energy levels from the lattice QCD calculation [890]. The $\mathcal{H}\varphi$ interactions were obtained by the LO scattering amplitude with the HHχPT. Two sets of the $c\bar{s}$ bare masses were employed [926]. The Lagrangian for

the coupling of the $\mathcal{H}\varphi$ channel with the bare $c\bar{s}$ mesons is given in Eq. (130) which contains a dimensionless LEC h. One should note that Eq. (130) has employed the heavy quark spin symmetry in the system. The authors constructed the unitarized T-matrix with the chiral unitary method and extended it to the finite volume with Eq. (274). They successfully described the energy levels in the 0^+ and 1^+ channels in lattice QCD simulations. With the Weinberg's compositeness condition in Eq. (278), their results showed that the $D_{s0}^*(2317)$ and $D_{s1}(2460)$ resonances have the predominantly hadronic molecular DK and D^*K components, with the probabilities being 65% and 56%, respectively. Moreover, one additional broad resonance was found in both the 0^+ and 1^+ channels. The similar formalism was also applied to study the analogue resonances of the two B_s^* states in the bottom sector [927] with the help of the lattice data [902]. They found two poles in the S-wave $\bar{B}^{(*)}K$ amplitude with the masses $5709 \pm 8\,\text{MeV}\,(0^+)$ and $5755 \pm 8\,\text{MeV}\,(1^+)$, corresponding to the $\bar{B}_{s0}^*$ and $\bar{B}_{s1}$. The molecular $\bar{B}^{(*)}K$ components were around 50%.

In Ref. [894], the authors included both the $c\bar{s}$ and the $D^{(*)}K$ components explicitly and systematically studied the four positive parity D_s states: $D_{s0}^*(2317)$, $D_{s1}(2460)$, $D_{s1}^*(2536)$ and $D_{s2}^*(2573)$ with the chiral unitary approach. The authors employed the Godfrey-Isgur (GI) quark model [20] to specify the $c\bar{s}$ core explicitly, and refitted the masses of the well-established mesons. The P-wave bare $c\bar{s}$ cores were almost automatically accommodated into the heavy quark spin basis without the pre-implementation of HQSS, which implies that the HQSS is a good approximation in the D_s sectors. The couple-channel effects (g) between the bare $c\bar{s}$ core and the $D^{(*)}K$ channels were described by the quark pair creation (QPC, aka, the $^3P_0$) model [928, 929, 930, 931, 932, 933, 911, 933, 911]. The interactions (v) between the two-meson channels $D^{(*)}K$ were derived with the vector meson exchange Lagrangians [934, 935, 936].

To use the lattice QCD data, they adopted the Hamiltonian effective field theory (HEFT) [937, 938, 939, 940]. The momentum is discretized according to Eq. (273) in a cubic box with the size L. However, instead of the loop function, the Hamiltonian matrix is discretized in the HEFT as follows

$$H_0 \quad = \quad \sum_{i=1,n} |B_i\rangle m_i \langle B_i| + \sum_{\alpha,k} |\vec{q}_k, -\vec{q}_k\rangle_\alpha \left(\sqrt{m_{\alpha_B}^2 + q_\alpha^2} + \sqrt{m_{\alpha_M}^2 + q_\alpha^2} \right)_\alpha \langle \vec{q}_k, -\vec{q}_k|, \qquad (279)$$

$$H_I \quad = \quad \sum_k \left(\frac{2\pi}{L}\right)^{3/2} \sum_\alpha \sum_{i=1,n} \left(|\vec{q}_k, -\vec{q}_k\rangle_\alpha g_{i,\alpha}^\dagger(s,\vec{q}_k)\langle B_i| + |B_i\rangle g_{i,\alpha}(s,\vec{q}_k)\langle \vec{q}_k, -\vec{q}_k| \right) \qquad (280)$$
$$+ \sum_{k,l} \left(\frac{2\pi}{L}\right)^{3/2} \sum_{\alpha,\beta} |\vec{q}_k, -\vec{q}_k\rangle_\alpha v_{\alpha,\beta}(s,\vec{q}_k - \vec{q}_l)_\beta \langle \vec{q}_l, -\vec{q}_l|,$$

where H_0 and H_I are the free and interacting Hamiltonian. The i, j and α, β represent the bare $c\bar{s}$ core and the $D^{(*)}K$ channels, respectively. k, l are the indices of the discretized momentum. The discretized energy levels were obtained from the eigenvalues of the Hamiltonian matrix for each L, which are used to compare with the ones in the lattice QCD as shown in Fig. 26. In the figure, the data in the 0^+ and 1^+ sectors was used as input. In the 0^+ channel, the 0^+ $c\bar{s}$ core and the S-wave DK channels were involved. In the 1^+ one, two $c\bar{s}$ cores with $J^P = 1^+$ as well as the S-wave and D-wave D^*K channels were considered. The lowest eigenvalue corresponded to the $D_{s1}(2460)$ and its $c\bar{s}$ core had a significant mass shift due to the coupling with the S-wave D^*K channel. In contrast, the $c\bar{s}$ core for the $D_{s1}^*(2536)$ mainly couples with the D-wave D^*K channel and its energy levels tended to be stable. With the increasing length, the kinetic energy of the D^*K channel decreased. When its eigenvalue approached that of the $D_{s1}^*(2536)$, an interesting crossing appeared around $L = 3.5$ fm. In the 2^+ sector, the results for the $D_{s2}^*(2573)$ are the predictions from the Hamiltonian matrix with the 2^+ $c\bar{s}$ core and the D-wave DK as well as the D^*K channels. The authors determined the parameters and got the unitarized T-matrix through the Lippmann-Schwinger equation in the infinite volume. The physical $D_{s0}^*(2317)$ and $D_{s1}(2460)$ are the mixtures of the bare $c\bar{s}$ core and $D^{(*)}K$ component with the probabilities $P_{D_{s0}^*(2317)}(DK) \approx 68.0\%$ and $P_{D_{s1}(2460)}(D^*K) \approx 47.6\%$, respectively. The $D_{s1}^*(2536)$ and $D_{s2}^*(2573)$ are almost dominated by the bare $c\bar{s}$ core with $P_{D_{s1}^*(2536)}(c\bar{s}) \approx 98.2\%$ and $P_{D_{s2}^*(2573)}(c\bar{s}) \approx 95.9\%$, respectively. The different mass shifts and mixing patterns of the four D_s states are governed by the heavy quark symmetry. In the heavy quark limit, the $c\bar{s}$ cores in the $D_{s0}^*(2317)$ and $D_{s1}(2460)$ can couple with the S-wave DK and D^*K channels, respectively. However, the coupling of the $c\bar{s}$ cores in the $D_{s1}^*(2536)$ and $D_{s2}^*(2573)$ with the S-wave two-meson channels are forbidden by HQSS. They can only couple with the D-wave ones which are significantly suppressed in the vicinity of the thresholds. Another prediction was that the mass of the $D_{s0}^*(2317)$ tended to be stable with increasing m_π which can be checked in the future lattice calculation.

With the interplay of the $c\bar{s}$ and D^*K components, the positive parity D_s states can take two forms: either a compact $c\bar{s}$ state dressed by the $D^{(*)}K$ or a molecular state dominated by the $D^{(*)}K$ components. Both scenarios can explain the mass shifts observed in comparison to the prediction from the conventional quark model. To distinguish these two scenarios, the experimental observations of the electromagnetic decays into $D_s^{(*)}\gamma$ or strong decays into the isospin-violating $D^{(*)}\pi^0$ channels will be very helpful. In Sec. 3.3.1, the significant differences in the decays of $D_{s0}^*(2317)$ and $D_{s1}(2460)$ in the compact and molecular scenarios were discussed. The decay widths for the $D^{(*)}\pi$ modes are less than 10 keV in the compact scenario [816, 761], while the molecular scenario leads to the enhanced decay widths due to the isospin-breaking effects in the K and $D^{(*)}$ meson masses via loops. For examples, the widths were around 100 keV in Refs. [818, 762, 763].

One may also compare the formation mechanisms of the molecular D^*K states. In Sec. 4.2.1, the molecular state is formed via the $D^{(*)}K$ interactions in χPT, which are then used as the kernel in the chiral unitary method. This subsection considers the interplay between the $c\bar{s}$ component and the $D^{(*)}K$. Besides the interactions in the D^*K channels, the $D^{(*)}K$ can also interact through exchanging the compact $c\bar{s}$ state. Both mechanisms without and with the $c\bar{s}$ component can describe the physical $D_{s0}^*(2317)$ and $D_{s1}(2460)$ masses as well as lattice QCD data and yield the consistent probabilities of the $D^{(*)}K$ components (over 60%). These probabilities were extracted using either the Weinberg's compositness relation or the wave function of the physical state. The contribution of the $c\bar{s}$ component to the $D^{(*)}K$ interactions in the latter case is short-range, which may be incorporated into the LECs in the chiral Lagrangian. These LECs can be determined from experiments or lattice simulations. Then both mechanisms contain physically similar information and can be considered more or less equivalent in this context as the results are consistent.
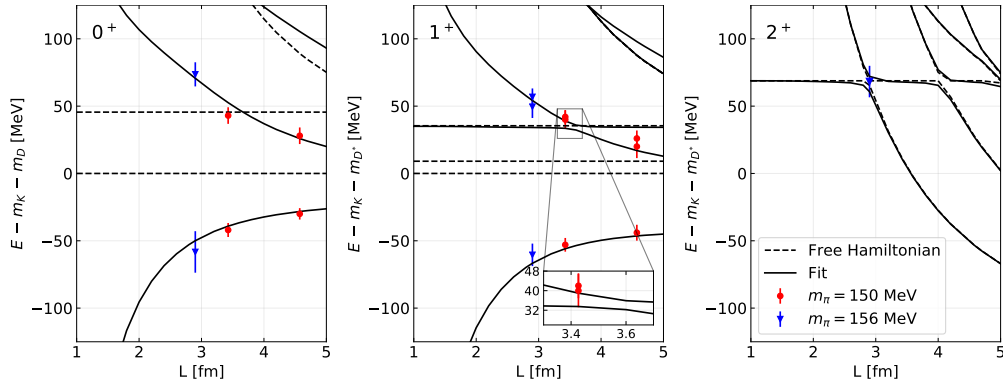
Figure 26: The comparison of the dependence of lattice binding energies on length L for the $D_{s0}^*(2317)$ (left), the $D_{s1}(2460)/D_{s1}^*(2536)$ (middle), and $D_{s2}^*(2573)$ (right) states with the pion mass $m_\pi = 150$ MeV [890] and $m_\pi = 156$ MeV [889]. The black curves stand for the eigenvalues using the finite-volume Hamiltonian, while the dashed lines represent those of the bare $c\bar{s}$ cores and $D^{(*)}K$ thresholds obtained with the free Hamiltonian H_0. Figures taken from Ref. [894].

4.2.3. Two-pole structures of $D_0^*(2300)$ and $D_1(2430)$

The structures of the $D_{s0}^*(2317)$ and the $D_{s1}(2460)$ have been successfully disentangled with the chiral unitary methods as discussed in Sec. 4.2.1. Under the SU(3) flavor symmetry, the unitarized scattering amplitude can be directly extended to study the other $\mathcal{H}\varphi$ scattering channels as shown in Fig. 24 and Table 5. The possible strangeness-isospin quantum numbers of the $\mathcal{H}\varphi$ channels are

$$(S, I) = (2, \tfrac{1}{2}),\ (1, 0),\ (1, 1),\ (0, \tfrac{1}{2}),\ (0, \tfrac{3}{2}),\ (-1, 0),\ (-1, 1). \tag{281}$$

One striking observation is that there are two poles in the channels with the strangeness-isospin quantum numbers $(S, I) = (0, 1/2)$ where the $D^{(*)}\pi$, $D^{(*)}\eta$ and $D_s^{(*)}\bar{K}$ are involved in the 0^+ (1^+) sector as illustrated in Fig. 27.

The presence of the two-pole structures originated from the Weinberg-Tomozawa terms at LO, which read [880,

Table 5: The possible strange-isospin quantum numbers (S, I) for the $\mathcal{H}\varphi$ system. The symbols "×", "⊗", and "○" represent that the pole does not exist, exists perhaps, does exist, respectively. The script "Irreps." denotes the irreducible representations in the SU(3) flavor symmetry.

(S, I)	Irreps.	channels	$\langle \boldsymbol{F}_{\mathcal{H}} \cdot \boldsymbol{F}_{\varphi} \rangle_{\mathcal{H}\varphi}$	Poles	References
$(2, \frac{1}{2})$	$\overline{\mathbf{15}}_f$	$D_s K$	$\frac{1}{2}$	×	
$(1, 1)$	$\overline{\mathbf{15}}_f, \mathbf{6}_f$	$\begin{pmatrix} DK \\ D_s\pi \end{pmatrix}$	$\begin{pmatrix} 0 & -\frac{1}{2} \\ -\frac{1}{2} & 0 \end{pmatrix}$	$\begin{pmatrix} \times \\ \times \end{pmatrix}$	cusp effect [37, 54], no experimental relavant pole [899, 39, 42].
$(1, 0)$	$\overline{\mathbf{15}}_f, \bar{\mathbf{3}}_f$	$\begin{pmatrix} DK \\ D_s\eta \end{pmatrix}$	$\begin{pmatrix} -1 & -\frac{\sqrt{3}}{2} \\ -\frac{\sqrt{3}}{2} & 0 \end{pmatrix}$	$\begin{pmatrix} \circ \\ \times \end{pmatrix}$	$D_{s0}^*(2317)$ (see Sec. 4.2.1)
$(0, \frac{3}{2})$	$\overline{\mathbf{15}}_f$	$D\pi$	$\frac{1}{2}$	×	
$(0, \frac{1}{2})$	$\overline{\mathbf{15}}_f, \mathbf{6}_f, \bar{\mathbf{3}}_f$	$\begin{pmatrix} D\pi \\ D\eta \\ D_s\bar{K} \end{pmatrix}$	$\begin{pmatrix} -1 & 0 & -\frac{\sqrt{6}}{4} \\ 0 & 0 & \frac{\sqrt{6}}{4} \\ -\frac{\sqrt{6}}{4} & \frac{\sqrt{6}}{4} & -\frac{1}{2} \end{pmatrix}$	$\begin{pmatrix} \circ \\ \times \\ \circ \end{pmatrix}$	two-pole structures (see Sec. 4.2.3)
$(-1, 1)$	$\overline{\mathbf{15}}_f$	$D\bar{K}$	$\frac{1}{2}$	×	
$(-1, 0)$	$\mathbf{6}_f$	$D\bar{K}$	$-\frac{1}{2}$	⊗	cusp effect [37, 54], virtual [899], bound states [39]
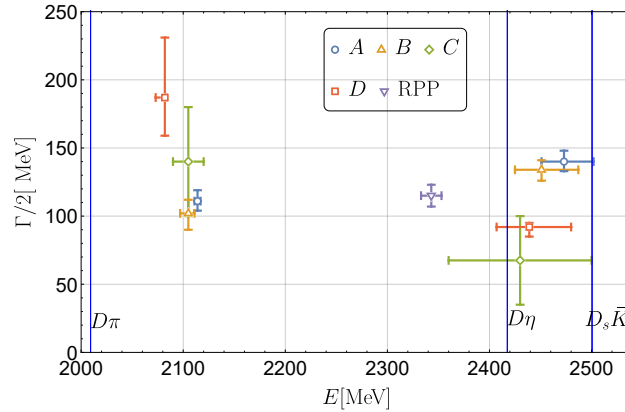
Figure 27: The comparison of the two-pole structures in the chiral unitary approaches for the channels with the strangeness-isospin number $(S, I) = (1, \frac{1}{2})$ and RPP [1]. The A, B, C, D represent the results in Ref. [51], Refs. [899, 901], Ref. [54], Refs. [895, 904], respectively.

881] [14]

$$V^{(\text{WT})}(s,u) \sim -C_{\alpha,\mathcal{H}\varphi}\frac{(s-u)}{4f_\varphi^2}, \qquad C_{\alpha,\mathcal{H}\varphi} = -\left\langle 2\boldsymbol{F}_{\mathcal{H}}\cdot\boldsymbol{F}_\varphi\right\rangle_\alpha = C_2(\mathcal{H}) - C_2(\alpha) + 3, \qquad (282)$$

with α the flavor representation of the $\mathcal{H}\varphi$ system. $\boldsymbol{F}_{\mathcal{H}}$ and $\boldsymbol{F}_\varphi$ are the SU(3) generators for the heavy meson and the light Goldstone boson. C_2 is the Casimir operator. For the $\overline{\mathbf{15}}_f \oplus \mathbf{6}_f \oplus \bar{\mathbf{3}}_f$ flavor representations as shown in Fig. 24, the LO potentials are $V^{\text{WT}} \sim (1,-1,-3)w$ where the w is positive. Thus, the $\mathcal{H}\varphi$ potentials are attractive in the $\mathbf{3}_f$ and $\mathbf{6}_f$ representation, while they are repulsive in the $\overline{\mathbf{15}}_f$ one. Furthermore, the attractive potentials in the anti-triplet channel are much stronger than that in the sextet one. In the SU(3) limit, the lower pole therefore belongs to the $\bar{\mathbf{3}}_f$ which is the partner state of the $D_{s0}^*(2317)$ $[D_{s1}(2460)]$ state with isospin $I=0$, while the higher pole belongs to the sextet. The two-pole structures have been predicted using the LO unitarized scattering amplitude in the chiral unitary method [37, 44, 42, 43, 900, 45] as mentioned in Sec. 4.2.1. In literature, there were extensive discussions of the similar two-pole structures [941] in the $K_1(1270)$ [556, 942, 943] and $\Lambda(1405)$ systems [551, 944, 586, 945].

The chiral amplitudes up to NLO [47, 884, 51, 899, 54] and N^{2}LO [895, 946] do not change the predictions. As mentioned in Sec. 4.2.1, the authors of Ref. [55] used the same NLO unitarized amplitude and the fixed LECs from the lattice scattering lengths in Ref. [884] to provide a good description of the energy levels in the 0^+ and 1^+ charm-strange channels from the later lattice QCD calculation [890]. In Ref. [899], the authors extended the same formalism to predict the finite volume energy levels of the strangeness-isospin $(S,I)=(0,1/2)$ channel with $J^P=0^+$. They considered the S-wave $D\pi$, $D\eta$ and $D_s\bar{K}$ coupled-channel scatterings and found two poles at $(2105^{+6}_{-8} - i102^{+10}_{-12})$ MeV and $(2451^{+36}_{-26} - i134^{+7}_{-8})$ MeV, which dominantly couples with the $D\pi$ and $D_s\bar{K}$ channels, respectively. Their results successfully described the finite volume energy levels of the coupled-channel $D\pi, D\eta$ and D_sK scattering from the later lattice QCD calculations [891] in the c.m.s as shown in Fig. 28. The consistence seemed to support the existence of the two pole structures. The same resonance patterns also occurred to their partners in the bottom sector. The authors also investigated the trajectories of the two poles from the physical to the SU(3) symmetric cases by varying the meson masses. In Ref. [54], the authors fitted the lattice data [891] in the strangeness-isospin $(S,I)=(0,\frac{1}{2})$ channels obtained in the c.m.s and the moving frames. The extracted parameters are similar to those in Ref. [899].

The successful descriptions of the lattice QCD results, for instance, the scattering lengths [884, 54, 47, 51, 895, 946], the phase shift [54, 895, 946], the finite energy levels in the charmed strange channels [55, 54] as well as the charmed channels with $(S,I)=(0,1/2)$ the Refs. [899, 54], tended to support the existence of the two-pole structures for the positive D_0^* and D_1^* charmed mesons.

Up to now, only one pole was reported in lattice QCD simulations [891, 898]. In Ref. [891], the Hadron Spectrum Collaboration reported a scalar D_0^* meson with $m_\pi \simeq 390$ MeV. Very recently, the Hadron Spectrum Collaboration computed the isospin-$\frac{1}{2}$ $D\pi$ scattering amplitudes using lattice QCD at $m_\pi \approx 239$MeV and found a broad D_0^* resonance around $2200 - i400$ MeV [898], which was lighter than $D_{s0}^*(2317)$. Its mass was consistent with the predictions for the lower D_0^* state in the chiral unitary approaches.

In Ref. [901], the authors argued that the amplitudes in lattice QCD simulations [891] contained an additional pole, but the pole position depended strongly on the parametrization. The pole might be located too deep in the complex plane to be captured at $m_\pi \simeq 390$MeV [899, 901, 54]. They concluded the existence of the additional pole was not ruled out. In Ref. [901], the authors studied the mass trajectory of the sextet pole with different Goldstone boson mass m_φ by varying the quark masses in the SU(3) symmetric case. The result is displayed in the right panel in Fig. 28. With the increasing m_φ, the energy-dependent LO WT terms become larger and lead to the stronger $\mathcal{H}\varphi$ potentials. The sextet pole changes from the resonance to the virtual state and even the bound state with a large enough m_φ [901]. The authors of Ref. [58] studied the lightest $D_{s0}^*(2317)$ and D_0^* as well as their axial vector partners at the SU(3) symmetric point using lattice QCD. They found the evidence for the nontrivial bound sextet state at $M_\pi = 612(90)$ MeV. More lattice calculations are needed to check the extra sextet pole.

There is only one scalar and one axial-vector charmed meson listed in the Review of Particle Physics [1], the $D_0^*(2300)$ and $D_1(2430)$. Their resonance parameters were extracted with a simple Breit-Wigner (BW) parametrization

---

[14]The potential is obtained with the scattering amplitude in Eq. (264). In some theoretical works, the $C_{\alpha,\mathcal{H}\varphi}$ is related to C_{LO} up to the additional form factors due to the renormalization, for instance $\sqrt{\left(m_{\mathcal{H}_i}+E_{\mathcal{H}_i}\right)\left(m_{\mathcal{H}_j}+E_{\mathcal{H}_j}\right)/\left(4m_{\mathcal{H}_i}m_{\mathcal{H}_j}\right)}$.
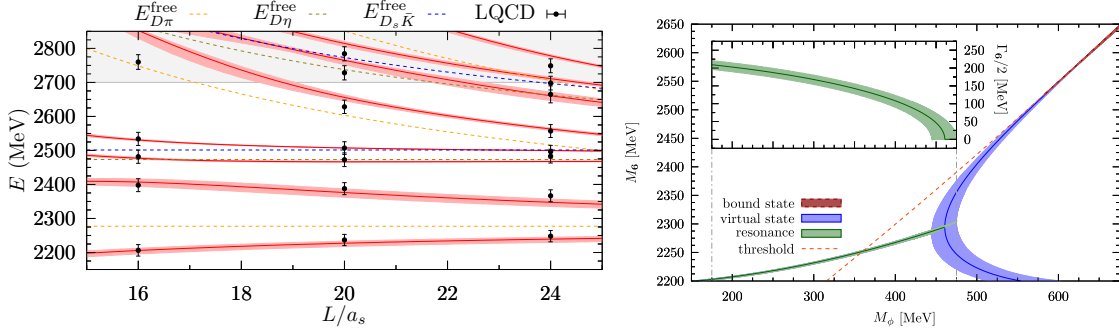
Figure 28: Left panel: Comparison of the predictions from Ref. [899] for the energy levels in the $(S, I) = (0, 1/2)$ channel with the lattice QCD data [891] (black dots) using $m_\pi \simeq 391$ MeV (red lines and bands). Right panel: Mass of the predicted sextet state M_6 at the SU(3) symmetric point as a function of the Goldstone boson mass M_φ. The left and right panel are taken from Ref. [899] and Ref. [901], respectively.

in the $D^{(*)}\pi$ invariant mass spectrum, which correspond to the constant interaction vertices. The pionic couplings contain the additional E_π dependence from the chiral symmetry (Goldstone theorem). The inclusion of the energy-dependent interaction results in a shift of the pole position from the simple Breit-Wigner parametrization [908]. Moreover, the $D^*_{s0}(2300)$ signal spreads in a wide range and the high energy region overlaps with the S-wave $D^{(*)}\eta$ and the $D^{(*)}_s \bar{K}$ thresholds. Thus, the coupled-channel effects should be taken into consideration [908, 947]. The $B^- \to D^+\pi^-\pi^-$ decay might help to confirm the molecular explanation of the D^*_{s0} states as well as the two-pole structures [947]. The unitarized $D\pi$ scattering amplitude seemed to describe the LHCb data quite well as shown in Fig. 29. In the vicinity of the $D^*_0(2300)$ and $D_1(2430)$, there are two broad D^*_0 and two D^*_1 states produced. The wide $D^*(2300)$ state in RPP is actually a combination of two D^*_0 poles. The mass of the lowest D^*_0 was predicted to be around 2.1 GeV.
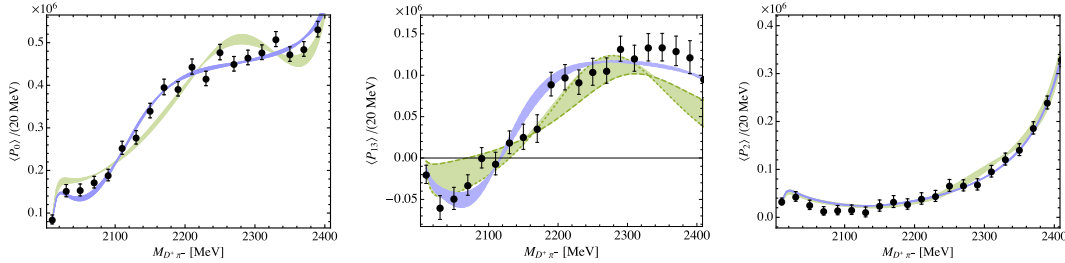
Figure 29: The best fits of the LHCb angular moments (denoted with the black dot) [909] using the Breit-Wigner parametrization (green band, $\chi^2/$d.o.f = 2.0) and the unitarized amplitude in the chiral unitary approach (blue band, $\chi^2/$d.o.f = 1.2).

The existence of the $D^*_{s0}(2317)$ [$D_{s1}(2460)$], and the two-pole structures of the charmed meson with $(S, I) = (0, \frac{1}{2})$ are closely related to the chiral dynamics through the WT terms. After the spontaneous breaking of the chiral symmetry, the remaining SU(3) flavor symmetry constrains the $\mathcal{H}\varphi$ molecules as the multiplet in Table 5. The flavor representation can be directly used to determine the existence of the pole in the SU(3) limit. According to Eq. (282), the potentials for the $\overline{\mathbf{15}}_f$, $\mathbf{6}_f$ and $\bar{\mathbf{3}}_f$ are repulsive, attractive, and more attractive, respectively. There are no poles in the $(S, I) = (2, \frac{1}{2})$, $(S, I) = (0, \frac{3}{2})$, and $(S, I) = (-1, 1)$ channels in the $\overline{\mathbf{15}}_f$ representation. The potential in the $(S, I) = (-1, 0)$ channel is attractive but weaker than that in the $\bar{\mathbf{3}}_f$ channel, hence the existence of the pole is uncertain and still in discussion.

With the SU(3) symmetry breaking, the states with the other (S, I) are composed of the $\mathcal{H}\varphi$ channels with different thresholds as shown in the lower panel of Fig. 24. The mass splittings between different channels break the SU(3) flavor symmetry and play an important role in the formation of the unnatural states. Especially, their underlying structures are sensitive to these thresholds. For instance, in the $(0, \frac{1}{2})$ sector, the $D_s\bar{K}$ is located around 490 MeV

higher than the $D\pi$ one. The lower D_0^* mainly couples to the $D\pi$ channel while the higher one couples to the $D_s\bar{K}$ channels. Thus, it may be more reasonable to categorize the states using the channels instead of the SU(3) flavor representations.

In the quark model, there only exists one non-strange scalar charmed meson below 2.4 GeV. In the molecular scenario, the positive parity D-states can be dynamically generated through the scattering of the pseudo-scalar meson and the ground state charm meson. Such an interaction arises from the Weinberg-Tomozawa terms at LO. In other words, the presence of the positive parity molecular D-states is closely related to the chiral symmetry. Moreover, there exist two broad molecular states. The higher state is around 2.45 GeV while the lower one is around 2.1 GeV. Both of them have a large width around $200 \sim 400$ MeV. The large widths of the $D_0^*(2300)$ and $D_1(2430)$ suggest that they may correspond to two distinct D_0^* and two D_1^* poles respectively. Up to now, the two-pole structures with a large decay width seemed to describe the experimental data successfully. More lattice QCD calculations from different groups are needed to examine the two-pole structures of the D_0^* and D_1^* mesons carefully.

4.3. Scatterings of Goldstone bosons off the heavy baryons

The frameworks developed to investigate the $D_{s0}^*(2317)$ and $D_{s1}(2460)$ were also used to explore the scattering of the light pseudoscalar mesons (φ) off the heavy baryons (B_Q or B_{QQ}) and predict the exotic states [948, 695, 949, 950, 951]. Among them, the φB_{QQ} systems are the most interesting ones [949, 950, 951] because the B_{QQ} can be related to the heavy-light mesons in the HDAS as discussed in Sec. 2.2.2. The same chiral dynamics between φB_{QQ} and $\varphi D(\bar{B})$ in the HDAS limit leads to the possible existence of the analogs of $D_{s0}^*(2317)$ and $D_{s1}(2460)$ in the doubly heavy sector. We review the calculation within the EFT frameworks. The above systems were also explored in other approaches (e.g. Refs. [952, 953]).

In Ref. [948], Liu *et al* investigated the pseudoscalar meson and decuplet baryon scattering lengths to N^{2}LO within HBχPT. The same framework was extended to calculate the scattering of the pseudoscalar meson off the singly charmed baryons in Ref. [695]. In their calculation, the mass splittings of the different multiplets were kept in the small scale expansion scheme [954, 955]. The chiral expansion was performed to N^{2}LO including the diagrams similar to Figs. 20, 21 and 23. In the numerical analysis, the authors adopted the SU(4) flavor symmetry to determine the LECs. From the signs of the scattering lengths, one can get a rough idea about the possible existence of the loosely bound state in each channel.

In Ref. [950], Meng and Zhu investigated the scattering lengths of $\varphi B_{cc}^{(*)}$ to $O(p^3)$ in the HBχPT. Within the HDAS, the LECs are related to those of the $\varphi D^{(*)}$ scattering in Ref. [877, 879]. The authors proved that the analytical results for the scattering lengths in the HDAS satisfy

$$a_{\varphi B_{cc}} = a_{\varphi B_{cc}^*} = a_{\bar{\varphi}D} = a_{\bar{\varphi}D^*}. \tag{283}$$

The corrections from the recoil effect and the mass splitting between spin-$\frac{1}{2}$ and spin-$\frac{3}{2}$ doubly charmed baryons were tiny. The LECs determined from fitting lattice QCD results [884] and using the resonance saturation model are consistent with each other. The interactions for the $[\pi\Xi_{cc}^{(*)}]^{(1/2)}$, $[K\Xi_{cc}^{(*)}]^{(0)}$, $[K\Omega_{cc}^{(*)}t]^{(1/2)}$, $[\eta\Xi_{cc}^{(*)}]^{(1/2)}$, $[\eta\Omega_{cc}^{(*)}]^{(0)}$, and $[\bar{K}\Xi_{cc}^{(*)}]^{(0)}$ channels are attractive, where the superscripts represent the isospin. Among them, the most attractive channel $[\bar{K}\Xi_{cc}^{(*)}]^{(0)}$ is likely to form the analogs of the $D_{s0}^*(2317)$ $[D_{s1}(2460)]$ in the doubly heavy sector.

In Ref. [949], Guo predicted several states by investigating the S-wave scattering of the doubly charmed baryons ($\Xi_{cc}^{++}, \Xi_{cc}^+, \Omega_{cc}^+$) and the light pseudoscalar mesons (π, K, η) in the unitarized LO chiral effective field theory. They predicted a $\Xi_{cc}\bar{K}$ bound state in the $(S, I) = (-1, 0)$ channel and two resonance structures in the $\Xi_{cc}\pi$, $\Xi_{cc}\eta$ and $\Omega_{cc}K$ coupled channels with $(S, I) = (0, 1/2)$. They are the analogs of the $D_{s0}^*(2317)$ and the two-pole structures for the D_0^* in the doubly charmed sector.

In Ref. [951], the authors predicted the negative-parity doubly charmed baryons by investigating the scattering of the light pseudoscalar off the ground doubly charmed baryons using the unitarized version of χPT up to NLO. The authors considered the mixing effect between the φB_{cc} molecules and the P-wave doubly charmed baryons B_{cc}^P. The B_{cc}^P is the conventional baryon with the P-wave excitation within the (cc) diquark, which is expected to be the lowest excitation of the doubly charmed baryons [956, 502, 504]. They predicted two narrow states in $(S, I) = (-1, 1/2)$ channel and one narrow state in the $(S, I) = (0, 1/2)$ channel, respectively.

5. Chiral effective field theory for heavy hadronic molecules

In this section, we will review the applications of the EFT in the hadronic molecules composed of two matter fields. An important analog is the deuteron in the *NN* systems. In order to investigate the deuteron-like states in the heavy flavor sector, numerous EFTs are constructed. In this section, we will first review these EFTs from the simple to complex ones, specifically from the single-channel EFTs to coupled-channel EFTs, from the pionless EFTs [πEFTs (contact EFTs)] to the chiral EFT, from the perturbative pion EFTs to nonperturbative pion EFTs. After that, we will review applications of these EFTs to specific hadronic molecular candidates. One may also consult the review in Ref. [11]. Since we are only interested in the energy regions close to two hadron thresholds, the EFTs for the hadronic molecules are usually nonrelativistic.

Unlike the χEFT for the *NN* systems which is constrained by the precise *NN* phase shifts from the experiments, the EFTs constructed for the hadronic molecules are still preliminary. In this section, we will also review some frameworks that are not rigorous EFTs but incorporate the spirits of EFT. From our perspective, an EFT is the quantum field theory which should include quantum fluctuations and renormalizations. Therefore, we will pay more attentions to the frameworks which include quantum fluctuations (either by calculating loop corrections or iterating nonperturbatively) and scale-independent renormalizations. After all, the tree-level results or the cutoff-sensitive results from the so-called EFTs are usually equivalent to some classical frameworks. Meanwhile, the EFTs are based on separated scales and specific symmetries. In this section, we will discuss some frameworks making use of separated scales and symmetries. In principle, the EFTs are performed according to the power counting which originates from the scale analysis and should manifest convergence in high order calculations. According to the present experimental status, it is usually hard to fix the LECs in higher order calculations. Therefore, in this section, we have to pay some attentions to the validity of the scale analysis.

5.1. Pionless EFT

5.1.1. Single-channel systems

We start from the LO pionless EFT in the single-channel for the S-wave systems. The interaction between particles A and B is $V(p, p') = v\Theta(\Lambda - p)\Theta(\Lambda - p')$. We choose a cutoff UV regulator $\Theta(\Lambda - p)$ in this section. One can also use other regularization schemes such as the PDS in Sec. 2.7.1, which will not change the results qualitatively. In order to reproduce a bound state or virtual state, we resum the interaction nonperturbatively via LSEs,

$$T(p, p') = V(p, p') + \int \frac{d^3q}{(2\pi)^3} V(p, q) G(E, q) T(q, p'), \qquad G(E, q) = \frac{1}{E - \frac{q^2}{2\mu} + i\epsilon}. \tag{284}$$

For such a separable interaction, we can assume the T-matrix is also separable, i.e., $T(p, p') = t\Theta(\Lambda - p)\Theta(\Lambda - p')$. Then the LSEs can be solved as

$$t = v + vFt, \implies t^{-1} = v^{-1} - F, \tag{285}$$

where the F is

$$F(E) = \int^{\Lambda} \frac{d^3q}{(2\pi)^3} \frac{1}{E - \frac{q^2}{2\mu} + i\epsilon} \approx \begin{cases} -\frac{\mu}{2\pi}\left(\frac{2}{\pi}\Lambda + ik\right) & \text{with } E > 0, \ k \equiv \sqrt{2\mu E} \\ -\frac{\mu}{2\pi}\left(\frac{2}{\pi}\Lambda - \kappa\right) & \text{with } E \leq 0, \ \kappa \equiv \sqrt{-2\mu E} \end{cases}. \tag{286}$$

In the cutoff regularization, the F has the linear UV behavior which is similar to that of PDS in Eq. (158) up to a factor for Λ. One can see the relation of the cutoff regularization and dimensional regularization for the nonrelativistic system in Ref. [957]. Meanwhile, the $(v^{-1} - F)$ should be cutoff-independent to make the T-matrix renormalization group invariant. The pole of the T-matrix obtained in the real axis from $v^{-1} - F(E) = 0$ corresponds to the bound state (in the first Riemann sheet) or virtual state (in the second Riemann sheet) of the AB system.

It was shown that the πEFT is equivalent to the ERE [628]. We will illustrate the equivalence at the LO. One can perform the ERE as

$$t^{-1} = -\frac{\mu}{2\pi}(k\cot\delta - ik) = -\frac{\mu}{2\pi}\left(-\frac{1}{a_s} - ik + \frac{1}{2}r_0 k^2 ...\right)$$

$$= v^{-1} - F = -\frac{\mu}{2\pi}\left(-\frac{2\pi}{\mu}v^{-1} - \frac{2}{\pi}\Lambda - ik\right). \tag{287}$$

One can obtain the k^0 and k^1 terms from the LO πEFT, which matches to the ERE truncated at the LO. The scattering length term and t^{-1} read, respectively,

$$\frac{1}{a_s} = \left(\frac{2\pi}{\mu}v^{-1} + \frac{2}{\pi}\Lambda\right), \qquad t^{-1} \sim \left(-\frac{1}{a_s} - ik\right). \tag{288}$$

The k^1 term is required by the unitarity. The approximation of using the contact interaction without derivative is equivalent to keeping the LO ERE (only the scattering length term). The effective range and higher order terms are neglected. For $a_s > 0$, one can see the $E = -\gamma^2/(2\mu) = -1/(2\mu a_s^2)$ corresponding to a bound state pole with the binding momentum $\gamma = 1/a_s$. For $a_s < 0$, one can see that $E = -1/(2\mu a_s^2)$ at the second Riemann sheet corresponds to a virtual state.

For the system with a bound state, the T-matrix can be reexpressed as

$$t^{-1} \sim (-\gamma - ik). \tag{289}$$

Another interesting quantity is the coupling constant g of the bound state X and its components A and B. As shown in Fig. 30(a), the vertex of XAB is $g\Theta(\Lambda - p)$. The T-matrix of the A and B scattering is saturated by the bound state. The coupling constant is obtained from the residue of t at its pole position [958, 959], i.e.,

$$t \sim \frac{g^2}{E - E_X}, \quad \Longrightarrow \quad g = \frac{4M_X \sqrt{\pi\gamma}}{\sqrt{\mu}}. \tag{290}$$

The coupling constant only depends on the binding energy which is determined by the scattering length. The relation between the coupling constant and $\sqrt{\gamma}$ is also derived from the Weinberg compositeness criterion [221] in the case of a pure molecule.

One can construct the composite operator $\hat{X}(x) \equiv \hat{A}(x)\hat{B}(x)$, where $\hat{A}$ and $\hat{B}$ are the field operators of A and B, respectively. The bound state can also be determined by the pole of the two-point Green's function of $\hat{X}$ [960],

$$G(E) = \int d^4x e^{-iEt}\langle 0|T\{X^\dagger(x)X(0)\}|0\rangle = i\frac{Z(E_X)}{E - E_X + i\epsilon}, \tag{291}$$

where $T\{...\}$ represents the time-ordered product. The Green's function can be calculated from the diagrams in Fig. 30(b) as

$$G = \Sigma + \Sigma(-iv\Sigma) + \Sigma(-iv\Sigma)^2 + ... = \frac{\Sigma(E)}{1 + iv\Sigma(E)} = \frac{iF}{1 - vF}, \tag{292}$$

where the $\Sigma = iF$ is used. We obtain the same equation of the binding energy $1 - vF = 0$ as that from the LSEs. The wave function renormalization factor Z is determined as

$$Z(E_X) = \frac{1}{2\pi}\left(\frac{2}{\pi}\Lambda - \gamma\right)^2 \gamma. \tag{293}$$

One notes that the dimension of Z is M^3. In our calculation, we adopt the fields of the $\hat{A}$ and $\hat{B}$ with the dimension $M^{3/2}$ as in most of the NREFT calculations. Thus, the composite operator $\hat{X}(x) \equiv \hat{A}(x)\hat{B}(x)$ carries the dimension M^3 and finally gives rise to the Z with M^3. In the present discussion, we focus on the relations of Z with the cutoff and binding momentum.

The above results about the bound state can also be obtained in the language of quantum mechanics. We investigate the same bound state in Schrödinger equation,

$$\frac{q^2}{2\mu}\phi(q) + \int \frac{d^3p}{(2\pi)^3} V(q,p)\phi(p) = -\frac{\gamma^2}{2\mu}\phi(q). \tag{294}$$
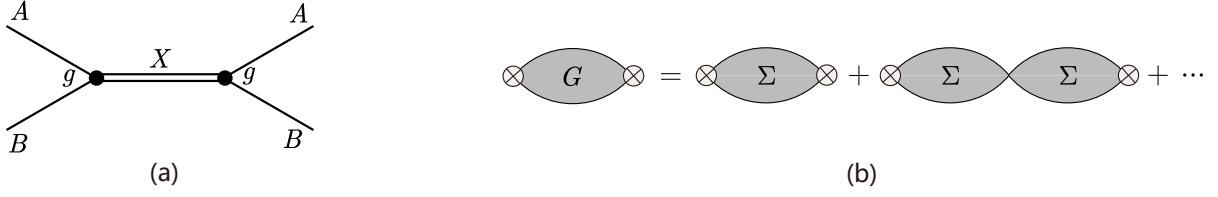
Figure 30: (a)The scattering of A and B is saturated by their bound state X. (b) The two point Green's function of $\hat{X}(x) \equiv \hat{A}(x)\hat{B}(x)$.

The wave function is

$$\phi(p) = \xi \frac{\Theta(\Lambda - p)}{-\frac{\gamma^2}{2\mu} - \frac{p^2}{2\mu}}, \qquad \xi^2 \approx \frac{\gamma}{4\pi^2\mu^2}, \tag{295}$$

where the normalization constant ξ is determined by $\int |\phi(p)|^2 d^3p = 1$. The wave function can be related to the scattering length as

$$\phi(p) = \frac{1}{\pi \sqrt{a_s}} \frac{1}{1/a_s^2 + p^2}, \qquad \varphi(r) = \frac{1}{\sqrt{2\pi a_s}} \frac{e^{-r/a_s}}{r}, \tag{296}$$

where we have taken the cutoff to infinity. $\varphi(r)$ is the wave function in the coordinate space. Another interesting quantity is the wave function at the origin,

$$\varphi(0) = -\frac{\gamma^{1/2}}{(2\pi)^{1/2}} \left(\frac{2}{\pi}\Lambda - \gamma \right), \tag{297}$$

which is cutoff-dependent and linear divergent.

One can set up two corresponding relations between the languages of quantum mechanics and quantum field theory,

$$\langle p|\hat{V}|\phi\rangle \sim g\Theta(\Lambda - p), \qquad \sqrt{Z} \sim \varphi(0). \tag{298}$$

One can take the approximation of the LSEs near the pole,

$$\hat{T} = \hat{V} + \hat{V}\frac{1}{E - \hat{H} + i\epsilon}\hat{V}, \implies T(p, p') \sim \frac{\langle p|\hat{V}|\phi\rangle\langle\phi|\hat{V}|p'\rangle}{E - E_X}, \tag{299}$$

with

$$\langle p|\hat{V}|\phi\rangle = \langle p|H - H_0|\phi\rangle = \left(E_0 - \frac{p^2}{2\mu} \right)\langle p|\phi\rangle = \xi\Theta(\Lambda - p). \tag{300}$$

One can see that the $\langle p|\hat{V}|\phi\rangle$ corresponds to the XAB vertex $g\Theta(\Lambda - p)$ in quantum field theory language. The bound state can be represented as

$$|X(\boldsymbol{P})\rangle \equiv \int \frac{d^3\boldsymbol{p}}{(2\pi)^3}\phi(\boldsymbol{p})|A(\boldsymbol{p}_1)B(\boldsymbol{p}_2)\rangle, \qquad \boldsymbol{P} \equiv \boldsymbol{p}_1 + \boldsymbol{p}_2, \quad \boldsymbol{p} \equiv \frac{\boldsymbol{p}_1 - \boldsymbol{p}_2}{2}. \tag{301}$$

From Eq. (291), we know the wave function renormalization factor Z can be extracted from

$$\langle X(P)|\hat{X}(x)|\Omega\rangle = \sqrt{Z}e^{iP\cdot x}. \tag{302}$$

With Eqs. (301) and (291), one notices that $\sqrt{Z} \sim \varphi(0)$ up to some constant factors. Both the quantum mechanics (e.g., [961, 962]) and quantum field theory (e.g., [963]) languages were used in literature.

From the above calculation, one can see that the binding energy, the wave function of the bound state and the low energy scattering properties are determined by one parameter a_s. For the two body system which admits a shallow bound state with an unnatural large scattering length, the low-energy behavior is universal and depends on the

scattering length only. For such a system, the LO ERE and LO contact interaction will be a good approximation (see Ref. [523] for a review of the universality).

In the LO single-channel contact interaction, since a_s is real, the pole of the T-matrix can only appear in the real axis corresponding to either the bound state or the virtual state. In order to interpret the resonance with a width, one can introduce the LO coupled-channel contact interaction or resort to the NLO contact interaction (e.g., [964, 311, 313]). In the LO coupled-channel contact scheme, one may obtain the effective a_s for the elastic channel with an imaginary part (e.g., [965]) considering the inelastic channel. It will be discussed in Sec. 5.1.2. Meanwhile, using the NLO contact interaction is equivalent to keeping the effective range term in ERE (e.g., see Refs. [346, 327, 605]).

We take the S-wave interaction to the NLO as an example,

$$V(p, p') = \frac{c_a}{\Lambda} + \frac{c_b}{\Lambda^3}(\boldsymbol{p}^2 + \boldsymbol{p'}^2), \tag{303}$$

where c_a and c_b are the LECs. For simplicity, we assume the interaction is independent on energy. For such a separable interaction, we adopt the techniques in Ref. [966] and obtain,

$$\frac{1}{T(k)} = \frac{-G_0\Lambda^5 c_a - 2G_2\Lambda^3 c_b + \left(G_2^2 - G_0 G_4\right)c_b^2 + \Lambda^6}{\Lambda^5 c_a + c_b\left[c_b\left(G_0 k^4 - 2G_2 k^2 + G_4\right) + 2k^2\Lambda^3\right]}, \quad \text{with } G_n = \int \frac{d^3 q}{(2\pi)^3} \frac{q^n}{E - \frac{q^2}{2\mu} + i\epsilon}. \tag{304}$$

In the hard cutoff regularization scheme, we obtain the analytical expressions of G_n as

$$G_0 = \frac{4\pi}{(2\pi)^3} 2\mu \left[k\tanh^{-1}\left(\frac{k}{\Lambda}\right) - \Lambda - i\frac{\pi}{2}k\right], \qquad G_n = k^2 G_{n-2} - \frac{\mu}{\pi^2}\frac{\Lambda^{n+1}}{n+1}. \tag{305}$$

Performing the effective range expansion, $T^{-1}(k) = -\frac{\mu}{2\pi}\left(-\frac{1}{a_s} - ik + \frac{1}{2}r_0 k^2 + ...\right)$, we obtain that

$$a_s = \frac{9\pi\mu\left(5\pi^2 c_a - \mu c_b^2\right)}{\Lambda\left(30\pi^2\mu\left(3c_a + 2c_b\right) - 8\mu^2 c_b^2 + 90\pi^4\right)}, \tag{306}$$

$$r_0 = \frac{4\left(30\pi^2\mu^2 c_b^2\left(10c_b - 9c_a\right) + 225\pi^4\mu\left(3c_a^2 + 5c_b^2\right) + 52\mu^3 c_b^4 + 1350\pi^6 c_b\right)}{27\pi\Lambda\mu\left(\mu c_b^2 - 5\pi^2 c_a\right)^2}. \tag{307}$$

Now, we obtain the non-vanishing r_0. The resonance poles can be obtained from $T^{-1} = 0$ in the NLO ERE formula [605].

With the above expressions, we can check the validity of of the extension of the argument of Landau and Smorodinsky in the non-local potential [536]. It was proved that the effective range is always positive ($r_0 > 0$) if the local potential is attractive everywhere, i.e., $V(r) < 0$ everywhere in their textbook [536]. The argument was cited in Ref. [222] to claim that "the molecular case gives always $r_0 > 0$". We use Eq. (303) as an example of the non-local potential case. For simplicity, we take $\Lambda = 1$ GeV and $\mu = 1$ GeV. We constrain the interaction in Eq. (303) via admitting a bound state with the binding energy $E_b = 1$ MeV, which will constrain the relation of the two LECs as shown in the left panel of Fig. 31. In the middle panel, we present the a_s and r_0 numerically. One can see that the negative r_0 is allowed for such a non-local interaction. In the right panel, we present the variation of the root-mean-square radii $r_{\rm rms}$ with the coupling constants. One can see these states are all loosely bound states with $r_{\rm rms}$ around 2−3 fm. Therefore, it is biased to conclude that the molecule solution implies the always positive effective range. See [540] for more detailed discussions on this issue.

5.1.2. Coupled-channel systems

In Ref. [967], Cohen, Galman and van Kolck proposed a coupled-channel EFT for two channels with different thresholds. For the LO contact interaction, the renormalization is given explicitly. Within the hard cutoff regularization, the interaction reads

$$V(p, p') = \begin{bmatrix} v_{11} & v_{12} \\ v_{12} & v_{22} \end{bmatrix} \Theta(\Lambda - p)\Theta(\Lambda - p'). \tag{308}$$
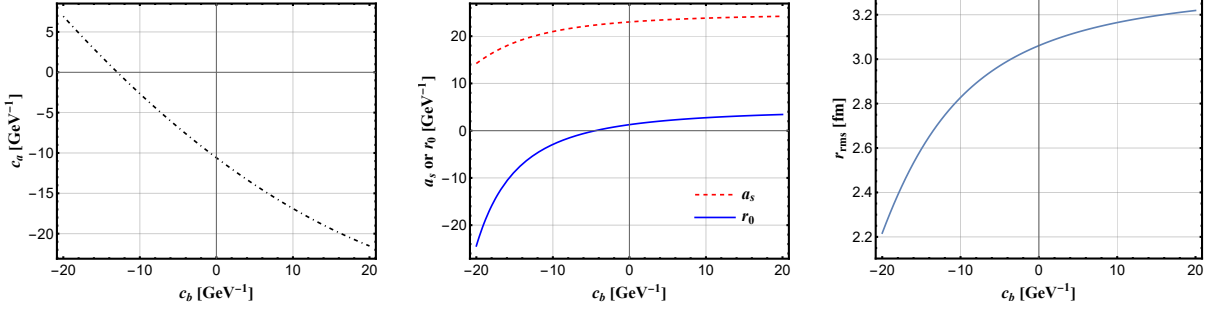
Figure 31: The scattering length and effective range for the system in the non-local interaction in Eq. (303) with a binding energy $E_b = 1$ MeV. The relation of c_a and c_b is constrained by permitting a bound state with the binding energy $E_b = 1$ MeV (left panel). The a_s and r_0 depend on the coupling constants (middle panel). The root-mean-square radii r_{rms} vary with the coupling constants (right panel).

For the separable interaction, one can transform the LSEs into the algebraic equation of the coefficient matrices v and t, i.e.,

$$T = V + VGT, \implies t = (1 - vF)^{-1}v, \tag{309}$$

where the $F = \text{diag}\{F_a, F_b\}$ with

$$F_a(E) = \int^\Lambda \frac{d^3 p''}{(2\pi)^3} \frac{1}{E - E_{a,p''}}, \qquad E_{a,p''} = \delta_a + \frac{p''^2}{2\mu_a}. \tag{310}$$

We can choose the $\delta_1 = 0$ and $\delta_2 = \delta$. We use the μ_i to represent the reduced masses of two channels. With the definitions $\kappa_1 \equiv \sqrt{-2\mu_1 E}$ and $\kappa_2 \equiv \sqrt{-2\mu_2(E - \delta)}$, the solution of the LSEs is

$$t^{-1} = \frac{1}{D} \begin{pmatrix} \frac{1}{\mu_1} b_{11} b_{12}^2 (1 - b_{22}\kappa_2) & \frac{1}{\sqrt{\mu_1\mu_2}} b_{11} b_{12} b_{22} \\ \frac{1}{\sqrt{\mu_1\mu_2}} b_{11} b_{12} b_{22} & \frac{1}{\mu_1} b_{12}^2 b_{22} (1 - b_{11}\kappa_1) \end{pmatrix}, \tag{311}$$

where $D = \frac{1}{2\pi} \left[b_{12}^2 (b_{11}\kappa_1 - 1)(b_{22}\kappa_2 - 1) - b_{11}b_{22} \right]$. The b_{11}, b_{22} and b_{12} are cutoff-independent parameters defined by

$$\begin{cases} \frac{1}{b_{11}} &= \frac{2\pi}{\mu_1} \left(\frac{v_{22}}{v_{11}v_{22} - v_{12}^2} - F_1 \right) + \kappa_1 \\ \frac{1}{b_{22}} &= \frac{2\pi}{\mu_2} \left(\frac{v_{11}}{v_{11}v_{22} - v_{12}^2} - F_2 \right) + \kappa_2 \\ \frac{1}{b_{12}} &= \frac{2\pi}{\sqrt{\mu_1\mu_2}} \frac{v_{12}}{v_{11}v_{22} - v_{12}^2} \end{cases} \tag{312}$$

The cutoff dependence in the F_1 and F_2 is canceled out by the cutoff-dependent coupling constants v_{ij}. Thus, the renormalization of the EFT is given explicitly. In literature, when a similar contact interaction as in Eq. (308) was used to depict the neutral and charged channels of $X(3872)$, it was often assumed that $v_{11} = v_{22} = v_{12} = v_{21}$, which is equivalent to the vanishing isovector interaction. However, we can see that the v_{12} and v_{11}, v_{22} in Eq. (312) have to cancel out the quite different divergent behavior. In such an EFT framework, one can set $v_{11} = v_{22}$. However, it is illegitimate to introduce the $v_{ii} = v_{12}$ or v_{21} in order to meet the renormalization group invariance.

For the coupled-channel system, if one expands the $1/t_{11}$ according to the ERE as

$$\frac{1}{t_{11}} = -\frac{\mu_1}{2\pi} \left[-\frac{1}{a_{\text{eff}}} + \frac{1}{2} r_{\text{eff}} k^2 - ik + \dots \right], \tag{313}$$

one can get the expression of the parameters a_{eff} and r_{eff} as

$$\frac{1}{a_{\text{eff}}} = \frac{1}{b_{11}} + \frac{1}{b_{12}^2} \left[\sqrt{2\delta\mu_2} - \frac{1}{b_{22}} \right]^{-1}, \qquad r_{\text{eff}} = -\frac{1}{\sqrt{2\delta\mu_2}} \frac{b_{22}^2}{\left(b_{12} \sqrt{2\delta\mu_2} - 1 \right)^2}, \tag{314}$$

82

where a_{eff} and r_{eff} represent the effective scattering length and effective range, respectively. If the second threshold is below the first one, i.e., $\delta < 0$, the inelastic channel (the second channel) renders a_{eff} a complex number. Another interesting conclusion is $r_{\text{eff}} < 0$ if the second threshold is larger than the first one, i.e., $\delta > 0$. In such a coupled-channel system, the bound state is allowable by tuning the parameters, but with the negative effective range, which is another example challenging the statement in Ref. [222].

Meanwhile, if a_{eff} is unnaturally large, the long-range behavior only depends on a_{eff}, which is the universality for the coupled-channel system [965]. From the expression of a_{eff}, one can see that the universality can be obtained by fine-tuning either the interaction or the threshold difference of the two channels.

If there exists the bound state solution with $E_0 < 0$, one can obtain the residues of the T-matrix (see Ref. [968] for details),

$$\lim_{E \to E_0} (E - E_0)t = \frac{2\pi}{\mu^2} \begin{bmatrix} \gamma_1 \cos^2 \theta & \sqrt{\gamma_1 \gamma_2} \sin \theta \cos \theta \\ \sqrt{\gamma_1 \gamma_2} \sin \theta \cos \theta & \gamma_2 \sin^2 \theta \end{bmatrix}, \tag{315}$$

with $\lim_{E \to E_0} \kappa_i \equiv \gamma_i$, and $\tan^2 \theta \equiv \frac{b_{22}\gamma_1(b_{11}\gamma_1-1)}{b_{11}\gamma_2(b_{22}\gamma_2-1)}$. The b_{12} is eliminated by setting $D = 0$. For convenience, we omit the difference of two reduced masses and set $\mu_1 = \mu_2 = \mu$. The coupling constants between the bound state and two channels are

$$g_1 = \frac{4M_T \sqrt{\pi\gamma_1}}{\sqrt{\mu}} \cos \theta, \qquad g_2 = \frac{4M_T \sqrt{\pi\gamma_2}}{\sqrt{\mu}} \sin \theta. \tag{316}$$

One can obtain similar results in quantum mechanics. The wave function of the bound states is

$$\langle \boldsymbol{p}|\psi\rangle = c_1\phi_1(p)|1\rangle + c_2\phi_2(p)|2\rangle, \qquad \phi_i(p) = \xi_i \frac{\Theta(\Lambda - p)}{E_0 - \frac{p^2}{2\mu} - \delta_i}, \qquad \xi_i^2 \approx \frac{\gamma_i}{4\pi^2\mu^2}. \tag{317}$$

Similar to the single-channel case, one gets

$$\langle \boldsymbol{p}, i|\hat{V}|\psi\rangle = \langle p, i|H - H_0|\psi\rangle = \left(E_0 - \frac{p^2}{2\mu} - \delta_i\right)\langle \boldsymbol{p}, i|\psi\rangle = c_i\phi_i(p) = c_i\xi_i\Theta(\Lambda - p). \tag{318}$$

When one relates $\langle \boldsymbol{p}, i|\hat{V}|\psi\rangle$ with $g_i\Theta(\Lambda - p)$, one can see that $c_1 = \cos\theta$ and $c_2 = \sin\theta$. Therefore, the θ angle defined in the quantum field theory language is just the mixing angle of the two channels.

5.2. XEFT

The XEFT is a nonrelativistic EFT to depict the long-range properties of the $X(3872)$, in which the D^{*0}, $\bar{D}^0$ and π^0 are explicit degrees of freedom [963]. It is very similar to the KSW scheme for the NN system in Sec. 2.7.1. In this section, we will take the $X \to D^0\bar{D}^0\pi^0$ and $D^0\bar{D}^{*0}/D^{*0}\bar{D}^0$ scattering as examples to illustrate this formalism.
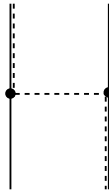
Figure 32: The one-pion exchange interaction for the $D^0\bar{D}^{*0}/D^{*0}\bar{D}^0$ scattering. The double (solid plus dashed) line denotes the $D^{*0}/\bar{D}^{*0}$, while the single solid and dashed lines denote the $D^0/\bar{D}^0$ and π^0, respectively.

For the $D^0\bar{D}^{*0}/\bar{D}^0D^{*0}$ scattering, the $D^{*0}D^0\pi^0/\bar{D}^{*0}\bar{D}^0\pi^0$ vertices contribute to the OPE interaction (see Fig. 32). The mass splitting $\Delta = M_{D^{*0}} - M_{D^0}$ will enter the pion propagator. The static OPE potential is [15]

---

[15]The f_π in Ref. [963] is different from that in this review by a factor $\sqrt{2}$.

Table 6: Some scales associated with the $X(3872)$. The $T^n = M_{D^{*0}} + M_{D^0}$ and $T^c = M_{D^{*+}} + M_{D^+}$ are the neutral and charged thresholds. $E_{\pi^0}^{\max} = (M_X^2 - 4M_{D^0}^2 + m_{\pi^0}^2)/(2M_X)$ is the maximum energy of the pion in the $X \to D^0 \bar{D}^0 \pi^0$ decay.

	$\Delta = M_{D^{*0}} - M_{D^0} = 142$ MeV,		$m_{\pi^0} = 135$ MeV	
Energy scale	$E_X^c \equiv T^c - M_X$	$E_X \equiv T^n - M_X$	$\delta = \Delta - m_{\pi^0}$	$E_{\pi^0}^{max} - m_{\pi^0}$
	8.4 MeV	0.2 MeV	7 MeV	6.6 MeV
Momentum	$\gamma^c = \sqrt{2\mu E_X^c}$ $\sim p_{D^*} \sim p_D$	$\gamma = \sqrt{2\mu E_X}$ $\sim p_{D^*} \sim p_D$	$u = \sqrt{\Delta^2 - m_{\pi^0}^2}$ $\sim \sqrt{2m_{\pi^0}\delta}$ $\sim p_\pi$	$p_\pi = \sqrt{2m_\pi(E_\pi^{max} - m_\pi)}$
	128 MeV	20 MeV	45 MeV	42 MeV
Velocity	$v_{D^{(*)}} = \frac{p_{D^{(*)}}}{M_{D^{(*)}}}$	$v_{D^{(*)}} = \frac{p_{D^{(*)}}}{M_{D^{(*)}}}$	$v_\pi = \frac{p_\pi}{m_\pi}$	$v_\pi = \frac{p_\pi}{m_\pi}$
	0.06	0.01	0.32	0.31
Process	−	−	OPE	$X \to D^0 \bar{D}^0 \pi^0$

$$\frac{g_b^2}{4f_\pi^2} \frac{(\boldsymbol{q} \cdot \boldsymbol{\varepsilon}'^\dagger)(\boldsymbol{q} \cdot \boldsymbol{\varepsilon})}{\boldsymbol{q}^2 - u^2}, \tag{319}$$

where u^2 is defined as $u^2 = \Delta^2 - m_{\pi^0}^2$. The above static propagator is an economy choice in most studies, but the cost is the analytic structure of OPE is changed due to the omission of the energy term, see Sec. 5.5.1 for details.

In Table 6, we list the estimation of different scales associated with $X(3872)$. One can see the momentum of the $D^{(*)0}$ estimated by the binding momentum of the $X(3872)$, the momentum of the π^0 in the OPE and the $X \to D^0 \bar{D}^0 \pi^0$ are all small scale. In comparison, the momentum associated with the charged channel is about $3 - 6$ times larger. Therefore, in the XEFT, the charged channel is integrated out. In fact, some KSW-type EFTs containing the charged channel have been developed . In this review, we use the terminology "XEFT" to denote the EFT without the charged channel as in the original paper [963]. Meanwhile, the Δ and m_{π^0} are also large scales compared with $u \sim p_\pi$. Thus, in XEFT, the expansion is performed in the powers of $p_D \sim p_{D^*} \sim p_\pi \sim u \sim \gamma$. We use Q to label these small scales. The velocities of the explicit degrees of freedom, D^0, $\bar{D}^{*0}$ and π^0 are much smaller than 1, thus they are all treated nonrelativistically. The Lagrangians are constructed as follows (convention-II in Table A.11),

$$
\begin{aligned}
\mathcal{L} = \ & \boldsymbol{D}^{*\dagger} \cdot \left(i\partial_t + \frac{\vec{\boldsymbol{\nabla}}^2}{2m_{D^*}}\right) \boldsymbol{D}^* + D^\dagger \left(i\partial_t + \frac{\vec{\boldsymbol{\nabla}}^2}{2m_D}\right) D + \bar{\boldsymbol{D}}^{*\dagger} \cdot \left(i\partial_t + \frac{\vec{\boldsymbol{\nabla}}^2}{2m_{D^*}}\right) \bar{\boldsymbol{D}}^* + \bar{D}^\dagger \left(i\partial_t + \frac{\vec{\boldsymbol{\nabla}}^2}{2m_D}\right) \bar{D} \\
& + \pi^\dagger \left(i\partial_t + \frac{\vec{\boldsymbol{\nabla}}^2}{2m_\pi} + \delta\right) \pi + \frac{g_b}{2f_\pi} \frac{1}{\sqrt{2m_\pi}} \left(D\boldsymbol{D}^{*\dagger} \cdot \vec{\boldsymbol{\nabla}}\pi + \bar{D}^\dagger \bar{\boldsymbol{D}}^* \cdot \vec{\boldsymbol{\nabla}}\pi^\dagger\right) + \text{H.c.} \\
& - \frac{C_0}{2} \left(\bar{\boldsymbol{D}}^* D + \boldsymbol{D}^* \bar{D}\right)^\dagger \cdot \left(\bar{\boldsymbol{D}}^* D + \boldsymbol{D}^* \bar{D}\right) + \frac{C_2}{16} \left(\bar{\boldsymbol{D}}^* D + \boldsymbol{D}^* \bar{D}\right)^\dagger \cdot \left(\bar{\boldsymbol{D}}^* (\overleftrightarrow{\boldsymbol{\nabla}})^2 D + \boldsymbol{D}^* (\overleftrightarrow{\boldsymbol{\nabla}})^2 \bar{D}\right) + \text{H.c.} \\
& + \frac{B_1}{\sqrt{2}} \frac{1}{\sqrt{2m_\pi}} \left(\bar{\boldsymbol{D}}^* D + \boldsymbol{D}^* \bar{D}\right)^\dagger \cdot D\bar{D}\vec{\boldsymbol{\nabla}}\pi + \text{H.c.} + \dots,
\end{aligned}
\tag{320}
$$

where $\overleftrightarrow{\boldsymbol{\nabla}} = \overleftarrow{\boldsymbol{\nabla}} - \overrightarrow{\boldsymbol{\nabla}}$. The power counting can be summarized as follows,

$$p_D \sim p_{D^*} \sim p_\pi \sim u \sim \gamma \sim Q, \tag{321}$$

$$\text{Propagators:} \sim \frac{1}{E_D} / \frac{1}{E_{D^*}} / \frac{1}{E_\pi} \sim Q^{-2}, \tag{322}$$
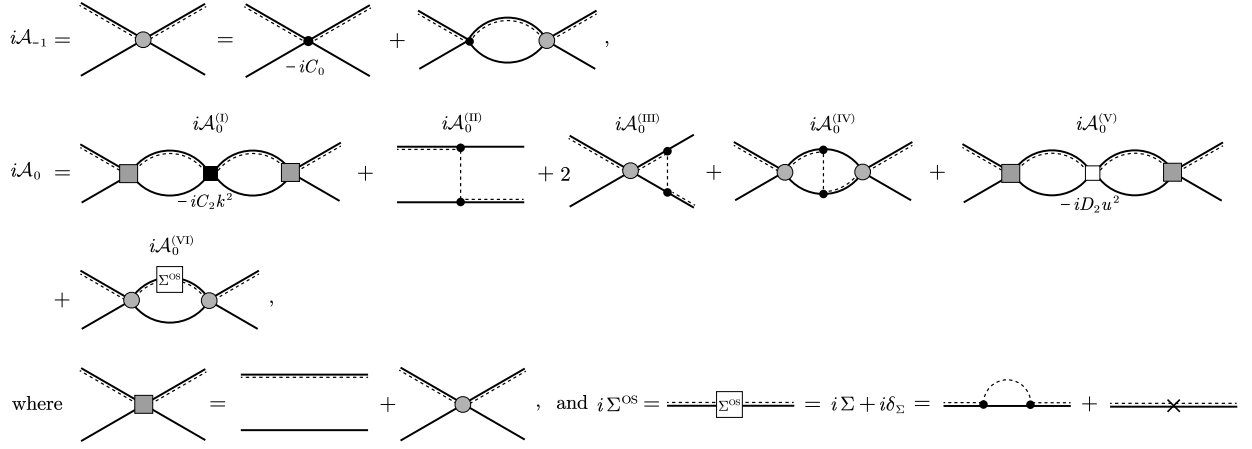
$$\text{Loop integrals:} \sim Q^5, \tag{323}$$

Figure 33: Feynman diagrams in Ref. [969] for the $D^0\bar{D}^{*0}/D^{*0}\bar{D}^0$ scattering in the $J^{PC} = 1^{++}$ channel to NLO.

$$D^{*0}D^0\pi^0 \text{ vertex: } \sim Q, \quad \text{OPE interaction: } \frac{g_b^2}{4f_\pi^2}\frac{\boldsymbol{q}\cdot\boldsymbol{\varepsilon}'^\dagger\boldsymbol{q}\cdot\boldsymbol{\varepsilon}}{\boldsymbol{q}^2-u^2} \sim Q^0. \tag{324}$$

Like the LO contact interaction in the KSW scheme, the NDA of C_0 is $1/(M_D\Lambda)$. However, for a system with unnaturally large scattering length, the scale of C_0 is $1/(M_D Q)$ as shown in Table 2. One can find that

$$C_0 = \frac{2\pi}{\mu_{DD^*}}\frac{1}{\frac{1}{a_s}-\mu}, \tag{325}$$

where μ is the renormalization scale in PDS, and μ_{DD^*} is the reduced mass of the D^0 and $\bar{D}^{*0}$ pair. The corresponding vertex is at the order of Q^{-1}. An extra loop with an extra vertex C_0 will introduce an extra factor at order 1 [$Q^5 \times (Q^{-2})^2 \times Q^{-1} \sim Q^0$] as shown in Sec. 2.7.1 (see Fig. 9). Therefore, the C_0 should be resummed nonperturbatively. In this unnatural case, the LEC C_2 is at the order of Q^{-2} and the Lagrangian with the C_2 term is at the order of Q^0, which is the NLO contribution as the OPE. The NLO and higher order vertices can be included perturbatively. It seems that the XEFT should be different from KSW because the pion mass is treated as a large scale in XEFT. However, the u is another small scale and serves as the similar role as the pion mass in the KSW framework. There also exists the KSW-type EFTs containing the $D^*\bar{D}^*$ system, where the pion mass is treated as a small scale as in Refs. [960, 522]. However, in this review, we restrict the terminology "XEFT" for the neutral $D^*\bar{D}$ system without the $D^*\bar{D}^*$ channel as in the original paper of Fleming *et al* [963], which is extended to investigate the D^*D system at most.

With XEFT, one can calculate the $D^0\bar{D}^{*0}/D^{*0}\bar{D}^0$ scattering process (e.g., [969]). The Feynman diagrams up to NLO are listed in Fig. 33. One can see that the C_0 term is treated nonperturbatively, while the OPE and NLO contact terms are calculated perturbatively. With the scattering amplitude, one can extract the coupling constants of the $X(3872)$ with $D^0\bar{D}^{*0}/D^{*0}\bar{D}^0$ by calculating the residue of the T-matrix as shown in Fig. 30(a).

The Feynman diagrams contributing to $X \to D^0\bar{D}^0\pi^0$ is presented in Fig. 34. The diagram (a) contributes to the LO decay widths. The circled cross represents the vertex (form factor) of $XD^*\bar{D}$ and its charge conjugations, which is obtained by iterating the C_0 terms. The diagrams (b)-(g) contributing to the NLO. The pion vertices, C_2 and B_1 are included as perturbation. The LEC B_1 is at the same order of Q^{-2} as C_2. The C_π and C_{0D} terms are omitted in the original work of XEFT [963] and first pointed out in Ref. [11], which will be discussed in details in Sec. 5.5.4.

5.3. Chiral effective field theory

In Sec. 5.1, we have discussed the πEFT, in which the pions are totally integrated out. In Sec. 5.2, we elucidated the XEFT, in which the pions are treated perturbatively. Modern theory of nuclear forces (χEFT) is built upon the Weinberg scheme (see Sec. 2.7), in which the pion is an explicit d.o.f and treated nonperturbatively. The EFTs with different treatment of the pion are valid in different low energy scales [970, 644], see Sec. 5.5.1 for details. In
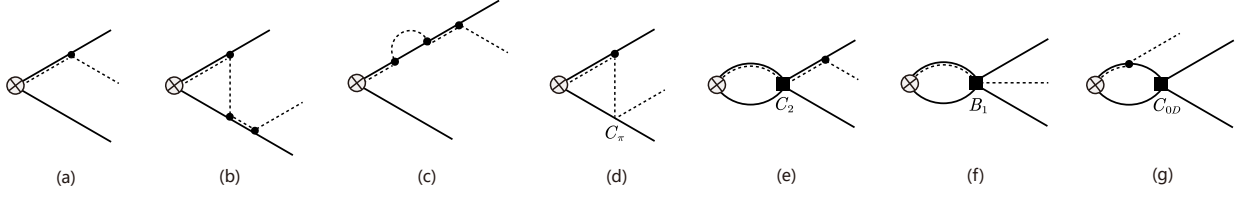
Figure 34: Feynman diagrams for $X \to D^0 \bar{D}^0 \pi^0$ up to NLO in XEFT. The circled cross represents the vertex (form factor)$XD^*\bar{D}$ and its charge conjugations.

this section, χEFT is generalized to heavy hadron systems combining both the chiral symmetry and the heavy quark symmetry. The expansion parameter in this case is Q/Λ, where the corresponding low energy scale Q can be either the pion mass m_π, the momentum of pion, or the residual momenta of heavy hadrons, while the high energy scale Λ can be either the chiral symmetry breaking scale Λ_χ or the heavy hadron masses. As stated in Sec. 2.7, Weinberg's proposal is to extract the effective potentials from the two particle irreducible diagrams. The importance of the corresponding irreducible diagrams is measured via the power counting given in Eq. (67). In this part, we take the $D\bar{D}^*/\bar{D}D^*$ system as an example to illustrate the generalizations of χEFT in the heavy hadron systems.

5.3.1. Leading order interactions

According to the power counting in Eq. (67), the LO effective potentials of $D\bar{D}^*/\bar{D}D^*$ receive contributions from the contact terms and one-pion exchange (OPE) interaction, see the diagrams in the first row of Fig. 35. For a more concrete case, we consider the $D\bar{D}^*/\bar{D}D^*$ system with $I^G(J^{PC}) = 1^+(1^{+-})$ (C-parity for the neutral systems only), which corresponds to the $Z_c(3900)$ with flavor wave function

$$|1^+(1^{+-})\rangle = \frac{1}{\sqrt{2}}(D\bar{D}^* + D^*\bar{D}), \tag{326}$$

where the relative sign is determined by the convention $\hat{C}D^* \to -\bar{D}^*$ (convention-I in Table A.11). One can derive the static OPE potential of this state with the LO chiral Lagrangians in Eqs. (123) and (124), which reads

$$V_{\text{OPE}} = -\frac{g_b^2}{4f_\pi^2} \frac{(\boldsymbol{q} \cdot \boldsymbol{\varepsilon})(\boldsymbol{q} \cdot \boldsymbol{\varepsilon}'^\dagger)}{\boldsymbol{q}^2 + m_\pi^2}, \tag{327}$$

with $\boldsymbol{q} = \boldsymbol{p} - \boldsymbol{p}'$ the transferred momentum. $\boldsymbol{p}$ ($\boldsymbol{p}'$) denotes the momentum of the initial (final) states in the center of mass system (c.m.s). $\boldsymbol{\varepsilon}$ ($\boldsymbol{\varepsilon}'^\dagger$) is the polarization vector of the initial (final) D^* or $\bar{D}^*$ meson. Besides, the Breit approximation $\mathcal{V} = -\mathcal{M}/\sqrt{\Pi_i 2m_i \Pi_f 2m_f}$ [m_i (m_f) stands for the mass of initial (final) state] has been used to relate the effective potential $\mathcal{V}$ to the scattering amplitude $\mathcal{M}$ [971]. Note that the term $p_0 - p_0' \approx m_{D^*} - m_D = \delta_b$ is ignored in the denominator of Eq. (327). One recovers the structure of Eq. (319) once the mass difference is considered.

In Refs. [972, 973], the time-ordered perturbation theory (TOPT) (see [974, 975] for the details of the Feynman rules in TOPT) is adopted to derive the nonstatic (energy dependent) OPE potential. Two typical contributions are shown in Figs. 36(a) and 36(b), which read

$$V_{\text{OPE}}^{(a)} = -\frac{g_b^2}{4f_\pi^2} \frac{(\boldsymbol{q} \cdot \boldsymbol{\varepsilon})(\boldsymbol{q} \cdot \boldsymbol{\varepsilon}'^\dagger)}{2E_\pi(E_\pi + E_{D^*} + E_{\bar{D}^*} - E - i\epsilon)}, \tag{328}$$

$$V_{\text{OPE}}^{(b)} = -\frac{g_b^2}{4f_\pi^2} \frac{(\boldsymbol{q} \cdot \boldsymbol{\varepsilon})(\boldsymbol{q} \cdot \boldsymbol{\varepsilon}'^\dagger)}{2E_\pi(E_\pi + E_D + E_{\bar{D}} - E - i\epsilon)}, \tag{329}$$

where

$$E_\pi = \sqrt{\boldsymbol{q}^2 + m_\pi^2}, \qquad E_i = m_i + \frac{\boldsymbol{p}_i^2}{2m_i}, \quad (i = D^*, \bar{D}^*, D, \bar{D}), \tag{330}$$

and E represents the total energy of the system.

86
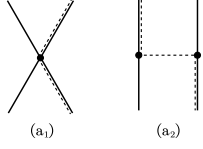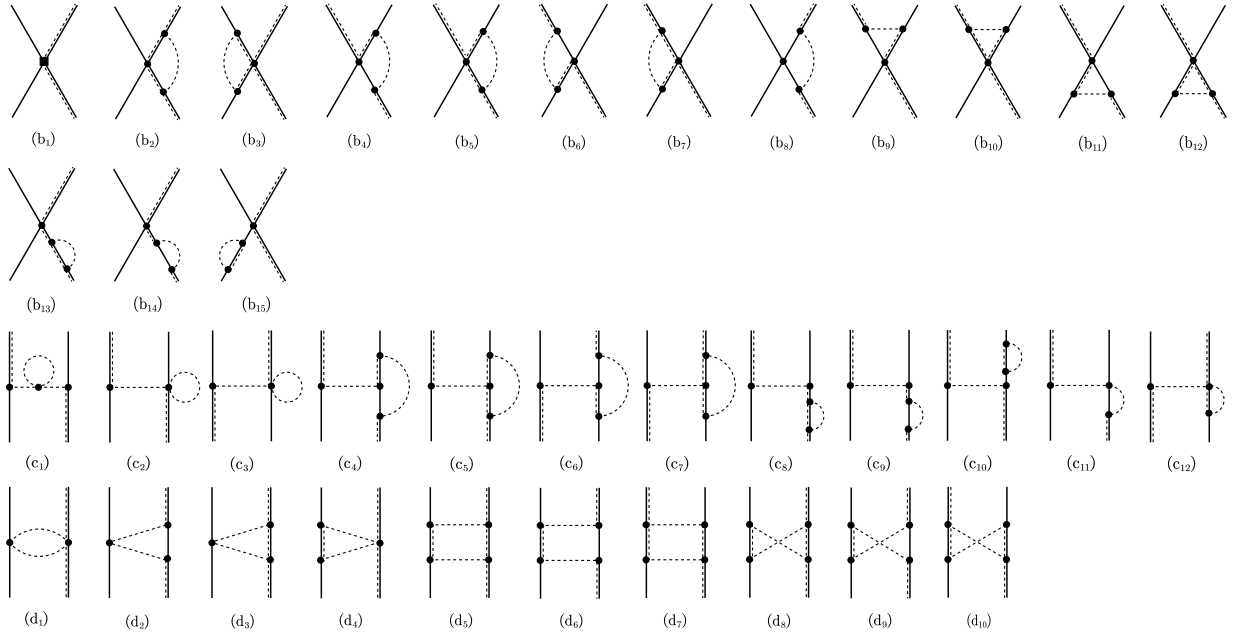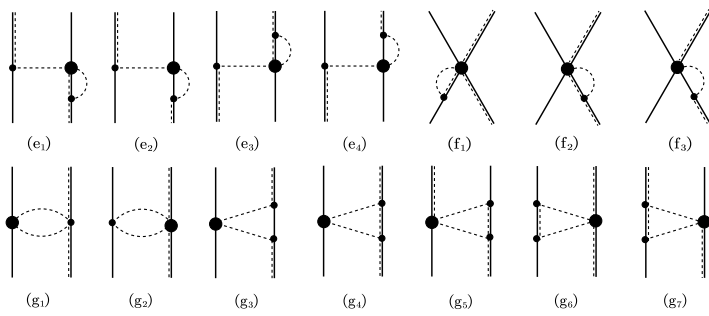
Figure 35: The LO, NLO and N^{2}LO Feynmann diagrams of the $D\bar{D}^*/\bar{D}D^*$ scatterings in χEFT, where the double (solid plus dashed) line denotes the $D^*/\bar{D}^*$, while the single solid line and dashed line denote the $D/\bar{D}$ and pion, respectively. The small dot ('•') denotes the LO vertex, such as the vertices in Lagrangias (331), (123) and (124). The vertex denoted by black square ('■') in diagram (b_1) comes from the NLO contact Lagrangian (335). The large dot ('●') denotes the NLO vertex, such as the two-pion coupling vertices in $(e_1) - (e_4)$ and $(g_1) - (g_7)$ from the NLO Lagrangian (344), and vertices in diagrams $(f_1) - (f_3)$ from the Lagrangian (345). The diagrams $(b_2) - (b_{15})$ represent the one-loop corrections to LO contact term, while the diagrams $(c_1) - (c_{12})$ are the one-loop corrections to OPE.
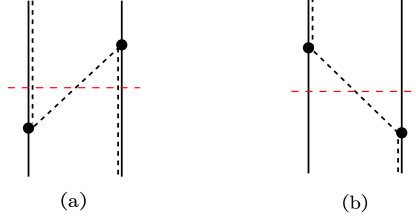
Figure 36: The OPE diagrams for the $D\bar{D}^*/\bar{D}D^*$ scattering in time-ordered perturbation theory. The notations are the same as those in Fig. 35. The red-dashed horizontal line indicates the time at which the intermediate state is evaluated. In diagrams (a) and (b), the propagators are retarded and advanced ones, respectively. The corresponding intermediate states in diagrams (a) and (b) are $D^*\bar{D}^*\pi$ and $D\bar{D}\pi$, respectively.

If we only focus on the SU(2) case [see Ref. [976] for the SU(3) case], the LO contact potential is obtained from the following Lagrangian without derivatives [976, 977, 978],

$$
\begin{aligned}
\mathcal{L}_{\text{ct}}^{(0)} &= D_a \langle \bar{\tilde{\mathcal{H}}} \tilde{\mathcal{H}} \rangle \langle \mathcal{H} \bar{\mathcal{H}} \rangle + D_b \langle \bar{\tilde{\mathcal{H}}} \gamma^\mu \gamma_5 \tilde{\mathcal{H}} \rangle \langle \mathcal{H} \gamma_\mu \gamma_5 \bar{\mathcal{H}} \rangle \\
&\quad + E_a \langle \bar{\tilde{\mathcal{H}}} \tau_i \tilde{\mathcal{H}} \rangle \langle \mathcal{H} \tau_i \bar{\mathcal{H}} \rangle + E_b \langle \bar{\tilde{\mathcal{H}}} \gamma^\mu \gamma_5 \tau_i \tilde{\mathcal{H}} \rangle \langle \mathcal{H} \gamma_\mu \gamma_5 \tau_i \bar{\mathcal{H}} \rangle,
\end{aligned}
\tag{331}
$$

where D_a, D_b, E_a and E_b are four LECs. The τ_i is the isospin Pauli matrix. There are other forms of couplings such as $\langle \bar{\tilde{\mathcal{H}}} \gamma_\mu \tilde{\mathcal{H}} \rangle \langle \mathcal{H} \gamma^\mu \bar{\mathcal{H}} \rangle$, which is equal to $\langle \bar{\tilde{\mathcal{H}}} v_\mu \tilde{\mathcal{H}} \rangle \langle \mathcal{H} v^\mu \bar{\mathcal{H}} \rangle$ with heavy field reduction and is absorbed by adjusting the D_a. The term $\langle \bar{\tilde{\mathcal{H}}} \gamma_5 \tilde{\mathcal{H}} \rangle \langle \mathcal{H} \gamma_5 \bar{\mathcal{H}} \rangle$ vanishes in the heavy quark limit. The remaining terms $\langle \bar{\tilde{\mathcal{H}}} \sigma_{\mu\nu} \tilde{\mathcal{H}} \rangle \langle \mathcal{H} \sigma^{\mu\nu} \bar{\mathcal{H}} \rangle$ and $\langle \bar{\tilde{\mathcal{H}}} \sigma_{\mu\nu} \gamma_5 \tilde{\mathcal{H}} \rangle \langle \mathcal{H} \sigma^{\mu\nu} \gamma_5 \bar{\mathcal{H}} \rangle$ can also be absorbed by adjusting the D_b (see the properties of the gamma matrices under the heavy field reduction in Ref. [477]).

It is worth mentioning that the contact Lagrangians introduced here as well as those in Secs. 5.1 and 5.2 should be regarded as the parameterization of the dynamics that occur at the scale which is much shorter than the scale we are working, but they are not the true zero-range interaction, e.g., see the discussions in Ref. [979], which implies that the regularization is necessary from the outset.

With the Lagrangian (331), the LO contact potential of the state (326) is

$$
V_{\text{ct}}^{(0)} = (-D_a - D_b + E_a + E_b) \boldsymbol{\varepsilon} \cdot \boldsymbol{\varepsilon}'^\dagger,
\tag{332}
$$

where the LECs may be separately determined either by fitting the experimental data or from the phenomenological meson exchange model such as the resonance saturation model (RSM) [599, 980].

Here, we append a brief introduction to the RSM. The basic idea of RSM is to localize the resonance-exchange contribution if one is interested in the region $q^2 \ll m_e^2$, e.g., see the illustration in Fig. 37. The exchanged resonances may contain many types with different quantum numbers, such as the scalar (s), pseudoscalar (p), vector (v), axial-vector (a), and tensor (t), etc. We take the NN interaction as an example. Within the framework of the one-boson exchange (OBE) model, the effective potential of NN can be written as

$$
V_{NN} = V_\pi + \sum_{e=s,p,v,a,t} V_e,
\tag{333}
$$

where V_π denotes the one-pion exchange contribution, which is usually regarded as the long-range force both in the OBE model and the χEFT. In the region $q^2 \ll m_e^2$, one can make the following expansion for V_e,

$$
V_e = (\bar{N}\Gamma_i N)\left(\frac{g_e^2 \delta^{ij}}{q^2 - m_e^2}\right)(\bar{N}\Gamma_j N) = -\frac{g_e^2}{m_e^2}\left[(\bar{N}\Gamma_i N)(\bar{N}\Gamma^i N) + \frac{q^2}{m_e^2}(\bar{N}\Gamma_i N)(\bar{N}\Gamma^i N) + \dots\right],
\tag{334}
$$

where g_e, q and m_e denote the coupling constant, the transferred momentum and the mass of the exchanged resonance in order. Γ_i are the projectors on the appropriate quantum numbers for a given resonance exchange. From Eq. (334), the interaction is changed into the contact form in the soft-momentum approximation. One then can estimate the LECs via comparing the structures in Eq. (334) and those from the contact chiral Lagrangians. The LECs estimated with

88

the RSM in the meson-meson [599], meson-baryon [981], and baryon-baryon [980] sectors are close to the values determined from the experimental data. The RSM is also applied to the heavy-heavy sectors [291, 329, 897]. One should note that the RSM can work only for a certain range of regulators. For example, the momentum cutoff for the OBE potentials in the NN case is in the range $1 - 2$ GeV, while it is commonly around 0.5 GeV for the chiral NN potentials [980]. Therefore, though one may use the RSM to estimate the LECs in EFTs, one should consistently use the cutoff constrained by the validity of the EFTs rather than that of the OBE model.
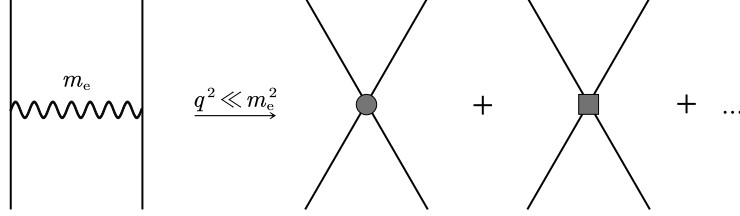
Figure 37: An illustration of the resonance saturation model. The wiggly line denotes the exchanged resonances. The circle and square blobs represent the contact vertices with zero and two derivatives, respectively. The ellipsis stands for the higher order terms (with more derivatives).

5.3.2. Next-to-leading order interactions

The NLO interactions can be divided into four parts. The first part is the one-loop corrections to the LO OPE [see Figs. 35(c_1)-(c_{12})], which include the corrections to the $D^*D\pi$ vertex, the renormalizations of the wave functions of the pion and D mesons. The second part arises from the one-loop corrections to the LO contact diagrams [see Figs. 35(b_2)-(b_{15})]. These two contributions have been systematically considered for the DD^* [268], BB^*[812] and $\Sigma_c N$ [982] systems. Partial diagrams were also calculated for the $X(3872)$ [983] (see the criticisms in Ref. [984]). However, these two parts do not induce new structures. Thus, if one does not care about the m_π dependence of the $D\bar{D}^*$ forces, their contributions can be included by using the physical values of m_π, g_b, f_π, m_D, m_{D^*} and the LO contact LECs (see also the discussions on the one-loop corrections in the NN cases [985, 475, 476], and the possible appearance of Goldberger-Treiman discrepancy at this order [986]).

The third part comes from the NLO contact Lagrangian [see diagram 35(b_1)], which carries two derivatives or has an insertion of the light quark mass terms,

$$\mathcal{L}_{ct}^{(2)} = \sum_{i=1}^{4} \mathcal{D}_\mu \mathcal{D}^\mu \langle \bar{\tilde{\mathcal{H}}} \mathbb{O}_i \tilde{\mathcal{H}} \rangle \langle \mathcal{H} \mathbb{O}_i \bar{\mathcal{H}} \rangle + \sum_{i=5}^{6} \mathcal{D}_\mu \mathcal{D}^\nu \langle \bar{\tilde{\mathcal{H}}} \mathbb{O}_i^\mu \tilde{\mathcal{H}} \rangle \langle \mathcal{H} \mathbb{O}_{i\nu} \bar{\mathcal{H}} \rangle + \sum_{i=1}^{4} \chi \langle \bar{\tilde{\mathcal{H}}} \mathbb{O}_i \tilde{\mathcal{H}} \rangle \langle \mathcal{H} \mathbb{O}_i \bar{\mathcal{H}} \rangle, \tag{335}$$

where the $\mathbb{O}_i$ are defined as $\mathbb{O}_1 = \mathbf{I}, \mathbb{O}_2 = \gamma^\mu \gamma_5, \mathbb{O}_3 = \tau_i, \mathbb{O}_4 = \gamma^\mu \gamma_5 \tau_i, \mathbb{O}_5^\mu = \gamma^\mu \gamma_5, \mathbb{O}_6^\mu = \gamma^\mu \gamma_5 \tau_i$. The two covariant derivatives terms stand for the following allocations,

$$
\begin{aligned}
\mathcal{D}_\mu \mathcal{D}^\mu \langle \bar{\tilde{\mathcal{H}}} \mathbb{O}_i \tilde{\mathcal{H}} \rangle \langle \mathcal{H} \mathbb{O}_i \bar{\mathcal{H}} \rangle \;\equiv\; & C_{i1}^d \left(\langle \mathcal{D}_\mu \bar{\tilde{\mathcal{H}}} \tilde{\mathcal{H}} \rangle \langle \mathcal{H} \mathcal{D}^\mu \bar{\mathcal{H}} \rangle + \langle \bar{\tilde{\mathcal{H}}} \mathcal{D}_\mu \tilde{\mathcal{H}} \rangle \langle \mathcal{D}^\mu \mathcal{H} \bar{\mathcal{H}} \rangle \right) \\
& + C_{i2}^d \left(\langle \mathcal{D}_\mu \bar{\tilde{\mathcal{H}}} \tilde{\mathcal{H}} \rangle \langle \mathcal{D}^\mu \mathcal{H} \bar{\mathcal{H}} \rangle + \langle \bar{\tilde{\mathcal{H}}} \mathcal{D}_\mu \tilde{\mathcal{H}} \rangle \langle \mathcal{H} \mathcal{D}^\mu \bar{\mathcal{H}} \rangle \right) \\
& + C_{i3}^d \left(\langle \mathcal{D}^2 \bar{\tilde{\mathcal{H}}} \tilde{\mathcal{H}} \rangle \langle \mathcal{H} \bar{\mathcal{H}} \rangle + \langle \bar{\tilde{\mathcal{H}}} \mathcal{D}^2 \tilde{\mathcal{H}} \rangle \langle \mathcal{H} \bar{\mathcal{H}} \rangle \right) \\
& + C_{i4}^d \left(\langle \bar{\tilde{\mathcal{H}}} \tilde{\mathcal{H}} \rangle \langle \mathcal{D}^2 \mathcal{H} \bar{\mathcal{H}} \rangle + \langle \bar{\tilde{\mathcal{H}}} \tilde{\mathcal{H}} \rangle \langle \mathcal{H} \mathcal{D}^2 \bar{\mathcal{H}} \rangle \right) \\
& + C_{i5}^d \left(\langle \mathcal{D}_\mu \bar{\tilde{\mathcal{H}}} \mathcal{D}^\mu \tilde{\mathcal{H}} \rangle \langle \mathcal{H} \bar{\mathcal{H}} \rangle + \langle \bar{\tilde{\mathcal{H}}} \tilde{\mathcal{H}} \rangle \langle \mathcal{D}_\mu \mathcal{H} \mathcal{D}^\mu \bar{\mathcal{H}} \rangle \right).
\end{aligned}
\tag{336}
$$

The $\chi \langle \bar{\tilde{\mathcal{H}}} \mathbb{O}_i \tilde{\mathcal{H}} \rangle \langle \mathcal{H} \mathbb{O}_i \bar{\mathcal{H}} \rangle$ terms are the m_π^2 related terms, allowing the following forms

$$\chi \langle \bar{\tilde{\mathcal{H}}} \mathbb{O}_i \tilde{\mathcal{H}} \rangle \langle \mathcal{H} \mathbb{O}_i \bar{\mathcal{H}} \rangle \equiv C_{i1}^\chi \langle \bar{\tilde{\mathcal{H}}} \mathbb{O}_i \tilde{\mathcal{H}} \rangle \langle \mathcal{H} \mathbb{O}_i \bar{\mathcal{H}} \rangle \mathrm{Tr}(\chi_+) + C_{i2}^\chi \langle \bar{\tilde{\mathcal{H}}} \hat{\chi}_+ \mathbb{O}_i \tilde{\mathcal{H}} \rangle \langle \mathcal{H} \mathbb{O}_i \bar{\mathcal{H}} \rangle + C_{i3}^\chi \langle \bar{\tilde{\mathcal{H}}} \mathbb{O}_i \tilde{\mathcal{H}} \rangle \langle \mathcal{H} \hat{\chi}_+ \mathbb{O}_i \bar{\mathcal{H}} \rangle, \tag{337}$$

where $\hat{\chi}_+ = \chi_+ - \frac{1}{2}\mathrm{Tr}(\chi_+)$ in the SU(2) case. These terms can be absorbed into the LO contact interaction, if one does not care about the pion mass dependence.

Similar to the *NN* case [987], it is more convenient to extract the operator structures of the $D\bar{D}^*/\bar{D}D^*$ interactions in momentum space. There are four independent operators for the $D\bar{D}^*/\bar{D}D^*$ system [988],

$$O_1 = \varepsilon'^\dagger \cdot \varepsilon, \qquad\qquad\qquad O_2 = (\varepsilon'^\dagger \times \varepsilon) \cdot (q \times k),$$
$$O_3 = (q \cdot \varepsilon'^\dagger)(q \cdot \varepsilon), \qquad\qquad\qquad O_4 = (k \cdot \varepsilon'^\dagger)(k \cdot \varepsilon), \qquad\qquad (338)$$

with $k = (p' + p)/2$ the average momentum. A similar term $[\varepsilon'^\dagger \cdot (q \times k)][\varepsilon \cdot (q \times k)]$ contributes to the N^{3}LO (or even higher order) potentials [987]. Note that the remaining two terms $(q \times \varepsilon'^\dagger) \cdot (q \times \varepsilon)$ and $(k \times \varepsilon'^\dagger) \cdot (k \times \varepsilon)$ in Ref. [988] are not independent since $(q \times \varepsilon'^\dagger) \cdot (q \times \varepsilon) = q^2(\varepsilon'^\dagger \cdot \varepsilon) - (q \cdot \varepsilon'^\dagger)(q \cdot \varepsilon)$. With the operators in Eq. (338), the NLO contact potential of the state (326) can be parameterized as follows,

$$V_{\text{ct}}^{(2)} = (C_1 q^2 + C_2 k^2)O_1 + \sum_{i=2}^{4} C_{i+1}O_i, \qquad\qquad (339)$$

in which the m_π^2 related terms are omitted. The C_is are the linear combinations of the LECs in Eq. (335). An additional term $C_6 m_\pi^2 O_1$ should be added into Eq. (339) if one is interested in the m_π dependence, see e.g., [969, 989, 990, 982, 991]. The $V_{\text{ct}}^{(2)}$ only contributes to the S- and P-wave interactions. The D-wave interaction needs contact terms at least at $O(p^4)$ [476]. Projecting the $V_{\text{ct}}^{(2)}$ into S-wave (considering the S- and D-wave mixing) with the partial wave decomposition (PWD) [992], one obtains

$$[V_{\text{ct}}^{(2)}]_{LL'} = \begin{bmatrix} V_{^3S_1} & V_{^3S_1-^3D_1} \\ V_{^3D_1-^3S_1} & V_{^3D_1} \end{bmatrix} = \begin{bmatrix} \tilde{C}_{\text{s}} + C_{\text{s}}(p^2 + p'^2) & C_{\text{sd}}p^2 \\ C_{\text{sd}}p'^2 & 0 \end{bmatrix}, \qquad\qquad (340)$$

where

$$\tilde{C}_{\text{s}} = 4\pi(-D_a - D_b + E_a + E_b),$$
$$C_{\text{s}} = \pi(4C_1 + C_2 + \frac{4}{3}C_4 + \frac{1}{3}C_5),$$
$$C_{\text{sd}} = -\frac{\sqrt{2}}{3}\pi(4C_4 + C_5). \qquad\qquad (341)$$

The C_3 does not appear in Eq. (341). Because the related operator O_2 is responsible for the spin-orbit (S-L) coupling, which vanishes in the S-wave ($L = 0$) case. In performing PWD, the polarization vectors ε and $\varepsilon'^\dagger$ are related to the conventional spin operators of the vector particles with the spin transition operators (see the Appendix C of Ref. [364]).

The fourth part of the NLO effective potential originates from the two-pion exchange (TPE) diagrams [see Figs. 35(d$_1$)-(d$_{10}$)], in which the one-pion and two-pion coupling vertices are governed by the axial coupling terms and chiral connections of the LO Langrangians (123) and (124), respectively. The TPE contributions up to NLO have been considered for heavy hadron systems in a series of works [976, 983, 268, 812, 355, 364, 993, 994, 982, 417, 93, 988, 312, 453, 995]. These systems will be discussed later. The planar box diagram 35(d$_6$) contains the 2PR component (see the definitions about 2PR and 2PIR in Sec. 2.7), which can also be generated from the iterated OPE when the OPE potential is fed into the nonrelativistic Lippmann-Schwinger equation via

$$V_{d_6}^{\text{it}}(p, p') = \int \frac{d^3q}{(2\pi)^3} V_{\text{OPE}}(p, q) \frac{2\mu_{DD^*}}{p^2 - q^2 + i\epsilon} V_{\text{OPE}}(q, p'). \qquad\qquad (342)$$

The $V_{d_6}^{\text{it}}$ is proportional to the reduced mass of $D\bar{D}^*$, thus it breaks the naive power counting in Eq. (67). Therefore, one needs to subtract the 2PR contribution in V_{d_6}, which can be done with the old-fashioned TOPT [996, 653] or the covariant perturbation theory [651]. In the Appendix B of Ref. [364], the authors demonstrated another trick to make the 2PR subtraction with the mass splitting δ_b kept, which is based on the principle-value integral within the framework of covariant perturbation theory. Notably, the 2PR contribution also emerges in the one-loop corrections of the LO contact term, e.g., diagrams 35(b$_9$) and 35(b$_{11}$), which can be easily seen via replacing one of the V_{OPE}s in Eq. (342) with the LO contact potential (332).

For the graphs 35(d_5), 35(b_{10}) and 35(b_{12}), there is no pinched singularity if one keeps the mass splittings of the intermediate states and outer legs. One can choose either to not perform 2PR subtraction or perform the 2PR subtraction with the inclusion of the inelastic channel $D\bar{D}^* \leftrightarrow D^*\bar{D}^*$ in the LO tree diagrams. In the first choice, the coupled-channel effect of $D^*\bar{D}^*$ is included via loop diagrams while in the second choice the coupled-channel effect is included by iterating the tree diagrams.

In strict heavy quark symmetry limit, i.e., $m_Q \to \infty$, the exact HQSS guarantees $\delta_b \to 0$. Then the 2PIR TPE potential at NLO can be formulated in a compact form [988],

$$
\begin{aligned}
V_{\text{TPE}} = & -O_1 \frac{24(4g_b^2+1)m_\pi^2 + (38g_b^2+5)\boldsymbol{q}^2}{2304\pi^2 f_\pi^4} + O_1 \frac{6(6g_b^2+1)m_\pi^2 + (10g_b^2+1)\boldsymbol{q}^2}{768\pi^2 f_\pi^4} \ln \frac{m_\pi^2}{(4\pi f_\pi)^2} \\
& + O_1 \frac{4(4g_b^2+1)m_\pi^2 + (10g_b^2+1)\boldsymbol{q}^2}{384\pi^2 f_\pi^4 y} \varpi \arctan \frac{y}{\varpi},
\end{aligned}
\tag{343}
$$

where $\varpi = \sqrt{\boldsymbol{q}^2 + 4m_\pi^2}$, and $y = \sqrt{2pp' \cos\vartheta - p^2 - p'^2}$ (with $p^{(')} = |\boldsymbol{p}^{(')}|$, and ϑ the scattering angle in the c.m.s of $D\bar{D}^*$). The $O_{2,\dots,4}$ terms vanish and only the central potential, i.e., the O_1 term survives [355].

5.3.3. Next-to-next-to-leading order interactions

The N^{2}LO interactions of the $D\bar{D}^*/\bar{D}D^*$ system are composed of three types of diagrams [see Figs. 35(e_1)-(e_4), (f_1)-(f_3) and (g_1)-(g_7)] due to the absence of the four-body contact Lagrangians at this order. In these diagrams, the following subleading vertices [997, 998, 471, 618] are inserted,

$$
\begin{aligned}
\mathcal{L}_{\mathcal{H}\varphi}^{(2)} = & \ \tilde{c}_1 \langle \mathcal{H}\bar{\mathcal{H}} \rangle \text{Tr}(\chi_+) + \tilde{c}_2 \langle \mathcal{H} u^\mu u^\nu v_\mu v_\nu \bar{\mathcal{H}} \rangle + \tilde{c}_3 \langle \mathcal{H} u^\mu u_\mu \bar{\mathcal{H}} \rangle \\
& + i\tilde{c}_4 \langle \mathcal{H}[u^\mu, u^\nu]\sigma_{\mu\nu}\bar{\mathcal{H}} \rangle + \tilde{c}_5 \langle \mathcal{H}\hat{\chi}_+\bar{\mathcal{H}} \rangle,
\end{aligned}
\tag{344}
$$

$$
\mathcal{L}_{\mathcal{H}\mathcal{H}\varphi}^{(1)} = \tilde{d}_1 \langle \bar{\tilde{\mathcal{H}}}\tilde{\mathcal{H}} \rangle \langle \mathcal{H}\psi\gamma_5\bar{\mathcal{H}} \rangle + \tilde{d}_2 \langle \bar{\tilde{\mathcal{H}}}\psi\gamma_5\tilde{\mathcal{H}} \rangle \langle \mathcal{H}\bar{\mathcal{H}} \rangle,
\tag{345}
$$

where the $\tilde{c}_i$ and $\tilde{d}_i$ are corresponding LECs. One can accordingly obtain the $\mathcal{L}_{\bar{\mathcal{H}}\varphi}^{(2)}$ for the anticharmed ones (see Sec. 2.6.1). Eq. (344) contributes to diagrams 35(e_1)-(e_4), (g_1)-(g_7), and Eq. (345) contributes to diagrams 35(f_1)-(f_3), respectively.

The subleading $NN\pi\pi$ couplings can be extracted [998, 981, 999, 1000] with the benefit of abundant πN scattering data [1001, 1002], while for the $\mathcal{H}\mathcal{H}\pi\pi$ ($\tilde{\mathcal{H}}\tilde{\mathcal{H}}\pi\pi$) couplings, only a few terms in Eq. (344) were estimated for specific problems [39, 37, 763, 877, 879, 882, 583, 51, 53, 901, 895], or see discussions in Sec. 4.2.

It is pointed out that calculating the TPE loop diagrams with dimensional regularization induces unphysically attractive forces in the isospin scalar NN channel [1003, 1004], which results from the heavily involved higher momentum modes of the intermediate states. An alternative approach, the spectral function regularization (SFR), was adopted to calculate the TPE contributions [1003, 1004], in which a cutoff $\tilde{\Lambda}$ (usually chosen to be $0.5 < \tilde{\Lambda} < 1.0$ GeV) is used in the dispersion relation to suppress the high momentum modes and restrict the potentials in the low-energy region where χEFT works healthily (see more details in [985]). Recently, in the new generation of nuclear force, the local or semi-local regularization is adopted for the pion exchange contributions [646, 645], which resolves all the issues mentioned above.

At present, the N^{2}LO TPE potentials for the DD^* system have been attained in Ref. [291]. The higher order contributions, such as the three-pion exchange interactions are still absent. However, they deserve the systematical studies in the future since they are crucial for us to establish a uniform picture between the nuclear forces and their analogues in the heavy hadron sectors.

5.3.4. Nonperturbative renormalizations

We have handled the regularization of the loop diagrams in deriving the effective potentials above. The potentials will be iterated into the LSEs to generate the possible molecular states in the $D\bar{D}^*/\bar{D}D^*$ system. Once again, one needs to impose regularization on LSEs to suppress the higher momentum contributions [655]. In addition, regularizing the LSEs is also required from the outset—the contact interaction is used to mimic (model) the short-distance physics but not the incarnation of the idealized zero-range forces [979]. The renormalization of the Weinberg scheme is not

as transparent as that of the KSW scheme but has been proved more practical in the NN systems (see discussions in Sec. 2.7). In practical calculations, the LSEs is regularized by multiplying a form factor on the potentials, i.e.,

$$V(p, p') \rightarrow V(p, p')\mathcal{F}(p, p', \Lambda), \tag{346}$$

where the regulator $\mathcal{F}(p, p', \Lambda)$ is usually chosen to be the Gaussian form

$$\mathcal{F}(p, p', \Lambda) = \exp\left[-\left(\frac{p}{\Lambda}\right)^{2n} - \left(\frac{p'}{\Lambda}\right)^{2n}\right], \text{ with } n \geq 1, \tag{347}$$

or the hard cutoff form

$$\mathcal{F}(p, p', \Lambda) = \Theta(\Lambda - p)\Theta(\Lambda - p'), \text{ with } \Theta \text{ the step function,} \tag{348}$$

in which Λ is the cutoff parameter.

The value of Λ is constrained in the applicable region of χEFT (such as $\Lambda \sim 0.5$ GeV in the NN case). Putting the Λ beyond the breaking scale of χEFT may render the results uncontrollable and lose its predictive power. Here, we adopt the elucidations of nonperturbative renormalizations in Refs. [655, 476], which are based on the spirit of Lepage [1005]: As long as the cutoff pertains to the working region of χEFT and the associated errors induced by its finite value are within the theoretical uncertainty at the given order, the χEFT gradually achieves 'nonperturbative renormalization' when the calculation is put to higher orders and the resulting physical observables become more and more insensitive to the different values of the cutoff, e.g., see the performance of nuclear forces [1006, 648].

5.4. Heavy quark symmetry and SU(3) flavor symmetry in heavy hadronic molecules

One prominent feature of the interactions in the heavy hadron systems is the embedding of heavy quark symmetry and light quark flavor symmetry simultaneously. In the light-meson-exchange picture, the interactions between the heavy hadrons are mediated by exchanging the soft light mesons [roughly the SU(3) flavor multiplets], which do not depend on the heavy quark masses and spins in the heavy quark limit. The interactions constrained by HQS and SU(3) flavor symmetry are reflected in the spectrum of the heavy hadronic molecules. With these symmetries, one can make abundant predictions with a few inputs. In the following, we take the S-wave $B^{(*)}\bar{B}^{(*)}$ system as an example to illustrate the HQS and SU(3) light flavor symmetry in the heavy hadronic molecules. The possible symmetry breaking effects are also discussed.

In the SU(3) flavor symmetry limit and the heavy quark limit, the di-meson spectrum is classified by the irreducible representation of SU(3) group and the total spin of the light d.o.fs. In the spin space, the total angular momentum of the $B^{(*)}\bar{B}^{(*)}$ system can be $J = 0, 1, 2$ if the S-wave orbital angular momentum is presumed. One can make the following decomposition for J,

$$\begin{cases} J = 0, & B\bar{B}, B^*\bar{B}^* \\ J = 1, & B\bar{B}^*(B^*\bar{B}), B^*\bar{B}^* \\ J = 2 & B^*\bar{B}^* \end{cases} \tag{349}$$

For the $B\bar{B}^*(B^*\bar{B})$ system, one can define the C parity even and C parity odd basis as [C parity for the neutral ones in the following]

$$C \text{ parity even}: \quad \frac{1}{\sqrt{2}}(B\bar{B}^* - B^*\bar{B}), \tag{350}$$

$$C \text{ parity odd}: \quad \frac{1}{\sqrt{2}}(B\bar{B}^* + B^*\bar{B}), \tag{351}$$

in which the convention $\hat{C}B^* \rightarrow -\bar{B}^*$ is implied (convention-I in Table A.11). For the $\bar{B}^{(*)}$ and $B^{(*)}$ mesons, we denote the spins of the mesons as the sum of the internal heavy quark and light quark as $j_1(\bar{B}^{(*)}) = s_1(b) + \ell_1(\bar{q})$, $j_2(B^{(*)}) = s_2(\bar{b}) + \ell_2(q)$. In the strict HQSS, it is more convenient to use the basis $|\ell_1\ell_2 S_\ell, s_1 s_2 S_h; JM\rangle$, where the
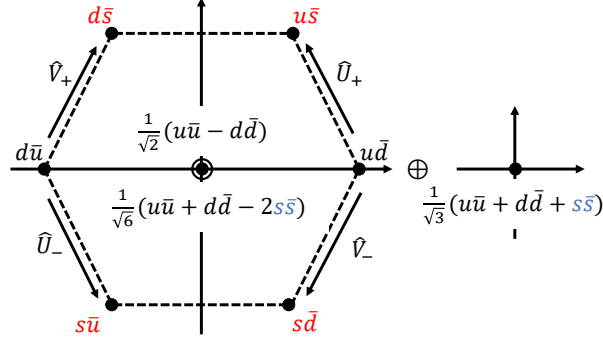
Figure 38: The SU(3) flavor multiplets with the strict flavor symmetry. We use red and blue to label the state with one and two (anti)strange quark, respectively.

heavy spin, light spin and total spin are defined as $S_h = s_1 + s_2$, $S_\ell = \ell_1 + \ell_2$, $J = j_1 + j_2 = S_h + S_\ell$. Since the interaction does not depend on the S_h, the hadronic molecules form two multiples labeled by the S_ℓ,

$$
\begin{aligned}
S_\ell = 0: \quad & \left\{ |0_h^{-+} \otimes 0_\ell^{-+}, 0^{++}\rangle, |1_h^{--} \otimes 0_\ell^{-+}, 1^{+-}\rangle \right\}, \\
S_\ell = 1: \quad & \left\{ |0_h^{-+} \otimes 1_\ell^{--}, 1^{+-}\rangle, |1_h^{--} \otimes 1_\ell^{--}, 0^{++}\rangle, |1_h^{--} \otimes 1_\ell^{--}, 1^{++}\rangle, |1_h^{--} \otimes 1_\ell^{--}, 2^{++}\rangle \right\}.
\end{aligned}
\tag{352}
$$

The above discussion in the spin space can be extended to the system with strange (anti)quark in the strict SU(3) flavor symmetry. The Eqs. (350) and (351) are also the states with fixed G parity once their isospin were determined. For the systems with (anti)strange quark, one can introduce $G_{U/V}$ parities to label the $B_s^* \bar{B}/B_s \bar{B}^*$ states [311]. With the strict SU(3) flavor symmetry, the $B_{(s)}^{(*)} \bar{B}_{(s)}^{(*)}$ will form two multplets $\mathbf{8}_F$ and $\mathbf{1}_F$ as shown in Fig. 38. With the strict HQSS and SU(3) flavor symmetry, the interaction of $q\bar{q}$ can be parameterized as

$$
V_{q\bar{q}} = c_1 + c_2 \boldsymbol{\ell}_1 \cdot \boldsymbol{\ell}_2 + c_3 \mathbb{C}_2 + c_4 (\boldsymbol{\ell}_1 \cdot \boldsymbol{\ell}_2) \mathbb{C}_2.
\tag{353}
$$

$\mathbb{C}_2 = -\sum_{i=1}^{8} \lambda_F^i \lambda_F^{i*}$ is the Casimir operator in the flavor space. There are four independent operators in spin and flavor space in the symmetry limits.

Apart from the interaction terms, the mass terms will violate the symmetries. There are two related mass splittings [see also Eqs. (61) and (62)],

$$
m_{B_{(s)}^{(*)}} - m_{B^{(*)}} \simeq 90 \text{ MeV}, \qquad m_{B_{(s)}^*} - m_{B_{(s)}} \simeq 45 \text{ MeV},
\tag{354}
$$

which break the SU(3) symmetry and HQSS, respectively. For the near-threshold states, the interaction is weak compared to the above mass splittings. Although we can still assume the interactions satisfy the symmetries, in Eq. (353), the mass splitting in the Eq. (354) will separate the di-meson systems into several blocks.

$$
\begin{aligned}
\text{spin space:} \quad & \{B_{(s)} \bar{B}_{(s)}\}, \{B_{(s)} \bar{B}_{(s)}^*/B_{(s)}^* \bar{B}_{(s)}\}, \{B_{(s)}^* \bar{B}_{(s)}^*\}, \\
\text{flavor space:} \quad & \{\bar{B}^{(*)} B^{(*)}\}, \{B_s^{(*)} \bar{B}^{(*)}\}, \{\bar{B}_s^{(*)} B^{(*)}\}, \{B_s^{(*)} \bar{B}_s^{(*)}\}.
\end{aligned}
\tag{355}
$$

The mixing between states in different blocks is suppressed by the mass splittings in Eq. (354). In fact, it is shown to be suppressed by at least two orders in EFT power counting in Ref. [978]. Thus, we need only focus on the mixing effect inside each block.

The two particle basis in Eq. (349) can be expanded with the HQSS basis $|S_h \otimes S_\ell\rangle$ via the $9j$ symbols, if the orbital angular momentum $L = 0$ is presumed. Then we have [1007]

$$
\left[\begin{array}{c} |B\bar{B}\rangle \\ |B^*\bar{B}^*\rangle \end{array} \right]_{0^{++}} = \left[\begin{array}{cc} \frac{1}{2} & \frac{\sqrt{3}}{2} \\ -\frac{\sqrt{3}}{2} & \frac{1}{2} \end{array} \right] \left[\begin{array}{c} |0_h^{-+} \otimes 0_\ell^{-+}\rangle \\ |1_h^{--} \otimes 1_\ell^{--}\rangle \end{array} \right],
\tag{356}
$$

93
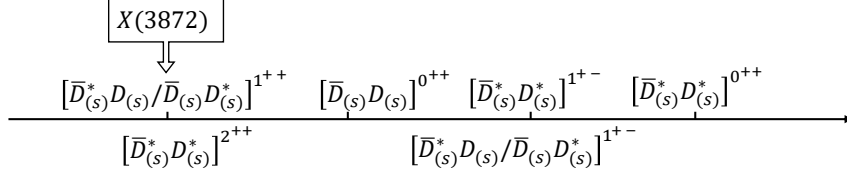
Figure 39: The order of the six $\bar{D}_{(s)^{(*)}}D^{(*)}_{(s)}$ states according to interaction in Eqs. (360)-(365). The arrows indicates that the interaction becomes more attractive or repulsive according to the sign of $\tilde{c}_2$.

$$|\frac{1}{\sqrt{2}}(B\bar{B}^* - B^*\bar{B})\rangle_{1^{++}} = -|1_h^{--} \otimes 1_\ell^{--}\rangle, \tag{357}$$

$$\left[\begin{array}{c} |\frac{1}{\sqrt{2}}(B\bar{B}^* + B^*\bar{B})\rangle \\ |B^*\bar{B}^*\rangle \end{array}\right]_{1^{+-}} = \left[\begin{array}{cc} \frac{1}{\sqrt{2}} & -\frac{1}{\sqrt{2}} \\ -\frac{1}{\sqrt{2}} & -\frac{1}{\sqrt{2}} \end{array}\right]\left[\begin{array}{c} |1_h^{--} \otimes 0_\ell^{-+}\rangle \\ |0_h^{-+} \otimes 1_\ell^{--}\rangle \end{array}\right], \tag{358}$$

$$|B^*\bar{B}^*\rangle_{2^{++}} = -|1_h^{--} \otimes 1_\ell^{--}\rangle, \tag{359}$$

where the subscripts at the left hand side denote the J^{PC} of the $B^{(*)}\bar{B}^{(*)}$ system, which are expressed by $S_h^{P_hC_h} \otimes S_\ell^{P_\ell C_\ell}$. One can also include the G parity, such as $|B^*\bar{B}^*\rangle_{0^+(2^{++})} = -|0^-(1_h^{--}) \otimes 0^-(1_\ell^{--})\rangle$, and $|B^*\bar{B}^*\rangle_{1^-(2^{++})} = -|0^-(1_h^{--}) \otimes 1^+(1_\ell^{--})\rangle$.

The simultaneous conservation of $\boldsymbol{J}$ and $\boldsymbol{S}_h$ means that the $\boldsymbol{S}_\ell$ is also a conserved quantity. Therefore, the interaction is largely simplified for an effective Hamiltonian $\hat{H}_{\text{eff}} \equiv \tilde{c}_1 + \tilde{c}_2\boldsymbol{\ell}_1 \cdot \boldsymbol{\ell}_2$ that satisfies the HQS. The conservation of $\boldsymbol{S}_\ell$ requires

$$C_0^\alpha = \langle S_h \otimes 0; \alpha|\hat{H}_{\text{eff}}|S_h \otimes 0; \alpha\rangle = \tilde{c}_1 - \frac{3}{4}\tilde{c}_2, \tag{360}$$

$$C_1^\alpha = \langle S_h \otimes 1; \alpha|\hat{H}_{\text{eff}}|S_h \otimes 1; \alpha\rangle = \tilde{c}_1 + \frac{1}{4}\tilde{c}_2, \tag{361}$$

where C_0^α and C_1^α (α denotes the other conserved quantities, such as the isospin) are the corresponding LECs in the $S_\ell = 0$ and $S_\ell = 1$ sectors, respectively. Then the effective potentials read

$$V_{0^{++}}^\alpha = \left[\begin{array}{cc} \frac{1}{4}(C_0^\alpha + 3C_1^\alpha) & \frac{\sqrt{3}}{4}(-C_0^\alpha + C_1^\alpha) \\ \frac{\sqrt{3}}{4}(-C_0^\alpha + C_1^\alpha) & \frac{1}{4}(3C_0^\alpha + C_1^\alpha) \end{array}\right] = \left[\begin{array}{cc} \tilde{c}_1 & \frac{\sqrt{3}}{4}\tilde{c}_2 \\ \frac{\sqrt{3}}{4}\tilde{c}_2 & \tilde{c}_1 - \frac{1}{2}\tilde{c}_2 \end{array}\right], \tag{362}$$

$$V_{1^{+-}}^\alpha = \left[\begin{array}{cc} \frac{1}{2}(C_0^\alpha + C_1^\alpha) & \frac{1}{2}(-C_0^\alpha + C_1^\alpha) \\ \frac{1}{2}(-C_0^\alpha + C_1^\alpha) & \frac{1}{2}(C_0^\alpha + C_1^\alpha) \end{array}\right] = \left[\begin{array}{cc} \tilde{c}_1 - \frac{1}{4}\tilde{c}_2 & \frac{1}{2}\tilde{c}_2 \\ \frac{1}{2}\tilde{c}_2 & \tilde{c}_1 - \frac{1}{4}\tilde{c}_2 \end{array}\right], \tag{363}$$

$$V_{1^{++}}^\alpha = C_1^\alpha = \tilde{c}_1 + \frac{1}{4}\tilde{c}_2, \tag{364}$$

$$V_{2^{++}}^\alpha = C_1^\alpha = \tilde{c}_1 + \frac{1}{4}\tilde{c}_2. \tag{365}$$

An equivalent description is performed through the superfield representations, e.g., see Refs. [1008, 1009, 1010]. Here we demonstrate Eqs. (364) and (365) by expanding the LO Lagrangian (331),

$$V_{1^{++}}^\alpha = (-D_a + D_b + E_a - E_b)\boldsymbol{\varepsilon}'^\dagger \cdot \boldsymbol{\varepsilon}, \tag{366}$$

$$V_{2^{++}}^\alpha = (E_a - D_a)(\boldsymbol{\varepsilon}^\dagger \cdot \boldsymbol{\varepsilon})(\boldsymbol{\varepsilon}'^\dagger \cdot \boldsymbol{\varepsilon}') + (E_b - D_b)\left[(\boldsymbol{\varepsilon}' \cdot \boldsymbol{\varepsilon})(\boldsymbol{\varepsilon}'^\dagger \cdot \boldsymbol{\varepsilon}^\dagger) - (\boldsymbol{\varepsilon}'^\dagger \cdot \boldsymbol{\varepsilon})(\boldsymbol{\varepsilon}^\dagger \cdot \boldsymbol{\varepsilon}')\right], \tag{367}$$

where $\alpha = 1$. One can easily verify that $V_{1^{++}}^\alpha = V_{2^{++}}^\alpha$ with the substitution $\boldsymbol{\varepsilon}'^\dagger \cdot \boldsymbol{\varepsilon} \to 1$, $(\boldsymbol{\varepsilon}^\dagger \cdot \boldsymbol{\varepsilon})(\boldsymbol{\varepsilon}'^\dagger \cdot \boldsymbol{\varepsilon}') \to 1$, $(\boldsymbol{\varepsilon}' \cdot \boldsymbol{\varepsilon})(\boldsymbol{\varepsilon}'^\dagger \cdot \boldsymbol{\varepsilon}^\dagger) \to (\boldsymbol{S}_1 \cdot \boldsymbol{S}_2)^2 - 1$, $(\boldsymbol{\varepsilon}'^\dagger \cdot \boldsymbol{\varepsilon})(\boldsymbol{\varepsilon}^\dagger \cdot \boldsymbol{\varepsilon}') \to \boldsymbol{S}_1 \cdot \boldsymbol{S}_2 + (\boldsymbol{S}_1 \cdot \boldsymbol{S}_2)^2 - 1$, where $\boldsymbol{S}_1$ and $\boldsymbol{S}_2$ denote the spin operators of the B^* and $\bar{B}^*$, respectively.

Since the mixing effect induced by the off-diagonal terms in Eqs. (362)-(365) is suppressed, we only focus on the diagonal terms. In the parameterization with $\tilde{c}_1$ and $\tilde{c}_2$, the interactions for the six states have the same coefficient of

94

$\tilde{c}_1$ and are arranged in order of $\tilde{c}_2$ in Fig. 39. The trivial prediction in the heavy quark symmetry is the existence of the $[D^*\bar{D}^*]^{2^{++}}$ molecule state whose interaction is the same as that of the $X(3872)$. In addition, if there exists any other bound state with the binding energy larger than that of the $X(3872)$ among the other four channels, one can naturally expect the existence of all the six molecular states [1009, 1011]. The arrow in Fig. 39 indicates the more attractive trend. See more related discussions in Refs. [1012, 1013, 1014, 1015, 257, 1016, 1017, 1018, 1019, 1020, 1021, 1022, 1023].

The above formalism can be extended to the other systems, such as the $\Sigma_c^{(*)}\bar{D}^{(*)}$. In this case,

$$I = \alpha : \begin{cases} J = \frac{1}{2}, & \Sigma_c\bar{D}, \Sigma_c\bar{D}^*, \Sigma_c^*\bar{D}^* \\ J = \frac{3}{2}, & \Sigma_c\bar{D}^*, \Sigma_c^*\bar{D}, \Sigma_c^*\bar{D}^*, \\ J = \frac{5}{2}, & \Sigma_c^*\bar{D}^* \end{cases} \tag{368}$$

where $\alpha = 1/2, 3/2$. The two particle basis can then be expanded with the HQSS basis as

$$\begin{bmatrix} |\Sigma_c\bar{D}\rangle \\ |\Sigma_c\bar{D}^*\rangle \\ |\Sigma_c^*\bar{D}^*\rangle \end{bmatrix}_{J=\frac{1}{2}} = \begin{bmatrix} \frac{1}{2} & -\frac{1}{2\sqrt{3}} & \sqrt{\frac{2}{3}} \\ -\frac{1}{2\sqrt{3}} & \frac{5}{6} & \frac{\sqrt{2}}{3} \\ \sqrt{\frac{2}{3}} & \frac{\sqrt{2}}{3} & -\frac{1}{3} \end{bmatrix} \begin{bmatrix} |0_h \otimes \frac{1}{2}_\ell\rangle \\ |1_h \otimes \frac{1}{2}_\ell\rangle \\ |1_h \otimes \frac{3}{2}_\ell\rangle \end{bmatrix}, \tag{369}$$

$$\begin{bmatrix} |\Sigma_c\bar{D}^*\rangle \\ |\Sigma_c^*\bar{D}\rangle \\ |\Sigma_c^*\bar{D}^*\rangle \end{bmatrix}_{J=\frac{3}{2}} = \begin{bmatrix} \frac{1}{3} & -\frac{1}{\sqrt{3}} & \frac{\sqrt{5}}{3} \\ -\frac{1}{\sqrt{3}} & \frac{1}{2} & \frac{1}{2}\sqrt{\frac{5}{3}} \\ \frac{\sqrt{5}}{3} & \frac{1}{2}\sqrt{\frac{5}{3}} & \frac{1}{6} \end{bmatrix} \begin{bmatrix} |1_h \otimes \frac{1}{2}_\ell\rangle \\ |0_h \otimes \frac{3}{2}_\ell\rangle \\ |1_h \otimes \frac{3}{2}_\ell\rangle \end{bmatrix}, \tag{370}$$

$$|\Sigma_c^*\bar{D}^*\rangle_{J=\frac{5}{2}} = |1_h \otimes \frac{3}{2}_\ell\rangle. \tag{371}$$

Similarly, there are two independent LECs,

$$C_{1/2}^\alpha = \langle S_h \otimes \frac{1}{2}; \alpha|\hat{H}_{\text{eff}}|S_h \otimes \frac{1}{2}; \alpha\rangle, \tag{372}$$

$$C_{3/2}^\alpha = \langle S_h \otimes \frac{3}{2}; \alpha|\hat{H}_{\text{eff}}|S_h \otimes \frac{3}{2}; \alpha\rangle. \tag{373}$$

It is straightforward to obtain the effective potentials $V_{1/2}^\alpha$, $V_{3/2}^\alpha$ and $V_{5/2}^\alpha$, see details in Ref. [411]. The related SU(3) flavor symmetry was investigated in Ref. [1024].

5.5. X(3872) and T_{cc}^+ states

There is no doubt that $X(3872)$ is the superstar in the exotic hadron family. In this section, we will review the theoretical progress of the $X(3872)$ and its analogue T_{cc}^+ as the hadronic molecules in EFTs.

5.5.1. Methodology

We will first review some characters of the $X(3872)$ and T_{cc}^+ from the theoretical perspectives. These characters will hint which kind of EFT is suitable for the $X(3872)$ and T_{cc}^+ states. In Fig. 40, we summarize the valid scales and relevant d.o.fs of different EFTs for the $X(3872)$. The details are as follows.

- *Molecular interpretation.* There are different interpretations for the $X(3872)$, e.g., the molecular picture [1025, 1026, 1027, 266], compact tetraquark state [66, 1028], radial excitation of the charmonium [1029, 1030], etc.. Naturally, one can blend the above mentioned pictures, e.g., the coupled-channel picture of the $c\bar{c}$ and di-meson d.o.fs [1031, 1032, 1033, 1034, 1035, 568, 1036]. We refer to Refs. [6, 9, 14] for general reviews and Ref. [1037] for the specialized review of the $X(3872)$ as a molecule. The evidences supporting the molecular interpretation of $X(3872)$ include its mass coinciding with the $D^0\bar{D}^{*0}/D^{*0}\bar{D}^0$ threshold $m_{D^0} + m_{D^{*0}} - m_{X(3872)} = (0.00 \pm 0.18)$ MeV and large branching ratio of $\mathcal{R}[X(3872) \to (D^0\bar{D}^0\pi^0, \bar{D}^{*0}D^0)] \approx 80\%$ [1]. In this section, we focus on the molecular picture, which suits to be depicted in the EFT at the hadronic level. For the EFT at the quark-gluon level, e.g., Born-Oppenheimer EFT, we refer to Ref. [14] for reviews.
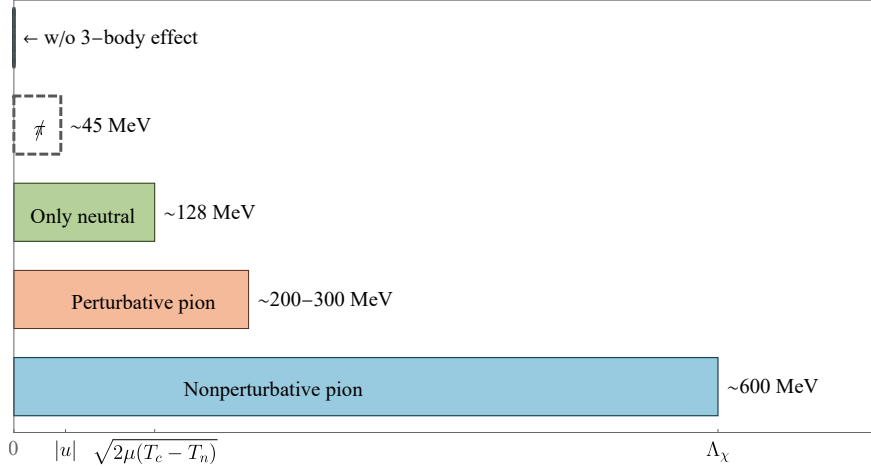
Figure 40: The validity range of the EFTs for the $X(3872)$. We here choose the $D^0\bar{D}^{*0}/D^{*0}\bar{D}^0$ threshold as the baseline. For simplicity, we use the "invalid energy range or scale" to denote the scale where the EFT breaks down. For the $X(3872)$, the invalid energy range of the EFTs without considering the three-body dynamics, pionless EFTs (conditionally valid), EFTs with only the neutral channel, EFTs with the perturbative pion and EFTs with the nonperturbative pion are given in order. The three-body dynamics should be considered from the $D^0\bar{D}^{*0}/D^{*0}\bar{D}^0$ threshold, because the $D^0\bar{D}^0\pi^0$ threshold is below it. Therefore, the pionless EFTs cannot work rigorously without considering the three-body effect. If one treats the D^{*0} as a stable state, the pionless EFTs will be valid conditionally up to the scale $|u| = \sqrt{|m_\pi^2 - (M_{D^*} - M_D)^2|}$. The invalid scale of the EFTs with only the neutral channel is estimated by the momentum corresponding to the threshold difference. In the figure, T_c, T_n and μ are the charged threshold, neutral threshold and reduced mass, respectively. The invalid scale of the perturbative pion is from Ref. [978]. The EFTs with the nonperturbative pion (e.g., the χEFT) will be valid to the chiral breaking scale Λ_χ.

- *Universality.* As shown in Fig. 41, the $X(3872)$ is below the $D^0\bar{D}^{*0}/D^{*0}\bar{D}^0$ threshold about 0.2 MeV. The T_{cc}^+ is below the $D^{*+}D^0$ threshold about 0.3 MeV. If we regard the $X(3872)$ or T_{cc}^+ as the bound state of the related particles, the binding energy is unnaturally small as compared to the typical scale $m_\pi^2/(2\mu_{DD^*}) \sim 10$ MeV. The shallow S-wave bound state indicates the unnaturally large scattering length as compared to $1/m_\pi$, and the low-energy universality. The universality motivated numerous works based on LO contact interaction to depict the long-range dynamics of the $X(3872)$, e.g., [961, 1031, 965]. However, the universality is a two-edged sword, which makes the long-range dynamics only depend on one parameter (binding-energy or scattering length), and also makes the mechanism of forming the $X(3872)$ hard to be detected. As pointed out in Ref. [1031], there are two fine-tuning mechanisms to form the $X(3872)$, the fine-tuning of the $D^0\bar{D}^{*0}/D^{*0}\bar{D}^0$ interaction and reduced mass to form a loosely bound state, and the fine-tuning of the P-wave charmonium, i.e., $\chi_{c1}(2P)$, to the proximity of the $D^0\bar{D}^{*0}/D^{*0}\bar{D}^0$ threshold. It is worthwhile to stress that in the latter mechanism, the $c\bar{c}$ component plays a crucial role to form the $X(3872)$ but its proportion could be very small (suppressed by $1/a_s$). In order to discriminate the two mechanisms, one has to detect the dynamics beyond the "universal" region—tens of MeV from the threshold. In Ref. [570], Artoisenet *et al* proposed an EFT mixing the zero-range amplitude and Flatté scattering amplitude [1038, 568] to discern the two different mechanisms from the line shape.

- *Pion-exchange interaction.* The OPE interaction in the $D\bar{D}^*/D^*\bar{D}$ and D^*D systems only allows the $D^*D\pi/\bar{D}^*\bar{D}\pi$ vertex as shown in Fig. 32. The mass difference of the D^* and D will appear in the propagator of the pion as

$$(q^2 - m_\pi^2)^{-1} = \left[(E_{D^*} - E_D)^2 - (\boldsymbol{q}^2 + m_\pi^2)\right]^{-1} \approx \left[(M_{D^*} - M_D)^2 - (\boldsymbol{q}^2 + m_\pi^2)\right]^{-1} \equiv -(\boldsymbol{q}^2 + \tilde{u}^2)^{-1}, \qquad (374)$$

where the energy dependence other than the mass splitting of the D^* and D is neglected (static approximation). $\tilde{u} \equiv \sqrt{m_\pi^2 - (M_{D^*} - M_D)^2}$ is introduced as the effective mass in the propagator. The values $\tilde{u}$ for the states with different charges are given in Table 7. If we use $\tilde{u}$ as a natural scale to estimate the natural binding energy, the result is $0.3-1.0$ MeV. Among them, the $D^{*0}D^0\pi^0$ one is about 1.0 MeV. The estimation hints that the convergent range of the πEFT is $p < |\tilde{u}| \sim 44.12$ MeV rather than $p < m_\pi$. The universality is valid in a smaller range. Therefore, the OPE interaction is needed to exploit the larger-range dynamics, e.g., in [963, 597]. It should be

96

stressed that for the T_{cc}^+ and $X(3872)$, the lowest relevant two-body thresholds are above some $DD\pi$ or $D\bar{D}\pi$ three-body thresholds as shown in Fig. 41. The pionless EFTs cannot work rigorously without considering the three-body effect. If one treats the D^* as a stable state, the pionless EFTs will be valid conditionally up to the scale $|\tilde{u}|$.

- *Perturbative pion versus nonperturbative pion.* In the $^3S_1$ NN system, the perturbative treatment of the OPE interaction fails in the expansion in the KSW scheme [637]. However, the relative ratios of the two-pion and one-pion exchange interaction for the NN system and $\bar{D}^*D$ system are estimated as

$$\bar{D}^*D: \ \frac{g_b^2 \mu_{DD^*}|\tilde{u}|}{8\pi f_\pi^2} \approx \frac{1}{16}, \quad NN: \ \frac{g_A^2 \mu_{NN} m_\pi}{8\pi f_\pi^2} \approx \frac{1}{2}. \tag{375}$$

Compared with the NN system, the expansion parameter for the $\bar{D}^*D$ system is relatively small. Therefore, one expects that the validity range of the perturbative pion for the $\bar{D}^*D$ system is larger. The OPE interaction is included perturbatively in XEFT [963]. In the Weinberg scheme, the OPE interaction is resummed nonperturbatively [972, 989, 990, 283, 268, 812, 597]. In Ref. [978], the breaking-down scale of the perturbative pions is estimated to be around $200-300$ MeV for the $X(3872)$ via a technique to analyze the scattering in the power law singular potentials based on the renormalization group [1039, 636].

- *Three-body dynamics.* One may notice that the effective mass $\tilde{u}$ defined in Eq. (374) can be imaginary as shown explicitly in Table 7. The corresponding potential from Eq. (374) in coordinate space is an oscillating function rather than the conventional Yukawa potential [1040]. In other words, the exchanged pion can be on mass-shell. The imaginary part of the potential arises from the opening of the three-body threshold. The $X(3872)$ is above the $D^0\bar{D}^0\pi^0$ threshold about 6.8 MeV and the T_{cc}^+ state is above the $D^0D^0\pi^+$ and $D^0D^+\pi^0$ thresholds about 5.5 MeV, e.g., see Fig. 41. In order to consider this effect, the three-body dynamics should be incorporated properly. There are two types of three-body cuts (see Fig. 42) that were studied in Refs. [1041, 972, 969, 597, 283]. In the previous discussions, the pion propagators in the OPE interactions are mentioned many times, see Eqs. (319), (327), (328), (329) and (374). However, among them, only Eqs. (328) and (329) keep the three-body cuts properly, which should be a better choice in the calculation.

- *Factorization versus non-factorization.* The productions and decays of the $X(3872)$ should be associated with the short-range dynamics unavoidably. For example, in the $X \to J/\psi \pi^+\pi^-$, the formation of the J/ψ would involve the short-distance interaction around its size, which is much shorter than the size of the $X(3872)$ as a hadronic molecule. In the process $B \to XK$, the production of the c and $\bar{c}$ quark is a high-energy dynamics compared with the binding momentum of the $X(3872)$. With the separated scale, Braaten *et al* proposed the factorization formula [1042], which can be derived from the operator product expansion in Ref [1043]. In the literature, the factorization formula was used either implicitly or explicitly [1044, 1045, 1046, 569, 1047, 1048, 1049, 1050, 1051, 1052]. We take the decays involving the short-range dynamics $X \to H$ [where H denotes the final states produced through short-range dynamics, such as $J/\psi\rho(\omega)$] as an example. The amplitude reads

$$\begin{aligned} \mathcal{T}[X \to H] &\sim \int \frac{d^3q}{(2\pi)^3} \psi(\boldsymbol{q}) \times \mathcal{A}_{\text{short}}[\{D(\boldsymbol{q})\bar{D}^*(-\boldsymbol{q})\}^+ \to H] \\ &\sim \mathcal{A}_{\text{long}}(E) \times \mathcal{A}_{\text{short}}[\{D\bar{D}^*\}^+ \to H], \end{aligned} \tag{376}$$

where $\psi(\boldsymbol{q})$ is the wave function of the $X(3872)$. The superscript of $\{D\bar{D}^*\}^+$ represents the even C parity state. Strictly speaking, the short-range part will (insensitively) depend on the momentum of $D(\bar{D}^*)$. One can ignore the $\boldsymbol{q}$-dependence and factorize out the long- and short-range parts. The long-range part is the molecular wave function at origin. The factorization formula can simplify the calculation by circumventing the complicated loop integrals sometimes. What is more important, it is easy to establish the relation between two processes with the same short- or long-range dynamics, within the factorization approach (this will be illustrated later). Meanwhile, one can depict the same dynamics by calculating the loop diagrams (non-factorization approach), which incorporates the long- and short-range dynamics simultaneously. In general, it aims to include more dynamical details than the factorization approach. However, apart from the tedious calculations, a caveat is

Table 7: Mass scales in the OPE interactions for the $D\bar{D}^*/D^*\bar{D}$ and D^*D systems (in units of MeV). The $\Delta^i \equiv D^{*i} - D^i$, m_π^i and $\tilde{u}_i \equiv \sqrt{m_\pi^{i2} - \Delta^{i2}}$ are listed in order, where i represents different charges.

$\Delta^i|m_\pi^i|\tilde{u}_i$	D^{*0}	D^{*+}
D^0	142.02 | 134.98 | i44.12	145.43 | 139.57 | i40.83
D^+	137.20 | 139.57 | 25.61	140.61 | 134.98 | 39.39

that the dynamics at different energy scales should be incorporated properly in a unified framework, which is a subtle work. We will compare the factorization and non-factorization frameworks in detail later.
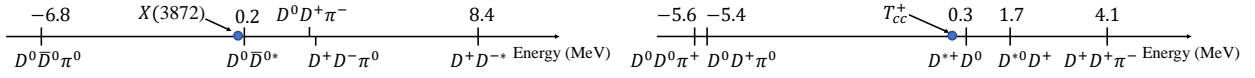
Figure 41: $X(3872)$ (left one) and T_{cc}^+ (right one) related two-body and three-body thresholds.
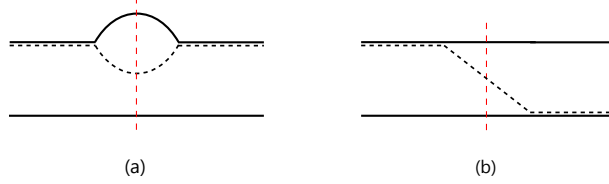
Figure 42: Two types of three-body cuts for the three-body dynamics of $X(3872)$ or T_{cc}^+.

In order to fit these characters of the $X(3872)$ or T_{cc}^+, many attempts have been made to include new ingredients in EFTs. We will review the progresses in EFT frameworks to investigate the $X(3872)$ or T_{cc}^+. We will discuss the XEFT with revised power counting, the Galilean invariant XEFT, the perturbative scale of the pion-exchange interaction, the formulation of the three-body dynamics, factorization and non-factorization schemes for the processes with short-distance dynamics.

In the original version of XEFT [963], the m_π and $M_{D^{(*)}}$ are integrated out as the large scales. However, they will appear in the kinetic energy terms in the calculation. In Ref. [963], the m_π/M_D expansion is performed to simplify the calculation, though it is not implemented systematically in the power counting scheme. In Ref. [1053], a modified power counting for XEFT is proposed. In this power counting, Δ and m_π is treated as $O(Q)$ and δ is treated as $O(Q^2)$. Accordingly, the power counting of other quantities is

$$
\begin{aligned}
\Delta, \ m_\pi, \ p_D &\sim Q, \\
u, \ p_\pi &\sim Q^{3/2}, \\
\delta, \ p_\pi^2/(2m_\pi), \ p_D^2/(2M_D) &\sim Q^2.
\end{aligned}
\tag{377}
$$

This power counting is very convenient to match with the HHχPT. In Ref. [1053], it was employed to simplify the loop diagrams rather than constructing the Lagrangians order by order.

It was pointed out by Braaten [1054] that there are several problems which prevented the original XEFT [963] from obtaining accurate predictions. First, in the original XEFT, the results are not frame-independent, which was specified, e.g., in the center-of-mass frame. Meanwhile, the UV divergence in the NLO calculation can be canceled out only when the low order m_π/M_D expansions are kept. In addition, the renormalization scheme in the original XEFT made it hard to include the decays with large momentum in the final state, such as $D^{*0} \to D^0\gamma$. In order to overcome

these shortcomings, Braaten proposed the Galilean-invariant XEFT based on the feature that $M_{D^*} \approx M_D + m_\pi$ [1054]. In a nonrelativistic theory, the Galilean boost with velocity $\boldsymbol{v}$ will change the momentum and energy as

$$\boldsymbol{p} \to \boldsymbol{p} + m\boldsymbol{v}, \qquad E \to E + m\boldsymbol{v} \cdot \boldsymbol{p} + \frac{1}{2}mv^2. \tag{378}$$

The combination $E - \frac{p^2}{2m}$ is Galilean invariant. Thus, the kinetic terms of the π^0 and D^0 in Eq. (320) satisfy the Galilean invariance. In Ref. [1054], the author chose a different baseline of the mass and eliminate the δ term in the π^0 kinetic term. In the Galilean-invariant XEFT, the D^* is regarded as the combination of D and π, thus its kinetic mass is $M + m$ (where M and m are the masses of D^0 and π^0, respectively). The kinetic term of the D^{*0} reads

$$\mathcal{L}_{D^{*0}} = \boldsymbol{D}^\dagger \cdot \left[i\partial_0 + \frac{\boldsymbol{\nabla}^2}{2(M+m)} - \left(\delta - i\frac{\Gamma_{*0}}{2} \right) \right] \boldsymbol{D}, \tag{379}$$

where Γ_{*0} denotes the D^{*0} width. The partial width of $D^{*0} \to D^0\gamma$ can be included in the Γ_{*0} term. For the interaction terms, the Galilean invariant Lagrangian can be obtained from modifying those in Eq. (320) as follows

- In the $\boldsymbol{D}^\dagger \cdot D\overrightarrow{\boldsymbol{\nabla}}\pi$ term, the operator $\overrightarrow{\boldsymbol{\nabla}}$ is replaced by $(M\overrightarrow{\boldsymbol{\nabla}} - m\overleftarrow{\boldsymbol{\nabla}})/(M+m)$;

- In the $(\bar{D}\boldsymbol{D})^\dagger \cdot \bar{D}(\overleftrightarrow{\boldsymbol{\nabla}})^2\boldsymbol{D}$, the $\overleftrightarrow{\boldsymbol{\nabla}}$ should be replaced by $4(M\overrightarrow{\boldsymbol{\nabla}} - (M+m)\overleftarrow{\boldsymbol{\nabla}})^2/(2M+m)^2$;

- In the interaction $(\bar{D}\boldsymbol{D})^\dagger \cdot \bar{D}D\overrightarrow{\boldsymbol{\nabla}}\pi$, the $\overrightarrow{\boldsymbol{\nabla}}$ should be replaced by $(2M\overrightarrow{\boldsymbol{\nabla}} - m\overleftarrow{\boldsymbol{\nabla}})/(2M+m)$.

The above results are obtained by satisfying two conditions—the Galilean invariance and recovery of the original XEFT in the center-of-mass frame. We can see the Galilean invariance easily in the form, e.g., $(m^{-1}\overrightarrow{\boldsymbol{\nabla}} - M^{-1}\overleftarrow{\boldsymbol{\nabla}})\mu_{M,m}$, where $m^{-1}\overrightarrow{\boldsymbol{\nabla}}$ and $M^{-1}\overleftarrow{\boldsymbol{\nabla}}$ are proportional to the velocity operators. In the Galilean-invariant XEFT, apart from the conservation of $N_c \equiv N_{D^0} + N_{D^{*0}}$ and $N_{\bar{c}} \equiv N_{\bar{D}^0} + N_{\bar{D}^{*0}}$, an extra conservation of the pion number $N_\pi \equiv N_{\pi^0} + N_{D^{*0}} + N_{\bar{D}^{*0}}$ is guaranteed by the Galilean symmetry. Constrained by the Galilean symmetry, it is hard to include the $D^*D^*\pi$ vertex. The heavy quark spin symmetry has to be given up. In the calculation, the complex on-shell renormalization scheme was used, which introduces an extra counter term,

$$\mathcal{L} = -\frac{\delta D_0}{2}(\bar{D}\boldsymbol{D})^\dagger \cdot \left[i\partial_0 + \frac{\boldsymbol{\nabla}^2}{2(2M+m)} \right] (\bar{D}\boldsymbol{D}). \tag{380}$$

With the constraints of the Galilean symmetry, the cutoff-dependence is eliminated to all orders of m/M. In Ref. [1055], the Galilean-invariant XEFT was reformulated in a more simple way by introducing the auxiliary field and adopting a new complex threshold renormalization scheme.

In Ref. [978], Valderrama investigated the power counting in the heavy meson molecules, such as the $X(3872)$, $Z_b(10610)$ and $Z_b(10650)$. They argued that the coupled-channel effect from the HQSS partner channels (e.g., $D\bar{D}$, $D\bar{D}^*/D^*\bar{D}$ and $D^*\bar{D}^*$) is suppressed by at least two orders, which can be safely neglected in the low order calculation. Meanwhile, the energy scale that the pion can be treated perturbatively was explored within a framework developed in atomic physics to handle the singular power-law potential [1039] (which was employed successfully in the NN system [644]). It was shown that the validity of the perturbative pion is related to the $1/r^3$ singularity in the short range part of the tensor force in the OPE interaction [644]. Expanding the Schrödinger equation with the power-law potential in the Bessel functions makes it possible to obtain the analytical solutions nonperturbatively and determine the radius of convergence [644]. In the Ref. [978], the approach was extended to the heavy meson systems. For the $I^G(J^{PC}) = 0^\pm(1^{+\pm})$, the critical momentum of the perturbative pion is about 290^{+120}_{-80} MeV, which corresponds to the critical binding energy 42^{+46}_{-19} MeV. Therefore, it is reasonable to adopt the perturbative pion in XEFT. One can see that the γ_c in Table 6 is below the critical momentum. Thus, in the EFT, considering the charged channel $D^+D^{*-}/D^{*+}D^-$, one can treat the OPE interaction as the NLO contribution perturbatively as well.

In Ref. [1041], the author proposed a toy model to investigate the three-body dynamics of the $X(3872)$ with an equivalently perturbative pion-exchange interaction, which is the first work to discuss the three-body dynamics of the
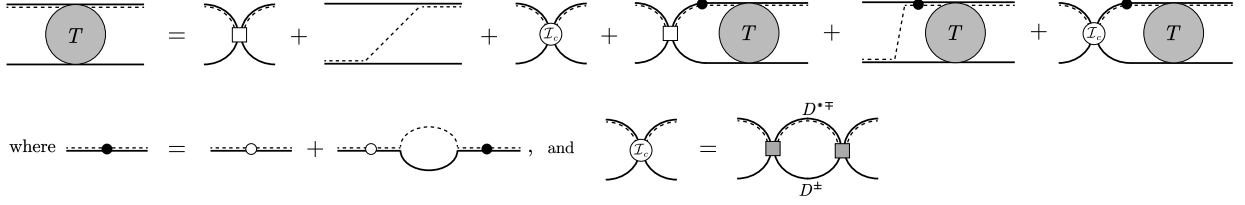
Figure 43: Nonperturbative $D\bar{D}^*$ amplitude in Ref. [597].

$X(3872)$. In this toy model, three spin-zero mesons D_1, D_2 and ϕ are used to mimic the D, D^* and pion, respectively. The Lagrangians are

$$\mathcal{L}_{\text{free}} = \sum_{i=1,2} D_i^\dagger \left(i\frac{\partial}{\partial t} - M_i + \frac{1}{2M_i}\nabla^2 \right) D_i + \phi^\dagger \left(i\frac{\partial}{\partial t} - m + \frac{1}{2m}\nabla^2 \right)\phi, \tag{381}$$

$$\mathcal{L}_{\text{int}} = -\lambda_0 D_1^\dagger D_2^\dagger D_1 D_2 - g(D_2^\dagger D_1 \phi + D_1^\dagger \phi^\dagger D_2) - \delta M D_2^\dagger D_2. \tag{382}$$

In the calculation, the vertex λ_0 is summed to all orders but the vertex g is treated perturbatively. The cutoff dependence was removed by renormalizing the D_2 mass, the λ_0 and short-range coefficients in the operator product expansion. In the NLO, the nonzero width of the D_2 mesons was introduced by either summing its self-energy correction to all orders or using the complex mass scheme to remove the nonphysical IR divergence. In Ref. [969], the binding energy of the $X(3872)$ is investigated up to NLO in XEFT, where the one-pion-exchange interaction is treated perturbatively. Two types of three-body cuts in Fig. 42 were considered, which will be reviewed in detail in Sec. 5.5.2.

In Ref. [972], the three-body dynamics of the $X(3872)$ was investigated in a Faddeev-type framework with non-perturbative pion dynamics for the first time. In Ref. [597], Schmidt *et al* proposed an EFT with D^0, $\bar{D}^0$ and π^0 as the basic degrees of freedom for the $X(3872)$ with the exact Galilean invariance. The D^{*0} is dynamically generated as the P-wave resonance of $D^0\pi^0$. The LO Lagrangians are (convention-II in Table A.11)

$$\mathcal{L} = \mathcal{L}_{\text{kin}} + (\mathcal{L}_{D\pi} + \mathcal{L}_{\bar{D}\pi}) + \mathcal{L}_{D\bar{D}\pi}, \tag{383}$$

$$\mathcal{L}_{\text{kin}} = D^\dagger \left[i\partial_0 + \frac{\nabla^2}{2M_D} \right] D + \bar{D}^\dagger \left[i\partial_0 + \frac{\nabla^2}{2M_D} \right] \bar{D} + \pi^\dagger \left[i\partial_0 + \frac{\nabla^2}{2m_\pi} \right] \pi, \tag{384}$$

$$\mathcal{L}_{D\pi} = \boldsymbol{D}^\dagger \left[\Delta_0 + \Delta_1 \, i\partial_{\text{cm}} + \sum_{n\geq 2} \Delta_n (i\partial_{\text{cm}})^n \right] \boldsymbol{D} + g\left[\boldsymbol{D}^\dagger \cdot (\pi \overleftrightarrow{\boldsymbol{\nabla}} D) + \text{H.c.} \right], \tag{385}$$

$$\mathcal{L}_{D\bar{D}\pi} = -C_0 \frac{1}{2} \left[\bar{D}\boldsymbol{D} + D\bar{\boldsymbol{D}} \right]^\dagger \cdot \left[\bar{D}\boldsymbol{D} + D\bar{\boldsymbol{D}} \right], \tag{386}$$

where $i\partial_{\text{cm}} \equiv i\partial_0 + \nabla^2/(2M)$ (with $M \equiv M_D + m_\pi$) and $\overleftrightarrow{\boldsymbol{\nabla}} \equiv \mu_{D\pi}(m_\pi^{-1}\overleftarrow{\boldsymbol{\nabla}} - M_D^{-1}\overrightarrow{\boldsymbol{\nabla}})$ are Galilean-invariant derivatives [1054, 1055]. $\mu_{D\pi}$ is the reduced mass of the D and π. The $\boldsymbol{D}$ ($\bar{\boldsymbol{D}}$) is the auxiliary vector field to embed the P-wave interaction. The auxiliary field can be eliminated by the path integral or the equations of motion. In general, the value Δ_1 can be taken as $\Delta_1 = \pm 1$, in which the $\Delta_1 = +1$ makes the $\boldsymbol{D}$ a physical field. The Feynman diagrams are presented in Fig. 43. The three-body cut associated with the self-energy of the D^* is included by incorporating the full propagator of the D^*. The pion exchange potential is given by

$$i V^{ij}(\boldsymbol{p}, \boldsymbol{q}; E) \equiv i g^2 \frac{(\alpha \boldsymbol{p} + \boldsymbol{q})^i (\alpha \boldsymbol{q} + \boldsymbol{p})^j}{E - \frac{p^2}{2\mu} - \frac{q^2}{2\mu} - \frac{\boldsymbol{p}\cdot\boldsymbol{q}}{m_\pi} + i\epsilon}, \tag{387}$$

where i and j are the indices of the polarization vector. The α is defined as $\alpha = M_D/M$. The three-body dynamics for the pion-exchange interaction is included as well. Meanwhile, at NLO the charged channel is included in the kernel $\mathcal{I}_c$ as shown in Fig. 43.

With the separated scale, Braaten *et al* adopted the factorization formula [1042] to explore the decays and productions of the $X(3872)$ when the short-range dynamics is involved. The amplitude of the decays involving short-rang

dynamics is given in Eq. (376). The long-range part involves the wave function at origin. Another equivalent approach to writing down the long-range dynamics is

$$\frac{d^3q}{(2\pi)^3}\psi(\boldsymbol{q}) \sim \int \frac{d^3q}{(2\pi)^3}\frac{g}{E - \frac{q^2}{2\mu}},\tag{388}$$

where the coupling constant and two-body nonrelativistic propagator are introduced. The equivalence has been shown in Sec. 5.1.1. According to Eq. (297), the long-range and short-range parts are both cutoff-dependent. One can define the cutoff-independent factorization formula by absorbing the linear divergent part in the wave function at origin into the short-range part,

$$\mathcal{T}[X \to H] \sim \tilde{\mathcal{A}}_{\text{long}}(E) \times \tilde{\mathcal{A}}_{\text{short}}[\{D\bar{D}^*\}^+ \to H],\tag{389}$$

where we use $\tilde{\mathcal{A}}$ to represent the cutoff-independent amplitude. Similarly, the production of the $X(3872)$ as shown in Fig. 44(b) can be formulated as

$$\mathcal{T}[B \to XK] \sim \tilde{\mathcal{A}}_{\text{short}}[B \to \{D\bar{D}^*\}^+K] \times \tilde{\mathcal{A}}_{\text{long}}[\{D\bar{D}^*\}^+ \to X].\tag{390}$$

If one wants to investigate the line shape of $B \to D\bar{D}^*K$ as shown in Fig. 44(c), the factorization reads

$$\mathcal{T}[B \to D\bar{D}^*K] \sim \tilde{\mathcal{A}}_{\text{short}}[B \to \{D\bar{D}^*\}^+K] \times \tilde{\mathcal{A}}_{\text{long}}[\{D\bar{D}^*\}^+ \to \{D\bar{D}^*\}^+].\tag{391}$$

For the line shape $B \to KJ/\psi\pi\pi$ in Fig. 44(d), the factorization is

$$\mathcal{T}[B \to HK] \sim \tilde{\mathcal{A}}_{\text{short}}[B \to \{D\bar{D}^*\}^+K] \times \tilde{\mathcal{A}}_{\text{long}}[\{D\bar{D}^*\}^+ \to \{D\bar{D}^*\}^+] \times \tilde{\mathcal{A}}_{\text{short}}[\{D\bar{D}^*\}^+ \to H].\tag{392}$$

It is worthwhile to mention that the charged $D^+D^{*-}/D^{*+}D^-$ channel can be regarded as either the short-range dynamics [965] or long-range dynamics [1050] depending on the specific framework.
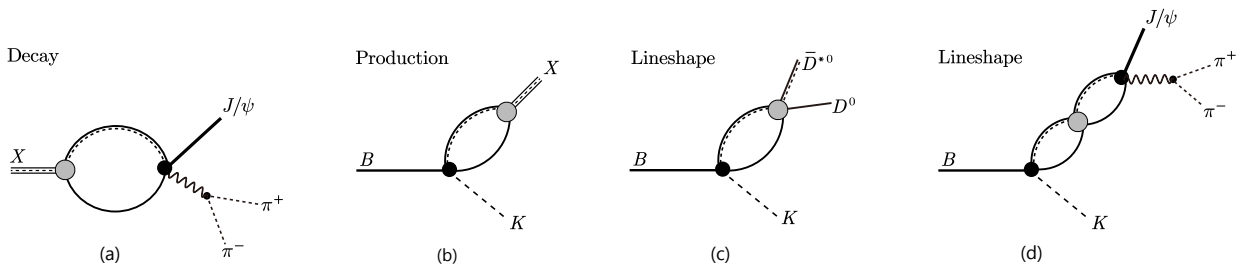
Figure 44: Examples to use the factorization formula in Ref. [1042].

Apart from the factorization framework, the non-factorization approach is also used when calculating these short-range involved dynamics. An example is the NREFT expanded with the velocity of particles [1056, 1057, 1058, 1059, 1060, 11]. We take the hadron loop diagrams in Fig. 45 as an example. In the loop diagrams, the momentum and energy of the three nonrelativistic intermediate states are counted as $O(v)$ and $O(v^2)$, respectively. Thus, the propagators are counted as $O(v^{-2})$ and the loop integral $\int d^4l$ is counted as $O(v^5)$. The general amplitude is counted as

$$\mathcal{M} \sim \frac{v^5q^n}{(v^2)^3}.\tag{393}$$

where q^n is the scale arising from the derivative coupling vertices.

The relation of these two approaches was investigated by Mehen [1061] with the $X(3872) \to \chi_{cJ}\pi^0$ process as an example. In the non-factorization approach (also known as the hadronic loop approach) the diagrams are listed in the Fig. 45. The $D\bar{D}\chi_{c0}$ and $D^*\bar{D}^*\chi_{c0}$ vertices were constructed in HMχPT. The loop integral in the non-factorization approach is finite (an extra regulator is not needed). In the factorization approach, the short-distance dynamics is depicted by the $D\bar{D}^*\chi_{c0}\pi$ vertex in XEFT, which is matched to the HMχPT diagrams. In the factorization approach,

the charged channel $D^+D^{*-}/D^{*+}D^-$ is integrated out. The short-distance dynamics in these two approaches arise from the same $D\bar{D}\chi_{c0}$ and $D^*\bar{D}^*\chi_{c0}$ vertices in HMχPT. However, one cannot expect these two approaches to give the same results. The two approaches do include the same dynamics in the region $p < \gamma_c$, where γ_c is the binding momentum with respect to the charged threshold. When the cutoff $\Lambda \sim \gamma_c$ is introduced, the non-factorization approach will give the same results as the factorization approach [1061]. However, in the region $p > \gamma_c$, these two approaches contain different UV behaviors, which will lead to different results. Mehen pointed out [1061] that the $X(3872) \to \chi_{cJ}\pi^0$ rate in the non-factorization approach including the charged channels will be similar to the results from the factorization approach because of the cancellations of the contribution from the UV region in the neutral and charged channels for the specific process. However, this is just a specific example. In Ref. [11], it was found that the contributions of the charged and neutral channels for $X(3872) \to \chi_{cJ}\pi\pi$ are constructive. Thus, these two approaches (even with the charged channel in the non-factorization approach) will give different results.
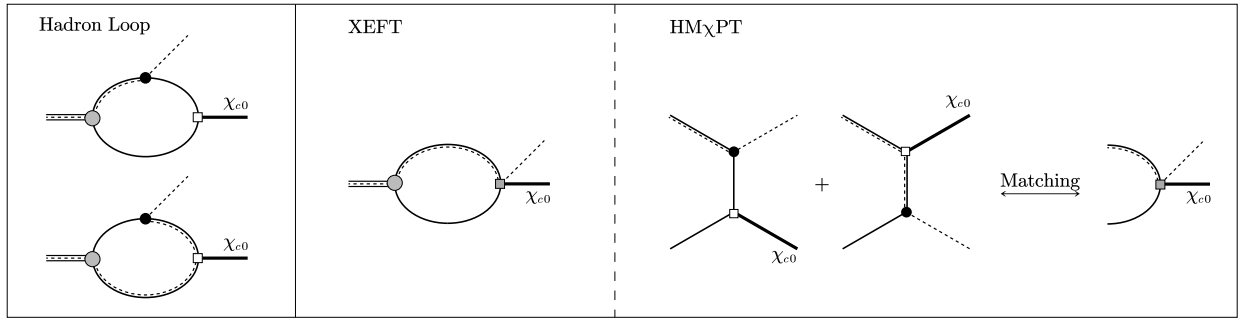
Figure 45: $X(3872) \to \chi_{c0}\pi$ in the non-factorization scheme (hadron loop) and factorization scheme (matching HMχPT to the XEFT).

We can analyze the scales appearing in the above example following Ref. [1062]. The binding momenta for the neutral and charged channels are $\gamma_n \sim 20$ MeV and $\gamma_c \sim 120$ MeV, respectively (see Table 6 for details). The vertex $X\bar{D}^*D$ is dressed by the one-pion exchange interaction with the typical scale $|u| \sim 45$ MeV. The typical scale of the vertex $D^*D\pi$ is estimated as $\sqrt{2m_\pi|m_{D^*} - m_D - m_\pi|} \sim |u| \sim 45$ MeV in the nonrelativistic approximation. The vertex $D^{(*)}\bar{D}^{(*)}\chi_{c0}$ is relevant to the rearrangement of the charmed quarks into a bound state. Here we use the binding momentum of the charmonium, $m_c v \sim 900$ MeV to estimate the typical scale, where the $v \sim 0.3$ is the typical velocity of charm quark. One can see that there are at least three well-separated scales in total, $|u| \sim \gamma_n$, γ_c and $m_c v$. In the above examples, one should be cautious of taking the cutoff Λ to infinity, because one cannot expect the hadronic vertices still work properly at very high energy scale. One cannot even expect that one single cutoff is enough to mimic all the form factors of the vertices at (widely) separated scale. Meanwhile, in the NREFT, there exist two velocities as pointed out in Ref. [11]. The power counting might fail due to the two separated velocities and the appearance of triangle singularity (see Ref. [1063] for reviews). However, in order to include the effect of triangle singularity, one has to resort to the non-factorization approach [1064, 1065, 1066, 1067, 1068]. Therefore, the non-factorization approach is trying to embed details of higher energy scales than those in the factorization approach. The cost for the non-factorization approach is the arbitrariness of choosing UV behaviors. Moreover, the appearance of multiple scales would destroy the convergence of EFT. In the specific process, the two approaches might give different results, which need to be checked by experiments.

5.5.2. Mass corrections

In Ref. [983], the authors investigated the $D\bar{D}^*/D^*\bar{D}$ scattering in the unitarized HHχPT with the pion exchange and a contact interaction. In the calculation, the $O(p^0)$ amplitudes come from the (a) and (b) diagrams in Fig. 46. The diagrams (c)-(f) are counted as $O(p^2)$ from Weinberg's power counting. However, the amplitudes of such two-particle reducible diagrams are enhanced by a factor M/p if one keeps the kinetic energy terms to remove the pinched singularity as shown in Eq. (152). The amplitudes in diagrams (c)-(f) counted as $O(p)$ can be generated by iterating the tree-level amplitudes in (a) and (b). The authors obtained a unitary amplitude $T^{\text{phy}} = T^{(0)2}/(T^{(0)} - T^{(1)})$ on the basis of the leading order Padé approximation (see Ref. [1069] for Padé approximation and see Ref. [577] for the similar

unitary method for the $\pi\pi$ scattering). The authors concluded that (i) the pion-exchange interaction is sufficient to form a bound state without the contact interaction, (ii) the result is not sensitive to the strength of the contact interaction, and (iii) the $X(3872)$ pole disappears when the pion mass is larger than 142 MeV.
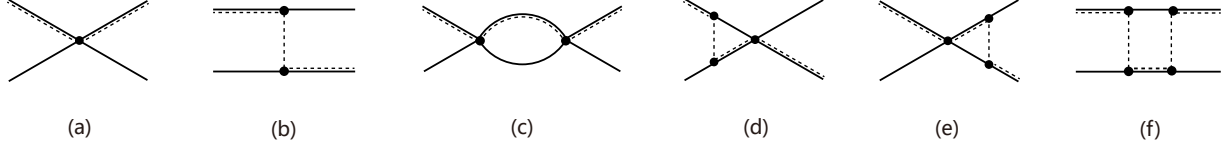

Figure 46: Feynman diagrams contribute to $T^{(0)}$ and $T^{(2)}$ in Ref. [983].

However, the authors of Ref. [984] illustrated in an explicit cutoff-regularization scheme that the OPE interaction is well defined only in the context of the definite contact interaction because the divergent part of the iterating pion-exchange interaction should be canceled out by the contact counter term. Thus, the separation of the pion-exchange and contact contributions is scheme-dependent. In Ref. [972], the cutoff dependence of the contact coupling constants was obtained (see Fig. 47), in which a bound state was imposed with a binding energy 0.5 MeV in an interaction with the dynamical pion. One notices that the $C_0 = 0$ corresponds to the cutoff $\Lambda \approx 1.0$ GeV. Thus, the bound state was naively attributed to the OPE interaction when the cutoff is around 1.0 GeV (e.g., [1025, 1070]), which seems a scheme-dependent conclusion.

In Ref. [989], the authors investigated the m_π-dependence of the binding energy of the $X(3872)$ within a nonrelativistic Faddeev-type three-body equation for the $D\bar{D}\pi$ system in the $J^{PC} = 1^{++}$ channel. In the calculation, the dynamical pion was included nonperturbatively, and the m_π-dependence of the $D^{(*)}$ mass [49], pion decay constant f_π [485] as well as the $D^*D\pi$ coupling constant g [732] were determined by χPT or lattice QCD. However, the m_π-dependence of the contact interaction is hard to determine, which is conjectured on the basis of the $X(3872)$ as a bound state and the cutoff-independent binding energy E_B. The form of the contact interaction is assumed as

$$C_0(\Lambda, \xi) = C_0^{\text{ph}}(\Lambda)\left[1 + f(\Lambda)\frac{m_\pi^{\text{ph2}}}{M^2}(\xi^2 - 1)\right]. \tag{394}$$

The superscript "ph" represents the quantities at the physical pion mass. The ξ is defined as $\xi \equiv m_\pi/m_\pi^{\text{ph}}$. M is a large scale around $m_\rho \approx 800$ MeV. The unknown $f(\Lambda)$ is evaluated with the requirement that the binding energy E_B^{ph} and its slope $S_{E_B} \equiv (\partial E_B/\partial m_\pi)|_{m_\pi = m_\pi^{\text{ph}}}$ should be cutoff-independent at the physical point. The final results depend on the specific value of S_{E_B}. A two-pion-exchange diagram was used to estimate the natural results of $f(\Lambda)$ and S_{E_B}. The final result is given with varying S_{E_B} in a natural scale as shown in the middle subfigure of Fig. 48. The results indicated that the behavior of the quark-mass dependence of the $X(3872)$ strongly depends on the contact interaction. In other words, ignoring the contact interaction might yield misleading results. Meanwhile, the $X(3872)$ can turn into a virtual state only when the S_{E_B} is in a unnatural range, which is different from the results in Ref. [983].

In Ref. [990], the chiral extrapolation of the binding energy of the $X(3872)$ was investigated in a similar framework with that in Ref. [989], but in the modified Weinberg formulation [1071]. The modified Weinberg formulation was
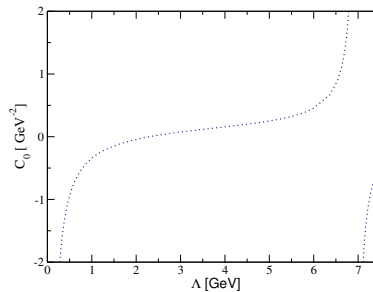
Figure 47: The cutoff dependence of the contact coupling constant obtained in Ref. [972] by imposing a bound state with a binding energy 0.5 MeV in an interaction with the dynamical pion.
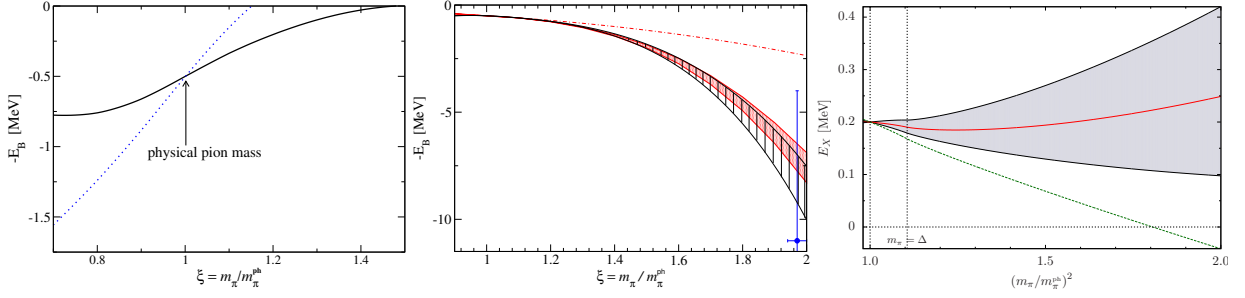
Figure 48: Left panel: The LO results including the fully three-body dynamics (black solid curve) and in the simple static OPE (blue dotted curve) in Ref. [990] within the modified Weinberg formulation. Middle panel: The NLO results in the conventional Weinberg formulation (black hatched band) in Ref. [989] and modified Weinberg formulation (red dotted band) in Ref. [990]. The dot-dashed curve comes from the calculation without pions. The dot with error bars represents the results from lattice QCD simulations [1073]. Right panel: The NLO results (gray band) in XEFT in Ref. [969], where the unknown d_2 and r_0 are estimated with naturalness. The red solid curve represents the result considering the LO contact and OPE interaction. The green dashed curve represents an example of unnatural parameters.

proposed to solve the problem which was referred to as the "inconsistency of Weinberg's approach" [1072]. The idea is to make the UV behavior milder by interchanging the expansion order of $1/\Lambda$ and $1/m$. For example, within the cutoff regularization, the relativistic loop function reads

$$I = \frac{4\,i}{(2\,\pi)^4} \int \frac{d^4k\,\theta(\Lambda - |\boldsymbol{k}|)}{[k^2 - m^2 + i\,0^+]\,[(P-k)^2 - m^2 + i\,0^+]}, \tag{395}$$

where $P = (2\sqrt{m^2 + \boldsymbol{p}^2}, \boldsymbol{0})$. The integral is logarithmically divergent. Our conventional nonrelativistic expansion based on $p \ll \Lambda \ll m$ will give rise to a linear divergence. However, if one first performs the $1/\Lambda$ expansion and then performs the $1/m$ expansion based on $p \ll m \ll \Lambda$, one can retrieve the logarithmic divergence and solve the inconsistency of Weinberg's approach. With this modified Weinberg formulation, the theory is perturbatively renormalizable and all divergence can be removed by renormalizing the LECs of the LO contact interaction. Unlike the approach of Ref. [989], where additional input is needed to maintain the renormalization, the modified Weinberg approach can predict the m_π-dependence of the binding energy without extra parameters. At the leading order the contact coupling constant C_0 is m_π-independent. The LO results are shown in the left subfigure of Fig. 48, in which the binding energy of the $X(3872)$ will decrease and finally become unbound with the increasing of m_π. However, the NLO results shown in the middle subfigure of Fig. 48 will change the tendency and become consistent with those in Ref. [989]. It is worthwhile to stress that the NLO results were based on some assumptions and naive dimensional analysis.

In Ref. [969], the binding energy of the $X(3872)$ was investigated in XEFT, where the $D^0\bar{D}^{*0}/D^{*0}\bar{D}^0$ scattering in the $J^{PC} = 1^{++}$ channel was calculated up to NLO as shown in the diagrams of Fig. 33. Apart from the Lagrangian (320), an extra NLO Lagrangian was introduced to include the m_π-dependence of the contact term (convention-II) in Table A.11,

$$\mathcal{L}^{\mathrm{NLO}} = -\frac{D_2 u^2}{2}(\bar{D}D + D\bar{D})^\dagger \cdot (\bar{D}D + D\bar{D}), \tag{396}$$

where u^2 is defined as $u^2 = \Delta^2 - m_\pi^2$. Compared with the KSW scheme for the NN system, a novel feature is the $\mathcal{A}_0^{(\mathrm{VI})}$. The contribution of the diagram for the NN system is canceled out by the counter term in the on-shell renormalization scheme because the pions are always off-shell which only contribute to the real part of the pole of the nucleon propagator. For the XEFT, the pions could be on-shell and contribute to the imaginary part of the pole of the D^* which cannot be removed in the on-shell renormalization scheme. In the calculation, the authors showed that the $\mathcal{A}_0^{(\mathrm{VI})}$ is IR divergent if one dresses the D^{*0} propagator with one loop. Instead, the author used the full propagator of the D^{*0} that is dressed to all orders. If the full propagator is used in $\mathcal{A}_{-1}$ and $\mathcal{A}_0^{(\mathrm{I},\ldots,\mathrm{V})}$, the contribution of $\mathcal{A}_0^{(\mathrm{VI})}$ is included automatically. To the NLO, the cutoff-dependence of the C_2 and D_2 is obtained by the renormalization up to two unknown parameters, r_0 and d_2. With the naturalness estimation of the two parameters, the m_π-dependence of the binding energy is given in the right subfigure of Fig. 48. In the numerical analysis, the m_π-dependence of the pion

decay constant, D meson axial coupling constant and masses of the $D^{(*)}$ were taken from Refs. [485, 1074, 732, 47]. One can see that the binding energy of the $X(3872)$ depends on the pion mass moderately. In Ref. [1075], the calculation was extended to the $X(3872)$ in the finite volume. The finite volume correction to the binding energy was obtained explicitly and fully determined by the infinite volume parameters. The numerical results showed that the finite volume effect is significant even for a large box with the length around 20 fm.

In Ref. [268], Xu et al calculated the DD^* interaction in χEFT up to NLO with the Weinberg scheme. In their calculation, the LO contact term, OPE and the NLO TPE interactions were investigated. The LECs of the LO contact terms were estimated in the resonance saturation model [599, 1076, 981, 980, 897]. The numerical results showed that there is no bound state in the isovector channel. In the isoscalar channel, there exists a bound state with the binding energy $17.5^{+4.1+18.3}_{-3.9-14.0}$ MeV, where the first and second uncertainties arise from the inclusion of the f_0, a_0 and a_1, f_1 mesons in the resonance saturation model, respectively. The prediction was confirmed by the observation of the T_{cc}^+ [5, 4]. The similar χEFT was adopted to investigate the $\bar{B}^{(*)}\bar{B}^{(*)}$ systems in Ref. [976, 812]. It was shown that there exist the $\bar{B}\bar{B}^*$ and $\bar{B}^*\bar{B}^*$ bound states with $I(J^P) = 0(1^+)$. The former one is naturally the heavy quark flavor symmetry partner of the T_{cc}^+ state.

5.5.3. Partners of X(3872)

The $X(3872)$ as a hadronic molecule implies the existence of other states which are related to the $X(3872)$ through various symmetries such as the heavy quark spin symmetry, heavy quark flavor symmetry, SU(3) flavor symmetry and so on. In this section, we review the partner states of the $X(3872)$ as predicted in various EFT frameworks. We will also pay attention to the caveats of these predictions.

In Ref. [977], the author adopted the πEFT with heavy quark symmetry to explore the partners of the $X(3872)$. It was found that the existence of the $D^0\bar{D}^{*0}/D^{*0}\bar{D}^0$ bound state does not exclude and support the existence of the $D^0\bar{D}^0$ bound state. As shown in Eqs. (362), (363) and (365) there are two independent coupling constants in the $D^{(*)}\bar{D}^{(*)}$ systems. The interactions for the $D\bar{D}^*/D^*\bar{D}$ and $D\bar{D}$ systems are independent in the heavy quark spin symmetry limit.

In Ref. [1020], Nieves et al discussed the $B\bar{B}^*$ bound states deduced from the weakly bound $X(3872)$ within EFT framework including the contact and OPE interactions. The heavy quark symmetry was used to relate the cutoffs in the charmed and bottom systems by $\Lambda_B = \Lambda_X + O(\frac{1}{m_Q})$. The contact dynamics is determined from the phenomenological model in Refs. [42, 900]. Within the phenomenological model, the contact interaction in the neutral-charged basis can be expressed as

$$\langle \boldsymbol{k}|V_C|\boldsymbol{k}'\rangle_{C=+1} = \langle \boldsymbol{k}|V_C|\boldsymbol{k}'\rangle_{C=-1} = C_0^{D\bar{D}^*} \begin{pmatrix} 1 & 1 \\ 1 & 1 \end{pmatrix}. \tag{397}$$

One can see that the model exerts two constrains. First, the diagonal and off-diagonal terms are constrained to be equal, which implies the vanishing interaction in the isovector channel. Meanwhile, the states with odd and even parities have the same interaction. With the relations, the authors predicted the $I^G(J^{PC}) = 0^\pm(1^{+\pm})$ $B\bar{B}^*/B^*\bar{B}$ bound states in the ${}^3S_1 - {}^3D_1$ waves and an even C parity ${}^3P_0$ states. The conclusions in Ref. [1020] strongly rely on the validity of the phenomenological model [42, 900].

Nieves et al investigated the heavy quark spin symmetry partners of the $X(3872)$ within the pionless EFT [1009]. Apart from the trivial prediction of the $J^{PC} = 2^{++}$ state [see Eq. (365)], the authors predicted a total six $D^{(*)}\bar{D}^{(*)}$ molecular states with the extra assignment of the $X(3915)$ as the 0^{++} $D^*\bar{D}^*$ molecule. The result is very natural, which has been explained in Sec. 5.4 according to Fig. 39. In Ref. [1009], the author also considered the subleading effect, like the HQSS breaking effect, OPE interaction and coupled-channel effect, which brought uncertainties of about $40 - 50$ MeV to the binding energy of the most bound cases.

In Ref. [1010], Hidalgo-Duque investigated the partner states of the $X(3872)$ in HQSS and light flavor symmetry. In this work, the coupled-channel effects related to the mass splittings $M_{D^*} - M_D$ and $M_{D_s} - M_D$ are neglected. As shown in Eq. (353), there are four independent coupling constants to depict the general $D^{(*)}\bar{D}^{(*)}$ systems in the HQSS and SU(3) flavor symmetry. The four independent coupling constants are determined by treating the $X(3872)$ as the $D\bar{D}^*/D^*\bar{D}$ state, $X(3915)$ as the $D^*\bar{D}^*$ state, $Y(4140)$ as the $D_s^*\bar{D}_s^*$ state and the isospin violating decay ratio of $X(3872)$ (the isospin violating decay ratio depends on the binding energy and mixing angle of the neutral and charged components, see Sec. 5.5.5). In the numerical analysis of Ref. [1010], the isospin partner of the $X(3872)$ is ruled out. Meanwhile, the author predicted the $D_{(s)}^{(*)}\bar{D}_{(s)}^{(*)}$ full molecular spectrum.

In Ref. [1011], Meng *et al* predicted the $[\bar{D}_s^* D_s^*]^{0^{++}}$, $[\bar{D}_s^* D_s / \bar{D}_s D_s^*]^{1^{+-}}$, and $[\bar{D}_s^* D_s^*]^{1^{+-}}$ bound states as the partners of the $X(3872)$ in the HQSS and SU(3) flavor symmetry, which is the consequence of the existence of the $[\bar{D}_s D_s]^{0^{++}}$ bound state supported by the lattice QCD calculation [1077] and the observation of $\chi_{c0}(3930)$ by the LHCb Collaboration [1078, 1079]. In the single-channel scheme, the authors obtained the results by assuming $X(3872)$ as the weakly bound $D^0 \bar{D}^{*0}/D^{*0} \bar{D}^0$ state, which can be related to the $\bar{D}_s^* D_s / D_s^* \bar{D}_s$ state in the SU(3) flavor symmetry. Then, according to Fig. 39, one can infer that the arrow in Fig. 39 represents the more attractive interaction if the $[\bar{D}_s D_s]^{0^{++}}$ is the deeper bound state. In the Ref. [1011], the authors also considered the coupled-channel effect for the $X(3872)$. Within a cutoff-independent framework, it was shown that treating $X(3872)$ as a coupled-channel molecule will not change the results qualitatively, instead will make it become a deeper bound state.

In Ref. [1021], the authors explored the consistence of the strict heavy quark limit and the OPE interaction. The calculation showed that the implication of HQSS, degeneration of $|0_H^{-+} \otimes 1_L^{--}, 1^{+-}\rangle$, $|1_H^{--} \otimes 1_L^{--}, 0^{++}\rangle$, $|1_H^{--} \otimes 1_L^{--}, 1^{++}\rangle$ [$X(3872)$], and $|1_H^{--} \otimes 1_L^{--}, 2^{++}\rangle$ are still robust considering the OPE interaction when all the partial waves and channels are included. The similar consistences of chiral dynamics and the heavy quark symmetry were also explored in Ref. [950]. In Ref. [1021], the 2^{++} channels were investigated with the nonperturbative pions considering the heavy quark symmetry breaking effect. The results showed that the nonperturbative pion approach will lead to significant shifts of the mass and width about 50 MeV as compared to the perturbative pion approach.

Recently, Xu explored the S-wave interaction for the $D\bar{D}^*$ system with $I^G(J^{PC}) = 0^+(1^{++})$, $0^-(1^{+-})$, $1^+(1^{+-})$ and $1^-(1^{++})$ within the χEFT [995]. The calculation was performed up to NLO, including the contact term, OPE and TPE interactions with the Weinberg scheme. The results indicated the existence of the $0^-(1^{+-})$ and $1^+(1^{+-})$ molecular states in addition to the $X(3872)$ as the $0^+(1^{++})$ molecule.

In Ref. [1023], the HDAS was used to investigate the triply heavy partners of $X(3872)$ in contact EFT. With this symmetry, $X(3872)$ as the molecule implies several isoscalar baryonic molecules composed of $\Xi_{QQ'}^{(*)} D^*$ and $\Xi_{QQ'}^{(*)} \bar{B}^*$.

In Ref. [1080], the hadronic atom $D^\pm D^{*\mp}$ was investigated, which is formed mainly by the Coulomb interaction. Unlike the conventional hadronic atoms [1081, 1082], the strong interaction correction to the Coulomb interaction is treated nonperturbatively due to the pole of the $X(3872)$. In their calculation, the strong interaction in the neutral and charged bases was introduced as

$$V = C_0 \begin{pmatrix} 1 & 1 \\ 1 & 1 \end{pmatrix}, \tag{398}$$

where the vanishing isovector interaction is presumed. With this interaction, the correction to the binding energy of the hadronic atom is

$$\Delta E_n = \frac{2\alpha^3 \mu_c^2}{n^3 \sqrt{2\mu_c \Delta}} \left[-1 - i + O\left(\alpha \sqrt{\frac{\mu_c}{\Delta}}\right) \right]^{-1}, \tag{399}$$

where μ_c is the reduced mass and n is the principal quantum number. Δ is the threshold difference of the charged and neutral channels. The correction is independent of the binding energy of the $X(3872)$ and depends on the threshold difference. The authors evaluated the ratio of the production rate of the X atom with respective to the $X(3872)$ in B decays and at hadron collider. The null observing of the X atom will give lower limit of the binding energy of the $X(3872)$.

Canham studied the scatterings of the D and D^* mesons off the $X(3872)$ as a weakly bound state of the $D^0 \bar{D}^{*0}/D^{*0} \bar{D}^0$ in a contact EFT [1083]. In Ref. [1084], the scattering of the ultrasoft pion and $X(3872)$ was investigated in XEFT. The breakup cross section of $\pi^+ X(3872) \to D^{*+} \bar{D}^{*0}$ was calculated. In Ref. [1085], the hadronic systems composed of three and four $X(3872)$ were investigated. A $4X(4^{++})$ octamer and a bound $3X(3^{++})$ were predicted with strict HQSS.

5.5.4. Long-range dynamics

In Ref. [961], Voloshin investigated the $X(3872) \to D^0 \bar{D}^0 \pi^0$ and $X(3872) \to D^0 \bar{D}^0 \gamma$ decays driven by $D^{*0} \to D^0 \pi^0(\gamma)$ and its charge conjugation $\bar{D}^{*0} \to \bar{D}^0 \pi^0(\gamma)$. The Feynman diagram of the $X(3872) \to D^0 \bar{D}^0 \pi^0$ decay corresponds to Fig. 34(a). The universal wave function in Eq. (296) up to a different normalization was adopted. The decay patterns for different C parities of the $X(3872)$ are distinct due to the different interference of the contributions from the D^{*0} and $\bar{D}^{*0}$ decays. Although the calculation was not performed in an EFT framework, it is equivalent to the results from the LO contact EFT as shown in Sec. 5.1.1.
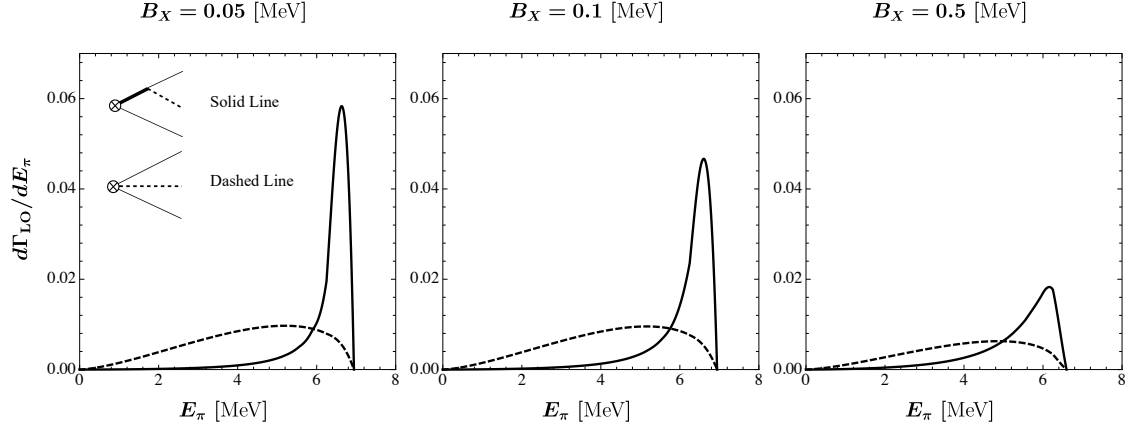
Figure 49: The differential distribution in the pion energy. The solid and dashed curves correspond to the decays driven by $D^{*0} \to D^0 \pi^0$ (or its charge conjugation) and contracting the D^{*0} propagator into a contact vertex, respectively.

In the original work of XEFT [963], the $X \to D^0 \bar{D}^0 \pi^0$ was calculated up to NLO. The contributions of Feynman diagrams (a), (b), (c), (e) and (f) in Fig. 34 were investigated. The decay rate for $X \to D^0 \bar{D}^0 \pi^0$ was given as a function of the binding energy. The results showed that the nonanalytical correction from the perturbative pion exchange is very small, about 1% of the decay rate. The calculation was updated in Ref. [1086] by including the $\pi^0 D^0$, $\pi^0 \bar{D}^0$ and $D^0 \bar{D}^0$ rescattering effect. Apart from the Lagrangians in Eq. (320), two extra terms were included, which were first pointed out in Ref. [11],

$$\mathcal{L}^{\mathrm{NLO}} = \frac{C_\pi}{2m_\pi}(D^\dagger \pi^\dagger D\pi + \bar{D}^\dagger \pi^\dagger \bar{D}\pi) + C_{0D} D^\dagger \bar{D}^\dagger D\bar{D}, \tag{400}$$

where the first and second terms correspond to the C_π and C_{0D} vertices in diagrams (d) and (g) of Fig. 34, respectively. The two new interactions change the uncertainties of the decay rate and the binding energy. In the calculation, the interaction of $D^0 \bar{D}^0$ was resummed to include the rescattering effect from the bubble diagram to all orders. The results showed that the rescattering effect of $D^0 \bar{D}^0$ only leads to a small modification. The differential distribution in the pion energy, i.e., $d\Gamma/dE_\pi$ was studied, which is sensitive to the binding energy and the correct inclusion of the virtual $D^{*0}/\bar{D}^{*0}$ propagator as shown in Fig. 49. The differential decay width becomes very different when one contracts the virtual $D^{*0}/\bar{D}^{*0}$ propagator into a contact vertex.

In Ref. [1087], Guo *et al* investigated the $X(3872) \to D^0 \bar{D}^0 \pi^0$ in the coupled-channel contact ($\not{\pi}$) EFT (see Sec. 5.1.2). The neutral ($D^0 \bar{D}^{*0}/D^{*0} \bar{D}^0$) and charged ($D^+ D^{*-}/D^{*+} D^-$) channels were both considered. The diagrams (a) and (g) in Fig. 34 were calculated considering the charged channel. The two coupling constants were fixed by fitting the $X \to J/\psi\rho$ and $X \to J/\psi\omega$ line shapes [1088] and those of $Z_b(10610)$ [307]. The cutoff is specified as $\Lambda = 0.5$ GeV and 1.0 GeV. In the calculation, the final state interaction of $D\bar{D}$ was induced by solving the LSEs, which is important numerically.

In Ref. [1050], Meng *et al* obtained the decay widths of $X(3872) \to D^0 \bar{D}^0 \pi^0$ and $X(3872) \to D^0 \bar{D}^0 \gamma$ as a by-product of investigating its isospin violating decays in the coupled-channel $\not{\pi}$EFT. The cutoff-dependence was removed in such an EFT. The LECs were determined by the isospin violating decay ratio and the binding energy of the $X(3872)$. The decay widths are presented in Fig. 54. The strong and radiative decay widths are about 30 keV and 10 keV, respectively, for the binding energy from -300 keV to -50 keV. The calculation details will be given in Sec. 5.5.5.

In Ref. [968], Meng *et al* investigated the kinetically allowed $T_{cc}^+ \to D^0 D^0 \pi^+$, $T_{cc}^+ \to D^+ D^0 \pi^0$ and $T_{cc}^+ \to D^+ D^0 \gamma$ decays within the coupled-channel EFT (see Sec. 5.1.2). The T_{cc}^+ was treated as the bound state of $D^{*0} D^+/D^{*+} D^0$. In the coupled-channel EFT, the coupling constants of the T_{cc}^+ with the two channels were related to the binding energy and mixing angle of two components. This framework includes the possible isospin violating effect and satisfies the renormalization group invariance. The numerical results were given in Fig. 50. The results showed that the largest decay mode is the $T_{cc}^+ \to D^0 D^0 \pi^+$, which is just the experimental discovery channel. The total width (strong plus radiative decays) in the single-channel and isospin singlet limits are $59.7^{+4.6}_{-4.4}$ keV and $46.7^{+2.7}_{-2.9}$ keV, respectively, which
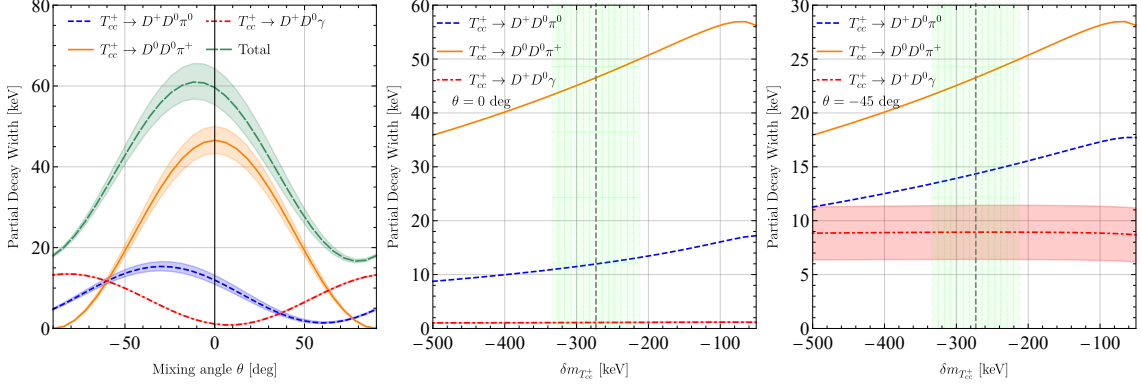
Figure 50: The strong and radiative decay widths of the T_{cc}^+ obtained in Ref. [968]. Left panel: the mixing angle dependence of the partial widths, where the colored shadow represents the uncertainties stemming from the T_{cc}^+ mass. Middle and right panels: the dependence of the partial widths on the binding energy of the T_{cc}^+ in single-channel limit ($\theta = 0°$) and isospin limit ($\theta = -45°$), respectively.
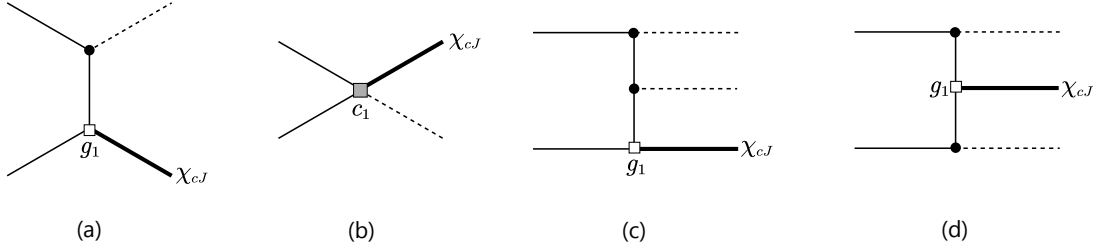

Figure 51: The topological diagrams contributing to $D\bar{D}^* \to \chi_{cJ}\pi$ and $D\bar{D}^* \to \chi_{cJ}\pi\pi$ in HMχPT [1089]. The thin solid line represents D or $\bar{D}^*$.

is much smaller than the width first reported (about 410 keV) in experiment [4]. However, the theoretical calculation was supported by the subsequent experimental analysis in a unitarized profile, which gives $\Gamma = 47.8 \pm 1.9$ keV [5]. In Ref. [278], Fleming *et al* obtained similar results with the similar two-channel contact EFT but in a relativistic form. Apart from the decay widths, the differential spectra as a function of the invariant mass of the final state DD pair was given. The effect of the possible bound state from the DD system was discussed. In Ref. [271], the authors obtained consistent results with those in Ref. [968] within a single-channel phenomenological approach in the presumed isoscalar channel.

In Ref. [275], the subleading contributions to the strong and electromagnetic decays of the T_{cc}^+ state were investigated within the framework of EFT, including the contribution of the seagull two-body operator, the DD final state interaction, the isospin violating effect of the molecular wave function and the contribution of the compact tetraquark component. Although it is hard to determine all the parameters in calculation, the authors provided some reasonable estimation of these effects.

Du *et al* [283] adopted a coupled-channel EFT including the three-body dynamics (e.g., see Fig. 42) to fit the observed line shape in the $D^0 D^0 \pi^+$ channel [4]. With the analysis, the scattering length and effective range of the $D^* D$ scattering was extracted and the compositeness parameter of the T_{cc}^+ was calculated, which is close to the unity indicating the molecular nature of the T_{cc}^+. Employing the HQSS, a $D^* D^*$ molecular partner of the T_{cc}^+ with $I(J^P) = 0(1^+)$ was predicted. In Ref. [282], the partners of the T_{cc}^+ state in the HQSS were investigated.

5.5.5. Short-range dynamics

In Ref. [1089], Fleming *et al* calculated the $X(3872) \to \chi_{cJ}(\pi^0, \pi\pi)$ processes with the factorization formula. The short-range dynamics is depicted by the local operators [for the $D^0 \bar{D}^0 \chi_{cJ}(\pi^0, \pi\pi)$ vertices] in XEFT. The coupling constants of the local operators are determined by matching to the HMχPT as shown in Fig. 51, where g_1 and c_1 are
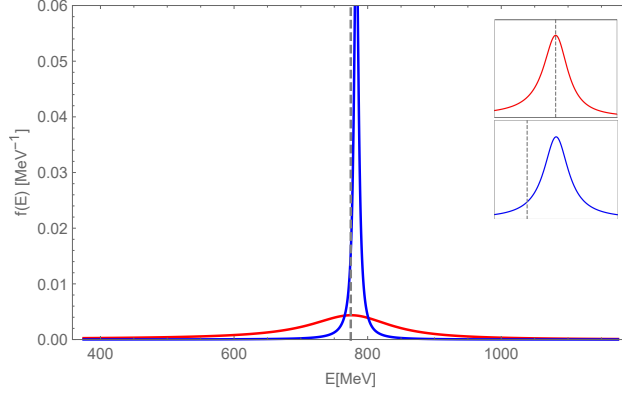
Figure 52: Schematic illustration of the kinematic mechanism of the large isospin violating decay of the $X(3872)$. The red and blue curves are the Breit-Wigner distribution of ρ and ω mesons. The dashed vertical line corresponds to the $M_{X(3872)} - M_{J/\psi}$. The two small subfigures are the rescaled plots.

unknown couplings. The results showed that the two pion transitions are highly suppressed compared with the one pion transition, except the $X \to \chi_{c1}\pi^0\pi^0$, which is almost at the same order as the $X \to \chi_{c1}\pi^0$. The enhancement of $X \to \chi_{c1}\pi^0\pi^0$ arises from regulating the IR divergence (when the D meson is on-shell) with the D^{*0} width. In Ref. [1052], the author corrected the calculation with the operator product expansion by regulating the IR divergence with the binding energy of the $X(3872)$. From the updated results, the $X \to \chi_{c1}\pi\pi$ process does not receive the large enhancement.

We move on to the $X \to J/\psi h$ decays (h denotes the light hadrons or photon). An interesting issue is the isospin violating decay of the $X(3872)$ as reviewed in Sec. 1.3.1. The isospin conserving decay mode driven by $X \to J/\psi\omega$ is strongly suppressed kinetically as shown in Fig. 52. Only a small portion of the Breit-Winger distribution of the ω meson is in the kinetically allowed region. In contrast, about half of the Breit-Winger distribution of the ρ meson is allowed by kinetics. In addition to the kinetic restriction, there are also dynamical reasons for the large isospin violating decays of $X(3872)$.

The $X \to J/\psi h$ was investigated by Braaten *et al* with the factorization formula [965], where h stands for $\pi^+\pi^-\pi^0$, $\pi^+\pi^-$, $\pi^0\gamma$ or γ. It was assumed that these decay modes are driven by the $X \to J/\psi\rho$ and $X \to J/\psi\omega$ (see Fig. 53). The amplitudes $V \to h$ ($V \equiv \rho$ or ω) were determined by the effective Lagrangian approaches with the partial decay widths of the ρ and ω as inputs. The isospin violating decay ratio was determined as

$$\frac{\Gamma\left[X \to J/\psi\pi^+\pi^-\pi^0\right]}{\Gamma\left[X \to J/\psi\pi^+\pi^-\right]} = 0.087 \frac{\left|G_{X\psi\omega}\right|^2}{\left|G_{X\psi\rho}\right|^2}. \tag{401}$$

The part-II ($V \to h$) of Fig. 53 contributes a factor about 0.087, which incorporates the kinetic effect. In the part-I ($X \to J/\psi V$) of Fig. 53, the author adopted the factorization formula. The long-range part was obtained by the universality, which is equivalent to the single-channel ($D^0\bar{D}^{*0}/D^{*0}\bar{D}^0$) πEFT, while the short-range part was fixed by a model proposed by Swanson [1090, 1091]. The partial width of $X \to J/\psi\pi^+\pi^-\pi^0$ was predicted as a function of the binding energy and total width of the $X(3872)$.

In Ref. [1050], Meng *et al* also investigated the isospin violating decays, in which the ratio is divided into two parts.

$$R \equiv \frac{\mathcal{B}^{I=0}(X \to J/\psi\pi^+\pi^-\pi^0)}{\mathcal{B}^{I=1}(X \to J/\psi\pi^+\pi^-)} = R_1 \times R_2, \tag{402}$$

where the R_2 includes the kinetic mechanism, and it was estimated in two approaches from Refs. [959, 965] (which give $R_2 = 0.147$ and 0.087, respectively). The R_1 was handled in the factorization formula. The long-range part is investigated in the coupled-channel EFT (see Sec. 5.1.2), in which the isospin violating effect in the wave function was considered. In the short-range part, the isospin symmetry is exact and the unknown matrix element cancels out in
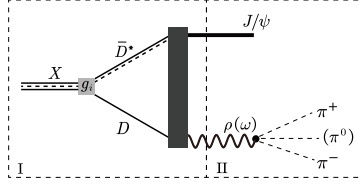
Figure 53: Isospin violating decays of $X(3872)$. The $X \to J/\psi\pi^+\pi^-(\pi^0)$ decays are divided into two pieces, the $X \to J/\psi V$ and $V \to \pi^+\pi^-(\pi^0)$ with $V \equiv \rho$ and ω.
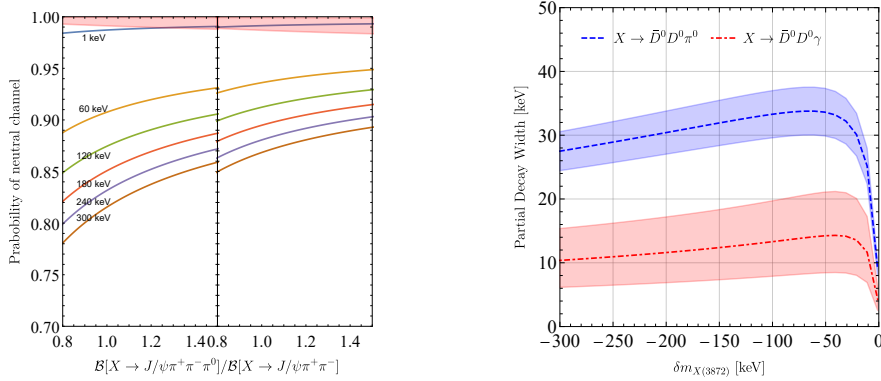

Figure 54: Numerical results in Ref. [1050]. Left panel: probability of the neutral channel in the wave function of the $X(3872)$. The binding energies are labeled near the related curves. Right panel: the partial widths of the $X(3872)$ with the mixing angle of neutral and charged channels extracted from the left subfigure.

the ratio while the isospin Clebsch-Gordon coefficients survive. The R_1 reads

$$R_1 = \left(\frac{g_1 F_1 - g_2 F_2}{g_1 F_1 + g_2 F_2}\right)^2 \approx \left(\frac{g_1 - g_2}{g_1 + g_2}\right)^2 = \left(\frac{c_1 \gamma_1^{1/2} - c_2 \gamma_2^{1/2}}{c_1 \gamma^{1/2} + c_2 \gamma^{1/2}}\right)^2, \tag{403}$$

where the F_i, g_i and γ_i are defined in Sec. 5.1.2. c_1 and c_2 are the coefficients of the neutral and charged channels in the wave function of the $X(3872)$, respectively. The proportion of the neutral channel was determined using the experimental R as shown in the left panel of Fig. 54. With both values of R_2, the proportion R is over 80%. With the proportion as input, the partial widths of the $X \to \bar{D}^0 D^0 \pi^0$ and $X \to \bar{D}^0 D^0 \gamma$ were calculated (see the right panel of Fig. 54). To derive Eq. (403), the difference of F_1 and F_2 is neglected, which is different from Ref. [958]. In Ref. [958], the authors presumed $g_1 = g_2$ and kept the difference of F_1 and F_2 to make R_1 non-vanishing. The isospin violation effect of the conventional hadrons can stem from the not fully offset loop integrals due to the displaced charged and neutral thresholds. However, such effects are usually tiny. For the case of the $X(3872)$, the isospin violation effects from the difference of F_1 and F_2 depend on the cutoff and are too small to explain the large isospin violation effect with a reasonable cutoff. Thus, the authors made a different assumption that g_1 and g_2 are different while F_1 and F_2 are the same as in Ref. [1050]. In fact, the relation $g_1 = g_2$ is by no means guaranteed. In Ref. [958], the validation of $g_1 = g_2$ is based on the constraint $v_{11} = v_{22} = v_{12}$ in Eq. (308), namely, the vanishing interaction in the isovector channel. However, the LECs v_{ij} are cutoff-dependent, which cannot be equal to each other with the varying cutoff [see Eq. (312)]. On the other hand, the couplings g_i are related to the mixing angle of the two channels, binding energy and mass difference of the two thresholds [see Eq. (316)], which are all physical observables. Therefore, it is reasonable to infer the more important effect resulting from different coupling constants. One can find comparisons of these two works in details in Ref. [1050].

Mehen *et al* calculated the radiative decays of $X(3872) \to \psi(2S)\gamma$ and $\psi(4040) \to X(3872)\gamma$ with the factorization formula by matching the short-range dynamics in HHχPT to the operators of XEFT [1051]. In these two decays, the photon energy is about 181 MeV and 165 MeV. In the long-range dynamics, the $X(3872)$ is regarded as a bound state
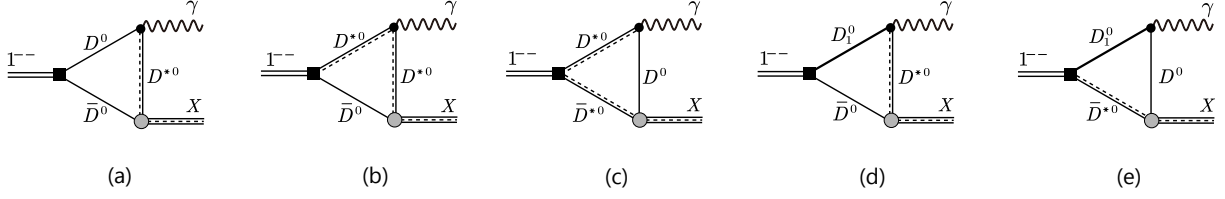
Figure 55: Feynman diagrams for the production of the $X(3872)$ in the radiative transitions of the vector charmonium(-like) states, including $\psi(4040)$, $\psi(4160)$, $\psi(4415)$ and the $Y(4260)$ in Ref. [1059].

of the $D^0\bar{D}^{*0}/D^{*0}\bar{D}^0$. In the $X \to J/\psi\gamma$ decay, the energy of the photon is about 700 MeV, which lies beyond the working range of HHχPT. Thus, in this framework, one cannot obtain the branching fraction

$$R = \Gamma[X \to \psi(2S)\gamma]/\Gamma[X \to J/\psi\gamma], \tag{404}$$

which has been measured in experiments [1092, 1093, 1094]. However, it was shown that the polarization of $\psi(2S)$ in $X \to \psi(2S)\gamma$ and the angular distribution of X in $\psi(4040)$ decays can be used to determine the quantum number of $X(3872)$. Similar framework was also used to study the $\psi(4160) \to X(3872)\gamma$ [1095], where the correlation between the polarization of $\psi(4160)$ and angular distribution of the final states can be utilized to explore the structure of the $X(3872)$.

Guo et al investigated the production of the $X(3872)$ in the radiative transitions of the vector charmonium(-like) states—including the $\psi(4040)$, $\psi(4160)$, $\psi(4415)$ and $Y(4260)$ [1059] within NREFT according to the powers of the velocities in Eq. (393). The Feynman diagrams are presented in Fig. 55. With the naturalness assumption of the vertices, the production of the $Y(4260) \to X(3872)\gamma$ is enhanced as compared to those of the other channels if the $Y(4260)$ is treated as the $D\bar{D}_1$ molecule. A similar approach was adopted to explore the production of the X_b—the HQFS partner of the $X(3872)$ from the decays of $\Upsilon(5S,6S) \to X_b\gamma$ [1096]. In Ref. [1060], the same NREFT was used to explore the radiative decays of the $X(3872)$, i.e., $X \to J/\psi\gamma$ and $X \to \psi(2S)\gamma$. With the naturalness assumption for the coupling constants, their results indicate that the experimental ratio in Eq. (404) does not conflict with the molecule-dominant structure of the $X(3872)$.

In Refs. [1044, 1045, 1046, 569, 1047, 1048, 1049], the productions of the $X(3872)$ and the related line shapes were investigated with the factorization formula, e.g., see Fig. 44. In fact, a heated topic about the $X(3872)$ is its substantial prompt production [209, 210, 211, 212, 213, 214], which was often used as an evidence against the molecular interpretation of the $X(3872)$ [208]. In the hadron collider, the $X(3872)$ can be produced from either bottom hadron decays or QCD mechanism. If X is produced by the QCD mechanism, its production vertices will be very close to the collision point, which is refereed as the prompt production. On the contrast, the production vertex from bottom hadron will be displace from the collision point (non-prompt production). Intuitively, the prompt production is the high energy process, in which only the almost relatively static two hadrons can form into loosely bound states. Thus, one would expect the suppressed prompt production for hadronic molecules. In general, the inclusive production of the $X(3872)$ can be formulated as follows (convention-II in Table A.11),

$$
\begin{aligned}
d\sigma[X(3872)] &= \frac{1}{\text{flux}} \sum_y \int d\Phi_{(D^*\bar{D})+y} \left| \int \frac{d^3k}{(2\pi)^3} \psi_X(\boldsymbol{k}) \frac{\mathcal{A}_{D^{*0}\bar{D}^0+y}(\boldsymbol{k}) + \mathcal{A}_{D^0\bar{D}^{*0}+y}(\boldsymbol{k})}{\sqrt{2}} \right|^2 \frac{1}{2\mu_{D^*D}} \\
&= \frac{1}{\text{flux}} \sum_y \int d\Phi_{(D^*\bar{D})+y} \left| \int \frac{d^3k}{(2\pi)^3} \psi_X(\boldsymbol{k}) \mathcal{A}_{D^{*0}\bar{D}^0+y}(\boldsymbol{k}) \right|^2 \frac{1}{2\mu_{D^*D}}
\end{aligned}
\tag{405}
$$

where y represents all the possible final states and $\Phi_{(D^*\bar{D})+y}$ is the phase space for the composite $(D^*\bar{D})$ and y. The validity of the second equality arises from the cancelling-out interference effect. In Ref. [208], the authors adopted the Schwarz inequality to obtain that

$$d\sigma[X(3872)] \leq \frac{1}{\text{flux}} \sum_y \int d\Phi_{(D^*\bar{D})+y} \int_{|\boldsymbol{k}|<k_{max}} \frac{d^3k}{(2\pi)^3} |\psi_X(\boldsymbol{k})|^2 \times \int_{|\boldsymbol{k}|<k_{max}} \frac{d^3k}{(2\pi)^3} \left| \mathcal{A}_{D^{*0}\bar{D}^0+y}(\boldsymbol{k}) \right|^2 \frac{1}{2\mu_{D^*D}} . \tag{406}$$
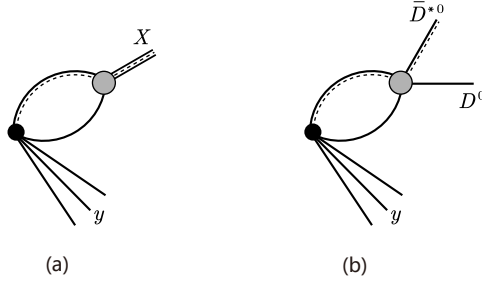
Figure 56: The Feynman diagrams for the inclusive productions of the $X(3872)$ and $D^0\bar{D}^{*0}/D^{*0}\bar{D}^0$.

One finally obtains the following inequality due to the normalized wave function $\psi_X(\boldsymbol{k})$,

$$\sigma[X(3872)] < \sigma[D^{*0}\bar{D}^0(|\boldsymbol{k}| < k_{max})]. \tag{407}$$

With the Monte Carlo event generators like Herwig and Pythia, the authors obtained $\sigma[D^{*0}\bar{D}^0(|\boldsymbol{k}| < k_{max})]$ truncated at k_{max} and then estimated the maximum production cross section of the $X(3872)$. The theoretical result is about two orders smaller than the experimental ones. Therefore, the authors concluded that the results refute the molecular nature of the $X(3872)$. However, one subtle issue in the above calculation is the choice of k_{max}. In Ref. [208], the authors argued that the momentum scale should be set by the binding momentum of the $X(3872)$ and took $k_{max} = 35$ MeV. However, the setting is challenged by Albaladejo *et al* [216], Artoisenet *et al* [215] and Braaten *et al* [217].

In Ref. [216], the authors argued that for the deuteron the $k_{max} \sim 300$ MeV $\sim 2m_\pi$ could be a good approximation of the effect of its wave function and the same k_{max} was expected for $X(3872)$. Meanwhile, the authors calculated the inclusive production of the $X(3872)$ by simulating the short-range dynamics with Monte Carlo event generators and combining the long-range interaction in an EFT with a Gaussian regulator cutoff Λ. The Λ can roughly amount to $2\sqrt{2/\pi}k_{max}$ in the sharp regulator. With a cutoff corresponding to $k_{max} \in [300, 600]$ MeV, the cross section is consistent with the experimental results. In Ref. [1097], the authors defended their own conclusions in Ref. [208] and argued that the k_{max} should be determined independently without surmising the explicit form of the wave function.

In Ref. [215], the authors challenged Ref. [208] and pointed out that the upper bound should be at the scale of m_π due to the rescattering effect of $D^*\bar{D}$, which leads to the consistent result with the experimental measurement. In Ref. [217], the authors established the relation of the production of the $X(3872)$ and $D\bar{D}^*$ as shown in Fig. 56 with the factorization formula. We show the derivation in Ref. [217] with the notation in Sec. 5.1.1. For the long-range dynamics, one has

$$
\begin{aligned}
\mathcal{M}(X) &\sim \int d^3q \, \psi_X(q) \sim \int d^3q \frac{g}{E_X - \frac{q^2}{2\mu} + i\epsilon}, \\
\mathcal{M}\left[\{D^0\bar{D}^{*0}(E)\}_+\right] &\sim \int d^3q \frac{1}{E - \frac{q^2}{2\mu} + i\epsilon} T(E),
\end{aligned}
\tag{408}
$$

where $g \sim \sqrt{\gamma_X}$ and $T \sim (i\sqrt{2\mu E} + \gamma_X)^{-1}$ are given in Eqs. (290) and (289), respectively. The integrals are linear divergent as shown in Eq. (286), thus one can eliminate the cutoff Λ by calculating the ratio of $\mathcal{M}(X)$ and $\mathcal{M}[\{D\bar{D}^{0*}(E)\}_+]$. One can set up the following relation,

$$\mathcal{M}\left[\{D^0\bar{D}^{*0}(E)\}_+\right] \sim \frac{\mathcal{M}(X)}{g} T(E) \sim \frac{\mathcal{M}(X)/\sqrt{\gamma_X}}{i\sqrt{2\mu E} + \gamma_X}. \tag{409}$$

The explicit result for the cross section was given in Ref. [217], which reads

$$d\sigma\left[D^0\bar{D}^{*0}\right] = d\sigma[X(3872)] \frac{\pi/\gamma_X}{\gamma_X^2 + k^2} \frac{d^3k}{(2\pi)^3}. \tag{410}$$
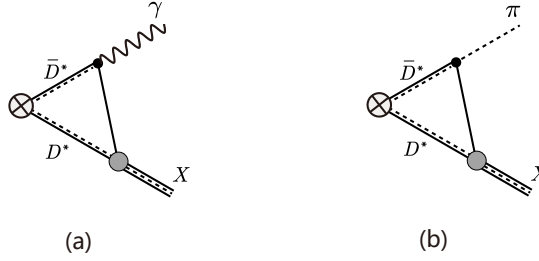
Figure 57: Two production processes for the $X(3872)$ with the triangle singularities.

In the derivation of Eq. (410), an implicit constraint is the cutoff Λ to regulate the linear divergence, which is at the scale of m_π. From Eq. (410), the authors obtained that $\sigma[X(3872)] = \sigma[D^0\bar{D}^{*0}(k < 7.73\gamma_X)]$. Thus, the upper bound is $k_{max} = 7.73\gamma_X$, in which the theoretical cross section for the prompt production of X is consistent with the experimental measurements.

Guo pointed out that the short-distance creation of the S-wave $D^0\bar{D}^{*0}$ pair [the Feynman diagram in Fig. 57(a)] can produce a narrow peak in the $X(3872)\gamma$ invariant mass spectrum due to the triangle singularity [1064]. Another similar narrow peak in the $X(3872)\pi$ from triangle singularity was pointed out by Braaten *et al* [1066, 1067] due to the short-range creation of the $D^*\bar{D}^*$ pair as shown in Fig. 57(b). Recently, the similar triangle singularity was investigated for the production of the T_{cc}^+ [286]. We refer to the review [1063] for details of triangle singularity. In order to investigate the triangle singularity, one has to adopt the non-factorization formula [1064, 1065, 1066, 1067, 1068]. In Refs. [1066, 1067], the productions of the $X(3872)$ accompanied by a soft pion at hadron colliders and in B meson decays were investigated, where the rescattering of $D^*\bar{D}^* \rightarrow X\pi$ is embedded in XEFT (which is similar to Ref. [1084]). The production of the T_{cc}^+ in heavy-ion collisions and in hadron colliders were investigated in Refs. [288, 1098], respectively.

5.6. Charged charmoniumlike and bottomoniumlike states without and with the strangeness

In this section, we review the applications of πEFT, χEFT and other related calculations in heavy hadron systems. The $Z_c(3900)$, $Z_c(4020)$, $Z_{cs}(3985)$, $Z_b(10610)$, $Z_b(10650)$ and so on are very good candidates of hadronic molecules due to their proximity to the corresponding thresholds. There are extensive studies and intensive debates on the inner configurations of these states, see Sec. 1.3.2 and some reviews [6, 11, 13, 8, 9, 14, 10, 12, 309, 200]. In the following we review the progress on how the EFTs help us understand the nature of these states (see an analogical analysis of nuclear forces and their counterparts in heavy hadron systems [1099]).

5.6.1. Z_c, Z_b and partners

In the BW fits which ignored the nearby thresholds, the $Z_c(3900)$, $Z_c(4020)$, $Z_b(10610)$ and $Z_b(10650)$ (in what follows we will denote them as Z_c, Z_c', Z_b, and Z_b', respectively) lie few MeV above the $D\bar{D}^*$, $D^*\bar{D}^*$, $B\bar{B}^*$ and $B^*\bar{B}^*$ thresholds, respectively. In addition to the similarities of their decay patterns, the mass differences of (Z_c, Z_c') and (Z_b, Z_b') almost equal to those of (D, D^*) and (B, B^*), respectively. Thus, they are suggested to be the molecular twin partners in HQSS and HQFS. It will be very instructive to classify these states into one group and study their behaviors in a uniform framework.

With the EFT formalism, there are two directions toward understanding the nature of these states. The first one is to calculate the mass spectrum with πEFT, in which the LO LECs are related with HQS and they are fixed with the help of the assumption that $X(3872)$ and Z_b are the $D\bar{D}^*$ and $B\bar{B}^*$ bound state respectively [1100]. The second one resorts to fitting the invariant mass spectrum from which the particle is observed [964, 1101, 1102, 915, 1103, 1104, 973, 988]. In this case, the $D^*\bar{D}^{(*)}/B^*\bar{B}^{(*)}$ rescatterings are treated perturbatively or nonperturbatively. For the former case, one deems that the $Z_Q^{(\prime)}$ ($Q \equiv c, b$) states are generated from the kinematic effect [1105, 1106, 1107, 1108]. But this is criticized in Ref. [1109], in which Guo *et al* built a solvable model to fit the elastic ($D\bar{D}^*$) and inelastic ($J/\psi\pi$) invariant mass distributions of the Z_c. In order to fit the experimental line shapes, the interaction strength of $D\bar{D}^*$ needs to be adjusted to large values, which in turn negates the perturbative assumptions. Therefore, the pronounced

near-threshold narrow peaks in experiments cannot be ascribed to the pure kinematic effect. The strong interacting $D\bar{D}^*$ should be resummed in an infinite series of loops, which generates pole(s) in the S-matrix.

There are several lattice QCD studies on the Z_c states. The corresponding results disfavored the Z_c state as a conventional resonance. The first kind is based on the finite volume energy levels. For example, Ref. [1110] considered the $D\bar{D}^*$ and $J/\psi\pi$ channels with $m_\pi = 266$ MeV, but did not find the signal of the Z_c except the non-interacting two meson energy levels (see also [1111, 1112] for similar results). Ref. [1113] simulated the single-channel—$(D\bar{D}^*)^\pm$ scattering with $m_\pi = 485, 420, 300$ MeV, where the authors found the $D\bar{D}^*$ interaction with three different m_π is weakly repulsive. In Refs. [526] and [1114], the coupled-channel Lüscher formula together with the Ross-Shaw theory is used to study the near-threshold scattering of the $D\bar{D}^*$. The results indicated that neither the threshold effect interpretation nor the resonance interpretation is favored. HAL QCD Collaboration considered the three channel couplings among $J/\psi\pi$, $D\bar{D}^*$, and $\eta_c\rho$ with $m_\pi = 410 - 700$ MeV [1115, 1116]. Their simulations revealed that the coupled-channel potentials are dominated by the off-diagonal terms, i.e., the couplings of $J/\psi\pi$-$D\bar{D}^*$ as well as $\eta_c\rho$-$D\bar{D}^*$, which makes the Z_c look more like a cusp effect but not a conventional resonance state.

Unlike the lattice QCD results, the combinations of EFT and experimental data do support the $Z_Q^{(\prime)}$ to be the virtual states or resonances generated from the nonrelativistic $D^*\bar{D}^{(*)}/B^*\bar{B}^{(*)}$ interactions. From Eq. (363), one obtains that

$$V_{1^{+-}}^\alpha(B\bar{B}^*) = V_{1^{+-}}^\alpha(B^*\bar{B}^*) \overset{\text{HQFS}}{=} V_{1^{+-}}^\alpha(D\bar{D}^*) = V_{1^{+-}}^\alpha(D^*\bar{D}^*), \qquad (411)$$

where the HQSS and HQFS are employed to relate the potentials of $[D^*\bar{D}^{(*)}, B^*\bar{B}^{(*)}]_{1^{+-}}$. For the single channel case, there is only one LEC if we define $C_{\alpha z} = (C_0^\alpha + C_1^\alpha)/2$. Assuming the Z_b as a $[B\bar{B}^*]_{1^{+-}}$ bound state, Ref. [1100] obtained the virtual state solution for the $Z_c^{(\prime)}$. However, one should be cautious about the HQFS relation in Eq. (411). For example, in Ref. [977], a general dimensional analysis shows that the LO contact LECs are scaled as $1/M$, where M is proportional to the heavy meson mass. In Ref. [1117], it is argued that the renormalizibility requires that the LO LECs introduced in Sec. 5.4 decreases at least as $1/M$ in the limit $M \to \infty$. Thus, it is even claimed that there cannot be a common EFT for different heavy quark masses. A coercive using of the HQFS to relate the double-charm and -bottom sectors may lead to predictions with uncontrolled uncertainties.

Albaladejo *et al* analyzed the pole distributions of the Z_c via fitting the $D\bar{D}^*$ and $J/\psi\pi$ invariant mass spectra [964], in which they modeled a coupled-channel—$J/\psi\pi$ and $D\bar{D}^*$ effective potential in the framework of $\not{\pi}$EFT,

$$V_{ij} = \begin{bmatrix} 0 & \tilde{C} \\ \tilde{C} & C + C'\boldsymbol{p}^2 \end{bmatrix}, \qquad (412)$$

where the interaction of $J/\psi\pi$ is set to be zero due to their weak coupling [1118, 1119]. The $D\bar{D}^*$-$J/\psi\pi$ coupling is momentum independent assuming it is dominated by the S-wave interaction, while the $D\bar{D}^*$ interaction is kept to the NLO. In Ref. [964], different explanations for the Z_c are given when the $C'\boldsymbol{p}^2$ term is switched on and off. When $C' \neq 0$, the Z_c state is a resonance that lies above the $D\bar{D}^*$ threshold. If $C' = 0$, the Z_c becomes a virtual state that lies below the $D\bar{D}^*$ threshold (with a small width from the $J/\psi\pi$ decay). For the case of the virtual state, the line shape of the inelastic channel—$J/\psi\pi$ peaks exactly at the threshold of the $D\bar{D}^*$, which is a generic feature that has been discussed by Frazer *et al* [1120] (for more general discussions on the pole distributions and classifications in different Riemann sheets, we refer to [1120, 1121, 547]). Besides, this approach is also reformulated in a box [1122] to compare with the lattice QCD energy levels [1111].

An elaborated approach to parameterizing the line shapes of the near-threshold states was developed in Refs. [1102, 915] based on the coupled-channel LSEs. The $Z_b^{(\prime)}$ states were observed in the $\Upsilon(5S) \to B^*\bar{B}^{(*)}\pi$, $\Upsilon(nS)\pi\pi$, and $h_b(mP)\pi\pi$ decays in the $B^*\bar{B}^{(*)}$, $\Upsilon(nS)\pi$ and $h_b(mP)\pi$ invariant mass spectra. For the $Z_b^{(\prime)}$ states, the relevant elastic and inelastic channels are $B\bar{B}^*$, $B^*\bar{B}^*$, and $\Upsilon(nS)\pi$ ($n = 1, 2, 3$), $h_b(mP)\pi$ ($m = 1, 2$), respectively. The coupled-channel effective potential (the bare pole is not considered here, see discussions in [973]) is given with the $(N_e + N_i) \times (N_e + N_i)$ matrix (with $N_e = 2$ and $N_i = 5$ the numbers of the elastic and inelastic channels, respectively),

$$V = \begin{bmatrix} \mathcal{V}_{\alpha\beta}(p, p') & \mathcal{V}_{\alpha i}(p, k_i) \\ \mathcal{V}_{j\beta}(k_j', p') & \mathcal{V}_{ji}(k_j', k_i) \end{bmatrix}, \qquad (413)$$

where the α, β denote the elastic channels and i, j denote the inelastic channels, respectively. In order to simplify the calculation, the authors made some assumptions and approximations such as the $\mathcal{V}_{ji} \approx 0$ because the coupling of

the heavy quarkonium and pion is rather weak [1118, 1119]. With this approximation, the inelastic channels can be disentangled from the elastic ones. The inelastic channel contributions are reduced to the additive terms in the contact potentials of $\mathcal{V}_{\alpha\beta}$ [1102, 915, 973], which is equivalent to using the description of the optical (complex) potential[16], i.e.,

$$\mathcal{V}_{\alpha\beta}^{\text{ct}}(E, p, p') = v_{\alpha\beta} - \frac{i}{2\pi E} \sum_i m_{H_i} m_{h_i} g_{i\alpha} g_{i\beta} k_i^{2l_i+1}, \tag{414}$$

with $v_{\alpha\beta}$ the contact potential of the elastic-to-elastic scattering. The m_{H_i} (m_{h_i}), k_i and l_i are the mass of the heavy (light) meson, the momentum and the angular momentum in the ith inelastic channel, respectively. The E represents the invariant mass of the system. The second term in Eq. (414) comes from the transition vertex of the elastic-to-inelastic

$$\mathcal{V}_{i\alpha}(k_i, p) = \mathcal{V}_{\alpha i}(p, k_i) = g_{i\alpha} k_i^{l_i}, \tag{415}$$

and the inelastic loop. For more details, see Refs. [1102, 915]. If one assumes that the direct production vertex is saturated by the $B^* \bar{B}^{(*)} \pi$ channels, the production amplitudes for the elastic and inelastic channels read, respectively,

$$\mathcal{U}_\alpha(E, \mathbf{p}) = \mathcal{M}_\alpha(E, \mathbf{p}) + \sum_\beta \int \frac{d^3\mathbf{q}}{(2\pi)^3} \mathcal{V}_{\alpha\beta}(E, \mathbf{p}, \mathbf{q}) \mathcal{G}_\beta(E, \mathbf{q}) \mathcal{U}_\beta(E, \mathbf{q}), \tag{416}$$

$$\mathcal{U}_i(E, \mathbf{k}) = \sum_\beta \int \frac{d^3\mathbf{q}}{(2\pi)^3} \mathcal{V}_{i\beta}(\mathbf{k}) \mathcal{G}_\beta(E, \mathbf{q}) \mathcal{U}_\beta(E, \mathbf{q}), \tag{417}$$

where

$$\mathcal{G}_\beta = \frac{2\mu_\beta}{\mathbf{p}_\beta^2 - \mathbf{q}^2 + i\epsilon}, \qquad \mathbf{p}_\beta^2 \equiv 2\mu_\beta(E - m_{\text{th}}^\beta), \tag{418}$$

with μ_β and m_{th}^β the reduced mass and threshold of the βth elastic channel, respectively. The Eqs. (416) and (417) were also illustrated via a diagrammatic representation in Fig. 58.

(a)   (b)   (c)
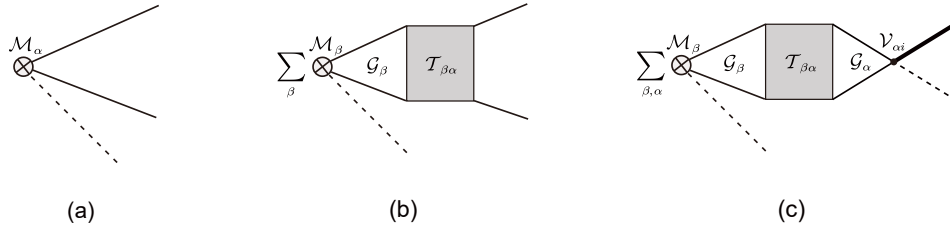
Figure 58: A diagrammatic representation of Eqs. (416) and (417), where the (thin) solid and dashed lines denote the vector (pseudoscalar) B mesons and pion, respectively, while the thick solid line denotes the bottomonium. The circled cross represents the production source. The shaded box stands for the rescattering T-matrix of the elastic channels.

With this approach, Refs. [1102, 915, 973] fitted the invariant mass spectrum of the $B^* \bar{B}^{(*)}$ and $h_b(mP)\pi$, as well as those of the $\Upsilon(nS)\pi$ in Ref. [1125] with the inclusion of the $\pi\pi$ final state interaction via the dispersion relation. In Refs. [1102, 915], the $B^* \bar{B}^{(*)}$ interactions are built upon the pionless framework, the LO contact potentials are constrained by the HQS (see Sec. 5.4). A good overall description of the data is consistent with the Z_b as a virtual state and Z_b' as a resonance. Their poles both reside very close to the $B\bar{B}^*$ and $B^*\bar{B}^*$ thresholds, respectively [915].

---

[16]The optical potential has both the real and imaginary parts, which is usually introduced to describe a process where the explicitly considered flux is not conserved. This is general in hadronic physics, such as the $p\bar{p}$ annihilation at low energies [1123], where the opened channels—multi light hadrons cannot be explicitly described by the theory, e.g., the χEFT [1124].

An improved fitting with the Weinberg scheme is given by Ref. [973] with the potential $\mathcal{V}_{\alpha\beta}$ of the contact terms (LO plus NLO), OPE and one-eta exchange (OEE),

$$\mathcal{V}_{\alpha\beta} = V_{\alpha\beta}^{\mathrm{ct}} + V_{\alpha\beta}^{\mathrm{OPE}} + V_{\alpha\beta}^{\mathrm{OEE}}, \tag{419}$$

where the three-body dynamics in OPE/OEE is considered via the TOPT formalism (see Sec. 5.3.1). Seven different fitting schemes are considered by including the OPE/OEE, $S-D$ mixing, HQSS violation and NLO contact potentials by order. They obtained that the line shapes are insensitive to the central part of the S-wave OPE potential since it can be absorbed by adjusting the LO LECs, while the effect of the tensor force from OPE (though it is partially balanced by the $S-D$ transition terms of the NLO contact terms) leads to visible modifications of the line shapes [where the regulator (348) is used and the (hard) cutoff is around 1.0 GeV]. The effect of the OEE interaction is rather weak, and the higher order terms for the contact potentials of the inelastic channels seem not necessary. The Fig. 59 shows the real and imaginary parts of the Z_b and Z_b' poles, where the fitting schemes A (only with the LO $V_{\alpha\beta}^{\mathrm{ct}}$) and G [with the full form of Eq. (419) as well as the $S-D$ mixing] indicate that the Z_b and Z_b' are virtual and resonant states residing below the $B\bar{B}^*$ and above the $B^*\bar{B}^*$ thresholds, respectively.
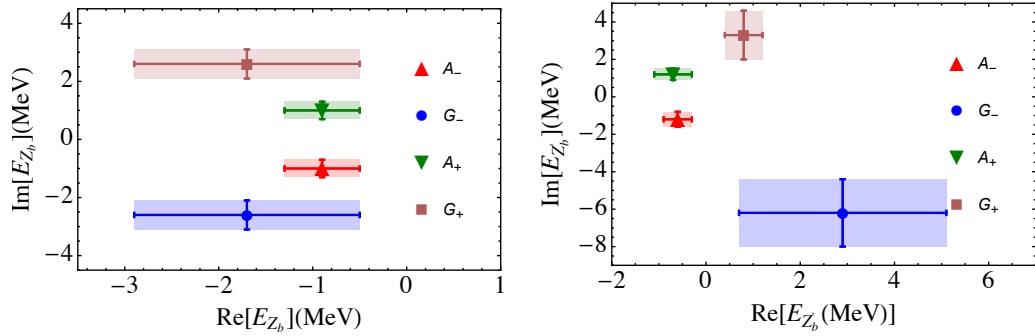
Figure 59: The real and imaginary parts of the poles of the Z_b (left panel) and Z_b' (right panel) states obtained in fit Scheme A and G, respectively [973], where the x-axes are defined as $E_{Z_b} = M_{Z_b}^{\mathrm{pole}} - m_B - m_{B^*}$, $E_{Z_b'} = M_{Z_b'}^{\mathrm{pole}} - 2m_{B^*}$.

An extensive study of the $Z_c^{(\prime)}$ and $Z_b^{(\prime)}$ states was provided by Ref. [988] in χEFT, in which the effective potentials of the $D^*\bar{D}^{(*)}$ and $B^*\bar{B}^{(*)}$ were calculated up to NLO (e.g., see Sec. 5.3.2). Unlike the Refs. [1102, 915, 973], this work is performed in the single-channel framework (ignoring the coupled-channel effect induced by the $S-D$ mixing), and the inelastic channels are not considered. The coupled-channel effect (e.g., $D\bar{D}^* \to D^*\bar{D}^*$ and $B\bar{B}^* \to B^*\bar{B}^*$) is (partially) included in the TPE diagrams. The corresponding invariant mass distributions of the elastic channels were fitted, see Fig. 60, and the extracted poles of the $Z_c^{(\prime)}$ and $Z_b^{(\prime)}$ all reside in the unphysical Riemann sheet and lie above the $D^*\bar{D}^{(*)}$ and $B^*\bar{B}^{(*)}$ thresholds, respectively. Therefore, they are explained as the $D^*\bar{D}^{(*)}$ and $B^*\bar{B}^{(*)}$ resonances, respectively. One virtue of Ref. [988] is that the soft cutoff Λ (≤ 0.5 GeV) is natural and consistent with the validity of χEFT (see discussions in Sec. 5.3.4). In Ref. [973], the typical momentum scale for the coupled-channel is $p^{\mathrm{ty}} = \sqrt{2\mu_{B^*\bar{B}^{(*)}}\delta_b} \approx 0.5$ GeV. In order to effectively involve the coupled-channels, the relatively hard cutoff (~ 1.0 GeV) was used.

In the HQSS limit, there are six $B^{(*)}\bar{B}^{(*)}$ systems in the isovector channel including the Z_b and Z_b', which were proposed by Bondar *et al* [1012]. The other four isovector states with negative G parities are named as $W_{bJ}^{(\prime)}$ [1013]

$$|B\bar{B}\rangle_{1^-(0^{++})} \quad : \quad W_{b0} \to \eta_b\pi, \chi_b\pi, \Upsilon\rho, \tag{420}$$

$$|B^*\bar{B}^*\rangle_{1^-(0^{++})} \quad : \quad W_{b0}' \to \eta_b\pi, \chi_b\pi, \Upsilon\rho, \tag{421}$$

$$|B\bar{B}^*\rangle_{1^-(1^{++})} \quad : \quad W_{b1} \to \chi_b\pi, \Upsilon\rho, \tag{422}$$

$$|B^*\bar{B}^*\rangle_{1^-(2^{++})} \quad : \quad W_{b2} \to \chi_b\pi, \Upsilon\rho, \tag{423}$$

where their possible decay modes are also presented. Because they have the negative G-parity, these states can be detected in the radiative decays of the $\Upsilon(5S)/\Upsilon(6S)$ rather than the of pionic transitions (for a review, see [1126]).

116

With pionfully nonperturbative treatment of the $B^*\bar{B}^{(*)}$ interactions and using the parameters of the $Z_b^{(\prime)}$ as inputs, the $W_{bJ}^{(\prime)}$ states are predicted as the virtual states or resonances that reside near their corresponding thresholds [1127, 1128].
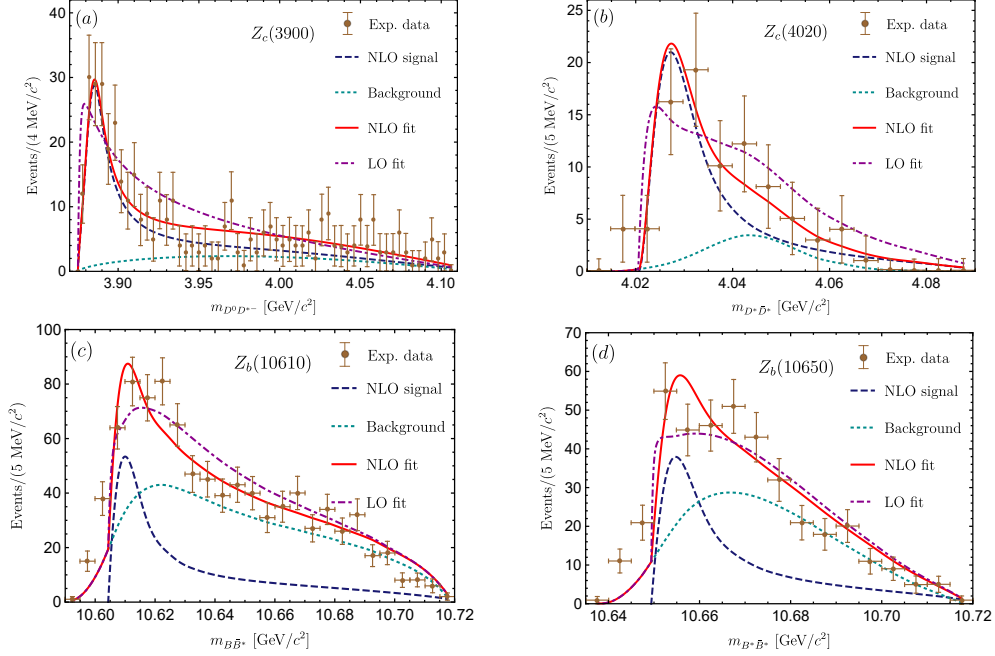

Figure 60: The fitted invariant mass spectra of the $D^*\bar{D}^{(*)}$ and $B^*\bar{B}^{(*)}$ distributions in $e^+e^- \to \pi V(V)P$ (where V and P denote the vector and pseudoscalar D (B) mesons, respectively) transitions from Ref. [988]. The data with error bars in figures (a), (b) and (c)/(d) are taken from Refs. [295], [297] and [301] at $\sqrt{s}$ = 4.26, 4.23, and 10.86 GeV, respectively. The figures are taken from Ref. [988].

5.6.2. Z_{cs} and partners

The above frameworks were also transplanted to study the recently observed $Z_{cs}(3985)$ by the BESIII Collaboration [310] as well as the $Z_{cs}(4000)$ and $Z_{cs}(4220)$ by the LHCb Collaboration [345].

In Ref. [311], the $Z_{cs}(3985)$ was treated as the U/V-spin partners of Z_c state in flavor SU(3) symmetry. The notion of the isospin was extended to the U and V-spins in exact SU(3) symmetry. The corresponding G_U and G_V parities were defined (see Sec. 2.1.2). The $Z_{cs}(3985)$ can be connected to the Z_c via

$$Z_c^-(c\bar{c}d\bar{u}) \overset{\hat{U}}{\longleftrightarrow} Z_{cs}^-(c\bar{c}s\bar{u}), \qquad Z_c^+(c\bar{c}u\bar{d}) \overset{\hat{V}}{\longleftrightarrow} \bar{Z}_{cs}^0(c\bar{c}s\bar{d}), \tag{424}$$

where $\hat{U}$ ($\hat{V}$) denotes the U (V)-spin rotation. One can consequently define the $G_{U/V}$ parity even and odd basis through the two particle basis $\bar{D}_s D^*$ and $\bar{D}_s^* D$ (convention-I in Table A.11) as

$$|G_U = \eta\rangle = \frac{1}{\sqrt{2}}\left(|D_s^- D^{*+}\rangle + \eta|D_s^{*-} D^+\rangle\right), \tag{425}$$

$$|G_V = \eta\rangle = \frac{1}{\sqrt{2}}\left(|D_s^- D^{*0}\rangle + \eta|D_s^{*-} D^0\rangle\right), \tag{426}$$

where $\eta = +1$ corresponds to the $\bar{Z}_{cs}^0$ and Z_{cs}^-, respectively. The potential (412) was expanded to the three-channel case, $(J/\psi\pi, D\bar{D}^*, \bar{D}^*D^*)$ for the Z_c and $(J/\psi K, \bar{D}_s D^*, \bar{D}_s^* D^*)$ for the $Z_{cs}(3985)$. The four LECs (see Ref. [311]) were fixed using the mass and width of the Z_c (Z_b) and Z_c' (Z_b') as inputs. In addition, the molecular resonances in the $\bar{D}_s^* D^*$, $B_s\bar{B}^*$ and $B_s^*\bar{B}^*$ channels were predicted.

The calculation for the $\bar{D}_s D^*$ system within χEFT was performed in Ref. [312], where the effective potential was given up to NLO including the OEE and two-kaon exchange (TKE) interactions. Based on the parameters by

117

fitting the line shapes of the $Z_c^{(\prime)}$ and $Z_b^{(\prime)}$ in Ref. [988], the line shape and resonance parameters of the $Z_{cs}(3985)$ were reproduced [312]. For example, a sharp peak automatically emerges in the $\bar{D}_s D^*$ invariant mass spectrum (see Fig. 61), and the extracted mass and width $(m, \Gamma) = (3982.4^{+4.8}_{-3.4}, 11.8^{+5.5}_{-5.2})$ MeV are very consistent with the experimental value. The possible resonances in the $\bar{D}_s^* D^*$, $B_s \bar{B}^*$ and $B_s^* \bar{B}^*$ systems were also predicted, which established a complete spectrum of the charged heavy quarkoniumlike states with the positive $G_{I/U/V}$ parities (see Fig. 61).

Other similar studies within the $\not\!\pi$EFT were presented in Refs. [313, 319, 339]. For example, with the framework of Ref. [964], Ref. [313] fitted the invariant mass spectrum of the $\bar{D}_s D^*$ with either the LO or NLO effective potential of the $\bar{D}_s D^*$ system in the energy range below 4.03 GeV, where the production is enhanced by the triangle singularity. As a consequence, the $Z_{cs}(3985)$ and its HQSS partner are virtual states or resonances depending on the potential. An extension to the whole energy region in experiments was performed through introducing the coupled-channel $\bar{D}_s^* D^*$ with the LO contact potential constrained by the HQSS [339]. Ref. [319] used the potential (363) with the parameters C_0^α, C_1^α fixed by fitting the data of the $Z_c^{(\prime)}$ and $Z_{cs}(3985)$. They predicted the possible existence of the $W_{cJ}^{(\prime)}$, $W_{csJ}^{(\prime)}$ either as the bound states or virtual states.
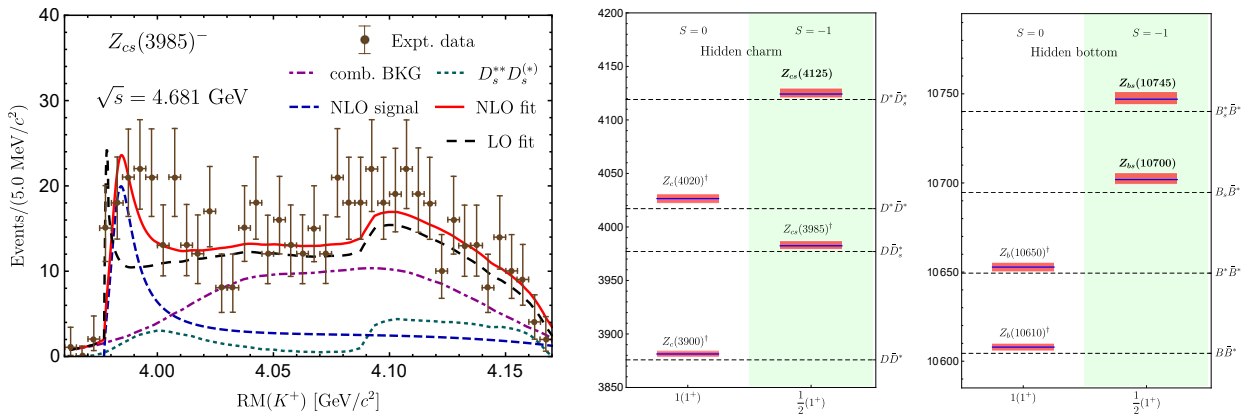
Figure 61: Left panel: the K^+ recoil-mass spectrum distributions obtained with the fitted parameters of the $Z_c(3900)$ [988] as inputs. The data with error bars are taken from [310] at $\sqrt{s} = 4.681$ GeV. Middle and right panels: the spectrum of the charmoniumlike and bottomoniumlike states with positive $G_{I/U/V}$ parities predicted in Ref. [312]. The blue solid line and red band denote the central value and range of errors of the mass. The observed and predicted states are marked with † and boldface, respectively. The figures are taken from Ref. [312].

About four months after the observation of $Z_{cs}(3985)$ [310], the LHCb discovered two states $Z_{cs}(4000)$ and $Z_{cs}(4220)$ in the invariant mass spectrum of $J/\psi K^+$ for the $B^+ \to J/\psi K^+ \phi$ decay with the significance of 15 σ and 5.9 σ, respectively [345]. The mass of the $Z_{cs}(4000)$ is also very close to the $\bar{D}_s D^*$ threshold but its width is around 130 MeV, which is about 10 times larger than that of the $Z_{cs}(3985)$ as shown in Fig. 62. The $Z_{cs}(4220)$ is also much broader than any theoretical predictions of the HQSS partners of $Z_{cs}(3985)$. Therefore, whether the $Z_{cs}(3985)$ and $Z_{cs}(4000)$ are the same states observed in different processes [330] or they are utterly two different states [346] deserves serious analyses.

From Eqs. (425) or (426) we know that there are two orthogonal basis with $\eta = +1$ and -1, respectively. In the above investigations [312, 311, 313, 319, 339], the $Z_{cs}(3985)$ was assigned as the $\eta = +1$ state. Meng *et al* derived some important implications by treating the $Z_{cs}(3985)$ and $Z_{cs}(4000)$ as two different states [346] corresponding to the states with $\eta = -1$ and $\eta = +1$, respectively. With this assumption, the SU(3) partners of the Z_c and Z_c' are assigned as the $Z_{cs}(4000)$ and $Z_{cs}(4220)$, respectively, see details in Fig. 63. In such a scenario, the SU(3) breaking effect in the $D^* \bar{D}^{(*)}$ and $\bar{D}_s^* D^{(*)}$ systems should be very significant since $\Gamma_{Z_{cs}(4000)} \gg \Gamma_{Z_c(3900)}$, $\Gamma_{Z_{cs}(4220)} \gg \Gamma_{Z_c(4020)}$, and $m_{Z_{cs}(4220)} - m_{Z_c(4020)} \approx 2[m_{Z_{cs}(4000)} - m_{Z_c(3900)}]$. With strict HQSS, the $G_{I/U/V}$ parity even and odd states are orthogonal, whereas the mixing occurs when the HQSS is broken to some extent. In Ref. [346] the HQSS breaking effect was investigated via introducing the following coupled-channel potential,

$$V_{1^+}(\boldsymbol{p}, \boldsymbol{p}')_{\{+,-\}} = \begin{bmatrix} \frac{c_a^+ + \delta c_a}{\Lambda} & \frac{\delta c_a}{\Lambda} \\ \frac{\delta c_a}{\Lambda} & \frac{c_a^- + \delta c_a}{\Lambda} \end{bmatrix} + \begin{bmatrix} \frac{c_b^+(p^2 + p'^2)}{\Lambda^3} & \\ & \frac{c_b^-(p^2 + p'^2)}{\Lambda^3} \end{bmatrix}, \tag{427}$$

where the c_a^+ (c_a^-) and c_b^+ (c_b^-) denote the LO and NLO LECs for the $\eta = +1$ (-1) channel, respectively. The δc_a designates the strength of the off-diagonal term. A conversion of the potential (427) into the $\{\bar{D}_s D^*, \bar{D}_s^* D\}$ basis defines a measure of the HQSS breaking scale, $R_{\mathrm{HQSSB}} = 4\delta c_a/|c_a^+ + c_a^-|$. Ref. [346] found that the pole trajectories of the $Z_{cs}(3985)$ and $Z_{cs}(4000)$ are not sensitive to R_{HQSSB} (the corresponding mixing angle θ changes from $-3°$ to $3°$) when the R_{HQSSB} is varied from -0.4 to 0.4, see Fig. 62.
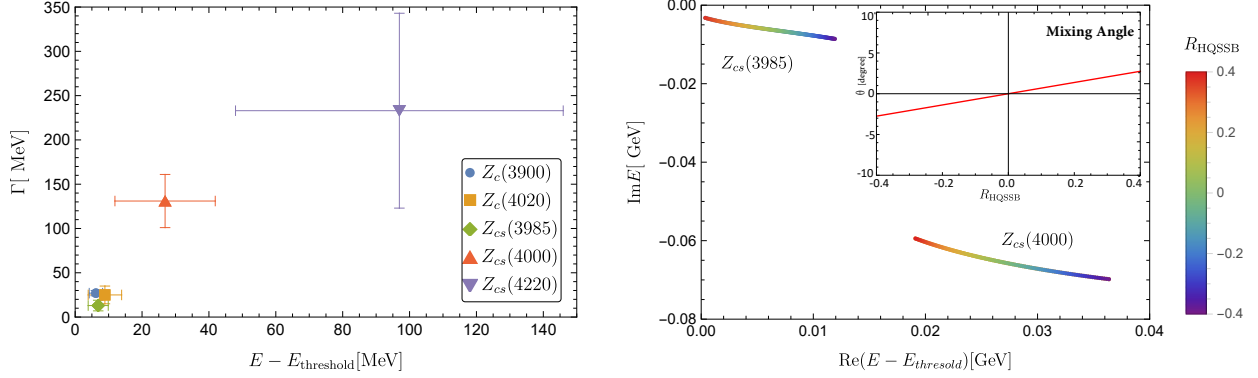
Figure 62: Left panel: the x-axis denotes the masses of the $Z_c(3900)$, $Z_c(4020)$, $Z_{cs}(3985)$, $Z_{cs}(4000)$ and $Z_{cs}(4220)$ with respect to the corresponding thresholds $\bar{D}D^*/\bar{D}^*D$, $D^*\bar{D}^*$, $\bar{D}_s D^*/\bar{D}_s^* D$, $\bar{D}^* D_s/\bar{D}D_s^*$ and $\bar{D}^* D_s^*$, respectively, while the y-axis represents their widths [295, 1129, 310, 345]. Right panel: the pole trajectories and the mixing angle range of $|\bar{D}_s D^*/\bar{D}_s^* D, +\rangle$ and $|\bar{D}_s D^*/\bar{D}_s^* D, -\rangle$ basis for the $Z_{cs}(3985)$ and $Z_{cs}(4000)$ states when varying R_{HQSSB} from -0.4 to 0.4. The figures are taken from Ref. [346].

If the $Z_{cs}(3985)$ and $Z_{cs}(4000)$ are different states [346]: (1) HQSS is a good symmetry for the $\bar{D}_s^{(*)} D^{(*)}$ systems. (2) The $Z_{cs}(4000)$ and $Z_{cs}(4220)$ are the HQSS partners. (3) The $Z_{cs}(3985)$ and $Z_{cs}(4000)$ are pure $G_{U/V}$ parity odd and even states, respectively. (4) There exists a tensor resonance $|\bar{D}_s^* D^*\rangle_{2^+}$ as the HQSS partner of the $Z_{cs}(3985)$. Its mass and width are predicted to be $(m, \Gamma) = (4126 \pm 3, 13 \pm 6)$ MeV. (5) For the $Z_{cs}(3985)$ and $Z_{cs}(4000)$, the branching ratio $\mathscr{R}(Z_{cs} \to \bar{D}_s^* D/Z_{cs} \to \bar{D}_s D^*) \approx 0.5$. (6) The decay mode $Z_{cs}(3985) \to J/\psi K$ is suppressed in the HQS limit [see Eq. (357)]. (7) The SU(3) breaking effect is significant for the systems without and with the strangeness. The implications (4) and (6) could serve as a criterion for experiments to test the scenario proposed in Ref. [346].
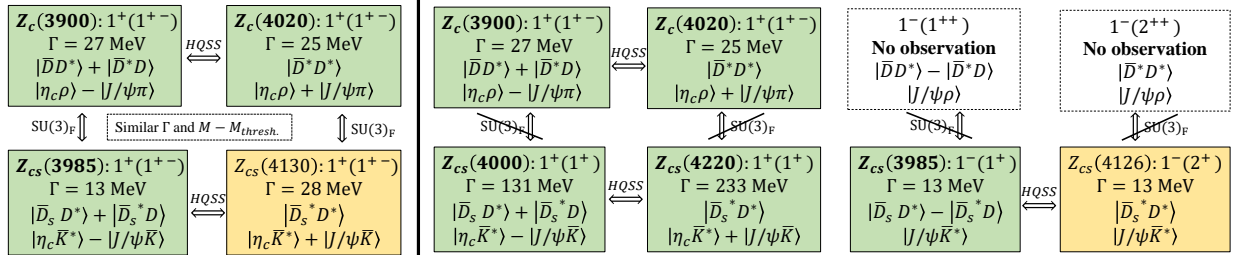
(a) $Z_{cs}(3985)$ as the SU(3)$_F$ partner of $Z_c(3900)$.

(b) Implications of $Z_{cs}(3985)$ and $Z_{cs}(4000)$ as two different states.

Figure 63: Two assignments for the $Z_{cs}(3985)$ and $Z_{cs}(4000)$ states in Ref. [346] and the corresponding consequences. Subfigure (a): The $Z_{cs}(3985)$ is treated as the SU(3) partner of the $Z_c(3900)$ with the positive $G_{I/U/V}$ parities. Subfigure (b): the SU(3) partner of the $Z_c(3900)$ is $Z_{cs}(4000)$ (with significant symmetry breaking), while the $Z_{cs}(3985)$ is assigned as a negative $G_{U/V}$ parity state. The projected flavor wave function in the open-charm and hidden-charm channels, as well as the corresponding $I^{G_I}/U^{G_U}/V^{G_V}(J^{PC})$ quantum numbers can be traced back to Sec. 5.4. The particles listed in green and yellow cards represent the observed and predicted states, respectively. The double head arrows denote the partner states in HQSS and SU(3) symmetries (the symmetries hold well in this case), while the ones slashed by the oblique lines represent the breaking of SU(3) symmetry. The two partner channels given in the white cards are required by the symmetry, but they are not considered in Ref. [346].

5.7. Hidden-charm molecular pentaquarks without and with the strangeness

5.7.1. P_c and partners

In 2019, the LHCb analyzed both the run-I and run-II data [3], and found the previously observed $P_c(4450)$ signal [2] actually contains two substructures—the $P_c(4440)$ and $P_c(4457)$. Meanwhile, another new structure $P_c(4312)$ was discovered, while the broad $P_c(4380)$ [2] lost its significance in the $J/\psi p$ invariant mass spectrum. One may still notice a bump around the 4.38 GeV. However, this bump is too narrow (see Ref. [385] for a quantitative fit) to be identified as the same state in the first analysis. Their isospin $I = 1/2$ can be easily inferred from the final state $J/\psi p$. The community instantly noticed that the $P_c(4312)$ and $P_c(4440)$, $P_c(4457)$ reside very close to (and below) the $\Sigma_c \bar{D}$ and $\Sigma_c \bar{D}^*$ thresholds, respectively. This triggered a flood of works toward the molecular explanations with various models, e.g., see Sec. 1.3.3.

In Ref. [352], the πEFT and HQSS was combined to parameterize the interactions of the $\Sigma_c \bar{D}$, $\Sigma_c \bar{D}^*$, $\Sigma_c^* \bar{D}$ and $\Sigma_c^* \bar{D}^*$ by two LECs, which are equivalent to the $C_{1/2}^\alpha$ and $C_{3/2}^\alpha$ of Eqs. (372) and (373) but within the uncoupled-channel framework. The two LECs are fixed using the binding energies of the $P_c(4440)$ and $P_c(4457)$ via treating them as the S-wave $\Sigma_c \bar{D}^*$ molecules with $J^P = \frac{1}{2}^-$ and $\frac{3}{2}^-$. The J^P quantum numbers of the $P_c(4440)$ and $P_c(4457)$ are not determined yet, so there are two options:

$$\text{canonical spin order:} \quad P_c(4440): J^P = \tfrac{1}{2}^-, \quad P_c(4457): J^P = \tfrac{3}{2}^-, \tag{428}$$

$$\text{non-canonical spin order:} \quad P_c(4440): J^P = \tfrac{3}{2}^-, \quad P_c(4457): J^P = \tfrac{1}{2}^-, \tag{429}$$

where the spin order in Eq. (428) is called *canonical* because the empirical pattern from the hadron spectra is that the higher spin states usually have larger masses [1]. It was shown that the canonical order is more preferable considering the induced binding energy of the $P_c(4312)$ is closer to the experimental data. Another four bound states in the $\Sigma_c^* \bar{D}$ and $\Sigma_c^* \bar{D}^*$ systems with $J^P = \frac{3}{2}^-$ and $\frac{1}{2}^-$, $\frac{3}{2}^-$, $\frac{5}{2}^-$ were predicted with binding energies around $3 - 27$ MeV. The fits in Ref. [356] show that the two arrangements in Eqs. (428) and (429) work equally well without pions. However, in a recent study based on the machine learning [1130], the authors claimed that the J^P quantum numbers of $P_c(4440)$ and $P_c(4457)$ can be discriminated even within the πEFT, and the canonical spin order is supported in the neural network-based approach.

The OPE interaction for the $\Sigma_c \bar{D}^*$ system was included in Refs. [363, 387] (see a more general discussion on the role of OPE for heavy hadron systems [1131]), in which the hard cutoff $\Lambda \gtrsim 1.0$ GeV was used to regularize the Schrödinger equation. The results showed that the J^P of the $P_c(4440)$ and $P_c(4457)$ turns into the non-canonical order of Eq. (429). A systematic study of the $\Sigma_c^{(*)} \bar{D}^{(*)}$ interactions within the χEFT was performed in Refs. [355, 364], where the contact interactions, the OPE and TPE were considered. The contact Lagrangian of the $\Sigma_c^{(*)} \bar{D}^{(*)}$ is given as

$$\begin{aligned}
\mathcal{L} &= \tilde{D}_a \langle \bar{\tilde{\mathcal{H}}} \tilde{\mathcal{H}} \rangle \text{Tr}(\bar{\psi}_Q^\mu \psi_{Q\mu}) + i\tilde{D}_b \epsilon_{\sigma\mu\nu\rho} v^\sigma \langle \bar{\tilde{\mathcal{H}}} \gamma^\rho \gamma_5 \tilde{\mathcal{H}} \rangle \text{Tr}(\bar{\psi}_Q^\mu \psi_Q^\nu) \\
&+ \tilde{E}_a \langle \bar{\tilde{\mathcal{H}}} \tau_i \tilde{\mathcal{H}} \rangle \text{Tr}(\bar{\psi}_Q^\mu \tau_i \psi_{Q\mu}) + i\tilde{E}_b \epsilon_{\sigma\mu\nu\rho} v^\sigma \langle \bar{\tilde{\mathcal{H}}} \gamma^\rho \gamma_5 \tau_i \tilde{\mathcal{H}} \rangle \text{Tr}(\bar{\psi}_Q^\mu \tau_i \psi_Q^\nu),
\end{aligned} \tag{430}$$

where the corresponding LECs are denoted as $\tilde{D}_a$, $\tilde{D}_b$, $\tilde{E}_a$ and $\tilde{E}_b$, respectively. The ψ_Q^μ represents the superfield of the singly heavy baryons in Sec. 2.6.3. Expanding Eq. (430) one obtains

$$\mathcal{V}_{\Sigma_c \bar{D}}^{\text{ct}} = -\tilde{D}_a - 2\tilde{E}_a (\boldsymbol{I}_1 \cdot \boldsymbol{I}_2), \tag{431}$$

$$\mathcal{V}_{\Sigma_c \bar{D}^*}^{\text{ct}} = -\tilde{D}_a - 2\tilde{E}_a (\boldsymbol{I}_1 \cdot \boldsymbol{I}_2) + \frac{2}{3} \Big[-\tilde{D}_b - 2\tilde{E}_b (\boldsymbol{I}_1 \cdot \boldsymbol{I}_2) \Big] \boldsymbol{\sigma} \cdot \boldsymbol{T}, \tag{432}$$

$$\mathcal{V}_{\Sigma_c^* \bar{D}}^{\text{ct}} = -\tilde{D}_a - 2\tilde{E}_a (\boldsymbol{I}_1 \cdot \boldsymbol{I}_2), \tag{433}$$

$$\mathcal{V}_{\Sigma_c^* \bar{D}^*}^{\text{ct}} = -\tilde{D}_a - 2\tilde{E}_a (\boldsymbol{I}_1 \cdot \boldsymbol{I}_2) + \Big[-\tilde{D}_b - 2\tilde{E}_b (\boldsymbol{I}_1 \cdot \boldsymbol{I}_2) \Big] \boldsymbol{\sigma}_{rs} \cdot \boldsymbol{T}, \tag{434}$$

where $\boldsymbol{I}_1$ ($\boldsymbol{I}_2$) denotes the isospin operator of the $\Sigma_c^{(*)}$ ($\bar{D}^{(*)}$). The spin operator of the Σ_c (Σ_c^*) is related to the $\boldsymbol{\sigma}$ ($\boldsymbol{\sigma}_{rs}$) via $\boldsymbol{S}_1 = \boldsymbol{\sigma}/2$ ($\boldsymbol{S}_1' = 3\boldsymbol{\sigma}_{rs}/2$), while the spin operator of the $\bar{D}^*$ is defined as $\boldsymbol{S}_2 = -\boldsymbol{T} = i\boldsymbol{\varepsilon}^\dagger \times \boldsymbol{\varepsilon}$, e.g., see the Appendix C of Ref. [364]. Meanwhile, the effective potentials from the OPE and NLO TPE interactions can be derived from Eqs. (124) and (139). The OPE only survives in the $\Sigma_c \bar{D}^*$ and $\Sigma_c^* \bar{D}^*$ systems, which read

$$\mathcal{V}_{\Sigma_c \bar{D}^*}^{\text{OPE}} = -(\boldsymbol{I}_1 \cdot \boldsymbol{I}_2) \frac{g g_1}{2 f_\pi^2} \frac{(\boldsymbol{q} \cdot \boldsymbol{\sigma})(\boldsymbol{q} \cdot \boldsymbol{T})}{\boldsymbol{q}^2 + m_\pi^2}, \tag{435}$$
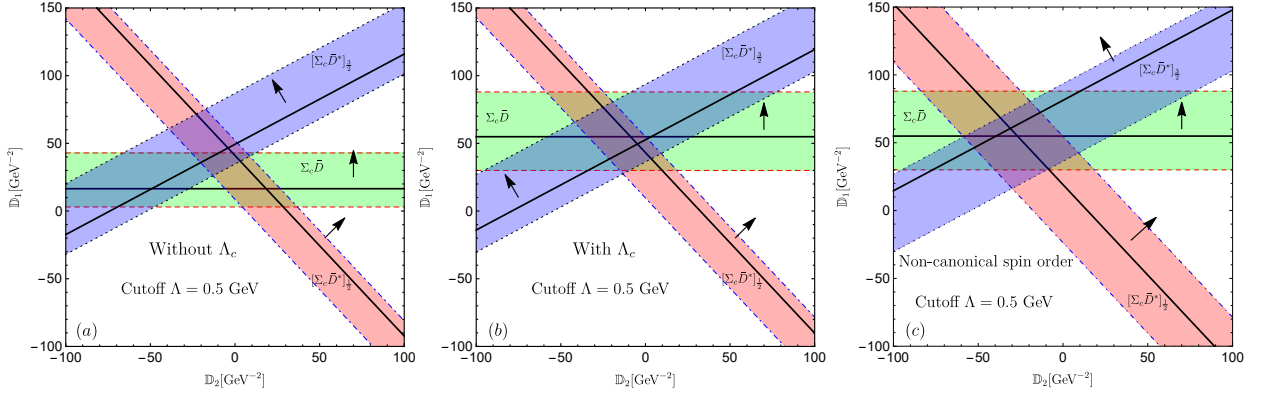
Figure 64: The parameter regions of three P_c states in the cases of (a)-not considering the contribution of the Λ_c in the loop diagrams, (b)-considering the contribution of the Λ_c in the loop diagrams, (c)-using the non-canonical spin order for the $P_c(4440)$ and $P_c(4457)$. The green, red and blue bands denote the binding energies of the $[\Sigma_c\bar{D}]_{J=1/2}$, $[\Sigma_c\bar{D}^*]_{J=1/2}$ and $[\Sigma_c\bar{D}^*]_{J=3/2}$ systems in the region $[-30, 0]$ MeV, respectively, while the arrow for each one denotes the direction that the binding becomes deeper. The corresponding three black straight lines represent the central values of the binding energies obtained from the experimental data [3].

$$\mathcal{V}^{\text{OPE}}_{\Sigma^*_c\bar{D}^*} = (\boldsymbol{I}_1 \cdot \boldsymbol{I}_2)\frac{gg_5}{2f^2_\pi}\frac{(\boldsymbol{q}\cdot\boldsymbol{\sigma}_{rs})(\boldsymbol{q}\cdot\boldsymbol{T})}{\boldsymbol{q}^2 + m^2_\pi}. \tag{436}$$

As in the *NN* interactions within the χEFT [475, 476], the static OPE potential is introduced for the $\Sigma_c\bar{D}^*$ and $\Sigma^*_c\bar{D}^*$ systems. For the OPE potential with the kinetic energies of the heavy particles in the framework of TOPT, e.g., the expressions like those in Eqs. (328) and (329), one can consult the supplemental materials of Ref. [356].

The TPE expressions including the mass splittings are lengthy and can be found in Refs. [355, 364]. For the specified total isospin $\boldsymbol{I} = \boldsymbol{I}_1 + \boldsymbol{I}_2$, the matrix element $\langle\boldsymbol{I}_1 \cdot \boldsymbol{I}_2\rangle = [I(I + 1) - I_1(I_1 + 1) - I_2(I_2 + 1)]/2$. From Eqs. (431)–(434), we can redefine

$$\mathbb{D}_1 = \tilde{D}_a + 2\tilde{E}_a(\boldsymbol{I}_1 \cdot \boldsymbol{I}_2), \qquad \mathbb{D}_2 = \tilde{D}_b + 2\tilde{E}_b(\boldsymbol{I}_1 \cdot \boldsymbol{I}_2), \tag{437}$$

where $\mathbb{D}_1$ and $\mathbb{D}_2$ represent the strength of the central potential and spin-spin interaction of the light d.o.f, respectively. One can build a connection between $\mathbb{D}_1$, $\mathbb{D}_2$ and $C^\alpha_{1/2}$, $C^\alpha_{3/2}$ through matching the potentials in the corresponding channels.

In Refs. [355, 364], the values of $\mathbb{D}_1$ and $\mathbb{D}_2$ were varied in the ranges $[-100, 150]$ GeV^{-2} and $[-100, 100]$ GeV^{-2} with the cutoff $\Lambda = 0.5$ GeV. They investigated the results without and with the Λ_c as the intermediate state in the TPE loop diagrams in the case of the canonical spin order for the $P_c(4440)$ and $P_c(4457)$, see Figs. 64(a) and 64(b). The result with the contributions of the Λ_c is better than that of without the Λ_c. This is a natural consequence of the strong coupling between $\Sigma^{(*)}_c$ and $\Lambda_c\pi$ as well as the accidental degeneration of the $\Sigma_c\bar{D}$ and $\Lambda_c\bar{D}^*$ (the mass difference $m_{\Sigma_c\bar{D}} - m_{\Lambda_c\bar{D}^*} \simeq 28$ MeV $\ll m_\pi$). With the configuration of the canonical spin order, one gets $|\mathbb{D}_1| \gg |\mathbb{D}_2|$ [see Fig. 64(b)], which implies that the potential is dominated by the central term and the spin-spin interaction only serves as a 'perturbation' to tune the binding energies of the $[\Sigma_c\bar{D}^*]_{1/2}$ and $[\Sigma_c\bar{D}^*]_{3/2}$ slightly (where the subscript denotes the total angular momentum J). It is worth noting that the role of Λ_c is still under debate. For example, it turns out that the inclusion of the Λ_c channels does not necessarily lead to improved fits in an updated fit in Ref. [385].

Wang *et al* also explored the possibility of the non-canonical spin order [364], see Fig. 64(c). It was shown that the experimental data can be equally well reproduced as that in Fig. 64(b), but one has to largely enhance the spin-spin interaction, such as $|\mathbb{D}_1| \sim |\mathbb{D}_2|$ in this case. From the experience of the *NN* interaction, the LECs C_T for the spin-spin interaction is much smaller than the C_S for the central interaction, which is a manifestation of the Wigner symmetry in the large N_c limit [1132]. With the help of the quark model as shown in the Appendix of Ref. [417], one can always relate the contact terms of the $\Sigma^{(*)}_c\bar{D}^{(*)}$ to those of the *NN* systems. Thus, one expects the suppression of the $\mathbb{D}_2$. Therefore, the canonical spin order is favored in Ref. [364].

With the fixed $\mathbb{D}_1$ and $\mathbb{D}_2$, the full spectrum of the $\Sigma^{(*)}_c\bar{D}^{(*)}$ hadronic molecules with $I = 1/2$ was established, see Fig. 65(a). The $[\Sigma^*_c\bar{D}]_{3/2}$ system is the most deeply bound one with a mass at 4348 MeV (but this result is sensitive to
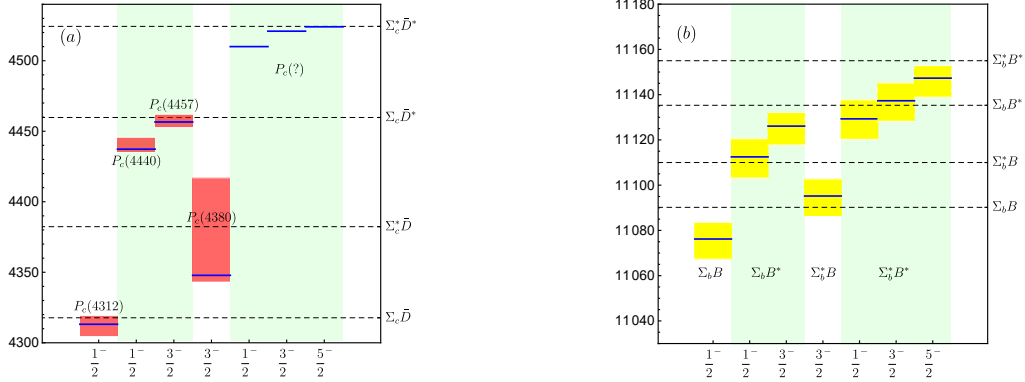
Figure 65: Left panel: The mass spectrum of the $\Sigma_c^{(*)}\bar{D}^{(*)}$ molecular pentaquarks. Right panel: The predicted mass spectrum of the $\Sigma_b^{(*)}B^{(*)}$ molecular pentaquarks. The mass ranges obtained from the experimental measurements and theoretical estimations are denoted by the red and yellow bands, respectively, while the central values calculated in Ref. [364] are represented by the blue solid line.

the cutoff, see Table 3 of Ref. [364]), which might correspond to the previously reported $P_c(4380)$ [2] or the recently announced $P_c(4337)$ [408] (for alternative explanations of the $P_c(4337)$, see [409, 381, 410]). A prediction of the possible molecular pentaquarks in the hidden-bottom $\Sigma_b^{(*)}B^{(*)}$ systems was also given, see Fig. 65(b).

The invariant mass spectrum of the $J/\psi p$ was fitted by Du *et al* [356] within the framework of Refs. [1102, 915, 973]. The LO contact potentials $V_{\alpha\beta}$ of the elastic channels $\Sigma_c^{(*)}\bar{D}^{(*)}$ were derived from Eqs. (369)-(373), and the contribution of the inelastic channel $J/\psi p$ was added into the $\mathcal{V}_{\alpha\beta}$ via an imaginary term due to the weak coupling of $J/\psi p$ [1133], which is analogous to Eq. (414). Besides, the OPE for the $\Sigma_c\bar{D}^*$ and $\Sigma_c^*\bar{D}^*$ systems was considered and treated nonperturbatively. The LSEs (416) and (417) were regularized with the hard cutoff [see Eq. (348)], where Λ is chosen to be in the range $1.0 - 1.5$ GeV. The fitted line shape is shown in Fig. 66. There are two schemes to fit the data: Scheme I—only the LO contact potential was considered; Scheme II—the OPE was incorporated. The results in Scheme I are shown in Fig. 66(I), where there are two solutions as those of Ref. [352], i.e., two optional spin orders in Eqs. (428) and (429), and the corresponding fitting quality $\chi^2/\text{d.o.f} = 1.01$ and 1.03, respectively. However, including the OPE (Scheme II) gives the unique solution with the slightly improved $\chi^2/\text{d.o.f} = 0.98$. In this case, the spin-parity of the $P_c(4440)$ and $P_c(4457)$ abide by the non-canonical spin order. In both schemes, a bound state was produced in the $[\Sigma_c^*\bar{D}]_{3/2}$ channel with a narrow width, which qualitatively matches the inconspicuous bump around 4.38 GeV. An improved fitting with the additional inelastic $\eta_c p$ and $\Lambda_c\bar{D}^{(*)}$ channels was done in Ref. [385] (see also Ref. [359]), which supported the conclusion of Ref. [356], and predicted the line shapes in the invariant mass spectra of the $\eta_c p$ and $\Lambda_c\bar{D}^{(*)}$, respectively.

The results in Refs. [364, 363, 352, 387, 356, 385] showed the $P_c(4440)$ and $P_c(4457)$ in the non-canonical spin order imply that the spin order in the $\Sigma^*\bar{D}^*$ system is also non-canonical, i.e., $m_{[\Sigma^*\bar{D}^*]_{1/2}} > m_{[\Sigma^*\bar{D}^*]_{3/2}} > m_{[\Sigma^*\bar{D}^*]_{5/2}}$. In Refs. [363, 387, 356, 385], the OPE was all included with a hard cutoff $\Lambda \gtrsim 1.0$ GeV to regularize the iterative equation with the coupled-channel dynamics, which is indeed a very hard scale from the experience of the single-channel NN interaction [475, 476]. In the single-channel NN case, choosing $\Lambda \sim m_\rho$ or even larger values was already found to result in spurious deeply bound states in the NN systems [646]. Besides, the nuclear lattice simulations of Refs. [1134, 1135] also correspond to smaller cutoff values.

The decays of the P_c states into the $J/\psi\Delta$, $J/\psi N$, and $\eta_c N$ were investigated within $\not\pi$EFT in Refs. [390, 388]. The $P_c(4457)$ is much closer to the $\Sigma_c\bar{D}^*$ threshold than the other P_c states to their corresponding thresholds. The isospin of the $\Sigma_c\bar{D}^*$ can either be 1/2 or 3/2, which can be expressed with the two particle state,

$$\begin{bmatrix} |\Sigma_c\bar{D}^*; I = \frac{1}{2}, I_3 = \frac{1}{2}\rangle \\ |\Sigma_c\bar{D}^*; I = \frac{3}{2}, I_3 = \frac{1}{2}\rangle \end{bmatrix} = \begin{bmatrix} \sqrt{\frac{2}{3}} & -\frac{1}{\sqrt{3}} \\ \frac{1}{\sqrt{3}} & \sqrt{\frac{2}{3}} \end{bmatrix} \begin{bmatrix} |\Sigma_c^{++}D^{*-}\rangle \\ |\Sigma_c^+\bar{D}^{*0}\rangle \end{bmatrix}. \tag{438}$$

Because the $P_c(4457)$ is very close to the thresholds, the difference of thresholds has a significant effect on the component of the $P_c(4457)$. The binding energies of the $P_c(4457)$ with respect to the $\Sigma_c^{++}D^{*-}$ and $\Sigma_c^+\bar{D}^{*0}$ thresholds
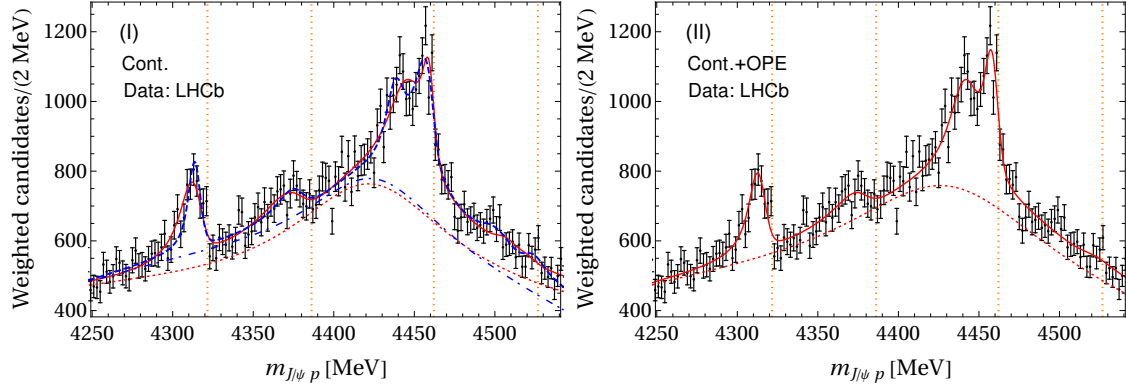
Figure 66: The fitted invariant mass spectrum of the $J/\psi p$ in Ref. [356]. The data with error bars are the weighted experimental data from Ref. [3]. Left panel: Only the contact potentials were considered in the fit. There exist two possible solutions with almost equal $\chi^2/\text{d.o.f}$ and they correspond to canonical (blue dashed curves) and non-canonical (red solid curves) spin orders for the $P_c(4440)$ and $P_c(4457)$. The blue dot-dashed and red dotted curves are the corresponding backgrounds, respectively. Right panel: Apart from the contact terms, the OPE interactions were also included in the fit (shown with the red solid curves).

read [390],

$$m_{\Sigma_c^{++}D^{*-}} - m_{P_c(4457)} = 6.9^{+1.8}_{-4.1}, \qquad m_{\Sigma_c^{+}\bar{D}^{*0}} - m_{P_c(4457)} = 2.5^{+1.8}_{-4.2}. \tag{439}$$

Since $m_{\Sigma_c^{+}\bar{D}^{*0}} - m_{P_c(4457)} \ll m_{\Sigma_c^{++}D^{*-}} - m_{P_c(4457)}$, one may expect the significant isospin violating decays for the $P_c(4457)$ as for the $X(3872)$ [for the isospin violating decays of the $X(3872)$, see Sec. 5.5.5]. In Ref. [390], Guo found that the isospin breaking ratio

$$\mathcal{R}_{\Delta^+/p} = \frac{\mathcal{B}[P_c(4457)^+ \to J/\psi\Delta^+]}{\mathcal{B}[P_c(4457)^+ \to J/\psi p]}, \tag{440}$$

is in the range from $O(10^{-2})$ to 30%, where the large uncertainty mainly comes from the mass of the $P_c(4457)$.

With the HQSS inspired potential for the $\Sigma_c^{(*)}\bar{D}^{(*)}$ systems [352], Sakai *et al* calculated their S-wave decays into the $J/\psi N$ and $\eta_c N$, respectively [388], i.e.,

$$\left\{[\Sigma_c\bar{D}]_{1/2}, [\Sigma_c^*\bar{D}]_{3/2}, [\Sigma_c\bar{D}^*]_{1/2}, [\Sigma_c\bar{D}^*]_{3/2}, [\Sigma_c^*\bar{D}^*]_{1/2}, [\Sigma_c^*\bar{D}^*]_{3/2}\right\} \to J/\psi N, \tag{441}$$

$$\left\{[\Sigma_c\bar{D}]_{1/2}, [\Sigma_c\bar{D}^*]_{1/2}, [\Sigma_c^*\bar{D}^*]_{1/2}\right\} \to \eta_c N. \tag{442}$$

They found that among the six states in Eq. (441), at least four states (including two $[\Sigma_c^*\bar{D}^*]_{1/2}$ and $[\Sigma_c^*\bar{D}^*]_{3/2}$) decay more easily into $J/\psi N$ than the $P_c(4312)$. Meanwhile, the partial width of the $P_c(4312) \to \eta_c N$ is larger than that of the $J/\psi N$. The ratio $\Gamma([\Sigma_c\bar{D}^*]_{1/2} \to J/\psi N)/\Gamma([\Sigma_c\bar{D}^*]_{1/2} \to \eta_c N)$ differs a lot for the canonical and non-canonical spin orders. See also the related calculations using a quark interchange model [360].

5.7.2. P_{cs} and partners

Based on Ref. [364], Wang *et al* studied the interactions of the $\Xi_c\bar{D}^{(*)}$, $\Xi_c'\bar{D}^{(*)}$ and $\Xi_c^*\bar{D}^{(*)}$ up to NLO [417], where the flavor symmetry group was enlarged to the SU(3) [the isospin Pauli matrix τ_i in Eq. (430) should be replaced by λ_i in this case]. In order to delineate the short-range interactions between the antitriplet singly heavy baryon $B_{\bar{3}}$ and anticharmed mesons, they constructed the following contact Lagrangian,

$$\begin{aligned}
\mathcal{L}_{\tilde{\mathcal{H}}B_{\bar{3}}} &= \tilde{D}'_a \langle \bar{\tilde{\mathcal{H}}}\tilde{\mathcal{H}}\rangle \text{Tr}(\bar{B}_{\bar{3}}B_{\bar{3}}) + \tilde{D}'_b \langle \bar{\tilde{\mathcal{H}}}\gamma^\rho\gamma_5\tilde{\mathcal{H}}\rangle \text{Tr}(\bar{B}_{\bar{3}}\gamma_\rho\gamma_5 B_{\bar{3}}) \\
&\quad + \tilde{E}'_a \langle \bar{\tilde{\mathcal{H}}}\lambda_i\tilde{\mathcal{H}}\rangle \text{Tr}(\bar{B}_{\bar{3}}\lambda_i B_{\bar{3}}) + \tilde{E}'_b \langle \bar{\tilde{\mathcal{H}}}\gamma^\rho\gamma_5\lambda_i\tilde{\mathcal{H}}\rangle \text{Tr}(\bar{B}_{\bar{3}}\gamma_\rho\gamma_5\lambda_i B_{\bar{3}}),
\end{aligned} \tag{443}$$

from which the contact potentials of the $\Xi_c\bar{D}$ and $\Xi_c\bar{D}^*$ are derived as

$$\mathcal{V}_{\Xi_c\bar{D}} = 2\tilde{D}'_a + 4(\boldsymbol{I}_1 \cdot \boldsymbol{I}_2 - 1/12)\tilde{E}'_a, \tag{444}$$

123

$$\mathcal{V}_{\Xi_c \bar{D}^*} = 2\tilde{D}'_a + 4\left(\boldsymbol{I}_1 \cdot \boldsymbol{I}_2 - 1/12\right)\tilde{E}'_a + \left[2\tilde{D}'_b + 4\left(\boldsymbol{I}_1 \cdot \boldsymbol{I}_2 - 1/12\right)\tilde{E}'_b\right]\boldsymbol{\sigma} \cdot \boldsymbol{T}. \tag{445}$$

The potentials of the $\Xi'_c \bar{D}^{(*)}$ and $\Xi^*_c \bar{D}^{(*)}$ are similar to those of the $\Sigma_c \bar{D}^{(*)}$ and $\Sigma^*_c \bar{D}^{(*)}$, respectively [the $\boldsymbol{I}_1 \cdot \boldsymbol{I}_2$ in Eqs. (431)–(434) should be replaced by $(\boldsymbol{I}_1 \cdot \boldsymbol{I}_2 - 1/12)$]. The HQSS cannot be used to relate the $\tilde{D}'_a, \ldots, \tilde{E}'_a$ to the $\tilde{D}_a, \ldots, \tilde{E}_a$, since the $B_{\bar{3}}$ and $B^{(*)}_6$ are not HQSS partners. In Refs. [982, 417], Meng *et al* proposed a 'microscopic' approach to build connections between the LECs in different systems containing the light quarks, e.g., Eqs. (443) and (430). Such an approach is analogous to the resonance saturation model [980], but carries the concepts of the quark-hadron duality and quark model. They constructed a quark level Lagrangian,

$$\mathcal{L}_{qq} = \tilde{g}_s \bar{q} \mathcal{S} q + \tilde{g}_a \bar{q} \gamma_\mu \gamma^5 \mathcal{A}^\mu q, \tag{446}$$

where $q = (u, d, s)^T$. Unlike the OBE model, the exchanged particles are not specified (e.g, $\rho, \omega, f_0, \ldots$). The scalar field $\mathcal{S}$ and axial-vector field $\mathcal{A}^\mu$ are two fictitious fields ($\tilde{g}_s$ and $\tilde{g}_a$ are the corresponding coupling constants). They are introduced to produce the central potential and spin-spin interaction between two light quarks, respectively. They are assumed to take the same matrix form as that of Eq. (41), but carry the quantum numbers of the scalar and axial-vector particles, respectively. The second terms is analogous to the axial-vector coupling of the light quarks and Goldstone bosons which stem from the chiral symmetry, e.g., see Sec. 2.1.1. The toy Lagrangian in Eq. (446) is introduced to predict the spectrum of P_{cs} states with the data of the P_c states as input. In principle, one should also include the vector-exchange interactions. However, if we only focus on the HQSS symmetry, the unit operator and spin-spin operator in the spin space have been included by the two terms in Eq. (446) after nonrelativisic reduction. The effect of the vector meson exchange interaction will be absorbed by the present two terms to some extent. For the predictions of the heavy flavor hadronic molecules using the above toy Lagrangian, see Refs. [281, 1136].

With the Lagrangian (446), the short-range interaction of the $\Sigma_c \bar{D}^*$ system can be written as

$$\mathcal{V}_{\Sigma_c \bar{D}^*} = \langle \Sigma_c \bar{D}^* | \mathcal{L}_{\bar{q}q} | \Sigma_c \bar{D}^* \rangle = -\frac{\tilde{g}_s^2}{6m_{\mathcal{S}}^2} - \frac{\tilde{g}_s^2}{m_{\mathcal{S}}^2}(\boldsymbol{I}_1 \cdot \boldsymbol{I}_2) + \frac{\tilde{g}_a^2}{9m_{\mathcal{A}}^2}\boldsymbol{\sigma} \cdot \boldsymbol{T} + \frac{2\tilde{g}_a^2}{3m_{\mathcal{A}}^2}(\boldsymbol{\sigma} \cdot \boldsymbol{T})(\boldsymbol{I}_1 \cdot \boldsymbol{I}_2), \tag{447}$$

where $q^2 \ll m_{\mathcal{S},\mathcal{A}}^2$ is assumed and $m_{\mathcal{S}}$ ($m_{\mathcal{A}}$) denotes the effective mass of the $\mathcal{S}$ ($\mathcal{A}^\mu$) field. Therefore, if one determines the square of the "charge-to-mass ratios" $\tilde{g}_s^2/m_{\mathcal{S}}^2$ and $\tilde{g}_a^2/m_{\mathcal{A}}^2$, one could use them to determine the short-range potentials of the other systems containing light quarks. The $\tilde{g}_s^2/m_{\mathcal{S}}^2$ and $\tilde{g}_a^2/m_{\mathcal{A}}^2$ are fixed by matching Eqs. (447) and (432) [also using the redefinition of Eq. (437)],

$$\frac{\tilde{g}_s^2}{m_{\mathcal{S}}^2} = -\frac{6}{5}\mathbb{D}_1, \qquad \frac{\tilde{g}_a^2}{m_{\mathcal{S}}^2} = \frac{6}{5}\mathbb{D}_2, \tag{448}$$

where the $\mathbb{D}_1$ and $\mathbb{D}_2$ are fixed using the data of the P_c states. Similarly, one can calculate the contact potentials of the $\Xi'_c \bar{D}^*$ and $\Xi_c \bar{D}^*$ with the quark level Lagrangian (446), and then match with the potentials obtained with the Lagrangians (430) and (443) in the SU(3) case, respectively (for more details, see Refs. [982, 417]).

Using the approach described above and the P_c data as inputs, Wang *et al* predicted ten molecular pentaquarks in the isoscalar $\Xi_c \bar{D}^{(*)}$, $\Xi'_c \bar{D}^{(*)}$ and $\Xi^*_c \bar{D}^{(*)}$ systems [417], see Table 8. The binding solutions in the $\Xi_c \bar{D}^{(*)}$ systems were also supported by the following works [416, 428, 432, 423]. The authors of Ref. [417] found that the contribution of the OEE is rather feeble, but the contribution of the TPE is very significant for the $\Xi'_c \bar{D}$ and $\Xi_c \bar{D}^*$ systems due to their approximate accidental degeneration, e.g., $m_{\Xi_c \bar{D}^*} - m_{\Xi'_c \bar{D}} \simeq 32$ MeV $\ll m_\pi$. They also found that no bound states exist in the isovector channels. They proposed to search for these isoscalar strange hidden-charm molecular pentaquarks in the $J/\psi \Lambda$ invariant mass spectrum from the decays $\Lambda_b(\Xi_b) \to J/\psi \Lambda K(\eta)$ [1137, 1138, 413]. There do not exist bound states in the $\Lambda_c \bar{D}_s^{(*)}$, $\Sigma_c^{(*)} \bar{D}_s^{(*)}$ and $\Omega_c^{(*)} \bar{D}_s^{(*)}$ systems [417]. The non-existence of the binding solution of the $\Lambda_c \bar{D}^{(*)}$ systems were pointed out long time ago in Refs. [1139, 347]. As for the $\Omega_c^{(*)} \bar{D}_s^{(*)}$ system, the bound states were obtained with a large cutoff in the OBE model in Ref. [1140].

Very recently, the LHCb Collaboration reported a structure in the $J/\psi \Lambda$ invariant mass spectrum in the $\Xi_b^- \to J/\psi \Lambda K^-$ decay with a significance of 3.1 σ [419]. The mass and width were measured to be $(m, \Gamma) = (4458.8 \pm 2.9^{+4.7}_{-1.1}, 17.3 \pm 6.5^{+8.0}_{-5.7})$ MeV. The mass of this structure is very consistent with that of the predicted state $[\Xi_c \bar{D}^*]_{1/2}$ in Ref. [417], see Table 8. There are two states in the $\Xi_c \bar{D}^*$ system with the total angular momentum $J = 1/2$ and $3/2$, respectively. The LHCb also tested the two-peak hypothesis, and found that in this case the masses and widths of

these two states are $(m, \Gamma) = (4454.9 \pm 2.7, 7.5 \pm 9.7)$ MeV and $(4467.8 \pm 3.7, 5.2 \pm 5.3)$ MeV, respectively. The data obtained with two peaks also support the predictions in Ref. [417], but the analysis of the current data sample cannot confirm or refute the two-peak hypothesis [419].

Table 8: The binding energies ΔE and masses M for the isoscalar $[\Xi'_c\bar{D}^{(*)}]_J$, $[\Xi^*_c\bar{D}^{(*)}]_J$ and $[\Xi_c\bar{D}^{(*)}]_J$ (where the subscript "J" denotes the total spin of the system) systems predicted in Ref. [417]. The state denoted by "$\sharp$" may be nonexistent at the upper limit. The results are given in units of MeV.

System	$[\Xi'_c\bar{D}]_{\frac{1}{2}}$	$[\Xi'_c\bar{D}^*]_{\frac{1}{2}}$	$[\Xi'_c\bar{D}^*]_{\frac{3}{2}}$	$[\Xi^*_c\bar{D}]_{\frac{3}{2}}$	$[\Xi^*_c\bar{D}^*]_{\frac{1}{2}}$	$[\Xi^*_c\bar{D}^*]_{\frac{3}{2}}$	$[\Xi^*_c\bar{D}^*]^{\sharp}_{\frac{5}{2}}$	$[\Xi_c\bar{D}]_{\frac{1}{2}}$	$[\Xi_c\bar{D}^*]_{\frac{1}{2}}$	$[\Xi_c\bar{D}^*]_{\frac{3}{2}}$
ΔE	$-18.5^{+6.4}_{-6.8}$	$-15.6^{+6.4}_{-7.2}$	$-2.0^{+1.8}_{-3.3}$	$-7.5^{+4.2}_{-5.3}$	$-17.0^{+6.7}_{-7.5}$	$-8.0^{+4.5}_{-5.6}$	$-0.7^{+0.7}_{-2.2}$	$-13.3^{+2.8}_{-3.0}$	$-17.8^{+3.2}_{-3.3}$	$-11.8^{+2.8}_{-3.0}$
M	$4423.7^{+6.4}_{-6.8}$	$4568.7^{+6.4}_{-7.2}$	$4582.3^{+1.8}_{-3.3}$	$4502.9^{+4.2}_{-5.3}$	$4635.4^{+6.7}_{-7.5}$	$4644.4^{+4.5}_{-5.6}$	$4651.7^{+0.7}_{-2.2}$	$4319.4^{+2.8}_{-3.0}$	$4456.9^{+3.2}_{-3.3}$	$4463.0^{+2.8}_{-3.0}$

Following the experiments of LHCb [419], the newly observed $P_{cs}(4459)$ was systematically studied in Ref. [420] with three closely connected methods: the effective range expansion (see Sec. 2.4), the extended Weinberg's compositeness relation [608], and fitting the line shape within $\not{\pi}$EFT, see Fig. 67. The authors considered the interplay between the three channels, $J/\psi\Lambda$, $\Xi'_c\bar{D}$ and $\Xi_c\bar{D}^*$, where their interactions are constrained by the HQSS. The two particle states $\Xi'_c\bar{D}$ and $\Xi_c\bar{D}^*$ are expanded with the $|S_h \otimes S_\ell\rangle$ basis as

$$|\Xi'_c\bar{D}\rangle_{J=\frac{1}{2}} = -\frac{1}{2}|0_h \otimes \frac{1}{2}_\ell\rangle + \frac{\sqrt{3}}{2}|1_h \otimes \frac{1}{2}_\ell\rangle, \tag{449}$$

$$|\Xi_c\bar{D}^*\rangle_{J=\frac{1}{2}} = \frac{\sqrt{3}}{2}|0_h \otimes \frac{1}{2}_\ell\rangle - \frac{1}{2}|1_h \otimes \frac{1}{2}_\ell\rangle, \tag{450}$$

$$|\Xi_c\bar{D}^*\rangle_{J=\frac{3}{2}} = |1_h \otimes \frac{1}{2}_\ell\rangle. \tag{451}$$

According to Sec. 5.4, there is only one LEC in principle, i.e., the $C^\alpha_{1/2}$. In Ref. [420], the following S-wave channel couplings were considered,

$$\text{I}: J/\psi\Lambda - \Xi_c\bar{D}^*, \ J = \frac{1}{2}, \frac{3}{2} \qquad \text{II}: J/\psi\Lambda - \Xi'_c\bar{D}, \ J = \frac{1}{2} \qquad \text{III}: J/\psi\Lambda - \Xi'_c\bar{D} - \Xi_c\bar{D}^*, \ J = \frac{1}{2}, \tag{452}$$

where J denotes the total angular momentum of the coupled system. The corresponding effective potentials for the $J = 1/2$ (3/2) in the two-channel and three-channel couplings may be read from Ref. [420]. The fitted line shapes of the three cases in Eq. (452) are shown in Fig. 67, where each subfigure is marked with (abc), and a, b, c refer to

$$a - \text{the number of channels}: 2 \equiv (J/\psi\Lambda - \Xi_c\bar{D}^* \text{ or } J/\psi\Lambda - \Xi'_c\bar{D}), \quad 3 \equiv (J/\psi\Lambda - \Xi'_c\bar{D} - \Xi_c\bar{D}^*), \tag{453}$$

$$b - \text{the number of partial waves}: 1 \equiv (J = \frac{1}{2} \text{ or } J = \frac{3}{2}), \quad 2 \equiv (J = \frac{1}{2} \text{ and } J = \frac{3}{2}), \tag{454}$$

$$c - \text{without or with the energy-dependent term in the potentials}: 0 \equiv (\text{without}), \quad 1 \equiv (\text{with}). \tag{455}$$

In Figs. 67(210) and 67(220), the authors considered the two-channel $J/\psi\Lambda - \Xi_c\bar{D}^*$ coupling. The dot-dashed line in Fig. 67(210) is obtained by solving the pole of the T-matrix with the mass and width of the $P_{cs}(4459)$ as inputs, while the solid line comes from the fit. The authors also introduced an energy-dependent term to mimic the role of the CDD pole in the case of the $\Xi_c\bar{D}^*$ single-channel scattering, but the resulting outputs are unacceptable, which implies the dynamically generated nature of the $P_{cs}(4459)$. In Fig. 67(220), the fit result of including the $J = 3/2$ partial wave is shown. The result is better than that of Fig. 67(210). There are two peaks in the line shape, which correspond to two poles of the T-matrix. In Fig. 67(210)′, the authors considered the $J/\psi\Lambda - \Xi'_c\bar{D}$ coupling. They tested permitting constant terms (the solid line) and CDD pole (dashed line) in the potential. Neither of them can well reproduce the data. In Fig. 67(320), the result with the three-channel $J/\psi\Lambda - \Xi'_c\bar{D} - \Xi_c\bar{D}^*$ coupling is illustrated. The fitting result contains two peaks as that of 67(220). They found the role of the $\Xi'_c\bar{D}$ channel is perturbative but it leads to the mass splitting between $J = 1/2$ and $J = 3/2$ states (see also Ref. [423]). From an overview of Fig. 67, the two fits in the right column are much better than those in the left one, which indicates both the partial waves $J = 1/2$ and
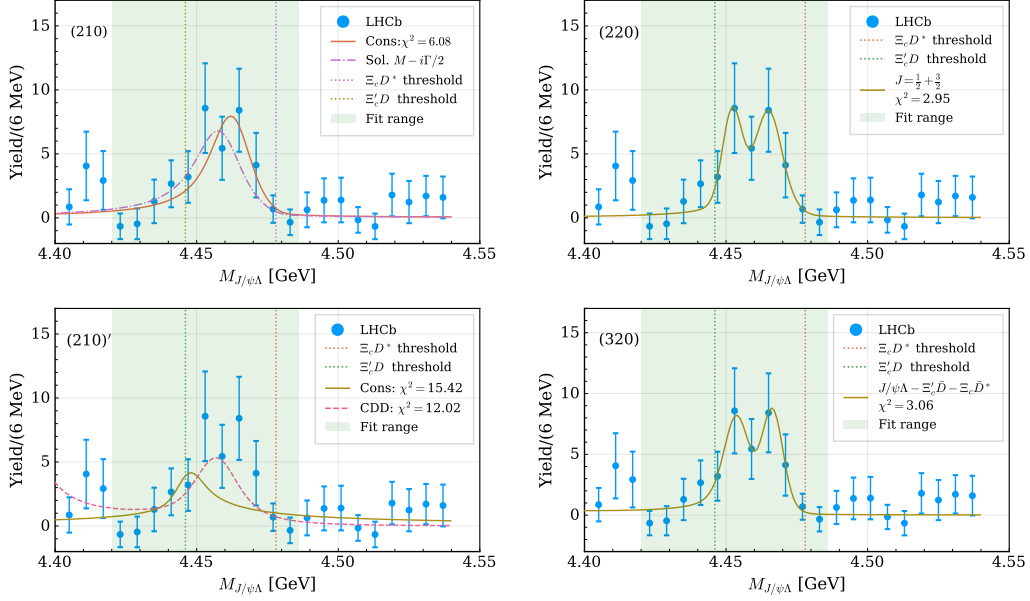
Figure 67: The fitted invariant mass spectrum of the $J/\psi\Lambda$ in Ref. [420], where the data with error bars are taken from Ref. [419]. The greenish area corresponds to the energy region used in the fit. The two dotted vertical lines from left to right correspond to the $\Xi'_c\bar{D}$ and $\Xi_c\bar{D}^*$ thresholds, respectively. The indications of the fitted curves are marked in each subfigure, and more explanations are given in the context.

$J = 3/2$ are important. However, in the signal region, the fits in the right column are both far too good. The lines almost go through all data points, which indicates it is hard to tell the different coupled-channel dynamic mechanisms forming the $P_{cs}(4459)$ under the present statistic significance. They also found the $J = 1/2$ and $J = 3/2$ states obey the canonical spin order, i.e., $m_{[\Xi_c\bar{D}^*]_{1/2}} < m_{[\Xi_c\bar{D}^*]_{3/2}}$, and the corresponding masses are consistent with those from the two-peak hypothesis of LHCb [419], but with smaller widths.

5.8. Other similar systems

In the above sections, we mainly focused on the experimentally observed molecular candidates. However, there exist theoretical predictions of many other hadronic molecules. Some of these predicted states may potentially be observed in the future experiments. Searching for these states would help us to assemble the jigsaw puzzles of the *hadronic molecular physics*. Therefore, we briefly review these efforts in this section.

It is instructive to enlarge the basis of the heavy matter fields. We consider the ground-state heavy matter fields containing light quarks, which include the nucleon[17], singly heavy mesons, singly heavy baryons, doubly heavy baryons and their antiparticles. Their possible combinations may lead to the molecular matrix with the following form,

$$
\begin{bmatrix} N \\ M_Q \\ B_Q \\ B_{QQ} \end{bmatrix} \hat{\otimes} \begin{bmatrix} N \\ M_Q \\ B_Q \\ B_{QQ} \\ \bar{N} \\ \bar{M}_Q \\ \bar{B}_Q \\ \bar{B}_{QQ} \end{bmatrix}^T \Rightarrow \begin{bmatrix} NN & NM_Q & NB_Q & NB_{QQ} & N\bar{N} \\ & M_QM_Q & M_QB_Q & M_QB_{QQ} & M_Q\bar{N} & M_Q\bar{M}_Q \\ & & B_QB_Q & B_QB_{QQ} & B_Q\bar{N} & B_Q\bar{M}_Q & B_Q\bar{B}_Q \\ & & & B_{QQ}B_{QQ} & B_{QQ}\bar{N} & B_{QQ}\bar{M}_Q & B_{QQ}\bar{B}_Q & B_{QQ}\bar{B}_{QQ} \end{bmatrix}
$$

---

[17]Sometimes, the K^* meson may be regarded as the heavy matter field to some extent ($m_{K^*} \sim m_N$). The $X_0(2900)$ and $X_1(2900)$ observed by the LHCb are very close to the $\bar{D}^*K^*$ threshold [1079, 1078]. They are explained as the S- and P-wave $\bar{D}^*K^*$ molecules, respectively [1141].

$$\Rightarrow \begin{bmatrix} \text{deuteron} & \Lambda_c(2940)?,\ldots & \square & \square & X(1835)? & & \\ & T_{cc},\ldots & \square & \square & \square & X(3872), Z^{(\prime)}_{c(s)}, Z^{(\prime)}_b, \ldots & \\ & & \square & \square & \square & P_{c(s)},\ldots & \square \\ & & \square & \square & \square & \square & \square & \square \end{bmatrix}, \quad (456)$$

where we use the N, M_Q, B_Q, and B_{QQ} to denote the sets of the nucleons, singly heavy mesons, singly heavy baryons and doubly heavy baryons in order, while the overhead bar represents their antiparticles. The charge conjugate is implied in the matrix of the first line, e.g., we only show the $M_Q \bar{N}$ explicitly, while its charge conjugate $N\bar{M}_Q$ is not given. The states in the matrix of the second line stand for the observed molecular candidates in the corresponding combinations, and the ellipses indicate that there might exist more states. The empty box denotes the observation in the corresponding combinations is still absent in experiments. If the future experiments could further fill up the empty boxes in Eq. (456) or give crucial evidences for the molecular nature of the observed states, the general pattern of the molecular spectrum would provide crucial insight into the underlying dynamics of the hadronic molecules.

5.8.1. $ND^{(*)}$, $N\Sigma_c^{(*)}$, $N\Xi_{cc}^{(*)}$

$ND^{(*)}$ systems

The interactions of the ND and ND^* are closely related to the inner structures of the charmed baryons $\Sigma_c(2800)$ and $\Lambda_c(2940)$, since these two states are very close to the thresholds of the ND and ND^* ($m_{ND} = 2805$ MeV, $m_{ND^*} = 2946$ MeV), respectively. The $I(J^P)$ quantum numbers of the $\Sigma_c(2800)$ and $\Lambda_c(2940)$ are $1(?^?)$ and $0(\frac{3}{2}^-)$ [note that the $J = 3/2$ for $\Lambda_c(2940)$ is favored but not certain], respectively [1]. Especially for the $\Lambda_c(2940)$, if it is the $2P$ state in the charmed baryon spectroscopy, its mass is about $60 - 100$ MeV smaller than the quark model calculations [1142, 80, 129, 106], which is very similar to what happened for the $\Lambda(1405)$, $D_{s0}^*(2317)$ and $X(3872)$. For more details, see Sec. 1.2 and the extensive discussions in the recent review [17]. Moreover, understanding the $ND^{(*)}$ interactions is important for investigating the charmed mesic nuclei [1143, 1144] and the properties of the charmed mesons in the nuclear matter [1145, 1146]. Haidenbauer *et al* have constructed the $N\bar{D}$ and ND interactions based on the meson-exchange model [1147, 1148, 1149].

In Ref. [93], Wang *et al* studied the $ND^{(*)}$ interactions in χEFT up to NLO, where the contribution of the $\Delta(1232)$ resonance was also included in the loops of the TPE. The LO LECs are fixed from the $N\bar{N}$ interactions [1124] with the help of quark model and SU(3) symmetry as in Eq. (446). Three singly charmed molecular pentaquarks in the isoscalar $ND^{(*)}$ [as well as the $\bar{B}^{(*)}N$] systems were predicted. However, there are no bound states in the isovector channels, which supports the interpretation of the $\Sigma_c(2800)$ as the compact charmed baryon. In Ref. [1150], by fitting the invariant mass spectrum of the pD^0 in the decay $\Lambda_b \to pD^0\pi^-$ [72], Sakai *et al* extracted the scattering length of the ND system (nD^+ and pD^0) in the coupled-channels [967]. They found the scattering length in the isovector channel is very large, and obtained a bound state pole in the isospin symmetry limit, which is assigned as the $\Sigma_c(2800)$.

If the $\Lambda_c(2940)$ is indeed the molecule of the ND^* [93], the observed peak of the $\Lambda_c(2940)$ by BaBar [70], Belle [71] and LHCb [72] should contain two subpeaks with $J = 1/2$ and $3/2$, respectively (recall that the similar story has happened for the P_c states after increasing the data sample, e.g., see Sec. 5.7.1). In this case, in contrast to the $J = 3/2$ one, the $J = 1/2$ component can easily decay into the pD^0 and $\Sigma_c\pi$ modes via the S-wave.

In Ref. [1151], the authors considered the interplay between the compact udc core and D^*N channel in an unquenched framework. They interpreted the recently observed $\Lambda_c(2910)$ [73] and the $\Lambda_c(2940)$ as the conventional charmed baryons but dressed with the D^*N channel. They also showed that the spin-parity of $\Lambda_c(2910)$ prefers $3/2^-$, while the $\Lambda_c(2940)$ is more likely to be $J^P = 1/2^-$ state.

$N\Sigma_c^{(*)}$ systems

The NY_c ($Y_c = \Sigma_c, \Lambda_c$) interactions are essential for understanding the charmed hypernuclei [1152, 1153, 1154] and the in-medium properties of the charmed baryons [1145]. In recent years, the experimental proposals at the J-PARC [1155] and GIS-FAIR [1156] have stimulated many investigations on the NY_c interactions and charmed hypernuclei [1157, 1158, 623, 1159, 1160, 1161, 1162, 1163, 1164]. In Refs. [1163, 1165], the HAL QCD Collaboration calculated the phase shifts of the $N\Lambda_c$ and $N\Sigma_c$ scatterings from lattice QCD at the unphysical pion mass $m_\pi = 410 - 570$ MeV. The extrapolations of lattice QCD results to the physical pion mass were done in Refs. [1164, 982, 991, 1166, 1167, 1168, 1169] with (covariant) χEFT. It was shown that the attractive interaction of
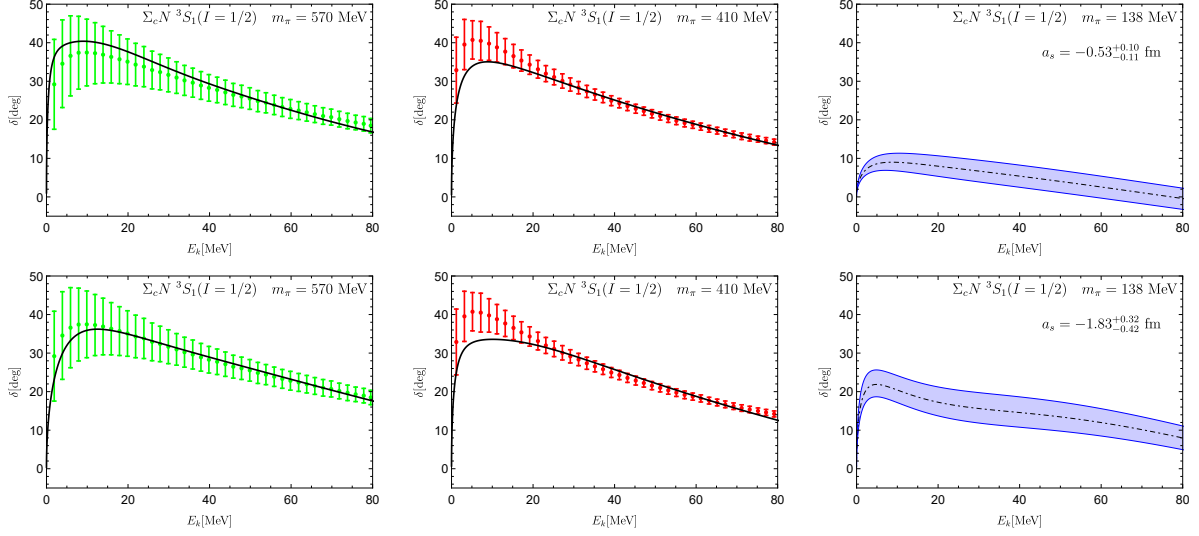
Figure 68: The fitted phase shifts of the $\Sigma_c N$ scattering in the $I = 1/2$ and $^3S_1$ channels at unphysical pion mass (black solid curves), and the chiral extrapolation of the phase shifts to the physical pion mass (given in the third column) [982]. The data with error bars are the phase shifts from lattice QCD calculations [1165]. The results in the first and second rows are fitted with $n = 1$, $\Lambda = 0.8$ GeV and $n = 2$, $\Lambda = 1.0$ GeV, respectively.

the $N\Lambda_c$ is too moderate to form a bound state in this system[18], while the bound states in the $4N\Lambda_c$ or $5N\Lambda_c$ might be possible [1164].

In Ref. [982], Meng *et al* performed the chiral extrapolation of the $N\Sigma_c$ interaction in χEFT up to NLO, where the one-loop corrections to OPE and LO contact interactions are explicitly considered due to their m_π-dependence. They introduced a Gauss form factor $\mathcal{F}(\boldsymbol{q}) = \exp(-\boldsymbol{q}^{2n}/\Lambda^{2n})$ to transform the momentum-space potential to the coordinate space. They considered two scenarios to fit the phase shifts of the $N\Sigma_c$ scatterings from lattice QCD [1165]. In scenario I: $n = 1$ and $\Lambda = 0.8$ GeV, while in scenario II: $n = 2$ and $\Lambda = 1.0$ GeV. The corresponding results from scenario I and II are shown in the first and second row of Fig. 68. An extrapolation of the $N\Sigma_c$ interaction to the physical pion mass gives the scattering length in scenario I and II as

$$\text{scenario I} : a_s = -0.53^{+0.10}_{-0.11} \text{ fm} ,$$
$$\text{scenario II} : a_s = -1.83^{+0.32}_{-0.42} \text{ fm}. \tag{457}$$

The result shows that the interaction in the $^3S_1(I = 1/2)$ $N\Sigma_c$ system is weakly attractive, but no bound solution can be found.

However, one should be aware that only the naive extrapolation was done in the above work, e.g., the finite volume effects were not considered. On the other hand, the lattice calculation was performed at a very large pion mass region (about $3m_\pi - 4m_\pi$). The chiral extrapolation uncertainties at such a large pion mass are hard to control.

$N\Xi_{cc}^{(*)}$ systems

The first calculation of the $N\Xi_{cc}$ interaction was given in Refs. [1170, 1171], in which $N\Xi_{cc}$ was linked to the NN system with the quark model, and the binding energy was predicted to be from several to several hundred MeVs depending on the concrete potential models. A recent calculation from the OBE model also predicted the bound states in the $N\Xi_{cc}$ and $\bar{N}\Xi_{cc}$ systems [1172].

5.8.2. $\Sigma_c^{(*)}D^{(*)}$, $\Sigma_c^{(*)}\bar{\Sigma}_c^{(*)}$, $\Sigma_c^{(*)}\Sigma_c^{(*)}$

$\Sigma_c^{(*)}D^{(*)}$ systems

---

[18]However, the phenomenological calculations in Refs. [623, 1159] yielded bound states in the $N\Lambda_c$ system with $J^P = 0^+$ and 1^+ once the coupled-channel effect among Λ_c, Σ_c and Σ_c^* are taken into account.

Based on Refs. [355, 364], the doubly charmed molecular pentaquarks P_{cc} composed of the $\Sigma_c^{(*)} D^{(*)}$ systems were explored by Chen *et al* [453]. They predicted seven analogous molecules as those of $\Sigma_c^{(*)} \bar{D}^{(*)}$ in the isospin $I = 1/2$ channels, see Fig. 69, while no bound states were found in the $I = 3/2$ channels. Since the quark components of the P_{cc} is $[cqq][c\bar{q}]$, the decay patterns are very different from those of the P_c states. There exist two types of decay modes for the P_{cc} states, i.e., the $[cqq] + [c\bar{q}]$ and $[ccq] + [q\bar{q}]$ modes. The $\Lambda_c\pi$ and $D\pi$ are the dominant decay modes of the $\Sigma_c^{(*)}$ and D^*, respectively. Thus the P_{cc} states with $J = 1/2$ can easily decay into $\Lambda_c D$ through S-wave via the OPE interaction. The lowest decay channel is $\Xi_{cc}\pi$ with the threshold at 3760 MeV, which is much lower than the P_{cc} states and it is not shown in Fig. 69. Besides, the P_{cc} states with the components $\Sigma_c^{(*)} D^*$ can also decay into $\Xi_{cc}\rho$ and $\Xi_{cc}\omega$. For more thresholds of the possible decay channels, such as the $\Lambda_c D\pi$ and $\Lambda_c D\pi\pi$, see Fig. 69. Ref. [453] also predicted possible molecules in the charmed-bottom $\Sigma_c^{(*)} \bar{B}^{(*)}$, $\Sigma_b^{(*)} D^{(*)}$, and doubly bottom $\Sigma_b^{(*)} \bar{B}^{(*)}$ systems.
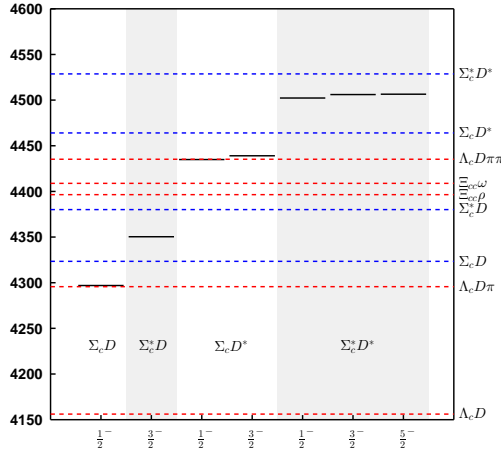
Figure 69: The mass spectrum of the P_{cc} molecular pentaquarks in the $I = 1/2$ $\Sigma_c^{(*)} D^{(*)}$ systems predicted in Ref. [453]. The thresholds of the $\Sigma_c^{(*)} D^{(*)}$ and possible decay channels are denoted with the blue and red dashed lines, respectively.

The doubly charmed pentaquarks were also investigated in the color-magnetic interaction model [448, 449], the chiral quark model [451], the QCD sum rule [1173], and the meson-exchange model [452, 952, 450, 273].

$\Sigma_c^{(*)} \bar{\Sigma}_c^{(*)}$ and $\Sigma_c^{(*)} \Sigma_c^{(*)}$ systems

The existence of the hidden-charm pentaquarks P_c stimulates the theorist to investigate whether the (double) hidden-charm hexaquarks exist likewise. In Ref. [1174], the authors found that the isoscalar $\Lambda_c\bar{\Lambda}_c$, $\Sigma_c^{(*)} \bar{\Sigma}_c^{(*)}$ and isovector $\Lambda_c\bar{\Sigma}_c^{(*)}$ as well as their doubly charmed and doubly bottom counterparts are good candidates of the molecular hexaquarks. The calculations in various models [1175, 622, 1176, 1177, 1178, 273, 358, 281, 1136, 1179, 1180] do indicate that the interactions in the isoscalar and isovector $\Sigma_c^{(*)} \bar{\Sigma}_c^{(*)}$ and $\Sigma_c^{(*)} \Sigma_c^{(*)}$ systems are strong enough to form bound states.

5.8.3. $\Xi_{cc}^{(*)} D^{(*)}$, $\Xi_{cc}^{(*)} \Sigma_c^{(*)}$, $\Xi_{cc}^{(*)} \Xi_{cc}^{(*)}$

The $\Xi_{cc}^{(*)}$ [$\bar{\Xi}_{cc}^{(*)}$] can be related to the $\bar{D}^{(*)}$ [$D^{(*)}$] with the heavy diquark-antiquark symmetry,

$$\Xi_{cc}^{(*)} \xleftrightarrow{\text{HDAS}} \bar{D}^{(*)}, \qquad \bar{\Xi}_{cc}^{(*)} \xleftrightarrow{\text{HDAS}} D^{(*)}. \qquad (458)$$

Therefore, the systems containing the doubly charmed baryons can be regarded as an extension of the systems with the charmed mesons. As a consequence of the HDAS, the $\Xi_{cc}^{(*)} D^{(*)}$, $\Xi_{cc}^{(*)} \Sigma_c^{(*)}$ and $\Xi_{cc}^{(*)} \Xi_{cc}^{(*)}$ systems can be related to the $\bar{D}^{(*)} D^{(*)}$, $\bar{D}^{(*)} \Sigma_c^{(*)}$ and $\bar{D}^{(*)} D^{(*)}$, respectively. Thus, the existence of the molecular states in the $\bar{D}^{(*)} D^{(*)}$ and $\bar{D}^{(*)} \Sigma_c^{(*)}$ systems should also imply the existence of the molecular states in the $\Xi_{cc}^{(*)} D^{(*)}$, $\Xi_{cc}^{(*)} \Sigma_c^{(*)}$ and $\Xi_{cc}^{(*)} \Xi_{cc}^{(*)}$ systems.

In Ref. [1023], the authors predicted the triply heavy pentaquarks with $I(J^P) = 0(\frac{3}{2}^-), 0(\frac{5}{2}^-)$ with the $X(3872)$ as input, as well as the $1(\frac{1}{2}^-)$ and $1(\frac{3}{2}^-)$ ones with the $Z_b(10650)$ as input (see also the calculations of Chen $et~al$ with the OBE model [1181]).

In Ref. [412], the authors proposed an alternative way to determine the spins of the $P_c(4440)$ and $P_c(4457)$ from the spectrum of the $\Xi_{cc}^{(*)}\Sigma_c^{(*)}$ systems with the help of lattice QCD [1182]. They predicted ten bound states in the $\Xi_{cc}^{(*)}\Sigma_c^{(*)}$ systems with the P_c states as inputs. Different spin orders of the $P_c(4440)$ and $P_c(4457)$ are also reflected in the $\Xi_{cc}^{(*)}\Sigma_c^{(*)}$ spectrum. For the possible molecular states in $\Xi_{cc}^{(*)}\Sigma_c^{(*)}$ systems, see also Ref. [1183].

In Ref. [1184], Yang $et~al$ investigated the possible bound states in the $\Xi_{cc}^{(*)}\Xi_{cc}^{(*)}/\bar{\Xi}_{cc}^{(*)}$ systems, and predicted the molecular candidates in the isoscalar and isovector channels.

6. Summary and outlook

The chiral dynamics is very important not only for the hadrons composed of light quarks (e.g. pion and nucleon) but also for the heavy flavor hadrons with one or two light quarks (e.g. heavy-light meson and singly heavy baryons). Combining the heavy quark symmetry, the chiral perturbation theory was successfully extended to the singly heavy systems to calculate the chiral correction to their masses, axial vector current, electromagnetic form factors and so on. Inspired by the recently observed Ξ_{cc} state, the χPT was also employed to investigate the chiral dynamics of the doubly heavy systems, especially the doubly charmed baryons. The heavy diquark-antiquark symmetry enhances the prediction powers of the χPT in the doubly heavy sector.

Since 2003, many exotic hadrons with heavy flavor were observed in experiments, some of which lie very close to the two-hadron threshold and are good candidates of the loosely bound hadronic molecules. The chiral effective field theories helped us understand the $\pi\pi$ scattering, πN scattering, NN scattering and related resonances in the past decades. The same chiral dynamics which plays a pivotal role in the formation of the $f_0(500)$, $\Lambda(1405)$ and deuteron also manifests themselves in the heavy flavor sector. The chiral effective field theories were also extended to explore these heavy flavor hadronic molecules.

Combining the lattice QCD simulation, the $\varphi D_{(s)}^{(*)}$ scattering were investigated with the unitarized χPT. The low mass puzzle of the $D_{s0}^*(2317)$ and $D_{s1}(2460)$ could be resolved either through the dynamical generation of the resonance in the molecular picture or through the channel couplings between the $c\bar{s}$ core and $\varphi D_{(s)}^{(*)}$ scattering state. Especially, the molecular picture leads to the two-pole structure of the $D_0^*(2300)$ and $D_1(2430)$, which awaits the confirmation of the experimental measurements and lattice QCD simulations in the future.

In the two matter field sector, there have been impressive progresses in the consistent description of the near-threshold states such as $X(3872)$, T_{cc}^+, Z_b, Z_c, Z_{cs}, P_c within the frameworks of the chiral effective field theory. Their masses, decays, lineshapes, production rates, etc. were reproduced well. The χEFT gives very useful predictions including their spin and flavor partner states, unobserved decay modes, branch ratios, production rates etc, which provide important clues for the future experiments.

However, the natures of the above exotic candidates have not been pinned down unambiguously. From the theoretical perspective, the nonperturbative QCD cannot be solved analytically. Except the $ab~initio$ lattice QCD formalism, it is still hard to set up the bottom-up theoretical frameworks with usability and predictive power. Meanwhile, the heavy flavor mesons and baryons are not available as the scattering target. The heavy flavor exotica were mainly observed in the complicated reactions or decay processes, which limit the experimental precision. Thus, in order to reveal their underlying structures, the joint efforts from the effective field theories, phenomenological models, lattice QCD simulations and more experimental measurements are necessary. In the following, we will summarize the wish list to clarify the main puzzles and challenges, focusing on the EFT perspective combining the lattice QCD and experiments.

- $X(3872)$

    - The masses of the $X(3872)$ coincides exactly with the $D^0\bar{D}^{*0}/D^{*0}\bar{D}^0$ threshold. Such a fine tuning is very interesting, which becomes acute when the similar fine tuning appears again in the T_{cc} system.

    - The refined measurement of the $X(3872)$ mass with respect to the $D^0\bar{D}^{*0}/D^{*0}\bar{D}^0$ threshold and the precise measurement of the lineshape of $X(3872) \to D^0\bar{D}^{*0}/D^{*0}\bar{D}^0$ will be very helpful. Now, the limiting factor

for the mass measurement is the experimental resolution. Thus, the measurement needed seems to be possible only at PANDA, once it will be in operation.

- – The experimental search of the partner states of the $X(3872)$ in the heavy quark symmetry and SU(3) flavor symmetry will help to explore its inner structure.

- – It should be figured out what clues the production of the $X(3872)$ in heavy ion collisions can provide regarding its underlying structure.

- T_{cc}

  - – The combined investigation and comparison of prompt productions of the doubly charm family, i.e. T_{cc}^+, Ξ_{cc}^{++} and Ξ_{cc}^+ (absent in the present observations) in pp collision may provide the clue to their structures.

  - – The similarity of the T_{cc} and $X(3872)$, especially their similar fine tuning, needs to be understood in an unified framework.

  - – The spin and flavor partner states of the T_{cc}^+.

- $D_{s0}^*(2317)$ and $D_{s1}(2460)$

  - – More independent lattice QCD simulations about the $D_{s0}^*(2317)/D_{s1}(2460)$ or D^*K scattering.

  - – There is only one scalar charm meson in quark model around 2.3 GeV, while the chiral unitary approaches generate two poles. These two models can be distinguished from the identification of the higher pole of the D_0^* in experiments and lattice QCD simulations.

- Z_c, Z_b and Z_{cs}

  - – The precise measurements of the lineshapes of the heavy quarkonia plus the pion can help to resolve the virtual state and resonance controversies of the $Z_{Q(s)}^{(\prime)}$ ($Q = c, b$).

  - – The experimental search of the HQSS partners of the $Z_{Q(s)}^{(\prime)}$, such as the $W_{cJ}^{(\prime)}$, $W_{bJ}^{(\prime)}$, Z_{cs}' and $Z_{bs}^{(\prime)}$.

  - – Lattice QCD simulations of the $D\bar{D}^*/B\bar{B}^*$ scattering near the physical pion mass will be very helpful.

  - – Whether the $Z_{cs}(3985)$ from BESIII and $Z_{cs}(4000)$ from LHCb are the same or different states should be checked carefully with the criteria in Ref. [346].

- P_c and P_{cs}

  - – The measurement of the J^P quantum numbers of the P_c states can resolve the spin-order problem of the $P_c(4440)$ and $P_c(4457)$.

  - – The experimental search of the predicted $\Sigma_c^*\bar{D}$ [$P_c(4380)$?] and $\Sigma_c^*\bar{D}^*$ molecular states.

  - – The experimental clarification of the relationship between the $P_c(4337)$ and $P_c(4312)/P_c(4380)$.

  - – The confirmation of the $P_{cs}(4459)$ as well as the search for the other $\Xi_c\bar{D}^{(*)}$, $\Xi_c'\bar{D}^{(*)}$ and $\Xi_c^*\bar{D}^{(*)}$ molecular candidates.

- General aspects of EFTs

  - – The EFTs with the resonances should be further developed (see [1185] for an example).

  - – The criteria to discern the "elementary" and "composite" particles in spirit of EFT, namely the decoupling of the high energy and low energy physics, need to be further developed. Distinguishing the "elementary" and "composite" particles should depend on the resolving scale. In the Weinberg's compositeness criterion, the low-energy scattering information (scattering length and effective range) is used. In principle, the short-range structure of a loosely bound state cannot be probed by the low-energy scattering. A quantity measuring compositeness should be defined in a resolving-scale-dependent way, which has been addressed in Refs. [609, 610, 612] to some extent.

131

- EFT based frameworks to extract the interactions and structures from the lattice QCD data (see [903, 1186, 573, 940] for examples) should be further developed, especially for the coupled-channel systems.

- EFT based amplitude analysis methods (see [203, 5] for two examples and the related review [1187]) should be further developed.

- Higher order calculations from χEFT are indispensable. The role of the large mass intermediate states should be examined carefully.

The discovery of the $X(3872)$ in 2003 launched the new era of hadron spectroscopy. The striking experimental progresses, like the discovery of many X, Y, Z states, the P_c states and T_{cc} state, remind us once again that this is a golden age of ambition and wisdom. We are essentially working on the clustering phenomena of the quark and gluon degrees of freedom of QCD and following the footsteps of the pioneers uncovering the structures at other levels such as the molecules, atoms, and nucleus. The few body physics of the quarks and gluons is very different from either the electron-electron interaction within the atom or the nucleon-nucleon interaction within the nucleus because the color confinement renders the basic d.o.fs nontransparent. Meanwhile, the underlying interactions (QCD) of hadrons are highly nonperturbative at the low energy scale. Although the endeavors in the past decades have brought us huge amounts of fresh perspectives, there is still a long long way to fully understand their internal structures. However, in the coming future, the accumulated data from the BaBar, Belle, BESIII, CDF, D0, LHCb, ATLAS and CMS Collaborations will continuously contribute to the discovery of the exotica with heavy flavors. At the same times, the ongoing, upgrading and upcoming experiments, including the GlueX [1188], Belle II [1189], BESIII [1190], LHCb [1191] and PANDA [1192, 1193] shall bring us more surprises. The amazing promotion of the computational capabilities will make more precise lattice QCD simulations available. The developments of theoretical frameworks, especially the EFTs, shall refresh our understanding about the exotic hadrons and add the new knowledge of the nonperturbative QCD dynamics.

Acknowledgments

Appendix A. Building blocks and the superfields

Appendix A.1. Building blocks

In order to fulfill the chiral symmetry, C, P, T symmetries and Hermitian, the chiral Lagrangians are often constructed using several 'building blocks' with known transformation behaviors under these symmetries. To avoid confusions, we use $\mathrm{Tr}(X)$ to represent the trace in the flavor space and $\langle X \rangle$ to represent the trace in the spinor space. The traceless building block $\hat{X}$ in the SU(3) case are defined as

$$\hat{X} = X - \frac{\mathbf{I}}{3}\mathrm{Tr}(X). \tag{A.1}$$

The corresponding results in SU(2) flavor symmetry can be deduced easily.

The building blocks to accommodate the Goldstone bosons were constructed as follows,

$$U = \xi^2 = \exp(i\varphi/f_\varphi), \quad \varphi = \begin{pmatrix} \pi^0 + \frac{1}{\sqrt{3}}\eta & \sqrt{2}\pi^+ & \sqrt{2}K^+ \\ \sqrt{2}\pi^- & -\pi^0 + \frac{1}{\sqrt{3}}\eta & \sqrt{2}K^0 \\ \sqrt{2}K^- & \sqrt{2}\bar{K}^0 & -\frac{2}{\sqrt{3}}\eta \end{pmatrix}, \tag{A.2}$$

where f_φ is the decay constant in the chiral limit. With the Goldstone bosons, left-handed external fields l_μ, right-handed external fields r_μ, scalar external fields s and pseudoscalar external fields p, one can construct the following building blocks.

$$\Gamma_\mu = \frac{1}{2}\left[\xi^\dagger(\partial_\mu - ir_\mu)\xi + \xi(\partial_\mu - il_\mu)\xi^\dagger\right], \tag{A.3}$$

$$u_\mu = \frac{i}{2}\left[\xi^\dagger(\partial_\mu - ir_\mu)\xi - \xi(\partial_\mu - il_\mu)\xi^\dagger\right], \tag{A.4}$$

$$\chi = 2B_0(s + ip), \tag{A.5}$$

$$\chi_\pm = \xi^\dagger\chi\xi^\dagger \pm \xi\chi^\dagger\xi, \tag{A.6}$$

$$f_{\mu\nu}^R = \partial_\mu r_\nu - \partial_\nu r_\mu - i[r_\mu, r_\nu], \tag{A.7}$$

$$f_{\mu\nu}^L = \partial_\mu l_\nu - \partial_\nu l_\mu - i[l_\mu, l_\nu], \tag{A.8}$$

$$f_{\mu\nu}^\pm = \xi^\dagger f_{\mu\nu}^R \xi \pm \xi f_{\mu\nu}^L \xi^\dagger, \tag{A.9}$$

$$\hat{f}_{\mu\nu}^\pm = f_{\mu\nu}^\pm - \frac{1}{3}\text{Tr}(f_{\mu\nu}^\pm). \tag{A.10}$$

The scalar external field $s = \text{diag}(m_u, m_d, m_s)$ is used to introduce the quark mass effect. If the pseudoscalar external field $p = 0$, the expansion of the χ_+ yields

$$\chi_+ = 2B_0\text{diag}(m_u, m_d, m_s) = \text{diag}(2m_\pi^2, 2m_\pi^2, 4m_K^2 - 2m_\pi^2), \tag{A.11}$$

where we have kept the leading order terms only. B_0 is related to the quark condensate, see Eq. (51) and its context for details.

If the external source is the electromagnetic field ($r_\mu = l_\mu = -e\mathcal{Q}A_\mu$), the right- and left- field strength tensors $f_{\mu\nu}^R$ and $f_{\mu\nu}^L$ are given as

$$f_{\mu\nu}^R = f_{\mu\nu}^L = -e\mathcal{Q}\left(\partial_\mu A_\nu - \partial_\nu A_\mu\right). \tag{A.12}$$

For the charmed and bottom mesons, $\mathcal{Q}$ denotes the electric charge matrix of their SU(3) multiplets, which reads $\mathcal{Q} = \text{diag}(0, -1, -1)$ for the $(\bar{D}^{(*)0}, D^{(*)-}, D_s^{(*)-})$, and $\mathcal{Q} = \text{diag}(1, 0, 0)$ for the $(B^{(*)+}, B^{(*)0}, B_s^{(*)0})$, respectively. Expanding the terms in Eqs. (A.9) and (A.10), respectively, one notes that $f_{\mu\nu}^+$ contains the $\mathcal{Q}$, while $\hat{f}_{\mu\nu}^+$ is proportional to the electric charge matrix $\mathcal{Q}_l$ of the light quark current $\mathcal{J}_\mu^\ell = \frac{2}{3}\bar{u}\gamma_\mu u - \frac{1}{3}\bar{d}\gamma_\mu d - \frac{1}{3}\bar{s}\gamma_\mu s$, i.e., $\mathcal{Q}_l = \text{diag}(2/3, -1/3, -1/3)$.

In order to investigate the isospin violation from the electromagnetic interaction, the left and right charges were often introduced [673, 674]. Their chiral transformations read

$$Q_{L/R} \to g_{L/R}Q_{L/R}g_{L/R}^\dagger \tag{A.13}$$

One can define the building block $Q_\pm$,

$$Q_\pm = \xi^\dagger Q_R \xi \pm \xi Q_L \xi^\dagger. \tag{A.14}$$

The chiral orders, chiral transformation, space inversion, charge conjugation and Hermitian conjugation of the above building blocks are given in Table A.9. The time reversal symmetry is usually guaranteed by the CPT theorem. In the practical calculation, there are some techniques to reduce the independent terms of the Lagrangians (see Refs. [998, 471, 618, 625] for examples).

Table A.9: The chiral order (D) and transformation properties of the building blocks under the chiral transformation (CH), space inversion (P), charge conjugation (C) and Hermitian conjugation (H.c.). We take the doublet nucleon ψ as an example, in which the covariant derivatives are defined as $\mathcal{D}_\mu = \partial_\mu + \Gamma_\mu$ and $\mathcal{D}'_\mu = \partial_\mu - \Gamma_\mu$. The covariant derivatives for the other mater fields are listed in the main text.

	U	ξ	χ	$f^R_{\mu\nu}$	$f^L_{\mu\nu}$
D	0	0	2	2	2
CH	$g_R U g_L^\dagger$	$g_R \xi K^\dagger$ or $K \xi g_L^\dagger$	$g_R \chi g_L^\dagger$	$g_R f^R_{\mu\nu} g_R^\dagger$	$g_L f^L_{\mu\nu} g_L^\dagger$
P	$U^\dagger$	$\xi^\dagger$	$\chi^\dagger$	$f^{L\mu\nu}$	$f^{R\mu\nu}$
C	U^T	ξ^T	χ^T	$-(f^L_{\mu\nu})^T$	$-(f^R_{\mu\nu})^T$
H.c.	$U^\dagger$	$\xi^\dagger$	$\chi^\dagger$	$f^R_{\mu\nu}$	$f^L_{\mu\nu}$

	$\chi_\pm$	$f^\pm_{\mu\nu}$	u_μ	$Q_\pm$	$h_{\mu\nu}$
D	2	2	1	1	2
CH	$K \chi_\pm K^\dagger$	$K f^\pm_{\mu\nu} K^\dagger$	$K u_\mu K^\dagger$	$K Q_\pm K^\dagger$	$K h_{\mu\nu} K^\dagger$
P	$\pm\chi_\pm$	$\pm f^{\pm\mu\nu}$	$-u^\mu$	$\pm Q_\pm$	$-h^{\mu\nu}$
C	$\chi_\pm^T$	$\mp(f^\pm_{\mu\nu})^T$	$(u_\mu)^T$	$Q_\pm^T$	$(h_{\mu\nu})^T$
H.c.	$\pm\chi_\pm$	$f^\pm_{\mu\nu}$	u_μ	$Q_\pm$	$h_{\mu\nu}$

	Γ_μ	ψ	$\bar\psi$	$\mathcal{D}_\mu\psi$	$g_{\mu\nu}$
D	1	0	0	0	0
CH	$K\Gamma^\mu K^\dagger - \partial^\mu K K^\dagger$	$K\psi$	$\bar\psi K^\dagger$	$K \mathcal{D}_\mu\psi$	$g_{\mu\nu}$
P	Γ^μ	$\gamma^0\psi$	$\bar\psi\gamma^0$	$\gamma^0 \mathcal{D}^\mu\psi$	$g^{\mu\nu}$
C	$-(\Gamma_\mu)^T$	$C\bar\psi^T$	$\psi^T C$	$C\mathcal{D}'^T_\mu \bar\psi^T$	$g_{\mu\nu}$
H.c.	$-\Gamma_\mu$	$\bar\psi\gamma_0$	$\gamma^0\psi$	$\psi^\dagger \overleftarrow{\mathcal{D}}'_\mu$	$g_{\mu\nu}$

	$\bar\psi\gamma^\mu\psi$	$\bar\psi\gamma^\mu\gamma_5\psi$	$\bar\psi\gamma_5\psi$	$\bar\psi\sigma_{\mu\nu}\psi$	$\epsilon_{\mu\nu\rho\sigma}$
D	1	0	1	0	0
CH	$\bar\psi\gamma^\mu\psi$	$\bar\psi\gamma^\mu\gamma_5\psi$	$\bar\psi\gamma_5\psi$	$\bar\psi\sigma_{\mu\nu}\psi$	$\epsilon_{\mu\nu\rho\sigma}$
P	$\bar\psi\gamma_\mu\psi$	$-\bar\psi\gamma_\mu\gamma_5\psi$	$-\bar\psi\gamma_5\psi$	$\bar\psi\sigma^{\mu\nu}\psi$	$-\epsilon^{\mu\nu\rho\sigma}$
C	$-\bar\psi\gamma^\mu\psi$	$\bar\psi\gamma^\mu\gamma_5\psi$	$\bar\psi\gamma_5\psi$	$-\bar\psi\sigma_{\mu\nu}\psi$	$\epsilon_{\mu\nu\rho\sigma}$
H.c.	$\bar\psi\gamma^\mu\psi$	$\bar\psi\gamma^\mu\gamma_5\psi$	$-\bar\psi\gamma_5\psi$	$\bar\psi\sigma_{\mu\nu}\psi$	$\epsilon_{\mu\nu\rho\sigma}$

The representation theory of SU(3) group can guide the construction of the Lagrangians to avoid omitting some terms. For example, for the heavy flavor system, the common and nontrivial reductions of the representation are as follows,

$$\mathbf{3} \otimes \mathbf{6} \quad = \quad \mathbf{8} \oplus \mathbf{10}, \tag{A.15}$$

$$\bar{\mathbf{6}} \otimes \mathbf{6} \quad = \quad \mathbf{1} \oplus \mathbf{8} \oplus \mathbf{27}, \tag{A.16}$$

$$\mathbf{8} \otimes \mathbf{8} \quad = \quad \mathbf{1} \oplus \mathbf{8}_1 \oplus \mathbf{8}_2 \oplus \mathbf{10} \oplus \overline{\mathbf{10}} \oplus \mathbf{27}, \tag{A.17}$$

$$\bar{\mathbf{3}} \otimes \mathbf{8} \quad = \quad \overline{\mathbf{15}} \oplus \mathbf{6} \oplus \bar{\mathbf{3}}. \tag{A.18}$$

The above $\mathbf{8}_1$ and $\mathbf{8}_2$ are actually the same irreducible representation (irrep.) of the SU(3) group, namely, $\{p, q\} = \{1, 1\}$ irrep., where the first row has one more box than the second row and the second row has one more box than the third row in Young diagram. However, in the tensor method to perform reduction (see [1194] for details), the irrep. with eight dimensions corresponds to a tensor with rank $(1, 1)$. The two $(1, 1)$ tensors A^i_j and B^i_j have two ways to form the new $(1, 1)$ tensors,

$$F^i_a = A^i_j B^j_a - B^i_j A^j_a, \quad D^i_a = A^i_j B^j_a + B^i_j A^j_a - \frac{2}{3} \delta^i_a S \tag{A.19}$$

where $S = A^i_a B^a_i$ is the tensor of rank $(0, 0)$. Apparently, the F and D are the antisymmetric and symmetric reductions, respectively. Therefore, we use $\mathbf{8}_1$ and $\mathbf{8}_2$ to label the two different reductions. In the Table A.10, we illustrate the reductions of two nonets X and Y, $\bar{B}_{\mathbf{6}}$ and $B_{\mathbf{6}}$, $\bar{B}_{\bar{\mathbf{3}}}$ and $B_{\mathbf{6}}$, respectively.

Table A.10: Reductions of two nonets X and Y, $\bar{B}_{\mathbf{6}}$ and $B_{\mathbf{6}}$, $\bar{B}_{\bar{\mathbf{3}}}$ and $B_{\mathbf{6}}$. The notations of the (anti)symmetrization are $(XY)_{\{a,b\}} = X_a Y_b + X_b Y_a$ and $(XY)_{[a,b]} = X_a Y_b - X_b Y_a$.

Group representation	$\mathbf{1} \otimes \mathbf{1} \to \mathbf{1}$	$\mathbf{1} \otimes \mathbf{8} \to \mathbf{8}$	$\mathbf{8} \otimes \mathbf{8} \to \mathbf{1}$	$\mathbf{8} \otimes \mathbf{8} \to \mathbf{8}_1$	
Flavor structure	$\mathrm{Tr}(X)\mathrm{Tr}(Y)$	$\mathrm{Tr}(X)\hat{Y}$ or $\mathrm{Tr}(Y)\hat{X}$	$\mathrm{Tr}(\hat{X}\hat{Y})$	$[\hat{X}, \hat{Y}]$	
Group representation	$\mathbf{8} \otimes \mathbf{8} \to \mathbf{8}_2$	$\mathbf{8} \otimes \mathbf{8} \to \mathbf{10}$	$\mathbf{8} \otimes \mathbf{8} \to \overline{\mathbf{10}}$	$\mathbf{8} \otimes \mathbf{8} \to \mathbf{27}$	
Flavor structure	$\{\hat{X}, \hat{Y}\}$	$(\hat{X}\hat{Y})^{\{i,j\}}_{[a,b]}$	$(\hat{X}\hat{Y})^{[i,j]}_{\{a,b\}}$	$(\hat{X}\hat{Y})^{\{i,j\}}_{\{a,b\}}$	
Group representation	$\bar{\mathbf{6}} \otimes \mathbf{6} \to \mathbf{1}$	$\bar{\mathbf{6}} \otimes \mathbf{6} \to \mathbf{8}$	$\bar{\mathbf{6}} \otimes \mathbf{6} \to \mathbf{27}$	$\mathbf{3} \otimes \mathbf{6} \to \mathbf{8}$	$\mathbf{3} \otimes \mathbf{6} \to \mathbf{10}$
Flavor structure	$\mathrm{Tr}(\bar{B}_{\mathbf{6}} B_{\mathbf{6}})$	$\bar{B}_{\mathbf{6}ab} B^{ca}_{\mathbf{6}}$	$\bar{B}_{\mathbf{6}ab} B^{ij}_{\mathbf{6}}$	$\bar{B}_{\bar{\mathbf{3}}ab} B^{ca}_{\mathbf{6}}$	$\bar{B}_{\bar{\mathbf{3}}ij} B^{ab}_{\mathbf{6}}$

In literature, there are two conventions of the charge conjugation transformation for D^* in constructing the di-meson states with fixed C-parity. The two conventions were spelled out in Ref. [1026] and Refs. [1070, 972], respectively. We summarize the them in Table A.11. In the main body, we will label the specific convention when the related Lagrangians or wave functions appear.

Table A.11: Two conventions for the charge conjugation of D^*. The convention-I and -II are spelled out in Ref. [1026] and Refs. [1070, 972], respectively.

	Interpolating current	Charge conjugation
convention-I	$D = \bar{q}\gamma_5 c, \ \bar{D} = \bar{c}\gamma_5 u$	$\hat{C}D\hat{C}^{-1} = \bar{D}, \ |\bar{D}\rangle = \hat{C}|D\rangle$
convention-II		
convention-I	$D^* = \bar{q}\gamma_\mu c, \ \bar{D}^* = \bar{c}\gamma_\mu q$	$\hat{C}D^*\hat{C}^{-1} = -\bar{D}^*, \ |\bar{D}^*\rangle = -\hat{C}|D^*\rangle$
convention-II	$D^* = \bar{q}\gamma_\mu c, \ \bar{D}^* = -\bar{c}\gamma_\mu q,$	$\hat{C}D^*\hat{C}^{-1} = \bar{D}^*, \ |\bar{D}^*\rangle = \hat{C}|D^*\rangle$

Appendix A.2. Superfields

The superfield is a technique to embed the heavy quark symmetry into the Lagrangians. In Ref. [615], Falk illustrated the constructions of the superfields with arbitrary spins. In this section, we present some commonly used

superfields. In principle, it is free to choose the relative phase of different components in the superfield. Therefore, one may see different definitions of superfields up to a phase in literature. We first introduce two projection operators, $\Lambda_+ = (1 + \rlap{/}{v})/2$ and $\Lambda_- = (1 - \rlap{/}{v})/2$.

The superfields for the ground state heavy mesons can be understood as the (tensor) product of the two spinors of the quark and antiquark [615],

$$\mathcal{H} \sim u_h \bar{v}_l, \quad \tilde{\mathcal{H}} \sim u_l \bar{v}_h, \quad \bar{\mathcal{H}} \sim v_l \bar{u}_h, \quad \bar{\tilde{\mathcal{H}}} \sim v_h \bar{u}_l, \tag{A.20}$$

where l and h represent the light and heavy quarks, respectively. At the hadronic level, the superfields read

$$\mathcal{H} = \Lambda_+ (P^*_\mu \gamma^\mu + iP\gamma_5), \qquad \tilde{\mathcal{H}} = (\tilde{P}^*_\mu \gamma^\mu + i\tilde{P}\gamma_5)\Lambda_-. \tag{A.21}$$

The $\tilde{\mathcal{H}}$ and $\mathcal{H}$ are related to each other through

$$\tilde{\mathcal{H}} = C[\mathcal{C}\mathcal{H}C^{-1}]^T C^{-1}, \tag{A.22}$$

where $\mathcal{C}$ and C are the charge conjugation acting on the field operator and Dirac matrix with

$$\mathcal{C}P_\mu \mathcal{C}^{-1} = -\tilde{P}_\mu, \quad \mathcal{C}P\mathcal{C}^{-1} = \tilde{P}, \quad C = i\gamma^2\gamma^0. \tag{A.23}$$

The conjugation of the fields are defined by $\bar{\mathcal{H}} = \gamma_0 \mathcal{H}^\dagger \gamma_0$ and $\bar{\tilde{\mathcal{H}}} = \gamma_0 \tilde{\mathcal{H}}^\dagger \gamma_0$. The general Lagrangians using the superfield were [e.g., see Eqs. (123) and (124)]

$$\mathcal{L} \sim \langle \bar{u}_l \Gamma_l u_l \bar{v}_h \Gamma_h v_h \rangle = \langle v_h \bar{u}_l \Gamma_l u_l \bar{v}_h \Gamma_h \rangle \sim \langle \bar{\tilde{\mathcal{H}}} \Gamma_l \tilde{\mathcal{H}} \Gamma_h \rangle, \tag{A.24}$$

$$\mathcal{L} \sim \langle \bar{u}_h \Gamma_h u_h \bar{v}_l \Gamma_l v_l \rangle = \langle u_h \bar{v}_l \Gamma_l v_l \bar{u}_h \Gamma_h \rangle \sim \langle \mathcal{H} \Gamma_l \bar{\mathcal{H}} \Gamma_h \rangle, \tag{A.25}$$

where Γ_h and Γ_l are the Dirac matrices in the bilinear forms of the heavy and light (anti)quarks, respectively . With Eqs. (A.24) and (A.25), one can easily construct the Lagrangians to keep or break the heavy quark spin symmetry by choosing the pertinent Γ_h.

For the excited P-wave heavy mesons, the superfield of the $(0^+, 1^+)$ doublet reads

$$\mathcal{S} = \Lambda_+ \left[R^{*\mu} \gamma_\mu \gamma_5 - R \right], \quad \text{with } \mathcal{S} \sim u_h \bar{v}_l \gamma_5, \quad \bar{\mathcal{S}} \sim -\gamma_5 v_l \bar{u}_h, \tag{A.26}$$

where the v_l is the effective spinor corresponding to combination of the light antiquark and the $l = 1$ angular momentum. The general form of the Lagrangians read [e.g., see Eq. (128)]

$$\mathcal{L} \sim \langle \bar{v}_l \Gamma_l v_l \bar{u}_h \Gamma_h u_h \rangle = \langle u_h \bar{v}_l \gamma_5 \gamma_5 \Gamma_l \gamma_5 \gamma_5 v_l \bar{u}_h \Gamma_h \rangle = -\langle \mathcal{S} \gamma_5 \Gamma_l \gamma_5 \bar{\mathcal{S}} \Gamma_h \rangle = -\langle \bar{\mathcal{S}} \Gamma_h \mathcal{S} \gamma_5 \Gamma_l \gamma_5 \rangle. \tag{A.27}$$

Meanwhile, the superfield of the $(1^+, 2^+)$ doublet reads

$$\mathcal{T}^\mu = \Lambda_+ \left\{ Y^{\mu\nu} \gamma_\nu - \sqrt{\frac{3}{2}} Y_\nu \gamma_5 \left[g^{\mu\nu} - \frac{1}{3} (\gamma^\mu - v^\mu)\gamma^\nu \right] \right\}, \quad \text{with } \mathcal{T} \sim u_h \bar{v}_l^\mu, \quad \bar{\mathcal{T}} \sim v_l^\mu \bar{u}_h, \tag{A.28}$$

where the v_l^μ denotes the vector-spinor of the light d.o.f with $j_l = \frac{3}{2}$. Similarly, the most general Lagrangians should have the following form [e.g., see Eq. (129)],

$$\mathcal{L} \sim \langle \bar{u}_h \Gamma_h u_h \bar{v}_l^\mu \Gamma_l^{\mu\nu} v_l^\nu \rangle = \langle v_l^\nu \bar{u}_h \Gamma_h u_h \bar{v}_l^\mu \Gamma_l^{\mu\nu} \rangle = \langle \bar{\mathcal{T}}^\nu \Gamma_h \mathcal{T}^\mu \Gamma_l^{\mu\nu} \rangle = \langle \mathcal{T}^\mu \Gamma_l^{\mu\nu} \bar{\mathcal{T}}^\nu \Gamma_h \rangle. \tag{A.29}$$

For the singly heavy baryon with the symmetric light diquark (flavor sextet), the spin-$\frac{1}{2}$ and -$\frac{3}{2}$ states form the doublet in the heavy quark spin symmetry. The superfield is constructed as [615]

$$\psi_Q^\mu = \mathcal{B}_{\mathbf{6}}^{*\mu} + \sqrt{\frac{1}{3}} (\gamma^\mu + v^\mu)\gamma^5 \mathcal{B}_{\mathbf{6}}. \tag{A.30}$$

136

The superfield can be understood as the

$$\psi_Q^\mu \sim u_h A_l^\mu, \tag{A.31}$$

where u_h and A_l^μ represent the spinor of the heavy quark and vector light diquark, respectively. A general interaction Lagrangian containing the ψ_Q^μ only has the following form [e.g., see Eq. (139)],

$$\mathcal{L} \sim \mathrm{Tr}[(\bar{u}_h\Gamma_h u_h)(A_l^{*\mu}\Gamma_{l\mu\nu}A_l^\nu)] \sim \mathrm{Tr}[\bar{u}_h A_l^{*\mu}\Gamma_h\Gamma_{l\mu\nu}u_h A_l^\nu)] \sim \mathrm{Tr}(\bar{\psi}_Q^\mu\Gamma_h\Gamma_{l\mu\nu}\psi_Q^\nu). \tag{A.32}$$

in which the Lorentz index of $\Gamma_{l\mu\nu}$ contracts with that of the light d.o.f. If one wants to keep the heavy quark spin symmetry, the Γ_h should be the unit matrix.

For the ground state doubly heavy baryons, two identical heavy quarks form a vector diquark. The spin-$\frac{1}{2}$ and spin-$\frac{3}{2}$ states form the spin doublet in the heavy quark spin symmetry. The superfield is constructed as [950]

$$\psi_{QQ}^\mu = \mathcal{B}_{QQ}^{*\,\mu} + \sqrt{\frac{1}{3}}(\gamma^\mu + \nu^\mu)\gamma^5\mathcal{B}_{QQ}. \tag{A.33}$$

The superfield can be understood as

$$\psi_{QQ}^\mu \sim u_l A_h^\mu, \tag{A.34}$$

where the u_l and A_h^μ denote the spinor of the light quark and vector heavy diquark, respectively. The general interaction may have the following form [e.g., see Eq. (146)],

$$\mathcal{L} \sim (\bar{u}_l\Gamma_l u_l)(A_h^{*\mu}\Gamma_{h\mu\nu}A_h^\nu) \sim (\bar{u}_l A_h^{*\mu}\Gamma_l\Gamma_{h\mu\nu}u_l A_h^\nu) \sim \bar{\psi}_{QQ}^\mu\Gamma_l\Gamma_{h\mu\nu}\psi_{QQ}^\nu. \tag{A.35}$$

If one wants to keep the heavy diquark spin symmetry, the Lorentz indices should contract with each other directly, i.e., $\Gamma_{h\mu\nu} = \alpha_h g_{\mu\nu}$ (with α_h a constant).

Although the superfields of the singly heavy and doubly heavy baryons have very similar forms, there are essential difference considering the light and heavy d.o.fs. The rules to construct the Lagrangians in the heavy (di)quark spin symmetry are totally different.

Appendix B. Heavy field expansion

We take the spin-$\frac{1}{2}$ fermion field Ψ as an example to illustrate the heavy field expansion. The momentum p of the field can be decomposed into the mass term and the residual momentum term,

$$p_\mu = M v_\mu + q_\mu, \tag{B.1}$$

where M is the mass, v_μ satisfies $v^2 = 1$, and q is the residual momentum. The field Ψ is divided into the light field H and the heavy field h,

$$H = e^{iMv\cdot x}\Lambda_+\Psi, \quad h = e^{iMv\cdot x}\Lambda_-\Psi, \tag{B.2}$$

where the projectors are defined as $\Lambda_\pm = \frac{1}{2}(1 \pm \slashed{v})$. With this decomposition, the most general Lagrangian becomes

$$\mathcal{L} = \bar{H}\mathcal{A}H + \bar{h}\mathcal{B}H + \bar{H}\gamma_0\mathcal{B}^\dagger\gamma_0 h - \bar{h}\mathcal{C}h. \tag{B.3}$$

Using the free Lagrangian $\mathcal{L} = \bar{\Psi}(i\slashed{D} - M)\Psi$ as an illustration, the corresponding $\mathcal{A}$, $\mathcal{B}$ and $\mathcal{C}$ are

$$\mathcal{A} = iv\cdot\mathcal{D}, \quad \mathcal{B} = i\slashed{D}_\perp, \quad \mathcal{C} = i(v\cdot\mathcal{D}) + 2M, \tag{B.4}$$

where $X_\perp^\mu \equiv X^\mu - (v\cdot X)v^\mu$. One can see that the H is massless, while the mass of the h is $2M$.

The meanings of the H and h is clear with the Dirac representation of the spinor and gamma matrices. The positive energy plane wave solution to the free Dirac equation reads

$$\psi_{\boldsymbol{p}}^s(x,t) = \sqrt{E(\boldsymbol{p}) + M}\left[\begin{array}{c}\chi^s \\ \frac{\sigma\cdot\boldsymbol{p}}{E(\boldsymbol{p})+M}\chi^s\end{array}\right]e^{-ip\cdot x}, \tag{B.5}$$

137

with χ^s the spin wave functions of two components. With a convenient choice $v^\mu = (1, \mathbf{0})$, one gets

$$
\begin{aligned}
H(x,t) &= \sqrt{E(\mathbf{p}) + M} \left[\begin{array}{c} \chi^s \\ 0 \end{array} \right] e^{-i[E(\mathbf{p})-M]t+i\mathbf{p}\cdot\mathbf{x}}, \\
h(x,t) &= \sqrt{E(\mathbf{p}) + M} \left[\begin{array}{c} 0 \\ \frac{\sigma\cdot\mathbf{p}}{E(\mathbf{p})+M}\chi^s \end{array} \right] e^{-i[E(\mathbf{p})-M]t+i\mathbf{p}\cdot\mathbf{x}}.
\end{aligned} \tag{B.6}
$$

Therefore, the light field H and heavy field h correspond to the large and small components of the wave function, respectively, in which h is $1/M$ suppressed in comparison with H.

In order to obtain the effective field theory with the light field H only, one can either substitute the h with the assistance of the equation of motion [474] (in the classical sense) or integrate out the heavy field h in the path integral approach [512, 474] (in the quantum sense). We here present the latter derivation explicitly. The generating functional of the Lagrangians is

$$
Z[\eta, \bar{\eta}, v, a, s, p] = \int [d\Psi][d\bar{\Psi}][du] e^{i[S + \int d^4 x(\bar{\eta}\Psi + \bar{\Psi}\eta)]}, \tag{B.7}
$$

where the η and $\bar{\eta}$ are the external fields. The v, a, s and p are possible external fields in the action S. u is the field (e.g., the Goldstone field) other than the fermion field Ψ. The external field η can be decomposed into the light part and heavy part,

$$
R = \frac{1}{2}(1 + \not v)e^{iMv\cdot x}\eta, \quad \rho = \frac{1}{2}(1 - \not v)e^{iMv\cdot x}\eta. \tag{B.8}
$$

The action corresponding to Lagrangian (B.3) can be rewritten as

$$
S + \int d^4 x(\bar{\eta}\Psi + \bar{\Psi}\eta) = \int d^4 x[\bar{H}\mathcal{A}H + \bar{H}\gamma^0\mathcal{B}^\dagger\gamma_0 C^{-1}\mathcal{B}H - \bar{h}'Ch' + \bar{R}H + \bar{H}R], \tag{B.9}
$$

with the substitution $h' = h - C^{-1}(\mathcal{B}H + \rho)$. Integrating out h', one obtains

$$
Z[\eta, \bar{\eta}, v, a, s, p] = \int [dH][d\bar{H}][du]\Delta_h e^{i \int d^4 x[\bar{H}\mathcal{A}H + \bar{H}\gamma^0\mathcal{B}^\dagger\gamma_0 C^{-1}\mathcal{B}H + \bar{R}H + \bar{H}R]}, \tag{B.10}
$$

where Δ_h is the resulting constant by integrating out h'. Therefore, we obtain the effective Lagrangian,

$$
\mathcal{L}_{\text{eff}} = \bar{H}(\mathcal{A} + \gamma^0\mathcal{B}^\dagger\gamma_0 C^{-1}\mathcal{B})H, \tag{B.11}
$$

where the $\bar{H}\mathcal{A}H$ is the LO in the heavy field expansion. The second term is the recoiling effect suppressed by the powers of $1/M$. In the example in Eq. (B.4), the expansion of C^{-1} read,

$$
C^{-1} = \frac{1}{2M} - \frac{i(v \cdot \mathcal{D})}{(2M)^2} + ... \tag{B.12}
$$

In the definition of H and h, we introduce a specific v with $v^2 = 1$. In the strict notation, the light field and heavy filed should be H_v and h_v depending on the choice of v. The introduction of v will break the Lorentz invariance. However, one can constrain the theory independent of the choice of v to restore the Lorentz symmetry partially, which is called the reparameterization invariance [811, 658]. For example, $i\bar{H}_v v \cdot \mathcal{D}H_v$, the Lagrangian in the heavy field limit of Eq. (B.4) cannot fulfill the reprarameterization invariance. One can introduce the flollowing tranformation,

$$
i\bar{H}_v v \cdot DH_v \rightarrow i\bar{H}_v v \cdot DH_v + \bar{H}_v \frac{(iD)^2}{M} H_v + O\left(\frac{1}{M^2}\right), \tag{B.13}
$$

where the recoiling effect is introduced to make the term the reparameterization invariant up to the discrepancy at $O(1/M^2)$.

In the heavy field expansion, it is very convenient to introduce the Pauli-Lubanski vector

$$
S^\mu = \frac{i}{2}\gamma_5\sigma^{\mu\nu}v_\nu = -\frac{1}{2}\gamma_5(\gamma^\mu\not v - v^\mu). \tag{B.14}
$$

138

Table B.12: The reductions of the Dirac matrices in heavy baryon formalism (H.B.F) via $\Lambda_+ \Gamma \Lambda_+$, where $\Lambda_+ = \frac{1}{2}(1 + \not{v})$.

Γ	$1_{4\times4}$	γ_5	γ^μ	$\gamma^\mu\gamma_5$	$\sigma^{\mu\nu}$	$\sigma^{\mu\nu}\gamma_5$
H.B.F	$1_{4\times4}$	0	v^μ	$2S^\mu$	$-2\varepsilon^{\mu\nu\rho\sigma}v_\rho S_\sigma$	$2i(v^\mu S^\nu - v^\nu S^\mu)$

The Dirac matrices can be reexpressed with the relations in Table B.12. In the spacetime with $d = 4$,

$$v \cdot S = 0, \quad \{S^\mu, S^\nu\} = \frac{1}{2}(v^\mu v^\nu - g^{\mu\nu}), \quad [S_v^\mu, S_v^\nu] = -i\varepsilon^{\mu\nu\rho\sigma}v_\rho S_\sigma^\nu. \tag{B.15}$$

where the Levi-Civita symbol is defined as [19]:

$$\varepsilon^{\mu\nu\alpha\beta} = \begin{cases} +1 & \text{even permutation} \\ -1 & \text{odd permutation} \\ 0 & \text{others} \end{cases}. \tag{B.16}$$

Under the heavy field reduction, the propagators of the spin-$\frac{1}{2}$ and spin-$\frac{3}{2}$ particles are

$$\mathcal{P}_{1/2} = \frac{i}{v \cdot q + i\varepsilon}, \qquad \mathcal{P}_{3/2}^{\mu\nu} = \frac{-iP^{\mu\nu}}{v \cdot q + i\varepsilon}, \tag{B.17}$$

where $P^{\mu\nu} = g^{\mu\nu} - v^\mu v^\nu + \frac{4}{d-1}S^\mu S^\nu$ is the projection operator which singles out the spin-$\frac{3}{2}$ component from the Rarita-Schwinger field.

For the scalar and vector fields, the free Lagrangian is

$$\mathcal{L} = \mathcal{D}_\mu \Phi \mathcal{D}^\mu \Phi^\dagger - M^2 \Phi \Phi^\dagger - \frac{1}{2}F^{\mu\nu}F_{\mu\nu}^\dagger + M^2 \Phi^{*\mu}\Phi_\mu^{*\dagger}, \tag{B.18}$$

where $F_{\mu\nu} = \partial_\mu \Phi_\nu^* - \partial_\nu \Phi_\mu^*$. The heavy field expansions for the particle $P^{(*\mu)}$ and antiparticle $\tilde{P}^{(*\mu)}$ are

$$\sqrt{M}\Phi^{(*\mu)} = e^{-iMv\cdot x}P^{(*\mu)}, \quad \Rightarrow \mathcal{L} = -2Piv \cdot \mathcal{D}P^\dagger + 2P^{*\mu}iv \cdot \mathcal{D}P_\mu^{*\dagger}, \tag{B.19}$$

$$\sqrt{M}\Phi^{(*\mu)} = e^{iMv\cdot x}\tilde{P}^{(*\mu)\dagger}, \quad \Rightarrow \mathcal{L} = 2\tilde{P}^\dagger iv \cdot \mathcal{D}\tilde{P} - 2\tilde{P}^{*\dagger\mu}iv \cdot \mathcal{D}\tilde{P}_\mu^*. \tag{B.20}$$

With the above reductions, the propagators of the scalar and vector heavy particles are

$$\mathcal{P}_0 = \frac{i}{2v \cdot q + i\varepsilon}, \qquad \mathcal{P}_1 = -\frac{i(g_{\mu\nu} - v_\mu v_\nu)}{2v \cdot q + i\varepsilon}. \tag{B.21}$$

Appendix C. Electromagnetic form factors

Appendix C.1. Vector mesons of spin-1

The magnetic moment of vector state is extracted from the matrix element of electromagnetic current as defined in Eq. (234). The explicit expression parameterized in a Lorentz covariant form reads [1196],

$$\begin{aligned}
\mathcal{G}^\mu(q^2) &= \langle V(p', \varepsilon'^*)| \mathcal{J}_{em}^\mu(q^2)|V(p, \varepsilon)\rangle \\
&= -\mathcal{G}_1(q^2)(\varepsilon \cdot \varepsilon'^*)(p + p')^\mu + \mathcal{G}_2(q^2)\left[(\varepsilon \cdot q)\varepsilon'^{*\mu} - (\varepsilon'^* \cdot q)\varepsilon^\mu\right] + \mathcal{G}_3(q^2)\frac{(\varepsilon \cdot q)(\varepsilon'^* \cdot q)}{2m_V^2}(p + p')^\mu, \tag{C.1}
\end{aligned}$$

---

[19]The Levi-Civita symbol is different from that in Refs. [477, 1195] by a sign.

where $p(p')$ and $\varepsilon(\varepsilon')$ are the momentum and polarization vector of initial (final) state. m_V is the mass of vector meson V. $\mathscr{G}_i(q^2)$ are called electromagnetic form factors that can be related to the charge, quadrupole and magnetic dipole form factors in the Breit frame. The kinetics in Breit frame are given as

$$q^\mu = (p - p')^\mu = (0, \boldsymbol{Q}), \qquad \boldsymbol{Q} = Q\hat{z}, \qquad p^\mu = (p^0, \tfrac{1}{2}\boldsymbol{Q}),$$
$$p'^\mu = (p^0, -\tfrac{1}{2}\boldsymbol{Q}), \qquad -q^2 = Q^2 \geq 0, \qquad p^0 = \sqrt{m_V^2 + \tfrac{1}{4}Q^2}. \tag{C.2}$$

The time and space components of Lorentz vector $\mathscr{G}^\mu(q^2)$ in Breit frame are derived as

$$\mathscr{G}^0(Q^2) \;=\; 2p^0\left\{\mathscr{G}_C(Q^2)(\boldsymbol{\varepsilon}\cdot\boldsymbol{\varepsilon}'^*) + \frac{\mathscr{G}_Q(Q^2)}{2m_V^2}\Big[(\boldsymbol{\varepsilon}\cdot\boldsymbol{Q})(\boldsymbol{\varepsilon}'^*\cdot\boldsymbol{Q}) - \frac{1}{3}(\boldsymbol{\varepsilon}\cdot\boldsymbol{\varepsilon}'^*)Q^2\Big]\right\}, \tag{C.3}$$

$$\boldsymbol{\mathscr{G}}(Q^2) \;=\; \mathscr{G}_2(Q^2)\left[(\boldsymbol{\varepsilon}'^*\cdot\boldsymbol{Q})\boldsymbol{\varepsilon} - (\boldsymbol{\varepsilon}\cdot\boldsymbol{Q})\boldsymbol{\varepsilon}'^*\right] = 2p^0\frac{\mathscr{G}_M(Q^2)}{2m_V}\left[(\boldsymbol{\varepsilon}'^*\cdot\boldsymbol{Q})\boldsymbol{\varepsilon} - (\boldsymbol{\varepsilon}\cdot\boldsymbol{Q})\boldsymbol{\varepsilon}'^*\right], \tag{C.4}$$

where $\mathscr{G}_C$, $\mathscr{G}_Q$ and $\mathscr{G}_M$ are the so-called charge, electric quadrupole and magnetic dipole form factors. They are bridged to $\mathscr{G}_i$ as defined in Eq. (C.1) via

$$\mathscr{G}_C \;=\; \mathscr{G}_1 + \frac{2}{3}\eta\mathscr{G}_Q, \qquad \mathscr{G}_Q = \mathscr{G}_3 + \mathscr{G}_2(1+\eta)^{-1} + \frac{1}{2}\mathscr{G}_1(1+\eta)^{-1}, \qquad \mathscr{G}_M = \mathscr{G}_2, \tag{C.5}$$

where $\eta = Q^2/(4m_V^2)$. Note that in deriving Eqs. (C.3) and (C.4), the transverse conditions $p \cdot \varepsilon = 0$, and $p' \cdot \varepsilon'^* = 0$ have been used. Then the magnetic moment of a vector meson is defined as

$$\mu_V = \mathscr{G}_M(Q^2)\big|_{Q^2\to 0}. \tag{C.6}$$

The radiative decay width can be expressed in terms of the transition magnetic moment $\mu'(q^2)$, and which is extracted from the following transition matrix element,

$$\langle P(p')|\,\mathscr{J}_{\mathrm{em}}^\mu(q^2)|V(p,\varepsilon)\rangle = e\,\sqrt{m_V m_P}\mu'(q^2)\epsilon^{\mu\nu\alpha\beta}v_\nu q_\alpha \varepsilon_\beta. \tag{C.7}$$

Performing the standard procedure for calculating the decay width of $1 \to 2$ process, the radiative decay width of $V \to P\gamma$ is given as

$$\Gamma[V \to P\gamma] = \frac{\alpha}{3}\frac{m_P}{m_V}\left|\mu'(0)\right|^2 |\boldsymbol{q}|^3, \tag{C.8}$$

with $\alpha = 1/137$ the fine structure constant. The transition magnetic moment $\mu_{V\to P\gamma}$ is defined as

$$\mu_{V\to P\gamma} = \frac{e}{2}\mu'(0). \tag{C.9}$$

Appendix C.2. Baryons of spin-$\frac{1}{2}$ and spin-$\frac{3}{2}$

The parameterizations of the electromagnetic currents for the spin-$\frac{1}{2}$ [857] and spin-$\frac{3}{2}$ [624] baryons (or the transition processes [858]) have been given with the relativistic and nonrelativistic forms (or see [1197, 1198, 1199, 1200]). The (transition) magnetic moments can be extracted from the corresponding electromagnetic form factors. We summarize the nonrelativistic froms in the following,

(1) *Spin-$\frac{1}{2}$ baryons*:

$$\langle B_{\bar{\mathbf{3}}}(p')|\,\mathscr{J}_{\mathrm{em}}^\mu\,|B_{\bar{\mathbf{3}}}(p)\rangle = \bar{u}(p')\left[v_\mu\mathscr{G}_E(q^2) + \frac{[S_\mu, S\cdot q]}{m_B}\mathscr{G}_M(q^2)\right]u(p), \tag{C.10}$$

where $\mathscr{G}_E$ and $\mathscr{G}_M$ are the electric and magnetic form factors, respectively. $S_\mu = \frac{i}{2}\gamma^5\sigma_{\mu\nu}v^\nu$ is the covariant spin operator. The magnetic moment is given by $\mu_B = \frac{e}{2m_B}\mathscr{G}_M(0)$. Although it is given with the $\bar{\mathbf{3}}_f$ baryons, the $\mathbf{6}_f$ ones take the same form.

(2) *Spin-$\frac{3}{2}$ baryons:*

$$\langle B_{\mathbf{6}}^{*}\left(p'\right)\left|\mathscr{J}_{\text{em}}^{\mu}\right|B_{\mathbf{6}}^{*}\rangle = \bar{u}^{\rho}\left(p'\right)\mathscr{O}_{\rho\mu\sigma}\left(p',p\right)u^{\sigma}(p),\tag{C.11}$$

with

$$\mathscr{O}_{\rho\mu\sigma}\left(p',p\right) = -g_{\rho\sigma}\left[v_{\mu}\left(\mathscr{F}_{1}-\tau\mathscr{F}_{2}\right)+\frac{[S_{\mu},S_{\alpha}]}{m_{B}}q^{\alpha}\left(\mathscr{F}_{1}+\mathscr{F}_{2}\right)\right]-\frac{q^{\rho}q^{\sigma}}{4m_{B}^{2}}\left[v_{\mu}\left(\mathscr{F}_{3}-\tau\mathscr{F}_{4}\right)+\frac{[S_{\mu},S_{\alpha}]}{m_{B}}q^{\alpha}\left(\mathscr{F}_{3}+\mathscr{F}_{4}\right)\right],\tag{C.12}$$

from which the charge, electric quadrupole, magnetic dipole, and magnetic octupole form factors are defined as

$$\begin{aligned}
\mathscr{G}_{C}(q^{2}) &= \mathscr{F}_{1}-\tau\mathscr{F}_{2}+\frac{2}{3}\tau\mathscr{G}_{E2}, & \mathscr{G}_{Q}(q^{2}) &= \mathscr{F}_{1}-\tau\mathscr{F}_{2}-\frac{1}{2}\left(1+\tau\right)\left(\mathscr{F}_{3}-\tau\mathscr{F}_{4}\right), \\
\mathscr{G}_{M}(q^{2}) &= \mathscr{F}_{1}+\mathscr{F}_{2}+\frac{4}{5}\tau\mathscr{G}_{M3}, & \mathscr{G}_{M3}(q^{2}) &= \mathscr{F}_{1}+\mathscr{F}_{2}-\frac{1}{2}\left(1+\tau\right)\left(\mathscr{F}_{3}+\mathscr{F}_{4}\right).
\end{aligned}\tag{C.13}$$

where $\tau = -q^{2}/(4m_{B}^{2})$. The magnetic moment is then given as $\mu_{B} = \frac{e}{2m_{B}}\mathscr{G}_{M}(0)$.

(3) *Spin-$\frac{1}{2}\rightarrow$spin-$\frac{1}{2}+\gamma$ transitions:*

$$\langle\psi\left(p'\right)\left|\mathscr{J}_{\text{em}}^{\mu}\right|\psi(p)\rangle = e\bar{u}\left(p'\right)\left[\left(v_{\mu}-\frac{\delta}{q^{2}}q_{\mu}\right)\mathscr{G}_{E}(q^{2})+\frac{2\left[S^{\mu},S^{\nu}\right]q_{\nu}}{m+m'}\mathscr{G}_{M}(q^{2})\right]u(p).\tag{C.14}$$

The decay width is expressed by the magnetic form factor $\mathscr{G}_{M}(0)$ as

$$\Gamma = \frac{4\alpha|\boldsymbol{p}_{\gamma}|^{3}}{(m+m')^{2}}\left|\mathscr{G}_{M}(0)\right|^{2}.\tag{C.15}$$

(4) *Spin-$\frac{3}{2}\rightarrow$spin-$\frac{1}{2}+\gamma$ transitions:*

$$\langle\psi_{6^{*}}\left|\mathscr{J}_{\text{em}\mu}\right|\psi\rangle = e\bar{u}^{\rho}\left(p'\right)\left[2\mathscr{G}_{1}(q^{2})\left(q_{\rho}S_{\mu}-q\cdot S\,g_{\rho\mu}\right)+\mathscr{G}_{2}(q^{2})\frac{2m'}{m+m'}\left(q_{\rho}v_{\mu}-q\cdot v g_{\rho\mu}\right)q\cdot S\right]u(p),\tag{C.16}$$

which is suitable for the on-shell transitions (for complete form, see Ref. [858]). This form factor corresponding to leading M1 and E2 transitions are given by

$$\begin{aligned}
\mathscr{G}_{M}(q^{2}) &= \frac{1}{4}\left[\mathscr{G}_{1}\frac{m_{+}\left(3m'+m\right)-q^{2}}{m'}+\mathscr{G}_{2}\left(m_{+}m_{-}-q^{2}\right)+2\left(\mathscr{G}_{3}+\mathscr{G}_{2}\right)q^{2}\right], \\
\mathscr{G}_{Q}(q^{2}) &= \frac{1}{4}\left[\mathscr{G}_{1}\frac{m_{+}m_{-}+q^{2}}{m'}+\mathscr{G}_{2}\left(m_{+}m_{-}-q^{2}\right)+2\left(\mathscr{G}_{2}+\mathscr{G}_{3}\right)q^{2}\right],
\end{aligned}\tag{C.17}$$

with $m_{\pm} = m'\pm m$. Then one can find the ratio

$$\frac{\mathscr{G}_{Q}(0)}{\mathscr{G}_{M}(0)} = \frac{m_{-}}{m}\left(\frac{1}{4}+\frac{\mathscr{G}_{2}}{4\mathscr{G}_{1}}\right)\tag{C.18}$$

shall be very small due to a suppressed factor m_{-}/m, which can qualitatively interpret the ratio obtained by Savage [853]. The decay widths are given with the helicity amplitudes as

$$\Gamma = \frac{mm'}{8\pi}\left(1-\frac{m^{2}}{m'^{2}}\right)^{2}\left[A_{3/2}^{2}(0)+A_{1/2}^{2}(0)\right],\tag{C.19}$$

with the helicity amplitudes

$$A_{3/2}\left(q^{2}\right) = -\sqrt{\frac{\pi\alpha\omega}{2m^{2}}}\left[\mathscr{G}_{M}\left(q^{2}\right)+\mathscr{G}_{Q}\left(q^{2}\right)\right], \qquad A_{1/2}\left(q^{2}\right) = -\sqrt{\frac{\pi\alpha\omega}{6m^{2}}}\left[\mathscr{G}_{M}\left(q^{2}\right)-3\mathscr{G}_{Q}\left(q^{2}\right)\right],\tag{C.20}$$

where $\omega = (m'^{2}-m^{2}+q^{2})/2m'$.

References

[1] R. L. Workman, et al., Review of Particle Physics, PTEP 2022 (2022) 083C01. `doi:10.1093/ptep/ptac097`.

[2] R. Aaij, et al., Observation of $J/\psi p$ Resonances Consistent with Pentaquark States in $\Lambda_b^0 \to J/\psi K^- p$ Decays, Phys. Rev. Lett. 115 (2015) 072001. `arXiv:1507.03414`, `doi:10.1103/PhysRevLett.115.072001`.

[3] R. Aaij, et al., Observation of a narrow pentaquark state, $P_c(4312)^+$, and of two-peak structure of the $P_c(4450)^+$, Phys. Rev. Lett. 122 (22) (2019) 222001. `arXiv:1904.03947`, `doi:10.1103/PhysRevLett.122.222001`.

[4] R. Aaij, et al., Observation of an exotic narrow doubly charmed tetraquark, Nature Phys. 18 (7) (2022) 751–754. `arXiv:2109.01038`, `doi:10.1038/s41567-022-01614-y`.

[5] R. Aaij, et al., Study of the doubly charmed tetraquark T_{cc}^+, Nature Commun. 13 (1) (2022) 3351. `arXiv:2109.01056`, `doi:10.1038/s41467-022-30206-w`.

[6] H.-X. Chen, W. Chen, X. Liu, S.-L. Zhu, The hidden-charm pentaquark and tetraquark states, Phys. Rept. 639 (2016) 1–121. `arXiv:1601.02092`, `doi:10.1016/j.physrep.2016.05.004`.

[7] H.-X. Chen, W. Chen, X. Liu, Y.-R. Liu, S.-L. Zhu, A review of the open charm and open bottom systems, Rept. Prog. Phys. 80 (7) (2017) 076201. `arXiv:1609.08928`, `doi:10.1088/1361-6633/aa6420`.

[8] R. F. Lebed, R. E. Mitchell, E. S. Swanson, Heavy-Quark QCD Exotica, Prog. Part. Nucl. Phys. 93 (2017) 143–194. `arXiv:1610.04528`, `doi:10.1016/j.ppnp.2016.11.003`.

[9] A. Esposito, A. Pilloni, A. D. Polosa, Multiquark Resonances, Phys. Rept. 668 (2017) 1–97. `arXiv:1611.07920`, `doi:10.1016/j.physrep.2016.11.002`.

[10] A. Hosaka, T. Iijima, K. Miyabayashi, Y. Sakai, S. Yasui, Exotic hadrons with heavy flavors: X, Y, Z, and related states, PTEP 2016 (6) (2016) 062C01. `arXiv:1603.09229`, `doi:10.1093/ptep/ptw045`.

[11] F.-K. Guo, C. Hanhart, U.-G. Meißner, Q. Wang, Q. Zhao, B.-S. Zou, Hadronic molecules, Rev. Mod. Phys. 90 (1) (2018) 015004. `arXiv:1705.00141`, `doi:10.1103/RevModPhys.90.015004`.

[12] A. Ali, J. S. Lange, S. Stone, Exotics: Heavy Pentaquarks and Tetraquarks, Prog. Part. Nucl. Phys. 97 (2017) 123–198. `arXiv:1706.00610`, `doi:10.1016/j.ppnp.2017.08.003`.

[13] Y.-R. Liu, H.-X. Chen, W. Chen, X. Liu, S.-L. Zhu, Pentaquark and Tetraquark states, Prog. Part. Nucl. Phys. 107 (2019) 237–320. `arXiv:1903.11976`, `doi:10.1016/j.ppnp.2019.04.003`.

[14] N. Brambilla, S. Eidelman, C. Hanhart, A. Nefediev, C.-P. Shen, C. E. Thomas, A. Vairo, C.-Z. Yuan, The XYZ states: experimental and theoretical status and perspectives, Phys. Rept. 873 (2020) 1–154. `arXiv:1907.07583`, `doi:10.1016/j.physrep.2020.05.001`.

[15] W. Lucha, D. Melikhov, H. Sazdjian, Tetraquarks in large-N_c QCD, Prog. Part. Nucl. Phys. 120 (2021) 103867. `arXiv:2102.02542`, `doi:10.1016/j.ppnp.2021.103867`.

[16] S. Chen, Y. Li, W. Qian, Z. Shen, Y. Xie, Z. Yang, L. Zhang, Y. Zhang, Heavy Flavour Physics and CP Violation at LHCb: a Ten-Year Review, Front. Phys. 18 (2023) 44601. `arXiv:2111.14360`, `doi:10.1007/s11467-022-1247-1`.

[17] H.-X. Chen, W. Chen, X. Liu, Y.-R. Liu, S.-L. Zhu, An updated review of the new hadron states, Rept. Prog. Phys. 86 (2) (2023) 026201. `arXiv:2204.02649`, `doi:10.1088/1361-6633/aca3b6`.

[18] M. Gell-Mann, A Schematic Model of Baryons and Mesons, Phys. Lett. 8 (1964) 214–215. `doi:10.1016/S0031-9163(64)92001-3`.

[19] G. Zweig, An SU(3) model for strong interaction symmetry and its breaking. Version 2, 1964, pp. 22–101.

[20] S. Godfrey, N. Isgur, Mesons in a Relativized Quark Model with Chromodynamics, Phys. Rev. D 32 (1985) 189–231. `doi:10.1103/PhysRevD.32.189`.

[21] S. Godfrey, R. Kokoski, The Properties of P-Wave Mesons with One Heavy Quark, Phys. Rev. D 43 (1991) 1679–1687. `doi:10.1103/PhysRevD.43.1679`.

[22] B. Aubert, et al., Observation of a narrow meson decaying to $D_s^+ \pi^0$ at a mass of 2.32 GeV/c^2, Phys. Rev. Lett. 90 (2003) 242001. `arXiv:hep-ex/0304021`, `doi:10.1103/PhysRevLett.90.242001`.

[23] D. Besson, et al., Observation of a narrow resonance of mass 2.46 GeV/c^2 decaying to $D_s^{*+} \pi^0$ and confirmation of the $D_{sJ}^*(2317)$ state, Phys. Rev. D 68 (2003) 032002, [Erratum: Phys.Rev.D 75, 119908 (2007)]. `arXiv:hep-ex/0305100`, `doi:10.1103/PhysRevD.68.032002`.

[24] Y. Mikami, et al., Measurements of the D_{sJ} resonance properties, Phys. Rev. Lett. 92 (2004) 012002. `arXiv:hep-ex/0307052`, `doi:10.1103/PhysRevLett.92.012002`.

[25] B. Aubert, et al., A Study of the $D_{sJ}^*(2317)$ and $D_{sJ}(2460)$ Mesons in Inclusive $c\bar{c}$ Production Near $\sqrt{s} = 10.6$ GeV, Phys. Rev. D 74 (2006) 032007. `arXiv:hep-ex/0604030`, `doi:10.1103/PhysRevD.74.032007`.

[26] B. Aubert, et al., Observation of a narrow meson decaying to $D_s^+ \pi^0 \gamma$ at a mass of 2.458 GeV/c^2, Phys. Rev. D 69 (2004) 031101. `arXiv:hep-ex/0310050`, `doi:10.1103/PhysRevD.69.031101`.

[27] Y.-B. Dai, C.-S. Huang, C. Liu, S.-L. Zhu, Understanding the $D_{sJ}^+(2317)$ and $D_{sJ}^+(2460)$ with sum rules in HQET, Phys. Rev. D 68 (2003) 114011. `arXiv:hep-ph/0306274`, `doi:10.1103/PhysRevD.68.114011`.

[28] D. S. Hwang, D.-W. Kim, Mass of $D_{sJ}^*(2317)$ and coupled-channel effect, Phys. Lett. B 601 (2004) 137–143. `arXiv:hep-ph/0408154`, `doi:10.1016/j.physletb.2004.09.040`.

[29] Y. A. Simonov, J. A. Tjon, The Coupled-channel analysis of the D and D_s mesons, Phys. Rev. D 70 (2004) 114013. `arXiv:hep-ph/0409361`, `doi:10.1103/PhysRevD.70.114013`.

[30] H.-Y. Cheng, F.-S. Yu, Near mass degeneracy in the scalar meson sector: Implications for $B_{(s)0}^*$ and $B_{(s)1}'$ mesons, Phys. Rev. D 89 (11) (2014) 114017. `arXiv:1404.3771`, `doi:10.1103/PhysRevD.89.114017`.

[31] Q.-T. Song, D.-Y. Chen, X. Liu, T. Matsuki, Charmed-strange mesons revisited: mass spectra and strong decays, Phys. Rev. D 91 (2015) 054031. `arXiv:1501.03575`, `doi:10.1103/PhysRevD.91.054031`.

[32] Y.-B. Dai, X.-Q. Li, S.-L. Zhu, Y.-B. Zuo, Contribution of DK continuum in the QCD sum rule for $D_{sJ}(2317)$, Eur. Phys. J. C 55 (2008) 249–258. `arXiv:hep-ph/0610327`, `doi:10.1140/epjc/s10052-008-0591-9`.

[33] H.-Y. Cheng, F.-S. Yu, Masses of Scalar and Axial-Vector B Mesons Revisited, Eur. Phys. J. C 77 (10) (2017) 668. `arXiv:1704.01208`, `doi:10.1140/epjc/s10052-017-5252-4`.

[34] S.-Q. Luo, B. Chen, X. Liu, T. Matsuki, Predicting a new resonance as charmed-strange baryonic analog of $D_{s0}^*(2317)$, Phys. Rev. D 103 (7) (2021) 074027. arXiv:2102.00679, doi:10.1103/PhysRevD.103.074027.

[35] Z.-Y. Zhou, Z. Xiao, Two-pole structures in a relativistic Friedrichs–Lee–QPC scheme, Eur. Phys. J. C 81 (6) (2021) 551. arXiv:2008.08002, doi:10.1140/epjc/s10052-021-09329-9.

[36] Y. Tan, J. Ping, $D_{s0}^*(2317)$ and $D_{s1}(2460)$ in an unquenched quark model (11 2021). arXiv:2111.04677.

[37] E. E. Kolomeitsev, M. F. M. Lutz, On Heavy light meson resonances and chiral symmetry, Phys. Lett. B 582 (2004) 39–48. arXiv:hep-ph/0307133, doi:10.1016/j.physletb.2003.10.118.

[38] A. P. Szczepaniak, Description of the $D_s^*(2320)$ resonance as the $D\pi$ atom, Phys. Lett. B 567 (2003) 23–26. arXiv:hep-ph/0305060, doi:10.1016/S0370-2693(03)00865-7.

[39] J. Hofmann, M. F. M. Lutz, Open charm meson resonances with negative strangeness, Nucl. Phys. A 733 (2004) 142–152. arXiv:hep-ph/0308263, doi:10.1016/j.nuclphysa.2003.12.013.

[40] E. van Beveren, G. Rupp, Observed $D_s(2317)$ and tentative $D(2100$–$2300)$ as the charmed cousins of the light scalar nonet, Phys. Rev. Lett. 91 (2003) 012003. arXiv:hep-ph/0305035, doi:10.1103/PhysRevLett.91.012003.

[41] T. Barnes, F. E. Close, H. J. Lipkin, Implications of a DK molecule at 2.32 GeV, Phys. Rev. D 68 (2003) 054006. arXiv:hep-ph/0305025, doi:10.1103/PhysRevD.68.054006.

[42] D. Gamermann, E. Oset, D. Strottman, M. J. Vicente Vacas, Dynamically generated open and hidden charm meson systems, Phys. Rev. D 76 (2007) 074016. arXiv:hep-ph/0612179, doi:10.1103/PhysRevD.76.074016.

[43] F.-K. Guo, P.-N. Shen, H.-C. Chiang, Dynamically generated 1^+ heavy mesons, Phys. Lett. B 647 (2007) 133–139. arXiv:hep-ph/0610008, doi:10.1016/j.physletb.2007.01.050.

[44] F.-K. Guo, P.-N. Shen, H.-C. Chiang, R.-G. Ping, B.-S. Zou, Dynamically generated 0^+ heavy mesons in a heavy chiral unitary approach, Phys. Lett. B 641 (2006) 278–285. arXiv:hep-ph/0603072, doi:10.1016/j.physletb.2006.08.064.

[45] J. M. Flynn, J. Nieves, Elastic S-wave $B\pi$, $D\pi$, DK and $K\pi$ scattering from lattice calculations of scalar form-factors in semileptonic decays, Phys. Rev. D 75 (2007) 074024. arXiv:hep-ph/0703047, doi:10.1103/PhysRevD.75.074024.

[46] A. Faessler, T. Gutsche, V. E. Lyubovitskij, Y.-L. Ma, Strong and radiative decays of the $D_{s0}^*(2317)$ meson in the DK-molecule picture, Phys. Rev. D 76 (2007) 014005. arXiv:0705.0254, doi:10.1103/PhysRevD.76.014005.

[47] F.-K. Guo, C. Hanhart, U.-G. Meissner, Interactions between heavy mesons and Goldstone bosons from chiral dynamics, Eur. Phys. J. A 40 (2009) 171–179. arXiv:0901.1597, doi:10.1140/epja/i2009-10762-1.

[48] Z.-X. Xie, G.-Q. Feng, X.-H. Guo, Analyzing $D_{s0}^*(2317)^+$ in the DK molecule picture in the Beth-Salpeter approach, Phys. Rev. D 81 (2010) 036014. doi:10.1103/PhysRevD.81.036014.

[49] M. Cleven, F.-K. Guo, C. Hanhart, U.-G. Meissner, Light meson mass dependence of the positive parity heavy-strange mesons, Eur. Phys. J. A 47 (2011) 19. arXiv:1009.3804, doi:10.1140/epja/i2011-11019-2.

[50] X.-G. Wu, Q. Zhao, The mixing of $D_{s1}(2460)$ and $D_{s1}(2536)$, Phys. Rev. D 85 (2012) 034040. arXiv:1111.4002, doi:10.1103/PhysRevD.85.034040.

[51] Z.-H. Guo, U.-G. Meißner, D.-L. Yao, New insights into the $D_{s0}^*(2317)$ and other charm scalar mesons, Phys. Rev. D 92 (9) (2015) 094008. arXiv:1507.03123, doi:10.1103/PhysRevD.92.094008.

[52] M. Albaladejo, D. Jido, J. Nieves, E. Oset, $D_{s0}^*(2317)$ and DK scattering in B decays from BaBar and LHCb data, Eur. Phys. J. C 76 (6) (2016) 300. arXiv:1604.01193, doi:10.1140/epjc/s10052-016-4144-3.

[53] M.-L. Du, F.-K. Guo, U.-G. Meißner, D.-L. Yao, Study of open-charm 0^+ states in unitarized chiral effective theory with one-loop potentials, Eur. Phys. J. C 77 (11) (2017) 728. arXiv:1703.10836, doi:10.1140/epjc/s10052-017-5287-6.

[54] Z.-H. Guo, L. Liu, U.-G. Meißner, J. A. Oller, A. Rusetsky, Towards a precise determination of the scattering amplitudes of the charmed and light-flavor pseudoscalar mesons, Eur. Phys. J. C 79 (1) (2019) 13. arXiv:1811.05585, doi:10.1140/epjc/s10052-018-6518-1.

[55] M. Albaladejo, P. Fernandez-Soler, J. Nieves, P. G. Ortega, Contribution of constituent quark model $c\bar{s}$ states to the dynamics of the $D_{s0}^*(2317)$ and $D_{s1}(2460)$ resonances, Eur. Phys. J. C 78 (9) (2018) 722. arXiv:1805.07104, doi:10.1140/epjc/s10052-018-6176-3.

[56] T.-W. Wu, M.-Z. Liu, L.-S. Geng, E. Hiyama, M. P. Valderrama, DK, DDK, and $DDDK$ molecules–understanding the nature of the $D_{s0}^*(2317)$, Phys. Rev. D 100 (3) (2019) 034029. arXiv:1906.11995, doi:10.1103/PhysRevD.100.034029.

[57] S.-Y. Kong, J.-T. Zhu, D. Song, J. He, Heavy-strange meson molecules and possible candidates $D_{s0}^*(2317)$, $D_{s1}(2460)$, and $X_0(2900)$, Phys. Rev. D 104 (9) (2021) 094012. arXiv:2106.07272, doi:10.1103/PhysRevD.104.094012.

[58] E. B. Gregory, F.-K. Guo, C. Hanhart, S. Krieg, T. Luu, Confirmation of the existence of an exotic state in the πD system (6 2021). arXiv:2106.15391.

[59] H.-Y. Cheng, W.-S. Hou, B decays as spectroscope for charmed four quark states, Phys. Lett. B 566 (2003) 193–200. arXiv:hep-ph/0305038, doi:10.1016/S0370-2693(03)00834-7.

[60] Y.-Q. Chen, X.-Q. Li, A Comprehensive four-quark interpretation of $D_s(2317)$, $D_s(2457)$ and $D_s(2632)$, Phys. Rev. Lett. 93 (2004) 232001. arXiv:hep-ph/0407062, doi:10.1103/PhysRevLett.93.232001.

[61] V. Dmitrasinovic, $D_{s0}^+(2317) - D_0(2308)$ mass difference as evidence for tetraquarks, Phys. Rev. Lett. 94 (2005) 162002. doi:10.1103/PhysRevLett.94.162002.

[62] H. Kim, Y. Oh, $D_s(2317)$ as a four-quark state in QCD sum rules, Phys. Rev. D 72 (2005) 074012. arXiv:hep-ph/0508251, doi:10.1103/PhysRevD.72.074012.

[63] J.-R. Zhang, Revisiting $D_{s0}^*(2317)$ as a 0^+ tetraquark state from QCD sum rules, Phys. Lett. B 789 (2019) 432–437. arXiv:1801.08725, doi:10.1016/j.physletb.2019.01.001.

[64] K. Terasaki, BABAR resonance as a new window of hadron physics, Phys. Rev. D 68 (2003) 011501. arXiv:hep-ph/0305213, doi:10.1103/PhysRevD.68.011501.

[65] T. E. Browder, S. Pakvasa, A. A. Petrov, Comment on the new $D_s^{(*)+}\pi^0$ resonances, Phys. Lett. B 578 (2004) 365–368. arXiv:hep-ph/0307054, doi:10.1016/j.physletb.2003.10.067.

[66] L. Maiani, F. Piccinini, A. D. Polosa, V. Riquer, Diquark-antidiquarks with hidden or open charm and the nature of $X(3872)$, Phys. Rev. D 71 (2005) 014028. arXiv:hep-ph/0412098, doi:10.1103/PhysRevD.71.014028.

[67] Y. Dong, A. Faessler, V. E. Lyubovitskij, Description of heavy exotic resonances as molecular states using phenomenological Lagrangians, Prog. Part. Nucl. Phys. 94 (2017) 282–310. `doi:10.1016/j.ppnp.2017.01.002`.

[68] D.-L. Yao, L.-Y. Dai, H.-Q. Zheng, Z.-Y. Zhou, A review on partial-wave dynamics with chiral effective field theory and dispersion relation, Rept. Prog. Phys. 84 (7) (2021) 076201. `arXiv:2009.13495`, `doi:10.1088/1361-6633/abfa6f`.

[69] V. M. Abazov, et al., Observation of the doubly strange b baryon Ω_b^-, Phys. Rev. Lett. 101 (2008) 232002. `arXiv:0808.4142`, `doi:10.1103/PhysRevLett.101.232002`.

[70] B. Aubert, et al., Observation of a charmed baryon decaying to $D^0 p$ at a mass near 2.94 GeV/c^2, Phys. Rev. Lett. 98 (2007) 012001. `arXiv:hep-ex/0603052`, `doi:10.1103/PhysRevLett.98.012001`.

[71] K. Abe, et al., Experimental constraints on the possible J^P quantum numbers of the $\Lambda_c(2880)^+$, Phys. Rev. Lett. 98 (2007) 262001. `arXiv:hep-ex/0608043`, `doi:10.1103/PhysRevLett.98.262001`.

[72] R. Aaij, et al., Study of the $D^0 p$ amplitude in $\Lambda_b^0 \to D^0 p \pi^-$ decays, JHEP 05 (2017) 030. `arXiv:1701.07873`, `doi:10.1007/JHEP05(2017)030`.

[73] Y. B. Li, et al., Evidence of a new excited charmed baryon decaying to $\Sigma_c(2455)^{0,++}\pi^{\pm}$, Phys. Rev. Lett. 130 (3) (2023) 031901. `arXiv:2206.08822`, `doi:10.1103/PhysRevLett.130.031901`.

[74] R. Mizuk, et al., Observation of an isotriplet of excited charmed baryons decaying to $\Lambda_c^+\pi$, Phys. Rev. Lett. 94 (2005) 122002. `arXiv:hep-ex/0412069`, `doi:10.1103/PhysRevLett.94.122002`.

[75] B. Aubert, et al., Measurements of $\mathcal{B}(\bar{B}^0 \to \Lambda_c^+ \bar{p})$ and $\mathcal{B}(B^- \to \Lambda_c^+ \bar{p}\pi^-)$ and Studies of $\Lambda_c^+\pi^-$ Resonances, Phys. Rev. D 78 (2008) 112003. `arXiv:0807.4974`, `doi:10.1103/PhysRevD.78.112003`.

[76] A. Valcarce, H. Garcilazo, J. Vijande, Towards an understanding of heavy baryon spectroscopy, Eur. Phys. J. A 37 (2008) 217–225. `arXiv:0807.2973`, `doi:10.1140/epja/i2008-10616-4`.

[77] D. Ebert, R. N. Faustov, V. O. Galkin, Masses of excited heavy baryons in the relativistic quark model, Phys. Lett. B 659 (2008) 612–620. `arXiv:0705.2957`, `doi:10.1016/j.physletb.2007.11.037`.

[78] W. Roberts, M. Pervin, Heavy baryons in a quark model, Int. J. Mod. Phys. A 23 (2008) 2817–2860. `arXiv:0711.2492`, `doi:10.1142/S0217751X08041219`.

[79] Q.-F. Lü, L.-Y. Xiao, Z.-Y. Wang, X.-H. Zhong, Strong decay of $\Lambda_c(2940)$ as a $2P$ state in the Λ_c family, Eur. Phys. J. C 78 (7) (2018) 599. `arXiv:1806.01076`, `doi:10.1140/epjc/s10052-018-6083-7`.

[80] D. Ebert, R. N. Faustov, V. O. Galkin, Spectroscopy and Regge trajectories of heavy baryons in the relativistic quark-diquark picture, Phys. Rev. D 84 (2011) 014025. `arXiv:1105.0583`, `doi:10.1103/PhysRevD.84.014025`.

[81] H.-Y. Cheng, C.-K. Chua, Strong Decays of Charmed Baryons in Heavy Hadron Chiral Perturbation Theory, Phys. Rev. D 75 (2007) 014006. `arXiv:hep-ph/0610283`, `doi:10.1103/PhysRevD.75.014006`.

[82] B. Chen, K.-W. Wei, X. Liu, T. Matsuki, Low-lying charmed and charmed-strange baryon states, Eur. Phys. J. C 77 (3) (2017) 154. `arXiv:1609.07967`, `doi:10.1140/epjc/s10052-017-4708-x`.

[83] H. Garcilazo, J. Vijande, A. Valcarce, Faddeev study of heavy baryon spectroscopy, J. Phys. G 34 (2007) 961–976. `arXiv:hep-ph/0703257`, `doi:10.1088/0954-3899/34/5/014`.

[84] K.-L. Wang, Y.-X. Yao, X.-H. Zhong, Q. Zhao, Strong and radiative decays of the low-lying S- and P-wave singly heavy baryons, Phys. Rev. D 96 (11) (2017) 116016. `arXiv:1709.04268`, `doi:10.1103/PhysRevD.96.116016`.

[85] X.-G. He, X.-Q. Li, X. Liu, X.-Q. Zeng, $\Lambda_c^+(2940)$: A Possible molecular state?, Eur. Phys. J. C 51 (2007) 883–889. `arXiv:hep-ph/0606015`, `doi:10.1140/epjc/s10052-007-0347-y`.

[86] J. He, Y.-T. Ye, Z.-F. Sun, X. Liu, The observed charmed hadron $\Lambda_c(2940)^+$ and the D^*N interaction, Phys. Rev. D 82 (2010) 114029. `arXiv:1008.1500`, `doi:10.1103/PhysRevD.82.114029`.

[87] P. G. Ortega, D. R. Entem, F. Fernandez, Quark model description of the $\Lambda_c(2940)^+$ as a molecular D^*N state and the possible existence of the $\Lambda_b(6248)$, Phys. Lett. B 718 (2013) 1381–1384. `arXiv:1210.2633`, `doi:10.1016/j.physletb.2012.12.025`.

[88] Y. Dong, A. Faessler, T. Gutsche, V. E. Lyubovitskij, Strong two-body decays of the $\Lambda_c(2940)^+$ in a hadronic molecule picture, Phys. Rev. D 81 (2010) 014006. `arXiv:0910.1204`, `doi:10.1103/PhysRevD.81.014006`.

[89] Y. Dong, A. Faessler, T. Gutsche, S. Kumano, V. E. Lyubovitskij, Radiative decay of $\Lambda_c(2940)^+$ in a hadronic molecule picture, Phys. Rev. D 82 (2010) 034035. `arXiv:1006.4018`, `doi:10.1103/PhysRevD.82.034035`.

[90] J.-R. Zhang, S-wave $D^{(*)}N$ molecular states: $\Sigma_c(2800)$ and $\Lambda_c(2940)^+$?, Phys. Rev. D 89 (9) (2014) 096006. `arXiv:1212.5325`, `doi:10.1103/PhysRevD.89.096006`.

[91] L. Zhao, H. Huang, J. Ping, ND and NB systems in quark delocalization color screening model, Eur. Phys. J. A 53 (2) (2017) 28. `arXiv:1612.00350`, `doi:10.1140/epja/i2017-12219-4`.

[92] D. Zhang, D. Yang, X.-F. Wang, K. Nakayama, Possible S-wave $ND^{(*)}$ and $N\bar{B}^{(*)}$ bound states in a chiral quark model (3 2019). `arXiv:1903.01207`.

[93] B. Wang, L. Meng, S.-L. Zhu, $D^{(*)}N$ interaction and the structure of $\Sigma_c(2800)$ and $\Lambda_c(2940)$ in chiral effective field theory, Phys. Rev. D 101 (9) (2020) 094035. `arXiv:2003.05688`, `doi:10.1103/PhysRevD.101.094035`.

[94] Y. Dong, A. Faessler, T. Gutsche, V. E. Lyubovitskij, Charmed baryon $\Sigma_c(2800)$ as a ND hadronic molecule, Phys. Rev. D 81 (2010) 074011. `arXiv:1002.0218`, `doi:10.1103/PhysRevD.81.074011`.

[95] C. E. Jimenez-Tejero, A. Ramos, I. Vidana, Dynamically generated open charmed baryons beyond the zero range approximation, Phys. Rev. C 80 (2009) 055206. `arXiv:0907.5316`, `doi:10.1103/PhysRevC.80.055206`.

[96] E. Klempt, J.-M. Richard, Baryon spectroscopy, Rev. Mod. Phys. 82 (2010) 1095–1153. `arXiv:0901.2055`, `doi:10.1103/RevModPhys.82.1095`.

[97] V. Crede, W. Roberts, Progress towards understanding baryon resonances, Rept. Prog. Phys. 76 (2013) 076301. `arXiv:1302.7299`, `doi:10.1088/0034-4885/76/7/076301`.

[98] H.-Y. Cheng, Charmed baryons circa 2015, Front. Phys. (Beijing) 10 (6) (2015) 101406. `doi:10.1007/s11467-015-0483-z`.

[99] Y. Kato, T. Iijima, Open charm hadron spectroscopy at B-factories, Prog. Part. Nucl. Phys. 105 (2019) 61–81. `arXiv:1810.03748`, `doi:10.1016/j.ppnp.2019.01.001`.

[100] H.-Y. Cheng, Phenomenological Study of Heavy Hadron Lifetimes, JHEP 11 (2018) 014. `arXiv:1807.00916`, `doi:10.1007/JHEP11(2018)014`.

[101] L. A. Copley, N. Isgur, G. Karl, Charmed Baryons in a Quark Model with Hyperfine Interactions, Phys. Rev. D 20 (1979) 768, [Erratum: Phys.Rev.D 23, 817 (1981)]. `doi:10.1103/PhysRevD.20.768`.

[102] T. Yoshida, E. Hiyama, A. Hosaka, M. Oka, K. Sadato, Spectrum of heavy baryons in the quark model, Phys. Rev. D 92 (11) (2015) 114029. `arXiv:1510.01067`, `doi:10.1103/PhysRevD.92.114029`.

[103] S. Capstick, N. Isgur, Baryons in a Relativized Quark Model with Chromodynamics, AIP Conf. Proc. 132 (1985) 267–271. `doi:10.1063/1.35361`.

[104] D. Ebert, R. N. Faustov, V. O. Galkin, Masses of heavy baryons in the relativistic quark model, Phys. Rev. D 72 (2005) 034026. `arXiv:hep-ph/0504112`, `doi:10.1103/PhysRevD.72.034026`.

[105] Z. Shah, K. Thakkar, A. K. Rai, P. C. Vinodkumar, Mass spectra and Regge trajectories of Λ_c^+, Σ_c^0, Ξ_c^0 and Ω_c^0 baryons, Chin. Phys. C 40 (12) (2016) 123102. `arXiv:1609.08464`, `doi:10.1088/1674-1137/40/12/123102`.

[106] Q.-F. Lü, Y. Dong, X. Liu, T. Matsuki, Puzzle of the Λ_c Spectrum, Nucl. Phys. Rev. 35 (1) (2018) 1–4. `arXiv:1610.09605`, `doi:10.11804/NuclPhysRev.35.01.001`.

[107] K. Gandhi, Z. Shah, A. K. Rai, Spectrum of nonstrange singly charmed baryons in the constituent quark model, Int. J. Theor. Phys. 59 (4) (2020) 1129–1156. `arXiv:1912.05859`, `doi:10.1007/s10773-020-04394-4`.

[108] R. N. Faustov, V. O. Galkin, Heavy Baryon Spectroscopy in the Relativistic Quark Model, Particles 3 (1) (2020) 234–244. `doi:10.3390/particles3010019`.

[109] S. Migura, D. Merten, B. Metsch, H.-R. Petry, Charmed baryons in a relativistic quark model, Eur. Phys. J. A 28 (2006) 41. `arXiv:hep-ph/0602153`, `doi:10.1140/epja/i2006-10017-9`.

[110] G. Yang, J. Ping, J. Segovia, The S- and P-Wave Low-Lying Baryons in the Chiral Quark Model, Few Body Syst. 59 (6) (2018) 113. `arXiv:1709.09315`, `doi:10.1007/s00601-018-1433-4`.

[111] E. Bagan, M. Chabab, H. G. Dosch, S. Narison, The Heavy baryons Σ_c, Σ_b from QCD spectral sum rules, Phys. Lett. B 278 (1992) 367–370. `doi:10.1016/0370-2693(92)90208-L`.

[112] X. Liu, H.-X. Chen, Y.-R. Liu, A. Hosaka, S.-L. Zhu, Bottom baryons, Phys. Rev. D 77 (2008) 014031. `arXiv:0710.0123`, `doi:10.1103/PhysRevD.77.014031`.

[113] H.-X. Chen, W. Chen, Q. Mao, A. Hosaka, X. Liu, S.-L. Zhu, P-wave charmed baryons from QCD sum rules, Phys. Rev. D 91 (5) (2015) 054034. `arXiv:1502.01103`, `doi:10.1103/PhysRevD.91.054034`.

[114] H.-X. Chen, Q. Mao, A. Hosaka, X. Liu, S.-L. Zhu, D-wave charmed and bottomed baryons from QCD sum rules, Phys. Rev. D 94 (11) (2016) 114016. `arXiv:1611.02677`, `doi:10.1103/PhysRevD.94.114016`.

[115] Z.-G. Wang, Analysis of $\Omega_c^*(css)$ and $\Omega_b^*(bss)$ with QCD sum rules, Eur. Phys. J. C 54 (2008) 231–237. `arXiv:0704.1106`, `doi:10.1140/epjc/s10052-008-0521-x`.

[116] H. Y. Jin, J. G. Korner, QCD sum rule for heavy baryons, Phys. Rev. D 64 (2001) 114006. `arXiv:hep-ph/0105023`, `doi:10.1103/PhysRevD.64.114006`.

[117] T. M. Aliev, K. Azizi, Y. Sarac, H. Sundu, Structure of the $\Xi_b(6227)^-$ resonance, Phys. Rev. D 98 (9) (2018) 094014. `arXiv:1808.08032`, `doi:10.1103/PhysRevD.98.094014`.

[118] P. Hasenfratz, R. R. Horgan, J. Kuti, J. M. Richard, Heavy Baryon Spectroscopy in the QCD Bag Model, Phys. Lett. B 94 (1980) 401–404. `doi:10.1016/0370-2693(80)90906-5`.

[119] D. Izatt, C. E. Detar, M. Stephenson, Spectroscopy of Hadrons Containing One Heavy Quark, Nucl. Phys. B 199 (1982) 269–289. `doi:10.1016/0550-3213(82)90347-9`.

[120] T. M. Aliev, K. Azizi, M. Savci, Spin-3/2 to spin-1/2 heavy baryons and pseudoscalar mesons transitions in QCD, Eur. Phys. J. C 71 (2011) 1675. `arXiv:1012.5935`, `doi:10.1140/epjc/s10052-011-1675-5`.

[121] W. Y. P. Hwang, D. B. Lichtenberg, Mass Splitting of Heavy Baryon Isospin Multiplets, Phys. Rev. D 35 (1987) 3526. `doi:10.1103/PhysRevD.35.3526`.

[122] I. M. Narodetskii, M. A. Trusov, The Heavy baryons in the nonperturbative string approach, Phys. Atom. Nucl. 65 (2002) 917–924. `arXiv:hep-ph/0104019`, `doi:10.1134/1.1481486`.

[123] E. E. Jenkins, Heavy baryon masses in the $1/m_Q$ and $1/N_c$ expansions, Phys. Rev. D 54 (1996) 4515–4531. `arXiv:hep-ph/9603449`, `doi:10.1103/PhysRevD.54.4515`.

[124] Y. Heo, X.-Y. Guo, M. F. M. Lutz, Framework for the chiral extrapolation of the charmed baryon ground-state masses, Phys. Rev. D 98 (5) (2018) 054012. `arXiv:1806.08602`, `doi:10.1103/PhysRevD.98.054012`.

[125] T. Ito, Y. Matsui, The $\Xi_Q - \Xi_Q'$ mixing and heavy baryon masses, Prog. Theor. Phys. 96 (1996) 659–664. `arXiv:hep-ph/9605289`, `doi:10.1143/PTP.96.659`.

[126] Y. Kim, E. Hiyama, M. Oka, K. Suzuki, Spectrum of singly heavy baryons from a chiral effective theory of diquarks, Phys. Rev. D 102 (1) (2020) 014004. `arXiv:2003.03525`, `doi:10.1103/PhysRevD.102.014004`.

[127] M. Harada, Y.-R. Liu, M. Oka, K. Suzuki, Chiral effective theory of diquarks and the $U_A(1)$ anomaly, Phys. Rev. D 101 (5) (2020) 054038. `arXiv:1912.09659`, `doi:10.1103/PhysRevD.101.054038`.

[128] Y.-s. Oh, B.-Y. Park, Excited states of heavy baryons in the Skyrme model, Phys. Rev. D 53 (1996) 1605–1615. `arXiv:hep-ph/9510268`, `doi:10.1103/PhysRevD.53.1605`.

[129] B. Chen, K.-W. Wei, A. Zhang, Assignments of Λ_Q and Ξ_Q baryons in the heavy quark-light diquark picture, Eur. Phys. J. A 51 (2015) 82. `arXiv:1406.6561`, `doi:10.1140/epja/i2015-15082-3`.

[130] K. C. Bowler, R. D. Kenway, O. Oliveira, D. G. Richards, P. Uberholz, L. Lellouch, J. Nieves, C. T. Sachrajda, N. Stella, H. Wittig, Heavy baryon spectroscopy from the lattice, Phys. Rev. D 54 (1996) 3619–3633. `arXiv:hep-lat/9601022`, `doi:10.1103/PhysRevD.54.3619`.

[131] A. Ali Khan, T. Bhattacharya, S. Collins, C. T. H. Davies, R. Gupta, C. Morningstar, J. Shigemitsu, J. H. Sloan, Heavy light mesons and baryons with b quarks, Phys. Rev. D 62 (2000) 054505. `arXiv:hep-lat/9912034`, `doi:10.1103/PhysRevD.62.054505`.

[132] J. M. Flynn, F. Mescia, A. S. B. Tariq, Spectroscopy of doubly charmed baryons in lattice QCD, JHEP 07 (2003) 066. `arXiv:hep-lat/`

0307025, doi:10.1088/1126-6708/2003/07/066.

[133] L. Liu, H.-W. Lin, K. Orginos, A. Walker-Loud, Singly and Doubly Charmed $J = 1/2$ Baryon Spectrum from Lattice QCD, Phys. Rev. D 81 (2010) 094505. arXiv:0909.3294, doi:10.1103/PhysRevD.81.094505.

[134] W. Detmold, C. J. D. Lin, S. Meinel, Axial couplings and strong decay widths of heavy hadrons, Phys. Rev. Lett. 108 (2012) 172003. arXiv:1109.2480, doi:10.1103/PhysRevLett.108.172003.

[135] H.-W. Lin, Review of Baryon Spectroscopy in Lattice QCD, Chin. J. Phys. 49 (2011) 827. arXiv:1106.1608.

[136] C. Alexandrou, J. Carbonell, D. Christaras, V. Drach, M. Gravina, M. Papinutto, Strange and charm baryon masses with two flavors of dynamical twisted mass fermions, Phys. Rev. D 86 (2012) 114501. arXiv:1205.6856, doi:10.1103/PhysRevD.86.114501.

[137] R. A. Briceno, H.-W. Lin, D. R. Bolton, Charmed-Baryon Spectroscopy from Lattice QCD with $N_f = 2 + 1 + 1$ Flavors, Phys. Rev. D 86 (2012) 094504. arXiv:1207.3536, doi:10.1103/PhysRevD.86.094504.

[138] W. Detmold, C. J. D. Lin, S. Meinel, Calculation of the heavy-hadron axial couplings g_1, g_2 and g_3 using lattice QCD, Phys. Rev. D 85 (2012) 114508. arXiv:1203.3378, doi:10.1103/PhysRevD.85.114508.

[139] Z. S. Brown, W. Detmold, S. Meinel, K. Orginos, Charmed bottom baryon spectroscopy from lattice QCD, Phys. Rev. D 90 (9) (2014) 094507. arXiv:1409.0497, doi:10.1103/PhysRevD.90.094507.

[140] A. R. Olamaei, K. Azizi, Radiative $\Xi_b^- \to \Xi^- \gamma$ decay, Eur. Phys. J. C 82 (1) (2022) 68. arXiv:2109.09783, doi:10.1140/epjc/s10052-022-10029-1.

[141] C. Alexandrou, C. Kallidonis, Low-lying baryon masses using $N_f = 2$ twisted mass clover-improved fermions directly at the physical pion mass, Phys. Rev. D 96 (3) (2017) 034511. arXiv:1704.02647, doi:10.1103/PhysRevD.96.034511.

[142] S. Durr, G. Koutsou, T. Lippert, Meson and Baryon dispersion relations with Brillouin fermions, Phys. Rev. D 86 (2012) 114514. arXiv:1208.6270, doi:10.1103/PhysRevD.86.114514.

[143] Y. Namekawa, et al., Charmed baryons at the physical point in 2 + 1 flavor lattice QCD, Phys. Rev. D 87 (9) (2013) 094512. arXiv:1301.4743, doi:10.1103/PhysRevD.87.094512.

[144] Y.-C. Chen, T.-W. Chiu, Lattice QCD with $N_f = 2 + 1 + 1$ domain-wall quarks, Phys. Lett. B 767 (2017) 193–198. arXiv:1701.02581, doi:10.1016/j.physletb.2017.01.068.

[145] C. Alexandrou, V. Drach, K. Jansen, C. Kallidonis, G. Koutsou, Baryon spectrum with $N_f = 2 + 1 + 1$ twisted mass fermions, Phys. Rev. D 90 (7) (2014) 074501. arXiv:1406.4310, doi:10.1103/PhysRevD.90.074501.

[146] P. Pérez-Rubio, S. Collins, G. S. Bali, Charmed baryon spectroscopy and light flavor symmetry from lattice QCD, Phys. Rev. D 92 (3) (2015) 034504. arXiv:1503.08440, doi:10.1103/PhysRevD.92.034504.

[147] H. Bahtiyar, K. U. Can, G. Erkol, P. Gubler, M. Oka, T. T. Takahashi, Charmed baryon spectrum from lattice QCD near the physical point, Phys. Rev. D 102 (5) (2020) 054513. arXiv:2004.08999, doi:10.1103/PhysRevD.102.054513.

[148] N. Mathur, M. Padmanath, Lattice QCD study of doubly-charmed strange baryons, Phys. Rev. D 99 (3) (2019) 031501. arXiv:1807.00174, doi:10.1103/PhysRevD.99.031501.

[149] M. Padmanath, R. G. Edwards, N. Mathur, M. Peardon, Spectroscopy of triply-charmed baryons from lattice QCD, Phys. Rev. D 90 (7) (2014) 074504. arXiv:1307.7022, doi:10.1103/PhysRevD.90.074504.

[150] M. Padmanath, R. G. Edwards, N. Mathur, M. Peardon, Spectroscopy of doubly-charmed baryons from lattice QCD, Phys. Rev. D 91 (9) (2015) 094502. arXiv:1502.01845, doi:10.1103/PhysRevD.91.094502.

[151] M. Padmanath, R. G. Edwards, N. Mathur, M. Peardon, Excited-state spectroscopy of singly, doubly and triply-charmed baryons from lattice QCD, in: 6th International Workshop on Charm Physics, 2013. arXiv:1311.4806.

[152] M. Padmanath, R. G. Edwards, N. Mathur, M. J. Peardon, Spectroscopy of charmed baryons from lattice QCD, PoS LATTICE2014 (2015) 084. arXiv:1410.8791, doi:10.22323/1.214.0084.

[153] H.-Y. Cheng, C.-K. Chua, Strong Decays of Charmed Baryons in Heavy Hadron Chiral Perturbation Theory: An Update, Phys. Rev. D 92 (7) (2015) 074014. arXiv:1508.05653, doi:10.1103/PhysRevD.92.074014.

[154] B. Chen, X. Liu, A. Zhang, Newly observed $\Lambda_c(2860)^+$ at LHCb and its D-wave partners $\Lambda_c(2880)^+$, $\Xi_c(3055)^+$ and $\Xi_c(3080)^+$, Phys. Rev. D 95 (7) (2017) 074022. arXiv:1702.04106, doi:10.1103/PhysRevD.95.074022.

[155] K. Gong, H.-Y. Jing, A. Zhang, Possible assignments of highly excited $\Lambda_c(2860)^+$, $\Lambda_c(2880)^+$ and $\Lambda_c(2940)^+$, Eur. Phys. J. C 81 (5) (2021) 467. doi:10.1140/epjc/s10052-021-09255-w.

[156] Q.-F. Lü, X.-H. Zhong, Strong decays of the higher excited Λ_Q and Σ_Q baryons, Phys. Rev. D 101 (1) (2020) 014017. arXiv:1910.06126, doi:10.1103/PhysRevD.101.014017.

[157] J.-J. Guo, P. Yang, A. Zhang, Strong decays of observed Λ_c baryons in the $^3P_0$ model, Phys. Rev. D 100 (1) (2019) 014001. arXiv:1902.07488, doi:10.1103/PhysRevD.100.014001.

[158] Y.-X. Yao, K.-L. Wang, X.-H. Zhong, Strong and radiative decays of the low-lying D-wave singly heavy baryons, Phys. Rev. D 98 (7) (2018) 076015. arXiv:1803.00364, doi:10.1103/PhysRevD.98.076015.

[159] H.-M. Yang, H.-X. Chen, E.-L. Cui, A. Hosaka, Q. Mao, Decay properties of P-wave bottom baryons within light-cone sum rules, Eur. Phys. J. C 80 (2) (2020) 80. arXiv:1909.13575, doi:10.1140/epjc/s10052-020-7637-z.

[160] H.-X. Chen, Q. Mao, W. Chen, A. Hosaka, X. Liu, S.-L. Zhu, Decay properties of P-wave charmed baryons from light-cone QCD sum rules, Phys. Rev. D 95 (9) (2017) 094008. arXiv:1703.07703, doi:10.1103/PhysRevD.95.094008.

[161] K.-L. Wang, X.-H. Zhong, Toward establishing the low-lying P-wave excited Σ_c baryon states, Chin. Phys. C 46 (2) (2021) 023103. arXiv:2110.12443, doi:10.1088/1674-1137/ac3123.

[162] R. Bijker, H. García-Tecocoatzi, A. Giachino, E. Ortiz-Pacheco, E. Santopinto, Masses and decay widths of $\Xi_{c/b}$ and $\Xi'_{c/b}$ baryons, Phys. Rev. D 105 (7) (2020) 074029. arXiv:2010.12437, doi:10.1103/PhysRevD.105.074029.

[163] K. U. Can, Lattice QCD study of the elastic and transition form factors of charmed baryons, Int. J. Mod. Phys. A 36 (23) (2021) 2130013. arXiv:2107.13159, doi:10.1142/S0217751X21300131.

[164] R.-X. Shi, L.-S. Geng, Magnetic moments of the spin-$\frac{3}{2}$ doubly charmed baryons in covariant baryon chiral perturbation theory, Phys. Rev. D 103 (11) (2021) 114004. arXiv:2103.07260, doi:10.1103/PhysRevD.103.114004.

[165] H. Bahtiyar, $\Lambda_c \to \Lambda$ Form Factors in Lattice QCD, Turk. J. Phys. 45 (2021) 4. arXiv:2107.13909, doi:10.3906/fiz-2104-28.

[166] H.-Y. Cheng, Charmed baryon physics circa 2021, Chin. J. Phys. 78 (2022) 324–362. arXiv:2109.01216, doi:10.1016/j.cjph.2022.06.021.

[167] M. Mattson, et al., First Observation of the Doubly Charmed Baryon Ξ_{cc}^+, Phys. Rev. Lett. 89 (2002) 112001. arXiv:hep-ex/0208014, doi:10.1103/PhysRevLett.89.112001.

[168] A. Ocherashvili, et al., Confirmation of the double charm baryon Ξ_{cc}^+(3520) via its decay to pD^+K^-, Phys. Lett. B 628 (2005) 18–24. arXiv:hep-ex/0406033, doi:10.1016/j.physletb.2005.09.043.

[169] M. A. Moinester, et al., First Observation of Doubly Charmed Baryons, Czech. J. Phys. 53 (2003) B201–B213. arXiv:hep-ex/0212029.

[170] S. P. Ratti, New results on c-baryons and a search for cc-baryons in FOCUS, Nucl. Phys. B Proc. Suppl. 115 (2003) 33–36. doi:10.1016/S0920-5632(02)01948-5.

[171] B. Aubert, et al., Search for doubly charmed baryons Ξ_{cc}^+ and Ξ_{cc}^{++} in BABAR, Phys. Rev. D 74 (2006) 011103. arXiv:hep-ex/0605075, doi:10.1103/PhysRevD.74.011103.

[172] R. Chistov, et al., Observation of new states decaying into $\Lambda_c^+K^-\pi^+$ and $\Lambda_c^+K_S^0\pi^-$, Phys. Rev. Lett. 97 (2006) 162001. arXiv:hep-ex/0606051, doi:10.1103/PhysRevLett.97.162001.

[173] R. Aaij, et al., Search for the doubly charmed baryon Ξ_{cc}^+, JHEP 12 (2013) 090. arXiv:1310.2538, doi:10.1007/JHEP12(2013)090.

[174] R. Aaij, et al., Observation of the doubly charmed baryon Ξ_{cc}^{++}, Phys. Rev. Lett. 119 (11) (2017) 112001. arXiv:1707.01621, doi:10.1103/PhysRevLett.119.112001.

[175] R. Aaij, et al., First Observation of the Doubly Charmed Baryon Decay $\Xi_{cc}^{++} \to \Xi_c^+\pi^+$, Phys. Rev. Lett. 121 (16) (2018) 162002. arXiv:1807.01919, doi:10.1103/PhysRevLett.121.162002.

[176] R. Aaij, et al., Precision measurement of the Ξ_{cc}^{++} mass, JHEP 02 (2020) 049. arXiv:1911.08594, doi:10.1007/JHEP02(2020)049.

[177] R. Aaij, et al., Measurement of the Lifetime of the Doubly Charmed Baryon Ξ_{cc}^{++}, Phys. Rev. Lett. 121 (5) (2018) 052002. arXiv:1806.02744, doi:10.1103/PhysRevLett.121.052002.

[178] S. Fleck, J. M. Richard, Baryons with double charm, Prog. Theor. Phys. 82 (1989) 760–774. doi:10.1143/PTP.82.760.

[179] R. L. Jaffe, J. E. Kiskis, Spectra of New Hadrons, Phys. Rev. D 13 (1976) 1355. doi:10.1103/PhysRevD.13.1355.

[180] W. Ponce, Heavy Quarks in a Spherical Bag, Phys. Rev. D 19 (1979) 2197. doi:10.1103/PhysRevD.19.2197.

[181] D.-H. He, K. Qian, Y.-B. Ding, X.-Q. Li, P.-N. Shen, Evaluation of spectra of baryons containing two heavy quarks in bag model, Phys. Rev. D 70 (2004) 094004. arXiv:hep-ph/0403301, doi:10.1103/PhysRevD.70.094004.

[182] D. Ebert, R. N. Faustov, V. O. Galkin, A. P. Martynenko, V. A. Saleev, Heavy baryons in the relativistic quark model, Z. Phys. C 76 (1997) 111–115. arXiv:hep-ph/9607314, doi:10.1007/s002880050534.

[183] S. M. Gerasyuta, D. V. Ivanov, Charmed baryons in bootstrap quark model, Nuovo Cim. A 112 (1999) 261–276. arXiv:hep-ph/0101310, doi:10.1007/BF03035848.

[184] C. Itoh, T. Minamikawa, K. Miura, T. Watanabe, Doubly charmed baryon masses and quark wave functions in baryons, Phys. Rev. D 61 (2000) 057502. doi:10.1103/PhysRevD.61.057502.

[185] J.-B. Wang, G. Li, C.-R. Deng, C.-S. An, J.-J. Xie, Ω_{cc} resonances with negative parity in the chiral constituent quark model, Phys. Rev. D 104 (9) (2021) 094008. arXiv:2110.06408, doi:10.1103/PhysRevD.104.094008.

[186] C. Albertus, E. Hernandez, J. Nieves, J. M. Verde-Velasco, Static properties and semileptonic decays of doubly heavy baryons in a nonrelativistic quark model, Eur. Phys. J. A 32 (2007) 183–199, [Erratum: Eur.Phys.J.A 36, 119 (2008)]. arXiv:hep-ph/0610030, doi:10.1140/epja/i2007-10364-y.

[187] M. H. Weng, X. H. Guo, A. W. Thomas, Bethe-Salpeter equation for doubly heavy baryons in the covariant instantaneous approximation, Phys. Rev. D 83 (2011) 056006. arXiv:1012.0082, doi:10.1103/PhysRevD.83.056006.

[188] J. Tarrús Castellà, Doubly heavy baryons in Born-Oppenheimer EFT, EPJ Web Conf. 258 (2022) 04003. arXiv:2111.09783, doi:10.1051/epjconf/202225804003.

[189] J. Soto, J. Tarrús Castellà, Nonrelativistic effective field theory for heavy exotic hadrons, Phys. Rev. D 102 (1) (2020) 014012. arXiv:2005.00552, doi:10.1103/PhysRevD.102.014012.

[190] K.-W. Wei, B. Chen, X.-H. Guo, Masses of doubly and triply charmed baryons, Phys. Rev. D 92 (7) (2015) 076008. arXiv:1503.05184, doi:10.1103/PhysRevD.92.076008.

[191] J. Oudichhya, K. Gandhi, A. K. Rai, Mass-spectra of singly, doubly, and triply bottom baryons, Phys. Rev. D 104 (11) (2021) 114027. arXiv:2111.00236, doi:10.1103/PhysRevD.104.114027.

[192] J.-R. Zhang, M.-Q. Huang, Doubly heavy baryons in QCD sum rules, Phys. Rev. D 78 (2008) 094007. arXiv:0810.5396, doi:10.1103/PhysRevD.78.094007.

[193] J.-R. Zhang, M.-Q. Huang, Deciphering triply heavy baryons in terms of QCD sum rules, Phys. Lett. B 674 (2009) 28–35. arXiv:0902.3297, doi:10.1016/j.physletb.2009.02.056.

[194] Z.-G. Wang, Analysis of the $1/2^-$ and $3/2^-$ heavy and doubly heavy baryon states with QCD sum rules, Eur. Phys. J. A 47 (2011) 81. arXiv:1003.2838, doi:10.1140/epja/i2011-11081-8.

[195] Z.-G. Wang, Analysis of the $\frac{3}{2}^+$ heavy and doubly heavy baryon states with QCD sum rules, Eur. Phys. J. C 68 (2010) 459–472. arXiv:1002.2471, doi:10.1140/epjc/s10052-010-1357-8.

[196] Z.-G. Wang, Analysis of the $\frac{1}{2}^+$ doubly heavy baryon states with QCD sum rules, Eur. Phys. J. A 45 (2010) 267–274. arXiv:1001.4693, doi:10.1140/epja/i2010-11004-3.

[197] X.-W. Wang, Z.-G. Wang, Search for the charmed baryonium and dibaryon structures via the QCD sum rules, Adv. High Energy Phys. 2022 (2021) 6224597. arXiv:2110.14133, doi:10.1155/2022/6224597.

[198] Y.-J. Shi, W. Wang, Z.-X. Zhao, U.-G. Meißner, Towards a Heavy Diquark Effective Theory for Weak Decays of Doubly Heavy Baryons, Eur. Phys. J. C 80 (5) (2020) 398. arXiv:2002.02785, doi:10.1140/epjc/s10052-020-7949-z.

[199] M. J. Savage, M. B. Wise, Spectrum of baryons with two heavy quarks, Phys. Lett. B 248 (1990) 177–180. doi:10.1016/0370-2693(90)90035-5.

[200] S. L. Olsen, T. Skwarnicki, D. Zieminska, Nonstandard heavy mesons and baryons: Experimental evidence, Rev. Mod. Phys. 90 (1) (2018) 015003. arXiv:1708.04012, doi:10.1103/RevModPhys.90.015003.

[201] S. K. Choi, et al., Observation of a narrow charmonium-like state in exclusive $B^{\pm} \to K^{\pm}\pi^{+}\pi^{-}J/\psi$ decays, Phys. Rev. Lett. 91 (2003) 262001. arXiv:hep-ex/0309032, doi:10.1103/PhysRevLett.91.262001.

[202] R. Aaij, et al., Determination of the $X(3872)$ meson quantum numbers, Phys. Rev. Lett. 110 (2013) 222001. arXiv:1302.6269, doi:10.1103/PhysRevLett.110.222001.

[203] R. Aaij, et al., Study of the lineshape of the $\chi_{c1}(3872)$ state, Phys. Rev. D 102 (9) (2020) 092005. arXiv:2005.13419, doi:10.1103/PhysRevD.102.092005.

[204] R. Aaij, et al., Study of the $\psi_2(3823)$ and $\chi_{c1}(3872)$ states in $B^+ \to (J\psi\pi^+\pi^-)K^+$ decays, JHEP 08 (2020) 123. arXiv:2005.13422, doi:10.1007/JHEP08(2020)123.

[205] K. Abe, et al., Evidence for $X(3872) \to \gamma J/\psi$ and the sub-threshold decay $X(3872) \to \omega J/\psi$, in: 22nd International Symposium on Lepton-Photon Interactions at High Energy (LP 2005), 2005. arXiv:hep-ex/0505037.

[206] P. del Amo Sanchez, et al., Evidence for the decay $X(3872) \to J/\psi\omega$, Phys. Rev. D 82 (2010) 011101. arXiv:1005.5190, doi:10.1103/PhysRevD.82.011101.

[207] M. Ablikim, et al., Study of $e^+e^- \to \gamma\omega J/\psi$ and Observation of $X(3872) \to \omega J/\psi$, Phys. Rev. Lett. 122 (23) (2019) 232002. arXiv:1903.04695, doi:10.1103/PhysRevLett.122.232002.

[208] C. Bignamini, B. Grinstein, F. Piccinini, A. D. Polosa, C. Sabelli, Is the $X(3872)$ Production Cross Section at Tevatron Compatible with a Hadron Molecule Interpretation?, Phys. Rev. Lett. 103 (2009) 162001. arXiv:0906.0882, doi:10.1103/PhysRevLett.103.162001.

[209] D. Acosta, et al., Observation of the narrow state $X(3872) \to J/\psi\pi^+\pi^-$ in $\bar{p}p$ collisions at $\sqrt{s}$ = 1.96 TeV, Phys. Rev. Lett. 93 (2004) 072001. arXiv:hep-ex/0312021, doi:10.1103/PhysRevLett.93.072001.

[210] S. Chatrchyan, et al., Measurement of the $X(3872)$ Production Cross Section Via Decays to $J/\psi\pi^+\pi^-$ in pp collisions at $\sqrt{s}$ = 7 TeV, JHEP 04 (2013) 154. arXiv:1302.3968, doi:10.1007/JHEP04(2013)154.

[211] M. Aaboud, et al., Measurements of $\psi(2S)$ and $X(3872) \to J/\psi\pi^+\pi^-$ production in pp collisions at $\sqrt{s}$ = 8 TeV with the ATLAS detector, JHEP 01 (2017) 117. arXiv:1610.09303, doi:10.1007/JHEP01(2017)117.

[212] V. M. Abazov, et al., Studies of $X(3872)$ and $\psi(2S)$ production in $p\bar{p}$ collisions at 1.96 TeV, Phys. Rev. D 102 (7) (2020) 072005. arXiv:2007.13420, doi:10.1103/PhysRevD.102.072005.

[213] R. Aaij, et al., Observation of Multiplicity Dependent Prompt $\chi_{c1}(3872)$ and $\psi(2S)$ Production in pp Collisions, Phys. Rev. Lett. 126 (9) (2021) 092001. arXiv:2009.06619, doi:10.1103/PhysRevLett.126.092001.

[214] R. Aaij, et al., Measurement of $\chi_{c1}(3872)$ production in proton-proton collisions at $\sqrt{s}$ = 8 and 13 TeV, JHEP 01 (2022) 131. arXiv:2109.07360, doi:10.1007/JHEP01(2022)131.

[215] P. Artoisenet, E. Braaten, Production of the $X(3872)$ at the Tevatron and the LHC, Phys. Rev. D 81 (2010) 114018. arXiv:0911.2016, doi:10.1103/PhysRevD.81.114018.

[216] M. Albaladejo, F.-K. Guo, C. Hanhart, U.-G. Meißner, J. Nieves, A. Nogga, Z. Yang, Note on $X(3872)$ production at hadron colliders and its molecular structure, Chin. Phys. C 41 (12) (2017) 121001. arXiv:1709.09101, doi:10.1088/1674-1137/41/12/121001.

[217] E. Braaten, L.-P. He, K. Ingles, Estimates of the $X(3872)$ Cross Section at a Hadron Collider, Phys. Rev. D 100 (9) (2019) 094024. arXiv:1811.08876, doi:10.1103/PhysRevD.100.094024.

[218] S. Chatrchyan, et al., Search for a New Bottomonium State Decaying to $\Upsilon(1S)\pi^+\pi^-$ in pp Collisions at $\sqrt{s}$ = 8 TeV, Phys. Lett. B 727 (2013) 57–76. arXiv:1309.0250, doi:10.1016/j.physletb.2013.10.016.

[219] G. Aad, et al., Search for the X_b and other hidden-beauty states in the $\pi^+\pi^-\Upsilon(1S)$ channel at ATLAS, Phys. Lett. B 740 (2015) 199–217. arXiv:1410.4409, doi:10.1016/j.physletb.2014.11.055.

[220] X. H. He, et al., Observation of $e^+e^- \to \pi^+\pi^-\pi^0\chi_{bJ}$ and Search for $X_b \to \omega\Upsilon(1S)$ at $\sqrt{s}$ = 10.867 GeV, Phys. Rev. Lett. 113 (14) (2014) 142001. arXiv:1408.0504, doi:10.1103/PhysRevLett.113.142001.

[221] S. Weinberg, Evidence That the Deuteron Is Not an Elementary Particle, Phys. Rev. 137 (1965) B672–B678. doi:10.1103/PhysRev.137.B672.

[222] A. Esposito, L. Maiani, A. Pilloni, A. D. Polosa, V. Riquer, From the line shape of the $X(3872)$ to its structure, Phys. Rev. D 105 (3) (2022) L031503. arXiv:2108.11413, doi:10.1103/PhysRevD.105.L031503.

[223] V. Baru, X.-K. Dong, M.-L. Du, A. Filin, F.-K. Guo, C. Hanhart, A. Nefediev, J. Nieves, Q. Wang, Effective range expansion for narrow near-threshold resonances, Phys. Lett. B 833 (2021) 137290. arXiv:2110.07484, doi:10.1016/j.physletb.2022.137290.

[224] A. Esposito, E. G. Ferreiro, A. Pilloni, A. D. Polosa, C. A. Salgado, The nature of $X(3872)$ from high-multiplicity pp collisions, Eur. Phys. J. C 81 (7) (2021) 669. arXiv:2006.15044, doi:10.1140/epjc/s10052-021-09425-w.

[225] E. Braaten, L.-P. He, K. Ingles, J. Jiang, Production of $X(3872)$ at High Multiplicity, Phys. Rev. D 103 (7) (2021) L071901. arXiv:2012.13499, doi:10.1103/PhysRevD.103.L071901.

[226] A. M. Sirunyan, et al., Evidence for $X(3872)$ in Pb-Pb Collisions and Studies of its Prompt Production at $\sqrt{s_{NN}}$ = 5.02 TeV, Phys. Rev. Lett. 128 (3) (2022) 032001. arXiv:2102.13048, doi:10.1103/PhysRevLett.128.032001.

[227] S. Cho, et al., Exotic hadrons from heavy ion collisions, Prog. Part. Nucl. Phys. 95 (2017) 279–322. arXiv:1702.00486, doi:10.1016/j.ppnp.2017.02.002.

[228] H. Zhang, J. Liao, E. Wang, Q. Wang, H. Xing, Deciphering the Nature of $X(3872)$ in Heavy Ion Collisions, Phys. Rev. Lett. 126 (1) (2021) 012301. arXiv:2004.00024, doi:10.1103/PhysRevLett.126.012301.

[229] B. Chen, L. Jiang, X.-H. Liu, Y. Liu, J. Zhao, $X(3872)$ Production in Relativistic Heavy-Ion Collisions, Phys. Rev. C 105 (5) (2021) 054901. arXiv:2107.00969, doi:10.1103/PhysRevC.105.054901.

[230] A. Esposito, C. A. Manzari, A. Pilloni, A. D. Polosa, Hunting for tetraquarks in ultraperipheral heavy ion collisions, Phys. Rev. D 104 (11) (2021) 114029. arXiv:2109.10359, doi:10.1103/PhysRevD.104.114029.

[231] J. Carlson, L. Heller, J. A. Tjon, Stability of Dimesons, Phys. Rev. D 37 (1988) 744. doi:10.1103/PhysRevD.37.744.

[232] B. Silvestre-Brac, C. Semay, Systematics of $L = 0$ $q^2\bar{q}^2$ systems, Z. Phys. C 57 (1993) 273–282. doi:10.1007/BF01565058.

[233] C. Semay, B. Silvestre-Brac, Diquonia and potential models, Z. Phys. C 61 (1994) 271–275. doi:10.1007/BF01413104.

[234] S. Pepin, F. Stancu, M. Genovese, J. M. Richard, Tetraquarks with color blind forces in chiral quark models, Phys. Lett. B 393 (1997) 119–123. arXiv:hep-ph/9609348, doi:10.1016/S0370-2693(96)01597-3.

[235] B. A. Gelman, S. Nussinov, Does a narrow tetraquark $cc\bar{u}\bar{d}$ state exist?, Phys. Lett. B 551 (2003) 296–304. arXiv:hep-ph/0209095, doi:10.1016/S0370-2693(02)03069-1.

[236] J. Vijande, F. Fernandez, A. Valcarce, B. Silvestre-Brac, Tetraquarks in a chiral constituent quark model, Eur. Phys. J. A 19 (2004) 383. arXiv:hep-ph/0310007, doi:10.1140/epja/i2003-10128-9.

[237] D. Janc, M. Rosina, The $T_{cc} = DD^*$ molecular state, Few Body Syst. 35 (2004) 175–196. arXiv:hep-ph/0405208, doi:10.1007/s00601-004-0068-9.

[238] Y. Cui, X.-L. Chen, W.-Z. Deng, S.-L. Zhu, The Possible Heavy Tetraquarks $qQ\bar{q}\bar{Q}$, $qq\bar{Q}\bar{Q}$ and $qQ\bar{Q}\bar{Q}$, HEPNP 31 (2007) 7–13. arXiv:hep-ph/0607226.

[239] F. S. Navarra, M. Nielsen, S. H. Lee, QCD sum rules study of $QQ-\bar{u}\bar{d}$ mesons, Phys. Lett. B 649 (2007) 166–172. arXiv:hep-ph/0703071, doi:10.1016/j.physletb.2007.04.010.

[240] J. Vijande, E. Weissman, A. Valcarce, N. Barnea, Are there compact heavy four-quark bound states?, Phys. Rev. D 76 (2007) 094027. arXiv:0710.2516, doi:10.1103/PhysRevD.76.094027.

[241] D. Ebert, R. N. Faustov, V. O. Galkin, W. Lucha, Masses of tetraquarks with two heavy quarks in the relativistic quark model, Phys. Rev. D 76 (2007) 114015. arXiv:0706.3853, doi:10.1103/PhysRevD.76.114015.

[242] S. H. Lee, S. Yasui, Stable multiquark states with heavy quarks in a diquark model, Eur. Phys. J. C 64 (2009) 283–295. arXiv:0901.2977, doi:10.1140/epjc/s10052-009-1140-x.

[243] Y. Yang, C. Deng, J. Ping, T. Goldman, S-wave $QQ\bar{q}\bar{q}$ state in the constituent quark model, Phys. Rev. D 80 (2009) 114023. doi:10.1103/PhysRevD.80.114023.

[244] M.-L. Du, W. Chen, X.-L. Chen, S.-L. Zhu, Exotic $QQ\bar{q}\bar{q}$, $QQ\bar{q}\bar{s}$ and $QQ\bar{s}\bar{s}$ states, Phys. Rev. D 87 (1) (2013) 014003. arXiv:1209.5134, doi:10.1103/PhysRevD.87.014003.

[245] G. Q. Feng, X. H. Guo, B. S. Zou, $QQ'\bar{u}\bar{d}$ bound state in the Bethe-Salpeter equation approach (9 2013). arXiv:1309.7813.

[246] Y. Ikeda, B. Charron, S. Aoki, T. Doi, T. Hatsuda, T. Inoue, N. Ishii, K. Murano, H. Nemura, K. Sasaki, Charmed tetraquarks T_{cc} and T_{cs} from dynamical lattice QCD simulations, Phys. Lett. B 729 (2014) 85–90. arXiv:1311.6214, doi:10.1016/j.physletb.2014.01.002.

[247] S.-Q. Luo, K. Chen, X. Liu, Y.-R. Liu, S.-L. Zhu, Exotic tetraquark states with the $qq\bar{Q}\bar{Q}$ configuration, Eur. Phys. J. C 77 (10) (2017) 709. arXiv:1707.01180, doi:10.1140/epjc/s10052-017-5297-4.

[248] M. Karliner, J. L. Rosner, Discovery of doubly-charmed Ξ_{cc} baryon implies a stable ($bb\bar{u}\bar{d}$) tetraquark, Phys. Rev. Lett. 119 (20) (2017) 202001. arXiv:1707.07666, doi:10.1103/PhysRevLett.119.202001.

[249] E. J. Eichten, C. Quigg, Heavy-quark symmetry implies stable heavy tetraquark mesons $Q_iQ_j\bar{q}_k\bar{q}_l$, Phys. Rev. Lett. 119 (20) (2017) 202002. arXiv:1707.09575, doi:10.1103/PhysRevLett.119.202002.

[250] Z.-G. Wang, Analysis of the axial-vector doubly heavy tetraquark states with QCD sum rules, Acta Phys. Polon. B 49 (2018) 1781. arXiv:1708.04545, doi:10.5506/APhysPolB.49.1781.

[251] G. K. C. Cheung, C. E. Thomas, J. J. Dudek, R. G. Edwards, Tetraquark operators in lattice QCD and exotic flavour states in the charm sector, JHEP 11 (2017) 033. arXiv:1709.01417, doi:10.1007/JHEP11(2017)033.

[252] W. Park, S. Noh, S. H. Lee, Masses of the doubly heavy tetraquarks in a constituent quark model, Nucl. Phys. A 983 (2019) 1–19. arXiv:1809.05257, doi:10.1016/j.nuclphysa.2018.12.019.

[253] A. Francis, R. J. Hudspith, R. Lewis, K. Maltman, Evidence for charm-bottom tetraquarks and the mass dependence of heavy-light tetraquark states from lattice QCD, Phys. Rev. D 99 (5) (2019) 054505. arXiv:1810.10550, doi:10.1103/PhysRevD.99.054505.

[254] P. Junnarkar, N. Mathur, M. Padmanath, Study of doubly heavy tetraquarks in Lattice QCD, Phys. Rev. D 99 (3) (2019) 034507. arXiv:1810.12285, doi:10.1103/PhysRevD.99.034507.

[255] C. Deng, H. Chen, J. Ping, Systematical investigation on the stability of doubly heavy tetraquark states, Eur. Phys. J. A 56 (1) (2020) 9. arXiv:1811.06462, doi:10.1140/epja/s10050-019-00012-y.

[256] G. Yang, J. Ping, J. Segovia, Doubly-heavy tetraquarks, Phys. Rev. D 101 (1) (2020) 014001. arXiv:1911.00215, doi:10.1103/PhysRevD.101.014001.

[257] M.-Z. Liu, T.-W. Wu, M. Pavon Valderrama, J.-J. Xie, L.-S. Geng, Heavy-quark spin and flavor symmetry partners of the X(3872) revisited: What can we learn from the one boson exchange model?, Phys. Rev. D 99 (9) (2019) 094018. arXiv:1902.03044, doi:10.1103/PhysRevD.99.094018.

[258] Y. Tan, W. Lu, J. Ping, Systematics of $QQ\bar{q}\bar{q}$ in a chiral constituent quark model, Eur. Phys. J. Plus 135 (9) (2020) 716. arXiv:2004.02106, doi:10.1140/epjp/s13360-020-00741-w.

[259] Q.-F. Lü, D.-Y. Chen, Y.-B. Dong, Masses of doubly heavy tetraquarks $T_{QQ'}$ in a relativized quark model, Phys. Rev. D 102 (3) (2020) 034012. arXiv:2006.08087, doi:10.1103/PhysRevD.102.034012.

[260] E. Braaten, L.-P. He, A. Mohapatra, Masses of doubly heavy tetraquarks with error bars, Phys. Rev. D 103 (1) (2021) 016001. arXiv:2006.08650, doi:10.1103/PhysRevD.103.016001.

[261] D. Gao, D. Jia, Y.-J. Sun, Z. Zhang, W.-N. Liu, Q. Mei, Masses of doubly heavy tetraquark states with isospin = $\frac{1}{2}$ and 1 and spin-parity $1^{+\pm}$ (7 2020). arXiv:2007.15213.

[262] J.-B. Cheng, S.-Y. Li, Y.-R. Liu, Z.-G. Si, T. Yao, Double-heavy tetraquark states with heavy diquark-antiquark symmetry, Chin. Phys. C 45 (4) (2021) 043102. arXiv:2008.00737, doi:10.1088/1674-1137/abde2f.

[263] S. Noh, W. Park, S. H. Lee, The Doubly-heavy Tetraquarks ($qq'\bar{Q}\bar{Q}'$) in a Constituent Quark Model with a Complete Set of Harmonic Oscillator Bases, Phys. Rev. D 103 (2021) 114009. arXiv:2102.09614, doi:10.1103/PhysRevD.103.114009.

[264] R. N. Faustov, V. O. Galkin, E. M. Savchenko, Heavy tetraquarks in the relativistic quark model, Universe 7 (4) (2021) 94. arXiv:2103.01763, doi:10.3390/universe7040094.

[265] J. M. Dias, S. Narison, F. S. Navarra, M. Nielsen, J. M. Richard, Relation between $T_{cc,bb}$ and $X_{c,b}$ from QCD, Phys. Lett. B 703 (2011) 274–280. arXiv:1105.5630, doi:10.1016/j.physletb.2011.07.082.

[266] N. Li, S.-L. Zhu, Isospin breaking, Coupled-channel effects and Diagnosis of X(3872), Phys. Rev. D 86 (2012) 074022. arXiv:1207.3954, doi:10.1103/PhysRevD.86.074022.

[267] N. Li, Z.-F. Sun, X. Liu, S.-L. Zhu, Coupled-channel analysis of the possible $D^{(*)}D^{(*)}$, $\bar{B}^{(*)}\bar{B}^{(*)}$ and $D^{(*)}\bar{B}^{(*)}$ molecular states, Phys. Rev. D

88 (11) (2013) 114008. `arXiv:1211.5007`, `doi:10.1103/PhysRevD.88.114008`.

[268] H. Xu, B. Wang, Z.-W. Liu, X. Liu, DD^* potentials in chiral perturbation theory and possible molecular states, Phys. Rev. D 99 (1) (2019) 014027, [Erratum: Phys.Rev.D 104, 119903 (2021)]. `arXiv:1708.06918`, `doi:10.1103/PhysRevD.99.014027`.

[269] L. Meng, G.-J. Wang, B. Wang, S.-L. Zhu, Long-range structure of T_{cc}^+ state, Nucl. Part. Phys. Proc. 324-329 (2023) 68–71. `doi:10.1016/j.nuclphysbps.2023.01.015`.

[270] S. S. Agaev, K. Azizi, H. Sundu, Newly observed exotic doubly charmed meson T_{cc}^+ , Nucl. Phys. B 975 (2022) 115650. `arXiv:2108.00188`, `doi:10.1016/j.nuclphysb.2022.115650`.

[271] X.-Z. Ling, M.-Z. Liu, L.-S. Geng, E. Wang, J.-J. Xie, Can we understand the decay width of the T_{cc}^+ state?, Phys. Lett. B 826 (2022) 136897. `arXiv:2108.00947`, `doi:10.1016/j.physletb.2022.136897`.

[272] R. Chen, Q. Huang, X. Liu, S.-L. Zhu, Predicting another doubly charmed molecular resonance $T_{cc}'^+$(3876), Phys. Rev. D 104 (11) (2021) 114042. `arXiv:2108.01911`, `doi:10.1103/PhysRevD.104.114042`.

[273] X.-K. Dong, F.-K. Guo, B.-S. Zou, A survey of heavy–heavy hadronic molecules, Commun. Theor. Phys. 73 (12) (2021) 125201. `arXiv:2108.02673`, `doi:10.1088/1572-9494/ac27a2`.

[274] A. Feijoo, W. H. Liang, E. Oset, $D^0 D^0 \pi^+$ mass distribution in the production of the T_{cc} exotic state, Phys. Rev. D 104 (11) (2021) 114015. `arXiv:2108.02730`, `doi:10.1103/PhysRevD.104.114015`.

[275] M.-J. Yan, M. P. Valderrama, Subleading contributions to the decay width of the T_{cc}^+ tetraquark, Phys. Rev. D 105 (1) (2022) 014007. `arXiv:2108.04785`, `doi:10.1103/PhysRevD.105.014007`.

[276] Q. Xin, Z.-G. Wang, Analysis of the doubly-charmed tetraquark molecular states with the QCD sum rules, Eur. Phys. J. A 58 (6) (2021) 110. `arXiv:2108.12597`, `doi:10.1140/epja/s10050-022-00752-4`.

[277] Y. Huang, H. Q. Zhu, L.-S. Geng, R. Wang, Production of T_{cc}^+ exotic state in the $\gamma p \to D^+ T_{cc}^- \Lambda_c^+$ reaction, Phys. Rev. D 104 (11) (2021) 116008. `arXiv:2108.13028`, `doi:10.1103/PhysRevD.104.116008`.

[278] S. Fleming, R. Hodges, T. Mehen, T_{cc}^+ decays: Differential spectra and two-body final states, Phys. Rev. D 104 (11) (2021) 116010. `arXiv:2109.02188`, `doi:10.1103/PhysRevD.104.116010`.

[279] K. Azizi, U. Özdem, Magnetic dipole moments of the T_{cc}^+ and Z_V^{++} tetraquark states, Phys. Rev. D 104 (11) (2021) 114002. `arXiv:2109.02390`, `doi:10.1103/PhysRevD.104.114002`.

[280] Y. Hu, J. Liao, E. Wang, Q. Wang, H. Xing, H. Zhang, Production of doubly charmed exotic hadrons in heavy ion collisions, Phys. Rev. D 104 (11) (2021) L111502. `arXiv:2109.07733`, `doi:10.1103/PhysRevD.104.L111502`.

[281] K. Chen, R. Chen, L. Meng, B. Wang, S.-L. Zhu, Systematics of the heavy flavor hadronic molecules, Eur. Phys. J. C 82 (7) (2022) 581. `arXiv:2109.13057`, `doi:10.1140/epjc/s10052-022-10540-5`.

[282] M. Albaladejo, Tcc+ coupled channel analysis and predictions, Phys. Lett. B 829 (2022) 137052. `arXiv:2110.02944`, `doi:10.1016/j.physletb.2022.137052`.

[283] M.-L. Du, V. Baru, X.-K. Dong, A. Filin, F.-K. Guo, C. Hanhart, A. Nefediev, J. Nieves, Q. Wang, Coupled-channel approach to T_{cc}^+ including three-body effects, Phys. Rev. D 105 (1) (2022) 014024. `arXiv:2110.13765`, `doi:10.1103/PhysRevD.105.014024`.

[284] C. Deng, S.-L. Zhu, T_{cc}^+ and its partners, Phys. Rev. D 105 (5) (2022) 054015. `arXiv:2112.12472`, `doi:10.1103/PhysRevD.105.054015`.

[285] S. S. Agaev, K. Azizi, H. Sundu, Hadronic molecule model for the doubly charmed state T_{cc}^+, JHEP 06 (2022) 057. `arXiv:2201.02788`, `doi:10.1007/JHEP06(2022)057`.

[286] E. Braaten, L.-P. He, K. Ingles, J. Jiang, Triangle Singularity in the Production of T_{cc}^+(3875) and a Soft Pion, Phys. Rev. D 106 (3) (2022) 034033. `arXiv:2202.03900`, `doi:10.1103/PhysRevD.106.034033`.

[287] J. He, X. Liu, The quasi-fission phenomenon of double charm T_{cc}^+ induced by nucleon, Eur. Phys. J. C 82 (4) (2022) 387. `arXiv:2202.07248`, `doi:10.1140/epjc/s10052-022-10363-4`.

[288] L. M. Abreu, F. S. Navarra, H. P. L. Vieira, The multiplicity of the doubly charmed state T_{cc}^+ in heavy-ion collisions, Phys. Rev. D 105 (11) (2022) 116029. `arXiv:2202.10882`, `doi:10.1103/PhysRevD.105.116029`.

[289] N. N. Achasov, G. N. Shestakov, Triangle Singularities in the $T_{cc}^+ \to D^{*+} D^0 \to \pi^+ D^0 D^0$ decay width, Phys. Rev. D 105 (9) (2022) 096038. `arXiv:2203.17100`, `doi:10.1103/PhysRevD.105.096038`.

[290] M. Mikhasenko, Effective-range expansion of the T_{cc}^+ state at the complex $D^{*+} D^0$ threshold (3 2022). `arXiv:2203.04622`.

[291] B. Wang, L. Meng, Revisiting the DD^* chiral interactions with the local momentum-space regularization up to the third order and the nature of T_{cc}^+ (12 2022). `arXiv:2212.08447`.

[292] Y. Lyu, S. Aoki, T. Doi, T. Hatsuda, Y. Ikeda, J. Meng, Doubly charmed tetraquark T_{cc}^+ from Lattice QCD near Physical Point (2 2023). `arXiv:2302.04505`.

[293] M. Ablikim, et al., Observation of a Charged Charmoniumlike Structure in $e^+ e^- \to \pi^+ \pi^- J/\psi$ at $\sqrt{s}$ =4.26 GeV, Phys. Rev. Lett. 110 (2013) 252001. `arXiv:1303.5949`, `doi:10.1103/PhysRevLett.110.252001`.

[294] M. Ablikim, et al., Observation of a charged $(D\bar{D}^*)^{\pm}$ mass peak in $e^+ e^- \to \pi D\bar{D}^*$ at $\sqrt{s}$ = 4.26 GeV, Phys. Rev. Lett. 112 (2) (2014) 022001. `arXiv:1310.1163`, `doi:10.1103/PhysRevLett.112.022001`.

[295] M. Ablikim, et al., Confirmation of a charged charmoniumlike state $Z_c(3885)^{\mp}$ in $e^+ e^- \to \pi^{\pm}(D\bar{D}^*)^{\mp}$ with double D tag, Phys. Rev. D 92 (9) (2015) 092006. `arXiv:1509.01398`, `doi:10.1103/PhysRevD.92.092006`.

[296] M. Ablikim, et al., Observation of a Charged Charmoniumlike Structure $Z_c(4020)$ and Search for the $Z_c(3900)$ in $e^+ e^- \to \pi^+ \pi^- h_c$, Phys. Rev. Lett. 111 (24) (2013) 242001. `arXiv:1309.1896`, `doi:10.1103/PhysRevLett.111.242001`.

[297] M. Ablikim, et al., Observation of a neutral charmoniumlike state $Z_c(4025)^0$ in $e^+ e^- \to (D^* \bar{D}^*)^0 \pi^0$, Phys. Rev. Lett. 115 (18) (2015) 182002. `arXiv:1507.02404`, `doi:10.1103/PhysRevLett.115.182002`.

[298] Z. Q. Liu, et al., Study of $e^+ e^- \to \pi^+ \pi^- J/\psi$ and Observation of a Charged Charmoniumlike State at Belle, Phys. Rev. Lett. 110 (2013) 252001, [Erratum: Phys.Rev.Lett. 111, 019901 (2013)]. `arXiv:1304.0121`, `doi:10.1103/PhysRevLett.110.252002`.

[299] T. Xiao, S. Dobbs, A. Tomaradze, K. K. Seth, Observation of the Charged Hadron $Z_c^{\pm}$(3900) and Evidence for the Neutral Z_c^0(3900) in $e^+ e^- \to \pi\pi J/\psi$ at $\sqrt{s}$ = 4170 MeV, Phys. Lett. B 727 (2013) 366–370. `arXiv:1304.3036`, `doi:10.1016/j.physletb.2013.10.041`.

[300] A. Bondar, et al., Observation of two charged bottomonium-like resonances in $\Upsilon(5S)$ decays, Phys. Rev. Lett. 108 (2012) 122001. `arXiv:`

1110.2251, doi:10.1103/PhysRevLett.108.122001.

[301] A. Garmash, et al., Observation of $Z_b(10610)$ and $Z_b(10650)$ Decaying to B Mesons, Phys. Rev. Lett. 116 (21) (2016) 212001. arXiv:1512.07419, doi:10.1103/PhysRevLett.116.212001.

[302] K. Chilikin, et al., Observation of a new charged charmoniumlike state in $\bar{B}^0 \rightarrow J/\psi K^- \pi^+$ decays, Phys. Rev. D 90 (11) (2014) 112009. arXiv:1408.6457, doi:10.1103/PhysRevD.90.112009.

[303] R. Aaij, et al., Model-Independent Observation of Exotic Contributions to $B^0 \rightarrow J/\psi K^+ \pi^-$ Decays, Phys. Rev. Lett. 122 (15) (2019) 152002. arXiv:1901.05745, doi:10.1103/PhysRevLett.122.152002.

[304] S. K. Choi, et al., Observation of a resonance-like structure in the $pi^\pm \psi'$ mass distribution in exclusive $B \rightarrow K\pi^\pm \psi'$ decays, Phys. Rev. Lett. 100 (2008) 142001. arXiv:0708.1790, doi:10.1103/PhysRevLett.100.142001.

[305] K. Chilikin, et al., Experimental constraints on the spin and parity of the $Z(4430)^+$, Phys. Rev. D 88 (7) (2013) 074026. arXiv:1306.4894, doi:10.1103/PhysRevD.88.074026.

[306] R. Aaij, et al., Observation of the resonant character of the $Z(4430)^-$ state, Phys. Rev. Lett. 112 (22) (2014) 222002. arXiv:1404.1903, doi:10.1103/PhysRevLett.112.222002.

[307] M. Cleven, F.-K. Guo, C. Hanhart, U.-G. Meissner, Bound state nature of the exotic Z_b states, Eur. Phys. J. A 47 (2011) 120. arXiv:1107.0254, doi:10.1140/epja/i2011-11120-6.

[308] T. Ji, X.-K. Dong, M. Albaladejo, M.-L. Du, F.-K. Guo, J. Nieves, Establishing the heavy quark spin and light flavor molecular multiplets of the $X(3872)$, $Z_c(3900)$, and $X(3960)$, Phys. Rev. D 106 (9) (2022) 094002. arXiv:2207.08563, doi:10.1103/PhysRevD.106.094002.

[309] S. L. Olsen, A New Hadron Spectroscopy, Front. Phys. (Beijing) 10 (2) (2015) 121–154. arXiv:1411.7738, doi:10.1007/S11467-014-0449-6.

[310] M. Ablikim, et al., Observation of a Near-Threshold Structure in the K^+ Recoil-Mass Spectra in $e^+ e^- \rightarrow K^+ (D_s^- D^{*0} + D_s^{*-} D^0)$, Phys. Rev. Lett. 126 (10) (2021) 102001. arXiv:2011.07855, doi:10.1103/PhysRevLett.126.102001.

[311] L. Meng, B. Wang, S.-L. Zhu, $Z_{cs}(3985)^-$ as the U-spin partner of $Z_c(3900)^-$ and implication of other states in the SU(3)$_F$ symmetry and heavy quark symmetry, Phys. Rev. D 102 (11) (2020) 111502. arXiv:2011.08656, doi:10.1103/PhysRevD.102.111502.

[312] B. Wang, L. Meng, S.-L. Zhu, Decoding the nature of $Z_{cs}(3985)$ and establishing the spectrum of charged heavy quarkoniumlike states in chiral effective field theory, Phys. Rev. D 103 (2) (2021) L021501. arXiv:2011.10922, doi:10.1103/PhysRevD.103.L021501.

[313] Z. Yang, X. Cao, F.-K. Guo, J. Nieves, M. P. Valderrama, Strange molecular partners of the $Z_c(3900)$ and $Z_c(4020)$, Phys. Rev. D 103 (7) (2021) 074029. arXiv:2011.08725, doi:10.1103/PhysRevD.103.074029.

[314] B.-D. Wan, C.-F. Qiao, About the exotic structure of Z_{cs}, Nucl. Phys. B 968 (2021) 115450. arXiv:2011.08747, doi:10.1016/j.nuclphysb.2021.115450.

[315] J.-Z. Wang, Q.-S. Zhou, X. Liu, T. Matsuki, Toward charged $Z_{cs}(3985)$ structure under a reflection mechanism, Eur. Phys. J. C 81 (1) (2021) 51. arXiv:2011.08628, doi:10.1140/epjc/s10052-021-08877-4.

[316] Z.-F. Sun, C.-W. Xiao, Explanation of the newly obseaved $Z_{cs}^-(3985)$ as a $D_s^{(*)-} D^{(*)0}$ molecular state (11 2020). arXiv:2011.09404.

[317] X. Cao, J.-P. Dai, Z. Yang, Photoproduction of strange hidden-charm and hidden-bottom states, Eur. Phys. J. C 81 (2) (2021) 184. arXiv:2011.09244, doi:10.1140/epjc/s10052-021-08858-7.

[318] R. Chen, Q. Huang, $Z_{cs}(3985)^-$: A strange hidden-charm tetraquark resonance or not?, Phys. Rev. D 103 (3) (2021) 034008. arXiv:2011.09156, doi:10.1103/PhysRevD.103.034008.

[319] M.-C. Du, Q. Wang, Q. Zhao, The nature of charged charmonium-like states $Z_c(3900)$ and its strange partner $Z_{cs}(3982)$ (11 2020). arXiv:2011.09225.

[320] B. Wang, L. Meng, S.-L. Zhu, Molecular tetraquarks and pentaquarks in chiral effective field theory, Nucl. Part. Phys. Proc. 324-329 (2023) 45–48. arXiv:2210.08227, doi:10.1016/j.nuclphysbps.2023.01.010.

[321] L. Meng, B. Wang, G.-J. Wang, S.-L. Zhu, Are the $Z_{cs}(3985)$ and $Z_{cs}(4000)$ the same state?, Nucl. Part. Phys. Proc. 318-323 (2022) 85–89. doi:10.1016/j.nuclphysbps.2022.09.018.

[322] Q.-N. Wang, W. Chen, H.-X. Chen, Exotic molecular states and tetraquark states with $J^P = 0^+, 1^+, 2^+$, Chin. Phys. C 45 (9) (2021) 093102. arXiv:2011.10495, doi:10.1088/1674-1137/ac0b3b.

[323] Z.-G. Wang, Analysis of $Z_{cs}(3985)$ as the axialvector tetraquark state, Chin. Phys. C 45 (7) (2021) 073107. arXiv:2011.10959, doi:10.1088/1674-1137/abfa83.

[324] X. Jin, Y. Wu, X. Liu, Y. Xue, H. Huang, J. Ping, B. Zhong, Strange hidden-charm tetraquarks in constituent quark model, Eur. Phys. J. C 81 (12) (2021) 1108. arXiv:2011.12230, doi:10.1140/epjc/s10052-021-09916-w.

[325] N. Ikeno, R. Molina, E. Oset, The $Z_{cs}(3985)$ as a threshold effect from the $\bar{D}_s^* D + \bar{D}_s D^*$ interaction, Phys. Lett. B 814 (2021) 136120. arXiv:2011.13425, doi:10.1016/j.physletb.2021.136120.

[326] Y.-J. Xu, Y.-L. Liu, C.-Y. Cui, M.-Q. Huang, $\bar{D}_s^{(*)} D^{(*)}$ molecular state with $J^P = 1^+$, Phys. Rev. D 104 (9) (2021) 094028. arXiv:2011.14313, doi:10.1103/PhysRevD.104.094028.

[327] Z.-H. Guo, J. A. Oller, Unified description of the hidden-charm tetraquark states $Z_{cs}(3985)$, $Z_c(3900)$, and $X(4020)$, Phys. Rev. D 103 (5) (2021) 054021. arXiv:2012.11904, doi:10.1103/PhysRevD.103.054021.

[328] U. Özdem, K. Azizi, Magnetic dipole moment of the $Z_{cs}(3985)$ state: diquark–antidiquark and molecular pictures, Eur. Phys. J. Plus 136 (9) (2021) 968. arXiv:2102.09231, doi:10.1140/epjp/s13360-021-01977-w.

[329] M.-J. Yan, F.-Z. Peng, M. Sánchez Sánchez, M. Pavon Valderrama, Axial meson exchange and the $Z_c(3900)$ and $Z_{cs}(3985)$ resonances as heavy hadron molecules, Phys. Rev. D 104 (11) (2021) 114025. arXiv:2102.13058, doi:10.1103/PhysRevD.104.114025.

[330] P. G. Ortega, D. R. Entem, F. Fernandez, The strange partner of the Z_c structures in a coupled-channels model, Phys. Lett. B 818 (2021) 136382. arXiv:2103.07871, doi:10.1016/j.physletb.2021.136382.

[331] H.-X. Chen, Hadronic molecules in B decays, Phys. Rev. D 105 (9) (2022) 094003. arXiv:2103.08586, doi:10.1103/PhysRevD.105.094003.

[332] L. Maiani, A. D. Polosa, V. Riquer, The new resonances $Z_{cs}(3985)$ and $Z_{cs}(4003)$ (almost) fill two tetraquark nonets of broken SU(3)$_f$, Sci. Bull. 66 (2021) 1616–1619. arXiv:2103.08331, doi:10.1016/j.scib.2021.04.040.

[333] P.-P. Shi, F. Huang, W.-L. Wang, Hidden charm tetraquark states in a diquark model, Phys. Rev. D 103 (9) (2021) 094038. arXiv:

2105.02397, doi:10.1103/PhysRevD.103.094038.

[334] J. F. Giron, R. F. Lebed, S. R. Martinez, Spectrum of hidden-charm, open-strange exotics in the dynamical diquark model, Phys. Rev. D 104 (5) (2021) 054001. arXiv:2106.05883, doi:10.1103/PhysRevD.104.054001.

[335] M. Karliner, J. L. Rosner, Configuration mixing in strange tetraquarks Z_{cs}, Phys. Rev. D 104 (3) (2021) 034033. arXiv:2107.04915, doi:10.1103/PhysRevD.104.034033.

[336] Z.-M. Ding, H.-Y. Jiang, D. Song, J. He, Hidden and doubly heavy molecular states from interactions $D_{(s)}^{(*)}\bar{D}_s^{(*)}/B_{(s)}^{(*)}\bar{B}_s^{(*)}$ and $D_{(s)}^{(*)}D_s^{(*)}/B_{(s)}^{(*)}B_s^{(*)}$, Eur. Phys. J. C 81 (8) (2021) 732. arXiv:2107.00855, doi:10.1140/epjc/s10052-021-09534-6.

[337] Q. Wu, D.-Y. Chen, Exploration of the hidden charm decays of $Z_{cs}(3985)$, Phys. Rev. D 104 (7) (2021) 074011. arXiv:2108.06700, doi:10.1103/PhysRevD.104.074011.

[338] G. Yang, J. Ping, J. Segovia, Hidden-charm tetraquarks with strangeness in the chiral quark model, Phys. Rev. D 104 (9) (2021) 094035. arXiv:2109.04311, doi:10.1103/PhysRevD.104.094035.

[339] V. Baru, E. Epelbaum, A. A. Filin, C. Hanhart, A. V. Nefediev, Is $Z_{cs}(3982)$ a molecular partner of $Z_c(3900)$ and $Z_c(4020)$ states?, Phys. Rev. D 105 (3) (2021) 034014. arXiv:2110.00398, doi:10.1103/PhysRevD.105.034014.

[340] J. Ferretti, E. Santopinto, The new $P_{cs}(4459)$, $Z_{cs}(3985)$, $Z_{cs}(4000)$ and $Z_{cs}(4220)$ and the possible emergence of flavor pentaquark octets and tetraquark nonets, Sci. Bull. 67 (2022) 1209. arXiv:2111.08650, doi:10.1016/j.scib.2022.04.010.

[341] Q. Wu, D.-Y. Chen, W.-H. Qin, G. Li, Production of Z_{cs} in B and B_s decays, Eur. Phys. J. C 82 (6) (2022) 520. arXiv:2111.13347, doi:10.1140/epjc/s10052-022-10465-z.

[342] M.-L. Du, M. Albaladejo, F.-K. Guo, J. Nieves, Combined analysis of the Zc(3900) and the Zcs(3985) exotic states, Phys. Rev. D 105 (7) (2022) 074018. arXiv:2201.08253, doi:10.1103/PhysRevD.105.074018.

[343] H. Chen, Q. Huang, R.-G. Ping, Spin and polarization analysis of Z_{cs} state, Phys. Rev. D 105 (3) (2022) 036002. arXiv:2201.09066, doi:10.1103/PhysRevD.105.036002.

[344] S. Han, L.-Y. Xiao, Aspects of $Z_{cs}(3985)$ and $Z_{cs}(4000)$, Phys. Rev. D 105 (5) (2022) 054008. doi:10.1103/PhysRevD.105.054008.

[345] R. Aaij, et al., Observation of New Resonances Decaying to $J/\psi K^+$ and $J/\psi \phi$, Phys. Rev. Lett. 127 (8) (2021) 082001. arXiv:2103.01803, doi:10.1103/PhysRevLett.127.082001.

[346] L. Meng, B. Wang, G.-J. Wang, S.-L. Zhu, Implications of the $Z_{cs}(3985)$ and $Z_{cs}(4000)$ as two different states, Sci. Bull. 66 (2021) 1516. arXiv:2104.08469, doi:10.1016/j.scib.2021.06.026.

[347] Z.-C. Yang, Z.-F. Sun, J. He, X. Liu, S.-L. Zhu, The possible hidden-charm molecular baryons composed of anti-charmed meson and charmed baryon, Chin. Phys. C 36 (2012) 6–13. arXiv:1105.2901, doi:10.1088/1674-1137/36/1/002.

[348] J.-J. Wu, R. Molina, E. Oset, B. S. Zou, Prediction of narrow N^* and Λ^* resonances with hidden charm above 4 GeV, Phys. Rev. Lett. 105 (2010) 232001. arXiv:1007.0573, doi:10.1103/PhysRevLett.105.232001.

[349] J.-J. Wu, L. Zhao, B. S. Zou, Prediction of super-heavy N^* and Λ^* resonances with hidden beauty, Phys. Lett. B 709 (2012) 70–76. arXiv:1011.5743, doi:10.1016/j.physletb.2012.01.068.

[350] H.-X. Chen, W. Chen, S.-L. Zhu, Possible interpretations of the $P_c(4312)$, $P_c(4440)$, and $P_c(4457)$, Phys. Rev. D 100 (5) (2019) 051501. arXiv:1903.11001, doi:10.1103/PhysRevD.100.051501.

[351] R. Chen, Z.-F. Sun, X. Liu, S.-L. Zhu, Strong LHCb evidence supporting the existence of the hidden-charm molecular pentaquarks, Phys. Rev. D 100 (1) (2019) 011502. arXiv:1903.11013, doi:10.1103/PhysRevD.100.011502.

[352] M.-Z. Liu, Y.-W. Pan, F.-Z. Peng, M. Sánchez Sánchez, L.-S. Geng, A. Hosaka, M. Pavon Valderrama, Emergence of a complete heavy-quark spin symmetry multiplet: seven molecular pentaquarks in light of the latest LHCb analysis, Phys. Rev. Lett. 122 (24) (2019) 242001. arXiv:1903.11560, doi:10.1103/PhysRevLett.122.242001.

[353] Z.-H. Guo, J. A. Oller, Anatomy of the newly observed hidden-charm pentaquark states: $P_c(4312)$, $P_c(4440)$ and $P_c(4457)$, Phys. Lett. B 793 (2019) 144–149. arXiv:1904.00851, doi:10.1016/j.physletb.2019.04.053.

[354] C. W. Xiao, J. Nieves, E. Oset, Heavy quark spin symmetric molecular states from $\bar{D}^{(*)}\Sigma_c^{(*)}$ and other coupled channels in the light of the recent LHCb pentaquarks, Phys. Rev. D 100 (1) (2019) 014021. arXiv:1904.01296, doi:10.1103/PhysRevD.100.014021.

[355] L. Meng, B. Wang, G.-J. Wang, S.-L. Zhu, The hidden charm pentaquark states and $\Sigma_c\bar{D}^{(*)}$ interaction in chiral perturbation theory, Phys. Rev. D 100 (1) (2019) 014031. arXiv:1905.04113, doi:10.1103/PhysRevD.100.014031.

[356] M.-L. Du, V. Baru, F.-K. Guo, C. Hanhart, U.-G. Meißner, J. A. Oller, Q. Wang, Interpretation of the LHCb P_c States as Hadronic Molecules and Hints of a Narrow $P_c(4380)$, Phys. Rev. Lett. 124 (7) (2020) 072001. arXiv:1910.11846, doi:10.1103/PhysRevLett.124.072001.

[357] F.-Z. Peng, M. Sánchez Sánchez, M.-J. Yan, M. Pavon Valderrama, Heavy-hadron molecular spectrum from light-meson exchange saturation, Phys. Rev. D 105 (3) (2022) 034028. arXiv:2101.07213, doi:10.1103/PhysRevD.105.034028.

[358] X.-K. Dong, F.-K. Guo, B.-S. Zou, A survey of heavy-antiheavy hadronic molecules, Progr. Phys. 41 (2021) 65–93. arXiv:2101.01021, doi:10.13725/j.cnki.pip.2021.02.001.

[359] C. W. Xiao, J. X. Lu, J. J. Wu, L. S. Geng, How to reveal the nature of three or more pentaquark states, Phys. Rev. D 102 (5) (2020) 056018. arXiv:2007.12106, doi:10.1103/PhysRevD.102.056018.

[360] G.-J. Wang, L.-Y. Xiao, R. Chen, X.-H. Liu, X. Liu, S.-L. Zhu, Probing hidden-charm decay properties of P_c states in a molecular scenario, Phys. Rev. D 102 (3) (2020) 036012. arXiv:1911.09613, doi:10.1103/PhysRevD.102.036012.

[361] T. Gutsche, V. E. Lyubovitskij, Structure and decays of hidden heavy pentaquarks, Phys. Rev. D 100 (9) (2019) 094031. arXiv:1910.03984, doi:10.1103/PhysRevD.100.094031.

[362] T. J. Burns, E. S. Swanson, Molecular interpretation of the $P_c(4440)$ and $P_c(4457)$ states, Phys. Rev. D 100 (11) (2019) 114033. arXiv:1908.03528, doi:10.1103/PhysRevD.100.114033.

[363] Y. Yamaguchi, H. García-Tecocoatzi, A. Giachino, A. Hosaka, E. Santopinto, S. Takeuchi, M. Takizawa, P_c pentaquarks with chiral tensor and quark dynamics, Phys. Rev. D 101 (9) (2020) 091502. arXiv:1907.04684, doi:10.1103/PhysRevD.101.091502.

[364] B. Wang, L. Meng, S.-L. Zhu, Hidden-charm and hidden-bottom molecular pentaquarks in chiral effective field theory, JHEP 11 (2019) 108. arXiv:1909.13054, doi:10.1007/JHEP11(2019)108.

[365] Y.-H. Lin, B.-S. Zou, Strong decays of the latest LHCb pentaquark candidates in hadronic molecule pictures, Phys. Rev. D 100 (5) (2019) 056005. arXiv:1908.05309, doi:10.1103/PhysRevD.100.056005.

[366] M. B. Voloshin, Some decay properties of hidden-charm pentaquarks as baryon-meson molecules, Phys. Rev. D 100 (3) (2019) 034020. `arXiv:1907.01476`, `doi:10.1103/PhysRevD.100.034020`.

[367] S.-Q. Kuang, L.-Y. Dai, X.-W. Kang, D.-L. Yao, Pole analysis on the hadron spectroscopy of $\Lambda_b \to J/\psi p K^-$, Eur. Phys. J. C 80 (5) (2020) 433. `arXiv:2002.11959`, `doi:10.1140/epjc/s10052-020-8008-5`.

[368] A. Ali, A. Y. Parkhomenko, Interpretation of the narrow $J/\psi p$ Peaks in $\Lambda_b \to J/\psi p K^-$ decay in the compact diquark model, Phys. Lett. B 793 (2019) 365–371. `arXiv:1904.00446`, `doi:10.1016/j.physletb.2019.05.002`.

[369] R. Zhu, X. Liu, H. Huang, C.-F. Qiao, Analyzing doubly heavy tetra- and penta-quark states by variational method, Phys. Lett. B 797 (2019) 134869. `arXiv:1904.10285`, `doi:10.1016/j.physletb.2019.134869`.

[370] Z.-G. Wang, Analysis of the $P_c(4312)$, $P_c(4440)$, $P_c(4457)$ and related hidden-charm pentaquark states with QCD sum rules, Int. J. Mod. Phys. A 35 (01) (2020) 2050003. `arXiv:1905.02892`, `doi:10.1142/S0217751X20500037`.

[371] J. F. Giron, R. F. Lebed, C. T. Peterson, The Dynamical Diquark Model: First Numerical Results, JHEP 05 (2019) 061. `arXiv:1903.04551`, `doi:10.1007/JHEP05(2019)061`.

[372] F. Stancu, Spectrum of the $uudc\bar{c}$ hidden charm pentaquark with an SU(4) flavor-spin hyperfine interaction, Eur. Phys. J. C 79 (11) (2019) 957. `arXiv:1902.07101`, `doi:10.1140/epjc/s10052-019-7474-0`.

[373] J. F. Giron, R. F. Lebed, Fine structure of pentaquark multiplets in the dynamical diquark model, Phys. Rev. D 104 (11) (2021) 114028. `arXiv:2110.05557`, `doi:10.1103/PhysRevD.104.114028`.

[374] J. Ferretti, E. Santopinto, M. Naeem Anwar, M. A. Bedolla, The baryo-quarkonium picture for hidden-charm and bottom pentaquarks and LHCb $P_c(4380)$ and $P_c(4450)$ states, Phys. Lett. B 789 (2019) 562–567. `arXiv:1807.01207`, `doi:10.1016/j.physletb.2018.09.047`.

[375] M. I. Eides, V. Y. Petrov, M. V. Polyakov, Narrow Nucleon-$\psi(2S)$ Bound State and LHCb Pentaquarks, Phys. Rev. D 93 (5) (2016) 054039. `arXiv:1512.00426`, `doi:10.1103/PhysRevD.93.054039`.

[376] M. I. Eides, V. Y. Petrov, M. V. Polyakov, New LHCb pentaquarks as hadro-charmonium states, Mod. Phys. Lett. A 35 (18) (2020) 2050151. `arXiv:1904.11616`, `doi:10.1142/S0217732320501515`.

[377] V. Kubarovsky, M. B. Voloshin, Formation of hidden-charm pentaquarks in photon-nucleon collisions, Phys. Rev. D 92 (3) (2015) 031502. `arXiv:1508.00888`, `doi:10.1103/PhysRevD.92.031502`.

[378] F.-K. Guo, U.-G. Meißner, W. Wang, Z. Yang, How to reveal the exotic nature of the $P_c(4450)$, Phys. Rev. D 92 (7) (2015) 071502. `arXiv:1507.04950`, `doi:10.1103/PhysRevD.92.071502`.

[379] X.-H. Liu, Q. Wang, Q. Zhao, Understanding the newly observed heavy pentaquark candidates, Phys. Lett. B 757 (2016) 231–236. `arXiv:1507.05359`, `doi:10.1016/j.physletb.2016.03.089`.

[380] M. Bayar, F. Aceti, F.-K. Guo, E. Oset, A Discussion on Triangle Singularities in the $\Lambda_b \to J/\psi K^- p$ Reaction, Phys. Rev. D 94 (7) (2016) 074039. `arXiv:1609.04133`, `doi:10.1103/PhysRevD.94.074039`.

[381] S. X. Nakamura, A. Hosaka, Y. Yamaguchi, $P_c(4312)^+$ and $P_c(4337)^+$ as interfering $\Sigma_c \bar{D}$ and $\Lambda_c \bar{D}^*$ threshold cusps, Phys. Rev. D 104 (9) (2021) L091503. `arXiv:2109.15235`, `doi:10.1103/PhysRevD.104.L091503`.

[382] J. He, Study of $P_c(4457)$, $P_c(4440)$, and $P_c(4312)$ in a quasipotential Bethe-Salpeter equation approach, Eur. Phys. J. C 79 (5) (2019) 393. `arXiv:1903.11872`, `doi:10.1140/epjc/s10052-019-6906-1`.

[383] J. He, D.-Y. Chen, Molecular states from $\Sigma_c^{(*)}\bar{D}^{(*)} - \Lambda_c\bar{D}^{(*)}$ interaction, Eur. Phys. J. C 79 (11) (2019) 887. `arXiv:1909.05681`, `doi:10.1140/epjc/s10052-019-7419-7`.

[384] M.-Z. Liu, T.-W. Wu, M. Sánchez Sánchez, M. P. Valderrama, L.-S. Geng, J.-J. Xie, Spin-parities of the $P_c(4440)$ and $P_c(4457)$ in the one-boson-exchange model, Phys. Rev. D 103 (5) (2021) 054004. `arXiv:1907.06093`, `doi:10.1103/PhysRevD.103.054004`.

[385] M.-L. Du, V. Baru, F.-K. Guo, C. Hanhart, U.-G. Meißner, J. A. Oller, Q. Wang, Revisiting the nature of the P_c pentaquarks, JHEP 08 (2021) 157. `arXiv:2102.07159`, `doi:10.1007/JHEP08(2021)157`.

[386] N. Yalikun, Y.-H. Lin, F.-K. Guo, Y. Kamiya, B.-S. Zou, Coupled-channel effects of the $\Sigma_c^{(*)}\bar{D}^{(*)} - \Lambda_c(2595)\bar{D}$ system and molecular nature of the P_c pentaquark states from one-boson exchange model, Phys. Rev. D 104 (9) (2021) 094039. `arXiv:2109.03504`, `doi:10.1103/PhysRevD.104.094039`.

[387] M. Pavon Valderrama, One pion exchange and the quantum numbers of the $P_c(4440)$ and $P_c(4457)$ pentaquarks, Phys. Rev. D 100 (9) (2019) 094028. `arXiv:1907.05294`, `doi:10.1103/PhysRevD.100.094028`.

[388] S. Sakai, H.-J. Jing, F.-K. Guo, Decays of P_c into $J/\psi N$ and $\eta_c N$ with heavy quark spin symmetry, Phys. Rev. D 100 (7) (2019) 074007. `arXiv:1907.03414`, `doi:10.1103/PhysRevD.100.074007`.

[389] C.-J. Xiao, Y. Huang, Y.-B. Dong, L.-S. Geng, D.-Y. Chen, Exploring the molecular scenario of $P_c(4312)$, $P_c(4440)$, and $P_c(4457)$, Phys. Rev. D 100 (1) (2019) 014022. `arXiv:1904.00872`, `doi:10.1103/PhysRevD.100.014022`.

[390] F.-K. Guo, H.-J. Jing, U.-G. Meißner, S. Sakai, Isospin breaking decays as a diagnosis of the hadronic molecular structure of the $P_c(4457)$, Phys. Rev. D 99 (9) (2019) 091501. `arXiv:1903.11503`, `doi:10.1103/PhysRevD.99.091501`.

[391] Y.-J. Xu, C.-Y. Cui, Y.-L. Liu, M.-Q. Huang, Partial decay widths of $P_c(4312)$ as a $\bar{D}\Sigma_c$ molecular state, Phys. Rev. D 102 (3) (2020) 034028. `arXiv:1907.05097`, `doi:10.1103/PhysRevD.102.034028`.

[392] X. Cao, J.-p. Dai, Confronting pentaquark photoproduction with new LHCb observations, Phys. Rev. D 100 (5) (2019) 054033. `arXiv:1904.06015`, `doi:10.1103/PhysRevD.100.054033`.

[393] X.-Z. Ling, J.-X. Lu, M.-Z. Liu, L.-S. Geng, $P_c(4457) \to P_c(4312)\pi/\gamma$ in the molecular picture, Phys. Rev. D 104 (7) (2021) 074022. `arXiv:2106.12250`, `doi:10.1103/PhysRevD.104.074022`.

[394] Y. Dong, P. Shen, F. Huang, Z. Zhang, Selected strong decays of pentaquark State $P_c(4312)$ in a chiral constituent quark model, Eur. Phys. J. C 80 (4) (2020) 341. `arXiv:2002.08051`, `doi:10.1140/epjc/s10052-020-7890-1`.

[395] P. Ling, X.-H. Dai, M.-L. Du, Q. Wang, Prompt production of the hidden charm pentaquarks in the LHC, Eur. Phys. J. C 81 (9) (2021) 819. `arXiv:2104.11133`, `doi:10.1140/epjc/s10052-021-09613-8`.

[396] I. W. Park, S. Cho, Y. Kim, S. H. Lee, Production of Pc(4312) state in electron-proton collisions, Phys. Rev. D 105 (11) (2022) 114023. `arXiv:2202.11631`, `doi:10.1103/PhysRevD.105.114023`.

[397] D. Winney, C. Fanelli, A. Pilloni, A. N. Hiller Blin, C. Fernández-Ramírez, M. Albaladejo, V. Mathieu, V. I. Mokeev, A. P. Szczepaniak, Double polarization observables in pentaquark photoproduction, Phys. Rev. D 100 (3) (2019) 034019. `arXiv:1907.09393`, `doi:10.1103/`

PhysRevD.100.034019.

[398] H.-X. Chen, Hidden-charm pentaquark states through current algebra: from their production to decay *, Chin. Phys. C 46 (9) (2022) 093105. arXiv:2011.07187, doi:10.1088/1674-1137/ac6ed2.

[399] Z. Yang, X. Cao, Y.-T. Liang, J.-J. Wu, Identifying hidden charm pentaquark signal from non-resonant background in electron–proton scattering, Chin. Phys. C 44 (8) (2020) 084102. arXiv:2003.06774, doi:10.1088/1674-1137/44/8/084102.

[400] A. Ali, et al., First Measurement of Near-Threshold J/ψ Exclusive Photoproduction off the Proton, Phys. Rev. Lett. 123 (7) (2019) 072001. arXiv:1905.10811, doi:10.1103/PhysRevLett.123.072001.

[401] M.-L. Du, V. Baru, F.-K. Guo, C. Hanhart, U.-G. Meißner, A. Nefediev, I. Strakovsky, Deciphering the mechanism of near-threshold J/ψ photoproduction, Eur. Phys. J. C 80 (11) (2020) 1053. arXiv:2009.08345, doi:10.1140/epjc/s10052-020-08620-5.

[402] M. Karliner, J. L. Rosner, Photoproduction of Exotic Baryon Resonances, Phys. Lett. B 752 (2016) 329–332. arXiv:1508.01496, doi:10.1016/j.physletb.2015.11.068.

[403] J.-J. Wu, T. S. H. Lee, B.-S. Zou, Nucleon resonances with hidden charm in γp reactions, Phys. Rev. C 100 (3) (2019) 035206. arXiv:1906.05375, doi:10.1103/PhysRevC.100.035206.

[404] G. Rossi, G. Veneziano, P_c Photo-production And Decay (9 2019). arXiv:1909.01753.

[405] G. C. Rossi, G. Veneziano, A Possible Description of Baryon Dynamics in Dual and Gauge Theories, Nucl. Phys. B 123 (1977) 507–545. doi:10.1016/0550-3213(77)90178-X.

[406] G. C. Rossi, G. Veneziano, Electromagnetic Mixing of Narrow Baryonium States, Phys. Lett. B 70 (1977) 255–259. doi:10.1016/0370-2693(77)90533-0.

[407] G. C. Rossi, G. Veneziano, Isospin mixing of narrow pentaquark states, Phys. Lett. B 597 (2004) 338–345. arXiv:hep-ph/0404262, doi:10.1016/j.physletb.2004.07.042.

[408] R. Aaij, et al., Evidence for a new structure in the $J/\psi p$ and $J/\psi \bar{p}$ systems in $B_s^0 \to J/\psi p \bar{p}$ decays, Phys. Rev. Lett. 128 (6) (2022) 062001. arXiv:2108.04720, doi:10.1103/PhysRevLett.128.062001.

[409] M.-J. Yan, F.-Z. Peng, M. Sánchez Sánchez, M. Pavon Valderrama, Interpretations of the new LHCb $P_c(4337)^+$ pentaquark state, Eur. Phys. J. C 82 (6) (2022) 574. arXiv:2108.05306, doi:10.1140/epjc/s10052-022-10522-7.

[410] J.-Z. Wang, X. Liu, T. Matsuki, Evidence supporting the existence of $P_c(4380)^{\pm}$ from the recent measurements of $B_s \to J/\psi p \bar{p}$, Phys. Rev. D 104 (11) (2021) 114020. arXiv:2110.09423, doi:10.1103/PhysRevD.104.114020.

[411] C. W. Xiao, J. Nieves, E. Oset, Combining heavy quark spin and local hidden gauge symmetries in the dynamical generation of hidden charm baryons, Phys. Rev. D 88 (2013) 056012. arXiv:1304.5368, doi:10.1103/PhysRevD.88.056012.

[412] Y.-W. Pan, M.-Z. Liu, F.-Z. Peng, M. Sánchez Sánchez, L.-S. Geng, M. Pavon Valderrama, Model independent determination of the spins of the $P_c(4440)$ and $P_c(4457)$ from the spectroscopy of the triply charmed dibaryons, Phys. Rev. D 102 (1) (2020) 011504. arXiv:1907.11220, doi:10.1103/PhysRevD.102.011504.

[413] H.-X. Chen, L.-S. Geng, W.-H. Liang, E. Oset, E. Wang, J.-J. Xie, Looking for a hidden-charm pentaquark state with strangeness $S = -1$ from Ξ_b^- decay into $J/\psi K^- \Lambda$, Phys. Rev. C 93 (6) (2016) 065203. arXiv:1510.01803, doi:10.1103/PhysRevC.93.065203.

[414] R. Chen, J. He, X. Liu, Possible strange hidden-charm pentaquarks from $\Sigma_c^{(*)} \bar{D}_s^*$ and $\Xi_c^{(',*)} \bar{D}^*$ interactions, Chin. Phys. C 41 (10) (2017) 103105. arXiv:1609.03235, doi:10.1088/1674-1137/41/10/103105.

[415] C.-W. Shen, J.-J. Wu, B.-S. Zou, Decay behaviors of possible $\Lambda_{c\bar{c}}$ states in hadronic molecule pictures, Phys. Rev. D 100 (5) (2019) 056006. arXiv:1906.03896, doi:10.1103/PhysRevD.100.056006.

[416] C. W. Xiao, J. Nieves, E. Oset, Prediction of hidden charm strange molecular baryon states with heavy quark spin symmetry, Phys. Lett. B 799 (2019) 135051. arXiv:1906.09010, doi:10.1016/j.physletb.2019.135051.

[417] B. Wang, L. Meng, S.-L. Zhu, Spectrum of the strange hidden charm molecular pentaquarks in chiral effective field theory, Phys. Rev. D 101 (3) (2020) 034018. arXiv:1912.12592, doi:10.1103/PhysRevD.101.034018.

[418] V. V. Anisovich, M. A. Matveev, J. Nyiri, A. V. Sarantsev, A. N. Semenova, Nonstrange and strange pentaquarks with hidden charm, Int. J. Mod. Phys. A 30 (32) (2015) 1550190. arXiv:1509.04898, doi:10.1142/S0217751X15501900.

[419] R. Aaij, et al., Evidence of a $J/\psi \Lambda$ structure and observation of excited Ξ^- states in the $\Xi_b^- \to J/\psi \Lambda K^-$ decay, Sci. Bull. 66 (2021) 1278–1287. arXiv:2012.10380, doi:10.1016/j.scib.2021.02.030.

[420] M.-L. Du, Z.-H. Guo, J. A. Oller, Insights into the nature of the $P_{cs}(4459)$, Phys. Rev. D 104 (11) (2021) 114034. arXiv:2109.14237, doi:10.1103/PhysRevD.104.114034.

[421] C.-R. Deng, Compact hidden charm pentaquark states and QCD isomers, Phys. Rev. D 105 (11) (2022) 116021. arXiv:2202.13570, doi:10.1103/PhysRevD.105.116021.

[422] F. Yang, Y. Huang, H. Q. Zhu, Strong decays of the $P_{cs}(4459)$ as a $\Xi_c \bar{D}^*$ molecule, Sci. China Phys. Mech. Astron. 64 (12) (2021) 121011. arXiv:2107.13267, doi:10.1007/s11433-021-1796-0.

[423] F.-Z. Peng, M.-J. Yan, M. Sánchez Sánchez, M. P. Valderrama, The $P_{cs}(4459)$ pentaquark from a combined effective field theory and phenomenological perspective, Eur. Phys. J. C 81 (7) (2021) 666. arXiv:2011.01915, doi:10.1140/epjc/s10052-021-09416-x.

[424] H.-X. Chen, W. Chen, X. Liu, X.-H. Liu, Establishing the first hidden-charm pentaquark with strangeness, Eur. Phys. J. C 81 (5) (2021) 409. arXiv:2011.01079, doi:10.1140/epjc/s10052-021-09196-4.

[425] R. Chen, Can the newly reported $P_{cs}(4459)$ be a strange hidden-charm $\Xi_c \bar{D}^*$ molecular pentaquark?, Phys. Rev. D 103 (5) (2021) 054007. arXiv:2011.07214, doi:10.1103/PhysRevD.103.054007.

[426] J.-T. Zhu, L.-Q. Song, J. He, $P_{cs}(4459)$ and other possible molecular states from $\Xi_c^{(*)} \bar{D}^{(*)}$ and $\Xi_c' \bar{D}^{(*)}$ interactions, Phys. Rev. D 103 (7) (2021) 074007. arXiv:2101.12441, doi:10.1103/PhysRevD.103.074007.

[427] J.-X. Lu, M.-Z. Liu, R.-X. Shi, L.-S. Geng, Understanding $P_{cs}(4459)$ as a hadronic molecule in the $\Xi_{bb} \to J/\psi \Lambda K^-$ decay, Phys. Rev. D 104 (3) (2021) 034022. arXiv:2104.10303, doi:10.1103/PhysRevD.104.034022.

[428] M.-Z. Liu, Y.-W. Pan, L.-S. Geng, Can discovery of hidden charm strange pentaquark states help determine the spins of $P_c(4440)$ and $P_c(4457)$?, Phys. Rev. D 103 (3) (2021) 034003. arXiv:2011.07935, doi:10.1103/PhysRevD.103.034003.

[429] S. Clymton, H.-J. Kim, H.-C. Kim, Production of hidden-charm strange pentaquarks P_{cs} from the $K^- p \to J/\psi \Lambda$ reaction, Phys. Rev. D 104 (1) (2021) 014023. arXiv:2102.08737, doi:10.1103/PhysRevD.104.014023.

154

[430] K. Azizi, Y. Sarac, H. Sundu, Investigation of $P_{cs}(4459)^0$ pentaquark via its strong decay to $\Lambda J/\psi$, Phys. Rev. D 103 (9) (2021) 094033. arXiv:2101.07850, doi:10.1103/PhysRevD.103.094033.

[431] Q. Wu, D.-Y. Chen, R. Ji, Production of $P_{cs}(4459)$ from Ξ_b Decay, Chin. Phys. Lett. 38 (7) (2021) 071301. arXiv:2103.05257, doi:10.1088/0256-307X/38/7/071301.

[432] C. W. Xiao, J. J. Wu, B. S. Zou, Molecular nature of $P_{cs}(4459)$ and its heavy quark spin partners, Phys. Rev. D 103 (5) (2021) 054016. arXiv:2102.02607, doi:10.1103/PhysRevD.103.054016.

[433] E. Santopinto, A. Giachino, Compact pentaquark structures, Phys. Rev. D 96 (1) (2017) 014014. arXiv:1604.03769, doi:10.1103/PhysRevD.96.014014.

[434] T. Gershon, Exotic hadron naming convention (6 2022). arXiv:2206.15233.

[435] Observation of a $J/\psi\Lambda$ resonance consistent with a strange pentaquark candidate in $B^- \to J/\psi\Lambda\bar{p}$ decays (10 2022). arXiv:2210.10346.

[436] M. Karliner, J. L. Rosner, New strange pentaquarks, Phys. Rev. D 106 (3) (2022) 036024. arXiv:2207.07581, doi:10.1103/PhysRevD.106.036024.

[437] L. Meng, B. Wang, S.-L. Zhu, Double thresholds distort the line shapes of the $P^\Lambda_{\psi s}(4338)^0$ resonance, Phys. Rev. D 107 (1) (2023) 014005. arXiv:2208.03883, doi:10.1103/PhysRevD.107.014005.

[438] K. Chen, Z.-Y. Lin, S.-L. Zhu, Comparison between the P^N_ψ and $P^\Lambda_{\psi s}$ systems, Phys. Rev. D 106 (11) (2022) 116017. arXiv:2211.05558, doi:10.1103/PhysRevD.106.116017.

[439] F.-L. Wang, X. Liu, Emergence of molecular-type characteristic spectrum of hidden-charm pentaquark with strangeness embodied in the $P^\Lambda_{\psi s}(4338)$ and $P_{cs}(4459)$, Phys. Lett. B 835 (2022) 137583. arXiv:2207.10493, doi:10.1016/j.physletb.2022.137583.

[440] T. J. Burns, E. S. Swanson, The LHCb state $P^\Lambda_{\psi s}(4338)$ as a triangle singularity, Phys. Lett. B 838 (2023) 137715. arXiv:2208.05106, doi:10.1016/j.physletb.2023.137715.

[441] M.-J. Yan, F.-Z. Peng, M. Sánchez Sánchez, M. Pavon Valderrama, The $P^\Lambda_{\psi s}(4338)$ pentaquark and its partners in the molecular picture (7 2022). arXiv:2207.11144.

[442] Z.-Y. Yang, F.-Z. Peng, M.-J. Yan, M. Sánchez Sánchez, M. Pavon Valderrama, Molecular P_ψ pentaquarks from light-meson exchange saturation (11 2022). arXiv:2211.08211.

[443] S. X. Nakamura, J. J. Wu, Pole determination of $P^\Lambda_{\psi s}(4338)$ and possible $P^\Lambda_{\psi s}(4255)$ in $B^- \to J/\psi\Lambda\bar{p}$ (8 2022). arXiv:2208.11995.

[444] A. Giachino, A. Hosaka, E. Santopinto, S. Takeuchi, M. Takizawa, Y. Yamaguchi, Rich structure of the hidden-charm pentaquarks near threshold regions (9 2022). arXiv:2209.10413.

[445] P. G. Ortega, D. R. Entem, F. Fernandez, Strange hidden-charm $P^\Lambda_{\psi s}(4459)$ and $P^\Lambda_{\psi s}(4338)$ pentaquarks and additional $P^\Lambda_{\psi s}$, $P^\Sigma_{\psi s}$ and $P^N_{\psi ss}$ candidates in a quark model approach, Phys. Lett. B 838 (2023) 137747. arXiv:2210.04465, doi:10.1016/j.physletb.2023.137747.

[446] U. Özdem, Investigation of magnetic moment of $P_{cs}(4338)$ and $P_{cs}(4459)$ pentaquark states, Phys. Lett. B 836 (2023) 137635. arXiv:2208.07684, doi:10.1016/j.physletb.2022.137635.

[447] F.-L. Wang, H.-Y. Zhou, Z.-W. Liu, X. Liu, What can we learn from the electromagnetic properties of hidden-charm molecular pentaquarks with single strangeness?, Phys. Rev. D 106 (5) (2022) 054020. arXiv:2208.10756, doi:10.1103/PhysRevD.106.054020.

[448] Q.-S. Zhou, K. Chen, X. Liu, Y.-R. Liu, S.-L. Zhu, Surveying exotic pentaquarks with the typical $QQqq\bar{q}$ configuration, Phys. Rev. C 98 (4) (2018) 045204. arXiv:1801.04557, doi:10.1103/PhysRevC.98.045204.

[449] W. Park, S. Cho, S. H. Lee, Where is the stable pentaquark?, Phys. Rev. D 99 (9) (2019) 094023. arXiv:1811.10911, doi:10.1103/PhysRevD.99.094023.

[450] R. Chen, N. Li, Z.-F. Sun, X. Liu, S.-L. Zhu, Doubly charmed molecular pentaquarks, Phys. Lett. B 822 (2021) 136693. arXiv:2108.12730, doi:10.1016/j.physletb.2021.136693.

[451] G. Yang, J. Ping, J. Segovia, Doubly Charmed Pentaquarks, Phys. Rev. D 101 (7) (2020) 074030. arXiv:2003.05253, doi:10.1103/PhysRevD.101.074030.

[452] Y. Shimizu, M. Harada, Hidden Charm Pentaquark $P_c(4380)$ and Doubly Charmed Baryon $\Xi^*_{cc}(4380)$ as Hadronic Molecule States, Phys. Rev. D 96 (9) (2017) 094012. arXiv:1708.04743, doi:10.1103/PhysRevD.96.094012.

[453] K. Chen, B. Wang, S.-L. Zhu, Exploration of the doubly charmed molecular pentaquarks, Phys. Rev. D 103 (11) (2021) 116017. arXiv:2102.05868, doi:10.1103/PhysRevD.103.116017.

[454] R. Chen, A. Hosaka, X. Liu, Heavy molecules and one-σ/ω-exchange model, Phys. Rev. D 96 (11) (2017) 116012. arXiv:1707.08306, doi:10.1103/PhysRevD.96.116012.

[455] K. Azizi, Y. Sarac, H. Sundu, Investigation of hidden-charm double strange pentaquark candidate P_{css} via its mass and strong decay to $\Xi^0 J/\psi$ (12 2021). arXiv:2112.15543.

[456] Y. Yan, Y. Wu, X. Hu, H. Huang, J. Ping, Fully heavy pentaquarks in quark models, Phys. Rev. D 105 (1) (2022) 014027. arXiv:2110.10853, doi:10.1103/PhysRevD.105.014027.

[457] H.-T. An, S.-Q. Luo, Z.-W. Liu, X. Liu, Fully heavy pentaquark states in constituent quark model, Phys. Rev. D 105 (7) (2022) 074032. arXiv:2203.03448, doi:10.1103/PhysRevD.105.074032.

[458] H.-T. An, K. Chen, X. Liu, Manifestly exotic pentaquarks with a single heavy quark, Phys. Rev. D 105 (3) (2022) 034018. arXiv:2010.05014, doi:10.1103/PhysRevD.105.034018.

[459] J.-M. Richard, A. Valcarce, J. Vijande, Pentaquarks with anticharm or beauty revisited, Phys. Lett. B 790 (2019) 248–250. arXiv:1901.03578, doi:10.1016/j.physletb.2019.01.031.

[460] C. Gignoux, B. Silvestre-Brac, J. M. Richard, Possibility of Stable Multi-Quark Baryons, Phys. Lett. B 193 (1987) 323. doi:10.1016/0370-2693(87)91244-5.

[461] H. J. Lipkin, New Possibilities for Exotic Hadrons: Anticharmed Strange Baryons, Phys. Lett. B 195 (1987) 484–488. doi:10.1016/0370-2693(87)90055-4.

[462] Y. Xing, W.-L. Liu, Y.-H. Xiao, The production of singly charmed pentaquark $\bar{c}qqqq$ from bottom baryon, Eur. Phys. J. C 82 (12) (2022) 1105. arXiv:2203.03248, doi:10.1140/epjc/s10052-022-11092-4.

[463] C.-W. Shen, U.-G. Meißner, Prediction of five-flavored pentaquarks, Phys. Lett. B 831 (2022) 137197. arXiv:2203.09804, doi:10.

1016/j.physletb.2022.137197.

[464] S. Weinberg, Phenomenological Lagrangians, Physica A 96 (1-2) (1979) 327–340. `doi:10.1016/0378-4371(79)90223-1`.

[465] U.-G. Meißner, A. Rusetsky, Effective Field Theories, Cambridge University Press, 2022. `doi:10.1017/9781108689038`.

[466] A. A. Petrov, A. E. Blechman, Effective Field Theories, WORLD SCIENTIFIC, 2016. `doi:10.1142/8619`.
URL `https://www.worldscientific.com/doi/abs/10.1142/8619`

[467] A. Manohar, H. Georgi, Chiral Quarks and the Nonrelativistic Quark Model, Nucl. Phys. B 234 (1984) 189–212. `doi:10.1016/0550-3213(84)90231-1`.

[468] G. Ecker, Chiral perturbation theory, Prog. Part. Nucl. Phys. 35 (1995) 1–80. `arXiv:hep-ph/9501357`, `doi:10.1016/0146-6410(95)00041-G`.

[469] V. Bernard, N. Kaiser, U.-G. Meissner, Chiral dynamics in nucleons and nuclei, Int. J. Mod. Phys. E 4 (1995) 193–346. `arXiv:hep-ph/9501384`, `doi:10.1142/S0218301395000092`.

[470] P. L. Cho, Heavy hadron chiral perturbation theory, Nucl. Phys. B 396 (1993) 183–204, [Erratum: Nucl.Phys.B 421, 683–686 (1994)]. `arXiv:hep-ph/9208244`, `doi:10.1016/0550-3213(93)90263-O`.

[471] N. Fettes, U.-G. Meissner, M. Mojzis, S. Steininger, The Chiral effective pion nucleon Lagrangian of order p^4, Annals Phys. 283 (2000) 273–302, [Erratum: Annals Phys. 288, 249–250 (2001)]. `arXiv:hep-ph/0001308`, `doi:10.1006/aphy.2000.6059`.

[472] S. Steininger, U.-G. Meissner, N. Fettes, On wave function renormalization and related aspects in heavy fermion effective field theories, JHEP 09 (1998) 008. `arXiv:hep-ph/9808280`, `doi:10.1088/1126-6708/1998/09/008`.

[473] V. Koch, Aspects of chiral symmetry, Int. J. Mod. Phys. E 6 (1997) 203–250. `arXiv:nucl-th/9706075`, `doi:10.1142/S0218301397000147`.

[474] M. Neubert, Heavy quark symmetry, Phys. Rept. 245 (1994) 259–396. `arXiv:hep-ph/9306320`, `doi:10.1016/0370-1573(94)90091-4`.

[475] E. Epelbaum, H.-W. Hammer, U.-G. Meissner, Modern Theory of Nuclear Forces, Rev. Mod. Phys. 81 (2009) 1773–1825. `arXiv:0811.1338`, `doi:10.1103/RevModPhys.81.1773`.

[476] R. Machleidt, D. R. Entem, Chiral effective field theory and nuclear forces, Phys. Rept. 503 (2011) 1–75. `arXiv:1105.2919`, `doi:10.1016/j.physrep.2011.02.001`.

[477] S. Scherer, Introduction to chiral perturbation theory, Adv. Nucl. Phys. 27 (2003) 277. `arXiv:hep-ph/0210398`.

[478] A. V. Manohar, M. B. Wise, Heavy quark physics, Vol. 10, 2000.

[479] A. Pich, Effective field theory: Course, in: Les Houches Summer School in Theoretical Physics, Session 68: Probing the Standard Model of Particle Interactions, 1998, pp. 949–1049. `arXiv:hep-ph/9806303`.

[480] J. Goldstone, Field Theories with Superconductor Solutions, Nuovo Cim. 19 (1961) 154–164. `doi:10.1007/BF02812722`.

[481] J. Goldstone, A. Salam, S. Weinberg, Broken Symmetries, Phys. Rev. 127 (1962) 965–970. `doi:10.1103/PhysRev.127.965`.

[482] Y. Nambu, G. Jona-Lasinio, Dynamical Model of Elementary Particles Based on an Analogy with Superconductivity. 1., Phys. Rev. 122 (1961) 345–358. `doi:10.1103/PhysRev.122.345`.

[483] M. Gell-Mann, M. Levy, The axial vector current in beta decay, Nuovo Cim. 16 (1960) 705. `doi:10.1007/BF02859738`.

[484] K.-C. Chou, On the pseudo-vector current and lepton decays of baryons and mesons, Soviet Phys. JETP 12 (1961) 492.

[485] J. Gasser, H. Leutwyler, Chiral Perturbation Theory to One Loop, Annals Phys. 158 (1984) 142. `doi:10.1016/0003-4916(84)90242-2`.

[486] J. Gasser, H. Leutwyler, Chiral Perturbation Theory: Expansions in the Mass of the Strange Quark, Nucl. Phys. B 250 (1985) 465–516. `doi:10.1016/0550-3213(85)90492-4`.

[487] S. R. Coleman, J. Wess, B. Zumino, Structure of phenomenological Lagrangians. 1., Phys. Rev. 177 (1969) 2239–2247. `doi:10.1103/PhysRev.177.2239`.

[488] C. G. Callan, Jr., S. R. Coleman, J. Wess, B. Zumino, Structure of phenomenological Lagrangians. 2., Phys. Rev. 177 (1969) 2247–2250. `doi:10.1103/PhysRev.177.2247`.

[489] J. Gasser, H. Leutwyler, Low-Energy Expansion of Meson Form-Factors, Nucl. Phys. B 250 (1985) 517–538. `doi:10.1016/0550-3213(85)90493-6`.

[490] J. Gasser, H. Leutwyler, $\eta \to 3\pi$ to One Loop, Nucl. Phys. B 250 (1985) 539–560. `doi:10.1016/0550-3213(85)90494-8`.

[491] H. D. Politzer, M. B. Wise, Leading Logarithms of Heavy Quark Masses in Processes with Light and Heavy Quarks, Phys. Lett. B 206 (1988) 681–684. `doi:10.1016/0370-2693(88)90718-6`.

[492] N. Isgur, M. B. Wise, Weak Decays of Heavy Mesons in the Static Quark Approximation, Phys. Lett. B 232 (1989) 113–117. `doi:10.1016/0370-2693(89)90566-2`.

[493] E. Eichten, B. R. Hill, An Effective Field Theory for the Calculation of Matrix Elements Involving Heavy Quarks, Phys. Lett. B 234 (1990) 511–516. `doi:10.1016/0370-2693(90)92049-O`.

[494] H. Georgi, An Effective Field Theory for Heavy Quarks at Low-energies, Phys. Lett. B 240 (1990) 447–450. `doi:10.1016/0370-2693(90)91128-X`.

[495] N. Isgur, M. B. Wise, Weak transition form-factors between heavy mesons, Phys. Lett. B 237 (1990) 527–530. `doi:10.1016/0370-2693(90)91219-2`.

[496] B. Grinstein, The Static Quark Effective Theory, Nucl. Phys. B 339 (1990) 253–268. `doi:10.1016/0550-3213(90)90349-I`.

[497] A. F. Falk, H. Georgi, B. Grinstein, M. B. Wise, Heavy Meson Form-factors From QCD, Nucl. Phys. B 343 (1990) 1–13. `doi:10.1016/0550-3213(90)90591-Z`.

[498] T. Mannel, W. Roberts, Z. Ryzak, A Derivation of the heavy quark effective Lagrangian from QCD, Nucl. Phys. B 368 (1992) 204–217. `doi:10.1016/0550-3213(92)90204-O`.

[499] M. Anselmino, E. Predazzi, S. Ekelin, S. Fredriksson, D. B. Lichtenberg, Diquarks, Rev. Mod. Phys. 65 (1993) 1199–1234. `doi:10.1103/RevModPhys.65.1199`.

[500] H. Georgi, M. B. Wise, Superflavor Symmetry for Heavy Particles, Phys. Lett. B 243 (1990) 279–283. `doi:10.1016/0370-2693(90)90851-V`.

[501] S. Fleming, T. Mehen, Doubly heavy baryons, heavy quark-diquark symmetry and NRQCD, Phys. Rev. D 73 (2006) 034502. `arXiv:`

hep-ph/0509313, doi:10.1103/PhysRevD.73.034502.

[502] D. Ebert, R. N. Faustov, V. O. Galkin, A. P. Martynenko, Mass spectra of doubly heavy baryons in the relativistic quark model, Phys. Rev. D 66 (2002) 014008. arXiv:hep-ph/0201217, doi:10.1103/PhysRevD.66.014008.

[503] R. Lewis, N. Mathur, R. M. Woloshyn, Charmed baryons in lattice QCD, Phys. Rev. D 64 (2001) 094509. arXiv:hep-ph/0107037, doi:10.1103/PhysRevD.64.094509.

[504] T. Mehen, Implications of Heavy Quark-Diquark Symmetry for Excited Doubly Heavy Baryons and Tetraquarks, Phys. Rev. D 96 (9) (2017) 094028. arXiv:1708.05020, doi:10.1103/PhysRevD.96.094028.

[505] T. C. Mehen, A. Mohapatra, Perturbative Corrections to Heavy Quark-Diquark Symmetry Predictions for Doubly Heavy Baryon Hyperfine Splittings, Phys. Rev. D 100 (7) (2019) 076014. arXiv:1905.06965, doi:10.1103/PhysRevD.100.076014.

[506] J. Hu, T. Mehen, Chiral Lagrangian with heavy quark-diquark symmetry, Phys. Rev. D 73 (2006) 054003. arXiv:hep-ph/0511321, doi:10.1103/PhysRevD.73.054003.

[507] N. Brambilla, A. Vairo, T. Rosch, Effective field theory Lagrangians for baryons with two and three heavy quarks, Phys. Rev. D 72 (2005) 034021. arXiv:hep-ph/0506065, doi:10.1103/PhysRevD.72.034021.

[508] T. D. Cohen, P. M. Hohler, Doubly heavy hadrons and the domain of validity of doubly heavy diquark-antiquark symmetry, Phys. Rev. D 74 (2006) 094003. arXiv:hep-ph/0606084, doi:10.1103/PhysRevD.74.094003.

[509] S. Weinberg, Effective chiral Lagrangians for nucleon-pion interactions and nuclear forces, Nucl. Phys. B 363 (1991) 3–18. doi:10.1016/0550-3213(91)90231-L.

[510] S. Weinberg, Three body interactions among nucleons and pions, Phys. Lett. B 295 (1992) 114–121. arXiv:hep-ph/9209257, doi:10.1016/0370-2693(92)90099-P.

[511] E. E. Jenkins, A. V. Manohar, Baryon chiral perturbation theory using a heavy fermion Lagrangian, Phys. Lett. B 255 (1991) 558–562. doi:10.1016/0370-2693(91)90266-S.

[512] V. Bernard, N. Kaiser, J. Kambor, U. G. Meissner, Chiral structure of the nucleon, Nucl. Phys. B 388 (1992) 315–345. doi:10.1016/0550-3213(92)90615-I.

[513] V. Bernard, Chiral Perturbation Theory and Baryon Properties, Prog. Part. Nucl. Phys. 60 (2008) 82–160. arXiv:0706.0312, doi:10.1016/j.ppnp.2007.07.001.

[514] T. Becher, H. Leutwyler, Baryon chiral perturbation theory in manifestly Lorentz invariant form, Eur. Phys. J. C 9 (1999) 643–671. arXiv:hep-ph/9901384, doi:10.1007/PL00021673.

[515] T. Becher, H. Leutwyler, Low energy analysis of $\pi N \to \pi N$, JHEP 06 (2001) 017. arXiv:hep-ph/0103263, doi:10.1088/1126-6708/2001/06/017.

[516] M. R. Schindler, J. Gegelia, S. Scherer, Infrared regularization of baryon chiral perturbation theory reformulated, Phys. Lett. B 586 (2004) 258–266. arXiv:hep-ph/0309005, doi:10.1016/j.physletb.2004.02.056.

[517] T. Fuchs, J. Gegelia, G. Japaridze, S. Scherer, Renormalization of relativistic baryon chiral perturbation theory and power counting, Phys. Rev. D 68 (2003) 056005. arXiv:hep-ph/0302117, doi:10.1103/PhysRevD.68.056005.

[518] D.-L. Yao, Analyses of pion-nucleon elastic scattering amplitudes up to $O(q^4)$ in extended-on-mass-shell subtraction scheme, Ph.D. thesis, Peking University (2013).

[519] H. A. Bethe, Theory of the Effective Range in Nuclear Scattering, Phys. Rev. 76 (1949) 38–50. doi:10.1103/PhysRev.76.38.

[520] J. M. Blatt, J. D. Jackson, On the Interpretation of Neutron-Proton Scattering Data by the Schwinger Variational Method, Phys. Rev. 76 (1949) 18–37. doi:10.1103/PhysRev.76.18.

[521] S. Weinberg, Elementary particle theory of composite particles, Phys. Rev. 130 (1963) 776–783. doi:10.1103/PhysRev.130.776.

[522] D. B. Kaplan, M. J. Savage, M. B. Wise, A New expansion for nucleon-nucleon interactions, Phys. Lett. B 424 (1998) 390–396. arXiv:nucl-th/9801034, doi:10.1016/S0370-2693(98)00210-X.

[523] E. Braaten, H. W. Hammer, Universality in few-body systems with large scattering length, Phys. Rept. 428 (2006) 259–390. arXiv:cond-mat/0410417, doi:10.1016/j.physrep.2006.03.001.

[524] V. Baru, E. Epelbaum, A. A. Filin, J. Gegelia, Low-energy theorems for nucleon-nucleon scattering at unphysical pion masses, Phys. Rev. C 92 (1) (2015) 014001. arXiv:1504.07852, doi:10.1103/PhysRevC.92.014001.

[525] C. Morningstar, J. Bulava, B. Singha, R. Brett, J. Fallica, A. Hanlon, B. Hörz, Estimating the two-particle K-matrix for multiple partial waves and decay channels from finite-volume energies, Nucl. Phys. B 924 (2017) 477–507. arXiv:1707.05817, doi:10.1016/j.nuclphysb.2017.09.014.

[526] T. Chen, Y. Chen, M. Gong, C. Liu, L. Liu, Y.-B. Liu, Z. Liu, J.-P. Ma, M. Werner, J.-B. Zhang, A coupled-channel lattice study on the resonance-like structure $Z_c(3900)$, Chin. Phys. C 43 (10) (2019) 103103. arXiv:1907.03371, doi:10.1088/1674-1137/43/10/103103.

[527] R. G. Newton, Scattering theory of waves and particles, Springer Science & Business Media, 2013.

[528] H. Ekstein, Equivalent Hamiltonians in Scattering Theory, Phys. Rev. 117 (6) (1960) 1590. doi:10.1103/PhysRev.117.1590.

[529] U. van Kolck, Effective field theory of short range forces, Nucl. Phys. A 645 (1999) 273–302. arXiv:nucl-th/9808007, doi:10.1016/S0375-9474(98)00612-5.

[530] N. Levinson, On the uniqueness of the potential in a Schrödinger equation for a given asymptotic phase, Kgl. Danske Videnskab Selskab. Mat. Fys. Medd. 25 (1949).

[531] Low-energy expansion. scattering length and effective range. bounds on the zero-energy cross section, in: F. Calogero (Ed.), Variable Phase Approach to Potential Scattering, Vol. 35 of Mathematics in Science and Engineering, Elsevier, 1967, pp. 67–76. doi:https://doi.org/10.1016/S0076-5392(08)60422-1.

[532] J. C. Polkinghorne, A note on the relation between scattering phase and bound states, Mathematical Proceedings of the Cambridge Philosophical Society 54 (4) (1958) 560–561. doi:10.1017/S0305004100003133.

[533] M. T. Vaughn, R. Aaron, R. D. Amado, Elementary and Composite Particles, Phys. Rev. 124 (4) (1961) 1258–1268. doi:10.1103/PhysRev.124.1258.

[534] M. I. Krivoruchenko, K. S. Tyrin, Generalization of the Levinson Theorem on the Asymptotic Value of the Scattering-Amplitude Phase Shift, Phys. Atom. Nucl. 84 (1) (2021) 29–33. arXiv:2006.09366, doi:10.1134/S1063778821010130.

[535] Y. Li, J.-J. Wu, Inverse scattering problem with a bare state, Phys. Rev. D 105 (11) (2022) 116024. `arXiv:2204.05510`, `doi:10.1103/PhysRevD.105.116024`.

[536] L. D. Landau, E. M. Lifshitz, Resonance scattering at low energies, in: Quantum mechanics: non-relativistic theory, Vol. 3 of Course of theoritical Physics, Elsevier, 2013, Ch. 133, p. 557.

[537] E. P. Wigner, Lower Limit for the Energy Derivative of the Scattering Phase Shift, Phys. Rev. 98 (1955) 145–147. `doi:10.1103/PhysRev.98.145`.

[538] D. R. Phillips, T. D. Cohen, How short is too short? Constraining contact interactions in nucleon-nucleon scattering, Phys. Lett. B 390 (1997) 7–12. `arXiv:nucl-th/9607048`, `doi:10.1016/S0370-2693(96)01411-6`.

[539] F. Tabakin, Inverse scattering problem for separable potentials, Phys. Rev. 177 (1969) 1443–1451. `doi:10.1103/PhysRev.177.1443`.

[540] Effective range for x(3872), A topical workshop, CERN, Switzerland (Nov. 2021).
URL `https://indico.cern.ch/event/1086301/`

[541] M. H. Ross, G. L. Shaw, Scattering length and effective range theory for multi-channel processes, Annals of Physics 9 (3) (1960) 391–415. `doi:https://doi.org/10.1016/0003-4916(60)90040-3`.

[542] M. H. Ross, G. L. Shaw, Multi-channel effective range theory, Annals of Physics 13 (2) (1961) 147–186. `doi:https://doi.org/10.1016/0003-4916(61)90078-1`.

[543] M. Pavon Valderrama, E. Ruiz Arriola, Low-energy NN scattering at next-to-next-to-next-to-next-to-leading order for partial waves with $j \leq 5$, Phys. Rev. C 72 (2005) 044007. `doi:10.1103/PhysRevC.72.044007`.

[544] J. R. Pelaez, F. J. Yndurain, The Pion-pion scattering amplitude, Phys. Rev. D 71 (2005) 074016. `arXiv:hep-ph/0411334`, `doi:10.1103/PhysRevD.71.074016`.

[545] H. van Haeringen, L. P. Kok, Modified effective range function, Phys. Rev. A 26 (1982) 1218–1225. `doi:10.1103/PhysRevA.26.1218`.

[546] B. Midya, J. Evrard, S. Abramowicz, O. L. Ramírez Suárez, J.-M. Sparenberg, Supersymmetric inversion of effective-range expansions, Phys. Rev. C 91 (5) (2015) 054004. `arXiv:1501.04011`, `doi:10.1103/PhysRevC.91.054004`.

[547] A. M. Badalian, L. P. Kok, M. I. Polikarpov, Y. A. Simonov, Resonances in Coupled-Channels in Nuclear and Particle Physics, Phys. Rept. 82 (1982) 31–177. `doi:10.1016/0370-1573(82)90014-X`.

[548] J. A. Oller, E. Oset, A. Ramos, Chiral unitary approach to meson-meson and meson-baryon interactions and nuclear applications, Prog. Part. Nucl. Phys. 45 (2000) 157–242. `arXiv:hep-ph/0002193`, `doi:10.1016/S0146-6410(00)00104-6`.

[549] J. A. Oller, Coupled-channel approach in hadron–hadron scattering, Prog. Part. Nucl. Phys. 110 (2020) 103728. `arXiv:1909.00370`, `doi:10.1016/j.ppnp.2019.103728`.

[550] J. A. Oller, A Brief Introduction to Dispersion Relations: With Modern Applications, Springer, 2019.

[551] J. A. Oller, U. G. Meissner, Chiral dynamics in the presence of bound states: Kaon-nucleon interactions revisited, Phys. Lett. B 500 (2001) 263–272. `arXiv:hep-ph/0011146`, `doi:10.1016/S0370-2693(01)00078-8`.

[552] J. A. Oller, E. Oset, J. R. Pelaez, Meson meson interaction in a nonperturbative chiral approach, Phys. Rev. D 59 (1999) 074001, [Erratum: Phys.Rev.D 60, 099906 (1999), Erratum: Phys.Rev.D 75, 099903 (2007)]. `arXiv:hep-ph/9804209`, `doi:10.1103/PhysRevD.59.074001`.

[553] J. A. Oller, E. Oset, J. R. Pelaez, Nonperturbative approach to effective chiral Lagrangians and meson interactions, Phys. Rev. Lett. 80 (1998) 3452–3455. `arXiv:hep-ph/9803242`, `doi:10.1103/PhysRevLett.80.3452`.

[554] J. A. Oller, E. Oset, N/D description of two meson amplitudes and chiral symmetry, Phys. Rev. D 60 (1999) 074023. `arXiv:hep-ph/9809337`, `doi:10.1103/PhysRevD.60.074023`.

[555] E. Oset, A. Ramos, Nonperturbative chiral approach to S-wave $\bar{K}N$ interactions, Nucl. Phys. A 635 (1998) 99–120. `arXiv:nucl-th/9711022`, `doi:10.1016/S0375-9474(98)00170-5`.

[556] L. Roca, E. Oset, J. Singh, Low lying axial-vector mesons as dynamically generated resonances, Phys. Rev. D 72 (2005) 014002. `arXiv:hep-ph/0503273`, `doi:10.1103/PhysRevD.72.014002`.

[557] J. A. Oller, E. Oset, Chiral symmetry amplitudes in the S-wave isoscalar and isovector channels and the σ, f_0(980), a_0(980) scalar mesons, Nucl. Phys. A 620 (1997) 438–456, [Erratum: Nucl.Phys.A 652, 407–409 (1999)]. `arXiv:hep-ph/9702314`, `doi:10.1016/S0375-9474(97)00160-7`.

[558] M. F. M. Lutz, E. E. Kolomeitsev, Relativistic chiral SU(3) symmetry, large N_c sum rules and meson baryon scattering, Nucl. Phys. A 700 (2002) 193–308. `arXiv:nucl-th/0105042`, `doi:10.1016/S0375-9474(01)01312-4`.

[559] B. Borasoy, R. Nissler, W. Weise, Chiral dynamics of kaon-nucleon interactions, revisited, Eur. Phys. J. A 25 (2005) 79–96. `arXiv:hep-ph/0505239`, `doi:10.1140/epja/i2005-10079-1`.

[560] U.-G. Meissner, J. A. Oller, Chiral unitary meson baryon dynamics in the presence of resonances: Elastic pion nucleon scattering, Nucl. Phys. A 673 (2000) 311–334. `arXiv:nucl-th/9912026`, `doi:10.1016/S0375-9474(00)00150-0`.

[561] V. Bernard, N. Kaiser, U. G. Meissner, Chiral perturbation theory in the presence of resonances: Application to $\pi\pi$ and πK scattering, Nucl. Phys. B 364 (1991) 283–320. `doi:10.1016/0550-3213(91)90586-M`.

[562] M. Jamin, J. A. Oller, A. Pich, S-wave $K\pi$ scattering in chiral perturbation theory with resonances, Nucl. Phys. B 587 (2000) 331–362. `arXiv:hep-ph/0006045`, `doi:10.1016/S0550-3213(00)00479-X`.

[563] M. F. M. Lutz, X.-Y. Guo, Y. Heo, C. L. Korpa, Coupled-channel dynamics with chiral long-range forces in the open-charm sector of QCD, Phys. Rev. D 106 (11) (2022) 114038. `arXiv:2209.10601`, `doi:10.1103/PhysRevD.106.114038`.

[564] M. F. M. Lutz, Y. Heo, X.-Y. Guo, On the convergence of the chiral expansion for the baryon ground-state masses, Nucl. Phys. A 977 (2018) 146–207. `arXiv:1801.06417`, `doi:10.1016/j.nuclphysa.2018.05.007`.

[565] G. F. Chew, S. Mandelstam, Theory of low-energy pion-pion interactions, Phys. Rev. 119 (1960) 467–477. `doi:10.1103/PhysRev.119.467`.

[566] L. Castillejo, R. H. Dalitz, F. J. Dyson, Low's scattering equation for the charged and neutral scalar theories, Phys. Rev. 101 (1956) 453–458. `doi:10.1103/PhysRev.101.453`.

[567] C. Hanhart, Y. S. Kalashnikova, A. V. Nefediev, Interplay of quark and meson degrees of freedom in a near-threshold resonance: multi-channel case, Eur. Phys. J. A 47 (2011) 101–110. `arXiv:1106.1185`, `doi:10.1140/epja/i2011-11101-9`.

[568] V. Baru, C. Hanhart, Y. S. Kalashnikova, A. E. Kudryavtsev, A. V. Nefediev, Interplay of quark and meson degrees of freedom in a near-threshold resonance, Eur. Phys. J. A 44 (2010) 93–103. arXiv:1001.0369, doi:10.1140/epja/i2010-10929-7.

[569] E. Braaten, M. Lu, Line shapes of the X(3872), Phys. Rev. D 76 (2007) 094028. arXiv:0709.2697, doi:10.1103/PhysRevD.76.094028.

[570] P. Artoisenet, E. Braaten, D. Kang, Using Line Shapes to Discriminate between Binding Mechanisms for the X(3872), Phys. Rev. D 82 (2010) 014013. arXiv:1005.2167, doi:10.1103/PhysRevD.82.014013.

[571] T. Hyodo, D. Jido, A. Hosaka, Origin of the resonances in the chiral unitary approach, Phys. Rev. C 78 (2008) 025203. arXiv:0803.2550, doi:10.1103/PhysRevC.78.025203.

[572] H.-X. Chen, E. Oset, $\pi\pi$ interaction in the ρ channel in finite volume, Phys. Rev. D 87 (1) (2013) 016014. arXiv:1202.2787, doi:10.1103/PhysRevD.87.016014.

[573] L. Meng, E. Epelbaum, Two-particle scattering from finite-volume quantization conditions using the plane wave basis, JHEP 10 (2021) 051. arXiv:2108.02709, doi:10.1007/JHEP10(2021)051.

[574] T. N. Truong, Chiral Perturbation Theory and Final State Theorem, Phys. Rev. Lett. 61 (1988) 2526. doi:10.1103/PhysRevLett.61.2526.

[575] T. N. Truong, Remarks on the unitarization methods, Phys. Rev. Lett. 67 (1991) 2260–2263. doi:10.1103/PhysRevLett.67.2260.

[576] A. Dobado, M. J. Herrero, T. N. Truong, Unitarized Chiral Perturbation Theory for Elastic Pion-Pion Scattering, Phys. Lett. B 235 (1990) 134–140. doi:10.1016/0370-2693(90)90109-J.

[577] A. Dobado, J. R. Pelaez, The Inverse amplitude method in chiral perturbation theory, Phys. Rev. D 56 (1997) 3057–3073. arXiv:hep-ph/9604416, doi:10.1103/PhysRevD.56.3057.

[578] J. R. Pelaez, From controversy to precision on the sigma meson: a review on the status of the non-ordinary f_0(500) resonance, Phys. Rept. 658 (2016) 1. arXiv:1510.00653, doi:10.1016/j.physrep.2016.09.001.

[579] M. Boglione, M. R. Pennington, Chiral poles and zeros and the role of the left hand cut, Z. Phys. C 75 (1997) 113–118. arXiv:hep-ph/9607266, doi:10.1007/s002880050452.

[580] S. L. Adler, Consistency conditions on the strong interactions implied by a partially conserved axial-vector current. II, Phys. Rev. 139 (1965) B1638–B1643. doi:10.1103/PhysRev.139.B1638.

[581] A. Gomez Nicola, J. R. Pelaez, G. Rios, The Inverse Amplitude Method and Adler Zeros, Phys. Rev. D 77 (2008) 056006. arXiv:0712.2763, doi:10.1103/PhysRevD.77.056006.

[582] A. Gomez Nicola, J. R. Pelaez, Meson meson scattering within one loop chiral perturbation theory and its unitarization, Phys. Rev. D 65 (2002) 054009. arXiv:hep-ph/0109056, doi:10.1103/PhysRevD.65.054009.

[583] D.-L. Yao, M.-L. Du, F.-K. Guo, U.-G. Meißner, One-loop analysis of the interactions between charmed mesons and Goldstone bosons, JHEP 11 (2015) 058. arXiv:1502.05981, doi:10.1007/JHEP11(2015)058.

[584] N. Kaiser, P. B. Siegel, W. Weise, Chiral dynamics and the low-energy kaon-nucleon interaction, Nucl. Phys. A 594 (1995) 325–345. arXiv:nucl-th/9505043, doi:10.1016/0375-9474(95)00362-5.

[585] B. Krippa, Chiral dynamics of the low-energy kaon-baryon interactions, Phys. Rev. C 58 (1998) 1333–1336. arXiv:hep-ph/9803332, doi:10.1103/PhysRevC.58.1333.

[586] C. Garcia-Recio, M. F. M. Lutz, J. Nieves, Quark mass dependence of S-wave baryon resonances, Phys. Lett. B 582 (2004) 49–54. arXiv:nucl-th/0305100, doi:10.1016/j.physletb.2003.11.073.

[587] E. E. Kolomeitsev, M. F. M. Lutz, On baryon resonances and chiral symmetry, Phys. Lett. B 585 (2004) 243–252. arXiv:nucl-th/0305101, doi:10.1016/j.physletb.2004.01.066.

[588] S. Sarkar, E. Oset, M. J. Vicente Vacas, Baryonic resonances from baryon decuplet-meson octet interaction, Nucl. Phys. A 750 (2005) 294–323, [Erratum: Nucl.Phys.A 780, 90–90 (2006)]. arXiv:nucl-th/0407025, doi:10.1016/j.nuclphysa.2005.01.006.

[589] T. Hyodo, S. I. Nam, D. Jido, A. Hosaka, Flavor SU(3) breaking effects in the chiral unitary model for meson baryon scatterings, Phys. Rev. C 68 (2003) 018201. arXiv:nucl-th/0212026, doi:10.1103/PhysRevC.68.018201.

[590] J. A. Oller, J. Prades, M. Verbeni, Surprises in threshold antikaon-nucleon physics, Phys. Rev. Lett. 95 (2005) 172502. arXiv:hep-ph/0508081, doi:10.1103/PhysRevLett.95.172502.

[591] M. F. M. Lutz, E. E. Kolomeitsev, On meson resonances and chiral symmetry, Nucl. Phys. A 730 (2004) 392–416. arXiv:nucl-th/0307039, doi:10.1016/j.nuclphysa.2003.11.009.

[592] A. Gasparyan, M. F. M. Lutz, Photon- and pion-nucleon interactions in a unitary and causal effective field theory based on the chiral Lagrangian, Nucl. Phys. A 848 (2010) 126–182. arXiv:1003.3426, doi:10.1016/j.nuclphysa.2010.08.006.

[593] R. L. Jaffe, Exotica, Phys. Rept. 409 (2005) 1–45. arXiv:hep-ph/0409065, doi:10.1016/j.physrep.2004.11.005.

[594] G. F. Chew, S. C. Frautschi, Potential Scattering as Opposed to Scattering Associated with Independent Particles in the S-Matrix Theory of Strong Interactions, Phys. Rev. 124 (1) (1961) 264. doi:10.1103/PhysRev.124.264.

[595] A. Martinez Torres, L. R. Dai, C. Koren, D. Jido, E. Oset, The KD, ηD_s interaction in finite volume and the nature of the D_{s0}^*(2317) resonance, Phys. Rev. D 85 (2012) 014027. arXiv:1109.0396, doi:10.1103/PhysRevD.85.014027.

[596] J. Nieves, E. Ruiz Arriola, Bethe-Salpeter approach for unitarized chiral perturbation theory, Nucl. Phys. A 679 (2000) 57–117. arXiv:hep-ph/9907469, doi:10.1016/S0375-9474(00)00321-3.

[597] M. Schmidt, M. Jansen, H. W. Hammer, Threshold Effects and the Line Shape of the X(3872) in Effective Field Theory, Phys. Rev. D 98 (1) (2018) 014032. arXiv:1804.00375, doi:10.1103/PhysRevD.98.014032.

[598] E. Witten, Baryons in the $1/n$ Expansion, Nucl. Phys. B 160 (1979) 57–115. doi:10.1016/0550-3213(79)90232-3.

[599] G. Ecker, J. Gasser, A. Pich, E. de Rafael, The Role of Resonances in Chiral Perturbation Theory, Nucl. Phys. B 321 (1989) 311–342. doi:10.1016/0550-3213(89)90346-5.

[600] J. R. Pelaez, On the Nature of light scalar mesons from their large N_c behavior, Phys. Rev. Lett. 92 (2004) 102001. arXiv:hep-ph/0309292, doi:10.1103/PhysRevLett.92.102001.

[601] V. Baru, J. Haidenbauer, C. Hanhart, Y. Kalashnikova, A. E. Kudryavtsev, Evidence that the a_0(980) and f_0(980) are not elementary particles, Phys. Lett. B 586 (2004) 53–61. arXiv:hep-ph/0308129, doi:10.1016/j.physletb.2004.01.088.

[602] T. Hyodo, D. Jido, A. Hosaka, Compositeness of dynamically generated states in a chiral unitary approach, Phys. Rev. C 85 (2012) 015201. `arXiv:1108.5524`, `doi:10.1103/PhysRevC.85.015201`.

[603] F. Aceti, E. Oset, Wave functions of composite hadron states and relationship to couplings of scattering amplitudes for general partial waves, Phys. Rev. D 86 (2012) 014012. `arXiv:1202.4607`, `doi:10.1103/PhysRevD.86.014012`.

[604] T. Sekihara, T. Hyodo, D. Jido, Comprehensive analysis of the wave function of a hadronic resonance and its compositeness, PTEP 2015 (2015) 063D04. `arXiv:1411.2308`, `doi:10.1093/ptep/ptv081`.

[605] T. Hyodo, Structure of Near-Threshold S-Wave Resonances, Phys. Rev. Lett. 111 (2013) 132002. `arXiv:1305.1999`, `doi:10.1103/PhysRevLett.111.132002`.

[606] G.-Y. Chen, W.-S. Huo, Q. Zhao, Identifying the structure of near-threshold states from the line shape, Chin. Phys. C 39 (9) (2015) 093101. `arXiv:1309.2859`, `doi:10.1088/1674-1137/39/9/093101`.

[607] Y. Kamiya, T. Hyodo, Structure of near-threshold quasibound states, Phys. Rev. C 93 (3) (2016) 035203. `arXiv:1509.00146`, `doi:10.1103/PhysRevC.93.035203`.

[608] Z.-H. Guo, J. A. Oller, Probabilistic interpretation of compositeness relation for resonances, Phys. Rev. D 93 (9) (2016) 096001. `arXiv:1508.06400`, `doi:10.1103/PhysRevD.93.096001`.

[609] Y. Li, F.-K. Guo, J.-Y. Pang, J.-J. Wu, Generalization of Weinberg's compositeness relations, Phys. Rev. D 105 (7) (2022) L071502. `arXiv:2110.02766`, `doi:10.1103/PhysRevD.105.L071502`.

[610] P. C. Bruns, Spatial interpretation of "compositeness" for finite-range potentials (5 2019). `arXiv:1905.09196`.

[611] P. C. Bruns, A toy model for "elementariness" (3 2022). `arXiv:2203.16909`.

[612] J. Song, L. R. Dai, E. Oset, How much is the compositeness of a bound state constrained by a and r_0? The role of the interaction range, Eur. Phys. J. A 58 (7) (2022) 133. `arXiv:2201.04414`, `doi:10.1140/epja/s10050-022-00753-3`.

[613] H. Georgi, Comment on heavy baryon weak form-factors, Nucl. Phys. B 348 (1991) 293–296. `doi:10.1016/0550-3213(91)90519-4`.

[614] T. Mannel, W. Roberts, Z. Ryzak, Baryons in the heavy quark effective theory, Nucl. Phys. B 355 (1991) 38–53. `doi:10.1016/0550-3213(91)90301-D`.

[615] A. F. Falk, Hadrons of arbitrary spin in the heavy quark effective theory, Nucl. Phys. B 378 (1992) 79–94. `doi:10.1016/0550-3213(92)90004-U`.

[616] M. B. Wise, Chiral perturbation theory for hadrons containing a heavy quark, Phys. Rev. D 45 (7) (1992) R2188. `doi:10.1103/PhysRevD.45.R2188`.

[617] H. Ohki, H. Matsufuru, T. Onogi, Determination of $B^*B\pi$ coupling in unquenched QCD, Phys. Rev. D 77 (2008) 094509. `arXiv:0802.1563`, `doi:10.1103/PhysRevD.77.094509`.

[618] S.-Z. Jiang, Y.-R. Liu, Q.-H. Yang, Chiral Lagrangians for mesons with a single heavy quark, Phys. Rev. D 99 (7) (2019) 074018. `arXiv:1901.09479`, `doi:10.1103/PhysRevD.99.074018`.

[619] U. Kilian, J. G. Korner, D. Pirjol, Excited charmed mesons in chiral perturbation theory, Phys. Lett. B 288 (1992) 360–366. `doi:10.1016/0370-2693(92)91115-P`.

[620] R. Casalbuoni, A. Deandrea, N. Di Bartolomeo, R. Gatto, F. Feruglio, G. Nardulli, Phenomenology of heavy meson chiral Lagrangians, Phys. Rept. 281 (1997) 145–238. `arXiv:hep-ph/9605342`, `doi:10.1016/S0370-1573(96)00027-0`.

[621] T.-M. Yan, H.-Y. Cheng, C.-Y. Cheung, G.-L. Lin, Y. C. Lin, H.-L. Yu, Heavy quark symmetry and chiral dynamics, Phys. Rev. D 46 (1992) 1148–1164, [Erratum: Phys.Rev.D 55, 5851 (1997)]. `doi:10.1103/PhysRevD.46.1148`.

[622] W. Meguro, Y.-R. Liu, M. Oka, Possible $\Lambda_c\Lambda_c$ molecular bound state, Phys. Lett. B 704 (2011) 547–550. `arXiv:1105.3693`, `doi:10.1016/j.physletb.2011.09.088`.

[623] Y.-R. Liu, M. Oka, $\Lambda_c N$ bound states revisited, Phys. Rev. D 85 (2012) 014015. `arXiv:1103.4624`, `doi:10.1103/PhysRevD.85.014015`.

[624] L. Meng, G.-J. Wang, C.-Z. Leng, Z.-W. Liu, S.-L. Zhu, Magnetic moments of the spin-$\frac{3}{2}$ singly heavy baryons, Phys. Rev. D 98 (9) (2018) 094013. `arXiv:1805.09580`, `doi:10.1103/PhysRevD.98.094013`.

[625] P.-C. Qiu, D.-L. Yao, Chiral effective Lagrangian for doubly charmed baryons up to $O(q^4)$, Phys. Rev. D 103 (3) (2021) 034006. `arXiv:2012.11117`, `doi:10.1103/PhysRevD.103.034006`.

[626] G. T. Bodwin, E. Braaten, G. P. Lepage, Rigorous QCD analysis of inclusive annihilation and production of heavy quarkonium, Phys. Rev. D 51 (1995) 1125–1171, [Erratum: Phys.Rev.D 55, 5853 (1997)]. `arXiv:hep-ph/9407339`, `doi:10.1103/PhysRevD.55.5853`.

[627] W. E. Caswell, G. P. Lepage, Effective Lagrangians for Bound State Problems in QED, QCD, and Other Field Theories, Phys. Lett. B 167 (1986) 437–442. `doi:10.1016/0370-2693(86)91297-9`.

[628] U. van Kolck, Effective field theory of nuclear forces, Prog. Part. Nucl. Phys. 43 (1999) 337–418. `arXiv:nucl-th/9902015`, `doi:10.1016/S0146-6410(99)00097-6`.

[629] D. B. Kaplan, M. J. Savage, M. B. Wise, Two nucleon systems from effective field theory, Nucl. Phys. B 534 (1998) 329–355. `arXiv:nucl-th/9802075`, `doi:10.1016/S0550-3213(98)00440-4`.

[630] S. Weinberg, Nuclear forces from chiral Lagrangians, Phys. Lett. B 251 (1990) 288–292. `doi:10.1016/0370-2693(90)90938-3`.

[631] T. Mehen, I. W. Stewart, A Momentum subtraction scheme for two nucleon effective field theory, Phys. Lett. B 445 (1999) 378–386. `arXiv:nucl-th/9809071`, `doi:10.1016/S0370-2693(98)01470-1`.

[632] T. Mehen, I. W. Stewart, Renormalization schemes and the range of two nucleon effective field theory, Phys. Rev. C 59 (1999) 2365–2383. `arXiv:nucl-th/9809095`, `doi:10.1103/PhysRevC.59.2365`.

[633] J. Gegelia, Chiral perturbation theory approach to NN scattering problem, in: Workshop on Methods of Nonperturbative Quantum Field Theory, 1998, pp. 30–35. `arXiv:nucl-th/9802038`.

[634] J. Gegelia, About the equivalence of cutoff and conventionally renormalized effective field theories, J. Phys. G 25 (1999) 1681–1693. `arXiv:nucl-th/9805008`, `doi:10.1088/0954-3899/25/8/310`.

[635] T. D. Cohen, J. M. Hansen, Systematic power counting in cutoff effective field theories for nucleon-nucleon interactions and the equivalence with PDS, Phys. Lett. B 440 (1998) 233–238. `arXiv:nucl-th/9808006`, `doi:10.1016/S0370-2693(98)01180-0`.

[636] M. C. Birse, J. A. McGovern, K. G. Richardson, A Renormalization group treatment of two-body scattering, Phys. Lett. B 464 (1999)

169–176. `arXiv:hep-ph/9807302`, `doi:10.1016/S0370-2693(99)00991-0`.

[637] S. Fleming, T. Mehen, I. W. Stewart, NNLO corrections to nucleon-nucleon scattering and perturbative pions, Nucl. Phys. A 677 (2000) 313–366. `arXiv:nucl-th/9911001`, `doi:10.1016/S0375-9474(00)00221-9`.

[638] T. D. Cohen, J. M. Hansen, Testing low-energy theorems in nucleon-nucleon scattering, Phys. Rev. C 59 (1999) 3047–3051. `arXiv:nucl-th/9901065`, `doi:10.1103/PhysRevC.59.3047`.

[639] S. R. Beane, D. B. Kaplan, A. Vuorinen, Perturbative nuclear physics, Phys. Rev. C 80 (2009) 011001. `arXiv:0812.3938`, `doi:10.1103/PhysRevC.80.011001`.

[640] D. B. Kaplan, Convergence of nuclear effective field theory with perturbative pions, Phys. Rev. C 102 (3) (2020) 034004. `arXiv:1905.07485`, `doi:10.1103/PhysRevC.102.034004`.

[641] J. Gegelia, Are pions perturbative in effective field theory? (6 1998). `arXiv:nucl-th/9806028`.

[642] J. Gegelia, Nucleon-nucleon scattering and effective field theory: Including pions nonperturbatively, Phys. Lett. B 463 (1999) 133–137. `arXiv:nucl-th/9908055`, `doi:10.1016/S0370-2693(99)00994-6`.

[643] T. D. Cohen, J. M. Hansen, Low-energy theorems for nucleon-nucleon scattering, Phys. Rev. C 59 (1999) 13–20. `arXiv:nucl-th/9808038`, `doi:10.1103/PhysRevC.59.13`.

[644] M. C. Birse, Power counting with one-pion exchange, Phys. Rev. C 74 (2006) 014003. `arXiv:nucl-th/0507077`, `doi:10.1103/PhysRevC.74.014003`.

[645] P. Reinert, H. Krebs, E. Epelbaum, Semilocal momentum-space regularized chiral two-nucleon potentials up to fifth order, Eur. Phys. J. A 54 (5) (2018) 86. `arXiv:1711.08821`, `doi:10.1140/epja/i2018-12516-4`.

[646] E. Epelbaum, H. Krebs, U. G. Meißner, Improved chiral nucleon-nucleon potential up to next-to-next-to-next-to-leading order, Eur. Phys. J. A 51 (5) (2015) 53. `arXiv:1412.0142`, `doi:10.1140/epja/i2015-15053-8`.

[647] E. Epelbaum, H. Krebs, U. G. Meißner, Precision nucleon-nucleon potential at fifth order in the chiral expansion, Phys. Rev. Lett. 115 (12) (2015) 122301. `arXiv:1412.4623`, `doi:10.1103/PhysRevLett.115.122301`.

[648] D. R. Entem, R. Machleidt, Y. Nosyk, High-quality two-nucleon potentials up to fifth order of the chiral expansion, Phys. Rev. C 96 (2) (2017) 024004. `arXiv:1703.05454`, `doi:10.1103/PhysRevC.96.024004`.

[649] E. Epelbaum, H. Krebs, P. Reinert, High-precision nuclear forces from chiral EFT: State-of-the-art, challenges and outlook, Front. in Phys. 8 (2020) 98. `arXiv:1911.11875`, `doi:10.3389/fphy.2020.00098`.

[650] H. W. Hammer, S. König, U. van Kolck, Nuclear effective field theory: status and perspectives, Rev. Mod. Phys. 92 (2) (2020) 025004. `arXiv:1906.12122`, `doi:10.1103/RevModPhys.92.025004`.

[651] N. Kaiser, R. Brockmann, W. Weise, Peripheral nucleon-nucleon phase shifts and chiral symmetry, Nucl. Phys. A 625 (1997) 758–788. `arXiv:nucl-th/9706045`, `doi:10.1016/S0375-9474(97)00586-1`.

[652] N. Kaiser, S. Gerstendorfer, W. Weise, Peripheral NN scattering: Role of delta excitation, correlated two pion and vector meson exchange, Nucl. Phys. A 637 (1998) 395–420. `arXiv:nucl-th/9802071`, `doi:10.1016/S0375-9474(98)00234-6`.

[653] C. Ordonez, L. Ray, U. van Kolck, The Two nucleon potential from chiral Lagrangians, Phys. Rev. C 53 (1996) 2086–2105. `arXiv:hep-ph/9511380`, `doi:10.1103/PhysRevC.53.2086`.

[654] E. Epelbaum, A. M. Gasparyan, J. Gegelia, U.-G. Meißner, How (not) to renormalize integral equations with singular potentials in effective field theory, Eur. Phys. J. A 54 (11) (2018) 186. `arXiv:1810.02646`, `doi:10.1140/epja/i2018-12632-1`.

[655] E. Epelbaum, J. Gegelia, Regularization, renormalization and 'peratization' in effective field theory for two nucleons, Eur. Phys. J. A 41 (2009) 341–354. `arXiv:0906.3822`, `doi:10.1140/epja/i2009-10833-3`.

[656] A. M. Gasparyan, E. Epelbaum, Nucleon-nucleon interaction in chiral effective field theory with a finite cutoff: Explicit perturbative renormalization at next-to-leading order, Phys. Rev. C 105 (2) (2022) 024001. `arXiv:2110.15302`, `doi:10.1103/PhysRevC.105.024001`.

[657] T. Mehen, R. P. Springer, Heavy-quark symmetry and the electromagnetic decays of excited charmed strange mesons, Phys. Rev. D 70 (2004) 074014. `arXiv:hep-ph/0407181`, `doi:10.1103/PhysRevD.70.074014`.

[658] C. G. Boyd, B. Grinstein, Chiral and heavy quark symmetry violation in B decays, Nucl. Phys. B 442 (1995) 205–227. `arXiv:hep-ph/9402340`, `doi:10.1016/S0550-3213(95)00005-4`.

[659] H.-Y. Cheng, C.-Y. Cheung, G.-L. Lin, Y. C. Lin, T.-M. Yan, H.-L. Yu, Corrections to chiral dynamics of heavy hadrons. 1. $1/M$ correction, Phys. Rev. D 49 (1994) 2490–2507. `arXiv:hep-ph/9308283`, `doi:10.1103/PhysRevD.49.2490`.

[660] E. E. Jenkins, Heavy meson masses in chiral perturbation theory with heavy quark symmetry, Nucl. Phys. B 412 (1994) 181–200. `arXiv:hep-ph/9212295`, `doi:10.1016/0550-3213(94)90499-5`.

[661] T. Mehen, R. P. Springer, Even- and odd-parity charmed meson masses in heavy hadron chiral perturbation theory, Phys. Rev. D 72 (2005) 034006. `arXiv:hep-ph/0503134`, `doi:10.1103/PhysRevD.72.034006`.

[662] M. H. Alhakami, Mass Spectra of Heavy-Light Mesons in Heavy Hadron Chiral Perturbation Theory, Phys. Rev. D 93 (9) (2016) 094007. `arXiv:1603.08848`, `doi:10.1103/PhysRevD.93.094007`.

[663] B. Ananthanarayan, S. Banerjee, K. Shivaraj, A. Upadhyay, Puzzles of excited charm meson masses, Phys. Lett. B 651 (2007) 124–128. `arXiv:0706.0942`, `doi:10.1016/j.physletb.2007.06.013`.

[664] M. H. Alhakami, Spectroscopy of excited charmed mesons, Phys. Rev. D 101 (1) (2020) 016001. `arXiv:1910.04409`, `doi:10.1103/PhysRevD.101.016001`.

[665] A. F. Falk, B. Grinstein, M. E. Luke, Leading mass corrections to the heavy quark effective theory, Nucl. Phys. B 357 (1991) 185–207. `doi:10.1016/0550-3213(91)90464-9`.

[666] J. L. Rosner, M. B. Wise, Meson masses from SU(3) and heavy quark symmetry, Phys. Rev. D 47 (1993) 343–345. `doi:10.1103/PhysRevD.47.343`.

[667] L. Randall, E. Sather, Heavy meson hyperfine splittings: A Puzzle for heavy quark chiral perturbation theory, Phys. Lett. B 303 (1993) 345–349. `arXiv:hep-ph/9211267`, `doi:10.1016/0370-2693(93)91443-Q`.

[668] N. Di Bartolomeo, R. Gatto, F. Feruglio, G. Nardulli, Heavy meson hyperfine splitting: A Complete $1/m_Q$ calculation, Phys. Lett. B 347 (1995) 405–412. `arXiv:hep-ph/9411210`, `doi:10.1016/0370-2693(95)00071-R`.

[669] G. Amoros, M. Beneke, M. Neubert, Two loop anomalous dimension of the chromomagnetic moment of a heavy quark, Phys. Lett. B 401

(1997) 81–90. arXiv:hep-ph/9701375, doi:10.1016/S0370-2693(97)00345-6.

[670] J. L. Goity, Chiral perturbation theory for SU(3) breaking in heavy meson systems, Phys. Rev. D 46 (1992) 3929–3936. arXiv:hep-ph/9206230, doi:10.1103/PhysRevD.46.3929.

[671] B. Blok, J. G. Korner, D. Pirjol, J. C. Rojas, Spectator effects in the heavy quark effective theory, Nucl. Phys. B 496 (1997) 358–374. arXiv:hep-ph/9607233, doi:10.1016/S0550-3213(97)00202-2.

[672] X.-H. Guo, A. W. Thomas, Chiral extrapolation of lattice data for the hyperfine splittings of heavy mesons, Phys. Rev. D 65 (2002) 074019. arXiv:hep-ph/0112040, doi:10.1103/PhysRevD.65.074019.

[673] U.-G. Meissner, G. Muller, S. Steininger, Virtual photons in SU(2) chiral perturbation theory and electromagnetic corrections to $\pi\pi$ scattering, Phys. Lett. B 406 (1997) 154–160, [Erratum: Phys.Lett.B 407, 454 (1997)]. arXiv:hep-ph/9704377, doi:10.1016/S0370-2693(97)00666-7.

[674] U. G. Meissner, S. Steininger, Isospin violation in pion nucleon scattering, Phys. Lett. B 419 (1998) 403–411. arXiv:hep-ph/9709453, doi:10.1016/S0370-2693(97)01418-4.

[675] F.-K. Guo, C. Hanhart, U.-G. Meissner, Mass splittings within heavy baryon isospin multiplets in chiral perturbation theory, JHEP 09 (2008) 136. arXiv:0809.2359, doi:10.1088/1126-6708/2008/09/136.

[676] F.-K. Guo, S. Krewald, U.-G. Meissner, Hadronic-loop induced mass shifts in scalar heavy-light mesons, Phys. Lett. B 665 (2008) 157–163. arXiv:0712.2953, doi:10.1016/j.physletb.2008.06.008.

[677] M. H. Alhakami, Predictions for the beauty meson spectrum, Phys. Rev. D 103 (3) (2021) 034009. arXiv:2006.16878, doi:10.1103/PhysRevD.103.034009.

[678] D. Becirevic, S. Fajfer, S. Prelovsek, On the mass differences between the scalar and pseudoscalar heavy-light mesons, Phys. Lett. B 599 (2004) 55. arXiv:hep-ph/0406296, doi:10.1016/j.physletb.2004.08.027.

[679] S. Fajfer, J. F. Kamenik, Chiral loop corrections to strong decays of positive and negative parity charmed mesons, Phys. Rev. D 74 (2006) 074023. arXiv:hep-ph/0606278, doi:10.1103/PhysRevD.74.074023.

[680] S. Fajfer, A. Prapotnik Brdnik, Isospin violating decays of positive parity B_s mesons in HMχPT, Eur. Phys. J. C 76 (10) (2016) 537. arXiv:1606.06943, doi:10.1140/epjc/s10052-016-4377-1.

[681] M. H. Alhakami, Low-energy constants of heavy meson effective theory in lattice QCD, Phys. Rev. D 98 (1) (2018) 016008. arXiv:1804.00019, doi:10.1103/PhysRevD.98.016008.

[682] W. A. Bardeen, E. J. Eichten, C. T. Hill, Chiral multiplets of heavy-light mesons, Phys. Rev. D 68 (2003) 054024. arXiv:hep-ph/0305049, doi:10.1103/PhysRevD.68.054024.

[683] W. A. Bardeen, C. T. Hill, Chiral dynamics and heavy quark symmetry in a solvable toy field theoretic model, Phys. Rev. D 49 (1994) 409–425. arXiv:hep-ph/9304265, doi:10.1103/PhysRevD.49.409.

[684] M. A. Nowak, M. Rho, I. Zahed, Chiral effective action with heavy quark symmetry, Phys. Rev. D 48 (1993) 4370–4374. arXiv:hep-ph/9209272, doi:10.1103/PhysRevD.48.4370.

[685] M. A. Nowak, M. Rho, I. Zahed, Chiral doubling of heavy light hadrons: BABAR 2317 MeV/c^2 and CLEO 2463 MeV/c^2 discoveries, Acta Phys. Polon. B 35 (2004) 2377–2392. arXiv:hep-ph/0307102.

[686] P. Colangelo, F. De Fazio, F. Giannuzzi, S. Nicotri, New meson spectroscopy with open charm and beauty, Phys. Rev. D 86 (2012) 054024. arXiv:1207.6940, doi:10.1103/PhysRevD.86.054024.

[687] P. Colangelo, F. De Fazio, R. Ferrandes, Bounding effective parameters in the chiral Lagrangian for excited heavy mesons, Phys. Lett. B 634 (2006) 235–239. arXiv:hep-ph/0511317, doi:10.1016/j.physletb.2006.01.021.

[688] G. Burdman, J. F. Donoghue, Union of chiral and heavy quark symmetries, Phys. Lett. B 280 (1992) 287–291. doi:10.1016/0370-2693(92)90068-F.

[689] H.-Y. Cheng, C.-Y. Cheung, G.-L. Lin, Y. C. Lin, T.-M. Yan, H.-L. Yu, Corrections to chiral dynamics of heavy hadrons: SU(3) symmetry breaking, Phys. Rev. D 49 (1994) 5857–5881, [Erratum: Phys.Rev.D 55, 5851–5852 (1997)]. arXiv:hep-ph/9312304, doi:10.1103/PhysRevD.49.5857.

[690] P. L. Cho, Chiral perturbation theory for hadrons containing a heavy quark: The Sequel, Phys. Lett. B 285 (1992) 145–152. arXiv:hep-ph/9203225, doi:10.1016/0370-2693(92)91314-Y.

[691] D. Pirjol, T.-M. Yan, Predictions for S-wave and P-wave heavy baryons from sum rules and constituent quark model. 1. Strong interactions, Phys. Rev. D 56 (1997) 5483–5510. arXiv:hep-ph/9701291, doi:10.1103/PhysRevD.56.5483.

[692] M. J. Savage, Charmed baryon masses in chiral perturbation theory, Phys. Lett. B 359 (1995) 189–193. arXiv:hep-ph/9508268, doi:10.1016/0370-2693(95)01060-4.

[693] X.-H. Guo, A. W. Thomas, Chiral extrapolation of lattice data for heavy baryons, Phys. Rev. D 67 (2003) 074005. arXiv:hep-ph/0210394, doi:10.1103/PhysRevD.67.074005.

[694] N. Jiang, X.-L. Chen, S.-L. Zhu, Mass and axial charge of heavy baryons, Phys. Rev. D 90 (7) (2014) 074011. arXiv:1403.5404, doi:10.1103/PhysRevD.90.074011.

[695] Z.-W. Liu, S.-L. Zhu, Pseudoscalar Meson and Charmed Baryon Scattering Lengths, Phys. Rev. D 86 (2012) 034009, [Erratum: Phys.Rev.D 93, 019901 (2016)]. arXiv:1205.0467, doi:10.1103/PhysRevD.86.034009.

[696] Z.-W. Liu, S.-L. Zhu, Pseudoscalar Goldstone Bosons Scattering off Charmed Baryons with Chiral Perturbation Theory, Nucl. Phys. A 914 (2013) 494–498. arXiv:1211.5013, doi:10.1016/j.nuclphysa.2012.12.023.

[697] M. J. Savage, Long distance contributions to the $\Lambda_b \to \Lambda_c e^- \bar{\nu}_e$ Isgur-Wise function, Phys. Lett. B 325 (1994) 488–494. arXiv:hep-ph/9401273, doi:10.1016/0370-2693(94)90044-2.

[698] M. J. Savage, Magnetic moment of the Λ_c, Ξ_{c1}^+ and Ξ_{c1}^0, Phys. Lett. B 326 (1994) 303–306. arXiv:hep-ph/9401345, doi:10.1016/0370-2693(94)91326-9.

[699] Y. Kim, Y.-R. Liu, M. Oka, K. Suzuki, Heavy baryon spectrum with chiral multiplets of scalar and vector diquarks, Phys. Rev. D 104 (5) (2021) 054012. arXiv:2105.09087, doi:10.1103/PhysRevD.104.054012.

[700] D. Suenaga, A. Hosaka, Novel pentaquark picture for singly heavy baryons from chiral symmetry, Phys. Rev. D 104 (3) (2021) 034009. arXiv:2101.09764, doi:10.1103/PhysRevD.104.034009.

[701] Y. Kawakami, M. Harada, M. Oka, K. Suzuki, Suppression of decay widths in singly heavy baryons induced by the $U_A(1)$ anomaly, Phys. Rev. D 102 (11) (2020) 114004. arXiv:2009.06243, doi:10.1103/PhysRevD.102.114004.

[702] V. Dmitrašinović, H.-X. Chen, Chiral $SU_L(3) \times SU_R(3)$ symmetry of baryons with one charmed quark, Phys. Rev. D 101 (11) (2020) 114016. doi:10.1103/PhysRevD.101.114016.

[703] D. Suenaga, Novel Pentaquark Picture of Single-Heavy Baryons in Chiral Effective Model, Few Body Syst. 62 (3) (2021) 49. doi:10.1007/s00601-021-01629-w.

[704] H.-X. Chen, V. Dmitrasinovic, A. Hosaka, K. Nagata, S.-L. Zhu, Chiral Properties of Baryon Fields with Flavor SU(3) Symmetry, Phys. Rev. D 78 (2008) 054021. arXiv:0806.1997, doi:10.1103/PhysRevD.78.054021.

[705] Z.-F. Sun, Z.-W. Liu, X. Liu, S.-L. Zhu, Masses and axial currents of the doubly charmed baryons, Phys. Rev. D 91 (9) (2015) 094030. arXiv:1411.2117, doi:10.1103/PhysRevD.91.094030.

[706] Z.-F. Sun, M. J. Vicente Vacas, Masses of doubly charmed baryons in the extended on-mass-shell renormalization scheme, Phys. Rev. D 93 (9) (2016) 094002. arXiv:1602.04714, doi:10.1103/PhysRevD.93.094002.

[707] D.-L. Yao, Masses and sigma terms of doubly charmed baryons up to $O(p^4)$ in manifestly Lorentz-invariant baryon chiral perturbation theory, Phys. Rev. D 97 (3) (2018) 034012. arXiv:1801.09462, doi:10.1103/PhysRevD.97.034012.

[708] H.-Z. Tong, H.-S. Li, Chiral corrections to the masses of the doubly heavy baryons, Commun. Theor. Phys. 74 (8) (2021) 085201. arXiv:2110.01380, doi:10.1088/1572-9494/ac78d7.

[709] H. Na, S. Gottlieb, Heavy baryon mass spectrum from lattice QCD with 2 + 1 dynamical sea quark flavors, PoS LATTICE2008 (2008) 119. arXiv:0812.1235, doi:10.22323/1.066.0119.

[710] Y. Namekawa, Charmed baryon spectroscopy on the physical point in 2 + 1 flavor lattice QCD, PoS LATTICE2012 (2012) 139. arXiv:1212.0073, doi:10.22323/1.164.0139.

[711] H.-S. Li, L. Meng, Z.-W. Liu, S.-L. Zhu, Magnetic moments of the doubly charmed and bottom baryons, Phys. Rev. D 96 (7) (2017) 076011. arXiv:1707.02765, doi:10.1103/PhysRevD.96.076011.

[712] T. Mehen, B. C. Tiburzi, Doubly heavy baryons and quark-diquark symmetry in quenched and partially quenched chiral perturbation theory, Phys. Rev. D 74 (2006) 054505. arXiv:hep-lat/0607023, doi:10.1103/PhysRevD.74.054505.

[713] S. J. Brodsky, F.-K. Guo, C. Hanhart, U.-G. Meissner, Isospin splittings of doubly heavy baryons, Phys. Lett. B 698 (2011) 251–255. arXiv:1101.1983, doi:10.1016/j.physletb.2011.03.014.

[714] C.-W. Hwang, C.-H. Chung, Isospin mass splittings of heavy baryons in HQS, Phys. Rev. D 78 (2008) 073013. arXiv:0804.4044, doi:10.1103/PhysRevD.78.073013.

[715] Y.-L. Ma, M. Harada, Doubly heavy baryons with chiral partner structure, Phys. Lett. B 748 (2015) 463–466. arXiv:1503.05373, doi:10.1016/j.physletb.2015.07.046.

[716] Y.-L. Ma, M. Harada, Degeneracy of doubly heavy baryons from heavy quark symmetry, Phys. Lett. B 754 (2016) 125–128. arXiv:1510.07481, doi:10.1016/j.physletb.2016.01.011.

[717] N. Isgur, M. B. Wise, Influence of the B^* Resonance on $\bar{B} \to \pi e \bar{\nu}_e$, Phys. Rev. D 41 (1990) 151. doi:10.1103/PhysRevD.41.151.

[718] G. Burdman, Z. Ligeti, M. Neubert, Y. Nir, The Decay $B \to \pi$ lepton neutrino in heavy quark effective theory, Phys. Rev. D 49 (1994) 2331–2345. arXiv:hep-ph/9309272, doi:10.1103/PhysRevD.49.2331.

[719] A. F. Falk, B. Grinstein, $\bar{B} \to \bar{K} e^+ e^-$ in Chiral Perturbation Theory, Nucl. Phys. B 416 (1994) 771–785. arXiv:hep-ph/9306310, doi:10.1016/0550-3213(94)90554-1.

[720] C. L. Y. Lee, M. Lu, M. B. Wise, B_{l4} and D_{l4} decay, Phys. Rev. D 46 (1992) 5040–5048. doi:10.1103/PhysRevD.46.5040.

[721] L. Randall, M. B. Wise, Chiral perturbation theory for $B \to D^*$ and $B \to D$ semileptonic transition matrix elements at zero recoil, Phys. Lett. B 303 (1993) 135–139. arXiv:hep-ph/9212315, doi:10.1016/0370-2693(93)90057-O.

[722] J. L. Goity, W. Roberts, Soft pion emission in semileptonic B meson decays, Phys. Rev. D 51 (1995) 3459–3477. arXiv:hep-ph/9406236, doi:10.1103/PhysRevD.51.3459.

[723] C. G. Boyd, B. Grinstein, SU(3) corrections to $B \to Dl\bar{\nu}$ form-factors at $O(1/M)$, Nucl. Phys. B 451 (1995) 177–193. arXiv:hep-ph/9502311, doi:10.1016/0550-3213(95)00339-T.

[724] Z. Ligeti, I. W. Stewart, M. B. Wise, Comment on V_{ub} from exclusive semileptonic B and D decays, Phys. Lett. B 420 (1998) 359–366. arXiv:hep-ph/9711248, doi:10.1016/S0370-2693(97)01518-9.

[725] B. Grinstein, E. E. Jenkins, A. V. Manohar, M. J. Savage, M. B. Wise, Chiral perturbation theory for f_{D_s}/f_D and B_{B_s}/B_B, Nucl. Phys. B 380 (1992) 369–376. arXiv:hep-ph/9204207, doi:10.1016/0550-3213(92)90248-A.

[726] M. Neubert, Symmetry breaking corrections to meson decay constants in the heavy quark effective theory, Phys. Rev. D 46 (1992) 1076–1087. doi:10.1103/PhysRevD.46.1076.

[727] G. M. de Divitiis, L. Del Debbio, M. Di Pierro, J. M. Flynn, C. Michael, J. Peisa, Towards a lattice determination of the $B^* B \pi$ coupling, JHEP 10 (1998) 010. arXiv:hep-lat/9807032.

[728] J. L. Goity, R. Lewis, M. Schvellinger, L.-Z. Zhang, The Goldberger-Treiman discrepancy in SU(3), Phys. Lett. B 454 (1999) 115–122. arXiv:hep-ph/9901374, doi:10.1016/S0370-2693(99)00217-8.

[729] D. Becirevic, B. Haas, $D^* \to D\pi$ and $D^* \to D\gamma$ decays: Axial coupling and Magnetic moment of D^* meson, Eur. Phys. J. C 71 (2011) 1734. arXiv:0903.2407, doi:10.1140/epjc/s10052-011-1734-y.

[730] D. Becirevic, B. Blossier, E. Chang, B. Haas, $g_{B^* B \pi}$-coupling in the static heavy quark limit, Phys. Lett. B 679 (2009) 231–236. arXiv:0905.3355, doi:10.1016/j.physletb.2009.07.031.

[731] A. Abada, D. Becirevic, P. Boucaud, G. Herdoiza, J. P. Leroy, A. Le Yaouanc, O. Pene, Lattice measurement of the couplings $\hat{g}_\infty$ and $g_{D^* D \pi}$, JHEP 02 (2004) 016. arXiv:hep-lat/0310050, doi:10.1088/1126-6708/2004/02/016.

[732] D. Becirevic, F. Sanfilippo, Theoretical estimate of the $D^* \to D\pi$ decay rate, Phys. Lett. B 721 (2013) 94–100. arXiv:1210.5410, doi:10.1016/j.physletb.2013.03.004.

[733] E. E. Jenkins, A. V. Manohar, Chiral corrections to the baryon axial currents, Phys. Lett. B 259 (1991) 353–358. doi:10.1016/0370-2693(91)90840-M.

[734] S.-L. Zhu, S. Puglia, M. J. Ramsey-Musolf, Recoil order chiral corrections to baryon octet axial currents, Phys. Rev. D 63 (2001) 034002.

arXiv:hep-ph/0009159, doi:10.1103/PhysRevD.63.034002.

[735] S.-L. Zhu, G. Sacco, M. J. Ramsey-Musolf, Recoil order chiral corrections to baryon octet axial currents and large N_c QCD, Phys. Rev. D 66 (2002) 034021. arXiv:hep-ph/0201179, doi:10.1103/PhysRevD.66.034021.

[736] T. R. Hemmert, M. Procura, W. Weise, Quark mass dependence of the nucleon axial vector coupling constant, Phys. Rev. D 68 (2003) 075009. arXiv:hep-lat/0303002, doi:10.1103/PhysRevD.68.075009.

[737] S. R. Beane, M. J. Savage, Baryon axial charge in a finite volume, Phys. Rev. D 70 (2004) 074029. arXiv:hep-ph/0404131, doi:10.1103/PhysRevD.70.074029.

[738] B. Smigielski, J. Wasem, Calculation of the axial charge in the ϵ and ϵ' regimes of HBChPT, Phys. Rev. D 76 (2007) 074503. arXiv:0706.3731, doi:10.1103/PhysRevD.76.074503.

[739] R. Flores-Mendieta, M. A. Hernandez-Ruiz, C. P. Hofmann, Renormalization of the baryon axial vector current in large-N_c chiral perturbation theory: Effects of the decuplet-octet mass difference and flavor symmetry breaking, Phys. Rev. D 86 (2012) 094041. arXiv:1210.8445, doi:10.1103/PhysRevD.86.094041.

[740] D.-L. Yao, L. Alvarez-Ruso, M. J. Vicente-Vacas, Extraction of nucleon axial charge and radius from lattice QCD results using baryon chiral perturbation theory, Phys. Rev. D 96 (11) (2017) 116022. arXiv:1708.08776, doi:10.1103/PhysRevD.96.116022.

[741] U. Sauerwein, M. F. M. Lutz, R. G. E. Timmermans, Axial-vector form factors of the baryon octet and chiral symmetry, Phys. Rev. D 105 (5) (2021) 054005. arXiv:2105.06755, doi:10.1103/PhysRevD.105.054005.

[742] I. W. Stewart, Extraction of the $D^* \to D\pi$ coupling from D^* decays, Nucl. Phys. B 529 (1998) 62–80. arXiv:hep-ph/9803227, doi:10.1016/S0550-3213(98)00374-5.

[743] J. E. Bartelt, et al., Observation of the radiative decay $D^{*+} \to D^+\gamma$, Phys. Rev. Lett. 80 (1998) 3919–3923. arXiv:hep-ex/9711011, doi:10.1103/PhysRevLett.80.3919.

[744] D. Guetta, P. Singer, Two photon decays of heavy vector mesons $B^* \to B\gamma\gamma$, $D^* \to D\gamma\gamma$, and the strong coupling $g_{B^*(D^*)B(D)\pi}$, Phys. Rev. D 61 (2000) 054014. arXiv:hep-ph/9904454, doi:10.1103/PhysRevD.61.054014.

[745] W. Detmold, C. J. D. Lin, S. Meinel, Axial couplings in heavy hadron chiral perturbation theory at the next-to-leading order, Phys. Rev. D 84 (2011) 094502. arXiv:1108.5594, doi:10.1103/PhysRevD.84.094502.

[746] C. W. Bernard, M. F. L. Golterman, Partially quenched gauge theories and an application to staggered fermions, Phys. Rev. D 49 (1994) 486–494. arXiv:hep-lat/9306005, doi:10.1103/PhysRevD.49.486.

[747] N. Li, S.-L. Zhu, Hadronic Molecular States Composed of Heavy Flavor Baryons, Phys. Rev. D 86 (2012) 014020. arXiv:1204.3364, doi:10.1103/PhysRevD.86.014020.

[748] J. Gronberg, et al., Observation of the isospin violating decay $D_s^{*+} \to D_s + \pi^0$, Phys. Rev. Lett. 75 (1995) 3232–3236. arXiv:hep-ex/9508001, doi:10.1103/PhysRevLett.75.3232.

[749] B. Aubert, et al., Measurement of the branching ratios $\Gamma(D_s^{*+} \to D_s^+\pi^0)/\Gamma(D_s^{*+} \to D_s^+\gamma)$ and $\Gamma(D^{*0} \to D^0\pi^0)/\Gamma(D^{*0} \to D^0\gamma)$, Phys. Rev. D 72 (2005) 091101. arXiv:hep-ex/0508039, doi:10.1103/PhysRevD.72.091101.

[750] P. L. Cho, M. B. Wise, Comment on $D_s^* \to D_s\pi^0$ decay, Phys. Rev. D 49 (1994) 6228–6231. arXiv:hep-ph/9401301, doi:10.1103/PhysRevD.49.6228.

[751] K. Terasaki, Decays of Charmed Vector Mesons-$\eta\pi^0$ mixing as an origin of isospin non-conservation (11 2015). arXiv:1511.05249.

[752] B. Yang, B. Wang, L. Meng, S.-L. Zhu, Isospin violating decay $D_s^* \to D_s\pi^0$ in chiral perturbation theory, Phys. Rev. D 101 (5) (2020) 054019. arXiv:1912.09616, doi:10.1103/PhysRevD.101.054019.

[753] B. Wang, B. Yang, L. Meng, S.-L. Zhu, Radiative transitions and magnetic moments of the charmed and bottom vector mesons in chiral perturbation theory, Phys. Rev. D 100 (1) (2019) 016019. arXiv:1905.07742, doi:10.1103/PhysRevD.100.016019.

[754] M. Ablikim, et al., Measurement of branching fraction of Ds*+→Ds+π0 relative to Ds*+→Ds+γ, Phys. Rev. D 107 (3) (2023) 032011. arXiv:2212.13361, doi:10.1103/PhysRevD.107.032011.

[755] C.-Y. Cheung, C.-W. Hwang, Three symmetry breakings in strong and radiative decays of strange heavy mesons, Eur. Phys. J. C 76 (1) (2016) 19. arXiv:1508.07686, doi:10.1140/epjc/s10052-016-3883-5.

[756] P. Gupta, A. Upadhyay, Analysis of strong decays of charmed mesons $D_2^*(2460)$, $D_0(2560)$, $D_2(2740)$, $D_1(3000)$, $D_2^*(3000)$ and their spin partners $D_1^*(2680)$, $D_3^*(2760)$ and $D_0^*(3000)$, Phys. Rev. D 97 (1) (2018) 014015. arXiv:1801.00404, doi:10.1103/PhysRevD.97.014015.

[757] K. Gandhi, A. K. Rai, Strong decays analysis of excited nonstrange charmed mesons: Implications for spectroscopy, Eur. Phys. J. A 57 (1) (2021) 23. arXiv:1911.06063, doi:10.1140/epja/s10050-020-00332-4.

[758] S. Anderson, et al., Observation of a broad $L = 1$ $c\bar{q}$ state in $B^- \to D^{*+}\pi^-\pi^-$ at CLEO, Nucl. Phys. A 663 (2000) 647–650. arXiv:hep-ex/9908009, doi:10.1016/S0375-9474(99)00697-1.

[759] K. Abe, et al., Study of $B \to D^0\pi^-(D^0 \to D^{(*)+}\pi^-)$ decays, Phys. Rev. D 69 (2004) 112002. arXiv:hep-ex/0307021, doi:10.1103/PhysRevD.69.112002.

[760] J. M. Link, et al., Measurement of masses and widths of excited charm mesons D_2^* and evidence for broad states, Phys. Lett. B 586 (2004) 11–20. arXiv:hep-ex/0312060, doi:10.1016/j.physletb.2004.02.017.

[761] S. Fajfer, A. Prapotnik Brdnik, Chiral loops in the isospin violating decays of $D_{s1}(2460)^+$ and $D*_{s0}(2317)^+$, Phys. Rev. D 92 (2015) 074047. arXiv:1506.02716, doi:10.1103/PhysRevD.92.074047.

[762] M. F. M. Lutz, M. Soyeur, Radiative and isospin-violating decays of D_s-mesons in the hadrogenesis conjecture, Nucl. Phys. A 813 (2008) 14–95. arXiv:0710.1545, doi:10.1016/j.nuclphysa.2008.09.003.

[763] F.-K. Guo, C. Hanhart, S. Krewald, U.-G. Meissner, Subleading contributions to the width of the $D_{s0}^*(2317)$, Phys. Lett. B 666 (2008) 251–255. arXiv:0806.3374, doi:10.1016/j.physletb.2008.07.060.

[764] R. Frisch, O. Stern, Magnetic Deviation of Hydrogen Molecules and the Magnetic Moment of the Proton. I, Z. Phys. 85 (1-2) (1933) 4–16. doi:10.1007/bf01330773.

[765] I. Esterman, O. Stern, Magnetic Deviation of Hydrogen Molecules and the Magnetic Moment of the Proton. II, Z. Phys. 85 (1-2) (1933) 17–24. doi:10.1007/bf01330774.

[766] G. Breit, I. Rabi, On the interpretation of present values of nuclear moments, Phys. Rev. 46 (3) (1934) 230–231. doi:10.1103/physrev.

46.230.

[767] H.-y. Gao, Nucleon electromagnetic form-factors, Int. J. Mod. Phys. E 12 (2003) 1–40, [Erratum: Int.J.Mod.Phys.E 12, 567 (2003)]. arXiv:nucl-ex/0301002, doi:10.1142/S021830130300117X.

[768] J. Arrington, C. D. Roberts, J. M. Zanotti, Nucleon electromagnetic form-factors, J. Phys. G 34 (2007) S23–S52. arXiv:nucl-th/0611050, doi:10.1088/0954-3899/34/7/S03.

[769] C. F. Perdrisat, V. Punjabi, M. Vanderhaeghen, Nucleon Electromagnetic Form Factors, Prog. Part. Nucl. Phys. 59 (2007) 694–764. arXiv:hep-ph/0612014, doi:10.1016/j.ppnp.2007.05.001.

[770] S. Pacetti, R. Baldini Ferroli, E. Tomasi-Gustafsson, Proton electromagnetic form factors: Basic notions, present achievements and future perspectives, Phys. Rept. 550-551 (2015) 1–103. doi:10.1016/j.physrep.2014.09.005.

[771] C. E. Carlson, The Proton Radius Puzzle, Prog. Part. Nucl. Phys. 82 (2015) 59–77. arXiv:1502.05314, doi:10.1016/j.ppnp.2015.01.002.

[772] T. Chupp, P. Fierlinger, M. Ramsey-Musolf, J. Singh, Electric dipole moments of atoms, molecules, nuclei, and particles, Rev. Mod. Phys. 91 (1) (2019) 015001. arXiv:1710.02504, doi:10.1103/RevModPhys.91.015001.

[773] N. Bezginov, T. Valdez, M. Horbatsch, A. Marsman, A. C. Vutha, E. A. Hessels, A measurement of the atomic hydrogen Lamb shift and the proton charge radius, Science 365 (6457) (2019) 1007–1012. doi:10.1126/science.aau7807.

[774] W. Xiong, et al., A small proton charge radius from an electron–proton scattering experiment, Nature 575 (7781) (2019) 147–150. doi:10.1038/s41586-019-1721-2.

[775] D. García Gudiño, G. Toledo Sánchez, Determination of the magnetic dipole moment of the ρ meson using 4 pion electroproduction data, Int. J. Mod. Phys. Conf. Ser. 35 (2014) 1460463. arXiv:1305.6345, doi:10.1142/S2010194514604633.

[776] G. Colangelo, M. Hoferichter, P. Stoffer, Two-pion contribution to hadronic vacuum polarization, JHEP 02 (2019) 006. arXiv:1810.00007, doi:10.1007/JHEP02(2019)006.

[777] S. K. Bose, L. P. Singh, Magnetic Moments of Charmed and B Flavored Hadrons in MIT Bag Model, Phys. Rev. D 22 (1980) 773. doi:10.1103/PhysRevD.22.773.

[778] H.-B. Deng, X.-L. Chen, W.-Z. Deng, Meson Decays in an Extended Nambu–Jona-Lasinio model with Heavy Quark Flavors, Chin. Phys. C 38 (1) (2014) 013103. arXiv:1304.5279, doi:10.1088/1674-1137/38/1/013103.

[779] Y.-L. Luan, X.-L. Chen, W.-Z. Deng, Meson electro-magnetic form factors in an extended Nambu–Jona-Lasinio model including heavy quark flavors, Chin. Phys. C 39 (11) (2015) 113103. arXiv:1504.03799, doi:10.1088/1674-1137/39/11/113103.

[780] V. Šimonis, Magnetic properties of ground-state mesons, Eur. Phys. J. A 52 (4) (2016) 90. arXiv:1604.05894, doi:10.1140/epja/i2016-16090-5.

[781] V. Simonis, Improved predictions for magnetic moments and M1 decay widths of heavy hadrons (3 2018). arXiv:1803.01809.

[782] T. M. Aliev, S. Bilmis, M. Savci, Multipole Moments of Heavy Vector and Axial-Vector Mesons in QCD, Phys. Rev. D 101 (5) (2020) 054009. arXiv:1912.05988, doi:10.1103/PhysRevD.101.054009.

[783] R. H. Hackman, N. G. Deshpande, D. A. Dicus, V. L. Teplitz, M1 Transitions in the MIT Bag Model, Phys. Rev. D 18 (1978) 2537–2546. doi:10.1103/PhysRevD.18.2537.

[784] E. Eichten, K. Gottfried, T. Kinoshita, K. D. Lane, T.-M. Yan, Charmonium: Comparison with Experiment, Phys. Rev. D 21 (1980) 203. doi:10.1103/PhysRevD.21.203.

[785] T. N. Pham, PCAC Condition in the Quark Model: G_a/G_V for Vector Meson and the $\omega\rho\pi$ Coupling Constant, Phys. Rev. D 25 (1982) 2955–2959. doi:10.1103/PhysRevD.25.2955.

[786] R. L. Thews, A. N. Kamal, Are D^* decays all right?, Phys. Rev. D 32 (1985) 810. doi:10.1103/PhysRevD.32.810.

[787] G. A. Miller, P. Singer, Radiative and Pionic Decays of the D^* Mesons and the Magnetic Moment of the Charmed Quark, Phys. Rev. D 37 (1988) 2564. doi:10.1103/PhysRevD.37.2564.

[788] A. N. Kamal, Q. P. Xu, Total width of the D^*, Phys. Lett. B 284 (1992) 421–426. doi:10.1016/0370-2693(92)90455-D.

[789] M. A. Ivanov, Y. M. Valit, Radiative and hadronic decays of heavy vector mesons, Z. Phys. C 67 (1995) 633–640. doi:10.1007/BF01553990.

[790] W. Jaus, Semileptonic, radiative, and pionic decays of B, B^* and D, D^* mesons, Phys. Rev. D 53 (1996) 1349, [Erratum: Phys.Rev.D 54, 5904 (1996)]. doi:10.1103/PhysRevD.53.1349.

[791] A. Deandrea, N. Di Bartolomeo, R. Gatto, G. Nardulli, A. D. Polosa, A Constituent quark meson model for heavy meson processes, Phys. Rev. D 58 (1998) 034004. arXiv:hep-ph/9802308, doi:10.1103/PhysRevD.58.034004.

[792] H.-M. Choi, Decay constants and radiative decays of heavy mesons in light-front quark model, Phys. Rev. D 75 (2007) 073016. arXiv:hep-ph/0701263, doi:10.1103/PhysRevD.75.073016.

[793] M. Priyadarsini, P. C. Dash, S. Kar, S. P. Patra, N. Barik, Electromagnetic form factors of heavy flavored vector mesons, Phys. Rev. D 94 (11) (2016) 113011. doi:10.1103/PhysRevD.94.113011.

[794] J. L. Goity, W. Roberts, Radiative transitions in heavy mesons in a relativistic quark model, Phys. Rev. D 64 (2001) 094007. arXiv:hep-ph/0012314, doi:10.1103/PhysRevD.64.094007.

[795] D. Ebert, R. N. Faustov, V. O. Galkin, Radiative M1 decays of heavy light mesons in the relativistic quark model, Phys. Lett. B 537 (2002) 241–248. arXiv:hep-ph/0204089, doi:10.1016/S0370-2693(02)01939-1.

[796] P. Colangelo, F. De Fazio, G. Nardulli, Radiative heavy meson transitions, Phys. Lett. B 316 (1993) 555–560. arXiv:hep-ph/9307330, doi:10.1016/0370-2693(93)91043-M.

[797] T. M. Aliev, E. Iltan, N. K. Pak, Radiative D^* meson decays in QCD sum rules, Phys. Lett. B 334 (1994) 169–174. doi:10.1016/0370-2693(94)90606-8.

[798] H. G. Dosch, S. Narison, $B^*B\pi(\gamma)$ couplings and $D^* \to D\pi(\gamma)$ decays within a $1/M$ expansion in full QCD, Phys. Lett. B 368 (1996) 163–170. arXiv:hep-ph/9510212, doi:10.1016/0370-2693(95)01417-9.

[799] S.-L. Zhu, W.-Y. P. Hwang, Z.-s. Yang, $D^* \to D\gamma$ and $B^* \to B\gamma$ as derived from QCD sum rules, Mod. Phys. Lett. A 12 (1997) 3027–3036. arXiv:hep-ph/9610412, doi:10.1142/S0217732397003150.

[800] H.-D. Li, C.-D. Lü, C. Wang, Y.-M. Wang, Y.-B. Wei, QCD calculations of radiative heavy meson decays with subleading power corrections,

JHEP 04 (2020) 023. `arXiv:2002.03825`, `doi:10.1007/JHEP04(2020)023`.

[801] P. L. Cho, H. Georgi, Electromagnetic interactions in heavy hadron chiral theory, Phys. Lett. B 296 (1992) 408–414, [Erratum: Phys.Lett.B 300, 410 (1993)]. `arXiv:hep-ph/9209239`, `doi:10.1016/0370-2693(92)91340-F`.

[802] J. F. Amundson, C. G. Boyd, E. E. Jenkins, M. E. Luke, A. V. Manohar, J. L. Rosner, M. J. Savage, M. B. Wise, Radiative D^* decay using heavy quark and chiral symmetry, Phys. Lett. B 296 (1992) 415–419. `arXiv:hep-ph/9209241`, `doi:10.1016/0370-2693(92)91341-6`.

[803] H.-Y. Cheng, C.-Y. Cheung, G.-L. Lin, Y. C. Lin, T.-M. Yan, H.-L. Yu, Chiral Lagrangians for radiative decays of heavy hadrons, Phys. Rev. D 47 (1993) 1030–1042. `arXiv:hep-ph/9209262`, `doi:10.1103/PhysRevD.47.1030`.

[804] P. Singer, Radiative decays of heavy mesons and the determination of the strong g coupling, Acta Phys. Polon. B 30 (1999) 3849–3859. `arXiv:hep-ph/9910558`.

[805] M. J. Savage, Heavy meson observables at one loop in partially quenched chiral perturbation theory, Phys. Rev. D 65 (2002) 034014. `arXiv:hep-ph/0109190`, `doi:10.1103/PhysRevD.65.034014`.

[806] W. M. Yao, et al., Review of Particle Physics, J. Phys. G 33 (2006) 1–1232. `doi:10.1088/0954-3899/33/1/001`.

[807] K. A. Olive, et al., Review of Particle Physics, Chin. Phys. C 38 (2014) 090001. `doi:10.1088/1674-1137/38/9/090001`.

[808] A. Anastassov, et al., First measurement of $\Gamma(D^{*+})$ and precision measurement of $m(D^{*+}) - m(D^0)$, Phys. Rev. D 65 (2002) 032003. `arXiv:hep-ex/0108043`, `doi:10.1103/PhysRevD.65.032003`.

[809] M. Tanabashi, et al., Review of Particle Physics, Phys. Rev. D 98 (3) (2018) 030001. `doi:10.1103/PhysRevD.98.030001`.

[810] V. M. Belyaev, V. M. Braun, A. Khodjamirian, R. Ruckl, $D^*D\pi$ and $B^*B\pi$ couplings in QCD, Phys. Rev. D 51 (1995) 6177–6195. `arXiv:hep-ph/9410280`, `doi:10.1103/PhysRevD.51.6177`.

[811] M. E. Luke, A. V. Manohar, Reparametrization invariance constraints on heavy particle effective field theories, Phys. Lett. B 286 (1992) 348–354. `arXiv:hep-ph/9205228`, `doi:10.1016/0370-2693(92)91786-9`.

[812] B. Wang, Z.-W. Liu, X. Liu, $\bar{B}^{(*)}\bar{B}^{(*)}$ interactions in chiral effective field theory, Phys. Rev. D 99 (3) (2019) 036007. `arXiv:1812.04457`, `doi:10.1103/PhysRevD.99.036007`.

[813] A. F. Falk, M. E. Luke, Strong decays of excited heavy mesons in chiral perturbation theory, Phys. Lett. B 292 (1992) 119–127. `arXiv:hep-ph/9206241`, `doi:10.1016/0370-2693(92)90618-E`.

[814] A. F. Falk, Excited heavy mesons and kaon loops in chiral perturbation theory, Phys. Lett. B 305 (1993) 268–274. `arXiv:hep-ph/9302265`, `doi:10.1016/0370-2693(93)90117-Z`.

[815] A. F. Falk, T. Mehen, Excited heavy mesons beyond leading order in the heavy quark expansion, Phys. Rev. D 53 (1996) 231–240. `arXiv:hep-ph/9507311`, `doi:10.1103/PhysRevD.53.231`.

[816] P. Colangelo, F. De Fazio, Understanding $D_{sJ}(2317)$, Phys. Lett. B 570 (2003) 180–184. `arXiv:hep-ph/0305140`, `doi:10.1016/j.physletb.2003.08.003`.

[817] P. Krokovny, et al., Observation of the $D_{sJ}(2317)$ and $D_{sJ}(2457)$ in B decays, Phys. Rev. Lett. 91 (2003) 262002. `arXiv:hep-ex/0308019`, `doi:10.1103/PhysRevLett.91.262002`.

[818] H.-L. Fu, H. W. Grießhammer, F.-K. Guo, C. Hanhart, U.-G. Meißner, Update on strong and radiative decays of the $D_{s0}^*(2317)$ and $D_{s1}(2460)$ and their bottom cousins, Eur. Phys. J. A 58 (4) (2022) 70. `arXiv:2111.09481`, `doi:10.1140/epja/s10050-022-00724-8`.

[819] M. Cleven, H. W. Grießhammer, F.-K. Guo, C. Hanhart, U.-G. Meißner, Strong and radiative decays of the $D_{s0}^*(2317)$ and $D_{s1}(2460)$, Eur. Phys. J. A 50 (2014) 149. `arXiv:1405.2242`, `doi:10.1140/epja/i2014-14149-y`.

[820] S. Aiola, et al., Progress towards the first measurement of charm baryon dipole moments, Phys. Rev. D 103 (7) (2021) 072003. `arXiv:2010.11902`, `doi:10.1103/PhysRevD.103.072003`.

[821] A. Bernotas, V. Simonis, Magnetic moments of heavy baryons in the bag model reexamined (9 2012). `arXiv:1209.2900`, `doi:10.3952/physics.v53i2.2668`.

[822] A. Bernotas, V. Šimonis, Radiative M1 transitions of heavy baryons in the bag model, Phys. Rev. D 87 (7) (2013) 074016. `arXiv:1302.5918`, `doi:10.1103/PhysRevD.87.074016`.

[823] W.-X. Zhang, H. Xu, D. Jia, Masses and magnetic moments of hadrons with one and two open heavy quarks: Heavy baryons and tetraquarks, Phys. Rev. D 104 (11) (2021) 114011. `arXiv:2109.07040`, `doi:10.1103/PhysRevD.104.114011`.

[824] N. Barik, M. Das, Magnetic moments of confined quarks and baryons in an independent quark model based on Dirac equation with power law potential, Phys. Rev. D 28 (1983) 2823–2829. `doi:10.1103/PhysRevD.28.2823`.

[825] M. A. Ivanov, V. E. Lyubovitskij, J. G. Korner, P. Kroll, Heavy baryon transitions in a relativistic three quark model, Phys. Rev. D 56 (1997) 348–364. `arXiv:hep-ph/9612463`, `doi:10.1103/PhysRevD.56.348`.

[826] M. A. Ivanov, J. G. Korner, V. E. Lyubovitskij, A. G. Rusetsky, Strong and radiative decays of heavy flavored baryons, Phys. Rev. D 60 (1999) 094002. `arXiv:hep-ph/9904421`, `doi:10.1103/PhysRevD.60.094002`.

[827] S. Tawfiq, J. G. Korner, P. J. O'Donnell, Electromagnetic transitions of heavy baryons in the $SU(2N_f) \times O(3)$ symmetry, Phys. Rev. D 63 (2001) 034005. `arXiv:hep-ph/9909444`, `doi:10.1103/PhysRevD.63.034005`.

[828] S. Julia-Diaz, D. O. Riska, Baryon magnetic moments in relativistic quark models, Nucl. Phys. A 739 (2004) 69–88. `arXiv:hep-ph/0401096`, `doi:10.1016/j.nuclphysa.2004.03.078`.

[829] S. Kumar, R. Dhir, R. C. Verma, Magnetic moments of charm baryons using effective mass and screened charge of quarks, J. Phys. G 31 (2) (2005) 141–147. `doi:10.1088/0954-3899/31/2/006`.

[830] A. Faessler, T. Gutsche, M. A. Ivanov, J. G. Korner, V. E. Lyubovitskij, D. Nicmorus, K. Pumsa-ard, Magnetic moments of heavy baryons in the relativistic three-quark model, Phys. Rev. D 73 (2006) 094013. `arXiv:hep-ph/0602193`, `doi:10.1103/PhysRevD.73.094013`.

[831] N. Sharma, H. Dahiya, P. K. Chatley, M. Gupta, Spin $1/2^+$, spin $3/2^+$ and transition magnetic moments of low lying and charmed baryons, Phys. Rev. D 81 (2010) 073001. `arXiv:1003.4338`, `doi:10.1103/PhysRevD.81.073001`.

[832] A. Majethiya, K. Thakkar, P. C. Vinodkumar, Spectroscopy and decay properties of Σ_b, Λ_b baryons in quark–diquark model, Chin. J. Phys. 54 (2016) 495–502. `arXiv:1102.4160`, `doi:10.1016/j.cjph.2016.06.008`.

[833] A. Hazra, S. Rakshit, R. Dhir, Radiative M1 transitions of heavy baryons: Effective quark mass scheme, Phys. Rev. D 104 (5) (2021) 053002. `arXiv:2108.01840`, `doi:10.1103/PhysRevD.104.053002`.

[834] S.-L. Zhu, W.-Y. P. Hwang, Z.-S. Yang, The Σ_c and Λ_c magnetic moments from QCD spectral sum rules, Phys. Rev. D 56 (1997) 7273–7275.

166

`arXiv:hep-ph/9708411`, `doi:10.1103/PhysRevD.56.7273`.

[835] S.-L. Zhu, Y.-B. Dai, Radiative decays of heavy hadrons from light cone QCD sum rules in the leading order of HQET, Phys. Rev. D 59 (1999) 114015. `arXiv:hep-ph/9810243`, `doi:10.1103/PhysRevD.59.114015`.

[836] T. M. Aliev, K. Azizi, A. Ozpineci, Magnetic Moments of Heavy Ξ_Q Baryons in Light Cone QCD Sum Rules, Phys. Rev. D 77 (2008) 114006. `arXiv:0803.4420`, `doi:10.1103/PhysRevD.77.114006`.

[837] T. M. Aliev, K. Azizi, A. Ozpineci, Mass and Magnetic Moments of the Heavy Flavored Baryons with $J = 3/2$ in Light Cone QCD Sum Rules, Nucl. Phys. B 808 (2009) 137–154. `arXiv:0807.3481`, `doi:10.1016/j.nuclphysb.2008.09.018`.

[838] Z.-G. Wang, Analysis of the vertexes $\Xi_Q^* \Xi'_Q V$, $\Sigma_Q^* \Sigma_Q V$ and radiative decays $\Xi_Q^* \to \Xi'_Q \gamma$, $\Sigma_Q^* \to \Sigma_Q \gamma$, Eur. Phys. J. A 44 (2010) 105–117. `arXiv:0910.2112`, `doi:10.1140/epja/i2010-10952-8`.

[839] T. M. Aliev, M. Savci, V. S. Zamiralov, Vector meson dominance and radiative decays of heavy spin-3/2 baryons to heavy spin-1/2 baryons, Mod. Phys. Lett. A 27 (2012) 1250054. `arXiv:1109.2473`, `doi:10.1142/S021773231250054X`.

[840] A. K. Agamaliev, T. M. Aliev, M. Savcı, Radiative decays of negative parity heavy baryons in the framework of the light cone QCD sum rules, Nucl. Phys. A 958 (2017) 38–47. `arXiv:1606.07666`, `doi:10.1016/j.nuclphysa.2016.11.005`.

[841] B. Patel, A. K. Rai, P. C. Vinodkumar, Masses and magnetic moments of heavy flavour baryons in hyper central model, J. Phys. G 35 (2008) 065001. `arXiv:0710.3828`, `doi:10.1088/0954-3899/35/6/065001`.

[842] Y.-s. Oh, D.-P. Min, M. Rho, N. N. Scoccola, Massive quark baryons as skyrmions: Magnetic moments, Nucl. Phys. A 534 (1991) 493–512. `doi:10.1016/0375-9474(91)90458-I`.

[843] Y.-s. Oh, B.-Y. Park, Magnetic moments of heavy baryons in the skyrme model, Mod. Phys. Lett. A 11 (1996) 653–662. `arXiv:hep-ph/9505269`, `doi:10.1142/S0217732396000679`.

[844] G.-S. Yang, H.-C. Kim, Magnetic moments of the lowest-lying singly heavy baryons, Phys. Lett. B 781 (2018) 601–606. `arXiv:1802.05416`, `doi:10.1016/j.physletb.2018.04.042`.

[845] G.-S. Yang, H.-C. Kim, Magnetic transitions and radiative decays of singly heavy baryons, Phys. Lett. B 801 (2020) 135142. `arXiv:1909.03156`, `doi:10.1016/j.physletb.2019.135142`.

[846] J.-Y. Kim, H.-C. Kim, G.-S. Yang, M. Oka, Electromagnetic transitions of the singly charmed baryons with spin 3/2, Phys. Rev. D 103 (7) (2021) 074025. `arXiv:2101.10653`, `doi:10.1103/PhysRevD.103.074025`.

[847] S. Scholl, H. Weigel, Magnetic moments of baryons with a single heavy quark, Nucl. Phys. A 735 (2004) 163–184. `arXiv:hep-ph/0312282`, `doi:10.1016/j.nuclphysa.2004.01.132`.

[848] H. Bahtiyar, K. U. Can, G. Erkol, M. Oka, $\Omega_c \gamma \to \Omega_c^*$ transition in lattice QCD, Phys. Lett. B 747 (2015) 281–286. `arXiv:1503.07361`, `doi:10.1016/j.physletb.2015.06.006`.

[849] H. Bahtiyar, K. U. Can, G. Erkol, M. Oka, T. T. Takahashi, $\Xi_c \gamma \to \Xi'_c$ transition in lattice QCD, Phys. Lett. B 772 (2017) 121–126. `arXiv:1612.05722`, `doi:10.1016/j.physletb.2017.06.022`.

[850] K. U. Can, G. Erkol, B. Isildak, M. Oka, T. T. Takahashi, Electromagnetic structure of charmed baryons in Lattice QCD, JHEP 05 (2014) 125. `arXiv:1310.5915`, `doi:10.1007/JHEP05(2014)125`.

[851] K. U. Can, G. Erkol, M. Oka, T. T. Takahashi, Look inside charmed-strange baryons from lattice QCD, Phys. Rev. D 92 (11) (2015) 114515. `arXiv:1508.03048`, `doi:10.1103/PhysRevD.92.114515`.

[852] P. L. Cho, Strong and electromagnetic decays of two new Λ_c^* baryons, Phys. Rev. D 50 (1994) 3295–3302. `arXiv:hep-ph/9401276`, `doi:10.1103/PhysRevD.50.3295`.

[853] M. J. Savage, E2 strength in the radiative charmed baryon decay $\Sigma_c^* \to \Lambda_c \gamma$, Phys. Lett. B 345 (1995) 61–66. `arXiv:hep-ph/9408294`, `doi:10.1016/0370-2693(94)01597-6`.

[854] M. C. Banuls, A. Pich, I. Scimemi, Electromagnetic decays of heavy baryons, Phys. Rev. D 61 (2000) 094009. `arXiv:hep-ph/9911502`, `doi:10.1103/PhysRevD.61.094009`.

[855] B. C. Tiburzi, Baryon electromagnetic properties in partially quenched heavy hadron chiral perturbation theory, Phys. Rev. D 71 (2005) 054504. `arXiv:hep-lat/0412025`, `doi:10.1103/PhysRevD.71.054504`.

[856] N. Jiang, X.-L. Chen, S.-L. Zhu, Electromagnetic decays of the charmed and bottom baryons in chiral perturbation theory, Phys. Rev. D 92 (5) (2015) 054017. `arXiv:1505.02999`, `doi:10.1103/PhysRevD.92.054017`.

[857] G.-J. Wang, L. Meng, H.-S. Li, Z.-W. Liu, S.-L. Zhu, Magnetic moments of the spin-$\frac{1}{2}$ singly charmed baryons in chiral perturbation theory, Phys. Rev. D 98 (5) (2018) 054026. `arXiv:1803.00229`, `doi:10.1103/PhysRevD.98.054026`.

[858] G.-J. Wang, L. Meng, S.-L. Zhu, Radiative decays of the singly heavy baryons in chiral perturbation theory, Phys. Rev. D 99 (3) (2019) 034021. `arXiv:1811.06208`, `doi:10.1103/PhysRevD.99.034021`.

[859] R.-X. Shi, Y. Xiao, L.-S. Geng, Magnetic moments of the spin-1/2 singly charmed baryons in covariant baryon chiral perturbation theory, Phys. Rev. D 100 (5) (2019) 054019. `arXiv:1812.07833`, `doi:10.1103/PhysRevD.100.054019`.

[860] S. R. Coleman, S. L. Glashow, Electrodynamic properties of baryons in the unitary symmetry scheme, Phys. Rev. Lett. 6 (1961) 423. `doi:10.1103/PhysRevLett.6.423`.

[861] E. E. Jenkins, M. E. Luke, A. V. Manohar, M. J. Savage, Chiral perturbation theory analysis of the baryon magnetic moments, Phys. Lett. B 302 (1993) 482–490, [Erratum: Phys.Lett.B 388, 866–866 (1996)]. `arXiv:hep-ph/9212226`, `doi:10.1016/0370-2693(93)90430-P`.

[862] U.-G. Meissner, S. Steininger, Baryon magnetic moments in chiral perturbation theory, Nucl. Phys. B 499 (1997) 349–367. `arXiv:hep-ph/9701260`, `doi:10.1016/S0550-3213(97)00313-1`.

[863] H.-S. Li, Z.-W. Liu, X.-L. Chen, W.-Z. Deng, S.-L. Zhu, Decuplet to octet baryon transitions in chiral perturbation theory, Eur. Phys. J. C 79 (1) (2019) 66. `arXiv:1706.06458`, `doi:10.1140/epjc/s10052-019-6592-z`.

[864] D. B. Lichtenberg, Magnetic Moments of Charmed Baryons in the Quark Model, Phys. Rev. D 15 (1977) 345. `doi:10.1103/PhysRevD.15.345`.

[865] S. N. Jena, D. P. Rath, Magnetic Moments of Light, Charmed and B Flavored Baryons in a Relativistic Logarithmic Potential, Phys. Rev. D 34 (1986) 196–200. `doi:10.1103/PhysRevD.34.196`.

[866] B. Silvestre-Brac, Spectrum and static properties of heavy baryons, Few Body Syst. 20 (1996) 1–25. `doi:10.1007/s006010050028`.

[867] B. Patel, A. K. Rai, P. C. Vinodkumar, Masses and Magnetic Moments of Charmed Baryons Using Hyper Central Model, in: 12th Interna-

tional Conference on Hadron Spectroscopy, 2008. `arXiv:0803.0221`.

[868] T. Branz, A. Faessler, T. Gutsche, M. A. Ivanov, J. G. Korner, V. E. Lyubovitskij, B. Oexl, Radiative decays of double heavy baryons in a relativistic constituent three-quark model including hyperfine mixing, Phys. Rev. D 81 (2010) 114036. `arXiv:1005.1850`, `doi:10.1103/PhysRevD.81.114036`.

[869] U. Özdem, Magnetic moments of doubly heavy baryons in light-cone QCD, J. Phys. G 46 (3) (2019) 035003. `arXiv:1804.10921`, `doi:10.1088/1361-6471/aafffc`.

[870] U. Özdem, Magnetic dipole moments of the spin-$\frac{3}{2}$ doubly heavy baryons, Eur. Phys. J. A 56 (2) (2020) 34. `arXiv:1906.08353`, `doi:10.1140/epja/s10050-020-00049-4`.

[871] K. U. Can, G. Erkol, B. Isildak, M. Oka, T. T. Takahashi, Electromagnetic properties of doubly charmed baryons in Lattice QCD, Phys. Lett. B 726 (2013) 703–709. `arXiv:1306.0731`, `doi:10.1016/j.physletb.2013.09.024`.

[872] H.-S. Li, W.-L. Yang, Spin-$\frac{3}{2}$ doubly charmed baryon contribution to the magnetic moments of the spin-$\frac{1}{2}$ doubly charmed baryons, Phys. Rev. D 103 (5) (2021) 056024. `arXiv:2012.14596`, `doi:10.1103/PhysRevD.103.056024`.

[873] L. Meng, H.-S. Li, Z.-W. Liu, S.-L. Zhu, Magnetic moments of the spin-$\frac{3}{2}$ doubly heavy baryons, Eur. Phys. J. C 77 (12) (2017) 869. `arXiv:1710.08283`, `doi:10.1140/epjc/s10052-017-5447-8`.

[874] H.-S. Li, L. Meng, Z.-W. Liu, S.-L. Zhu, Radiative decays of the doubly charmed baryons in chiral perturbation theory, Phys. Lett. B 777 (2018) 169–176. `arXiv:1708.03620`, `doi:10.1016/j.physletb.2017.12.031`.

[875] M.-Z. Liu, Y. Xiao, L.-S. Geng, Magnetic moments of the spin-1/2 doubly charmed baryons in covariant baryon chiral perturbation theory, Phys. Rev. D 98 (1) (2018) 014040. `arXiv:1807.00912`, `doi:10.1103/PhysRevD.98.014040`.

[876] A. N. Hiller Blin, Z.-F. Sun, M. J. Vicente Vacas, Electromagnetic form factors of spin-1/2 doubly charmed baryons, Phys. Rev. D 98 (5) (2018) 054025. `arXiv:1807.01059`, `doi:10.1103/PhysRevD.98.054025`.

[877] Y.-R. Liu, X. Liu, S.-L. Zhu, Light Pseudoscalar Meson and Heavy Meson Scattering Lengths, Phys. Rev. D 79 (2009) 094026. `arXiv:0904.1770`, `doi:10.1103/PhysRevD.79.094026`.

[878] B.-L. Huang, Z.-Y. Lin, S.-L. Zhu, Light pseudoscalar meson and heavy meson scattering lengths to $O(p^4)$ in heavy meson chiral perturbation theory, Phys. Rev. D 105 (3) (2021) 036016. `arXiv:2112.13702`, `doi:10.1103/PhysRevD.105.036016`.

[879] Z.-W. Liu, Y.-R. Liu, X. Liu, S.-L. Zhu, The Pseudoscalar Meson and Heavy Vector Meson Scattering Lengths, Phys. Rev. D 84 (2011) 034002. `arXiv:1104.2726`, `doi:10.1103/PhysRevD.84.034002`.

[880] S. Weinberg, Pion scattering lengths, Phys. Rev. Lett. 17 (1966) 616–621. `doi:10.1103/PhysRevLett.17.616`.

[881] Y. Tomozawa, Axial vector coupling renormalization and the meson baryon scattering lengths, Nuovo Cim. A 46 (1966) 707–717. `doi:10.1007/BF02857517`.

[882] M. Altenbuchinger, L. S. Geng, W. Weise, Scattering lengths of Nambu-Goldstone bosons off D mesons and dynamically generated heavy-light mesons, Phys. Rev. D 89 (1) (2014) 014026. `arXiv:1309.4743`, `doi:10.1103/PhysRevD.89.014026`.

[883] L. S. Geng, N. Kaiser, J. Martin-Camalich, W. Weise, Low-energy interactions of Nambu-Goldstone bosons with D mesons in covariant chiral perturbation theory, Phys. Rev. D 82 (2010) 054022. `arXiv:1008.0383`, `doi:10.1103/PhysRevD.82.054022`.

[884] L. Liu, K. Orginos, F.-K. Guo, C. Hanhart, U.-G. Meissner, Interactions of charmed mesons with light pseudoscalar mesons from lattice QCD and implications on the nature of the $D_{s0}^*(2317)$, Phys. Rev. D 87 (1) (2013) 014508. `arXiv:1208.4535`, `doi:10.1103/PhysRevD.87.014508`.

[885] L. Liu, H.-W. Lin, K. Orginos, Charmed Hadron Interactions, PoS LATTICE2008 (2008) 112. `arXiv:0810.5412`, `doi:10.22323/1.066.0112`.

[886] D. Mohler, C. B. Lang, L. Leskovec, S. Prelovsek, R. M. Woloshyn, $D_{s0}^*(2317)$ Meson and D-Meson-Kaon Scattering from Lattice QCD, Phys. Rev. Lett. 111 (22) (2013) 222001. `arXiv:1308.3175`, `doi:10.1103/PhysRevLett.111.222001`.

[887] M.-L. Du, F.-K. Guo, U.-G. Meißner, One-loop renormalization of the chiral Lagrangian for spinless matter fields in the SU(N) fundamental representation, J. Phys. G 44 (2017) 014001. `arXiv:1607.00822`, `doi:10.1088/0954-3899/44/1/014001`.

[888] M. Altenbuchinger, L.-S. Geng, Off-shell effects on the interaction of Nambu-Goldstone bosons and D mesons, Phys. Rev. D 89 (5) (2014) 054008. `arXiv:1310.5224`, `doi:10.1103/PhysRevD.89.054008`.

[889] C. B. Lang, L. Leskovec, D. Mohler, S. Prelovsek, R. M. Woloshyn, D_s mesons with DK and D^*K scattering near threshold, Phys. Rev. D 90 (3) (2014) 034510. `arXiv:1403.8103`, `doi:10.1103/PhysRevD.90.034510`.

[890] G. S. Bali, S. Collins, A. Cox, A. Schäfer, Masses and decay constants of the $D_{s0}^*(2317)$ and $D_{s1}(2460)$ from $N_f = 2$ lattice QCD close to the physical point, Phys. Rev. D 96 (7) (2017) 074501. `arXiv:1706.01247`, `doi:10.1103/PhysRevD.96.074501`.

[891] G. Moir, M. Peardon, S. M. Ryan, C. E. Thomas, D. J. Wilson, Coupled-Channel $D\pi$, $D\eta$ and $D_s\bar{K}$ Scattering from Lattice QCD, JHEP 10 (2016) 011. `arXiv:1607.07093`, `doi:10.1007/JHEP10(2016)011`.

[892] D. Mohler, S. Prelovsek, R. M. Woloshyn, $D\pi$ scattering and D meson resonances from lattice QCD, Phys. Rev. D 87 (3) (2013) 034501. `arXiv:1208.4059`, `doi:10.1103/PhysRevD.87.034501`.

[893] P. Wang, X. G. Wang, Study on 0^+ states with open charm in unitarized heavy meson chiral approach, Phys. Rev. D 86 (2012) 014030. `arXiv:1204.5553`, `doi:10.1103/PhysRevD.86.014030`.

[894] Z. Yang, G.-J. Wang, J.-J. Wu, M. Oka, S.-L. Zhu, Novel Coupled Channel Framework Connecting the Quark Model and Lattice QCD for the Near-threshold Ds States, Phys. Rev. Lett. 128 (11) (2022) 112001. `arXiv:2107.04860`, `doi:10.1103/PhysRevLett.128.112001`.

[895] X.-Y. Guo, Y. Heo, M. F. M. Lutz, On chiral extrapolations of charmed meson masses and coupled-channel reaction dynamics, Phys. Rev. D 98 (1) (2018) 014510. `arXiv:1801.10122`, `doi:10.1103/PhysRevD.98.014510`.

[896] V. Bernard, N. Kaiser, U. G. Meissner, Chiral corrections to the S-wave pion-nucleon scattering lengths, Phys. Lett. B 309 (1993) 421–425. `arXiv:hep-ph/9304275`, `doi:10.1016/0370-2693(93)90956-I`.

[897] M.-L. Du, F.-K. Guo, U.-G. Meißner, D.-L. Yao, Aspects of the low-energy constants in the chiral Lagrangian for charmed mesons, Phys. Rev. D 94 (9) (2016) 094037. `arXiv:1610.02963`, `doi:10.1103/PhysRevD.94.094037`.

[898] L. Gayer, N. Lang, S. M. Ryan, D. Tims, C. E. Thomas, D. J. Wilson, Isospin-1/2 $D\pi$ scattering and the lightest D_0^* resonance from lattice QCD, JHEP 07 (2021) 123. `arXiv:2102.04973`, `doi:10.1007/JHEP07(2021)123`.

[899] M. Albaladejo, P. Fernandez-Soler, F.-K. Guo, J. Nieves, Two-pole structure of the $D_0^*(2400)$, Phys. Lett. B 767 (2017) 465–469. `arXiv:`

1610.06727, doi:10.1016/j.physletb.2017.02.036.

[900] D. Gamermann, E. Oset, Axial resonances in the open and hidden charm sectors, Eur. Phys. J. A 33 (2007) 119–131. arXiv:0704.2314, doi:10.1140/epja/i2007-10435-1.

[901] M.-L. Du, M. Albaladejo, P. Fernández-Soler, F.-K. Guo, C. Hanhart, U.-G. Meißner, J. Nieves, D.-L. Yao, Towards a new paradigm for heavy-light meson spectroscopy, Phys. Rev. D 98 (9) (2018) 094018. arXiv:1712.07957, doi:10.1103/PhysRevD.98.094018.

[902] C. B. Lang, D. Mohler, S. Prelovsek, R. M. Woloshyn, Predicting positive parity B_s mesons from lattice QCD, Phys. Lett. B 750 (2015) 17–21. arXiv:1501.01646, doi:10.1016/j.physletb.2015.08.038.

[903] M. Doring, U.-G. Meissner, E. Oset, A. Rusetsky, Unitarized Chiral Perturbation Theory in a finite volume: Scalar meson sector, Eur. Phys. J. A 47 (2011) 139. arXiv:1107.3988, doi:10.1140/epja/i2011-11139-7.

[904] X.-Y. Guo, Y. Heo, M. F. M. Lutz, On chiral excitations with exotic quantum numbers, Phys. Lett. B 791 (2019) 86–91. arXiv:1809.01311, doi:10.1016/j.physletb.2019.02.022.

[905] X.-Y. Guo, M. F. M. Lutz, Chiral excitations of open-beauty systems, Phys. Rev. D 104 (5) (2021) 054035. arXiv:2103.11323, doi:10.1103/PhysRevD.104.054035.

[906] J. P. Lees, et al., Dalitz plot analyses of $B^0 \to D^- D^0 K^+$ and $B^+ \to \bar{D}^0 D^0 K^+$ decays, Phys. Rev. D 91 (5) (2015) 052002. arXiv:1412.6751, doi:10.1103/PhysRevD.91.052002.

[907] R. Aaij, et al., Dalitz plot analysis of $B_s^0 \to \bar{D}^0 K^- \pi^+$ decays, Phys. Rev. D 90 (7) (2014) 072003. arXiv:1407.7712, doi:10.1103/PhysRevD.90.072003.

[908] M.-L. Du, F.-K. Guo, U.-G. Meißner, Implications of chiral symmetry on S-wave pionic resonances and the scalar charmed mesons, Phys. Rev. D 99 (11) (2019) 114002. arXiv:1903.08516, doi:10.1103/PhysRevD.99.114002.

[909] R. Aaij, et al., Amplitude analysis of $B^- \to D^+ \pi^- \pi^-$ decays, Phys. Rev. D 94 (7) (2016) 072001. arXiv:1608.01289, doi:10.1103/PhysRevD.94.072001.

[910] E. van Beveren, G. Rupp, Continuum bound states K_L, $D_1(2420)$, $D_{s1}(2536)$ and their partners K_s, $D_1(2400)$, $D_{sJ}^*(2463)$, Eur. Phys. J. C 32 (2004) 493–499. arXiv:hep-ph/0306051, doi:10.1140/epjc/s2003-01465-0.

[911] Molecular components in P-wave charmed-strange mesons, Phys. Rev. D 94 (7) (2016) 074037. arXiv:1603.07000, doi:10.1103/PhysRevD.94.074037.

[912] D. Mohler, R. M. Woloshyn, D and D_s meson spectroscopy, Phys. Rev. D 84 (2011) 054505. arXiv:1103.5506, doi:10.1103/PhysRevD.84.054505.

[913] C. Hanhart, A. Nefediev, Do near-threshold molecular states mix with neighboring $\bar{Q}Q$ states?, Phys. Rev. D 106 (11) (2022) 114003. arXiv:2209.10165, doi:10.1103/PhysRevD.106.114003.

[914] H. Sazdjian, The Interplay between Compact and Molecular Structures in Tetraquarks, Symmetry 14 (3) (2022) 515. arXiv:2202.01081, doi:10.3390/sym14030515.

[915] F. K. Guo, C. Hanhart, Y. S. Kalashnikova, P. Matuschek, R. V. Mizuk, A. V. Nefediev, Q. Wang, J. L. Wynen, Interplay of quark and meson degrees of freedom in near-threshold states: A practical parametrization for line shapes, Phys. Rev. D 93 (7) (2016) 074031. arXiv:1602.00940, doi:10.1103/PhysRevD.93.074031.

[916] Constituent quark model study of the meson spectra, J. Phys. G 31 (2005) 481. arXiv:hep-ph/0411299, doi:10.1088/0954-3899/31/5/017.

[917] Quark-model study of few-baryon systems, Rept. Prog. Phys. 68 (2005) 965–1042. arXiv:hep-ph/0502173, doi:10.1088/0034-4885/68/5/R01.

[918] J. Segovia, D. R. Entem, F. Fernandez, E. Hernandez, Constituent quark model description of charmonium phenomenology, Int. J. Mod. Phys. E 22 (2013) 1330026. arXiv:1309.6926, doi:10.1142/S0218301313300269.

[919] A. Le Yaouanc, L. Oliver, O. Pene, J. C. Raynal, Naive quark pair creation model of strong interaction vertices, Phys. Rev. D 8 (1973) 2223–2234. doi:10.1103/PhysRevD.8.2223.

[920] Y. C. Tang, M. Lemere, D. R. Thompson, Resonating-group method for nuclear many-body problems, Phys. Rept. 47 (1978) 167–223. doi:10.1016/0370-1573(78)90175-8.

[921] C. Alexandrou, J. Berlin, J. Finkenrath, T. Leontiou, M. Wagner, Tetraquark interpolating fields in a lattice QCD investigation of the $D_{s0}^*(2317)$ meson, Phys. Rev. D 101 (3) (2020) 034502. arXiv:1911.08435, doi:10.1103/PhysRevD.101.034502.

[922] G. K. C. Cheung, C. E. Thomas, D. J. Wilson, G. Moir, M. Peardon, S. M. Ryan, DK $I = 0$, $D\bar{K}$ $I = 0, 1$ scattering and the $D_{s0}^*(2317)$ from lattice QCD, JHEP 02 (2021) 100. arXiv:2008.06432, doi:10.1007/JHEP02(2021)100.

[923] A. Martínez Torres, E. Oset, S. Prelovsek, A. Ramos, Reanalysis of lattice QCD spectra leading to the $D_{s0}^*(2317)$ and $D_{s1}^*(2460)$, JHEP 05 (2015) 153. arXiv:1412.1706, doi:10.1007/JHEP05(2015)153.

[924] T. Hyodo, Structure and compositeness of hadron resonances, Int. J. Mod. Phys. A 28 (2013) 1330045. arXiv:1310.1176, doi:10.1142/S0217751X13300457.

[925] F. Aceti, L. R. Dai, L. S. Geng, E. Oset, Y. Zhang, Meson-baryon components in the states of the baryon decuplet, Eur. Phys. J. A 50 (2014) 57. arXiv:1301.2554, doi:10.1140/epja/i2014-14057-2.

[926] J. Segovia, C. Albertus, E. Hernandez, F. Fernandez, D. R. Entem, Nonleptonic $B \to D^{(*)} D_{sJ}^{(*)}$ decays and the nature of the orbitally excited charmed-strange mesons, Phys. Rev. D 86 (2012) 014010. arXiv:1203.4362, doi:10.1103/PhysRevD.86.014010.

[927] M. Albaladejo, P. Fernandez-Soler, J. Nieves, P. G. Ortega, Lowest-lying even-parity $\bar{B}_s$ mesons: heavy-quark spin-flavor symmetry, chiral dynamics, and constituent quark-model bare masses, Eur. Phys. J. C 77 (3) (2017) 170. arXiv:1612.07782, doi:10.1140/epjc/s10052-017-4735-7.

[928] A. Le Yaouanc, L. Oliver, O. Pene, J. C. Raynal, Strong Decays of $\psi''(4028)$ as a Radial Excitation of Charmonium, Phys. Lett. B 71 (1977) 397–399. doi:10.1016/0370-2693(77)90250-7.

[929] R. Kokoski, N. Isgur, Meson Decays by Flux Tube Breaking, Phys. Rev. D 35 (1987) 907. doi:10.1103/PhysRevD.35.907.

[930] P. R. Page, Excited charmonium decays by flux tube breaking and the ψ' anomaly at CDF, Nucl. Phys. B 446 (1995) 189–210. arXiv:hep-ph/9502204, doi:10.1016/0550-3213(95)00171-N.

[931] H. G. Blundell, Meson properties in the quark model: A look at some outstanding problems, Other thesis (7 1996). arXiv:hep-ph/

9608473.

[932] E. S. Ackleh, T. Barnes, E. S. Swanson, On the mechanism of open flavor strong decays, Phys. Rev. D 54 (1996) 6811–6829. arXiv:hep-ph/9604355, doi:10.1103/PhysRevD.54.6811.

[933] D. Morel, S. Capstick, Baryon meson loop effects on the spectrum of nonstrange baryons (4 2002). arXiv:nucl-th/0204014.

[934] Z.-w. Lin, C. M. Ko, A Model for J/ψ absorption in hadronic matter, Phys. Rev. C 62 (2000) 034903. arXiv:nucl-th/9912046, doi:10.1103/PhysRevC.62.034903.

[935] E. Oset, A. Ramos, Dynamically generated resonances from the vector octet-baryon octet interaction, Eur. Phys. J. A 44 (2010) 445–454. arXiv:0905.0973, doi:10.1140/epja/i2010-10957-3.

[936] L. Zhao, L. Ma, S.-L. Zhu, Spin-orbit force, recoil corrections, and possible $B\bar{B}^*$ and $D\bar{D}^*$ molecular states, Phys. Rev. D 89 (9) (2014) 094026. arXiv:1403.4043, doi:10.1103/PhysRevD.89.094026.

[937] J. M. M. Hall, A. C.-P. Hsu, D. B. Leinweber, A. W. Thomas, R. D. Young, Finite-Volume Matrix Hamiltonian Model for a $\Delta \to \pi N$ System, Phys. Rev. D 87 (9) (2013) 094510. arXiv:1303.4157, doi:10.1103/PhysRevD.87.094510.

[938] J.-J. Wu, T.-S. H. Lee, A. W. Thomas, R. D. Young, Finite-Volume Hamiltonian Method for Coupled Channel Interactions in Lattice QCD, Phys. Rev. C 90 (5) (2014) 055206. arXiv:1402.4868, doi:10.1103/PhysRevC.90.055206.

[939] J. M. M. Hall, W. Kamleh, D. B. Leinweber, B. J. Menadue, B. J. Owen, A. W. Thomas, R. D. Young, Lattice QCD Evidence That the Λ(1405) Resonance Is an Antikaon-Nucleon Molecule, Phys. Rev. Lett. 114 (13) (2015) 132002. doi:10.1103/PhysRevLett.114.132002.

[940] Z.-W. Liu, W. Kamleh, D. B. Leinweber, F. M. Stokes, A. W. Thomas, J.-J. Wu, Hamiltonian Effective Field Theory Study of the $N^*(1535)$ Resonance in Lattice QCD, Phys. Rev. Lett. 116 (8) (2016) 082004. arXiv:1512.00140, doi:10.1103/PhysRevLett.116.082004.

[941] U.-G. Meißner, Two-pole structures in QCD: Facts, not fantasy!, Symmetry 12 (6) (2020) 981. arXiv:2005.06909, doi:10.3390/sym12060981.

[942] L. S. Geng, E. Oset, L. Roca, J. A. Oller, The WA3 data and the two $K_1(1270)$ resonances, in: 12th International Conference on Hadron Spectroscopy, 2007. arXiv:0711.4778.

[943] C. García-Recio, L. S. Geng, J. Nieves, L. L. Salcedo, E. Wang, J.-J. Xie, Low-lying even parity meson resonances and spin-flavor symmetry revisited, Phys. Rev. D 87 (9) (2013) 096006. arXiv:1304.1021, doi:10.1103/PhysRevD.87.096006.

[944] D. Jido, J. A. Oller, E. Oset, A. Ramos, U. G. Meissner, Chiral dynamics of the two Λ(1405) states, Nucl. Phys. A 725 (2003) 181–200. arXiv:nucl-th/0303062, doi:10.1016/S0375-9474(03)01598-7.

[945] S. S. Gubser, S. S. Pufu, F. D. Rocha, A. Yarom, Energy loss in a strongly coupled thermal medium and the gauge-string duality, 2010, pp. 1–59. arXiv:0902.4041, doi:10.1142/9789814293297_0001.

[946] X.-Y. Guo, Y. Heo, M. F. M. Lutz, On chiral extrapolations of coupled-channel reaction dynamics for charmed mesons, PoS LATTICE2018 (2018) 085. arXiv:1811.00478, doi:10.22323/1.334.0085.

[947] M.-L. Du, F.-K. Guo, C. Hanhart, B. Kubis, U.-G. Meißner, Where is the lightest charmed scalar meson?, Phys. Rev. Lett. 126 (19) (2021) 192001. arXiv:2012.04599, doi:10.1103/PhysRevLett.126.192001.

[948] Z.-W. Liu, Y.-R. Liu, S.-L. Zhu, Pseudoscalar Meson and Decuplet Baryon Scattering Lengths, Phys. Rev. D 83 (2011) 034004. arXiv:1011.3613, doi:10.1103/PhysRevD.83.034004.

[949] Z.-H. Guo, Prediction of exotic doubly charmed baryons within chiral effective field theory, Phys. Rev. D 96 (7) (2017) 074004. arXiv:1708.04145, doi:10.1103/PhysRevD.96.074004.

[950] L. Meng, S.-L. Zhu, Light pseudoscalar meson and doubly charmed baryon scattering lengths with heavy diquark-antiquark symmetry, Phys. Rev. D 100 (1) (2019) 014006. arXiv:1811.07320, doi:10.1103/PhysRevD.100.014006.

[951] M.-J. Yan, X.-H. Liu, S. Gonzàlez-Solís, F.-K. Guo, C. Hanhart, U.-G. Meißner, B.-S. Zou, New spectrum of negative-parity doubly charmed baryons: Possibility of two quasistable states, Phys. Rev. D 98 (9) (2018) 091502. arXiv:1805.10972, doi:10.1103/PhysRevD.98.091502.

[952] J. M. Dias, V. R. Debastiani, J. J. Xie, E. Oset, Doubly charmed Ξ_{cc} molecular states from meson-baryon interaction, Phys. Rev. D 98 (9) (2018) 094017. arXiv:1805.03286, doi:10.1103/PhysRevD.98.094017.

[953] Q.-X. Yu, J. M. Dias, W.-H. Liang, E. Oset, Molecular Ξ_{bc} states from meson-baryon interaction, Eur. Phys. J. C 79 (12) (2019) 1025. arXiv:1909.13449, doi:10.1140/epjc/s10052-019-7543-4.

[954] T. R. Hemmert, B. R. Holstein, J. Kambor, Systematic $1/M$ expansion for spin-3/2 particles in baryon chiral perturbation theory, Phys. Lett. B 395 (1997) 89–95. arXiv:hep-ph/9606456, doi:10.1016/S0370-2693(97)00049-X.

[955] T. R. Hemmert, B. R. Holstein, J. Kambor, Chiral Lagrangians and Δ(1232) interactions: Formalism, J. Phys. G 24 (1998) 1831–1859. arXiv:hep-ph/9712496, doi:10.1088/0954-3899/24/10/003.

[956] S. S. Gershtein, V. V. Kiselev, A. K. Likhoded, A. I. Onishchenko, Spectroscopy of doubly heavy baryons, Phys. Rev. D 62 (2000) 054021. doi:10.1103/PhysRevD.62.054021.

[957] D. R. Phillips, S. R. Beane, M. C. Birse, Scheming in dimensional regularization, J. Phys. A 32 (1999) 3397–3407. arXiv:hep-th/9810049, doi:10.1088/0305-4470/32/18/313.

[958] D. Gamermann, E. Oset, Isospin breaking effects in the X(3872) resonance, Phys. Rev. D 80 (2009) 014003. arXiv:0905.0402, doi:10.1103/PhysRevD.80.014003.

[959] D. Gamermann, J. Nieves, E. Oset, E. Ruiz Arriola, Couplings in coupled channels versus wave functions: application to the X(3872) resonance, Phys. Rev. D 81 (2010) 014029. arXiv:0911.4407, doi:10.1103/PhysRevD.81.014029.

[960] D. B. Kaplan, M. J. Savage, M. B. Wise, A Perturbative calculation of the electromagnetic form-factors of the deuteron, Phys. Rev. C 59 (1999) 617–629. arXiv:nucl-th/9804032, doi:10.1103/PhysRevC.59.617.

[961] M. B. Voloshin, Interference and binding effects in decays of possible molecular component of X(3872), Phys. Lett. B 579 (2004) 316–320. arXiv:hep-ph/0309307, doi:10.1016/j.physletb.2003.11.014.

[962] M. B. Voloshin, X(3872) diagnostics with decays to $D\bar{D}\gamma$, Int. J. Mod. Phys. A 21 (2006) 1239–1250. arXiv:hep-ph/0509192, doi:10.1142/S0217751X06029041.

[963] S. Fleming, M. Kusunoki, T. Mehen, U. van Kolck, Pion interactions in the X(3872), Phys. Rev. D 76 (2007) 034006. arXiv:hep-ph/0703168, doi:10.1103/PhysRevD.76.034006.

170

[964] M. Albaladejo, F.-K. Guo, C. Hidalgo-Duque, J. Nieves, $Z_c(3900)$: What has been really seen?, Phys. Lett. B 755 (2016) 337–342. `arXiv:1512.03638`, `doi:10.1016/j.physletb.2016.02.025`.

[965] E. Braaten, M. Kusunoki, Decays of the $X(3872)$ into J/ψ and light hadrons, Phys. Rev. D 72 (2005) 054022. `arXiv:hep-ph/0507163`, `doi:10.1103/PhysRevD.72.054022`.

[966] E. Epelbaum, J. Gegelia, U.-G. Meißner, Wilsonian renormalization group versus subtractive renormalization in effective field theories for nucleon–nucleon scattering, Nucl. Phys. B 925 (2017) 161–185. `arXiv:1705.02524`, `doi:10.1016/j.nuclphysb.2017.10.008`.

[967] T. D. Cohen, B. A. Gelman, U. van Kolck, An Effective field theory for coupled channel scattering, Phys. Lett. B 588 (2004) 57–66. `arXiv:nucl-th/0402054`, `doi:10.1016/j.physletb.2004.03.020`.

[968] L. Meng, G.-J. Wang, B. Wang, S.-L. Zhu, Probing the long-range structure of the T_{cc}^+ with the strong and electromagnetic decays, Phys. Rev. D 104 (5) (2021) 051502. `arXiv:2107.14784`, `doi:10.1103/PhysRevD.104.L051502`.

[969] M. Jansen, H. W. Hammer, Y. Jia, Light quark mass dependence of the $X(3872)$ in an effective field theory, Phys. Rev. D 89 (1) (2014) 014033. `arXiv:1310.6937`, `doi:10.1103/PhysRevD.89.014033`.

[970] T. Barford, M. C. Birse, A Renormalization group approach to two-body scattering in the presence of long range forces, Phys. Rev. C 67 (2003) 064006. `arXiv:hep-ph/0206146`, `doi:10.1103/PhysRevC.67.064006`.

[971] V. B. Berestetsky, E. M. Lifshitz, L. P. Pitaevsky, Quantum electrodynamics (1982) (1982).

[972] V. Baru, A. A. Filin, C. Hanhart, Y. S. Kalashnikova, A. E. Kudryavtsev, A. V. Nefediev, Three-body $D\bar{D}\pi$ dynamics for the X(3872), Phys. Rev. D 84 (2011) 074029. `arXiv:1108.5644`, `doi:10.1103/PhysRevD.84.074029`.

[973] Q. Wang, V. Baru, A. A. Filin, C. Hanhart, A. V. Nefediev, J. L. Wynen, Line shapes of the $Z_b(10610)$ and $Z_b(10650)$ in the elastic and inelastic channels revisited, Phys. Rev. D 98 (7) (2018) 074023. `arXiv:1805.07453`, `doi:10.1103/PhysRevD.98.074023`.

[974] M. D. Schwartz, Quantum Field Theory and the Standard Model, Cambridge University Press, 2014.

[975] G. F. Sterman, An Introduction to quantum field theory, Cambridge University Press, 1993.

[976] Z.-W. Liu, N. Li, S.-L. Zhu, Chiral perturbation theory and the $\bar{B}B$ strong interaction, Phys. Rev. D 89 (7) (2014) 074015. `arXiv:1211.3578`, `doi:10.1103/PhysRevD.89.074015`.

[977] M. T. AlFiky, F. Gabbiani, A. A. Petrov, $X(3872)$: Hadronic molecules in effective field theory, Phys. Lett. B 640 (2006) 238–245. `arXiv:hep-ph/0506141`, `doi:10.1016/j.physletb.2006.07.069`.

[978] M. P. Valderrama, Power Counting and Perturbative One Pion Exchange in Heavy Meson Molecules, Phys. Rev. D 85 (2012) 114037. `arXiv:1204.2400`, `doi:10.1103/PhysRevD.85.114037`.

[979] T. D. Cohen, Regularization, renormalization and range: The Nucleon-nucleon interaction from effective field theory, Phys. Rev. C 55 (1997) 67–72. `arXiv:nucl-th/9606044`, `doi:10.1103/PhysRevC.55.67`.

[980] E. Epelbaum, U. G. Meissner, W. Gloeckle, C. Elster, Resonance saturation for four nucleon operators, Phys. Rev. C 65 (2002) 044001. `arXiv:nucl-th/0106007`, `doi:10.1103/PhysRevC.65.044001`.

[981] V. Bernard, N. Kaiser, U.-G. Meissner, Aspects of chiral pion-nucleon physics, Nucl. Phys. A 615 (1997) 483–500. `arXiv:hep-ph/9611253`, `doi:10.1016/S0375-9474(97)00021-3`.

[982] L. Meng, B. Wang, S.-L. Zhu, $\Sigma_c N$ interaction in chiral effective field theory, Phys. Rev. C 101 (6) (2020) 064002. `arXiv:1912.09661`, `doi:10.1103/PhysRevC.101.064002`.

[983] P. Wang, X. G. Wang, Study on $X(3872)$ from effective field theory with pion exchange interaction, Phys. Rev. Lett. 111 (4) (2013) 042002. `arXiv:1304.0846`, `doi:10.1103/PhysRevLett.111.042002`.

[984] V. Baru, E. Epelbaum, A. A. Filin, F. K. Guo, H. W. Hammer, C. Hanhart, U. G. Meißner, A. V. Nefediev, Remarks on study of $X(3872)$ from effective field theory with pion-exchange interaction, Phys. Rev. D 91 (3) (2015) 034002. `arXiv:1501.02924`, `doi:10.1103/PhysRevD.91.034002`.

[985] E. Epelbaum, Few-nucleon forces and systems in chiral effective field theory, Prog. Part. Nucl. Phys. 57 (2006) 654–741. `arXiv:nucl-th/0509032`, `doi:10.1016/j.ppnp.2005.09.002`.

[986] E. Epelbaum, U.-G. Meissner, W. Gloeckle, Nuclear forces in the chiral limit, Nucl. Phys. A 714 (2003) 535–574. `arXiv:nucl-th/0207089`, `doi:10.1016/S0375-9474(02)01393-3`.

[987] K. Erkelenz, R. Alzetta, K. Holinde, Momentum space calculations and helicity formalism in nuclear physics, Nucl. Phys. A 176 (1971) 413–432. `doi:10.1016/0375-9474(71)90279-X`.

[988] B. Wang, L. Meng, S.-L. Zhu, Deciphering the charged heavy quarkoniumlike states in chiral effective field theory, Phys. Rev. D 102 (2020) 114019. `arXiv:2009.01980`, `doi:10.1103/PhysRevD.102.114019`.

[989] V. Baru, E. Epelbaum, A. A. Filin, C. Hanhart, U. G. Meissner, A. V. Nefediev, Quark mass dependence of the $X(3872)$ binding energy, Phys. Lett. B 726 (2013) 537–543. `arXiv:1306.4108`, `doi:10.1016/j.physletb.2013.08.073`.

[990] V. Baru, E. Epelbaum, A. A. Filin, J. Gegelia, A. V. Nefediev, Binding energy of the $X(3872)$ at unphysical pion masses, Phys. Rev. D 92 (11) (2015) 114016. `arXiv:1509.01789`, `doi:10.1103/PhysRevD.92.114016`.

[991] J. Haidenbauer, A. Nogga, I. Vidaña, Predictions for charmed nuclei based on $Y_c N$ forces inferred from lattice QCD simulations, Eur. Phys. J. A 56 (7) (2020) 195. `arXiv:2003.07768`, `doi:10.1140/epja/s10050-020-00185-x`.

[992] J. Golak, et al., A new way to perform partial wave decompositions of few-nucleon forces, Eur. Phys. J. A 43 (2010) 241–250. `arXiv:0911.4173`, `doi:10.1140/epja/i2009-10903-6`.

[993] L. Meng, B. Wang, G.-J. Wang, S.-L. Zhu, Hidden charm pentaquark states and $\Sigma_c^{(*)}\bar{D}^{(*)}$ interaction in chiral perturbation theory, in: 18th International Conference on Hadron Spectroscopy and Structure, 2020, pp. 313–317. `arXiv:1911.09250`, `doi:10.1142/9789811219313_0052`.

[994] Z.-W. Liu, B. Wang, H. Xu, N. Li, X. Liu, S.-L. Zhu, Interactions between two heavy mesons within heavy meson chiral effective field theory, in: 18th International Conference on Hadron Spectroscopy and Structure, 2020, pp. 453–457. `arXiv:1911.10840`, `doi:10.1142/9789811219313_0076`.

[995] H. Xu, Study of the hidden charm $D\bar{D}^*$ interactions in chiral effective field theory, Phys. Rev. D 105 (3) (2021) 034013. `arXiv:2112.10722`, `doi:10.1103/PhysRevD.105.034013`.

[996] C. Ordonez, L. Ray, U. van Kolck, Nucleon-nucleon potential from an effective chiral Lagrangian, Phys. Rev. Lett. 72 (1994) 1982–1985.

171

doi:10.1103/PhysRevLett.72.1982.

[997] J. Gasser, M. E. Sainio, A. Svarc, Nucleons with Chiral Loops, Nucl. Phys. B 307 (1988) 779–853. doi:10.1016/0550-3213(88)90108-3.

[998] N. Fettes, U.-G. Meissner, S. Steininger, Pion-nucleon scattering in chiral perturbation theory. 1. Isospin symmetric case, Nucl. Phys. A 640 (1998) 199–234. arXiv:hep-ph/9803266, doi:10.1016/S0375-9474(98)00452-7.

[999] N. Fettes, U. G. Meissner, Pion - nucleon scattering in an effective chiral field theory with explicit spin 3/2 fields, Nucl. Phys. A 679 (2001) 629–670. arXiv:hep-ph/0006299, doi:10.1016/S0375-9474(00)00368-7.

[1000] H. Krebs, A. Gasparyan, E. Epelbaum, Chiral three-nucleon force at N^{4}LO I: Longest-range contributions, Phys. Rev. C 85 (2012) 054006. arXiv:1203.0067, doi:10.1103/PhysRevC.85.054006.

[1001] R. Koch, A Calculation of Low-Energy πN Partial Waves Based on Fixed-t Analyticity, Nucl. Phys. A 448 (1986) 707–731. doi:10.1016/0375-9474(86)90438-0.

[1002] R. A. Arndt, W. J. Briscoe, I. I. Strakovsky, R. L. Workman, Extended partial-wave analysis of πN scattering data, Phys. Rev. C 74 (2006) 045205. arXiv:nucl-th/0605082, doi:10.1103/PhysRevC.74.045205.

[1003] E. Epelbaum, W. Gloeckle, U.-G. Meissner, Improving the convergence of the chiral expansion for nuclear forces. 1. Peripheral phases, Eur. Phys. J. A 19 (2004) 125–137. arXiv:nucl-th/0304037, doi:10.1140/epja/i2003-10096-0.

[1004] E. Epelbaum, W. Gloeckle, U.-G. Meissner, Improving the convergence of the chiral expansion for nuclear forces. 2. Low phases and the deuteron, Eur. Phys. J. A 19 (2004) 401–412. arXiv:nucl-th/0308010, doi:10.1140/epja/i2003-10129-8.

[1005] G. P. Lepage, How to renormalize the Schrödinger equation, in: 8th Jorge Andre Swieca Summer School on Nuclear Physics, 1997, pp. 135–180. arXiv:nucl-th/9706029.

[1006] D. R. Entem, R. Machleidt, Accurate charge dependent nucleon nucleon potential at fourth order of chiral perturbation theory, Phys. Rev. C 68 (2003) 041001. arXiv:nucl-th/0304018, doi:10.1103/PhysRevC.68.041001.

[1007] A. Ozpineci, C. W. Xiao, E. Oset, Hidden beauty molecules within the local hidden gauge approach and heavy quark spin symmetry, Phys. Rev. D 88 (2013) 034018. arXiv:1306.3154, doi:10.1103/PhysRevD.88.034018.

[1008] T. Mehen, J. W. Powell, Heavy Quark Symmetry Predictions for Weakly Bound B-Meson Molecules, Phys. Rev. D 84 (2011) 114013. arXiv:1109.3479, doi:10.1103/PhysRevD.84.114013.

[1009] J. Nieves, M. P. Valderrama, The Heavy Quark Spin Symmetry Partners of the X(3872), Phys. Rev. D 86 (2012) 056004. arXiv:1204.2790, doi:10.1103/PhysRevD.86.056004.

[1010] C. Hidalgo-Duque, J. Nieves, M. P. Valderrama, Light flavor and heavy quark spin symmetry in heavy meson molecules, Phys. Rev. D 87 (7) (2013) 076006. arXiv:1210.5431, doi:10.1103/PhysRevD.87.076006.

[1011] L. Meng, B. Wang, S.-L. Zhu, Predicting the $D_s^{(*)}D_s^{(*)}$ bound states as the partners of X(3872), Sci. Bull. 66 (2021) 1413. arXiv:2012.09813, doi:10.1016/j.scib.2021.03.016.

[1012] A. E. Bondar, A. Garmash, A. I. Milstein, R. Mizuk, M. B. Voloshin, Heavy quark spin structure in Z_b resonances, Phys. Rev. D 84 (2011) 054010. arXiv:1105.4473, doi:10.1103/PhysRevD.84.054010.

[1013] M. B. Voloshin, Radiative transitions from $\Upsilon(5S)$ to molecular bottomonium, Phys. Rev. D 84 (2011) 031502. arXiv:1105.5829, doi:10.1103/PhysRevD.84.031502.

[1014] F.-K. Guo, C. Hanhart, U.-G. Meissner, Implications of heavy quark spin symmetry on heavy meson hadronic molecules, Phys. Rev. Lett. 102 (2009) 242004. arXiv:0904.3338, doi:10.1103/PhysRevLett.102.242004.

[1015] M. Albaladejo, F. K. Guo, C. Hidalgo-Duque, J. Nieves, M. P. Valderrama, Decay widths of the spin-2 partners of the X(3872), Eur. Phys. J. C 75 (11) (2015) 547. arXiv:1504.00861, doi:10.1140/epjc/s10052-015-3753-6.

[1016] M. B. Voloshin, Light Quark Spin Symmetry in Z_b Resonances?, Phys. Rev. D 93 (7) (2016) 074011. arXiv:1601.02540, doi:10.1103/PhysRevD.93.074011.

[1017] M. B. Voloshin, Heavy quark spin selection rule and the properties of the X(3872), Phys. Lett. B 604 (2004) 69–73. arXiv:hep-ph/0408321, doi:10.1016/j.physletb.2004.11.003.

[1018] M. B. Voloshin, Z_c(3900)-what is inside?, Phys. Rev. D 87 (9) (2013) 091501. arXiv:1304.0380, doi:10.1103/PhysRevD.87.091501.

[1019] M. B. Voloshin, Quark spin structures of bottom-charmed threshold molecular states, Phys. Rev. D 98 (7) (2018) 074004. arXiv:1808.00427, doi:10.1103/PhysRevD.98.074004.

[1020] J. Nieves, M. P. Valderrama, Deriving the existence of $B\bar{B}^*$ bound states from the X(3872) and Heavy Quark Symmetry, Phys. Rev. D 84 (2011) 056015. arXiv:1106.0600, doi:10.1103/PhysRevD.84.056015.

[1021] V. Baru, E. Epelbaum, A. A. Filin, C. Hanhart, U.-G. Meißner, A. V. Nefediev, Heavy-quark spin symmetry partners of the X(3872) revisited, Phys. Lett. B 763 (2016) 20–28. arXiv:1605.09649, doi:10.1016/j.physletb.2016.10.008.

[1022] M. Cleven, F.-K. Guo, C. Hanhart, Q. Wang, Q. Zhao, Employing spin symmetry to disentangle different models for the XYZ states, Phys. Rev. D 92 (1) (2015) 014005. arXiv:1505.01771, doi:10.1103/PhysRevD.92.014005.

[1023] F.-K. Guo, C. Hidalgo-Duque, J. Nieves, M. P. Valderrama, Heavy-antiquark–diquark symmetry and heavy hadron molecules: Are there triply heavy pentaquarks?, Phys. Rev. D 88 (5) (2013) 054014. arXiv:1305.4052, doi:10.1103/PhysRevD.88.054014.

[1024] F.-Z. Peng, M.-Z. Liu, Y.-W. Pan, M. Sánchez Sánchez, M. Pavon Valderrama, Five-flavor pentaquarks and other light- and heavy-flavor symmetry partners of the LHCb hidden-charm pentaquarks, Nucl. Phys. B 983 (2022) 115936. arXiv:1907.05322, doi:10.1016/j.nuclphysb.2022.115936.

[1025] N. A. Tornqvist, Isospin breaking of the narrow charmonium state of Belle at 3872 MeV as a deuson, Phys. Lett. B 590 (2004) 209–215. arXiv:hep-ph/0402237, doi:10.1016/j.physletb.2004.03.077.

[1026] Y.-R. Liu, X. Liu, W.-Z. Deng, S.-L. Zhu, Is X(3872) Really a Molecular State?, Eur. Phys. J. C 56 (2008) 63–73. arXiv:0801.3540, doi:10.1140/epjc/s10052-008-0640-4.

[1027] X. Liu, Z.-G. Luo, Y.-R. Liu, S.-L. Zhu, X(3872) and Other Possible Heavy Molecular States, Eur. Phys. J. C 61 (2009) 411–428. arXiv:0808.0073, doi:10.1140/epjc/s10052-009-1020-4.

[1028] L. Maiani, A. D. Polosa, V. Riquer, Indications of a Four-Quark Structure for the X(3872) and X(3876) Particles from Recent Belle and

BABAR Data, Phys. Rev. Lett. 99 (2007) 182003. `arXiv:0707.3354`, `doi:10.1103/PhysRevLett.99.182003`.

[1029] T. Barnes, S. Godfrey, Charmonium options for the $X(3872)$, Phys. Rev. D 69 (2004) 054008. `arXiv:hep-ph/0311162`, `doi:10.1103/PhysRevD.69.054008`.

[1030] Y. S. Kalashnikova, A. V. Nefediev, $X(3872)$ as a $^1D_2$ charmonium state, Phys. Rev. D 82 (2010) 097502. `arXiv:1008.2895`, `doi:10.1103/PhysRevD.82.097502`.

[1031] E. Braaten, M. Kusunoki, Low-energy universality and the new charmonium resonance at 3870 MeV, Phys. Rev. D 69 (2004) 074005. `arXiv:hep-ph/0311147`, `doi:10.1103/PhysRevD.69.074005`.

[1032] Y. S. Kalashnikova, Coupled-channel model for charmonium levels and an option for $X(3872)$, Phys. Rev. D 72 (2005) 034010. `arXiv:hep-ph/0506270`, `doi:10.1103/PhysRevD.72.034010`.

[1033] T. Barnes, E. S. Swanson, Hadron loops: General theorems and application to charmonium, Phys. Rev. C 77 (2008) 055206. `arXiv:0711.2080`, `doi:10.1103/PhysRevC.77.055206`.

[1034] P. G. Ortega, J. Segovia, D. R. Entem, F. Fernandez, Coupled channel approach to the structure of the $X(3872)$, Phys. Rev. D 81 (2010) 054023. `arXiv:0907.3997`, `doi:10.1103/PhysRevD.81.054023`.

[1035] B.-Q. Li, C. Meng, K.-T. Chao, Coupled-Channel and Screening Effects in Charmonium Spectrum, Phys. Rev. D 80 (2009) 014012. `arXiv:0904.4068`, `doi:10.1103/PhysRevD.80.014012`.

[1036] Y. Yamaguchi, A. Hosaka, S. Takeuchi, M. Takizawa, Heavy hadronic molecules with pion exchange and quark core couplings: a guide for practitioners, J. Phys. G 47 (5) (2020) 053001. `arXiv:1908.08790`, `doi:10.1088/1361-6471/ab72b0`.

[1037] Y. S. Kalashnikova, A. V. Nefediev, $X(3872)$ in the molecular model, Phys. Usp. 62 (6) (2019) 568–595. `arXiv:1811.01324`, `doi:10.3367/UFNe.2018.08.038411`.

[1038] C. Hanhart, Y. S. Kalashnikova, A. E. Kudryavtsev, A. V. Nefediev, Reconciling the $X(3872)$ with the near-threshold enhancement in the $D^0\bar{D}^{*0}$ final state, Phys. Rev. D 76 (2007) 034007. `arXiv:0704.0605`, `doi:10.1103/PhysRevD.76.034007`.

[1039] B. Gao, Repulsive $1/r^3$ interaction, Physical Review A 59 (4) (1999) 2778.

[1040] M. Suzuki, The $X(3872)$ boson: Molecule or charmonium, Phys. Rev. D 72 (2005) 114013. `arXiv:hep-ph/0508258`, `doi:10.1103/PhysRevD.72.114013`.

[1041] E. Braaten, M. Lu, J. Lee, Weakly-bound Hadronic Molecule near a 3-body Threshold, Phys. Rev. D 76 (2007) 054010. `arXiv:hep-ph/0702128`, `doi:10.1103/PhysRevD.76.054010`.

[1042] E. Braaten, M. Kusunoki, Factorization in the production and decay of the $X(3872)$, Phys. Rev. D 72 (2005) 014012. `arXiv:hep-ph/0506087`, `doi:10.1103/PhysRevD.72.014012`.

[1043] E. Braaten, M. Lu, Operator Product Expansion in the Production and Decay of the $X(3872)$, Phys. Rev. D 74 (2006) 054020. `arXiv:hep-ph/0606115`, `doi:10.1103/PhysRevD.74.054020`.

[1044] E. Braaten, M. Kusunoki, S. Nussinov, Production of the $X(3870)$ in B meson decay by the coalescence of charm mesons, Phys. Rev. Lett. 93 (2004) 162001. `arXiv:hep-ph/0404161`, `doi:10.1103/PhysRevLett.93.162001`.

[1045] E. Braaten, M. Kusunoki, Exclusive production of the $X(3872)$ in B meson decay, Phys. Rev. D 71 (2005) 074005. `arXiv:hep-ph/0412268`, `doi:10.1103/PhysRevD.71.074005`.

[1046] E. Braaten, Inclusive production of the $X(3872)$, Phys. Rev. D 73 (2006) 011501. `arXiv:hep-ph/0408230`, `doi:10.1103/PhysRevD.73.011501`.

[1047] E. Braaten, M. Lu, The Effects of charged charm mesons on the line shapes of the $X(3872)$, Phys. Rev. D 77 (2008) 014029. `arXiv:0710.5482`, `doi:10.1103/PhysRevD.77.014029`.

[1048] E. Braaten, J. Stapleton, Analysis of $J/\psi\pi^+\pi^-$ and $D^0\bar{D}^0\pi^0$ Decays of the $X(3872)$, Phys. Rev. D 81 (2010) 014019. `arXiv:0907.3167`, `doi:10.1103/PhysRevD.81.014019`.

[1049] E. Braaten, D. Kang, $J/\psi\omega$ Decay Channel of the $X(3872)$ Charm Meson Molecule, Phys. Rev. D 88 (1) (2013) 014028. `arXiv:1305.5564`, `doi:10.1103/PhysRevD.88.014028`.

[1050] L. Meng, G.-J. Wang, B. Wang, S.-L. Zhu, Revisit the isospin violating decays of $X(3872)$, Phys. Rev. D 104 (9) (2021) 094003. `arXiv:2109.01333`, `doi:10.1103/PhysRevD.104.094003`.

[1051] T. Mehen, R. Springer, Radiative Decays $X(3872) \to \psi(2S)\gamma$ and $\psi(4040) \to X(3872)\gamma$ in Effective Field Theory, Phys. Rev. D 83 (2011) 094009. `arXiv:1101.5175`, `doi:10.1103/PhysRevD.83.094009`.

[1052] S. Fleming, T. Mehen, The decay of the $X(3872)$ into χ_{cJ} and the Operator Product Expansion in XEFT, Phys. Rev. D 85 (2012) 014016. `arXiv:1110.0265`, `doi:10.1103/PhysRevD.85.014016`.

[1053] M. H. Alhakami, M. C. Birse, Power counting for three-body decays of a near-threshold state, Phys. Rev. D 91 (5) (2015) 054019. `arXiv:1501.06750`, `doi:10.1103/PhysRevD.91.054019`.

[1054] E. Braaten, Galilean-invariant effective field theory for the $X(3872)$, Phys. Rev. D 91 (11) (2015) 114007. `arXiv:1503.04791`, `doi:10.1103/PhysRevD.91.114007`.

[1055] E. Braaten, L.-P. He, J. Jiang, Galilean-invariant effective field theory for the $X(3872)$ at next-to-leading order, Phys. Rev. D 103 (3) (2021) 036014. `arXiv:2010.05801`, `doi:10.1103/PhysRevD.103.036014`.

[1056] F.-K. Guo, C. Hanhart, U.-G. Meissner, On the extraction of the light quark mass ratio from the decays $\psi' \to J/\psi\pi^0(\eta)$, Phys. Rev. Lett. 103 (2009) 082003, [Erratum: Phys.Rev.Lett. 104, 109901 (2010)]. `arXiv:0907.0521`, `doi:10.1103/PhysRevLett.103.082003`.

[1057] F.-K. Guo, C. Hanhart, G. Li, U.-G. Meissner, Q. Zhao, Novel analysis of the decays $\psi' \to h_c\pi^0$ and $\eta_c' \to \chi_{c0}\pi^0$, Phys. Rev. D 82 (2010) 034025. `arXiv:1002.2712`, `doi:10.1103/PhysRevD.82.034025`.

[1058] F.-K. Guo, C. Hanhart, G. Li, U.-G. Meissner, Q. Zhao, Effect of charmed meson loops on charmonium transitions, Phys. Rev. D 83 (2011) 034013. `arXiv:1008.3632`, `doi:10.1103/PhysRevD.83.034013`.

[1059] F.-K. Guo, C. Hanhart, U.-G. Meißner, Q. Wang, Q. Zhao, Production of the $X(3872)$ in charmonia radiative decays, Phys. Lett. B 725 (2013) 127–133. `arXiv:1306.3096`, `doi:10.1016/j.physletb.2013.06.053`.

[1060] F.-K. Guo, C. Hanhart, Y. S. Kalashnikova, U.-G. Meißner, A. V. Nefediev, What can radiative decays of the $X(3872)$ teach us about its nature?, Phys. Lett. B 742 (2015) 394–398. `arXiv:1410.6712`, `doi:10.1016/j.physletb.2015.02.013`.

[1061] T. Mehen, Hadronic loops versus factorization in effective field theory calculations of $X(3872) \to \chi_{cJ}\pi^0$, Phys. Rev. D 92 (3) (2015)

173

034019. arXiv:1503.02719, doi:10.1103/PhysRevD.92.034019.

[1062] C. Hanhart, Y. S. Kalashnikova, A. E. Kudryavtsev, A. V. Nefediev, Two-photon decays of hadronic molecules, Phys. Rev. D 75 (2007) 074015. arXiv:hep-ph/0701214, doi:10.1103/PhysRevD.75.074015.

[1063] F.-K. Guo, X.-H. Liu, S. Sakai, Threshold cusps and triangle singularities in hadronic reactions, Prog. Part. Nucl. Phys. 112 (2020) 103757. arXiv:1912.07030, doi:10.1016/j.ppnp.2020.103757.

[1064] F.-K. Guo, Novel Method for Precisely Measuring the $X(3872)$ Mass, Phys. Rev. Lett. 122 (20) (2019) 202002. arXiv:1902.11221, doi:10.1103/PhysRevLett.122.202002.

[1065] E. Braaten, L.-P. He, K. Ingles, Triangle Singularity in the Production of $X(3872)$ and a Photon in e^+e^- Annihilation, Phys. Rev. D 100 (3) (2019) 031501. arXiv:1904.12915, doi:10.1103/PhysRevD.100.031501.

[1066] E. Braaten, L.-P. He, K. Ingles, Production of $X(3872)$ Accompanied by a Pion in B Meson Decay, Phys. Rev. D 100 (7) (2019) 074028. arXiv:1902.03259, doi:10.1103/PhysRevD.100.074028.

[1067] E. Braaten, L.-P. He, K. Ingles, Production of $X(3872)$ Accompanied by a Soft Pion at Hadron Colliders, Phys. Rev. D 100 (9) (2019) 094006. arXiv:1903.04355, doi:10.1103/PhysRevD.100.094006.

[1068] E. Braaten, L.-P. He, K. Ingles, Production of $X(3872)$ and a Photon in e^+e^- Annihilation, Phys. Rev. D 101 (1) (2020) 014021. arXiv:1909.03901, doi:10.1103/PhysRevD.101.014021.

[1069] W. Glöckle, The quantum mechanical few-body problem, Texts and monographs in physics, Springer, Berlin, 1983. doi:10.1007/978-3-642-82081-6.
URL https://cds.cern.ch/record/99109

[1070] C. E. Thomas, F. E. Close, Is $X(3872)$ a molecule?, Phys. Rev. D 78 (2008) 034007. arXiv:0805.3653, doi:10.1103/PhysRevD.78.034007.

[1071] E. Epelbaum, J. Gegelia, Weinberg's approach to nucleon–nucleon scattering revisited, Phys. Lett. B 716 (2012) 338–344. arXiv:1207.2420, doi:10.1016/j.physletb.2012.08.025.

[1072] M. J. Savage, Including pions, in: Caltech / INT Mini Workshop on Nuclear Physics with Effective Field Theories, 1998, pp. 247–267. arXiv:nucl-th/9804034.

[1073] M. Padmanath, C. B. Lang, S. Prelovsek, $X(3872)$ and $Y(4140)$ using diquark-antidiquark operators with lattice QCD, Phys. Rev. D 92 (3) (2015) 034501. arXiv:1503.03257, doi:10.1103/PhysRevD.92.034501.

[1074] G. Colangelo, J. Gasser, H. Leutwyler, $\pi\pi$ scattering, Nucl. Phys. B 603 (2001) 125–179. arXiv:hep-ph/0103088, doi:10.1016/S0550-3213(01)00147-X.

[1075] M. Jansen, H. W. Hammer, Y. Jia, Finite volume corrections to the binding energy of the $X(3872)$, Phys. Rev. D 92 (11) (2015) 114031. arXiv:1505.04099, doi:10.1103/PhysRevD.92.114031.

[1076] J. F. Donoghue, C. Ramirez, G. Valencia, The Spectrum of QCD and Chiral Lagrangians of the Strong and Weak Interactions, Phys. Rev. D 39 (1989) 1947. doi:10.1103/PhysRevD.39.1947.

[1077] S. Prelovsek, S. Collins, D. Mohler, M. Padmanath, S. Piemonte, Charmonium-like resonances with $J^{PC} = 0^{++}, 2^{++}$ in coupled $D\bar{D}, D_s\bar{D}_s$ scattering on the lattice, JHEP 06 (2021) 035. arXiv:2011.02542, doi:10.1007/JHEP06(2021)035.

[1078] R. Aaij, et al., Amplitude analysis of the $B^+ \to D^+D^-K^+$ decay, Phys. Rev. D 102 (2020) 112003. arXiv:2009.00026, doi:10.1103/PhysRevD.102.112003.

[1079] R. Aaij, et al., A model-independent study of resonant structure in $B^+ \to D^+D^-K^+$ decays, Phys. Rev. Lett. 125 (2020) 242001. arXiv:2009.00025, doi:10.1103/PhysRevLett.125.242001.

[1080] Z.-H. Zhang, F.-K. Guo, $D^\pm D^{*\mp}$ Hadronic Atom as a Key to Revealing the $X(3872)$ Mystery, Phys. Rev. Lett. 127 (1) (2021) 012002. arXiv:2012.08281, doi:10.1103/PhysRevLett.127.012002.

[1081] B. R. Holstein, Hadronic atoms and effective interactions, Phys. Rev. D 60 (1999) 114030. arXiv:nucl-th/9901041, doi:10.1103/PhysRevD.60.114030.

[1082] J. Gasser, V. E. Lyubovitskij, A. Rusetsky, Hadronic atoms in QCD + QED, Phys. Rept. 456 (2008) 167–251. arXiv:0711.3522, doi:10.1016/j.physrep.2007.09.006.

[1083] D. L. Canham, H. W. Hammer, R. P. Springer, On the scattering of D and D^* mesons off the $X(3872)$, Phys. Rev. D 80 (2009) 014009. arXiv:0906.1263, doi:10.1103/PhysRevD.80.014009.

[1084] E. Braaten, H. W. Hammer, T. Mehen, Scattering of an Ultrasoft Pion and the $X(3872)$, Phys. Rev. D 82 (2010) 034018. arXiv:1005.1688, doi:10.1103/PhysRevD.82.034018.

[1085] L. Contessi, J. Kirscher, M. Pavon Valderrama, Triple-X and beyond: hadronic systems of three and more $X(3872)$, Phys. Rev. D 103 (5) (2021) 056001. arXiv:2008.12268, doi:10.1103/PhysRevD.103.056001.

[1086] L. Dai, F.-K. Guo, T. Mehen, Revisiting $X(3872) \to D^0\bar{D}^0\pi^0$ in an effective field theory for the $X(3872)$, Phys. Rev. D 101 (5) (2020) 054024. arXiv:1912.04317, doi:10.1103/PhysRevD.101.054024.

[1087] F. K. Guo, C. Hidalgo-Duque, J. Nieves, A. Ozpineci, M. P. Valderrama, Detecting the long-distance structure of the $X(3872)$, Eur. Phys. J. C 74 (5) (2014) 2885. arXiv:1404.1776, doi:10.1140/epjc/s10052-014-2885-4.

[1088] C. Hanhart, Y. S. Kalashnikova, A. E. Kudryavtsev, A. V. Nefediev, Remarks on the quantum numbers of $X(3872)$ from the invariant mass distributions of the $\rho J/\psi$ and $\omega J/\psi$ final states, Phys. Rev. D 85 (2012) 011501. arXiv:1111.6241, doi:10.1103/PhysRevD.85.011501.

[1089] S. Fleming, T. Mehen, Hadronic Decays of the $X(3872)$ to χ_{cJ} in Effective Field Theory, Phys. Rev. D 78 (2008) 094019. arXiv:0807.2674, doi:10.1103/PhysRevD.78.094019.

[1090] E. S. Swanson, Short range structure in the $X(3872)$, Phys. Lett. B 588 (2004) 189–195. arXiv:hep-ph/0311229, doi:10.1016/j.physletb.2004.03.033.

[1091] E. S. Swanson, Diagnostic decays of the $X(3872)$, Phys. Lett. B 598 (2004) 197–202. arXiv:hep-ph/0406080, doi:10.1016/j.physletb.2004.07.059.

[1092] B. Aubert, et al., Evidence for $X(3872) \to \psi(2S)\gamma$ in $B^\pm \to X(3872)K^\pm$ decays, and a study of $B \to c\bar{c}\gamma K$, Phys. Rev. Lett. 102 (2009) 132001. arXiv:0809.0042, doi:10.1103/PhysRevLett.102.132001.

[1093] V. Bhardwaj, et al., Observation of $X(3872) \to J/\psi\gamma$ and search for $X(3872) \to \psi'\gamma$ in B decays, Phys. Rev. Lett. 107 (2011) 091803.

arXiv:1105.0177, doi:10.1103/PhysRevLett.107.091803.

[1094] R. Aaij, et al., Evidence for the decay $X(3872) \to \psi(2S)\gamma$, Nucl. Phys. B 886 (2014) 665–680. arXiv:1404.0275, doi:10.1016/j.nuclphysb.2014.06.011.

[1095] A. Margaryan, R. P. Springer, Using the decay $\psi(4160) \to X(3872)\gamma$ to probe the molecular content of the $X(3872)$, Phys. Rev. D 88 (1) (2013) 014017. arXiv:1304.8101, doi:10.1103/PhysRevD.88.014017.

[1096] Q. Wu, G. Li, F. Shao, Q. Wang, R. Wang, Y. Zhang, Y. Zheng, Production of X_b in $\Upsilon(5S, 6S) \to \gamma X_b$ Radiative Decays, Adv. High Energy Phys. 2016 (2016) 3729050. arXiv:1606.05118, doi:10.1155/2016/3729050.

[1097] A. Esposito, B. Grinstein, L. Maiani, F. Piccinini, A. Pilloni, A. D. Polosa, V. Riquer, Comment on 'Note on $X(3872)$ production at hadron colliders and its molecular structure', Chin. Phys. C 42 (11) (2018) 114107. arXiv:1709.09631, doi:10.1088/1674-1137/42/11/114107.

[1098] Y. Jin, S.-Y. Li, Y.-R. Liu, Q. Qin, Z.-G. Si, F.-S. Yu, Color and baryon number fluctuation of preconfinement system in production process and T_{cc} structure, Phys. Rev. D 104 (11) (2021) 114009. arXiv:2109.05678, doi:10.1103/PhysRevD.104.114009.

[1099] M. Pavon Valderrama, Heavy hadron molecules in effective field theory: the emergence of exotic nuclear landscapes, Eur. Phys. J. A 56 (4) (2020) 109. arXiv:1906.06491, doi:10.1140/epja/s10050-020-00099-8.

[1100] F.-K. Guo, C. Hidalgo-Duque, J. Nieves, M. P. Valderrama, Consequences of Heavy Quark Symmetries for Hadronic Molecules, Phys. Rev. D 88 (2013) 054007. arXiv:1303.6608, doi:10.1103/PhysRevD.88.054007.

[1101] T. Mehen, J. Powell, Line shapes in $\Upsilon(5S) \to B^*\bar{B}(*)\pi$ with $Z_b(10610)$ and $Z_b(10650)$ using effective field theory, Phys. Rev. D 88 (3) (2013) 034017. arXiv:1306.5459, doi:10.1103/PhysRevD.88.034017.

[1102] C. Hanhart, Y. S. Kalashnikova, P. Matuschek, R. V. Mizuk, A. V. Nefediev, Q. Wang, Practical Parametrization for Line Shapes of Near-Threshold States, Phys. Rev. Lett. 115 (20) (2015) 202001. arXiv:1507.00382, doi:10.1103/PhysRevLett.115.202001.

[1103] F. Aceti, M. Bayar, E. Oset, A. Martinez Torres, K. P. Khemchandani, J. M. Dias, F. S. Navarra, M. Nielsen, Prediction of an $I = 1$ $D\bar{D}^*$ state and relationship to the claimed $Z_c(3900)$, $Z_c(3885)$, Phys. Rev. D 90 (1) (2014) 016003. arXiv:1401.8216, doi:10.1103/PhysRevD.90.016003.

[1104] J. He, The $Z_c(3900)$ as a resonance from the $D\bar{D}^*$ interaction, Phys. Rev. D 92 (3) (2015) 034004. arXiv:1505.05379, doi:10.1103/PhysRevD.92.034004.

[1105] D. V. Bugg, An Explanation of Belle states $Z_b(10610)$ and $Z_b(10650)$, EPL 96 (1) (2011) 11002. arXiv:1105.5492, doi:10.1209/0295-5075/96/11002.

[1106] D.-Y. Chen, X. Liu, $Z_b(10610)$ and $Z_b(10650)$ structures produced by the initial single pion emission in the $\Upsilon(5S)$ decays, Phys. Rev. D 84 (2011) 094003. arXiv:1106.3798, doi:10.1103/PhysRevD.84.094003.

[1107] D.-Y. Chen, X. Liu, T. Matsuki, Reproducing the $Z_c(3900)$ structure through the initial-single-pion-emission mechanism, Phys. Rev. D 88 (3) (2013) 036008. arXiv:1304.5845, doi:10.1103/PhysRevD.88.036008.

[1108] E. S. Swanson, Z_b and Z_c Exotic States as Coupled Channel Cusps, Phys. Rev. D 91 (3) (2015) 034009. arXiv:1409.3291, doi:10.1103/PhysRevD.91.034009.

[1109] F.-K. Guo, C. Hanhart, Q. Wang, Q. Zhao, Could the near-threshold XYZ states be simply kinematic effects?, Phys. Rev. D 91 (5) (2015) 051504. arXiv:1411.5584, doi:10.1103/PhysRevD.91.051504.

[1110] S. Prelovsek, L. Leskovec, Search for $Z_c^+(3900)$ in the 1^{+-} Channel on the Lattice, Phys. Lett. B 727 (2013) 172–176. arXiv:1308.2097, doi:10.1016/j.physletb.2013.10.009.

[1111] S. Prelovsek, C. B. Lang, L. Leskovec, D. Mohler, Study of the Z_c^+ channel using lattice QCD, Phys. Rev. D 91 (1) (2015) 014504. arXiv:1405.7623, doi:10.1103/PhysRevD.91.014504.

[1112] S.-h. Lee, C. DeTar, D. Mohler, H. Na, Searching for the $X(3872)$ and $Z_c^+(3900)$ on HISQ Lattices (11 2014). arXiv:1411.1389.

[1113] Y. Chen, et al., Low-energy scattering of the $(D\bar{D}^*)^{\pm}$ system and the resonance-like structure $Z_c(3900)$, Phys. Rev. D 89 (9) (2014) 094506. arXiv:1403.1318, doi:10.1103/PhysRevD.89.094506.

[1114] C. Liu, L. Liu, K.-L. Zhang, Towards the understanding of $Z_c(3900)$ from lattice QCD, Phys. Rev. D 101 (5) (2020) 054502. arXiv:1911.08560, doi:10.1103/PhysRevD.101.054502.

[1115] Y. Ikeda, S. Aoki, T. Doi, S. Gongyo, T. Hatsuda, T. Inoue, T. Iritani, N. Ishii, K. Murano, K. Sasaki, Fate of the Tetraquark Candidate $Z_c(3900)$ from Lattice QCD, Phys. Rev. Lett. 117 (24) (2016) 242001. arXiv:1602.03465, doi:10.1103/PhysRevLett.117.242001.

[1116] Y. Ikeda, The tetraquark candidate $Z_c(3900)$ from dynamical lattice QCD simulations, J. Phys. G 45 (2) (2018) 024002. arXiv:1706.07300, doi:10.1088/1361-6471/aa9afd.

[1117] V. Baru, E. Epelbaum, J. Gegelia, C. Hanhart, U. G. Meißner, A. V. Nefediev, Remarks on the Heavy-Quark Flavour Symmetry for doubly heavy hadronic molecules, Eur. Phys. J. C 79 (1) (2019) 46. arXiv:1810.06921, doi:10.1140/epjc/s10052-019-6560-7.

[1118] W. Detmold, S. Meinel, Z. Shi, Quarkonium at nonzero isospin density, Phys. Rev. D 87 (9) (2013) 094504. arXiv:1211.3156, doi:10.1103/PhysRevD.87.094504.

[1119] X.-H. Liu, F.-K. Guo, E. Epelbaum, Extracting $\pi\pi$ S-wave scattering lengths from cusp effect in heavy quarkonium dipion transitions, Eur. Phys. J. C 73 (1) (2013) 2284. arXiv:1212.4066, doi:10.1140/epjc/s10052-013-2284-2.

[1120] W. R. Frazer, A. W. Hendry, S-Matrix Poles Close to Threshold, Phys. Rev. 134 (1964) B1307–B1314. doi:10.1103/PhysRev.134.B1307.

[1121] R. J. Eden, J. R. Taylor, Poles and Shadow Poles in the Many-Channel S-Matrix, Phys. Rev. 133 (1964) B1575–B1580. doi:10.1103/PhysRev.133.B1575.

[1122] M. Albaladejo, P. Fernandez-Soler, J. Nieves, $Z_c(3900)$: Confronting theory and lattice simulations, Eur. Phys. J. C 76 (10) (2016) 573. arXiv:1606.03008, doi:10.1140/epjc/s10052-016-4427-8.

[1123] C. B. Dover, T. Gutsche, M. Maruyama, A. Faessler, The Physics of nucleon-antinucleon annihilation, Prog. Part. Nucl. Phys. 29 (1992) 87–174. doi:10.1016/0146-6410(92)90004-L.

[1124] X.-W. Kang, J. Haidenbauer, U.-G. Meißner, Antinucleon-nucleon interaction in chiral effective field theory, JHEP 02 (2014) 113. arXiv:1311.1658, doi:10.1007/JHEP02(2014)113.

[1125] V. Baru, E. Epelbaum, A. A. Filin, C. Hanhart, R. V. Mizuk, A. V. Nefediev, S. Ropertz, Insights into $Z_b(10610)$ and $Z_b(10650)$ from dipion

transitions from $\Upsilon(10860)$, Phys. Rev. D 103 (3) (2021) 034016. `arXiv:2012.05034`, `doi:10.1103/PhysRevD.103.034016`.

[1126] A. G. Drutskoy, F.-K. Guo, F. J. Llanes-Estrada, A. V. Nefediev, J. M. Torres-Rincon, Hadron physics potential of future high-luminosity *B*-factories at the $\Upsilon(5S)$ and above, Eur. Phys. J. A 49 (2013) 7–32. `arXiv:1210.6623`, `doi:10.1140/epja/i2013-13007-x`.

[1127] V. Baru, E. Epelbaum, A. A. Filin, C. Hanhart, A. V. Nefediev, Spin partners of the $Z_b(10610)$ and $Z_b(10650)$ revisited, JHEP 06 (2017) 158. `arXiv:1704.07332`, `doi:10.1007/JHEP06(2017)158`.

[1128] V. Baru, E. Epelbaum, A. A. Filin, C. Hanhart, A. V. Nefediev, Q. Wang, Spin partners W_{bJ} from the line shapes of the $Z_b(10610)$ and $Z_b(10650)$, Phys. Rev. D 99 (9) (2019) 094013. `arXiv:1901.10319`, `doi:10.1103/PhysRevD.99.094013`.

[1129] M. Ablikim, et al., Observation of a charged charmoniumlike structure in $e^+e^- \rightarrow (D^*\bar{D}^*)^{\pm}\pi^{\mp}$ at $\sqrt{s} = 4.26$ GeV, Phys. Rev. Lett. 112 (13) (2014) 132001. `arXiv:1308.2760`, `doi:10.1103/PhysRevLett.112.132001`.

[1130] Z. Zhang, J. Liu, J. Hu, Q. Wang, U.-G. Meißner, Revealing the nature of hidden charm pentaquarks with machine learning (1 2023). `arXiv:2301.05364`.

[1131] M. Karliner, J. L. Rosner, New Exotic Meson and Baryon Resonances from Doubly-Heavy Hadronic Molecules, Phys. Rev. Lett. 115 (12) (2015) 122001. `arXiv:1506.06386`, `doi:10.1103/PhysRevLett.115.122001`.

[1132] D. B. Kaplan, M. J. Savage, The Spin flavor dependence of nuclear forces from large *N* QCD, Phys. Lett. B 365 (1996) 244–251. `arXiv:hep-ph/9509371`, `doi:10.1016/0370-2693(95)01277-X`.

[1133] U. Skerbis, S. Prelovsek, Nucleon-J/ψ and nucleon-η_c scattering in P_c pentaquark channels from LQCD, Phys. Rev. D 99 (9) (2019) 094505. `arXiv:1811.02285`, `doi:10.1103/PhysRevD.99.094505`.

[1134] E. Epelbaum, H. Krebs, D. Lee, U.-G. Meissner, Lattice effective field theory calculations for $A = 3, 4, 6, 12$ nuclei, Phys. Rev. Lett. 104 (2010) 142501. `arXiv:0912.4195`, `doi:10.1103/PhysRevLett.104.142501`.

[1135] B. Borasoy, E. Epelbaum, H. Krebs, D. Lee, U.-G. Meissner, Lattice Simulations for Light Nuclei: Chiral Effective Field Theory at Leading Order, Eur. Phys. J. A 31 (2007) 105–123. `arXiv:nucl-th/0611087`, `doi:10.1140/epja/i2006-10154-1`.

[1136] K. Chen, B. Wang, S.-L. Zhu, Heavy flavor molecular states with strangeness, Phys. Rev. D 105 (9) (2022) 096004. `arXiv:2112.13203`, `doi:10.1103/PhysRevD.105.096004`.

[1137] J.-X. Lu, E. Wang, J.-J. Xie, L.-S. Geng, E. Oset, The $\Lambda_b \rightarrow J/\psi K^0 \Lambda$ reaction and a hidden-charm pentaquark state with strangeness, Phys. Rev. D 93 (2016) 094009. `arXiv:1601.00075`, `doi:10.1103/PhysRevD.93.094009`.

[1138] A. Feijoo, V. K. Magas, A. Ramos, E. Oset, A hidden-charm $S = -1$ pentaquark from the decay of Λ_b into $J/\psi, \eta\Lambda$ states, Eur. Phys. J. C 76 (8) (2016) 446. `arXiv:1512.08152`, `doi:10.1140/epjc/s10052-016-4302-7`.

[1139] W. L. Wang, F. Huang, Z. Y. Zhang, B. S. Zou, $\Sigma_c \bar{D}$ and $\Lambda_c \bar{D}$ states in a chiral quark model, Phys. Rev. C 84 (2011) 015203. `arXiv:1101.0453`, `doi:10.1103/PhysRevC.84.015203`.

[1140] F.-L. Wang, X.-D. Yang, R. Chen, X. Liu, Hidden-charm pentaquarks with triple strangeness due to the $\Omega_c^{(*)}\bar{D}_s^{(*)}$ interactions, Phys. Rev. D 103 (5) (2021) 054025. `arXiv:2101.11200`, `doi:10.1103/PhysRevD.103.054025`.

[1141] B. Wang, S.-L. Zhu, How to understand the X(2900)?, Eur. Phys. J. C 82 (5) (2022) 419. `arXiv:2107.09275`, `doi:10.1140/epjc/s10052-022-10396-9`.

[1142] S. Capstick, N. Isgur, Baryons in a relativized quark model with chromodynamics, Phys. Rev. D 34 (9) (1986) 2809–2835. `doi:10.1103/physrevd.34.2809`.

[1143] K. Tsushima, D.-H. Lu, A. W. Thomas, K. Saito, R. H. Landau, Charmed mesic nuclei, Phys. Rev. C 59 (1999) 2824–2828. `arXiv:nucl-th/9810016`, `doi:10.1103/PhysRevC.59.2824`.

[1144] C. Garcia-Recio, J. Nieves, L. Tolos, *D* mesic nuclei, Phys. Lett. B 690 (2010) 369–375. `arXiv:1004.2634`, `doi:10.1016/j.physletb.2010.05.056`.

[1145] A. Hosaka, T. Hyodo, K. Sudoh, Y. Yamaguchi, S. Yasui, Heavy Hadrons in Nuclear Matter, Prog. Part. Nucl. Phys. 96 (2017) 88–153. `arXiv:1606.08685`, `doi:10.1016/j.ppnp.2017.04.003`.

[1146] G. Krein, A. W. Thomas, K. Tsushima, Nuclear-bound quarkonia and heavy-flavor hadrons, Prog. Part. Nucl. Phys. 100 (2018) 161–210. `arXiv:1706.02688`, `doi:10.1016/j.ppnp.2018.02.001`.

[1147] J. Haidenbauer, G. Krein, U.-G. Meissner, $\bar{D}N$ interaction from meson-exchange and quark-gluon dynamics, Eur. Phys. J. A 33 (2007) 107–117. `arXiv:0704.3668`, `doi:10.1140/epja/i2007-10417-3`.

[1148] J. Haidenbauer, G. Krein, U.-G. Meissner, A. Sibirtsev, Charmed meson rescattering in the reaction $\bar{p}d \rightarrow \bar{D}D n$, Eur. Phys. J. A 37 (2008) 55–67. `arXiv:0803.3752`, `doi:10.1140/epja/i2008-10602-x`.

[1149] J. Haidenbauer, G. Krein, U.-G. Meissner, L. Tolos, DN interaction from meson exchange, Eur. Phys. J. A 47 (2011) 18. `arXiv:1008.3794`, `doi:10.1140/epja/i2011-11018-3`.

[1150] S. Sakai, F.-K. Guo, B. Kubis, Extraction of ND scattering lengths from the $\Lambda_b \rightarrow \pi^- pD^0$ decay and properties of the $\Sigma_c(2800)^+$, Phys. Lett. B 808 (2020) 135623. `arXiv:2004.09824`, `doi:10.1016/j.physletb.2020.135623`.

[1151] Z.-L. Zhang, Z.-W. Liu, S.-Q. Luo, F.-L. Wang, B. Wang, H. Xu, $\Lambda c(2910)$ and $\Lambda c(2940)$ as conventional baryons dressed with the D*N channel, Phys. Rev. D 107 (3) (2023) 034036. `arXiv:2210.17188`, `doi:10.1103/PhysRevD.107.034036`.

[1152] G. Bhamathi, Light Supernuclei and SU(4) Symmetry, Phys. Rev. C 24 (1981) 1816–1818. `doi:10.1103/PhysRevC.24.1816`.

[1153] H. Bando, S. Nagata, Flavor nuclei one boson exchange potentials, Prog. Theor. Phys. 69 (1983) 557–564. `doi:10.1143/PTP.69.557`.

[1154] N. I. Starkov, V. A. Tsarev, Charmed nuclei, Nucl. Phys. A 450 (1986) 507C–516C. `doi:10.1016/0375-9474(86)90584-1`.

[1155] H. Fujioka, et al., Extension of the J-PARC Hadron Experimental Facility-summary report (6 2017). `arXiv:1706.07916`.

[1156] U. Wiedner, Future Prospects for Hadron Physics at PANDA, Prog. Part. Nucl. Phys. 66 (2011) 477–518. `arXiv:1104.3961`, `doi:10.1016/j.ppnp.2011.04.001`.

[1157] H. Garcilazo, A. Valcarce, T. F. Caramés, $J = 3/2$ charmed hypertriton, Phys. Rev. C 92 (2) (2015) 024006. `arXiv:1508.03535`, `doi:10.1103/PhysRevC.92.024006`.

[1158] I. Vidaña, A. Ramos, C. E. Jimenez-Tejero, Charmed nuclei within a microscopic many-body approach, Phys. Rev. C 99 (4) (2019) 045208. `arXiv:1901.09644`, `doi:10.1103/PhysRevC.99.045208`.

[1159] S. Maeda, M. Oka, A. Yokota, E. Hiyama, Y.-R. Liu, A model of charmed baryon–nucleon potential and two- and three-body bound states with charmed baryon, PTEP 2016 (2) (2016) 023D02. `arXiv:1509.02445`, `doi:10.1093/ptep/ptv194`.

[1160] S. Maeda, M. Oka, Y.-R. Liu, Resonance states in the Y_cN potential model, Phys. Rev. C 98 (3) (2018) 035203. arXiv:1803.11349, doi:10.1103/PhysRevC.98.035203.

[1161] H. Huang, J. Ping, F. Wang, $N\Sigma_c$ and $N\Sigma_b$ resonances in the quark-delocalization color-screening model, Phys. Rev. C 87 (3) (2013) 034002. doi:10.1103/PhysRevC.87.034002.

[1162] H. Garcilazo, A. Valcarce, T. F. Caramés, Charmed baryon–nucleon interaction, Eur. Phys. J. C 79 (7) (2019) 598. arXiv:1907.05022, doi:10.1140/epjc/s10052-019-7110-z.

[1163] T. Miyamoto, et al., Λ_cN interaction from lattice QCD and its application to Λ_c hypernuclei, Nucl. Phys. A 971 (2018) 113–129. arXiv:1710.05545, doi:10.1016/j.nuclphysa.2018.01.015.

[1164] J. Haidenbauer, G. Krein, Scattering of charmed baryons on nucleons, Eur. Phys. J. A 54 (11) (2018) 199. arXiv:1711.06470, doi:10.1140/epja/i2018-12638-7.

[1165] T. Miyamoto, Coupled-channel $\Lambda_cN - \Sigma_cN$ interaction from lattice QCD, PoS Hadron2017 (2018) 146. doi:10.22323/1.310.0146.

[1166] J. Haidenbauer, G. Krein, T. C. Peixoto, Femtoscopic correlations and the Λ_cN interaction, Eur. Phys. J. A 56 (7) (2020) 184. arXiv:2004.08136, doi:10.1140/epja/s10050-020-00190-0.

[1167] J. Song, Y. Xiao, Z.-W. Liu, C.-X. Wang, K.-W. Li, L.-S. Geng, Λ_cN interaction in leading-order covariant chiral effective field theory, Phys. Rev. C 102 (6) (2020) 065208. arXiv:2010.06916, doi:10.1103/PhysRevC.102.065208.

[1168] J. Haidenbauer, G. Krein, Comment on "Λ_cN interaction in leading order covariant chiral effective field theory" (1 2021). arXiv:2101.07160.

[1169] J. Song, Y. Xiao, Z.-W. Liu, K.-W. Li, L.-S. Geng, $^3S_1$–$^3D_1$ coupled channel Λ_c N interactions: chiral effective field theory versus lattice QCD, Commun. Theor. Phys. 75 (1) (2023) 015202. arXiv:2104.02380, doi:10.1088/1572-9494/ac9a3d.

[1170] B. Julia-Diaz, D. O. Riska, Nuclei of double charm hyperons, Nucl. Phys. A 755 (2005) 431–434. arXiv:nucl-th/0405061, doi:10.1016/j.nuclphysa.2005.03.050.

[1171] F. Froemel, B. Julia-Diaz, D. O. Riska, Bound states of double flavor hyperons, Nucl. Phys. A 750 (2005) 337–356. arXiv:nucl-th/0410034, doi:10.1016/j.nuclphysa.2005.01.022.

[1172] L. Meng, N. Li, S.-l. Zhu, Possible hadronic molecules composed of the doubly charmed baryon and nucleon, Eur. Phys. J. A 54 (9) (2018) 143. arXiv:1707.03598, doi:10.1140/epja/i2018-12578-2.

[1173] Z.-G. Wang, Analysis of the doubly heavy baryon states and pentaquark states with QCD sum rules, Eur. Phys. J. C 78 (10) (2018) 826. arXiv:1808.09820, doi:10.1140/epjc/s10052-018-6300-4.

[1174] J.-X. Lu, L.-S. Geng, M. P. Valderrama, Heavy baryon-antibaryon molecules in effective field theory, Phys. Rev. D 99 (7) (2019) 074026. arXiv:1706.02588, doi:10.1103/PhysRevD.99.074026.

[1175] N. Lee, Z.-G. Luo, X.-L. Chen, S.-L. Zhu, Possible Deuteron-like Molecular States Composed of Heavy Baryons, Phys. Rev. D 84 (2011) 014031. arXiv:1104.4257, doi:10.1103/PhysRevD.84.014031.

[1176] H. Huang, J. Ping, F. Wang, Possible H-like dibaryon states with heavy quarks, Phys. Rev. C 89 (3) (2014) 035201. arXiv:1311.4732, doi:10.1103/PhysRevC.89.035201.

[1177] T. F. Carames, A. Valcarce, Heavy flavor dibaryons, Phys. Rev. D 92 (3) (2015) 034015. arXiv:1507.08278, doi:10.1103/PhysRevD.92.034015.

[1178] H. Garcilazo, A. Valcarce, Doubly charmed multibaryon systems, Eur. Phys. J. C 80 (8) (2020) 720. arXiv:2008.00675, doi:10.1140/epjc/s10052-020-8320-0.

[1179] X.-Z. Ling, M.-Z. Liu, L.-S. Geng, Masses and strong decays of open charm hexaquark states $\Sigma_c^{(*)}\Sigma_c^{(*)}$, Eur. Phys. J. C 81 (12) (2021) 1090. arXiv:2110.13792, doi:10.1140/epjc/s10052-021-09867-2.

[1180] Z. Liu, H.-T. An, Z.-W. Liu, X. Liu, Where are the hidden-charm hexaquarks?, Phys. Rev. D 105 (3) (2022) 034006. arXiv:2112.02510, doi:10.1103/PhysRevD.105.034006.

[1181] R. Chen, A. Hosaka, X. Liu, Prediction of triple-charm molecular pentaquarks, Phys. Rev. D 96 (11) (2017) 114030. arXiv:1711.09579, doi:10.1103/PhysRevD.96.114030.

[1182] P. Junnarkar, N. Mathur, Deuteronlike Heavy Dibaryons from Lattice Quantum Chromodynamics, Phys. Rev. Lett. 123 (16) (2019) 162003. arXiv:1906.06054, doi:10.1103/PhysRevLett.123.162003.

[1183] R. Chen, F.-L. Wang, A. Hosaka, X. Liu, Exotic triple-charm deuteronlike hexaquarks, Phys. Rev. D 97 (11) (2018) 114011. arXiv:1804.02961, doi:10.1103/PhysRevD.97.114011.

[1184] B. Yang, L. Meng, S.-L. Zhu, Possible molecular states composed of doubly charmed baryons with coupled-channel effect, Eur. Phys. J. A 56 (2) (2020) 67. arXiv:1906.04956, doi:10.1140/epja/s10050-020-00028-9.

[1185] J. B. Habashi, S. Fleming, U. van Kolck, Nonrelativistic Effective Field Theory with a Resonance Field, Eur. Phys. J. A 57 (5) (2021) 169. arXiv:2012.14995, doi:10.1140/epja/s10050-021-00452-5.

[1186] M. Doring, U. G. Meissner, E. Oset, A. Rusetsky, Scalar mesons moving in a finite volume and the role of partial wave mixing, Eur. Phys. J. A 48 (2012) 114. arXiv:1205.4838, doi:10.1140/epja/i2012-12114-6.

[1187] M. Albaladejo, et al., Novel approaches in hadron spectroscopy, Prog. Part. Nucl. Phys. 127 (2022) 103981. arXiv:2112.13436, doi:10.1016/j.ppnp.2022.103981.

[1188] A. Ali, et al., Future Physics in Hall D with the GlueX Detector (2019). URL https://halldweb.jlab.org/DocDB/0038/003870/011/gluex_future.pdf

[1189] W. Altmannshofer, et al., The Belle II Physics Book, PTEP 2019 (12) (2019) 123C01, [Erratum: PTEP 2020, 029201 (2020)]. arXiv:1808.10567, doi:10.1093/ptep/ptz106.

[1190] M. Ablikim, et al., Future Physics Programme of BESIII, Chin. Phys. C 44 (4) (2020) 040001. arXiv:1912.05983, doi:10.1088/1674-1137/44/4/040001.

[1191] R. Aaij, et al., Physics case for an LHCb Upgrade II - Opportunities in flavour physics, and beyond, in the HL-LHC era (8 2018). arXiv:1808.08865.

[1192] M. F. M. Lutz, et al., Physics Performance Report for PANDA: Strong Interaction Studies with Antiprotons (3 2009). arXiv:0903.3905.

[1193] G. Barucca, et al., PANDA Phase One, Eur. Phys. J. A 57 (6) (2021) 184. arXiv:2101.11877, doi:10.1140/epja/

s10050-021-00475-y.

[1194] T. Lee, Particle physics and introduction to field theory, Harwood Academic, 1981, Ch. 12, p. 258.

[1195] S. Scherer, M. R. Schindler, A Primer for Chiral Perturbation Theory, Vol. 830, 2012. `doi:10.1007/978-3-642-19254-8`.

[1196] R. G. Arnold, C. E. Carlson, F. Gross, Elastic electron-Deuteron Scattering at High-Energy, Phys. Rev. C 21 (1980) 1426. `doi:10.1103/PhysRevC.21.1426`.

[1197] H. F. Jones, M. D. Scadron, Multipole $\gamma N\Delta$ form-factors and resonant photoproduction and electroproduction, Annals Phys. 81 (1973) 1–14. `doi:10.1016/0003-4916(73)90476-4`.

[1198] S. Nozawa, D. B. Leinweber, Electromagnetic form-factors of spin-3/2 baryons, Phys. Rev. D 42 (1990) 3567–3571. `doi:10.1103/PhysRevD.42.3567`.

[1199] A. Faessler, T. Gutsche, B. R. Holstein, V. E. Lyubovitskij, D. Nicmorus, K. Pumsa-ard, Light baryon magnetic moments and $N \rightarrow \Delta\gamma$ transition in a Lorentz covariant chiral quark approach, Phys. Rev. D 74 (2006) 074010. `arXiv:hep-ph/0608015`, `doi:10.1103/PhysRevD.74.074010`.

[1200] T. Ledwig, J. Martin-Camalich, V. Pascalutsa, M. Vanderhaeghen, The Nucleon and $\Delta(1232)$ form factors at low momentum-transfer and small pion masses, Phys. Rev. D 85 (2012) 034013. `arXiv:1108.2523`, `doi:10.1103/PhysRevD.85.034013`.